UNIVERSITÀ
DEGLI STUDI
DI TRIESTE

UNIVERSITÀ DEGLI STUDI DI TRIESTE
UNIVERSITÀ CA' FOSCARI VENEZIA

XXXV CICLO DEL DOTTORATO DI RICERCA IN

CHIMICA

PO FRIULI VENEZIA GIULIA - FONDO SOCIALE EUROPEO 2014/2020

THE IMPORTANCE OF SECONDARY INTERACTIONS IN Pd(II) CATALYZED SYNTHESIS OF FUNCTIONALIZED POLYOLEFINS.

Settore scientifico-disciplinare: **CHIM/03**

DOTTORANDO / A
CHIARA ALBERONI

COORDINATORE
PROF. ENZO ALESSIO

SUPERVISORE DI TESI
PROF. BARBARA MILANI

ANNO ACCADEMICO 2021/2022

TABLE OF CONTENTS

LIST OF ABBREVIATIONS

Ar-BIAN: Acenaphthene/bis(aryl-imino)acenaphthene based α-diimines

Ar-BIP: Phenanthrene based α-diimines

Ar-DAB: 1,4-diaza-1,3-butadiene or 1,4-diaza-2,3-methyl-buta-1,3-diene based α-diimines

BArF: $B(3,5–(CF_3)_2C_6H_3)_4^-$ (tetrakis[3,5-bis(trifluoromethyl)phenyl]borate)

Bd: branching degree

$CDCl_3$: deuterated chloroform

CD_2Cl_2: deuterated dichloromethane

CO: carbon monoxide

Cod: *cis*,*cis*–1,5–ciclooctadiene

COSY: correlation spectroscopy

CP: copolymer

DCM: dichloromethane

DFT: density functional theory

DMA: *N*,*N*-dimethylacrylamide

DQCOSY: double quantum correlation spectroscopy

E or Et: ethylene

FPO: functionalized polyolefins

GP: growing polymeric chain

GPC: gel permeation chromatography or growing polymeric chain

HMBC: heteronuclear multiple bond correlation

HSQC: heteronuclear single quantum coherence/correlation spectroscopy

L: labile ligand

lut: lutidine

MA: methyl acrylate

MC4: 4-membered metallacycle

MC5: 5-membered metallacycle

MC6: 6-membered metallacycle

M(MA): methyl acrylate in chain

M_w: mass average molar mass

M_n: number average molar mass

NIPAM: *N*-isopropylacrylamide

NMR: Nuclear magnetic resonance

NOESY: Nuclear Overhauser effect spectroscopy

ORTEP: Oak Ridge Thermal Ellipsoid Plot

OTf: triflate, $CF_3SO_3^-$

pic: picoline

pyr: pyridine

PE: polyethylene

PF_6: hexafluorophosphate

TFE: 2,2,2-trifluoroethanol

T(MA): methyl acrylate at the end of the branches

TOCSY: total correlation spectroscopy

TON: turnover number

TOF: turnover frequency

ABSTRACT

Among all the thermoplastic materials produced on industrial scale, polyolefins are the most versatile ones. However, due to the apolarity of polymer chains, they suffer from poor surface properties that can be improved thanks to the incorporation of low percentages of polar monomers (less than 20 mol %) into the polymer skeleton, leading to the so called "functionalized polyolefins" (FPO). Nowadays, FPO are produced by using radical polymerization processes, requiring harsh reaction conditions and resulting in a poor control over the polymer microstructure. The direct, controlled, homogeneously catalyzed copolymerization of terminal alkenes, such as ethylene (E), with polar vinyl monomers, such as methyl acrylate (MA), is considered one of the most promising and environmentally friendly approach to obtain FPO. From the industrial point of view, the ideal catalyst should show a high productivity and a good thermal stability, and it should exert a precise control over the macromolecule microstructure, in particular over the value of the molecular weight, the length and distribution of polymer branches, the amount of inserted polar monomer and its way of enchainment.

The aim of this PhD thesis is the development of palladium catalysts bearing α-diimine ligands for the synthesis of FPO. In particular, the secondary coordination sphere effects on the catalytic outcome are investigated. The synthesis and characterization of neutral and monocationic Pd(II) complexes will be reported, together with the study of their catalytic behaviour including the characterization of the catalytic products.

Chapter 1 deals with an overview of the principal catalytic systems reported in literature for the synthesis of FPO, with a focus on Pd(II) complexes showing functionalized groups on the N-N ligand. In addition the aim of the work is elucidated.

Chapter 2 focuses on the introduction of a hemilabile, potentially bidentate ligand such as a thiophenimine N-S, in the fourth coordination site of Pd(II) complexes replacing the more labile acetonitrile, usually present in the literature precatalysts. The obtained cationic Pd(II) complexes, $[Pd(CH_3)(N\text{-}N)(N\text{-}S)][PF_6]$, generate active species for the copolymerization of ethylene with methyl acrylate leading to the desired copolymer with a different percentage of the polar monomer incorporation. The inserted MA is present both into the main chain (M(MA)) and at the end of the branches (T(MA)), in a ratio that goes from 9:91 to 45:55 depending on both the solvent (moving from dichloromethane (DCM) to 2,2,2-trifluoroethanol (TFE)) and the nature of the N-S ligand. These new precatalysts, together with the CH_3CN parent compound, are used to perform accurate *in situ* NMR investigations on the reactions with both comonomers, ethylene and methyl acrylate.

These studies, supported by DFT calculations, allowed to discover that when the fluorinated solvent is the reaction medium, an open-chain intermediate is formed stabilized by a network of hydrogen bonds between the oxygen atom of the ester group of the inserted polar monomer and the hydroxyl groups of TFE. This intermediate is recognised as a novel catalyst resting state for this reaction.

In *Chapter 3* additional information about the Pd···S interaction are obtained studying two series of complexes with hemilabile potentially tridentate molecules, N-N'-S, having the thiophene group directly bonded to the N-N' fragment of the ligand itself. These complexes generate active species for the E/MA cooligomerization under mild reaction conditions leading to either unsaturated esters or cooligomers depending on the N-N' moiety. It was found that the thiophene pendant arm contributes to increase the catalyst stability and to affect the branching degree of the obtained macromolecules. Kinetic studies are performed connecting the reactor to a *mass flow control* device that allows to keep constant the ethylene pressure during the catalysis and to measure the consumed ethylene. We found that the consumed ethylene is higher than that found in the isolated cooligomers, thus suggesting the formation of two catalytic species: one active in the cooligomerization and the other in ethylene di- and trimerization, as it was confirmed by *in situ* NMR investigations about the reaction of the precatalysts with ethylene.

Pursuing the study of the effect of the ligand in the fourth coordination site of palladium, in *Chapter 4* a new class of Pd(II) complexes of general formula $[Pd(CH_3)(N\text{-}N)(N^{pyr})][PF_6]$, having a highly coordinating ligand, such as pyridine or its derivatives, is studied. These new complexes, as all those reported in the thesis, have been characterized both in solution by NMR spectroscopy and in solid state by X-Ray analysis. Their catalytic behavior is tested in the E/MA copolymerization by studying the effect of both the solvent and other reaction parameters. The most significant results are related to the macromolecules microstructure and the way of MA enchainment in the synthesized copolymers. When the catalysis are carried out in DCM, the produced copolymers are hyperbranched macromolecules with MA inserted in a junction point of a branch (J(MA)), indicating that the pyridine ligand affects the chain walking process after the insertion of both comonomers, thus suggesting that it remains close to the metal center during the catalysis. This hypothesis is also supported by the observation that when the catalysis are carried out in TFE, no effect of pyridine on the macromolecule microstructure is observed. In addition, both DFT calculations and *in situ* NMR studies confirm that a new open-chain intermediate having both the pyridine ligand and the growing polymeric chain bonded to palladium ion is formed.

Since the migratory insertion reaction of the polar vinyl monomer into the Pd-alkyl bond is one of the key steps of the catalytic cycle and considering the industrial interest in FPO containing amide moieties, in *Chapter 5* a detailed NMR investigation about the reactivity of two Pd(II) complexes bearing a N-N' bidentate pyridyl-pyridylidene amide ligand (PYA), with either MA or *N*,*N*-dimethylacrylamide (DMA), has been performed. Palladacycle intermediates, originated by the insertion of the polar monomer into the Pd-methyl bond are always detected, but in different amount depending on both the precursor and the polar monomer. The presence, or not, of acetonitrile in the palladium coordination sphere affects the reactivity of the complexes, suggesting that it plays a crucial role in the chain walking process. In the case of the reaction with DMA, suitable crystals for X-Ray analysis were obtained in the solution kept at 277 K for 2 weeks. In the unit cell the 5-membered palladacycle, resulting from the DMA migratory insertion reaction into the Pd-CH_3 bond, followed by the chain walking process, was found, confirming the high stability of this intermediate. This result represent the first solid state structure of a chelate DMA-inserted palladacycle. The reaction of this palladacycle with ethylene and carbon monoxide is investigated. No activity was found in the case of ethylene, whereas the migratory insertion of carbon monoxide into the Pd-alkyl bond of the metallacycles took place leading to a palladium-acyl carbonyl intermediate. The studies reported in this chapter are the result of a collaboration with Prof. Martin Albrecht of University of Bern (CH).

RIASSUNTO

Di tutti i materiali termoplastici prodotti su scala industriale, le poliolefine rappresentano la componente più versatile. Ciò nonostante, questi materiali, a causa del carattere apolare delle catene polimeriche che li costituiscono, presentano delle scarse proprietà di superficie, che possono essere migliorate grazie all'incorporazione, nello scheletro della poliolefina, di piccole percentuali di gruppi funzionali polari (meno del 20 %), portando all'ottenimento delle "poliolefine funzionalizzate". Attualmente queste vengono prodotte tramite reazioni di polimerizzazione radicalica che richiedono drastiche condizioni di reazione e che non permettono un controllo sulla microstruttura delle macromolecole ottenute. La copolimerizzazione diretta e controllata, via catalisi omogenea, di alcheni terminali, come l'etilene (E), con monomeri vinilici polari, come l'acrilato di metile (MA), è considerata l'approccio più promettente e sostenibile per ottenere questo tipo di macromolecole.

Per un'applicazione a livello industriale, il catalizzatore ideale, oltre ad avere un'elevata produttività, deve essere in grado di controllare la microstruttura del copolimero e, in particolare, la modalità di incorporazione del monomero vinilico polare.

Lo scopo di questa tesi di dottorato riguarda proprio lo sviluppo di nuovi catalizzatori omogenei, basati su complessi di palladio(II) con leganti bidentati azotati (N-N), e il loro utilizzo nella sintesi di poliolefine funzionalizzate. Il progetto di ricerca si è basato sullo studio degli effetti che le specie presenti nella seconda sfera di coordinazione del centro metallico possono avere a livello catalitico e come possono modificare la macromolecola sintetizzata. In ogni capitolo è riportata la sintesi e la caratterizzazione di complessi di Pd(II), che poi sono stati testati quali catalizzatori per la reazione di copolimerizzazione dell'etilene con l'acrilato di metile. Infine i prodotti catalitici sono stati caratterizzati in soluzione attraverso spettroscopia NMR a temperatura ambiente.

Il *Capitolo 1* consiste in una panoramica sui principali sistemi catalitici riportati in letteratura per la sintesi delle poliolefine funzionalizzate, con un approfondimento sui sistemi che presentano dei leganti con gruppi funzionali che possono dare luogo a interazioni secondarie. Successivamente viene descritto nel dettaglio lo scopo di questo lavoro di tesi.

Il *Capitolo 2* riguarda l'introduzione di un legante emilabile, potenzialmente bidentato come una tiofenimmina N-S, nel quarto sito di coordinazione del palladio sostituendo l'acetonitrile, il legante labile solitamente riportato nei sistemi di letteratura. Questi complessi, $[Pd(CH_3)(N\text{-}N)(N\text{-}S)][PF_6]$, generano catalizzatori attivi per la copolimerizzazione etilene/acrilato di metile lavorando in blande condizioni di reazione e portando all'ottenimento di copolimeri.

In essi l'acrilato è inserito sia in catena principale (M(MA)) che in terminazione di ramificazione (T(MA)), in un rapporto che varia da 9:91 a 45:55, passando da diclorometano (DCM) a trifluoroetanolo (TFE) come solvente per le catalisi, e variando la struttura del legante N-S. Dettagliati studi NMR di reattività *in situ* dei nuovi complessi con entrambi i comonomeri, etilene e MA, hanno dimostrato che, utilizzando il solvente fluorurato, si ottiene un intermedio a catena aperta avente la catena polimerica in crescita e o l'acetonitrile, o il legante N-S, coordinati al centro metallico. Questo intermedio rappresenta un nuovo *resting state* del ciclo catalitico. Questi risultati sperimentali sono supportati e confermati anche da calcoli computazionali DFT.

Nel *Capitolo 3* sono state ricavate ulteriori informazioni riguardo l'interazione Pd···S, studiando due serie di complessi che mostrano un legante potenzialmente tridentato, N-N'-S, con l'anello tiofenico direttamente legato ad esso. Questi nuovi complessi sono stati testati quali catalizzatori nella reazione di interesse, ottenendo esteri insaturi o cooligomeri a seconda della struttura dello scheletro del legante. Il braccio tiofenico aumenta la stabilità del complesso e influisce sul suo comportamento catalitico, in particolare sul grado di ramificazione dei prodotti. Alcune catalisi sono state condotte collegando il reattore ad un apparato per il *mass flow control* che permette di tenere costante la pressione di etilene durante la catalisi e di misurare contemporaneamente la quantità di monomero gassosa consumata. Questi studi hanno evidenziato che la quantità di etilene assorbita era maggiore di quella presente nei prodotti catalitici isolati, suggerendo la presenza di due specie catalitiche in soluzione: una che porta all'ottenimento dei cooligomeri e una che catalizza la di- e la trimerizzazione dell'etilene. Questa ipotesi è in accordo con i risultati ottenuti da studi NMR di reattività *in situ* dei precatalizzatori con l'etilene.

Seguendo sempre un approccio alternativo al *ligand design*, nel *Capitolo 4* è stata sintetizzata una nuova classe di complessi di Pd(II), $[Pd(CH_3)(N\text{-}N)(N^{pyr})][PF_6]$, avente in quarta posizione un legante più coordinante rispetto all'acetonitrile, appartenente alla famiglia delle piridine. Questi nuovi complessi cationici sono stati caratterizzati in soluzione e allo stato solido e testati nella copolimerizzazione E/MA. Il dato più significativo riguarda la modalità di incorporazione del monomero polare nei copolimeri ottenuti: quando la catalisi viene condotta in DCM, si ottengono dei copolimeri iper ramificati con l'acrilato di metile inserito in un punto di giunzione di una ramificazione (J(MA)), suggerendo che il legante piridinico influisca sul processo di crescita della catena polimerica. Questa ipotesi è supportata dal fatto che quando le catalisi vengono condotte in TFE, non si osserva alcun effetto della piridina sulla struttura delle macromolecole ottenute. Gli studi NMR *in situ* e i calcoli DFT confermano che durante la reazione la piridina non si allontana dalla sfera di coordinazione formando un intermedio stabile a catena aperta.

Considerando che la reazione di inserzione migratoria del monomero polare nel legame Pd-alchile è uno degli step fondamentali del ciclo catalitico e l'interesse crescente a livello industriale di poliolefine funzionalizzate che presentano gruppi amidici nelle loro catene polimeriche, nel *Capitolo 5* sono riportati i risultati di studi NMR di reattività *in situ* di complessi di Pd(II) con un legante bidentato caratterizzato da uno scheletro piridil-piridilidene amidico (PYA) sia con l'acrilato di metile che con la *N*,*N*-dimetil-acrilamide (DMA). Si osserva sempre la formazione di intermedi metallaciclici, ma in percentuale differente a seconda del precursore impiegato nella reazione e del monomero vinilico polare utilizzato. La presenza o meno dell'acetonitrile nella sfera di coordinazione del centro metallico influisce sulla reattività dei complessi suggerendo che il legante labile abbia un ruolo cruciale nel processo di *chain walking*. Nel caso della reattività di uno dei complessi con la DMA, nella soluzione sono stati ottenuti dei cristalli singoli adatti per la diffrattometria ai Raggi X. La struttura ottenuta è quella di un metallaciclo a 5 termini risultante dalla reazione di inserzione migratoria della DMA nel legame Pd-CH_3, seguita dal processo di *chain walking*. Si è poi studiata la reattività di questo metallaciclo sia con l'etilene che con il monossido di carbonio. Nel primo caso non si osserva alcuna reazione, mentre nel secondo caso il monossido di carbonio inserisce nel legame Pd-alchile del metallaciclo portando alla formazione di un intermedio stabile Pd-acil-carbonile.
I risultati riportati in questo capitolo sono stati ottenuti in collaborazione con il gruppo di ricerca del Prof. Martin Albrecht dell'Università di Berna (CH).

CHAPTER 1

Introduction

1.1 Functionalized polyolefins: from simple polyolefins to better performing macromolecules.

Polyolefins dominate global plastics production covering about the 65 % of the total demand of plastics, that in 2021 reached the value of 390.7 million tons.[1] As such, family of polyethylene (PE) and polypropylene (PP) thermoplastics are the most valuable polyolefins. One reason for their dominance is the versatility. They have an incredibly broad spectrum of applications, including rigid forms of plastics (such as plastic sheeting and bottles) and more flexible products (such as films, pouches and bubble wrap). In addition, in 2021 the sectors of packaging and construction represented the largest end-use markets for European plastics (about 60 %), while the third position was occupied by the automotive sector.[1] However, due to the apolarity of polymeric chains, these materials suffer from poor surface properties, such as adhesivity, dyeability, miscibility and mechanical compatibility with other materials.[2,3] Several studies attested that such properties can be improved thanks to the incorporation of low percentages of polar monomers into the polymer skeleton, leading to the "functionalized polyolefins" (FPO). Still, the molar percentage of inserted polar monomer should be less than 20 mol %, in order to maintain the thermoplastic features of pristine polyolefins.[2] Nowadays, FPO are industrially produced by using radical polymerization processes that require harsh reaction conditions and result in no control over the copolymer microstructure.[4] A second synthetic procedure to obtain FPO is based on post-polymerization functionalization, which also requires high temperatures due to the inertness of C–H bonds of the polymeric chain and it is limited to only few functional groups that can be inserted.[5,6]

The direct, controlled, homogeneously catalyzed copolymerization of olefins (e. g. ethylene, E) with polar vinyl monomers, such as methyl acrylate (MA), methyl methacrylate (MMA), acrylonitrile (AN), *N*-isopropylacrylamide (NIPAM) and *N*,*N*-dimethylacrylamide (DMA), represents an alternative and environmentally friendly technology to obtain FPO (Scheme 1.1). In particular the copolymerization of ethylene with methyl acrylate is taken as the model reaction for the synthesis of FPO.[7]

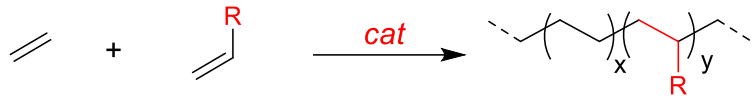

Scheme 1.1. Ethylene/generic acrylic ester copolymerization for the synthesis of FPO.

The first Pd(II)-based catalysts were developed by Brookhart and they were tested in the ethylene homopolymerization and E/MA copolymerization.[8] The Pd(II) cationic complexes, of general formula [Pd(CH_3)(N-N)(OEt_2)][BArF], bear a bidentate nitrogen-donor ancillary ligand (N-N) belonging to the class of α-diimines, that differs from both the skeleton, either 1,4-diaza-1,3-butadiene (DAB – **1** and **2**) or 1,2-bis(imino)-acenaphthene (BIAN – **L3**), and the *ortho*-substituents on the aryl rings, methyl (**1**) or isopropyl (**2** and **L3**) groups (Figure 1.1). The fourth site of the palladium coordination sphere is completed by a labile ligand, such as diethyl ether, and the tetrakis[3,5-bis(trifluoromethyl)phenyl]borate ($BArF^-$) is the counterion of choice.

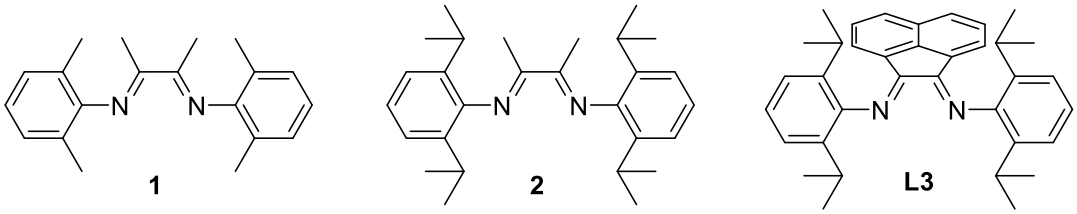

1.24 kg CP/mol Pd·h
14.2 mol % MA
M_n = 7 000

6.05 kg CP/mol Pd·h
4.0 mol % MA
M_n = 42 000

0.65 kg CP/mol Pd·h
4.7 mol % MA
M_n = 10 000

Figure 1.1. Classic Brookhart type α-diimine ligands and activities of the relevant Pd(II) catalysts.[7,8]

The copolymerization reaction was carried out under mild reaction conditions in terms of temperature (T = 303 K) and ethylene pressure (P_E = 1.0 – 6.0 atm), using dichloromethane (DCM) as a solvent. The obtained E/MA copolymers are branched macromolecules. Moving from catalysts with DAB to BIAN ligand a decrease in catalyst activity is shown (6.05 kg CP/mol Pd·h for $\mathbf{2^{Pd}}$ *vs* 0.65 kg CP/mol Pd·h for $\mathbf{L3^{Pd}}$). The substituted groups on the aryl rings affect both the M_n value of E/MA copolymers, that decreases when methyl groups are present with respect to isopropyl ones (7 kDa *vs* 42 kDa, respectively), and the content of polar monomer, that reaches the highest value of 14.2 mol % when [Pd(CH_3)(**1**)(OEt_2)][BArF], $\mathbf{1^{Pd}}$, is used. In all cases MA is inserted exclusively at the end of the branches (T(MA)) (Figure 1.2a).

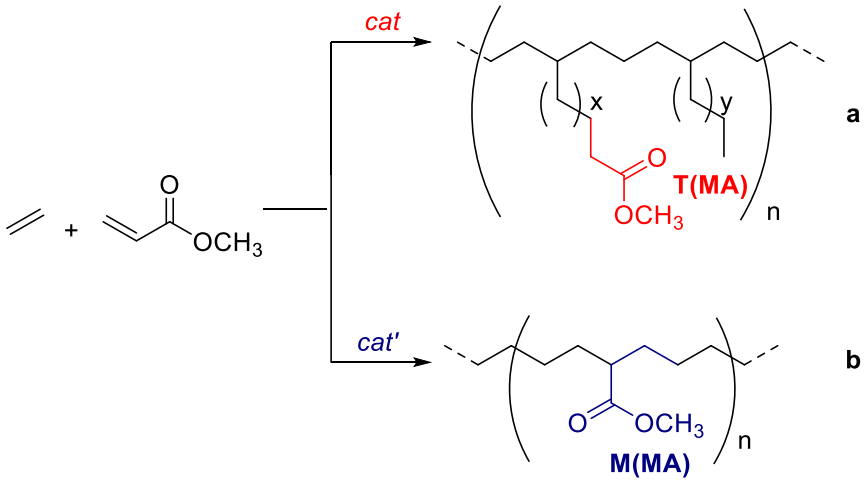

Figure 1.2. Obtained (a) branched and (b) linear functionalized polyolefins *via* direct, controlled, homogeneously catalyzed copolymerization of ethylene with methyl acrylate.

NMR studies at low temperature were performed to detect the key intermediates involved in the catalytic reaction. Starting from the coordination/insertion of methyl acrylate into the Pd-CH_3 bond with secondary regiochemistry, the 4-membered palladacycle, **MC4^{NN}**, was detected at 173 K. Increasing the temperature to 213 K, it evolves to the 5-membered palladacycle, **MC5^{NN}**, through the chain walking process. Finally, at 253 K the stable 6-membered palladacycle, **MC6^{NN}**, was observed and it represents the catalyst resting state. Afterwards the coordination/insertion of ethylene takes place and the copolymer is formed (Scheme 1.2). Since the chain walking process takes place after the insertion of polar monomer, MA goes at the end of a branch and it is exclusively inserted as T(MA). The absence of methyl acrylate units in the main chain (M(MA)) (Figure 1.2b), generated by the immediate coordination/insertion of ethylene into **MC4^{NN}**, indicates that chain walking process is kinetically favored with respect to the gaseous monomer coordination/insertion reaction.

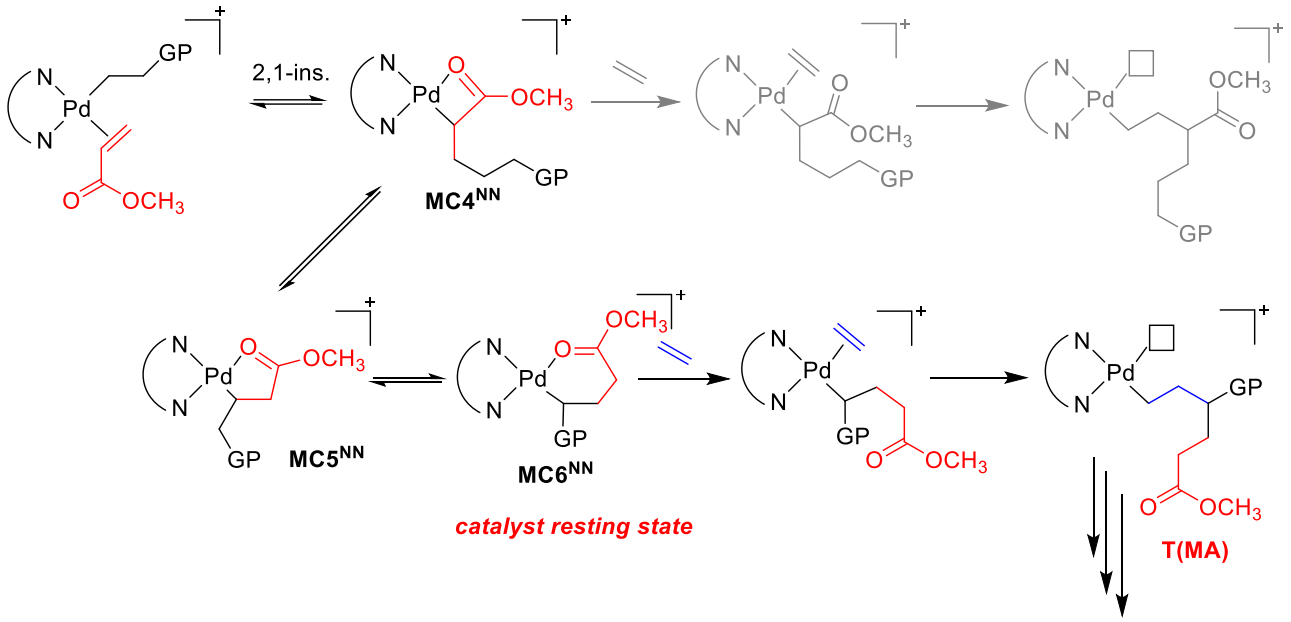

Scheme 1.2. Reaction mechanism of ethylene/methyl acrylate copolymerization with Brookhart catalysts; GP = growing polymer.

In 2002, Drent and Pugh reported that ethylene/methyl acrylate copolymerization was also performed by using a Pd(II) catalyst produced *in situ* from $Pd_2(dba)_3$ (dba = dibenzylidenacetone) or $Pd(OAc)_2$ and di(2-methoxyphenyl)benzene-2-sulfonic acid as ancillary ligand (**L4**, Figure 1.3).[9] Only in 2006, Nozaki *et al.* carried out E/MA copolymerization with the first well-defined catalyst bearing **L4**. The obtained copolymers are linear macromolecules with inserted acrylate (13 mol %) exclusively present as M(MA) with the average molecular weight of copolymers around 3.2 kDa.[10] Few years later, **L4^{Pd}** was slightly modified by introducing a labile ligand, the dimethylsulfoxide (dmso), in the fourth coordination site of palladium ion, [Pd(CH_3)(**L4**)(dmso)] (Figure 1.3).[11] Catalysis are carried out in toluene at 368 K under 5.0 bar of ethylene pressure and the polar monomer is incorporated in higher molar percentage, up to 52 mol %, always inserted as M(MA).

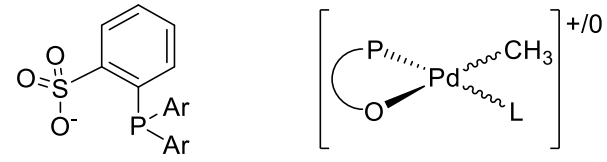

L4 **L4^{Pd}**

Figure 1.3. Example of a phosphino-sulfonate derivative and the relevant Pd(II) complexes.

NMR studies and DFT calculations allowed to investigate the chain growing mechanism with these catalysts. Since the phosphino-sulfonate ligands are nonsymmetric molecules which coordinate to the Pd(II) ion in a nonsymmetric chemical environment, two different geometrical isomers are possible. The *cis* isomer is the complex bearing the Pd-alkyl bond in relative *cis* position to the phosphorus atom, while the *trans* isomer is the complex bearing the Pd-alkyl bond in the opposite position with respect to the phosphorus atom. The migratory insertion of MA into the Pd-alkyl bond takes place with either primary or secondary regiochemistry,[12] leading to the formation of the 5-membered palladacycle **MC5$^{PO'}$** or 4-membered palladacycle **MC4^{PO}**, respectively. In both cases the functional group is preferentially coordinated in *trans* position with respect to the oxygen atom of the ligand. The chain walking process is suppressed and so the coordination/insertion reaction of incoming ethylene molecules takes place immediately after the insertion of the polar monomer. In this way the polymeric chain growths with inserted MA into it (Scheme 1.3). For this system the catalyst resting state is the insertion of the monomer, either ethylene or methyl acrylate, into the Pd-alkyl bond.

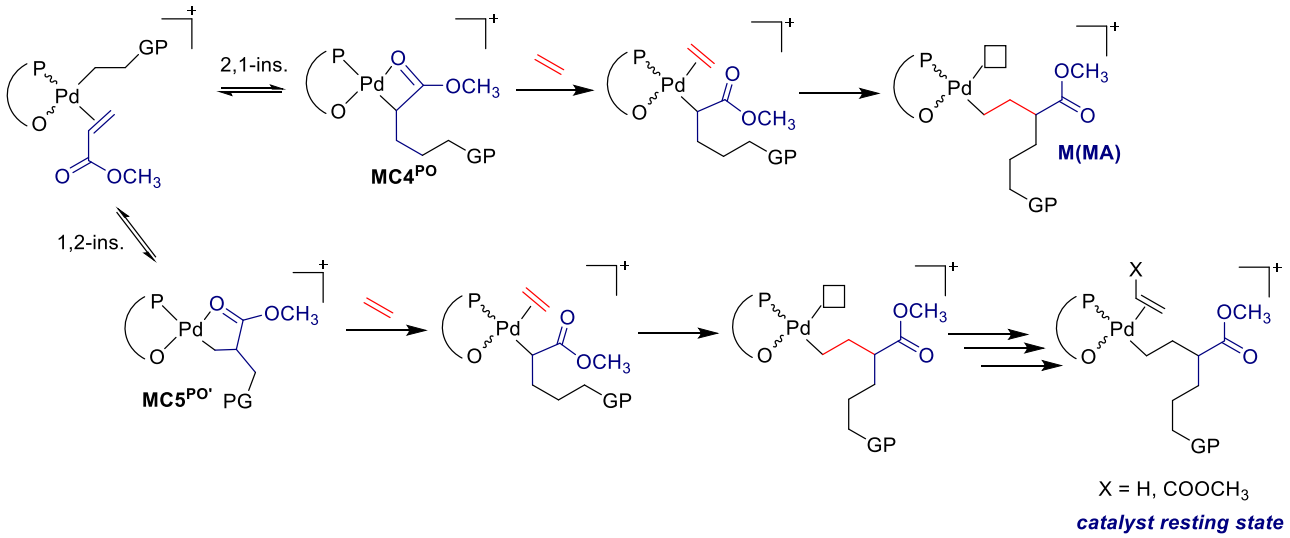

Scheme 1.3. Reaction mechanism of ethylene/methyl acrylate copolymerization with phosphino-sulfonate catalysts; GP = growing polymer.

For many years, ethylene/acrylic esters copolymerization reactions were thought to be efficiently performed by using Pd(II) catalysts only. In fact, Ni(II) complexes with α-diimine, which are extremely more active in ethylene homopolymerization than Pd(II) analogues,[8] are instead not suitable for the target copolymerization, due to the higher oxophilicity of the metal center.

The first Ni(II)-based catalyst with a sterically hindered salicyl-aldiminato ligand **L5** (Figure 1.4) was reported by Grubbs *et al.*.[13] It generates active species in the ethylene/hydroxyl-substituted norbornenes, but obtained copolymers have not found any industrial applications yet.

In 2017, one of the first Ni(II) catalysts able to perform E/MA copolymerization was synthesized, with a phosphino-phenolate ligand, **L6** (Figure 1.4).[14] Catalysis are carried out at 343 K under 30 atm of ethylene pressure and the complex [Ni(cod)(**L6**)], **L6^{Ni}**, shows an activity of about 86 kg CP/mol Ni·h. The obtained copolymers are linear macromolecules with an average M_n value of 68 kDa and the amount of inserted MA is about 4.5 mol %, exclusively present as M(MA). Later, another Ni(II)/[P-O] catalyst was developed bearing **L7** (Figure 1.4), active in the copolymerization of ethylene with both methyl acrylate and *N*,*N*-dimethylacrylamide.[15] About the model reaction, it shows an increase in the catalyst productivity (3.2 kg CP/mol Ni for **L7^{Ni}** *vs* 2.3 kg CP/mol Ni for **L6^{Ni}**, at T = 343 K and P_E = 10 bar), in the M_n values and in the amount of inserted MA reaching the highest value of 108 kDa and 5.4 mol %, respectively.

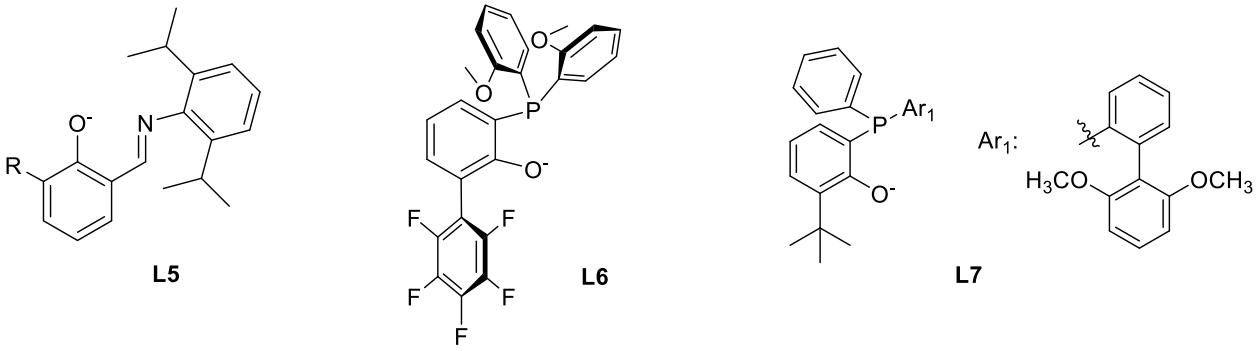

Figure 1.4. Examples of ligands using in Ni(II)-based catalysts.

The ideal catalyst, in addition to show a high productivity and a good thermal stability, might exert a precise control over the macromolecule microstructure, in particular over molecular weight and its distribution, lengths and distribution of the polymer branches, amount and way of enchainment of the polar monomer. The homogeneously catalyzed copolymerization potentially allows to carry out the reaction under mild conditions in terms of temperature and pressure and to tune the polymer architecture. From the industrial point of view, the target macromolecule is a linear copolymer with the functionalized groups present into the main chain. Despite the extensive research in this field, no industrial application is currently operative for the catalytic ethylene/polar vinyl monomer copolymerization reaction, which is recognized as "the polar monomer problem".[16,17]

1.2 The Brookhart catalysts with α-diimine ligands.

The poor thermal stability is one of the major disadvantage of Brookhart catalysts[18] and this is reasonably due to decomposition of the $[Pd(H)(N\text{-}N)]^+$ intermediate, obtained after the chain transfer process, to inactive Pd(0) (Scheme 1.4).

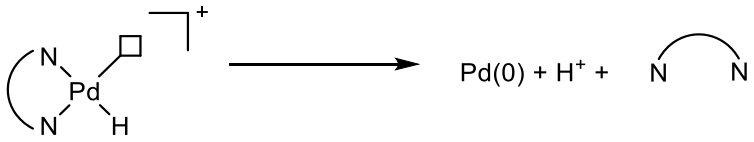

Scheme 1.4. Decomposition mechanism of the $[Pd(H)(N\text{-}N)]^+$ intermediate to inactive Pd(0).

Across the past decades, a huge number of modified Ni(II)- and Pd(II)-based Brookhart catalysts has been studied and the investigated structural variations give steric and electronic effects the in catalysis. They are related to modifications of α-diimine skeleton, variations on aryl fragments and synthesis of dinuclear complexes.

About the first approach recently, Milani *et al.* achieved a relevant increase in the catalysts productivity by using Pd(II) complexes bearing a bis(imino)-phenanthrene α-diimine (BIP, **L8**, **L9**, Figure 1.5) ligand.[19] Catalysis were carried out under mild reaction conditions (T = 308 K and P_E = 2.5 atm) in 2,2,2-trifluoroethanol (TFE) as a solvent. The best performing catalyst of the series bears **L8** ligand with isopropyl groups on the aryl rings, showing a productivity of 21 kg CP/mol Pd and an average M_n value of E/MA copolymers about 33 kDa. The highest amount of inserted MA (up to 2.4 mol %) was reported for catalyst with **L9** and the polar monomer is inserted preferentially at the end of the branches, but also into the main chain. The better performances of BIP catalysts with respect to DAB or BIAN derivatives were attributed to the higher Lewis basicity of the nitrogen donor atoms, which was supposed to destabilize the six-membered palladacycle. Gao *et al.* also tested the variation of the ligand backbone from α-diimine to imino-amine one (**L10**, Figure 1.5).[20] At 298 K, ethylene/methyl acrylate copolymers were obtained with a productivity of 4.8 kg CP/mol Pd, with a M_n value of $1.53 \cdot 10^4$ g/mol and a low content of inserted acrylate (1.1 mol %), which is preferentially present in the main chain (M(MA):T(MA) = 64:36). Detailed NMR investigations allowed to detect the 4- and 5-membered metallacycles, generated by the insertion of MA into the Pd-alkyl bond followed by the chain walking process, at room temperature. This indicated that the chain walking process is slowed down with this kind of ligands.

Moreover, catalysts bearing camphyl-based α-diimine (**L11**, Figure 1.5) showed a higher thermal stability with respect to Brookhart ones producing copolymers with 1.2 mol % of inserted MA.[21] A dibenzo-barrelene skeleton was also reported by the same research group (**L12**, Figure 1.5): the highest content of inserted MA about 4.64 mol % was found for the copolymerization test at 323 K when dichloromethane is the reaction medium.[22]

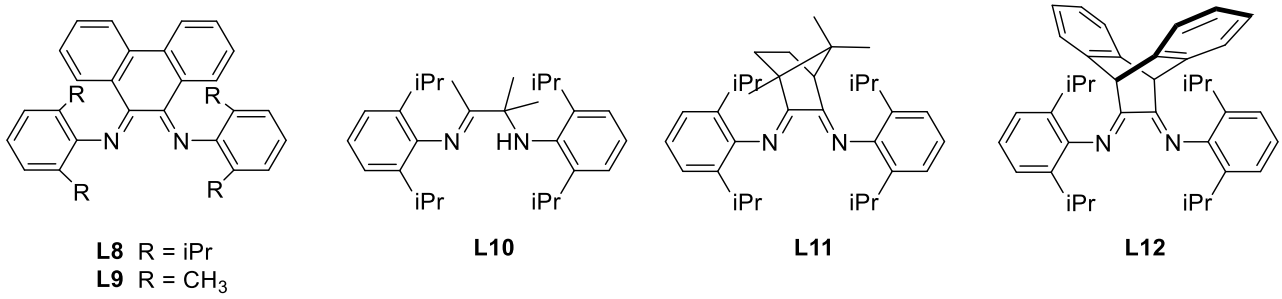

L8 R = iPr
L9 R = CH_3

L10 **L11** **L12**

Figure 1.5. Examples of structural modifications on α-diimine skeleton.

Another strategy of the ligand design is composed by varying the substituents on the aryl rings generating a nonsymmetric ligand and the relevant Pd(II) complexes might modulate the properties of the obtained copolymers.[18] Such kind of structural variations was firstly investigated by Milani *et al.* with both DAB and BIAN ligands having different substituents on the aryl rings (**L13** – **L15**, Figure 1.6).[23,24,25] The relevant Pd(II) complexes generate active species for the E/MA copolymerization with better performances than those of the catalysts with the corresponding symmetric analogues in terms of productivity and amount of inserted MA (up to 14.7 mol %). On the other hand, the absence of the steric hindrance in one half of the ligand did not allow to obtain copolymers, but the catalytic products are ethylene/MA cooligomers and higher alkenes. Recently, Dai *et al.* studied Pd(II) hybrid complexes active in the copolymerization reaction of ethylene with MA. They are characterized by bearing non-symmetric DAB ligand combining *ortho*-diarylmethyl and *ortho*-phenyl moieties (**L16**, Figure 1.6).[26] They are able to insert a percentage of MA in the range of 1.81 – 4.83 mol % and the obtained copolymers show moderate values of M_n (4.4 – 18.6 kg/mol). In this case MA units are present in the copolymers as T(MA).

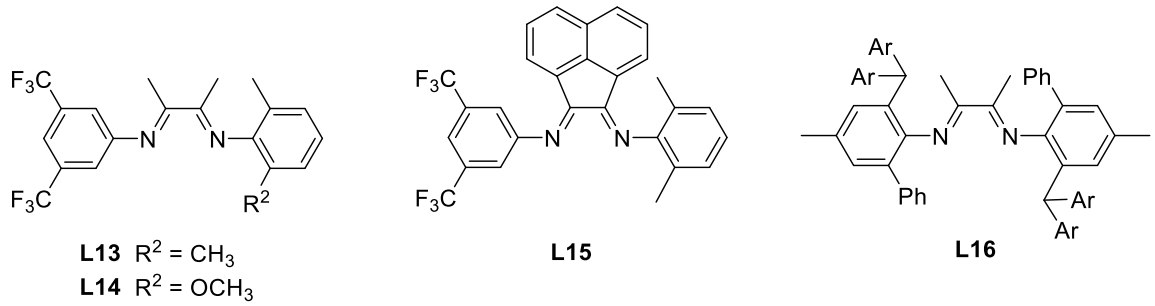

Figure 1.6. Examples of structural modifications on aryl fragments.

The increase in the congestion and the steric hindrance near the metal center modulate the properties of the obtained copolymers, too. In 2020, Jian *et al.* introduced a new α-diimine ligand starting from **L12** having, in addition to the dibenzo-barrelene skeleton, pentiptycene-based substituents on the nitrogen atoms (**L17**, Figure 1.7).[27] The relevant Pd(II) complex is active in the target reaction and it is stable in a huge range of temperature (from 303 to 363 K). The highest value of productivity (14.8 kg CP/mol Pd·h) was reached at 363 K and the obtained branched copolymer shows a M_n value of 85 kDa with 1.5 mol % of inserted MA. While at 303 K, the catalytic activity decreases to 1.9 kg CP/mol Pd·h, leading to an "ultra-highly branched" copolymer (degree of branches of 213/1000C) with M_n of $1.9 \cdot 10^4$ g/mol and a lower content of MA (0.6 mol %), which is mostly inserted in the main chain (98 % selectivity). Detail NMR mechanistic studies about the reaction of [Pd(CH_3)Cl(**L17**)], **L17^{Pd}**, activated *in situ* with sodium tetrakis[3,5-bis(trifluoromethyl) phenyl]borate (NaBArF), with MA highlighted that this effect is ascribed to the regioselectivity of MA insertion reaction.[28] It takes place in a 1,2-fashion instead of the typical secondary regiochemistry for catalysts with α-diimines. The formation of the 5-membered palladacycle, **MC5$^{NN'}$**, favored the subsequent insertion of ethylene molecule rather than the chain walking process (Scheme 1.5).

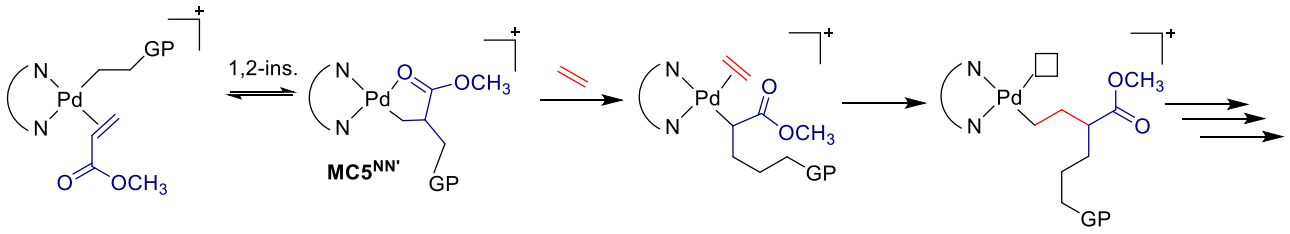

Schema 1.5. Investigated mechanism in the ethylene/methyl acrylate copolymerization using **L17^{Pd}**; GP = growing polymer.

Pd(II) complexes with a macrocyclic α-diimine ligand (**L18**, Figure 1.7) were tested in the target copolymerization with very low productivities.[29] On the other hand, they were able to insert a high percentage of the polar monomer (up to 21.8 mol %) as T(MA) due to the hindrance in the axial positions of the metal center. The peculiar orientation of such hindered substituents, which are located in the apical position with respect to the metal center, disfavors the termination of chain growth, that takes places through an associative mechanism. A similar effect was found also by Brookhart research group introducing a "sandwich structure", characterized by having 8-(p-tolyl)-naphthyl groups on the nitrogen atoms of the ligand (**L19**, Figure 1.7).[30] The obtained branched macromolecules show a high content of inserted MA about 13.8 mol %.

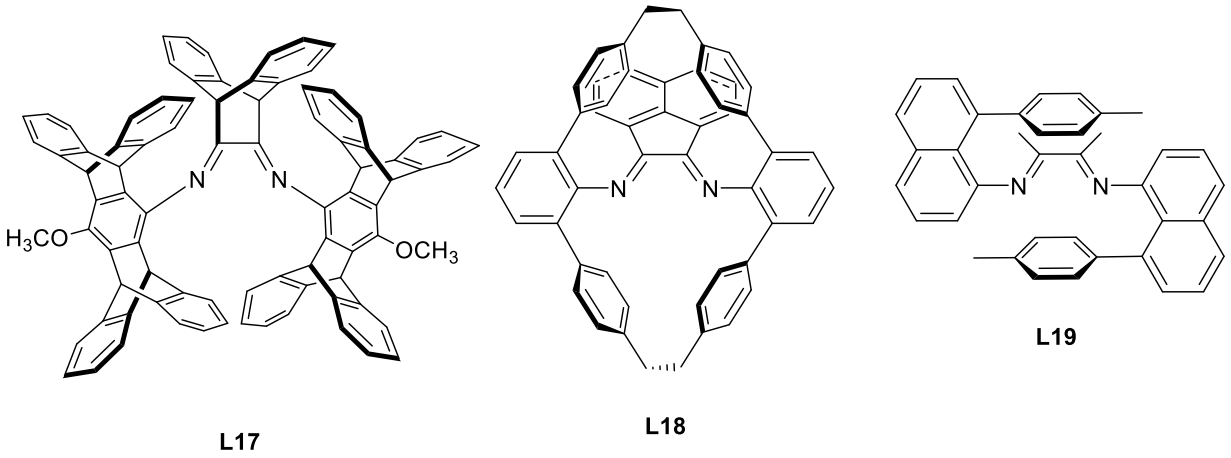

Figure 1.7. Examples of increased steric hindrance on the α-diimine ligands.

At least, the synthesis of dinuclear catalysts is to potentially get access to productivity values higher than the sum of the productivities of the two single mononuclear catalysts with analogous structure and also to different macromolecular architectures.[31,32] The first dinuclear Pd(II) catalyst active in the E/MA copolymerization (**L20**, Figure 1.8) was studied by Takeuchi and Osakada.[33] The ancillary ligand of choice is based on two BIAN coordinating fragments, connected by two parallel planes at a distance of 3.49 Å, leading to a "double-decker" structure. In particular reaction conditions ([MA] = 1.7 mol/L and P_E = 20 atm), [Pd(CH_3)Cl]$_2$[**L20**], **L20^{Pd}**, shows the highest value of activity about 2.72 kg CP/mol Pd·h with 3.4 mol % of inserted MA in a ratio of M(MA):T(MA) = 85:15. When catalysis are carried out under 10 atm of ethylene pressure, the M(MA):T(MA) ratio is 77:23, while with [Pd(CH_3)Cl(**L21)**], **L21^{Pd}**, under the same reaction conditions, is 21:79.

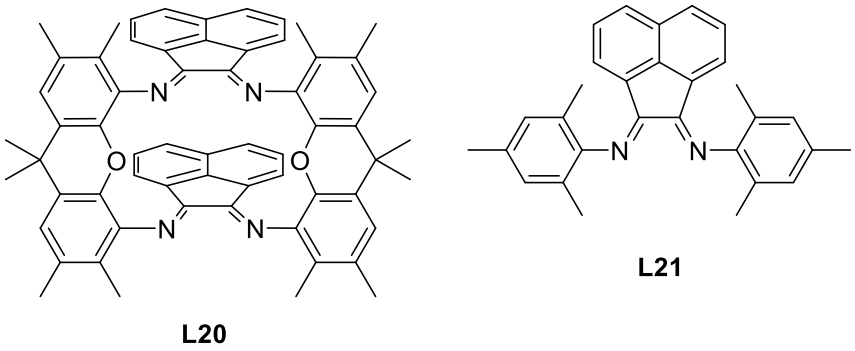

Figure 1.8. The bis-bidentate ligand synthesized by Takeuchi and Osakada **L20** and the bidentate one **L21**.[33]

The difference way of the polar monomer enchainment strongly suggests the existence of cooperativity effects between the two metal ions in the dinuclear catalysts and the higher percentage of M(MA) is supposed to be due to a weak interaction between the oxygen atom of the carbonyl group of inserted MA and the Pd(II) center that is not involved in the insertion of the polar monomer. In this way, an incoming ethylene molecule might be bonded to the vacant coordination site of the first palladium ion and the polar monomer is trapped in the main chain of growing polymer (Scheme 1.6).

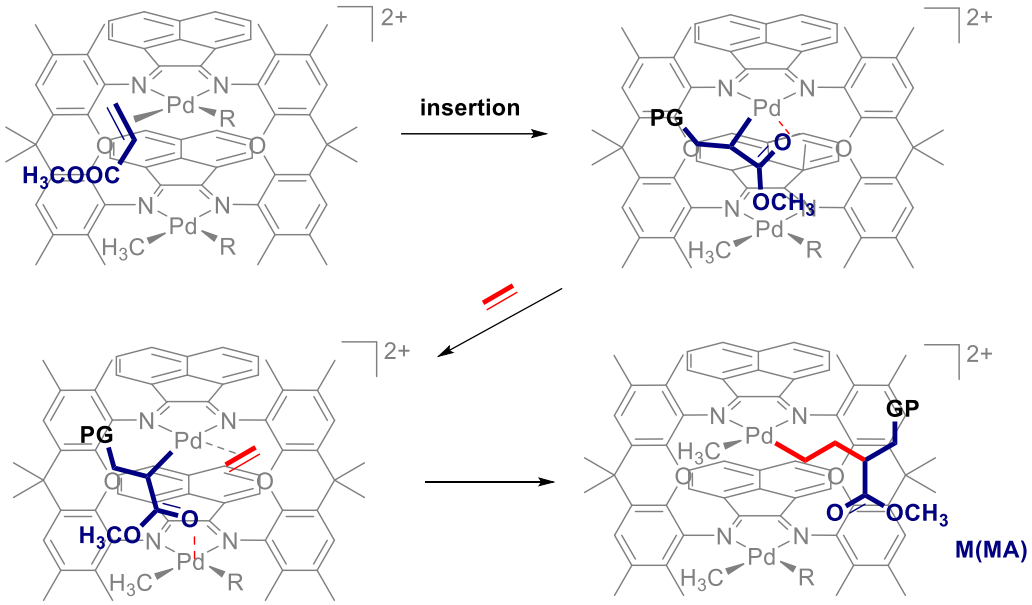

Scheme 1.6. Proposed mechanism in the ethylene/methyl acrylate copolymerization; GP = growing polymer.

1.3 An overview about P-X ligands.

In the past years, several structural variations of the original Pd(II) complex bearing the phosphino-sulfonate **L4** were explored introducing P-X ligands in the coordination sphere of palladium ion. The Bis-Phosphine Mono-Oxide ligands (BPMO) are characterized by having a one strong and one weak σ-donor site. This unbalance should be beneficial in obtaining highly linear copolymers. Firstly, Nozaki *et al.* in 2016 proposed two ligands that differ from specific functional groups on the *ortho* positions of the aryl rings bonded to the phosphorous atom: either methoxy (**L22**, Figure 1.9) or trifluoromethyl (**L23**, Figure 1.9) groups.[34] The relevant Pd(II) complexes, **L22^{Pd}** and **L23^{Pd}**, were tested in the E/MA copolymerization reaction. Moving from **L22^{Pd}** to **L23^{Pd}**, the precatalyst activity increases from 4.1 to 5.9 kg CP/mol Pd·h, while the M_n value decreases (33 kDa for **L22^{Pd}** *vs* 14 kDa for **L23^{Pd}**) as well as the content of inserted MA, from 2.3 to 0.9 mol %, respectively. On the basis of these catalytic results, the synthesis of new bidentate species of the same class was inspired. Phosphino-phosphonate derivatives (**L24** and **L25**, Figure 1.9) were studied by Jordan *et al.*.[35] Precatalysts with **L24** as the ancillary ligand showed an activity of 58 kg CP/mol Pd·h when catalysis is carried out at 353 K under 28 atm of ethylene pressure. The obtained linear copolymers molecular weight is about 1.5 kDa and the amount of inserted MA is 1.5 mol %, preferentially present as M(MA) (95 % of selectivity). Instead, **L25^{Pd}** is more active reaching the value of 150 kg CP/mol Pd·h with respect to **L24^{Pd}**. The most interesting catalytic data is related to the way of polar monomer enchainment: in this case only 60 % of the total amount of inserted MA (2.6 mol %) was present into the main chain.

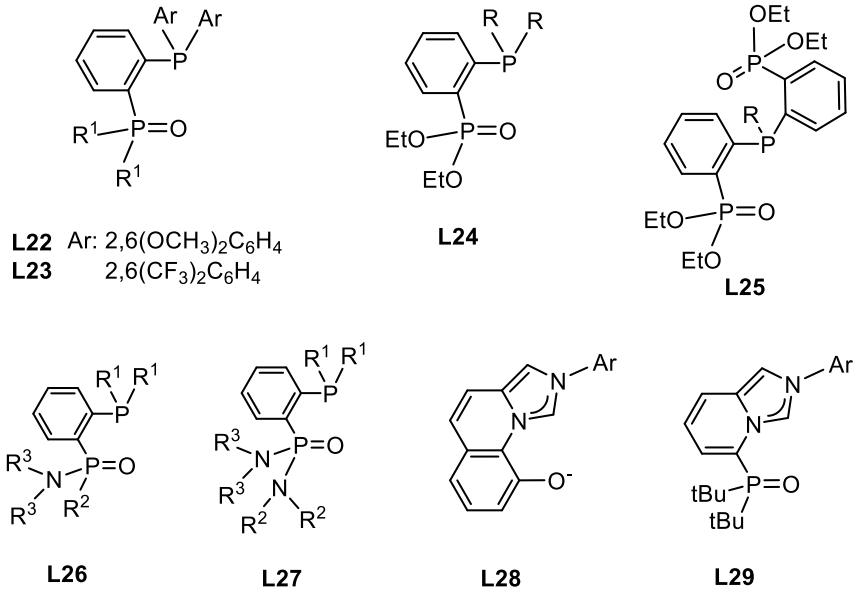

Figure 1.9. Examples of structural modifications of phosphino-sulfonate ligands.

Phosphino-phosphonamide (**L26**, Figure 1.9) and phosphino-phosphon(bisamide) ligands (**L27**, Figure 1.9) were introduced by Chen *et al.*[36] and by Carrow *et al.*[37], respectively. Copolymerization reactions with the relevant **L26**-Pd(II) complexes are performed at 373 K under 5 atm of ethylene pressure reaching the activity value of 8.7 kg CP/mol Pd·h. Obtained copolymers present 16 mol % of inserted MA. Also **L27^{Pd}** is tested in the target reaction and the amount of inserted MA decreases (5.4 mol %) and it is present as M(MA) with a high selectivity (> 97 %).

In addition, Nozaki tested the substitution of the phosphorus atom with an N-heterocyclic carbene (NHC) fragment (**L28** and **L29**, Figure 1.9), which also shows a strongly σ-donating behavior.[38,39] Despite the high thermal stability of the precatalysts obtained with these ligands, the copolymers show low values of both the M_n (17 kDa for **L28^{Pd}** and 7.0 kDa for **L29^{Pd}**) and the amount of inserted polar monomer (0.8 and 0.27 mol %, respectively).

Regardless of some of the above mentioned structural variations lead to higher productivities or improve the copolymer properties, in most cases the classes of Pd(II)/[P-O] and Pd(II)/[P-X] catalysts show comparable performances to those of Pd(II)/[N-N] derivatives only when the copolymerization reactions are carried out under harsh reaction conditions (temperature up to 373 K and ethylene pressure of 10 – 40 bar).

1.4 The secondary interactions in Pd(II) complexes with α-diimine ligands.

In the last years a new approach based on the studied of the secondary interactions is taking hold, suggesting that this might control the catalytic performances and increase the stability of the catalysts.[40] It involves the introduction of specific functionalized groups directly bonded to the N-N ligand itself. Jordan and co-workers modified the substituents on the *ortho* positions of only one aryl ring, introducing an amide-moiety (**L30**, Figure 1.10).[41] The solid state structure of [Pd(CH_3)Cl(**L30**)], **L30^{Pd}**, was solved and the distance between nitrogen atom of amide functionality and Pd–Cl fragment of 3.541(9) Å suggests a weak interaction between them. The precatalyst is tested in the ethylene/methyl acrylate copolymerization obtaining copolymers with a lower degree of branching and a higher amount of inserted MA (more than 1.3 mol %) with respect to the catalyst where this functionalized group is not present. In all cases MA is inserted as T(MA). Other examples of Pd(II) complexes, used as precatalysts in the target copolymerization that take advantage of secondary interactions, were reported by Chen *et al.*. The α-diimine ligand presents on the aryl rings very bulky substituent groups such as either benzothiophene (**L31**, Figure 1.10) or naphthalene (**L32**, Figure 1.10) moieties.[42]

Suitable single crystals of **L32^{Pd}** for X-ray analysis were obtained and in its ORTEP drawing a π-π stacking interaction between the *ortho* substituents and the aryl rings of the α-diimine ligand is observed. Both neutral Pd(II) complexes, activated *in situ* with NaBArF, were tested in the ethylene homopolymerization showing high activity, about $41 \cdot 10^5$ g PE/mol Pd·h, and generating almost linear polyethylene (PE) with high molecular weight. When ethylene/methyl acrylate copolymerization was carried out, the obtained copolymers showed an elevate M_n value, up to $44.7 \cdot 10^3$ kDa, and the percentage of inserted MA was about 0.88 mol % (at P_E = 8 atm, t = 12 h and [MA] = 1.0 M). The degree of branches was low (9 per 1000 C atoms) suggesting the chain walking process is slowed down after the insertion of the gaseous monomer. A detailed catalytic study performed with [Ni(Br)$_2$(**L31**)], **L31^{Ni}**, allowed to discover that at low temperature (T = 293 K), an interaction between the sulfur atom of the coordinated **L31** and the hydrogen atom on the beta position of the growing copolymeric chain might inhibit the β-H elimination reaction and consequently suppress the chain walking process.[43]

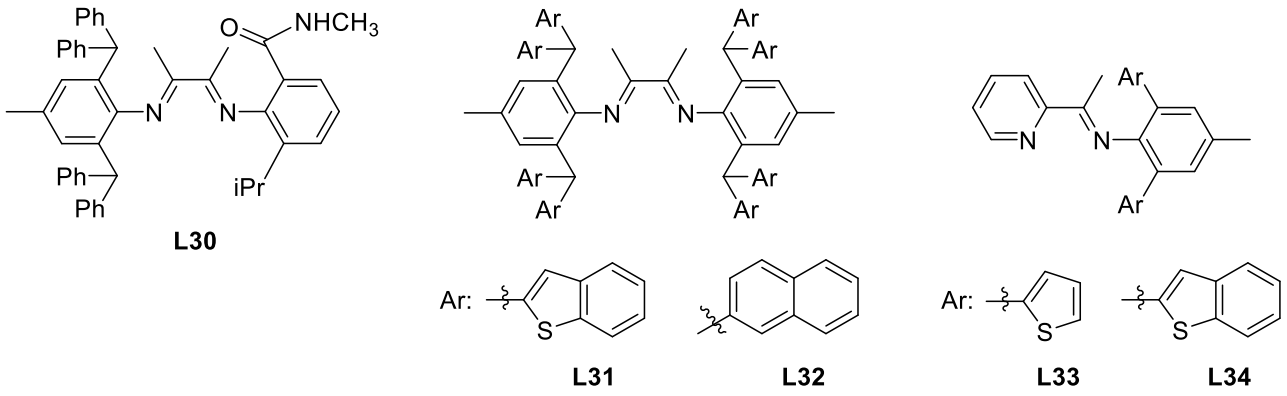

Figure 1.10. Examples of N-N' ligands which might generate secondary interactions with Pd ion.

Very recently, Dai and coworkers reported other efficient Ni(II) and Pd(II) complexes with nitrogen donor ligand with iminopyridyl skeleton (**L33** – **L34**, Figure 1.10).[44] The solid state molecular structure of **L33^{Pd}** reveales that one of the thiophene ring is located close to the Pd(II) ion with a Pd···S distance of 3.612 Å, suggesting a π-interaction of this thiophene ring with the metal center. They are tested in the target reaction and **L33^{Pd}** exhibited moderate activities ($9.92 \cdot 10^3$ g CP/mol Pd·h) leading to low molecular weight E/MA cooligomers (579 g/mol) with high incorporation ratio of the polar monomer (4.09 mol %), inserted as T(MA). On the other hand, **L34^{Pd}** with benzothiophene moiety, is almost ineffective in the E/MA cooligomerization reaction.

1.5 Aim of the work.

The aim of this PhD thesis is the development of palladium catalysts bearing α-diimine ligands for the synthesis of functionalized polyolefins. In particular, the secondary coordination sphere effects on the catalytic outcome are investigated.

The research activity encompasses all the typical steps for a project in homogeneous catalysis moving from the synthesis and characterization of molecules to be used as spectator ligands to the synthesis and characterization of the relevant Pd(II) complexes and the study of their catalytic behavior in the E/MA copolymerization. In addition, the *in situ* NMR mechanistic investigations and the characterization of catalytic products are performed.

Three new families of organometallic Pd(II) complexes have been investigating, differing for one of the ligand bonded to the metal center. The first, of general formula $[Pd(CH_3)(N\text{-}N)(N\text{-}S)][PF_6]$ (Figure 1.11a), are characterized to have a hemilabile, potentially bidentate ligand in the fourth coordination site of palladium, such as a thiophenimine N-S. The second one, $[Pd(CH_3)(N\text{-}N'\text{-}S)(L)][X]$ (Figure 1.11b), presents a potentially tridentate molecule with the thiophene group directly bonded to the N-N' skeleton. At least, Pd(II) complexes with a highly coordinating ligand belonging to the family of pyridines, $[Pd(CH_3)(N\text{-}N)(N^{pyr})][PF_6]$, are studied (Figure 1.11c).

Finally, *in situ* NMR reactions of both the neutral and the cationic Pd(II) complexes having a N-N' bidentate pyridyl-pyridylidene amide (PYA) ligand (Figure 1.11d) with methyl acrylate and *N,N*-dimethylacrylamide (DMA) are performed. The last part of the project is based on a collaboration between the group of Prof. Barbara Milani at the University of Trieste and the group of Prof. Martin Albrecht at the University of Bern.

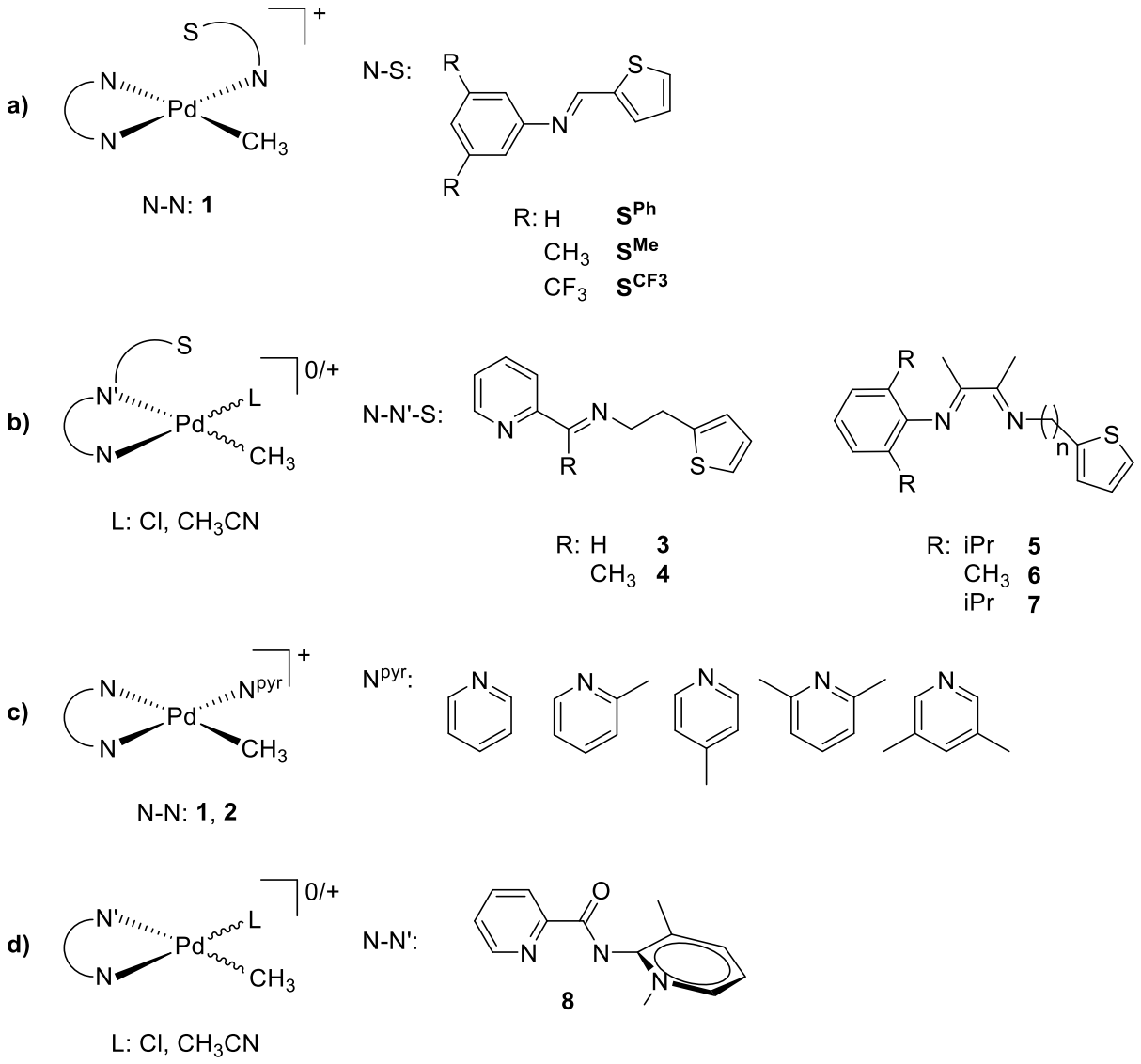

Figure 1.11. The Pd(II) complexes under investigation.

The following tasks have been personally carried out by the author of this thesis: synthesis and purification of all organometallic compounds; characterization by NMR spectroscopy, IR and mass analysis of ligands and Pd(II) complexes; crystallization of Pd(II) complexes for X-Ray analysis; catalysis preparation, experiment setup, data interpretation and characterization in solution of the catalytic products; *in situ* NMR investigations to detect intermediates involved in the catalytic reaction.

1.6 References.

(1) Plastics – the Facts 2022. **2022**, No. October.

(2) Nakamura, A.; Ito, S.; Nozaki, K. Coordination-Insertion Copolymerization of Fundamental Polar Monomers. *Chem. Rev.* **2009**, *109* (11), 5215–5244.

(3) Tan, C.; Zou, C.; Chen, C. Material Properties of Functional Polyethylenes from Transition-Metal-Catalyzed Ethylene-Polar Monomer Copolymerization. *Macromolecules* **2022**, *55* (6), 1910–1922.

(4) Birajdar, R. S.; Chikkali, S. H. Insertion Copolymerization of Functional Olefins: Quo Vadis? *Eur. Polym. J.* **2021**, *143* (September 2020).

(5) Tan, C.; Qasim, M.; Pang, W.; Chen, C. Ligand-Metal Secondary Interactions in Phosphine-Sulfonate Palladium and Nickel Catalyzed Ethylene (Co)Polymerization. *Polym. Chem.* **2020**, *11* (2), 411–416.

(6) Rodriguez, G. M.; Díaz-Requejo, M. M.; Pérez, P. J. Metal-Catalyzed Postpolymerization Strategies for Polar Group Incorporation into Polyolefins Containing C-C, C=C, and Aromatic Rings. *Macromolecules* **2021**, *54* (11), 4971–4985.

(7) Johnson, L. K.; Mecking, S.; Brookhart, M. Copolymerization of Ethylene and Propylene with Functionalized Vinyl Monomers by Palladium(II) Catalysts. *J. Am. Chem. Soc.* **1996**, *118* (1), 267–268.

(8) Brookhart, M.; Johnson, L. K.; Killian, C. M. New Pd(II)- and Ni(II)-Based Catalysts for Polymerization of Ethylene and α-Olefins. **1995**, *117*, 6414–6415.

(9) Drent, E.; Van Dijk, R.; Van Ginkel, R.; Van Oort, B.; Pugh, R. I. Palladium Catalysed Copolymerisation of Ethene with Alkylacrylates: Polar Comonomer Built into the Linear Polymer Chain. *Chem. Commun.* **2002**, *2* (7), 744–745.

(10) Kochi, T.; Yoshimura, K.; Nozaki, K. Synthesis of Anionic Methylpalladium Complexes with Phosphine-Sulfonate Ligands and Their Activities for Olefin Polymerization. *Dalt. Trans.* **2006**, No. 1, 25–27.

(11) Guironnet, D.; Roesle, P.; Rünzi, T.; Göttker-Schnetmann, I.; Mecking, S. Insertion Polymerization of Acrylate. *J. Am. Chem. Soc.* **2009**, *131* (2), 422–423.

(12) Nakamura, A.; Anselment, T. M. J.; Claverie, J.; Goodall, B.; Jordan, R. F.; Mecking, S.; Rieger, B.; Sen, A.; Van Leeuwen, P. W. N. M.; Nozaki, K. Ortho-Phosphinobenzenesulfonate: A Superb Ligand for Palladium-Catalyzed Coordination-Insertion Copolymerization of Polar Vinyl Monomers. *Acc. Chem. Res.* **2013**, *46* (7), 1438–1449.

(13) Younkin, T. R.; Connor, E. F.; Henderson, J. I.; Friedrich, S. K.; Grubbs, R. H.; Bansleben, D. A. Neutral Single-Component Nickel (II) Polyolefin Catalysts That Tolerate Heteroatoms. *Science (80-.).* **2000**, *287* (5452), 460–462.

(14) Xin, B. S.; Sato, N.; Tanna, A.; Oishi, Y.; Konishi, Y.; Shimizu, F. Nickel Catalyzed Copolymerization of Ethylene and Alkyl Acrylates. *J. Am. Chem. Soc.* **2017**, *139* (10), 3611–3614.

(15) Zhang, Y.; Mu, H.; Pan, L.; Wang, X.; Li, Y. Robust Bulky [P,O] Neutral Nickel Catalysts for Copolymerization of Ethylene with Polar Vinyl Monomers. *ACS Catal.* **2018**, *8* (7), 5963–5976.

(16) Luckham, S. L. J.; Nozaki, K. Toward the Copolymerization of Propylene with Polar Comonomers. *Acc. Chem. Res.* **2021**, *54* (2), 344–355.

(17) Keyes, A.; Basbug Alhan, H. E.; Ordonez, E.; Ha, U.; Beezer, D. B.; Dau, H.; Liu, Y. S.; Tsogtgerel, E.; Jones, G. R.; Harth, E. Olefins and Vinyl Polar Monomers: Bridging the Gap for Next Generation Materials. *Angew. Chemie - Int. Ed.* **2019**, *58* (36), 12370–12391.

(18) Wang, F.; Chen, C. A Continuing Legend: The Brookhart-Type α-Diimine Nickel and Palladium Catalysts. *Polym. Chem.* **2019**, *10* (19), 2354–2369.

(19) Dall'Anese, A.; Rosar, V.; Cusin, L.; Montini, T.; Balducci, G.; D'Auria, I.; Pellecchia, C.; Fornasiero, P.; Felluga, F.; Milani, B. Palladium-Catalyzed Ethylene/Methyl Acrylate Copolymerization: Moving from the Acenaphthene to the Phenanthrene Skeleton of α-Diimine Ligands. *Organometallics* **2019**, *38* (19), 3498–3511.

(20) Hu, H.; Chen, D.; Gao, H.; Zhong, L.; Wu, Q. Amine-Imine Palladium Catalysts for Living Polymerization of Ethylene and Copolymerization of Ethylene with Methyl Acrylate: Incorporation of Acrylate Units into the Main Chain and Branch End. *Polym. Chem.* **2016**, *7* (3), 529–537.

(21) Guo, L.; Gao, H.; Guan, Q.; Hu, H.; Deng, J.; Liu, J.; Liu, F.; Wu, Q. Substituent Effects of the Backbone in α-Diimine Palladium Catalysts on Homo- and Copolymerization of Ethylene with Methyl Acrylate. *Organometallics* **2012**, *31* (17), 6054–6062.

(22) Zhong, S.; Tan, Y.; Zhong, L.; Gao, J.; Liao, H.; Jiang, L.; Gao, H.; Wu, Q. Precision Synthesis of Ethylene and Polar Monomer Copolymers by Palladium-Catalyzed Living Coordination Copolymerization. *Macromolecules* **2017**, *50* (15), 5661–5669.

(23) Meduri, A.; Montini, T.; Ragaini, F.; Fornasiero, P.; Zangrando, E.; Milani, B. Palladium-Catalyzed Ethylene/Methyl Acrylate Cooligomerization: Effect of a New Nonsymmetric α-Diimine. *ChemCatChem* **2013**, *5* (5), 1170–1183.

(24) Rosar, V.; Montini, T.; Balducci, G.; Zangrando, E.; Fornasiero, P.; Milani, B. Palladium-Catalyzed Ethylene/Methyl Acrylate Co-Oligomerization: The Effect of a New Nonsymmetrical α-Diimine with the 1,4-Diazabutadiene Skeleton. *ChemCatChem* **2017**, *9* (17), 3402–3411.

(25) Rosar, V.; Meduri, A.; Montini, T.; Fornasiero, P.; Zangrando, E.; Milani, B. The Contradictory Effect of the Methoxy-Substituent in Palladium-Catalyzed Ethylene/Methyl Acrylate Cooligomerization. *Dalt. Trans.* **2018**, *47* (8), 2778–2790.

(26) Lu, W.; Wang, H.; Fan, W.; Dai, S. Exploring the Relationship between the Polyethylene Microstructure and Spatial Structure of α-Diimine Pd(II) Catalysts via a Hybrid Steric Strategy. *Inorg. Chem.* **2022**, *61*, 6799–6806.

(27) Zhang, Y.; Wang, C.; Mecking, S.; Jian, Z. Ultrahigh Branching of Main-Chain-Functionalized Polyethylenes by Inverted Insertion Selectivity. *Angew. Chemie* **2020**, *132* (34), 14402–14408.

(28) Zhang, Y.; Jian, Z. Comprehensive Picture of Functionalized Vinyl Monomers in Chain-Walking Polymerization. *Macromolecules* **2020**, *53* (20), 8858–8866.

(29) Popeney, C. S.; Camacho, D. H.; Guan, Z. Efficient Incorporation of Polar Comonomers in Copolymerizations with Ethylene Using a Cyclophane-Based Pd(II) α-Diimine Catalyst. *J. Am. Chem. Soc.* **2007**, *129* (33), 10062–10063.

(30) Allen, K. E.; Campos, J.; Daugulis, O.; Brookhart, M. Living Polymerization of Ethylene and Copolymerization of Ethylene/Methyl Acrylate Using "Sandwich" Diimine Palladium Catalysts. *ACS Catal.* **2015**, *5* (1), 456–464.

(31) Carrow, B. P.; Nozaki, K. Transition-Metal-Catalyzed Functional Polyolefin Synthesis: Effecting Control through Chelating Ancillary Ligand Design and Mechanistic Insights. *Macromolecules* **2014**, *47* (8), 2541–2555.

(32) Delferro, M.; Marks, T. J. Multinuclear Olefin Polymerization Catalysts. *Chem. Rev.* **2011**, *111* (3), 2450–2485.

(33) Takano, S.; Takeuchi, D.; Osakada, K.; Akamatsu, N.; Shishido, A. Dipalladium Catalyst for Olefin Polymerization: Introduction of Acrylate Units into the Main Chain of Branched Polyethylene. *Angew. Chemie - Int. Ed.* **2014**, *53* (35), 9246–9250.

(34) Mitsushige, Y.; Carrow, B. P.; Ito, S.; Nozaki, K. Ligand-Controlled Insertion Regioselectivity Accelerates Copolymerisation of Ethylene with Methyl Acrylate by Cationic Bisphosphine Monoxide-Palladium Catalysts. *Chem. Sci.* **2016**, *7* (1), 737–744.

(35) Contrella, N. D.; Sampson, J. R.; Jordan, R. F. Copolymerization of Ethylene and Methyl Acrylate by Cationic Palladium Catalysts That Contain Phosphine-Diethyl Phosphonate Ancillary Ligands. *Organometallics* **2014**, *33* (13), 3546–3555.

(36) Sui, X.; Dai, S.; Chen, C. Ethylene Polymerization and Copolymerization with Polar Monomers by Cationic Phosphine Phosphonic Amide Palladium Complexes. *ACS Catal.* **2015**, *5* (10), 5932–5937.

(37) Zhang, W.; Waddell, P. M.; Tiedemann, M. A.; Padilla, C. E.; Mei, J.; Chen, L.; Carrow, B. P. Electron-Rich Metal Cations Enable Synthesis of High Molecular Weight, Linear Functional Polyethylenes. *J. Am. Chem. Soc.* **2018**, *140* (28), 8841–8850.

(38) Nakano, R.; Nozaki, K. Copolymerization of Propylene and Polar Monomers Using Pd/IzQO Catalysts. *J. Am. Chem. Soc.* **2015**, *137* (34), 10934–10937.

(39) Tao, W.; Akita, S.; Nakano, R.; Ito, S.; Hoshimoto, Y.; Ogoshi, S.; Nozaki, K. Copolymerisation of Ethylene with Polar Monomers by Using Palladium Catalysts Bearing an N-Heterocyclic Carbene-Phosphine Oxide Bidentate Ligand. *Chem. Commun.* **2017**, *53* (17), 2630–2633.

(40) Li, M.; Wang, X.; Luo, Y.; Chen, C. A Second-Coordination-Sphere Strategy to Modulate Nickel- and Palladium-Catalyzed Olefin Polymerization and Copolymerization. *Angew. Chemie - Int. Ed.* **2017**, *56* (38), 11604–11609.

(41) Zhai, F.; Solomon, J. B.; Jordan, R. F. Copolymerization of Ethylene with Acrylate Monomers by Amide-Functionalized α-Diimine Pd Catalysts. *Organometallics* **2017**, *36* (9), 1873–1879.

(42) Dai, S.; Chen, C. Direct Synthesis of Functionalized High-Molecular-Weight Polyethylene by Copolymerization of Ethylene with Polar Monomers. *Angew. Chemie - Int. Ed.* **2016**, *55* (42), 13281–13285.

(43) Wang, H.; Duan, G.; Fan, H.; Dai, S. Second Coordination Sphere Effect of Benzothiophene Substituents on Chain Transfer and Chain Walking in Ethylene Insertion Polymerization. *Polymer*. **2022**, *245* (February), 124707.

(44) Fan, H.; Xu, G.; Wang, H.; Dai, S. Direct Synthesis of Hyperbranched Ethene Oligomers and Ethene-MA Co-Oligomers Using Iminopyridyl Systems with Weak Neighboring Group Interactions. *J. Polym. Sci.* **2022**, *60* (13), 1944–1953.

CHAPTER 2

Tunable "*in-chain*" and "*at the end of the branches*" methyl acrylate incorporation in polyolefin skeleton through Pd(II) catalysis

Overview

In this chapter, monocationic palladium(II) complexes of general formula [Pd(CH_3)(N-S)(**1**)][PF_6] having a thiophenimine molecule (N-S) as a hemilabile, potentially bidentate ligand bonded to the metal center in the place of acetonitrile have been studied. The new family of synthesized complexes generates active species for the ethylene/methyl acrylate copolymerization and their catalytic behavior is investigated. We have discovered that the N-S ligand present on the fourth coordination site of the metal center is able to affect the way of the polar monomer enchainment. The catalytic behavior of the new complexes is compared to that of the parent compound [Pd(CH_3)($NCCH_3$)(**1**)][PF_6] highlighting the fact that when trifluoroethanol is the reaction medium, this complex is also able to produce the E/MA copolymer with MA inserted both in the main chain and at the end of the branches. Detailed NMR studies on the reaction of the precatalyst with the two comonomers allowed to discover that in the fluorinated solvent, the catalyst resting state is an open-chain intermediate having both the organic fragment, originated from the migratory insertion of MA into the Pd-CH_3 bond, and the acetonitrile coordinated to palladium and not the six-membered palladacycle typically observed for the Pd-α-diimine catalysts.

Part of this Chapter was published as:

Alberoni, C., D'Alterio, M. C., Balducci, G., Immirzi, B., Polentarutti, M., Pellecchia, C., Milani, B. *ACS Catal.* **2022**, *12*, 3430.

2.1. Introduction.

Starting from the results obtained by the pioneering work of Brookhart in the middle of 90's (**1**, Figure 2.1),[1] where branched E/MA copolymers with methyl acrylate inserted at the end of the branches (T(MA)) were obtained, in the last two decades a huge number of α-diimine ligands with a DAB skeleton and different substituents on the aryl rings has been developed. The relevant Pd(II) complexes generate active species for the copolymerization of ethylene with polar vinyl monomers.[2] By modifying specific substituents on the ancillary ligand, it is possible to tune some parameters of the produced copolymers, such as the amount of inserted polar monomer, its way of enchainment, the degree of branching, etc.. In particular, the presence of dibenzhydryl groups on the aryl rings (**L35**, Figure 2.1) leads to semicrystalline, high molecular weight E/MA copolymers (M_n up to $1.9 \cdot 10^4$ Da), with branching degree about 25 per 1000 C atoms with the 1.8 mol % of polar monomer inserted at the end of long chain branches.[3] From these results, Chen *et al.* synthesized new ligands with an increased steric hindrance by replacing the phenyl groups with benzothiophene (**L31**, Figure 2.1) or naphthalene units (**L32**, Figure 2.1).[4] The X-ray analysis of the corresponding Pd(II) complexes highlights the presence of π-π stacking interactions between the *ortho* substituents and the aryl ring of the ligand skeleton that can influence the catalytic behavior of the complexes. These catalysts lead to semicrystalline E/MA copolymers with a high molecular weight and a low degree of branching (9 branches per 1000 C atoms), while the percentage of inserted MA is in the range of 0.60 - 0.88 mol %. These experimental data indicate that the high steric bulk of the ligand and the thermal stability of precatalysts disfavor the coordination/insertion of the polar monomer and significantly slow down the phenomenon of the chain walking with respect to the growth phase of the polymer chain.

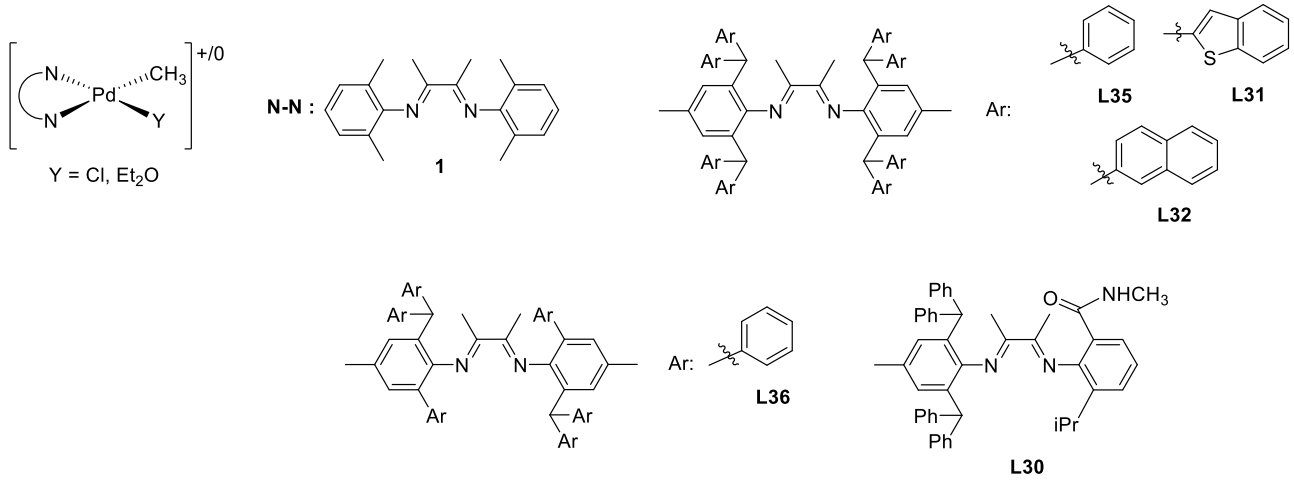

Figure 2.1. General structure of a Pd catalyst and examples of reported DAB ancillary ligands.

Ni(II) compounds with **L31** and **L32** are also synthesized and tested in the ethylene homopolymerization.[5] The results outline that the Ni(II) catalyst containing **L31** displays high activity and generates slightly branched (15 – 37/1000 C) polyethylene with particularly high molecular weight (M_n up to 2017.6 kg/mol) at low temperature (T = 293 K). The interaction between the sulfur atom of the coordinated **L31** and the hydrogen atom on the beta position of the growing copolymer chain is considered to be responsible to inhibit the β-H elimination reaction by suppressing both the chain walking process and the chain transfer reaction (Figure 2.2).

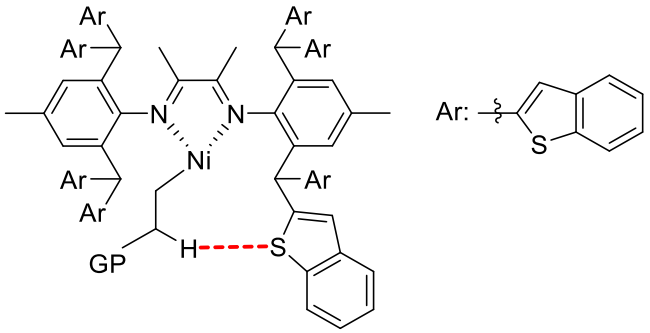

Figure 2.2. The proposed second coordination sphere effect of **L31** in ethylene polymerization at low temperatures; GP = growing polymer.

During the last year Dai *et al.* studied a compromised molecule between the previously reported ligands **L31** and **L35**, characterized by combining *ortho*-diarylmethyl and *ortho*-phenyl moieties (**L36**, Figure 2.1).[6] When **L36** is coordinated to palladium ion, it should create a more open spatial environment around the metal center responsible to tune the catalytic performance of these catalysts. The obtained E/MA copolymers have a modest molecular weight (4.4 – 18.6 kg/mol) and a moderate amount of inserted MA (1.8 – 4.8 mol %), predominately incorporated as T(MA).

Other authors are focused on the introduction on the α-diimine of some functionalities without increasing the steric bulkiness around the metal ion. Their presence can establish secondary interactions with the other ligands in the first coordination sphere of the metal center, tuning their catalytic properties. As an example, the catalyst with **L30** (Figure 2.1) proposed by Jordan *et al.* shows a H-bonding interaction between the amide-functionality and the Pd-Cl fragment of the complex (Cl···N of 3.541(9) Å).[7] This leads to copolymers with a lower branching degree than those obtained with the catalyst without it (74 *vs* 77 per 1000 C atoms) and a higher incorporation, up to 1.3 mol %, of MA, predominantly inserted at branch ends.

One possible explanation for these experimental results is that the H-bond donor properties of **L30** assist the insertion of MA into Pd−R bond and the opening of chelate metallacycle after the MA insertion (Figure 2.3).

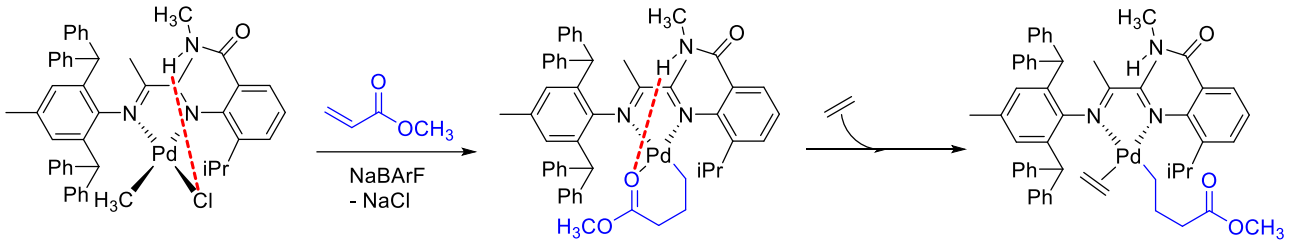

Figure 2.3. The proposed second coordination sphere effect of **L30** in ethylene/methyl acrylate polymerization.

Remembering that an ideal catalyst, in addition to be stable and to show a high productivity, should control some structural parameters over the synthesized copolymers, such as molecular weight and molecular weight distribution, the amount of polar monomer incorporation, macromolecule microstructure (i.e., linear or branched polymers), and the way of polar monomer enchainment, and considering the approach reported in literature for the study of the secondary interactions between the substituents on the α-diimmine ligand and the metal center, as an alternative strategy to ligand design, we decided to introduce in the palladium coordination sphere, in addition to the α-diimine, a hemilabile, potentially bidentate ligand, such as a thiophenimine N-S. With this aim we studied the monocationic Pd(II) complexes of general formula [Pd(CH_3)(N-S)(**1**)][PF_6], where N-S is a thiophenimine ligand with different substituents on the *meta* positions of the aryl ring. The catalytic behaviour of these complexes in the ethylene/methyl acrylate copolymerization was investigated in detailed and compared with that of the parent compound [Pd(CH_3)($NCCH_3$)(**1**)][PF_6], **1b**. Accurate *in situ* NMR studies of such complexes with ethylene, MA and both comonomers were also performed to gain information about the mechanism of the copolymerization reaction.

2.2. Results and discussion.

2.2.1 Synthesis and characterization of ligands S^{Ph}, S^{Me} *and* S^{CF3}.

The synthetic route applied to obtain the thiophenimine ligands is based on the condensation reaction of 2-thiophenecarboxaldehyde with the proper aniline (Scheme 2.1).

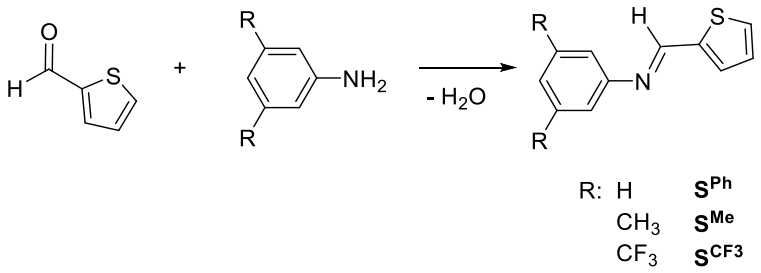

Scheme 2.1. Synthesis of N-S ligands.

In particular, the synthesis of $\mathbf{S^{Ph}}$ is reported in literature[8] and we synthesized $\mathbf{S^{Me}}$ with slight modifications of this procedure, while ligand $\mathbf{S^{CF3}}$ is obtained following a new procedure based on the use of microwave irradiation and it is obtained as a mixture of the desired product and 2-thiophenecarboxaldehyde. It is purified by flash chromatography to have the desired ligand. $\mathbf{S^{Ph}}$ and $\mathbf{S^{CF3}}$ have been isolated as red-yellow oils in high yields (93 % and 91 %, respectively), while $\mathbf{S^{Me}}$ is obtained like an orange solid in a yield about 90 %.

The mono- and bi-dimensional NMR spectroscopy is the technique of choice to characterize the obtained ligands (Figure S2.1-S2.2). For $\mathbf{S^{CF3}}$, the ^{19}F NMR spectrum is recorded on the pure ligand showing a singlet at -63.28 ppm (Figure 2.4).

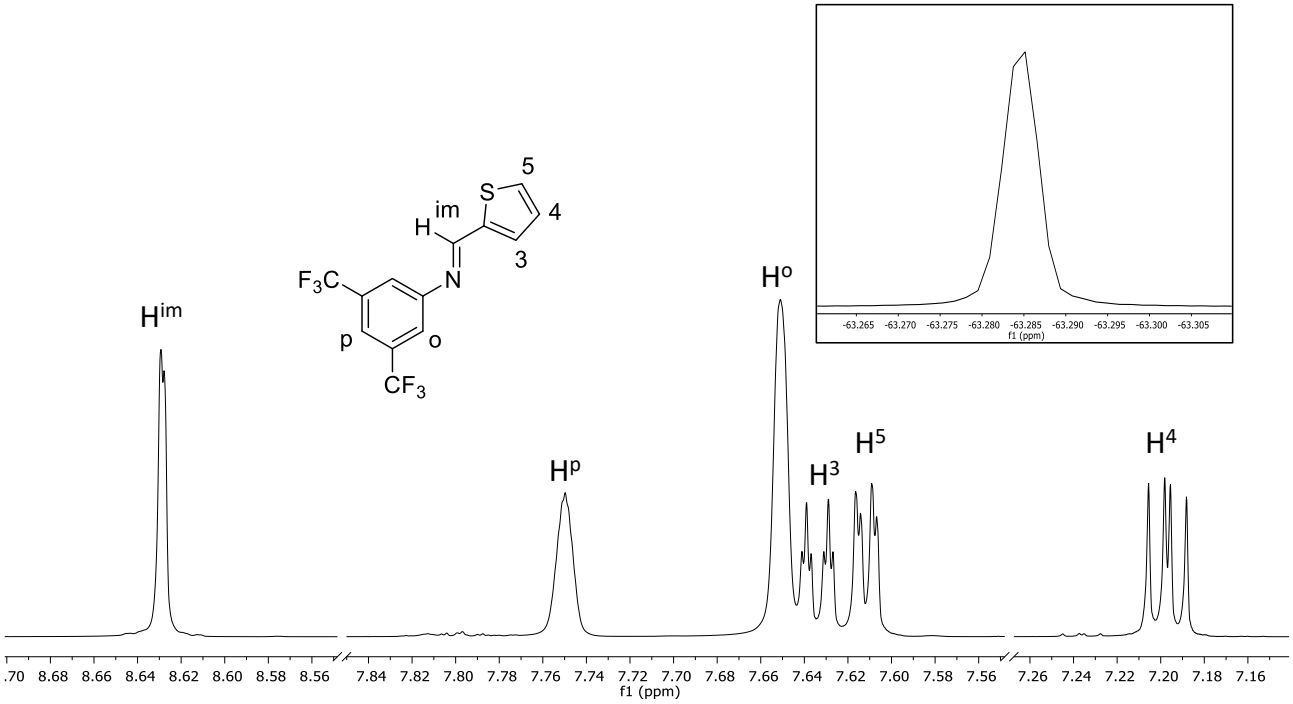

Figure 2.4. ^{1}H NMR spectrum (CD_2Cl_2, 298 K) of $\mathbf{S^{CF3}}$; inset: ^{19}F NMR spectrum.

The peak assigned to the iminic proton, H^{im}, confirms the formation of the ligand. It resonates at slightly different chemical shift depending on the substituents in *meta* positions of the aryl ring: at 8.60 ppm for $\mathbf{S^{Ph}}$, 8.57 ppm for $\mathbf{S^{Me}}$ and 8.63 ppm for $\mathbf{S^{CF3}}$ (Figure 2.5).

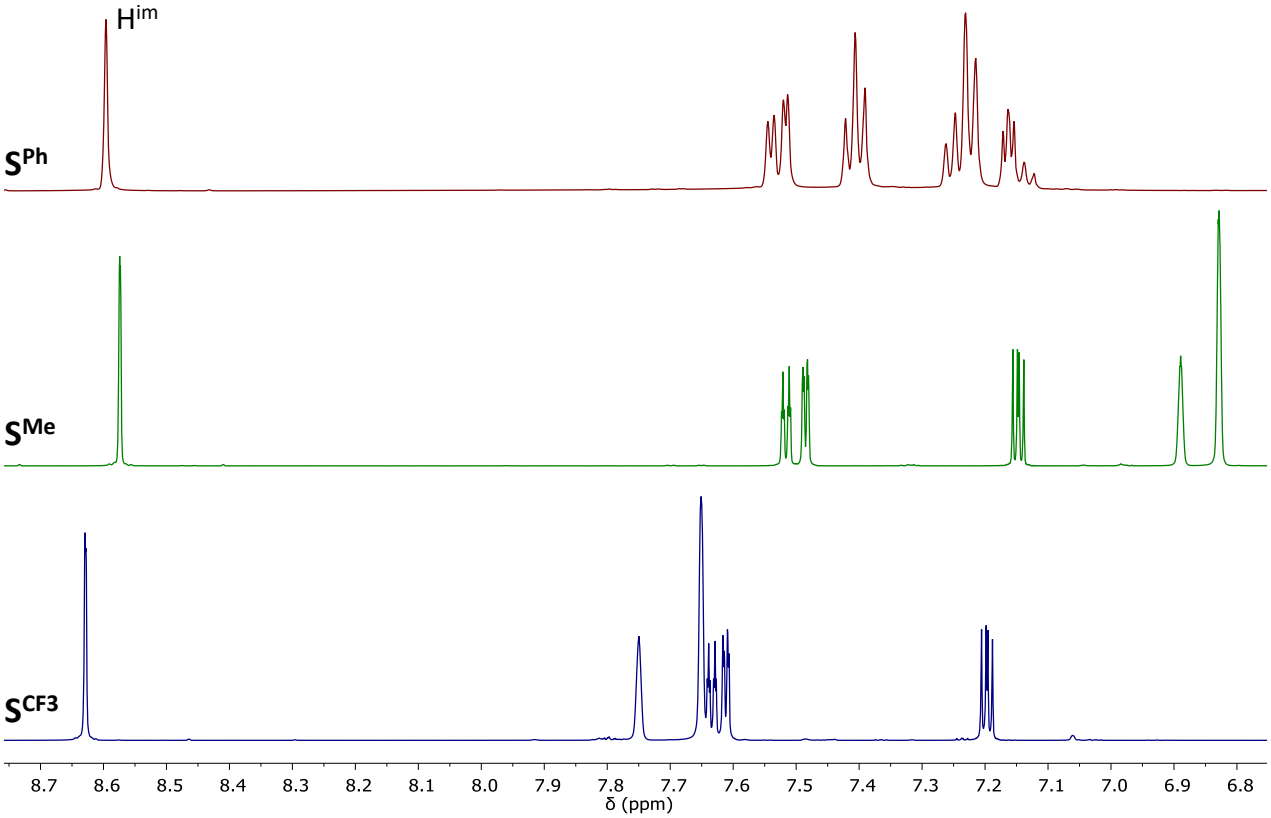

Figure 2.5. ^{1}H NMR spectra (CD_2Cl_2, 298 K) of ligands under investigation; aromatic region.

2.2.2 Synthesis and characterization of cationic Pd-complexes ***1S^{Ph}***, ***1S^{Me}*** *and* ***1S^{CF3}***.

The characterized thiophenimine ligands are used to synthesize the monocationic Pd(II) complexes $\mathbf{1S^{Ph}}$, $\mathbf{1S^{Me}}$ and $\mathbf{1S^{CF3}}$ starting from the reported cationic complex bearing the acetonitrile in the fourth coordination site, [Pd(CH_3)($NCCH_3$)(**1**)][PF_6], **1b**.[9] The desired complexes are isolated as yellow solids in moderate – high yields (from 66 % to 94 %) (Scheme 2.2).

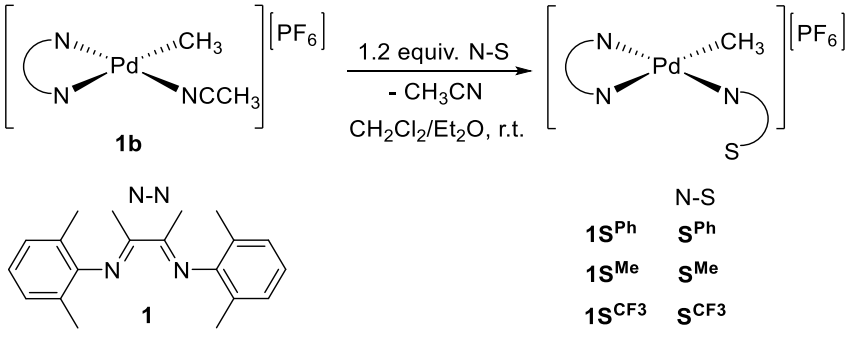

Scheme 2.2. Synthesis of the Pd(II) complexes under investigation.

They are characterized in solution by mono- and bi-dimensional NMR experiments (Figures S2.3-S2.5) at room temperature. The presence of one single species is confirmed by the one set of signals in the ^{1}H NMR spectrum and in particular by the singlet relative to the Pd-CH_3 moiety (Figure 2.6).

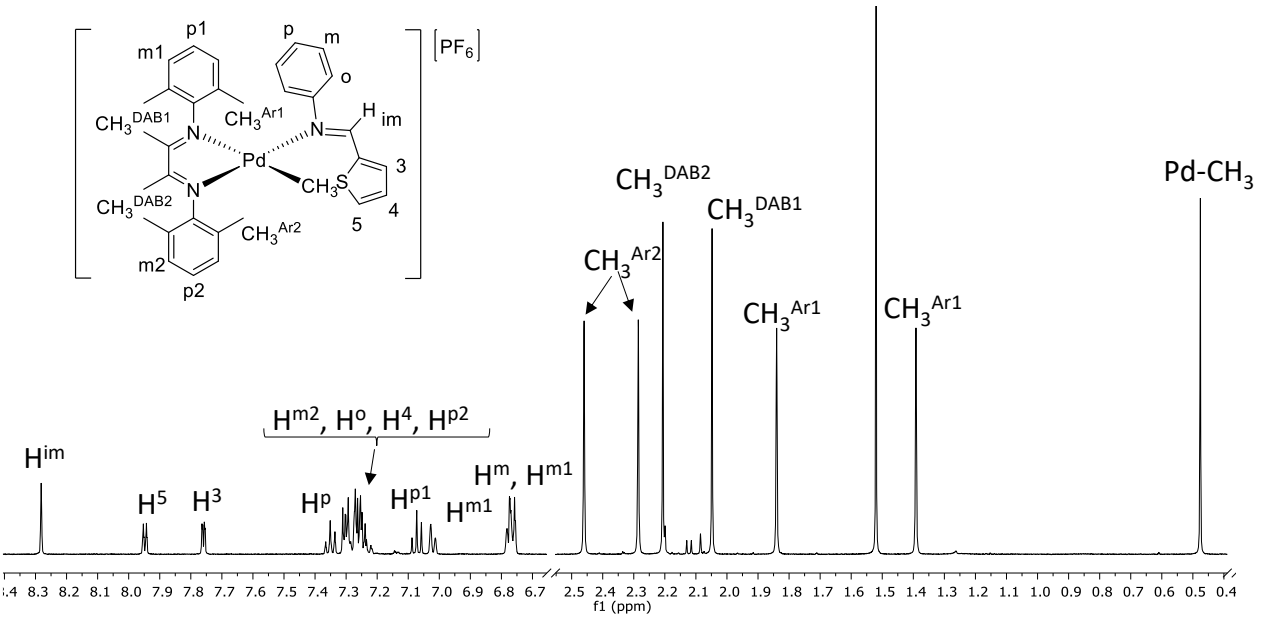

Figure 2.6. ^{1}H NMR spectrum (CD_2Cl_2, 298 K) of **1S^{Ph}**.

As for **1S^{Ph}**, on the basis of ^{1}H,^{1}H COSY spectrum (Figure S2.3) it is possible to recognize the signals due to CH_3^{Ar} that show correlation peaks with H^m and H^p of the aryl rings. The resonance at 1.39 ppm (CH_3^{Ar1}) has a correlation peak with that at 6.77 ppm (H^{m1}), while that at 1.84 ppm with the signal at 7.02 ppm (H^{m1}). Resonances of H^5 (7.95 ppm) and H^3 (7.76 ppm) of the thiophene ring are confirmed by ^{1}H,^{13}C HSQC spectrum due to characteristic chemical shifts of their carbon atoms at 136.2 ppm and 141.3 ppm respectively, as for H^{im} at 161.7 ppm (Figure 2.7).

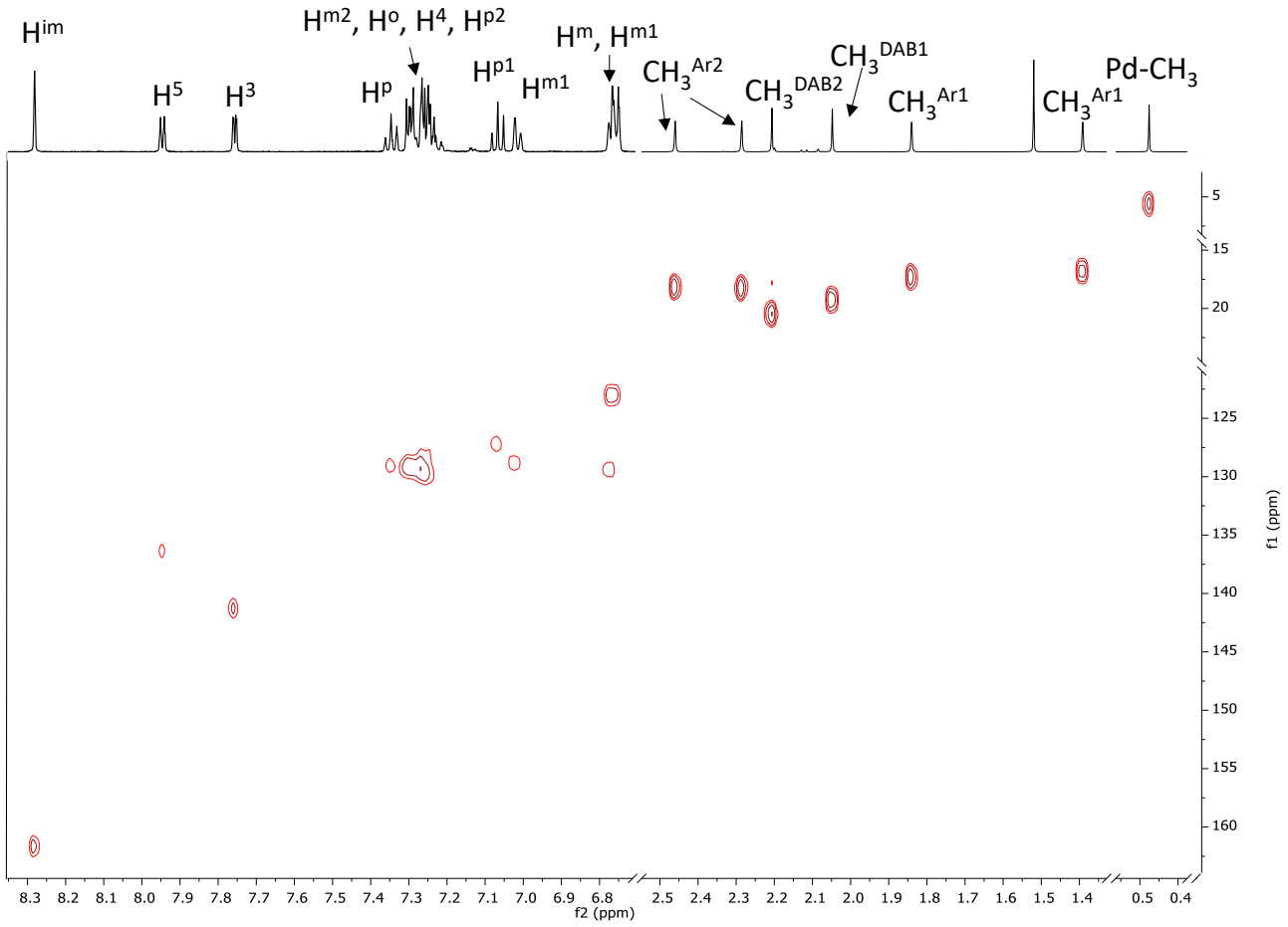

Figure 2.7. $^{1}H,^{13}C$ HSQC spectrum (CD_2Cl_2, 298 K) of **1S^{Ph}** (aromatic and aliphatic region not on scale).

In general the coordination of N-S ligand to Pd ion is clearly demonstrated by different factors. Firstly, the signals of ligand protons are at different chemical shifts from those of the free ligand, in particular the singlet of the diagnostic H^{im} of coordinated N-S shifts to lower frequency with respect to the free molecule (Figure 2.8). In **S^{Ph}** H^{im} resonates at 8.60 ppm, while in **1S^{Ph}** at 8.28 ppm, in the complex **1S^{Me}** it shifts from 8.57 to 8.29 ppm, while considering **S^{CF3}** and **1S^{CF3}** H^{im} resonates at 8.63 and 8.40 ppm, respectively.

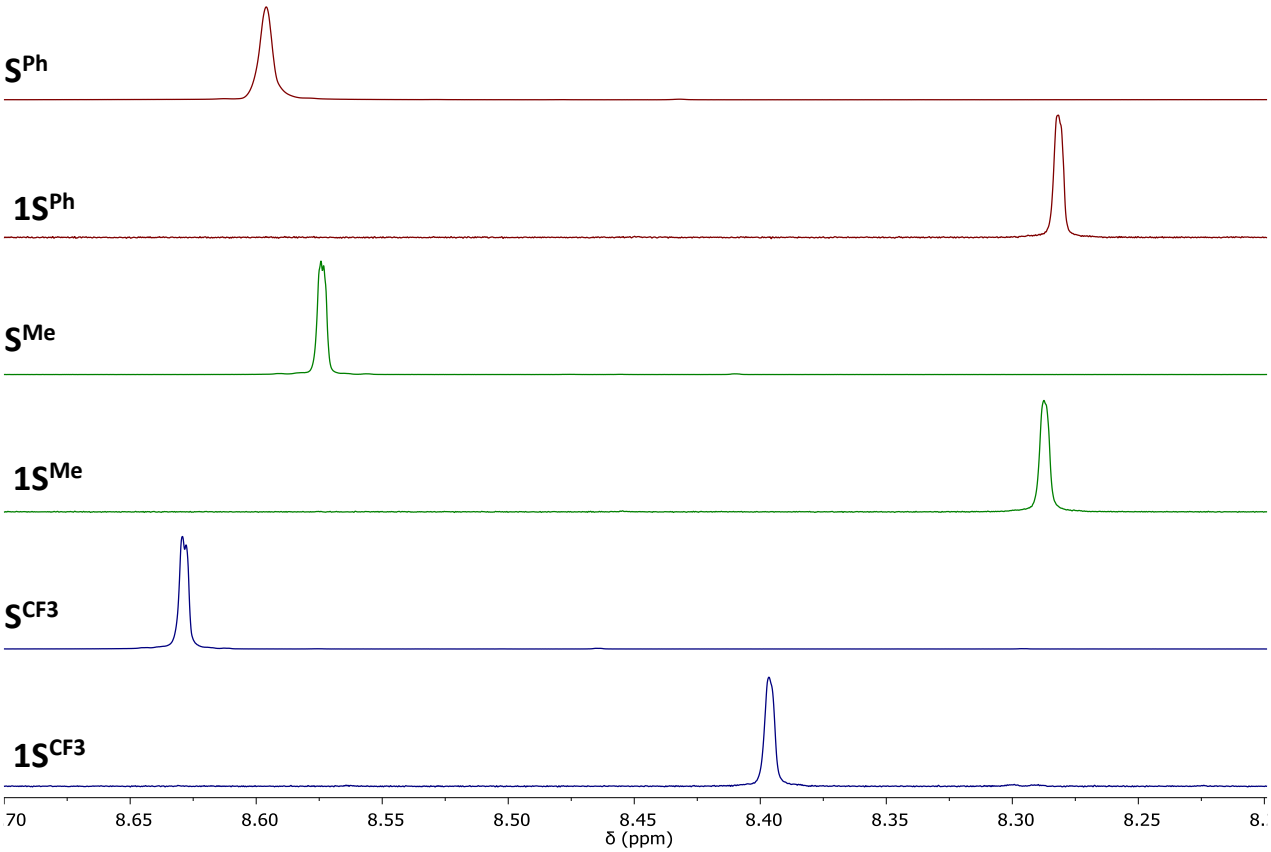

Figure 2.8. ^{1}H NMR spectra (CD_2Cl_2, 298 K) of ligands and complexes; signal of the iminic proton.

In analogy to the palladium coordination of pyridylimines,[10,11,12] this shift indicates that in the complex the N-S ligand is in the *E,syn* conformation (Scheme 2.3), suggesting the orientation of the sulfur atom toward the palladium ion.

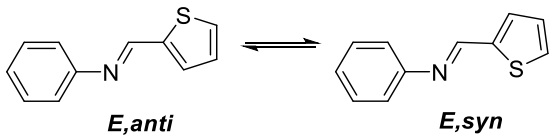

Scheme 2.3. *E,anti* and *E,syn* conformations for the N-S ligand.

The second factor of the coordination of the N-S ligand to the metal center is the change in the resonance frequency for protons of both **1** and Pd-CH_3 fragment with respect to **1b**. The singlet of Pd-CH_3 is shifted to higher frequencies from 0.34 ppm in **1b** to 0.47 ppm in **1S^{Ph}**, 0.45 ppm in **1S^{Me}** and 0.47 ppm in **1S^{CF3}**.

The last factor is the increase in the number of peaks of **1** protons due to the square planar plane not being a symmetry element any more. The proton-signal assignments of the two different halves of **1** are done thanks to the 2D experiments.

In particular in the $^{1}H,^{1}H$ NOESY spectrum a peak generated by the Overhauser effect between singlets of the methyl group on one of the two aryl rings at 2.46 and 2.29 ppm (CH_3^{Ar2}) and the Pd-CH_3 fragment at 0.47 ppm allows to understand which half of **1** is in *cis* position with respect to the Pd-CH_3 moiety (Figure 2.9).

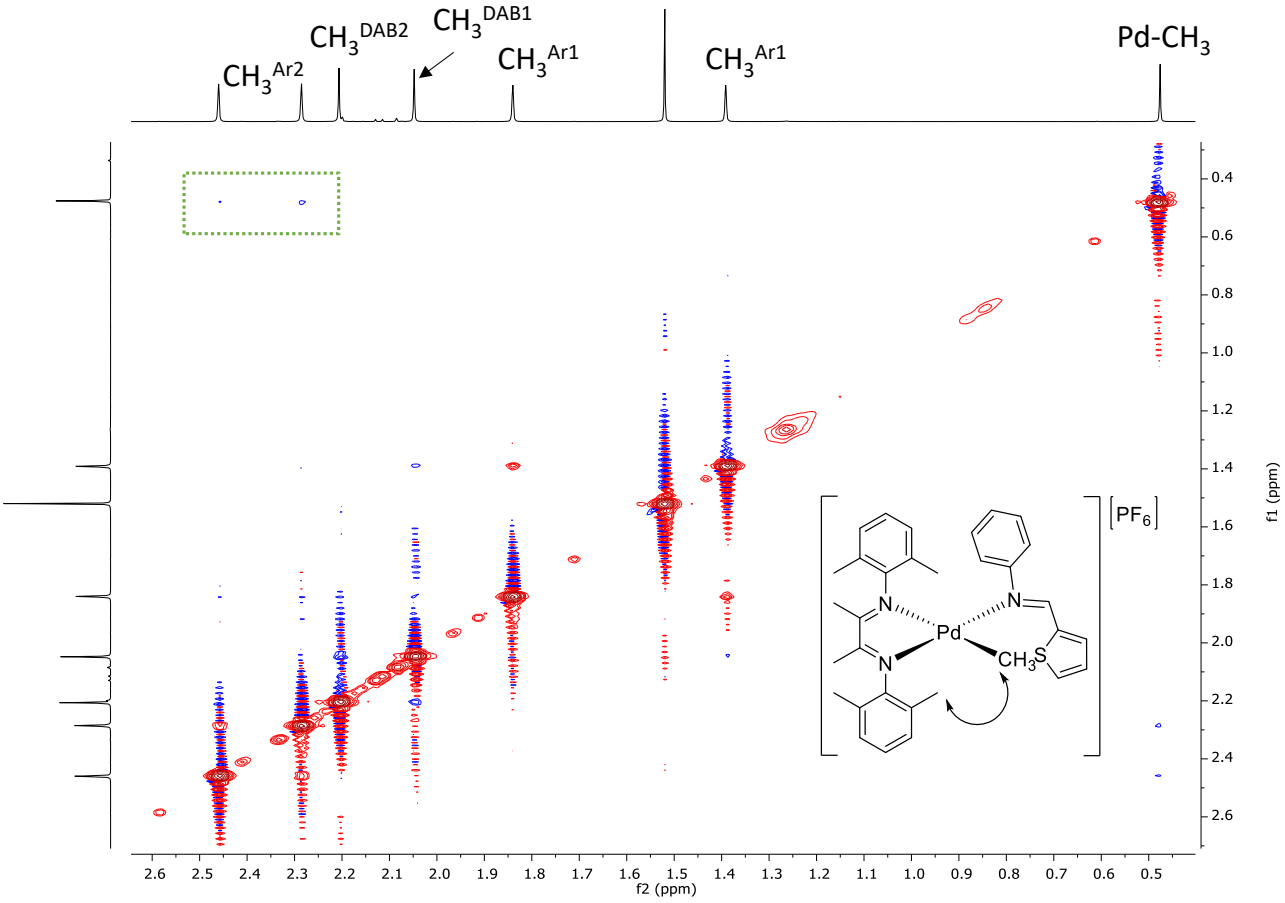

Figure 2.9. $^{1}H,^{1}H$ NOESY spectrum (CD_2Cl_2, 298 K) of **1S^{Ph}**.

Suitable single crystals for X-Ray analysis are obtained upon slow diffusion of *n*-hexane in a CD_2Cl_2 solution of the desired complex. For both **1S^{Ph}** and **1S^{Me}**, Pd ion shows the expected square planar geometry with the α-diimine **1** bonded as a chelating ligand and the thiophenimine as a monodentate one (Figure 2.10a and Figure S2.6). In the unit cell of **1S^{Ph}** only one molecule is present, while for **1S^{Me}** two independent molecules of this compound are found in the crystal structure that differ for the orientation and the distance of the sulfur atom with respect to the palladium ion.

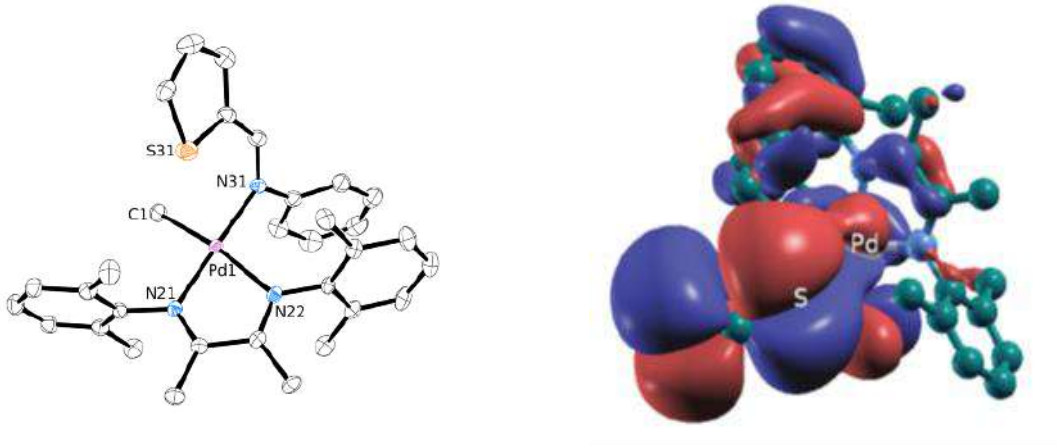

(a) (b)

Figure 2.10. (a) ORTEP drawing (50% probability ellipsoids) of the molecule of **1S^{Ph}**. Hydrogen atoms and the PF_6^- anion have been omitted for the sake of clarity; (b) Isosurface plot for the π symmetrical molecular orbital which extends over both Pd and S atoms.

The crystal structure confirms that the N-S ligand is coordinated through the nitrogen atom and the sulfur occupies an apical position with respect to the metal ion, at the distance of 3.100(1) Å and 3.328(2)/3.125(2) Å in **1S^{Ph}** and **1S^{Me}**, respectively, suggesting a weak interaction between them. In the case of **1S^{Ph}**, a π-π stacking interaction between the aryl ring of the N-S ligand and the substituted aryl of **1** in *cis* to it is suggested by the pertinent geometrical parameters (dihedral angle made by the least-squares planes through the rings: 9.0° and centroid−centroid distance: 3.8 Å). On the other hand, for **1S^{Me}**, the geometrical parameters for the same intramolecular π-π stacking interaction are less favourable (ring−ring dihedral angle and centroid distance are 16.5°, 4.3 Å and 17.8°, 4.7 Å for the two independent molecules of the unit cell, respectively), suggesting that the crystal packing plays a significant role in determining this kind of weak interaction. The Pd···S interaction in the solid state for complex **1S^{Ph}** is characterized by application of the methodology of quantum theory of atoms in molecules (QTAIM). The projection of the density of states (DOS) onto the atomic orbitals of Pd and S shows a small but noticeable overlap of Pd-d and S-p orbitals (Figure S2.7), which can be further evidenced with the isosurface plot of the square modulus of the corresponding molecular orbitals (Figure 2.10b). This structural analysis clearly supports the presence of a weak interaction between the Pd ion and sulfur atom in the complexes under investigation.

2.2.3 Ethylene/methyl acrylate copolymerization with ***1S^{Ph}***, ***1S^{Me}*** *and* ***1S^{CF3}***.

All complexes are tested in the ethylene/methyl acrylate copolymerization. They generate active species for the target reaction leading to branched copolymers. Catalysis are carried out under mild reaction conditions of temperature (308 K) and ethylene pressure, for a proper time (t = 6 h), in both dichloromethane (DCM) and 2,2,2-trifluoroethanol (TFE) as reaction media.

Considering the precursor **1b**, we carried out a detailed catalytic investigation about the proper ratio of the two comonomers with the aim to reach the highest amount of inserted M(MA) (Table 2.1). Upon increasing the [MA]/[Pd] ratio, by adding more polar monomer, and keeping constant the ethylene pressure at 2.5 bar, a decrease in productivity is observed together with an increase in the amount of inserted MA, as expected, but no difference in the way of MA enchainment is detected (M(MA):T(MA) = 24:76; Table 2.1, entries 1 and 2). Instead when the ethylene pressure is 5.0 bar and the [MA]/[Pd] is 1188, the precatalyst **1b** shows a moderate productivity of about 49 kg CP/mol Pd, incorporating 4.0 mol % of MA, but in this case the amount of M(MA) is the highest ever reported for a catalyst with the simple α-diimine of 40 % (Table 2.1, entry 4).

Table 2.1. Ethylene/methyl acrylate copolymerization: effect of amount of comonomers. Precatalyst: [Pd(CH$_3$)(NCCH$_3$)(1)][PF$_6$], 1b[a]

entry	P_E (bar)	[MA]/[Pd]	yield (g)	kg CP/mol Pd[b]	MA (mol %)[c]	Bd[d]	M(MA)[e]	T(MA)[e]
1	2.5	594	1.3917	66.27	3.6	93	24	76
2	2.5	1188	1.0033	47.78	4.9	93	24	76
3	5.0	594	1.0269	48.90	1.9	102	31	69
4	5.0	1188	1.2045	48.78	4.0	93	40	60

[a] Reaction conditions: $n_{Pd} = 2.1 \cdot 10^{-5}$ mol, V_{TFE} = 21 mL, T = 308 K, t = 6 h. [b] Productivity in kg CP/mol Pd = kilograms of copolymer per mol of palladium calculated on isolated yield. [c] Amount of inserted MA in mol % calculated by ^{1}H NMR spectroscopy on isolated product. [d] Branching degree expressed as number of branches per 1000 carbon atoms. [e] Way of MA enchainment, as calculated by ^{13}C NMR spectroscopy on isolated product (M(MA) = methyl acrylate in chain; T(MA) = methyl acrylate at the end of the branches).

So, two sets of reaction conditions have been chosen: set A with P_E = 2.5 bar and [MA]/[Pd] = 594 and set B having P_E = 5.0 bar and [MA]/[Pd] = 1188 (Tables 2.2 and 2.3). The obtained copolymers are similar to gums when they are synthesized in TFE or as oils when the catalysis are performed in DCM. Their microstructures and the amount of inserted polar monomer are studied in solution by NMR spectroscopy and their M_n is calculated using GPC analysis.

Table 2.2. Ethylene/methyl acrylate copolymerization: effect of N-S and solvent.

Precatalyst: [Pd(CH$_3$)(N-S/L)(1)][PF$_6$][a]

entry	precat.	Solvent	yield (g)	kg CP/mol Pd[b]	MA (mol %)[c]	TON[d]		M_n kDa[e] (Mw/Mn)	Bd[f]
						E	MA		
1	**1b**	TFE	1.3917	66.27	3.6	2095	79	24.6 (1.88)	93
2	**1S^{CF3}**	TFE	1.2608	60.04	3.2	1919	72	27.0 (2.12)	98
3	**1S^{Ph}**	TFE	0.5130	24.43	3.1	793	25	20.0 (1.64)	101
4	**1S^{Me}**	TFE	0.3521	16.77	2.9	546	16	14.7 (1.77)	103
5	**1b**	DCM	0.9692	46.15	4.8	1425	72	6.0 (2.18)	90
6	**1S^{CF3}**	DCM	1.0134	48.26	4.9	1446	78	8.2 (2.11)	87
7	**1S^{Ph}**	DCM	0.7411	35.29	3.2	1141	38	10.0 (2.03)	92
8	**1S^{Me}**	DCM	0.4105	19.55	3.6	625	23	12.4 (2.00)	95

[a] Reaction conditions: Set A: $n_{Pd} = 2.1 \cdot 10^{-5}$ mol, $V_{solvent} = 21$ mL, $V_{MA} = 1.130$ mL, [MA]/[Pd] = 594, $P_E = 2.5$ bar, T = 308 K, t = 6 h. [b] Productivity in kg CP/mol Pd = kilograms of copolymer per mol of palladium calculated on isolated yield. [c] Amount of inserted MA in mol % calculated by ^{1}H NMR spectroscopy on isolated product. [d] Turnover number = mol of substrate converted per mol of Pd. [e] Determined by GPC. [f] Branching degree expressed as number of branches per 1000 carbon atoms.

Table 2.3. Ethylene/methyl acrylate copolymerization: effect of N-S and solvent.

Precatalyst: [Pd(CH$_3$)(N-S/L)(1)][PF$_6$][a]

entry	precat.	Solvent	yield (g)	kg CP/mol Pd[b]	MA (mol %)[c]	TON[d]		M_n kDa[e] (Mw/Mn)	Bd[f]
						E	MA		
1	**1b**	TFE	1.2045	48.78	4.0	1524	84	23.4 (1.19)	93
2	**1S^{CF3}**	TFE	0.9874	46.89	3.2	1519	50	30.4 (1.81)	100
3	**1S^{Ph}**	TFE	0.5509	26.23	3.4	844	30	18.0 (1.98)	98
4	**1S^{Me}**	TFE	0.3924	18.68	3.4	601	21	12.3 (1.89)	97
5	**1b**	DCM	1.0380	49.43	4.8	1532	64	5.0 (2.00)	93
6	**1S^{CF3}**	DCM	0.9935	47.31	5.1	1446	78	5.4 (1.94)	93
7	**1S^{Ph}**	DCM	0.6266	29.84	4.0	943	39	11.0 (2.22)	90
8	**1S^{Me}**	DCM	0.4410	21.15	3.9	670	27	9.0 (1.89)	88

[a] Reaction conditions: Set B: $n_{Pd} = 2.1 \cdot 10^{-5}$ mol, $V_{solvent} = 21$ mL, $V_{MA} = 2.260$ mL, [MA]/[Pd] = 1188, $P_E = 5.0$ bar, T = 308 K, t = 6 h. [b] Productivity in kg CP/mol Pd = kilograms of copolymer per mol of palladium calculated on isolated yield. [c] Amount of inserted MA in mol % calculated by ^{1}H NMR spectroscopy on isolated product. [d] Turnover number = mol of substrate converted per mol of Pd. [e] Determined by GPC. [f] Branching degree expressed as number of branches per 1000 carbon atoms.

A decrease in productivity is observed moving from **1b** to the new family of precatalysts having the N-S ligands, according to the coordinating capability of thiophenimines. On the other hand these new complexes are very stable and no Pd(0) is formed when the catalysis are performed in TFE, but it is observed only in traces when **1b** and **1S^{CF3}** are used as precatalysts in the copolymerization carried out in DCM. This is due to the capability of the fluorinated reaction medium to stabilize the Pd-hydride intermediate, responsible of the precatalyst decomposition to inactive palladium metal.[13]

Also the amount of inserted MA decreases moving from CH_3CN to thiophenimine ligands, but it is in the range 5.1 – 2.9 mol %. Regardless of the reaction conditions and the precatalyst, the copolymers synthesized in dichloromethane have a slightly higher content of methyl acrylate than those obtained in trifluoroethanol.

The produced copolymers have M_n values in the range 5 − 30 kDa and rather narrow molecular weight distributions (M_w/M_n range between 1.2 and 2.2). The most relevant trend is the significantly higher molecular weight of the copolymers prepared in TFE with respect to those obtained in DCM, for all the catalysts and for both sets of conditions. **1S^{CF3}** in TFE produces the copolymer with the highest M_n (27.0 and 30.4 kDa under set A and set B of reaction conditions, respectively) and the same catalyst gives the lowest M_n in DCM (8.2 and 5.4 kDa).

The value of the degree of branches confirms that the copolymers are branched macromolecules and under both sets of reaction conditions it is not affected by either the solvent or the ligand in the fourth coordination site. It is in the range of 87 – 103 per 1000 C atoms and in general the Bd for the copolymers synthesized in TFE is higher than the one relative to the macromolecules produced in DCM.

The most interesting effect of both the solvent and the N-S ligand is relative to the way of the polar monomer enchainment (Figure 2.11). The obtained copolymers are characterized by NMR spectroscopy and the ^{13}C NMR spectroscopy is the technique of choice to detect the way of MA incorporation.

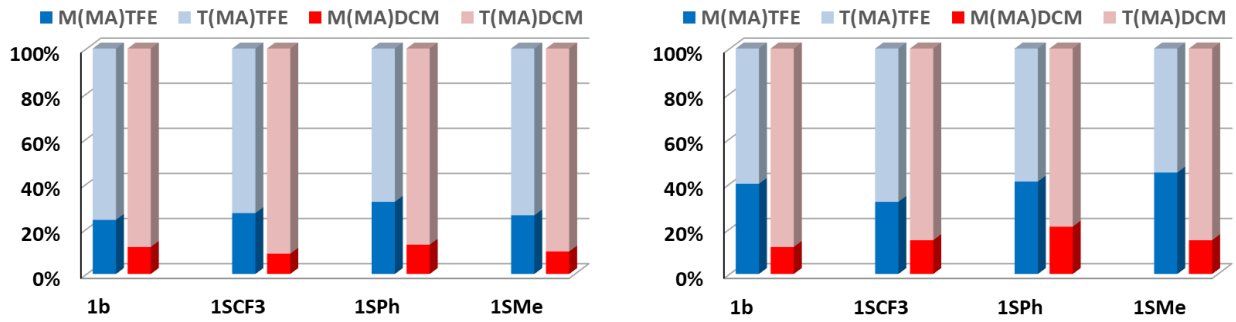

(a) (b)

Figure 2.11. Ethylene/MA copolymerization: effect of precatalyst and solvent on the way of MA enchainment (M(MA) of copolymers synthesized in TFE and DCM, blue and red bars, respectively; T(MA) of copolymers synthesized in TFE and DCM, light blue and light red bars, respectively). Reaction conditions: (a) Set A, Table 2.2; (b) Set B, Table 2.3.

From ^{13}C NMR spectra of the copolymers synthesized in DCM, we observe that methyl acrylate is almost exclusively inserted at the end of the branches (T(MA)), according to the literature,[9] with a small amount into the main chain (M(MA)). As mentioned above, even when the precatalysts with the N-S ligand are used, if the copolymerization is carried out in TFE, methyl acrylate is inserted as both M(MA) and T(MA), with a preference for the latter (Figure 2.12). The M(MA):T(MA) ratio varies with the precatalyst, the solvent and the set of reaction conditions (Tables S2.2 and S2.3). Under set B, considering the precatalyst **1b**, the macromolecule synthesized in TFE shows M(MA):T(MA) = 40:60, whereas for that one obtained in DCM, the ratio is 12:88 (Table S2.3, entries 1 and 5). The highest value of M(MA) is reached in the copolymer obtained in TFE using the Pd(II) complex bearing the methyl disubstituted thiophenimine, **1S^{Me}**, and a ratio about 1:1 is found between M(MA) and T(MA) (Table 2.3, entry 4).

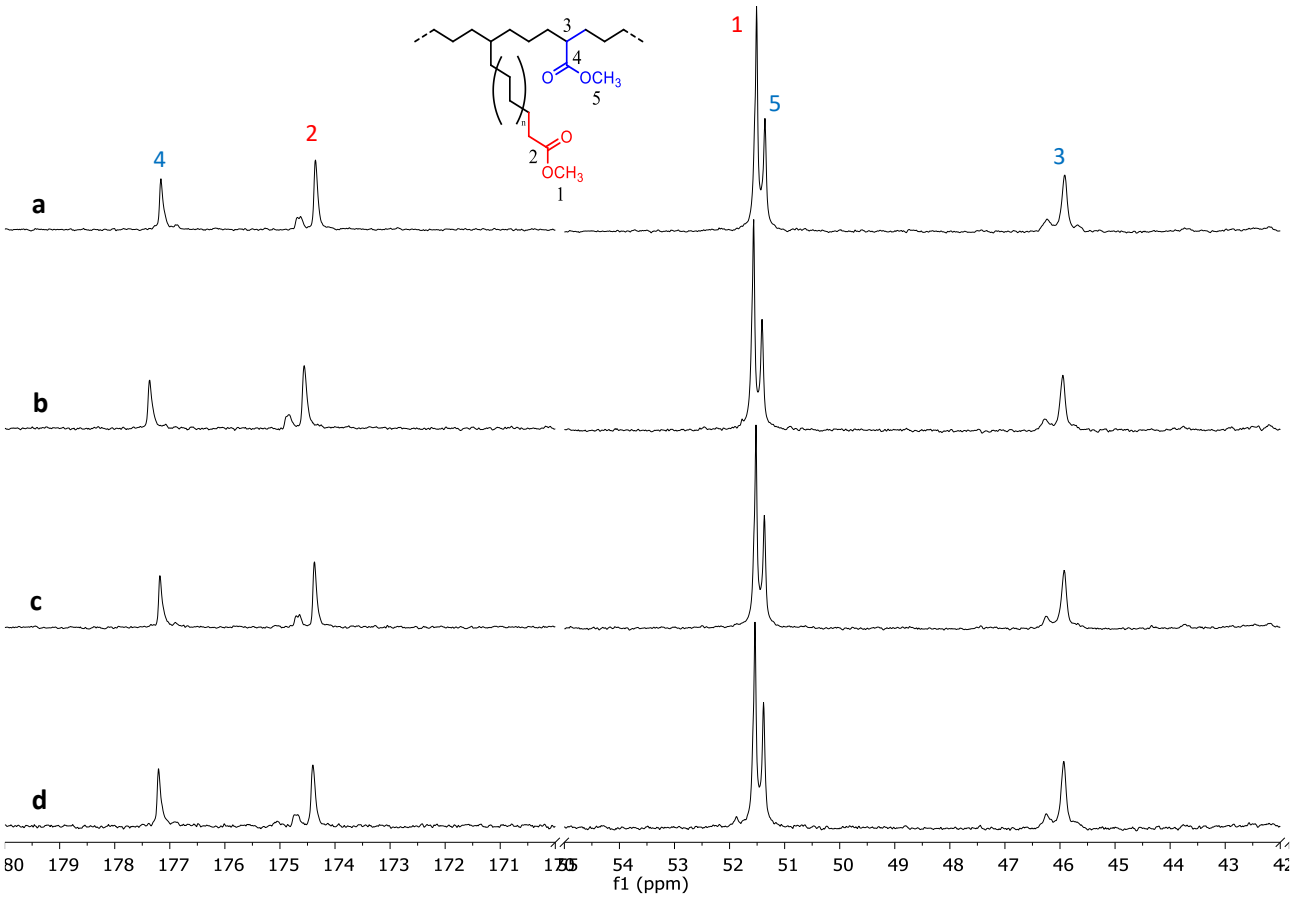

Figure 2.12. ^{13}C NMR spectra ($CDCl_3$, 298 K) of E/MA copolymers synthesized in TFE with (a) **1b**, (b) **1S^{CF3}**, (c) **1S^{Ph}** and (d) **1S^{Me}** under set B of reaction conditions (Table 2.3, entries 1 - 4); (left) carbonyl region; (right) methoxy and methinic region.

Moreover, under Set B in TFE, a clear trend of the M(MA):T(MA) with the N-S ligand is evident: moving from **1S^{CF3}** to **1S^{Ph}** and then to **1S^{Me}** the ratio increases, up to 0.82. Whereas using DCM as reaction medium, the best performing catalyst considering this catalytic parameter is **1S^{Ph}** (Tables S2.2 and S2.3, entry 7). These data indicate that the peculiar MA enchainment is due to both the solvent and the N-S ligand present in the palladium coordination sphere.

On the basis of these results, a detailed catalytic investigation is carried out using **1S^{Ph}** as precatalyst, in TFE. Temperature is the first operative parameter investigated in the range 308 – 328 K (Table 2.4).

Table 2.4. Ethylene/methyl acrylate copolymerization: effect of temperature.

Precatalyst: [Pd(CH$_3$)(S^{Ph})(1)][PF$_6$], 1S^{Ph} [a]

entry	T (K)	yield (g)	kg CP/mol Pd[b]	MA (mol %)[c]	M(MA)[d]	T(MA)[d]	M(MA): T(MA)	Bd[e]
1	308	0.5130	24.43	3.1	32	68	0.47	101
2	318	0.8960	42.67	3.8	21	79	0.26	100
3	328	1.5899	78.71	5.5	10	90	0.11	101

[a]Reaction conditions: $n_{Pd} = 2.1 \cdot 10^{-5}$ mol, V_{TFE} = 21 mL, V_{MA} = 1.130 mL, [MA]/[Pd] = 594, P_E = 2.5 bar, t = 6 h; [b]Productivity in kg CP/mol Pd = kilograms of copolymer per mol of palladium; [c]Calculated by ^{1}H NMR spectroscopy on isolated product; [d]Way of MA enchainment, as calculated by ^{13}C NMR spectroscopy on isolated product (M(MA) = methyl acrylate in chain; T(MA) = methyl acrylate at the end of the branches); [e]Branching degree calculated by ^{1}H NMR spectroscopy on isolated product and expressed as branches per 1000 carbon atoms.

An increase in productivity, reaching the value of about 79 kg CP/mol Pd, and in the amount of inserted MA, up to 5.5 mol %, is found moving from 308 to 328 K, together with a decrease in the M(MA):T(MA) ratio according to the fact that the temperature favors the chain walking process. At T = 328 K, the formation of traces of inactive palladium black is evident at the end of catalysis.

Then the effect of [MA]/[Pd] ratio is studied in the range 297-1188, by increasing the precatalyst concentration (Table S2.4). It results in a decrease in productivity together with an increase in the content of the inserted MA, suggesting that polynuclear species might be involved in catalyst deactivation, as we previously observed for catalysts with α-diimine ligands having a phenanthrene skeleton.[14] In agreement with literature, [1,9,14] when the influence of [MA]/[Pd] ratio is investigated by varying the amount of the polar monomer in the reaction mixture and keeping constant the amount of **1S^{Ph}** (Table S2.5), a linear increase in the content of inserted MA (up to 7.9 mol % at [MA]/[Pd] = 1782) together with a decrease in both productivity and degree of branching are observed. A slight increase in the M(MA) to T(MA) ratio is also found. The whole trend of parameters is in line with the inhibiting effect of the polar monomer.

The catalytic behavior of **1b** and **1S^{Ph}** is also studied with the use of the *mass flow control* device to measure the ethylene consumption during the catalytic process, under set A of reaction conditions by carrying out the copolymerization in TFE (Figure 2.13). After an induction period of 10 min for both complexes, the rate of ethylene uptake is the same up to half an hour, afterward **1b** remains very active for all the monitoring time, while **1S^{Ph}** slows down. This confirms the decrease in the terms of productivity observed moving from **1b** to **1S^{Ph}** and their stability by the absence of Pd(0) during catalysis.

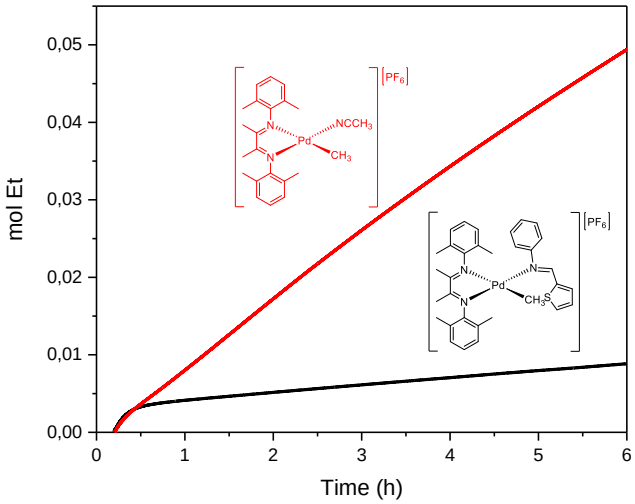

Figure 2.13. Ethylene/methyl acrylate copolymerization: kinetic profiles. Precatalyst: **1b** (red curve) and **1S^{Ph}** (black curve). Reaction conditions: see Table 2.2.

Complexes **1S^{Ph}**, **1S^{Me}** and **1S^{CF3}** generate active catalysts also for ethylene homopolymerization, in both trifluoroethanol and dichloromethane, leading to highly branched macromolecules (Table 2.5).

Table 2.5. Ethylene homopolymerization: effect of precatalyst and solvent.
Precatalyst: [Pd(CH$_3$)(N-S/L)(1)][PF$_6$],[a]

entry	precat.	solvent	yield (g)	kg PE/mol Pd[b]	Bd[c]
1	**1b**	TFE	3.0802	146.68	112
2	**1S^{CF3}**	TFE	3.2262	153.63	120
3	**1S^{Ph}**	TFE	0.9988	47.56	119
4	**1S^{Me}**	TFE	0.5846	27.84	117
5[d]	**1S^{CF3}**	DCM	2.7665	131.74	107
6	**1S^{Ph}**	DCM	2.3316	111.03	107
7	**1S^{Me}**	DCM	1.1376	54.17	106

[a]Reaction conditions: n_{Pd} = 2.1·10^{-5} mol, $V_{solvent}$ = 21 mL, P_E = 2.5 bar, t = 6 h; [b]Productivity in kg PE/mol Pd = kilograms of polyethylene per mol of palladium; [c]Branching degree calculated by ^{1}H NMR spectroscopy on isolated product and expressed as branches per 1000 carbon atoms; [d]t = 3h.

Complex **1S^{CF3}** generates the most productive catalyst in both solvents, whereas, in analogy to what has been found in the copolymerization, the productivity decreases moving to **1S^{Ph}** and **1S^{Me}**, this latter being the less productive catalyst of the series in both reactions. In addition, the polyethylene produced in TFE with the new family of precatalysts has a degree of branching higher than the PE obtained with **1b**, thus suggesting that the N−S ligand affects the chain walking process.

*2.2.4 Reactivity of **1b** and **1S^{Ph}** with ethylene, methyl acrylate and both comonomers.*

The novel catalytic results prompted us to investigate in more detail the reactivity of complexes with ethylene, methyl acrylate, separately and both comonomers together. The complexes of choice are **1b** and **1S^{Ph}** and the reactions are carried in either CD_2Cl_2 or TFE-d_3.

Focusing on **1b** dissolved in CD_2Cl_2, the first experiment is performed saturating the complex solution with ethylene. In the spectrum recorded after 5 min, resonances of branched PE and Pd-$NCCH_3$ are observed and no signals of **1b** or free ethylene (singlet at 5.40 ppm) are present, indicating the fast conversion of this complex into the active species for the homopolymerization reaction (Figures S2.8 and S2.9).

Then to a new solution of **1b**, 2 eq. of MA are added and the reaction is followed over time at room temperature (Figure 2.14). In the ^{1}H NMR spectrum recorded after 1 min from the addition of the polar monomer, the signals of the expected six-membered palladacycle (**MC6^{NS}**) are observed together with those of **1b**, five- and four- membered palladacycles (**MC5^{NS}** and **MC4^{NS}**, respectively) and the singlet of free acetonitrile at 1.99 ppm. After 2 h, all the precatalyst is consumed.

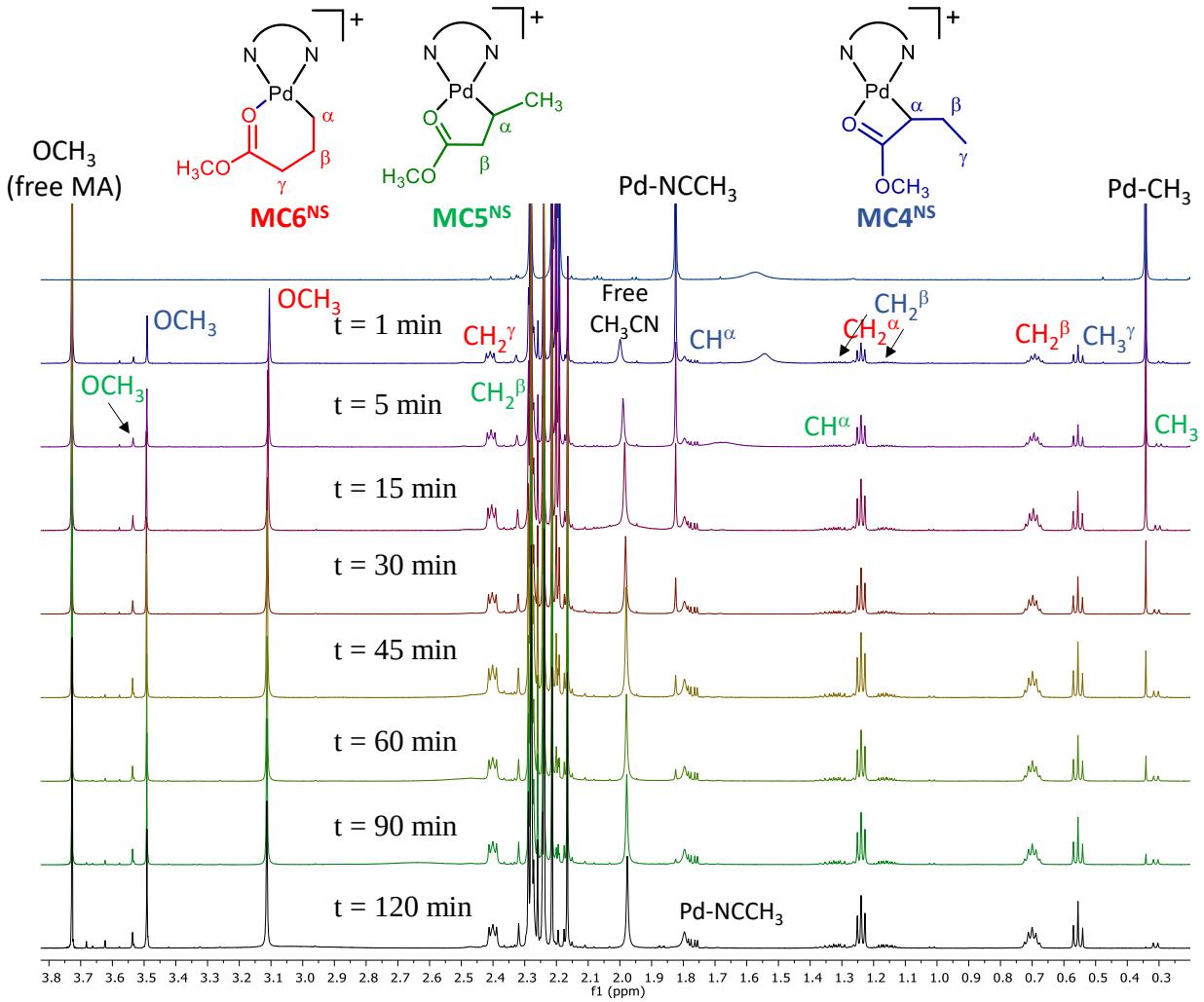

Figure 2.14. ^{1}H NMR spectra (CD_2Cl_2, 298 K) of **1b** (top spectrum) and of **1b** after the addition of methyl acrylate at different reaction times.

The assignments are done on the basis of a detailed bidimensional NMR investigation and the multiplicity of the signals. In the ^{1}H,^{1}H COSY spectrum (Figure S2.10) the triplet at 0.56 ppm (CH_3^{γ}) shows correlation peaks with signals at 1.17 and 1.33 ppm, relative to the diastereotopic protons of CH_2^{β}, which on turn correlate with the peak at 1.77 ppm (CH^{α}). All these resonances are in the same spin system and they are characteristic of **MC4^{NS}** intermediate. In the same spectrum also the multiplet at 0.70 ppm has extra diagonal peaks with signals at 1.23 and 2.41 ppm. In the ^{1}H,^{13}C HSQC spectrum (Figure 2.15) all these three resonances are assigned to CH_2 groups and they are CH_2^{β}, CH_2^{α} and CH_2^{γ} of **MC6^{NS}**, respectively. The peaks of the methoxy group at 3.49 ppm (**MC4^{NS}**) and at 3.12 ppm (**MC6^{NS}**) are assigned to the relevant metallacycles on the basis of the ^{1}H,^{13}C HMBC spectrum (Figure S2.11) and the value of their carbonyl group of 177.2 ppm for **MC4^{NS}** and 183.1 for **MC6^{NS}**. The assignments of **MC5^{NS}** are done in the same way as above.

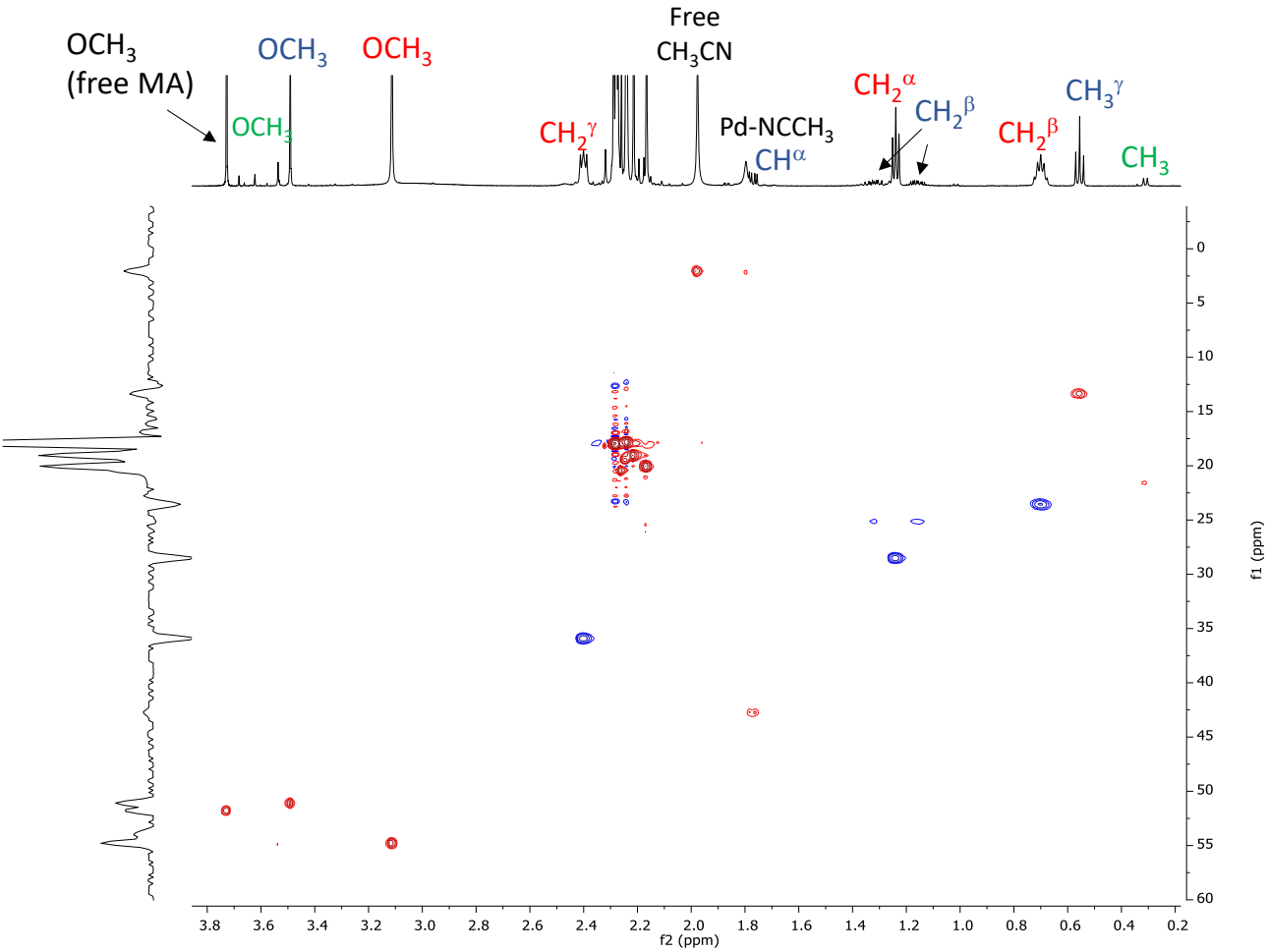

Figure 2.15. $^{1}H,^{13}C$ HSQC spectrum (CD_2Cl_2, 298 K) of the reaction mixture of **1b** with methyl acrylate at t = 120 min.

The metallacycle intermediates are the result of the migratory insertion of MA into the Pd-CH_3 bond followed by the chain walking process.[1] **MC4^{NS}** is detected in this work for the first time at room temperature with a Pd(II) complex bearing an α-diimine ligand. Recently, our research group in collaboration with Prof. Martin Albrecht of University of Bern observed this metallacycle at room temperature in the reaction between MA and a monocationic Pd(II)-PYA complex [Pd(CH_3)($NCCH_3$)(**8**)][PF_6], **8b**, where **8** is a N-N' bidentate pyridyl-pyridylidene amide (PYA) ligand (See Chapter 5).[15]

The solution containing the three metallacycles is then saturated with ethylene and the signals due to the growth of the E/MA copolymer are clearly observed in the NMR spectra. All ethylene is consumed in 1 h (the singlet at 5.40 ppm disappears) (Figure 2.16) and the singlet at 3.64 ppm is characteristic of the methoxy group of inserted MA in the copolymeric chain.

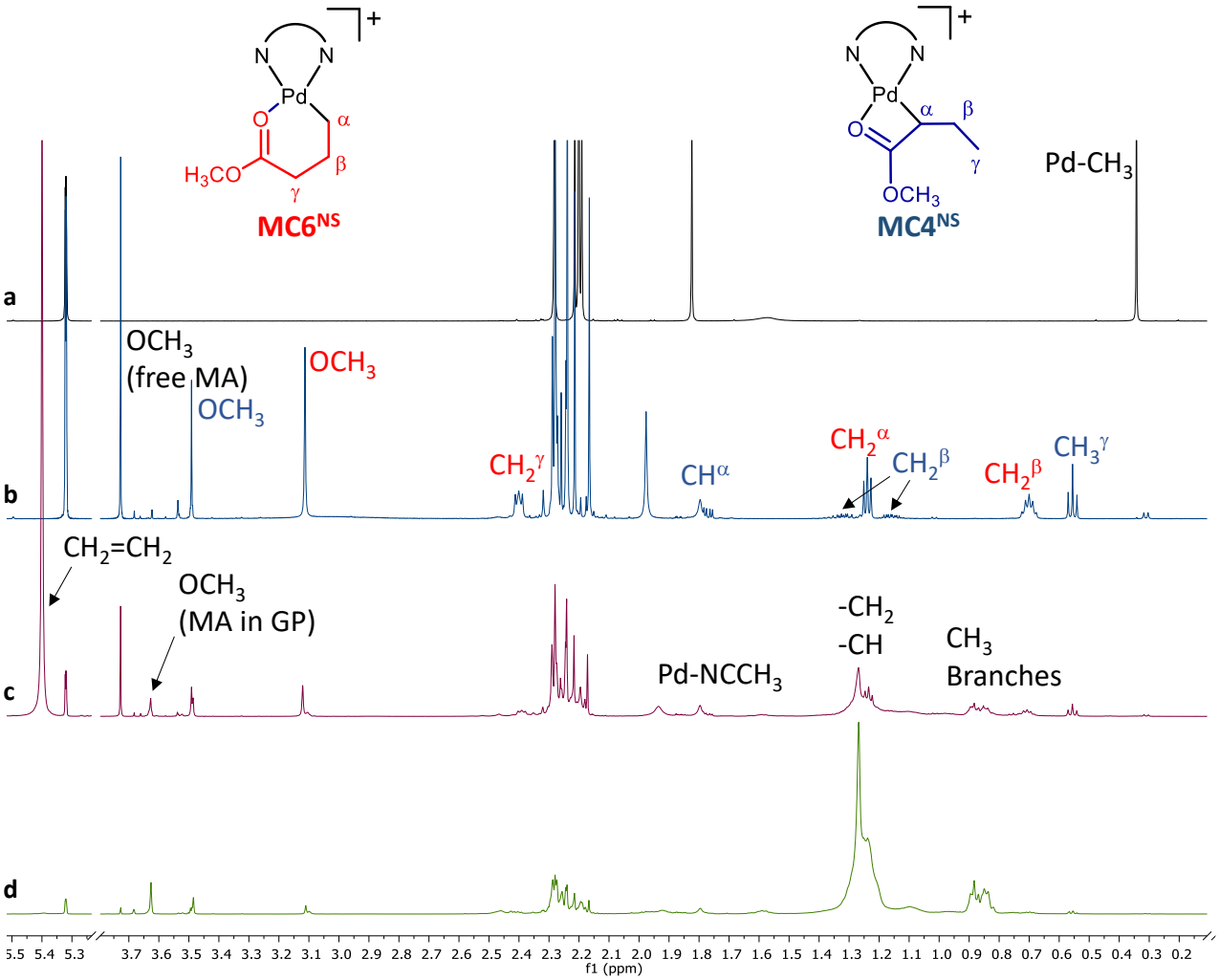

Figure 2.16. ^{1}H NMR spectra (CD_2Cl_2, 298 K) of: (a) **1b**; (b) **1b** + MA at t = 120 min; **1b** + MA + ethylene at (c) t = 5 min and (d) t = 60 min. GP = growing polymer.

The same NMR experiments are performed starting from a 10 mM solution of **1b** in TFE-d_3. Also in this case, the first reaction investigated is with the gaseous monomer and the results are analogous to those obtained in CD_2Cl_2. In the spectrum recorded after 5 min from the saturation with the gaseous monomer, resonances of branched PE are observed together with the singlet of Pd-$NCCH_3$, no signals of **1b** or free ethylene are present (Figure S2.12).

Moving to the reaction with MA, in the spectrum recorded immediately after the addition of the polar monomer, resonances assigned to **MC6^{NS}** and **1b** are present together with new signals. After 30 min all the precatalyst is converted and a bidimensional NMR analysis is carried out (Figure 2.17).

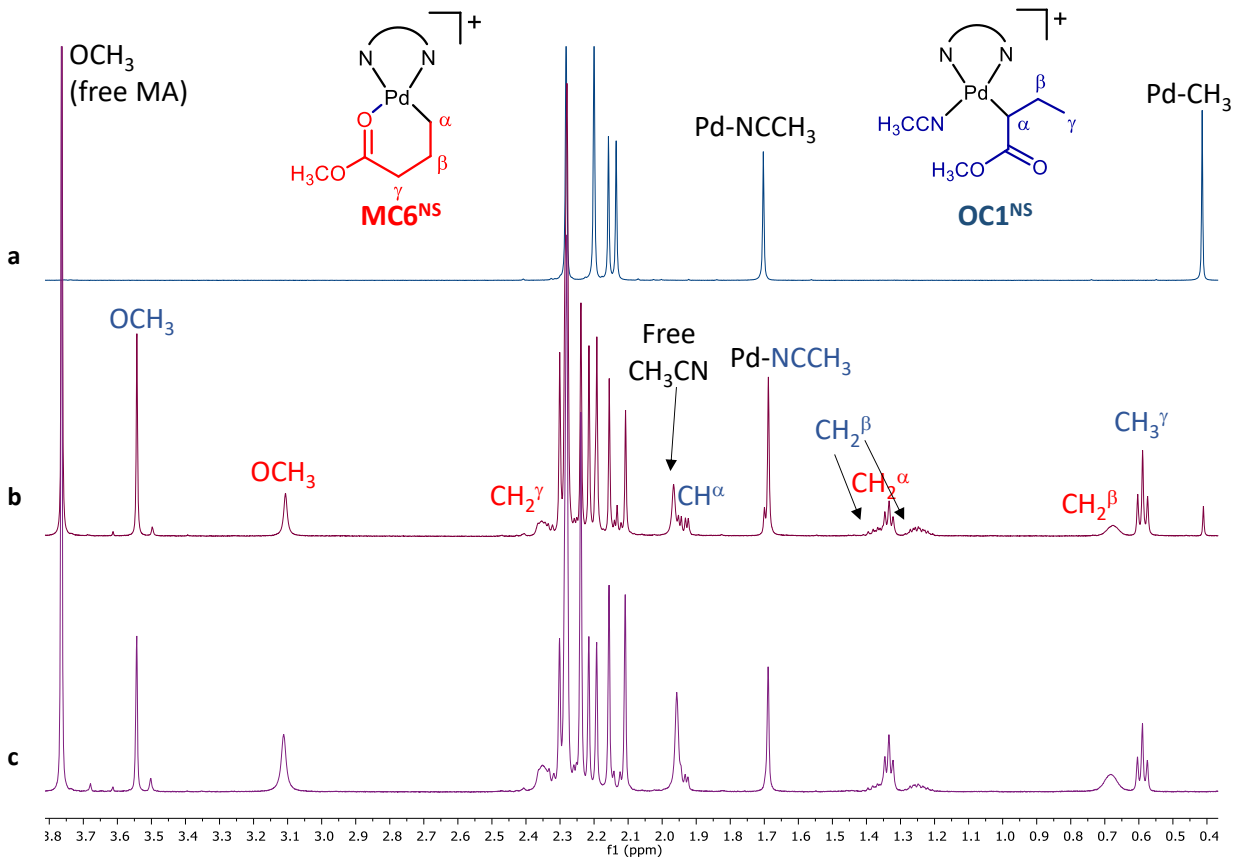

Figure 2.17. ^{1}H NMR spectra (TFE-d_3, 298 K) of: (a) **1b**; and **1b** + methyl acrylate at (b) t = 1 min and (c) t = 30 min.

In the ^{1}H,^{1}H COSY spectrum (Figure 2.18) correlation peaks between the triplet at 0.59 ppm (CH_3^{γ}) and the multiplets in the range 1.26 – 1.40 ppm (CH_2^{β}) are observed, together with a long range coupling cross peak with the signal at 1.93 ppm (CH^{α}). The new singlet at 1.68 ppm is assigned to a Pd-$NCCH_3$ fragment from ^{1}H,^{13}C HSQC spectrum on the basis of the chemical shift value of the carbon atom of the acetonitrile at -0.6 ppm (Figure S2.13). These data indicate the presence of an open-chain intermediate (**OC1^{NS}**) having coordinated to the metal center both the CH_3CN and the organic fragment, generated by the insertion of MA into the Pd-CH_3 bond with secondary regiochemistry. This work represents the first time that an open-chain intermediate is observed for this kind of reaction.

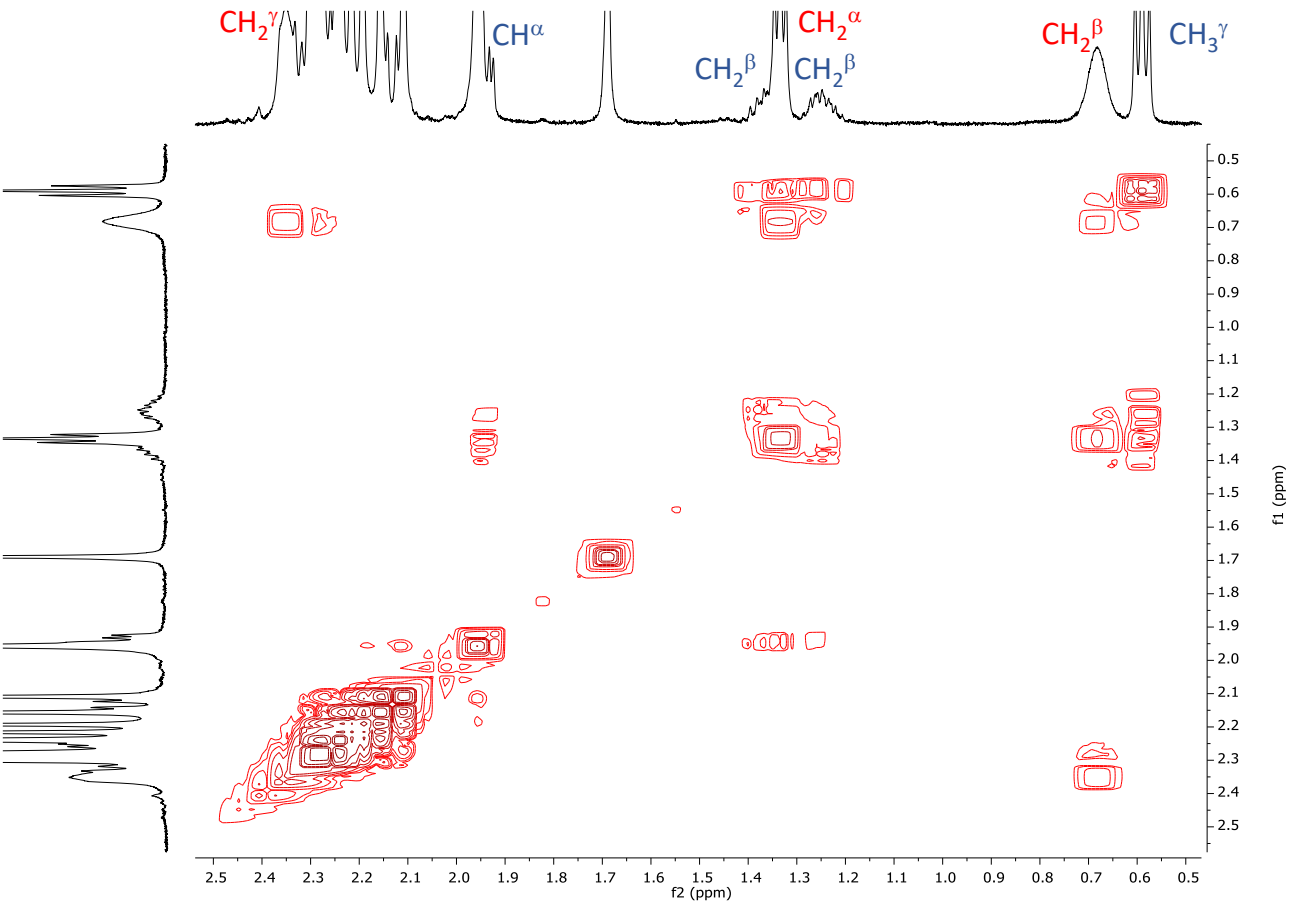

Figure 2.18. ^{1}H,^{1}H COSY spectrum (TFE-d_3, 298 K) of the reaction mixture of **1b** with methyl acrylate at t = 30 min.

The **MC6^{NS}**:**OC1^{NS}** is about 6:4 that recalls the ratio between T(MA) and M(MA) detected in the copolymer obtained with **1b** in TFE under set B of reaction conditions (Table S2.3, entry 1). The conversion of **1b** into the active species is faster than that performed in CD_2Cl_2 and no Pd(0) is observed in the NMR tube. The solution is monitored over time and in the ^{1}H NMR spectrum recorded after 19 h at room temperature a new open-chain intermediate (**OC2^{NS}**) is present. It is in equilibrium with its chelate form (**MC6^{NS}**) as indicated by the broadness of the signals of the latter species. When ethylene is bubbled in this solution, the resonances of E/MA copolymer are observed together with the singlet of free ethylene, that is completely consumed after 15 min (Figure 2.19).

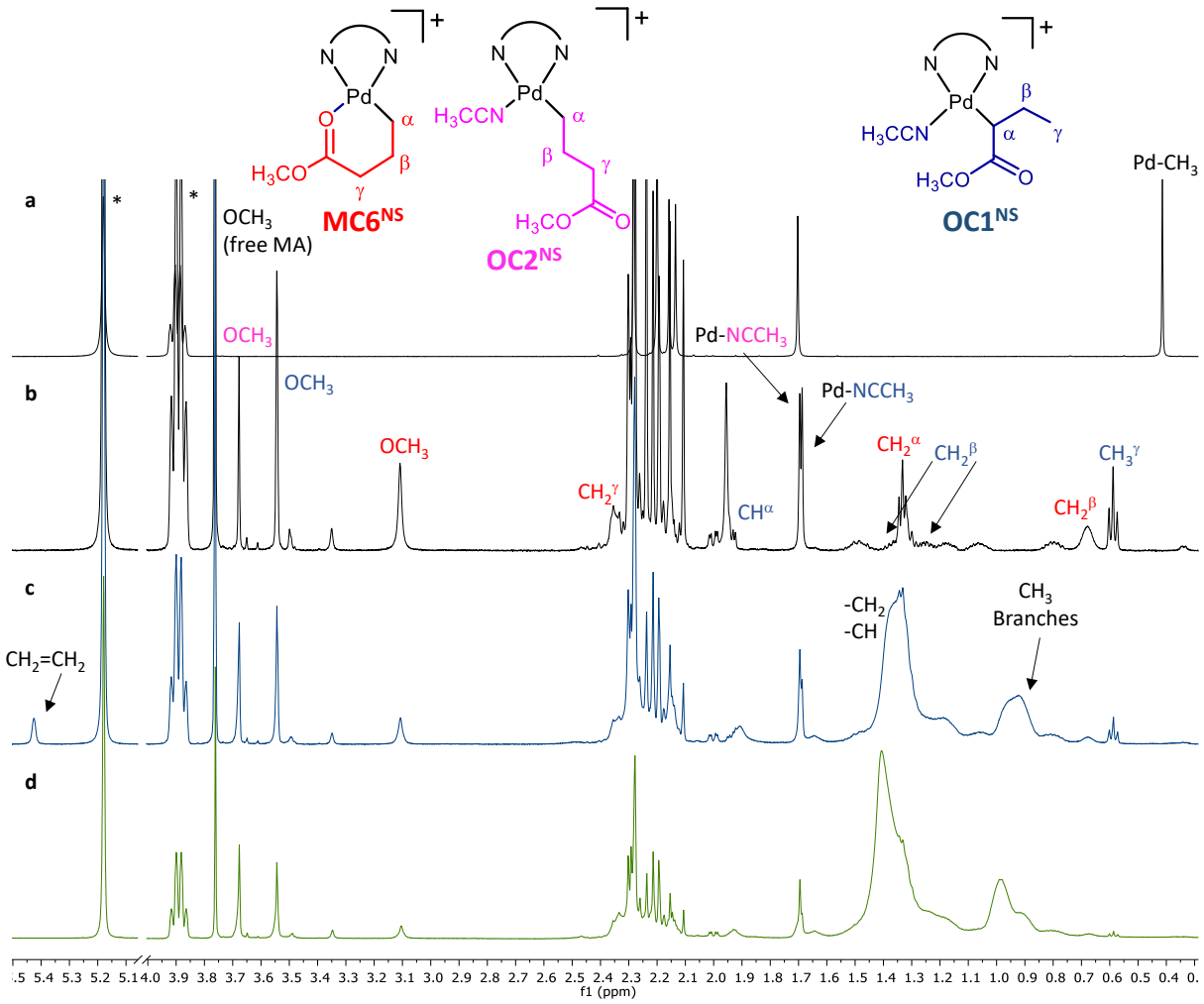

Figure 2.19. ^{1}H NMR spectra (TFE-d_3, 298 K) of: (a) **1b**; (b) **1b** + MA at t = 19 h; **1b** + MA + ethylene at (c) t = 5 min and (d) t = 15 min; *residual TFE.

In the ^{1}H NMR spectrum of the solution kept at room temperature for 3 days, the resonances assigned to **OC1^{NS}** are still present suggesting that, in the fluorinated solvent, the open-chain intermediate is the catalyst resting state (Figures S2.15 and S2.16). In this NMR tube after one week at room temperature the CP precipitates (Figures 2.20 and 2.21).

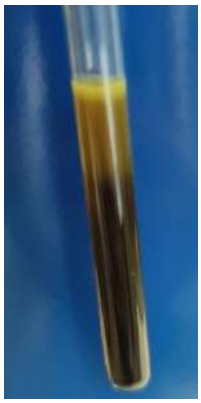

Figure 2.20. NMR tube of the mixture of **1b** + MA + E in TFE-d_3 after one week at room temperature: the precipitated copolymer is evident.

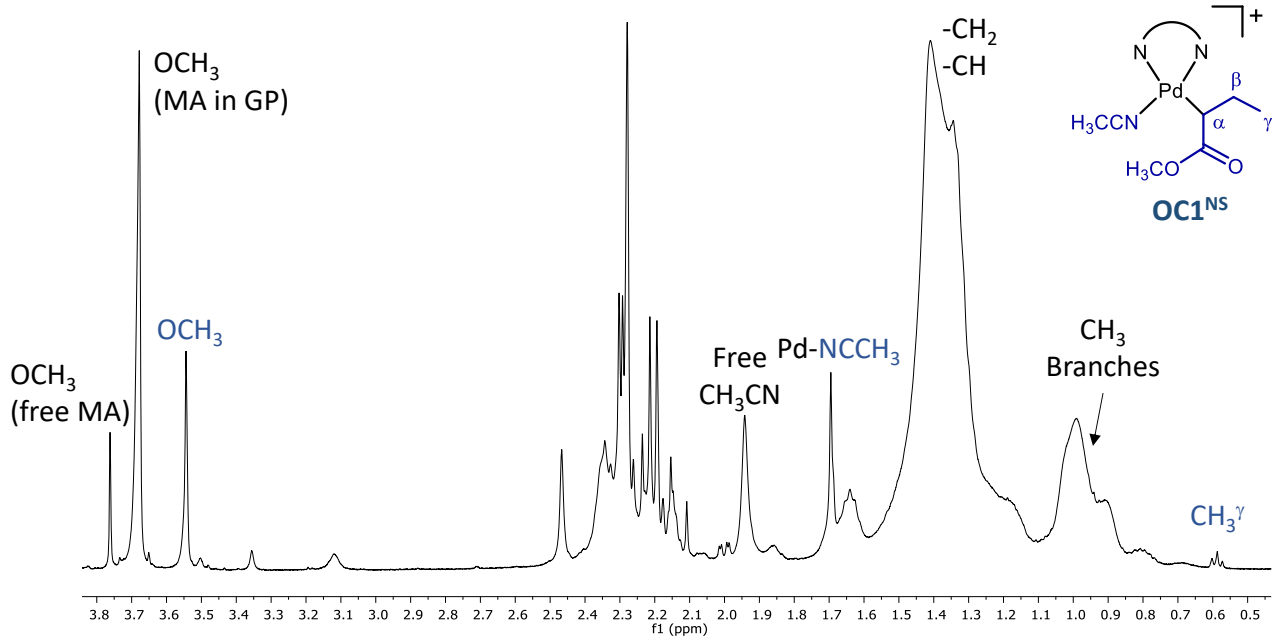

Figure 2.21. ^{1}H NMR spectrum (TFE-d_3, 298 K) of the reaction mixture of **1b** with methyl acrylate and ethylene at t = 3 days.

Analogous NMR investigations are performed using **1S^{Ph}** as precatalyst in both solvents. When a 10 mM CD_2Cl_2 solution of the complex is saturated with ethylene, the reaction is found to be slower than the same reaction observed for **1b** as the precursor. Resonances of branched PE are observed in the NMR spectrum recorded after 5 min from the addition of the gaseous monomer (Figure S2.17). In the spectrum recorded when ethylene is totally consumed (t = 45 min), together with resonances of PE and **1S^{Ph}**, signals of low intensity, as the broad peak at 8.37 ppm due to the iminic proton of **S^{Ph}** bonded to the metal center, are present. These indicate the presence of a new Pd species in solution that might have the growing polyethylene and **S^{Ph}** bonded to the palladium ion.

Both this new species and **1S^{Ph}** might represent the catalyst resting state of the reaction. This behaviour is completely different from that typical of other Pd-α-diimine complexes.[1,14,16] Moreover, no signals of free **S^{Ph}** are evident as well as no formation of Pd(0) is found in the NMR tube for the whole monitoring time.

Considering the reactivity of **1S^{Ph}** with the polar monomer in CD_2Cl_2, no reaction takes place within 2 h (Figure S2.18). So, this solution is saturated with ethylene. The peaks originated from its insertion into the Pd-CH_3 bond are observed after 5 min and, after 90 min from the addition of the gaseous monomer, the resonances of branched E/MA copolymer are present together with those of free E, free MA and **1S^{Ph}** (Figure 2.22 and Figures S2.19-S2.20). No resonances of free **S^{Ph}** and metallacycle intermediates are observed.

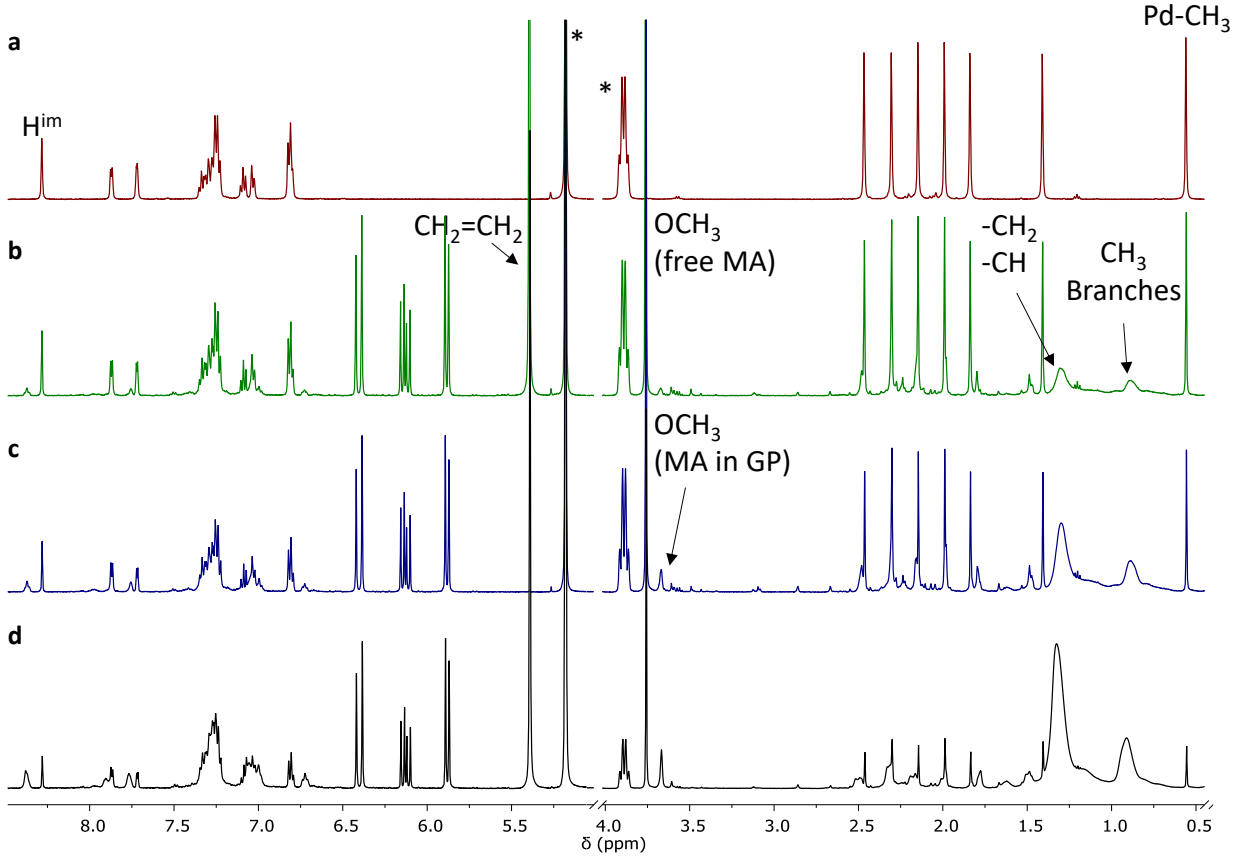

Figure 2.22. ^{1}H NMR spectra (CD_2Cl_2, 298 K) of: (a) **1S^{Ph}**; **1S^{Ph}** + MA + ethylene at (b) t = 5 min, (c) t = 45 min and (d) t = 90 min; aromatic and aliphatic region not on scale. GP = growing polymer.

When TFE-d_3 is the solvent, **1S^{Ph}** reacts immediately with ethylene producing a branched macromolecules. Also in the fluorinated solvent the new palladium species having the N-S ligand coordinated to the metal center is present with a set of broad signals and in this case its amount is higher than when CD_2Cl_2 is the reaction medium (**1S^{Ph}**:new species = 0.87:0.13 in CD_2Cl_2 at 45 min, **1S^{Ph}**:new species = 0.45:0.55 in TFE-d_3 at 55 min, as calculated from the integrals of the relevant iminic proton signal) (Figure 2.23).

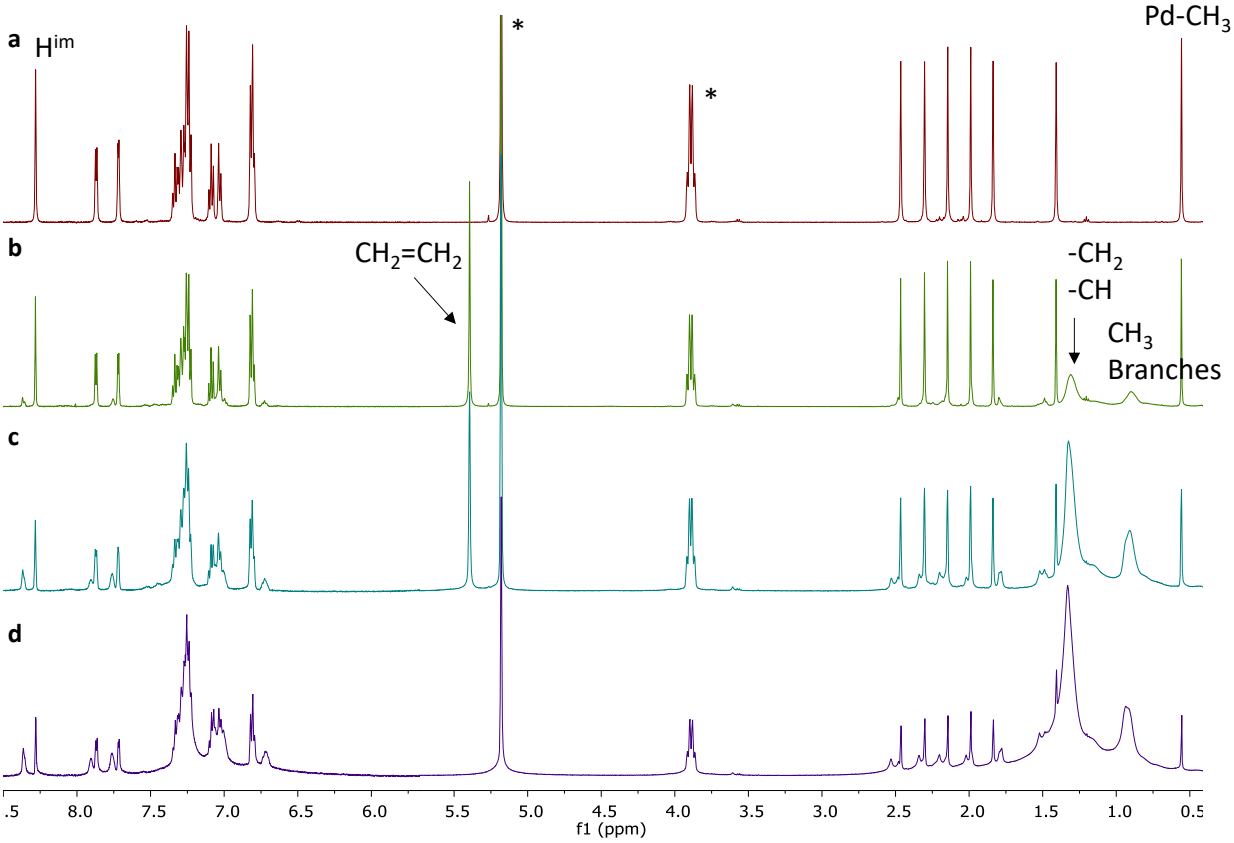

Figure 2.23. ^{1}H NMR spectra (TFE-d_3, 298 K) of: (a) **1S^{Ph}**; **1S^{Ph}** + ethylene at (b) t = 5 min, (c) t = 10 min and (d) t = 55 min; aromatic and aliphatic region not on scale; *residual TFE.

In analogy to the experiment in CD_2Cl_2, even in TFE-d_3, no reaction with MA takes place (Figure S2.21). While when both comonomers are added to the solution of the complex, the activation of **1S^{Ph}** is made by the reaction with ethylene, that is completely consumed after 45 min, followed by that of MA. The saturation with additional ethylene results in the proceeding of the copolymerization, as pointed out by the signals observed in the ^{1}H NMR spectrum recorded after 2 h, that are those of the growing copolymer chain, **1S^{Ph}** and a new palladium species. No signals of free **S^{Ph}** or metallacycles are observed (Figures S2.22 and S2.23).

In the $^{1}H,^{1}H$ NOESY spectrum (Figures 2.24 and S2.24) there are cross peaks among the resonances of $\mathbf{S^{Ph}}$ bonded to palladium (e.g. at 8.38 ppm (H^{im}), 7.91 ppm (H^{5}) and 7.78 ppm (H^{3})) and the peak of the growing copolymer chain at 1.32 ppm, thus demonstrating that the new species is a palladium intermediate with **1**, $\mathbf{S^{Ph}}$ and the growing chain bonded to the metal center. The signals are broad because of the presence of dynamic processes that might involve the exchange of the donor atoms of both bidentate ligands with the incoming polar monomer to allow the growth of the macromolecule together with the possible formation of pentacoordinated transient species[17] having the sulfur atom directly coordinated to palladium.

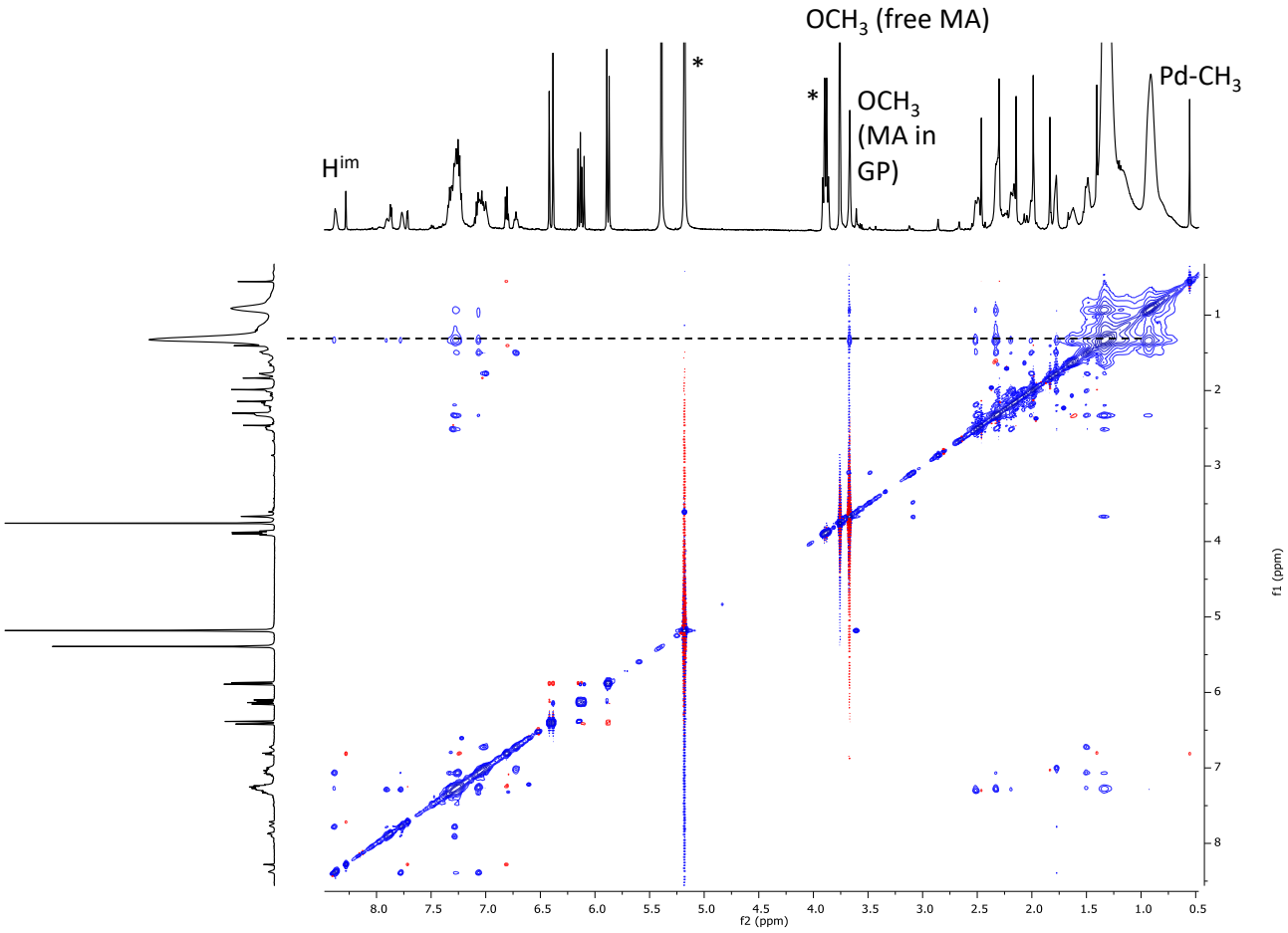

Figure 2.24. $^{1}H,^{1}H$ NOESY spectrum (TFE-d_3, 298 K) of reaction mixture of $\mathbf{1S^{Ph}}$ with methyl acrylate and ethylene at t = 2 h; *residual TFE. GP = growing polymer.

Moreover the cross peak between the singlet of the residual OH of TFE-d_3 and the peak of a methoxy group at 3.61 ppm assigned to MA inserted into the growing copolymer chain bonded to palladium indicates that they are in very close spatial proximity (Figure 2.25).

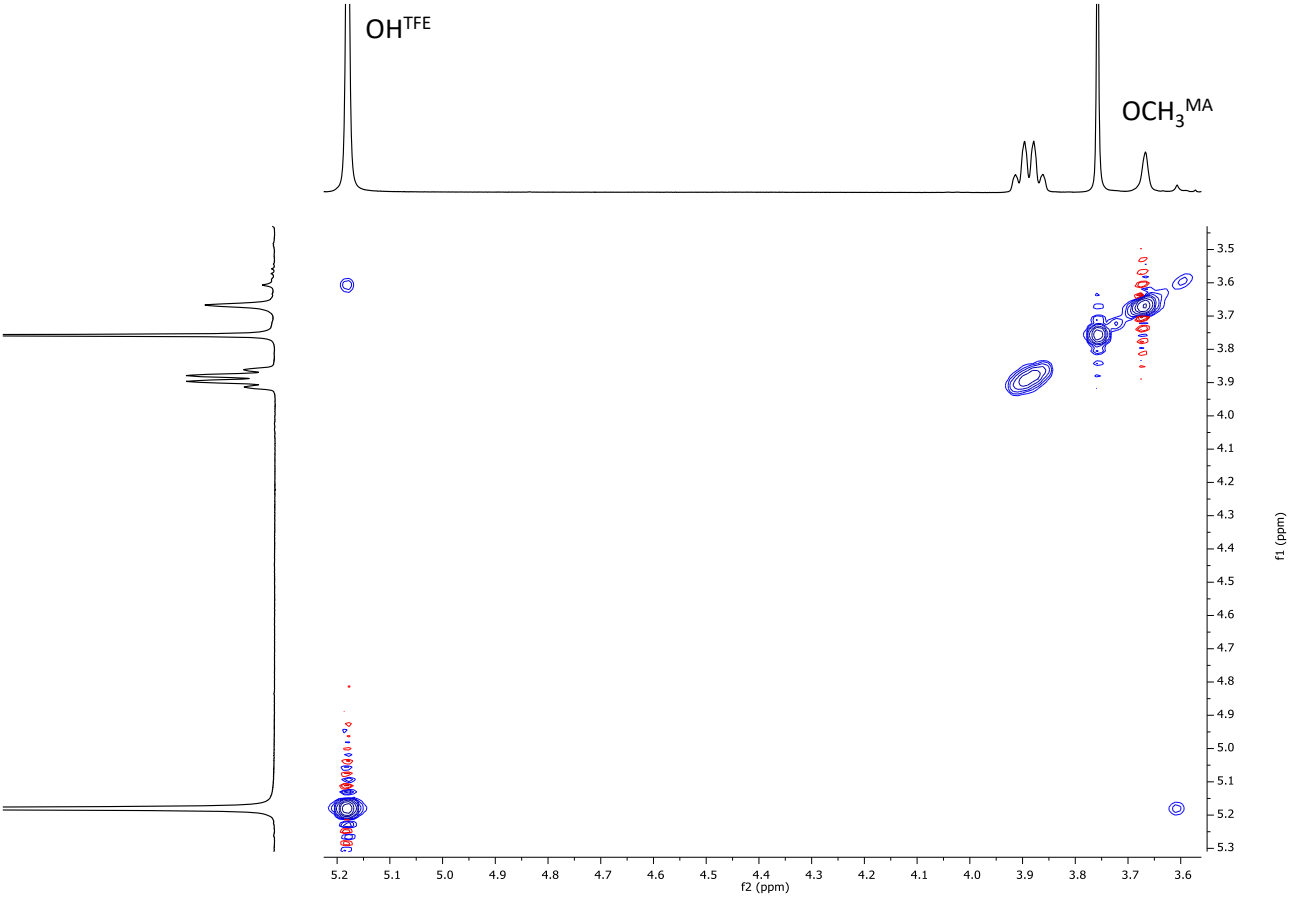

Figure 2.25. ^{1}H,^{1}H NOESY spectrum (TFE-d_3, 298 K) of reaction mixture of **1S^{Ph}** with MA and ethylene at t = 2 h: cross peak between the singlet of the residual OH of TFE-d_3 and the peak of a methoxy group of inserted MA.

For the two complexes (**1b** and **1S^{Ph}**) the main steps of the copolymerization are modelled by DFT calculations and the minimum energy paths (MEPs) are reported (Figure 2.26), assigning **1b** on the left side. The starting point for both calculations are the monocationic complexes (**1b** or **1S^{Ph}**) and the reactants at infinite distances. The reaction starts with a η^2-coordination of ethylene (**INT1**) followed by its insertion reaction (**TS1**). This is the rate-limiting step of both MEPs and for **1b** it is 4.2 kcal/mol lower than for **1S^{Ph}**, according to the lower productivity obtained by using **1S^{Ph}** and to the results of the *in situ* NMR experiments. From **TS1**, two intermediates are generated: **INT2′** (in red) leading to the β-H elimination on the propyl chain and/or **INT2** (in black) related to the copolymerization with the MA η^2-coordination to palladium. Focusing on the first pathway, β-H elimination of propene takes place through **TS2′** leading to the Pd−H species (**INT3′**) which is slightly more stable for **1S^{Ph}** than for **1b**, in agreement with the absence of palladium black during the catalysis carried out with complexes with the N–S ligand in both solvents.

Moving to the copolymerization mechanism (black path), starting from **INT2**, the insertion of MA into the Pd−C bond of the propyl chain with secondary regiochemistry takes place through **TS2**, and this step for **1b** is 4.5 kcal/mol lower than for **1S^{Ph}**, in agreement with the *in situ* NMR experiments where the conversion of **1S^{Ph}** into the active species is slower with respect to **1b**. Different intermediates are obtained depending on the considered complex. For **1b**, the 4-membered palladacycle **INT3-MC4** is the first product that evolves to the 6-membered palladacycle **INT-MC6**. In the case of **1S^{Ph}**, **INT3** with the open methyl-hexenoyl chain intermediate is formed. This is more stable than both the corresponding **INT3-MC4^{NS}** and all the other possible metallacycles (Chart S2.1), in agreement with the *in situ* NMR data about the reaction of **1S^{Ph}** with both comonomers, where no signals due to the metallacycles are detected. From **INT3**, β-H elimination takes place through **TS3** leading to the Pd−H species, **INT4**. This step costs 22.2 kcal/mol and it is higher with respect to the energy required for the β-H elimination of the propene taking place through **TS2′** (15.2 kcal/mol). By comparing the Pd···N distances in the relevant **TS2′** and **TS3**, we can see that the lower is the distance, the higher is the energetic barrier to overcome. In addition, the shorter Pd···N distance in **TS3** (3.07 Å) than in **TS2′** (3.43 Å) results in a stronger Pd···N interaction of the thiophenimine ligand and it allows to discriminate the rate of the chain walking process, if it takes place after the insertion of either the gaseous monomer or the polar monomer.

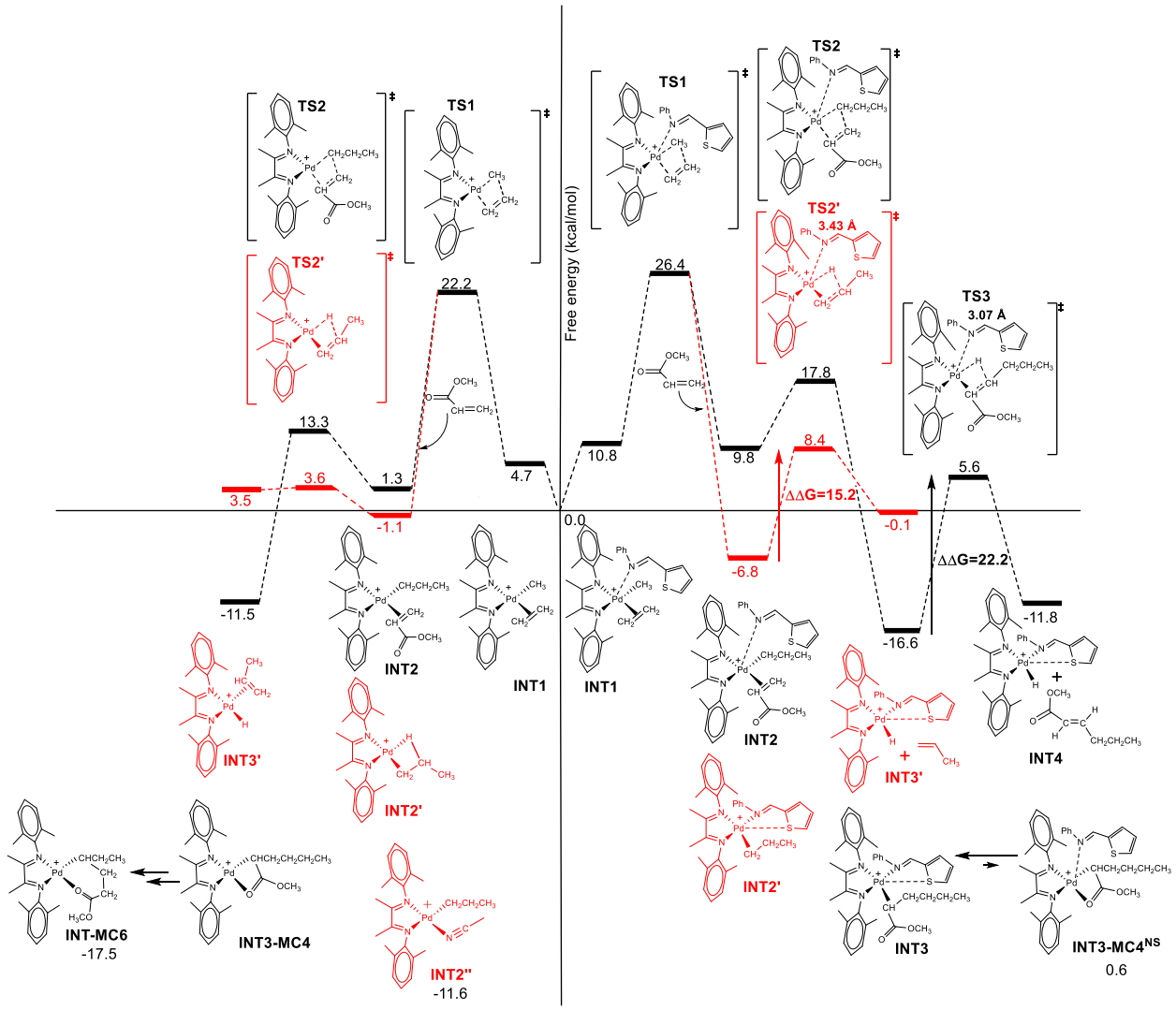

Figure 2.26. MEPs of the ethylene/MA copolymerization mechanism: MEP for **1S^{Ph}** (right) and MEP for **1b** (left).

On the basis of both the NMR experiments and DFT calculations, we propose different mechanism pathways for E/MA copolymerization carried out in either DCM or TFE. Considering complex **1b**, bearing acetonitrile in the fourth coordination site of Pd ion, the microstructure of obtained copolymer in DCM is in agreement with literature, indicating the it follows the growing mechanism investigated by Brookhart.[9] After the coordination and the migratory insertion of MA into the growing polymeric chain **a1**, the 4-membered metallacycle **b1** is formed that evolves in the 6-membered palladacycle **c1** through the chain walking process and, after some insertions of ethylene, the fragment of copolymer with MA at the end of the branches (T(MA)) **e1** is produced (Scheme 2.4).

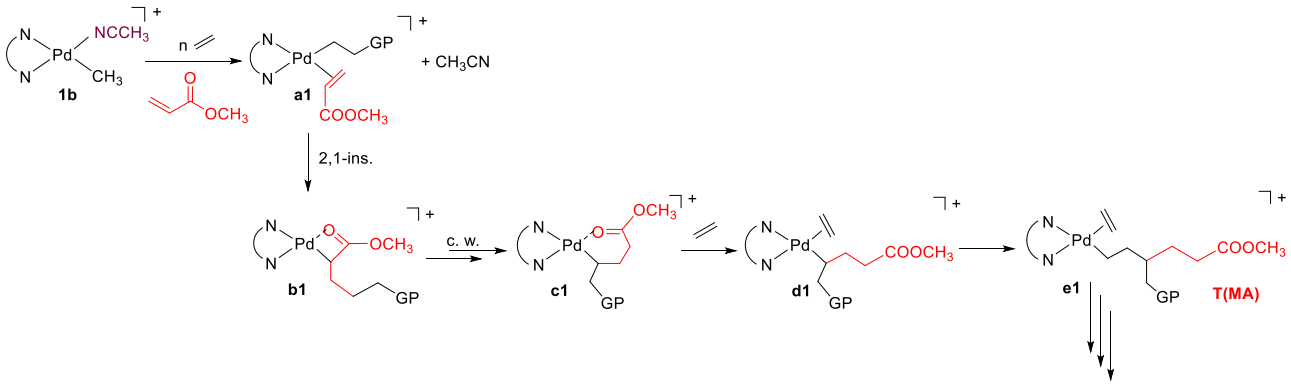

Scheme 2.4. Proposed mechanism for E/MA copolymerization with **1b** in DCM.

Moving to TFE, after the migratory insertion of MA, two intermediates are possible and they allow to explain because MA remains into the main chain or it is inserted as T(MA): the open-chain intermediate **f1** where the solvent is in close proximity to the methoxy group of inserted MA is responsible for the enchainment of MA as M(MA) (**i1**) because the H-bonds network traps the polar monomer into the main chain, while **c1**, that is in equilibrium with its open chain intermediate **g1**, follows the pathway described above leading to T(MA) (Scheme 2.5). The intermediate **f1** represents a novel catalyst resting state.

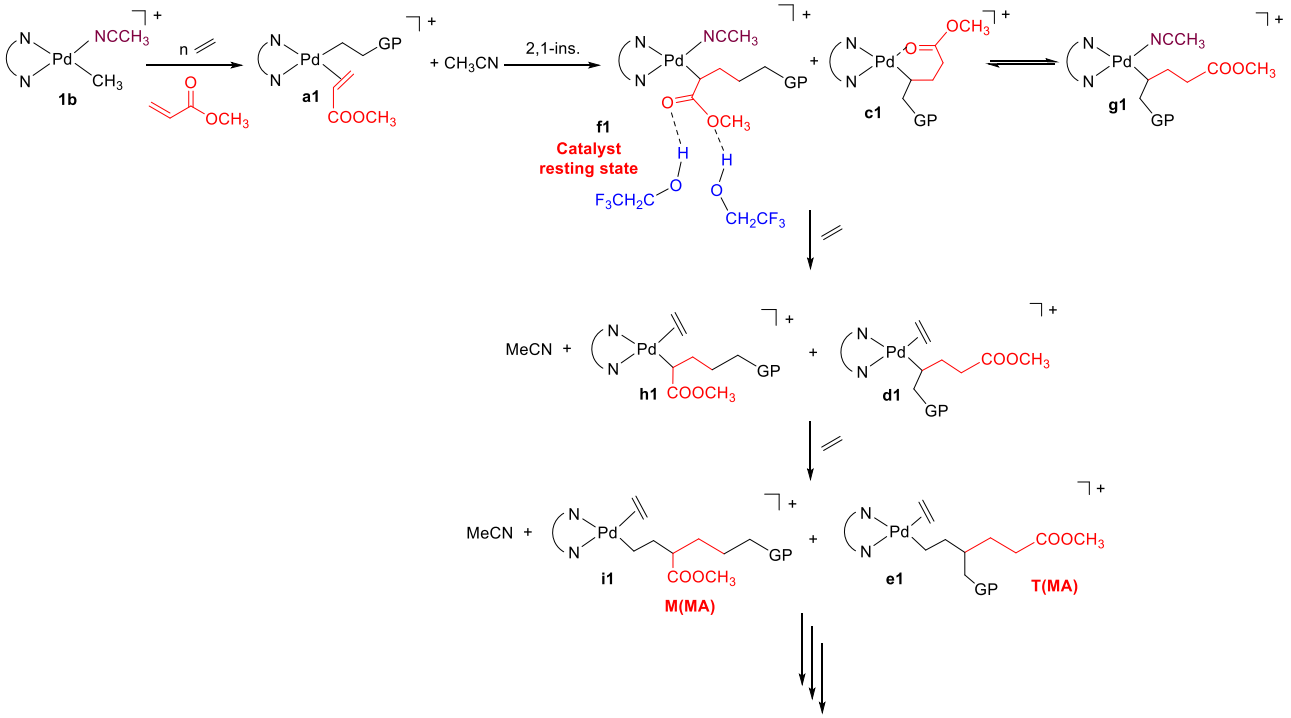

Scheme 2.5. Proposed mechanism for E/MA copolymerization with **1b** in TFE.

When the copolymerization is catalyzed by **1S^{Ph}** in DCM, MA is preferentially inserted as T(MA) and this indicates that the reaction follows the typical pathway of the Pd-α-diimiine complexes, but in this case the N–S ligand remains in close proximity to the metal centre (Scheme 2.6 – left). In TFE we observed intermediates analogous to those proposed for **1b**, but with the N–S ligand always bonded to palladium. In addition, in this case the catalyst resting state is the intermediate **f^{NS}** having both the thiophenimine and the growing copolymeric chain coordinated to the Pd ion (Scheme 2.6 – right).

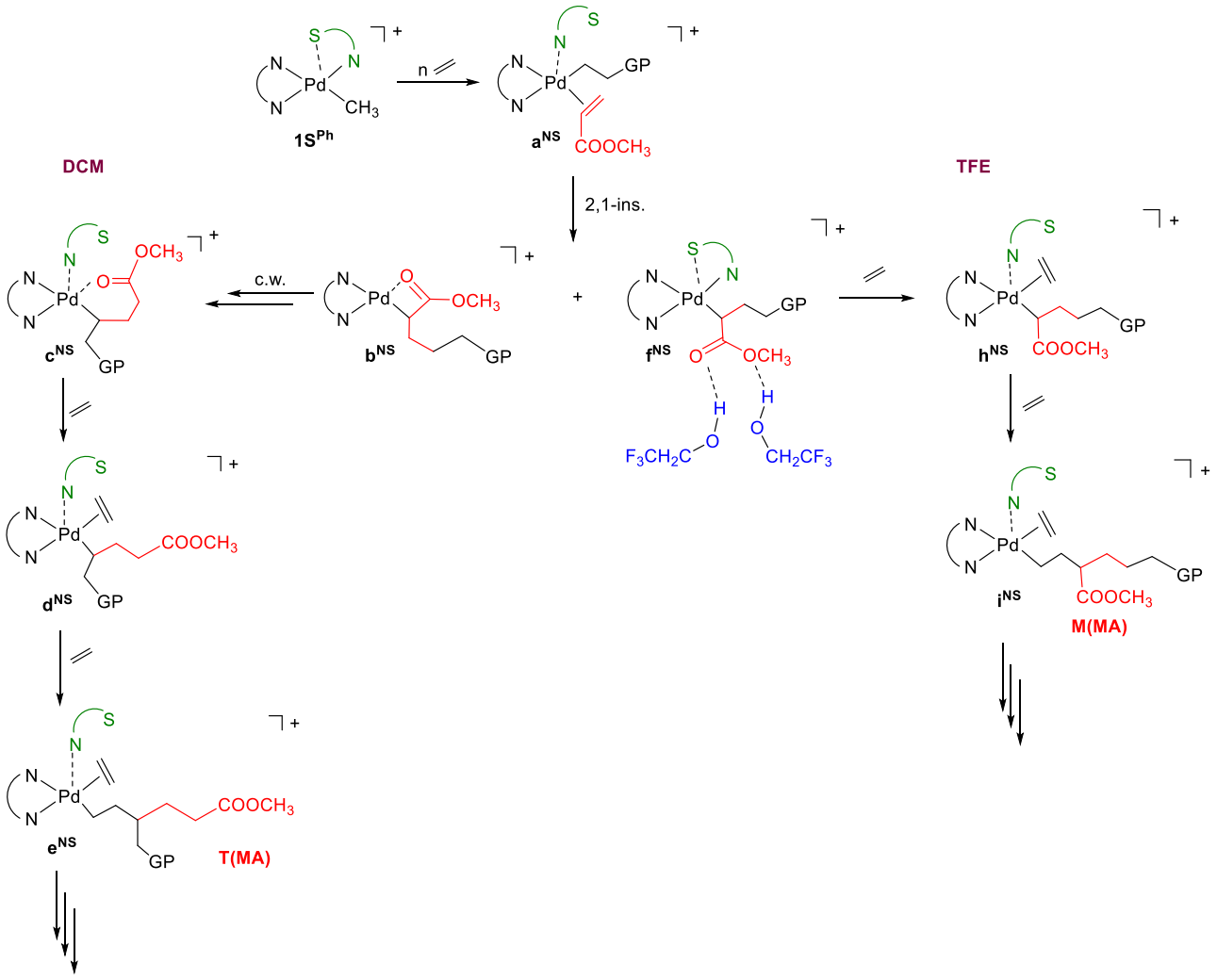

Scheme 2.6. Proposed mechanism for E/MA copolymerization with **1S^{Ph}**.

The presence of the N–S ligand and the H-bonds network produced by TFE around the polar monomer are responsible for the higher amount of M(MA) in these copolymers rather than in those obtained in DCM.

2.3. Conclusions.

Pd(II) complexes **1S^{Ph}**, **1S^{Me}** and **1S^{CF3}** of general formula [Pd(CH_3)(N-S)(**1**)][PF_6], where N-S is a hemilabile potentially bidentate ligand belonging to the family of the thiophenimines, are synthesized starting from the precursor [Pd(CH_3)($NCCH_3$)(**1**)][PF_6], **1b**. They are characterized in solution by NMR spectroscopy confirming the coordination of the N-S ligand to the metal centre and the presence of only single species in solution. Some suitable single crystals allowed us to characterize them also in the solid state with X-ray diffraction. This analysis evidences that the N–S is coordinated to the Pd ion through the nitrogen atom, while the sulfur atom occupies an apical position with respect to the metal center. Their distance indicates a weak interaction Pd···S between them, confirmed by theoretical calculation.

This new series of monocationic complexes is tested in the copolymerization of ethylene with methyl acrylate under mild reaction conditions of temperature and ethylene pressure by carrying out the catalysis in two different solvents, dichloromethane or trifluoroethanol. These compounds generate active species for the target reaction producing branched macromolecules. The highest productivity achieved is about 60 kg CP/mol Pd and the produced copolymers have M_n values in the range 5 − 30 kDa. The products, characterized by the ^1H and ^{13}C NMR spectroscopy, have the polar monomer inserted both in the main chain and at the end of the branches in a ratio that ranges from 9:91 to 45:55 depending on the solvent used for the catalysis and on the N-S ligand.

The *in situ* NMR studies about the reaction of both comonomers with **1b** at room temperature, in either CD_2Cl_2 or TFE-d_3, confirm the effect of the solvent. The reaction with the polar monomer in CD_2Cl_2 leads to the formation for the first time of the 4-membered metallacycle together with the expected 5- and 6-membered metallacycles. When the same reaction is performed in TFE-d_3, in addition to the expected 6-membered palladacycle, the formation of an open-chain intermediate, having both the organic fragment, generated from the migratory insertion of MA into the Pd-CH_3 bond, and the acetonitrile coordinated to palladium is detected for the first time. This intermediate represents a novel catalyst resting state. A detailed NMR investigation is performed with **1S^{Ph}**, too. It highlights that the N-S ligand remains in close proximity of the metal center and this favours the open-chain intermediate formation, that is responsible for trapping MA into the main chain together with H-bonds network generated by the neighbour of TFE molecules with the methoxy group of the polar monomer.

These results might open the way to the discovery of new, efficient catalytic systems for the synthesis of functionalized polyolefins based on secondary interactions and on the nature of the ligand in the fourth coordination site of palladium.

2.4. Experimental.

All complex manipulations were performed using standard Schlenk techniques under argon. Anhydrous dichloromethane was freshly obtained by distillation over CaH_2 under argon atmosphere. Deuterated solvents (Cambridge Isotope Laboratories, Inc. (CIL) and Sigma Aldrich) were stored as recommended by sellers. Ethylene (purity ≥ 99.9 %) supplied by SIAD and methyl acrylate (99.9%, with 0.02% of hydroquinone monomethyl ether) supplied by Aldrich were used as received. TFE and all the other reagents and solvents were purchased from Sigma-Aldrich/Merck and used without further purification for synthetic, spectroscopic and catalytic purposes. [$Pd(OCOCH_3)_2$] (BASF Italia) was used as source of the metal to obtain the corresponding Pd(II) complexes. Mono- and bidimensional NMR spectra of ligands and complexes were recorded on a Varian 500 spectrometer (500 MHz for ^1H, 125.68 MHz for ^{13}C), and of copolymers on a Varian 400 (400 MHz for ^1H, 100.55 MHz for ^{13}C). The resonances are reported in ppm (δ) and referenced to the residual solvent peak versus $Si(CH_3)_4$: CD_2Cl_2: at δ 5.32 (^1H) and δ 54.00 (^{13}C); $CDCl_3$: at δ 7.26 (^1H) and δ 77.16 (^{13}C); TFE-d_3: at δ 5.18 (^1H). ^{19}F–NMR spectra were recorded on a Varian 400 spectrometer at 376.3 MHz and referenced with respect to CCl_3F. NMR experiments were performed employing the automatic software parameters. In the case of NOESY experiments a mixing time of 500 ms was used. Mass spectra (ESI-MS) were recorded on a Massa Esquire 4000 – Bruker in positive ion polarity (HV capillary of 4000 V and dry gas of 5.00 L/min). Samples were dissolved in methanol and the analysis was carried out immediately. A CEM Discover microwave reactor was used for the microwave-assisted reactions preformed in 10 mL vessels. The average molecular weights (M_n and M_w) and polydispersity (M_w/M_n) values of copolymer samples were measured through gel permeation chromatography. Samples were dissolved in Romil chloroform stabilized with ethanol and analyzed using a GPC Max Viscotek system equipped with a TDA 305 detectors (Refractive Index, Low Angle Light Scattering, Right Angle Light Scattering and Viscometer) and UV detector. Columns set was composed by a pre-column Phenogel Phenomenex and two columns 10^6 and 10^3 $g \cdot mol^{-1}$, respectively. Polymers were eluted at a concentration of about 3-5 mg/mL at 308 K. The injection volume was 100 μL, the flow rate 0.8 ml/min. The chosen method of analysis was universal calibration with PS standard ranging from 1,280 kDa to 1060 Da. The measurements, performed at 308 K according to the temperatures of columns and detectors, were ran for 50 min in duplicate.

2.4.1 Synthesis and characterization of thiophenimine ligands ***S^{Ph}*** *and* ***S^{Me}***.

To a CH_2Cl_2 solution of tiophene-2-carboxaldehyde (8.9 mmol in 10 mL) 1.1 equiv. of the proper aniline (aniline for **S^{Ph}**; 3,5-dimethyl-aniline for **S^{Me}**) were added, together with molecular sieves (3 Å). The solution was stirred at room temperature for 16 h and filtered over Celite©. The solvent was removed leading to a red oil for **S^{Ph}** and an orange solid for **S^{Me}**.

S^{Ph}. (red oil, yield = 93 %); ^{1}H NMR (500 MHz, CD_2Cl_2, 298 K) δ = 8.60 (s, 1H, H^{im}), 7.56-7.51 (m, 2H, H^3, H^5), 7.43-7.41 (m, 1H, H^m), 7.27-7.21 (m, 3H, H^p, H^o), 7.17-7.15 (dd, 1H, H^4). ^{13}C NMR (125.68 MHz, CD_2Cl_2, 298 K, from the HSQC spectrum) δ = 153.22 (C^{im}), 130.53 (C^3), 132.63 (C^5), 129.15 (C^m), 126.27-121.19 (C^p, C^o), 128.12 (C^4).

S^{Me}. (orange solid, yield = 90 %); ^{1}H NMR (500 MHz, CD_2Cl_2, 298 K) δ = 8.57 (s, 1H, H^{im}), 7.52 (dt, 1H, H^3), 7.49 (dd, 1H, H^5), 7.15 (dd, 1H, H^4), 6.89 (b, 1H, H^p), 6.83 (b, 1H, H^o), 2.34 (s, 6H, CH_3^{NS}). ^{13}C NMR (125.68 MHz, CD_2Cl_2, 298 K, from the HSQC spectrum) δ = 152.76 (C^{im}), 130.34 (C^3), 130.68 (C^5), 128.10 (C^4), 128.01 (C^p), 118.94 (C^o), 21.29 (CH_3^{NS}).

2.4.2 Synthesis and characterization of thiophenimine ligand ***S^{CF3}***.

Tiophene-2-carboxaldehyde (4.45 mmol) was dissolved in 3 mL of CH_2Cl_2 in a microway vessel. After adding 3,5-bisfluoromethyl-aniline (1 equiv.) and molecular sieves (3 Å), the solution was heated in the MW reactor for 1 h at 373 K, leading to 315 K. Afterward it was filtered over Celite©, the solvent was removed leading to a yellow oil, that was purified by column flash chromatography (hexane: ethyl acetate = 100 : 1) under argon atmosphere, The desired product is a light yellow oil.

S^{CF3}. (yellow oil, yield = 91%); ^{1}H NMR (500 MHz, CD_2Cl_2, 298 K) δ = 8.63 (s, 1H, H^{im}), 7.75 (s, 1H, H^p), 7.65 (s, 2H, H^o), 7.63 (dt, 1H, H^3), 7.61 (dd, 1H, H^5), 7.20 (dd, 1H, H^4). ^{13}C NMR (125.68 MHz, CD_2Cl_2, 298 K, from the HSQC spectrum) δ = 156.14 (C^{im}), 119.50 (C^p), 134.52-121.73 (C^o, C^3, C^5), 128.53 (C^4). ^{19}F NMR (376.3 MHz, CD_2Cl_2, 298 K) δ = -63.28 (s). ESI-MS: m/z = 324.0 (S^{CF3}).

2.4.3 Synthesis and characterization of cationic complexes ***1S^{Ph}***, ***1S^{Me}***, ***1S^{CF3}***.

The cationic complexes were synthesized starting from [Pd(CH_3)(**1**)($NCCH_3$)][PF_6], **1b**, that, on turn, was prepared from [Pd($OCOCH_3$)$_2$] following the literature procedure.[18,19,20]

To a stirred solution of **1b** in CH_2Cl_2 (0.1 mmol in 5 mL), at 313 K, a dichloromethane solution of N-S (1.1 equiv. in 2 mL) was added. The reaction mixture was left under stirring, in the dark, for the proper reaction time (3 h for **S^{Ph}**, 4 h for **S^{Me}**, 7 h for **S^{CF3}**). Afterward it was concentrated to a few milliliters of volume and upon addition of cold diethyl ether the product was precipitated. It was filtered under vacuum after a night at 277 K and washed with Et_2O.

1S^{Ph}. (yellow solid, yield = 94 %); ^{1}H NMR (500 MHz, CD_2Cl_2, 298 K) δ = 8.28 (s, 1H, H^{im}), 7.95 (dd, 1H, H^5), 7.76 (dt, 1H, H^3), 7.35 (t, 1H, H^p), 7.32 – 7.19 (m, 6H, H^4, H^{m2}, H^{p2}, H^o), 7.07 (t, 1H, H^{p1}), 7.02 (dd, 1H, H^{m1}), 6.79 – 6.75 (m, 3H, H^{m1}, H^m), 2.46 (s, 3H, CH_3^{Ar2}), 2.29 (s, 3H, CH_3^{Ar2}), 2.21 (s, 3H, CH_3^{DAB2}), 2.05 (s, 3H, CH_3^{DAB1}), 1.84 (s, 3H, CH_3^{Ar1}), 1.39 (s, 3H, CH_3^{Ar1}), 0.47 (s, 3H, Pd-CH_3). ^{13}C NMR (125.68 MHz, CD_2Cl_2, 298 K, from the HSQC spectrum) δ = 161.55 (C^{im}), 136.30 (C^5), 141.15 (C^3), 129.35 (C^p), 129.01 (C^4), 128.91 (C^p), c.a. 129.75- 128.78 (C^{m1}, C^{p2}, C^{m2}), 127.08 (C^{p1}), 129.41 (C^m), 123.01 (C^{m1}), 18.16 (CH_3^{Ar2}), 18.26 (CH_3^{Ar2}), 20.46 (CH_3^{DAB2}), 19.25 (CH_3^{DAB1}), 17.30 (CH_3^{Ar1}), 16.81 (CH_3^{Ar1}), 5.55 (Pd-CH_3). MS-ESI: m/z = 397.1 [Pd(CH_3)(**1**)(**S^{Ph}**)]$^+$, m/z = 291.2 (**1**), m/z = 188.0 (**S^{Ph}**), m/z = 146.0 [Pd(CH_3)(**1**)(**S^{Ph}**)]$^+$ - {**S^{Ph}**, **1**} + {Na^+}.

1S^{Me}. (yellow solid, yield = 82 %); ^{1}H NMR (500 MHz, CD_2Cl_2, 298 K) δ = 8.29 (s, 1H, H^{im}), 7.93-7.92 (dd, 1H, H^5), 7.75-7.74 (dt, 1H, H^3), 7.31-7.23 (m, 4H, H^4, H^{m2}, H^{p2}), 7.08-6.98 (m, 3H, H^{m1}, H^p), 6.78-6.76 (d, 1H, H^{p1}), 6.41 (s, 2H, H^o), 2.45 (s, 3H, CH_3^{Ar2}), 2.30 (s, 3H, CH_3^{Ar2}), 2.26 (s, 6H, CH_3^{NS}), 2.20 (s, 3H, CH_3^{DAB2}), 2.04 (s, 3H, CH_3^{DAB1}), 1.85 (s, 3H, CH_3^{Ar1}), 1.44 (s, 3H, CH_3^{Ar1}), 0.45 (s, 3H, Pd-CH_3). ^{13}C NMR (125.68 MHz, CD_2Cl_2, 298 K, from the HSQC spectrum) δ = 160.74 (C^{im}), 135.96 (C^5), 140.86 (C^3), 128.97 (C^4, C^{m2}, C^{p2}), 126.89-130.36 (C^{m1}, C^p), 128.73 (C^{p1}), 120.73 (C^o), 18.05 (CH_3^{Ar2}), 17.98 (CH_3^{Ar2}), 21.18 (CH_3^{NS}), 20.32 (CH_3^{DAB2}), 19.12 (CH_3^{DAB1}), 17.24 (CH_3^{Ar1}), 16.65 (CH_3^{Ar1}), 5.53 (Pd-CH_3). MS-ESI: m/z = 628.3 [Pd(CH_3)(**1**)(**S^{Me}**)]$^+$, m/z = 612.2 [Pd(CH_3)(**1**)(**S^{Me}**)]$^+$ - {CH_3}, m/z = 291.2 (**1**).

1S^{CF3}. (yellow solid, yield = 66%); ^{1}H NMR (500 MHz, CD_2Cl_2, 298 K) δ = 8.39 (s, 1H, H^{im}), 8.12 (dd, 1H, H^5), 7.92 (dt, 1H, H^3), 7.88 (s, 1H, H^p), 7.38 (s, 1H, H^o), 7.37 (m, 2H, H^4), 7.30-7.25 (m, 3H, H^{p2}, H^{m2}), 7.06 (m, 2H, H^{p1}, H^{m1}), 6.72 (t, 1H, H^{m1}), 2.48 (s, 3H, CH_3^{Ar2}), 2.29 (s, 3H, CH_3^{Ar2}), 2.25 (s, 3H, CH_3^{DAB2}), 2.08 (s, 3H, CH_3^{DAB1}), 1.86 (s, 3H, CH_3^{Ar1}), 1.47 (s, 3H, CH_3^{Ar1}), 0.47 (s, 3H, Pd-CH_3). ^{13}C NMR (125.68 MHz, CD_2Cl_2, 298 K, from the HSQC spectrum) δ = 163.63 (C^{im}), 138.86 (C^5), 143.44 (C^3), 122.38 (C^{p1}), 129.48 (C^4), 129.22-128.13 (C^{m2}, C^{p2}), 129.18-127.63 (C^{p1}, C^{m1}), 128.83 (C^{m1}), 18.12 (CH_3^{Ar2}), 17.89 (CH_3^{Ar2}), 20.46 (CH_3^{DAB2}), 19.29 (CH_3^{DAB1}), 17.23 (CH_3^{Ar1}), 16.94 (CH_3^{Ar1}), 6.03 (Pd-CH_3). ^{19}F NMR (376.3 MHz, CD_2Cl_2, 298 K) δ = -63.20 (s), -72.92 (d).

2.4.4 Ethylene/methyl acrylate copolymerization reaction.

All catalytic experiments are carried out in a Büchi "tinyclave" reactor equipped with an interchangeable 50 mL glass vessel. The vessel is loaded with the desired complex (21 μmol), TFE (21 mL) or distilled CH_2Cl_2 (21 mL) and methyl acrylate. The reactor is placed in a preheated oil bath and connected to the ethylene tank. The ethylene is bubbled for 10 min, then the reactor is pressurized. The reaction mixture is stirred at constant temperature (308 K). After the proper time (6 h), the reactor is cooled to room temperature and vented.

The reaction mixture is poured in a 50 mL round flask, together with dichloromethane (3 x 2 mL) used to wash the glass vessel. Volatiles were removed under reduced pressure and the residual gum or oil is dried at constant weight and analyzed by NMR spectroscopy. The ethylene uptake was measured by performing the catalysis in the same Büchi "tinyclave" reactor connected to a thermal mass flow meter (Bronkhorst EL-FLOW Select model F-111B) and forward pressure controller device (Bronkhorst EL-PRESS model P-602). Gas flow needed to feed the reactor at a constant pressure was computer-recorded using the FlowPlot interface. At the end E/MA obtained copolymers are dissolving in $CHCl_3$ solution and the inactive palladium metal is filtered off over Celite® and the filtrate solution is dried at reduced pressure.

2.4.5 General procedures for in situ NMR reactivities.

*General procedure for the in situ NMR reactivity of **1b** and **1S^{Ph}** with ethylene.*

A 10 mM solution of the desired cationic complex in CD_2Cl_2 is prepared, and a first ^{1}H NMR spectrum is recorded. Ethylene is bubbled into the NMR tube for 5 min. The reaction is followed over time, at T = 298 K.

*General procedure for the in situ ^{1}H NMR reactivity of **1b** and **1S^{Ph}** with methyl acrylate.*

A 10 mM solution of the desired cationic complex in CD_2Cl_2 is prepared, and a first ^{1}H NMR spectrum is recorded. Methyl acrylate (2 equiv.) is then added to the solution. The reaction is followed over time, at T = 298 K.

*General procedure for the in situ ^{1}H NMR reactivity of **1b** and **1S^{Ph}** with both comonomers.*

A 10 mM solution of the desired cationic complex in CD_2Cl_2 is prepared, and a first ^{1}H NMR spectrum is recorded. Methyl acrylate (2 equiv.) is added to the solution, immediately followed by bubbling of ethylene into the NMR tube for 5 min. The reaction is followed over time, at T = 298 K.

The in situ NMR studies in TFE-d_3 were performed following the same three procedures reported above, just in the different solvent.

2.5. References.

(1) Mecking, S. Mechanistic Studies of the Palladium-Catalyzed Copolymerization of Ethylene and α-Olefins with Methyl Acrylate. *J. Am. Chem. Soc.* **1998**, *120* (5), 888–899.

(2) Tan, C.; Chen, C. Emerging Palladium and Nickel Catalysts for Copolymerization of Olefins with Polar Monomers. *Angew. Chemie - Int. Ed.* **2019**, *58* (22), 7192–7200.

(3) Dai, S.; Sui, X.; Chen, C. Highly Robust Palladium(II) α-Diimine Catalysts for Slow-Chain-Walking Polymerization of Ethylene and Copolymerization with Methyl Acrylate. *Angew. Chemie - Int. Ed.* **2015**, *54* (34), 9948–9953.

(4) Dai, S.; Chen, C. Direct Synthesis of Functionalized High-Molecular-Weight Polyethylene by Copolymerization of Ethylene with Polar Monomers. *Angew. Chemie - Int. Ed.* **2016**, *55* (42), 13281–13285.

(5) Wang, H.; Duan, G.; Fan, H.; Dai, S. Second Coordination Sphere Effect of Benzothiophene Substituents on Chain Transfer and Chain Walking in Ethylene Insertion Polymerization. *Polymer* **2022**, *245* (February), 124707.

(6) Lu, W.; Wang, H.; Fan, W.; Dai, S. Exploring the Relationship between the Polyethylene Microstructure and Spatial Structure of α-Diimine Pd(II) Catalysts via a Hybrid Steric Strategy. *Inorg. Chem.* **2022**, *61*, 6799–6806.

(7) Zhai, F.; Solomon, J. B.; Jordan, R. F. Copolymerization of Ethylene with Acrylate Monomers by Amide-Functionalized α-Diimine Pd Catalysts. *Organometallics* **2017**, *36* (9), 1873–1879.

(8) Bourque, A. N.; Dufresne, S.; Skene, W. G. Thiophene-Phenyl Azomethines with Varying Rotational Barriers-Model Compounds for Examining Imine Fluorescence Deactivation. *J. Phys. Chem. C* **2009**, *113* (45), 19677–19685.

(9) Johnson, L. K.; Mecking, S.; Brookhart, M. Copolymerization of Ethylene and Propylene with Functionalized Vinyl Monomers by Palladium(II) Catalysts. *J. Am. Chem. Soc.* **1996**, *118* (1), 267–268.

(10) Canil, G.; Rosar, V.; Dalla Marta, S.; Bronco, S.; Fini, F.; Carfagna, C.; Durand, J.; Milani, B. Unprecedented Comonomer Dependence of the Stereochemistry Control in Pd-Catalyzed CO/Vinyl Arene Polyketone Synthesis. *ChemCatChem* **2015**, *7* (14), 2255–2264.

(11) Rosar, V.; Dedeic, D.; Nobile, T.; Fini, F.; Balducci, G.; Alessio, E.; Carfagna, C.; Milani, B. Palladium Complexes with Simple Iminopyridines as Catalysts for Polyketone Synthesis. *Dalt. Trans.* **2016**, *45* (37), 14609–14619.

(12) Dall'Anese, A.; Fiorindo, M.; Olivieri, D.; Carfagna, C.; Balducci, G.; Alessio, E.; Durand, J.; Milani, B. Pd-Catalyzed CO/Vinyl Arene Copolymerization: When the Stereochemistry Is Controlled by the Comonomer. *Macromolecules* **2020**, *53* (18), 7783–7794.

(13) Scarel, A.; Durand, J.; Franchi, D.; Zangrando, E.; Mestroni, G.; Milani, B.; Gladiali, S.; Carfagna, C.; Binotti, B.; Bronco, S.; Gragnoli, T. Trifluoroethanol: Key Solvent for Palladium-Catalyzed Polymerization Reactions. *J. Organomet. Chem.* **2005**, *690* (8 SPEC. ISS.), 2106–2120.

(14) Dall'Anese, A.; Rosar, V.; Cusin, L.; Montini, T.; Balducci, G.; D'Auria, I.; Pellecchia, C.; Fornasiero, P.; Felluga, F.; Milani, B. Palladium-Catalyzed Ethylene/Methyl Acrylate Copolymerization: Moving from the Acenaphthene to the Phenanthrene Skeleton of α-Diimine Ligands. *Organometallics* **2019**, *38* (19), 3498–3511.

(15) Ó Máille, G. M.; Dall'Anese, A.; Grossenbacher, P.; Montini, T.; Milani, B.; Albrecht, M. Modulation of N^N′-Bidentate Chelating Pyridyl-Pyridylidene Amide Ligands Offers Mechanistic Insights into Pd-Catalysed Ethylene/Methyl Acrylate Copolymerisation. *Dalt. Trans.* **2021**, *50* (18), 6133–6145.

(16) Meduri, A.; Montini, T.; Ragaini, F.; Fornasiero, P.; Zangrando, E.; Milani, B. Palladium-Catalyzed Ethylene/Methyl Acrylate Cooligomerization: Effect of a New Nonsymmetric α-Diimine. *ChemCatChem* **2013**, *5* (5), 1170–1183.

(17) Milani, B.; Marson, A.; Zangrando, E.; Mestroni, G.; Ernsting, J. M.; Elsevier, C. J. New Monocationic Methylpalladium(II) Compounds with Several Bidentate Nitrogen-Donor Ligands: Synthesis, Characterisation and Reactivity with CO. *Inorganica Chim. Acta* **2002**, *327* (1), 188–201.

(18) Durand, J.; Zangrando, E.; Stener, M.; Fronzoni, G.; Carfagna, C.; Binotti, B.; Kamer, P. C. J.; Müller, C.; Caporali, M.; Van Leeuwen, P. W. N. M.; Vogt, D.; Milani, B. Long-Lived Palladium Catalysts for CO/Vinyl Arene Polyketones Synthesis: A Solution to Deactivation Problems. *Chem. - A Eur. J.* **2006**, *12* (29), 7639–7651.

(19) Brookhart, M.; Johnson, L. K.; Killian, C. M. New Pd(II)- and Ni(II)-Based Catalysts for Polymerization of Ethylene and α-Olefins. **1995**, *17* (23), 6414–6415.

(20) Rosar, V.; Montini, T.; Balducci, G.; Zangrando, E.; Fornasiero, P.; Milani, B. Palladium-Catalyzed Ethylene/Methyl Acrylate Co-Oligomerization: The Effect of a New Nonsymmetrical α-Diimine with the 1,4-Diazabutadiene Skeleton. *ChemCatChem* **2017**, *9* (17), 3402–3411.

CHAPTER 3

The effect of potentially tridentate ligands in Pd(II) catalysts for functionalized polyolefin synthesis

Overview

On the basis of the catalytic results obtained in the ethylene/methyl acrylate copolymerization using Pd(II) complexes with a thiophenimine ligand, [Pd(CH_3)(N-S)(**1**)][PF_6] (Chapter 2), we now investigate two series of Pd(II) complexes with hemilabile potentially tridentate molecules, N-N'-S, having the thiophene group directly bonded to the N-N' fragment of the ligand itself. The new ligands show either a pyridylimine fragment or a DAB skeleton and the relevant Pd(II) complexes generate active species for the target reaction leading to either unsaturated esters or cooligomers depending on the N-N' fragment. The catalytic reactions are carried out under mild reaction conditions in terms of temperature and ethylene pressure in either dichloromethane (DCM) or 2,2,2-trifluoroethanol (TFE). The thiophene pendant arm contributes to increase the catalyst stability and to affect the branching degree of the obtained macromolecules. A kinetic study is performed together with *in situ* NMR investigations to detect intermediates involved in the catalytic reaction.

3.1. Introduction.

The catalytic results obtained in the ethylene/methyl acrylate copolymerization using Pd(II) complexes with a hemilabile, potentially bidentate ligand such as a thiophenimine N-S, [Pd(CH_3)(N-S)(**1**)][PF_6] (Chapter 2), are promising in terms of catalyst stability and control over the way of polar monomer enchainment.[1] The catalytic reactions were carried out in either TFE or DCM and we found that the copolymer microstructure was affected by the solvent in terms of M_n values, degree of branches and way of polar monomer incorporation. Indeed, under specific reaction conditions, in the macromolecules synthesized in TFE, methyl acrylate is inserted both at the end of the branches (T(MA)) and into the main chain (M(MA)) in a ratio of about 55:45. Accurate *in situ* NMR investigations were performed in both deuterated solvents, TFE-d_3 and CD_2Cl_2, to have some insights about the nature of the effect of both the solvent and the N-S ligand on the catalyst performances. The reaction of [Pd(CH_3)($NCCH_3$)(**1**)][PF_6], **1b**, with the polar monomer in CD_2Cl_2 resulted in the formation of palladacycle intermediates (**MC4^{NS}**, **MC5^{NS}** and **MC6^{NS}**, Figure 2.14, Chapter 2), while when the same experiment was performed in TFE-d_3, in addition to the expected **MC6^{NS}**, an open-chain intermediate, having both CH_3CN and the organic fragment, generated by the insertion of MA into the Pd-CH_3 bond, was detected for the first time (**OC1^{NS}**, Figure 2.17, Chapter 2). We demonstrated that **OC1^{NS}** represents a novel catalyst resting state for this reaction (Figure 3.1).

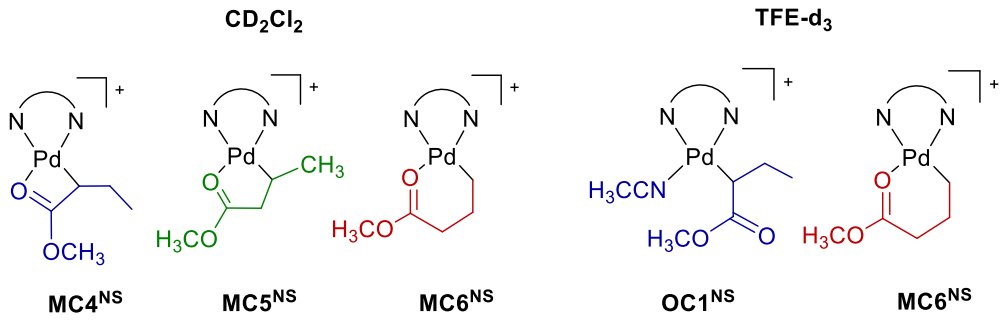

Figure 3.1. Detected intermediates in *in situ* NMR studies about the reaction of **1b** with MA.

Considering the Pd(II) complex bearing the simple thiophenimine, [Pd(CH_3)(**S^{Ph}**)(**1**)][PF_6], (**1S^{Ph}**, Scheme 2.2), when both comonomers, ethylene and methyl acrylate, are added to its CD_2Cl_2 solution (Figure 2.22, Chapter 2), **1S^{Ph}** was activated through the reaction with the gaseous monomer, followed by that with MA, leading to the growth of the copolymer chain.

No signals of the expected metallacycles were observed and on the basis of the bidimensional NMR analysis it was pointed out that during the process the N-S ligand remains coordinated to the metal center.

When the same experiment was performed in TFE-d_3 again the precatalyst activation took place through the insertion of ethylene followed by that of MA. In this case a new intermediate having ligands **1** and **S^{Ph}** and the growing chain bonded to palladium was detected. In addition, in a bidimensional ^{1}H,^{1}H NOESY spectrum the correlation peak between the methoxy group of inserted MA and the residual OH of deuterated TFE indicates their close spatial proximity (Figure 2.25, Chapter 2), suggesting that the ester group of the inserted polar monomer is involved in a network of hydrogen bonding interactions with the fluorinated solvent. Due to this network the oxygen atom of the carbonyl group of inserted MA is less available for the formation of the palladacycle intermediates involved in the chain walking process. Therefore, thanks to this H-bonds network MA is trapped into the main chain of the copolymer.

Focusing on the control of the polar monomer enchainment and by taking into account Pd(II) complexes with α-diimine ligands only, in literature, to the best of my knowledge, just two examples of Pd(II) catalysts of this family are reported to be able to insert methyl acrylate almost exclusively into the main chain. The first ligand is a very bulky α-diimine having a dibenzo-barrelene skeleton and pentiptycene-based substituents (**L17**, Figure 3.2).[2] The relevant Pd-catalyst leads to branched copolymers with MA mostly inserted into the main chain (98 % selectivity). This is due to the different regiochemistry of the polar monomer insertion, that, as discovered by detailed NMR mechanistic studies, takes place in a 1,2-fashion instead of the secondary regiochemistry typical for catalysts based on α-diimines.[3] In this way the formed 5-membered palladacycle preferentially reacts with the gaseous monomer to continue the growth of the copolymer chain disfavoring the chain walking process (Scheme 1.5, Chapter 1). The second example involves a dinuclear Pd(II) complex with a BIAN ligand having two bidentate compartments for the coordination of two palladium ions (**L20**, Figure 3.2).[4] The produced E/MA copolymers show MA inserted as both T(MA) and M(MA) in a ratio of about 23:77. The higher percentage of M(MA) is supposed to be due to a weak interaction between the oxygen atom of the C=O group of the inserted polar monomer and the second palladium ion that is not involved in the growth of the copolymer chain. In this way, on the first palladium ion a vacant coordination site is available for the binding of ethylene leading to the growth of the macromolecule with MA inserted in the main chain (Figure 3.2).

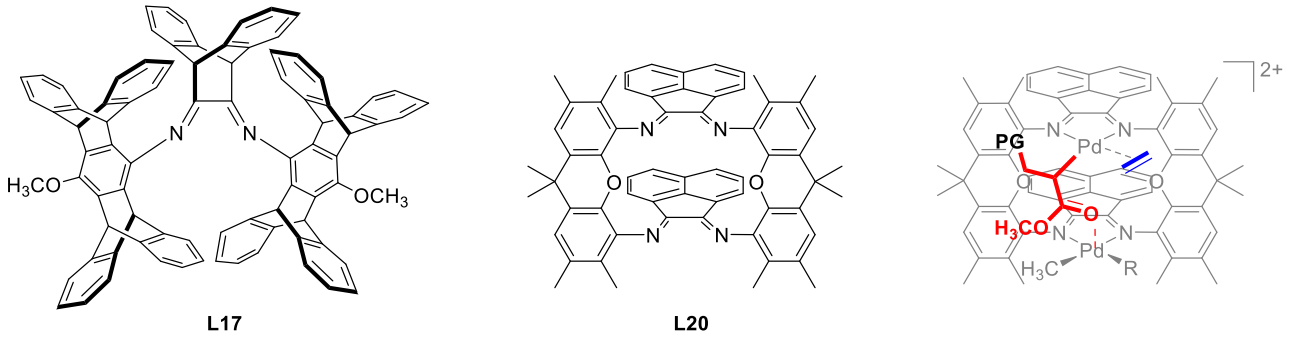

Figure 3.2. Examples of α-diimine ancillary ligands and of the proposed intermediate; GP = growing polymer.

On the basis of the results obtained with Pd(II) complexes bearing the N-S ligand, and considering that only tridentate *o*-aryloxide-NHC palladium complexes are reported active in the copolymerization of norbornene with butyl vinyl ether (BVE) and methyl 10-undecenoate (UA),[5] but never applied in catalysts for the target copolymerization, we have now studied two new families of molecules characterized by α-diimine bidentate fragment N-N' and a thiophene pendant arm attached to it, leading to hemilabile, potentially tridentate ligands, N-N'-S (Figure 3.3). The diimine bidentate compartment is chosen with either a pyridylimine moiety, ligands **3** and **4**, or a DAB skeleton, ligands **5** – **7**.

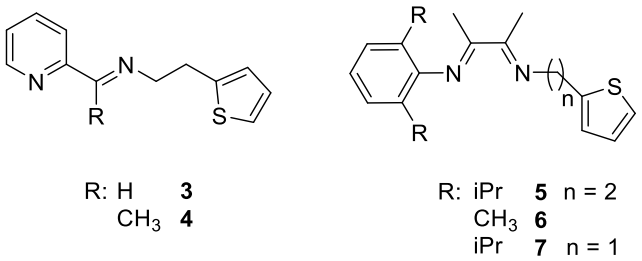

Figure 3.3. Investigated N-N'-S ligands.

Ligands **3** – **7** are used to obtain the relevant neutral and cationic Pd(II) complexes, that, after detailed characterization, both in solution and in solid state, have been tested as catalysts for the ethylene/methyl acrylate copolymerization under mild reaction conditions.

For the sake of clarity the section "Results and discussion" is divided into two parts: the first one (Part A) is focused on the complexes with N-N'-S ligands having the pyridylimine moiety, while in the second part (Part B) Pd(II) complexes having the N-N'-S ligands with the DAB skeleton are reported.

3.2 Results and discussion – Part A.

*3.2.1 Synthesis and characterization of thiophene-pyridylimine ligands **3** and **4**.*

The thiophene-pyridylimine ligands, **3** and **4**, are synthesized through the condensation reaction of 2-thiophene ethylamine with the proper pyridine in a water solution, according to the literature (Scheme 3.1).[6] Ligand **3** is obtained as a dark yellow oil in a high yield (83 %) with some traces of 2-thiophene ethylamine, while **4** is an orange oil with traces of 2-acetyl-pyridine in a yield about 86 %.

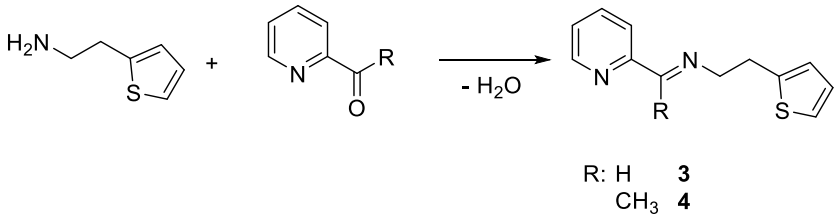

Scheme 3.1. Synthesis of ligands **3** and **4**.

Ligands **3** and **4** are characterized in solution by mono- and bidimensional NMR spectroscopy at room temperature. The ^{1}H NMR spectrum of **3** is in agreement with that one reported in literature[6,7] and the presence of one set of signals indicates only one product in solution (Figure 3.4a).

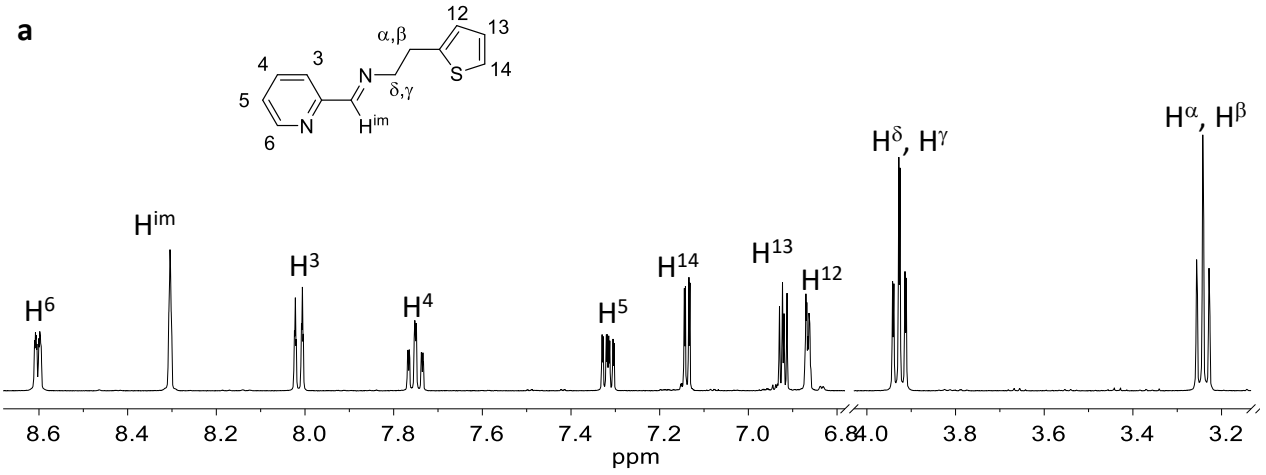

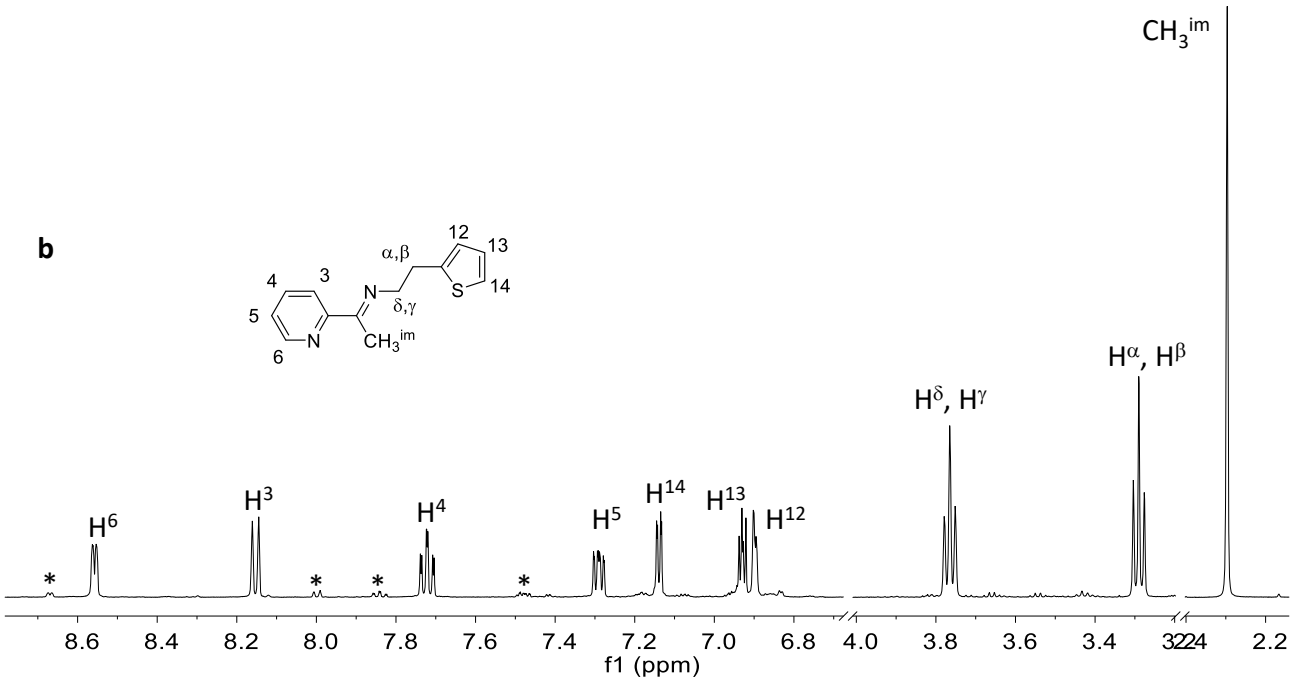

Figure 3.4. ^{1}H NMR spectra (CD_2Cl_2, 298 K) of (a) **3** and (b) **4**; *2-acetyl-pyridine.

Ligand **4** is reported in this work for the first time. In its ^{1}H NMR spectrum (Figure 3.4b) the assignments signal to proton are made as follows. The resonance at 8.56 ppm is assigned to H^6 in analogy to other pyridylimine molecules,[8] the singlet at 2.30 ppm is due to CH_3^{im} as indicated by the characteristic chemical shift value of its carbon atom at 14.0 ppm, reported in the $^{1}H,^{13}C$ HSQC spectrum (Figure 3.5). Focusing on H^6, thanks to $^{1}H,^{1}H$ DQCOSY and $^{1}H,^{1}H$ COSY spectra (Figures 3.6 and 3.7), other signal-proton assignments are made for the pyridyl ring (e.g. H^5 at 7.29 ppm, H^4 at 7.72 ppm and H^3 at 8.15 ppm). Triplets at 3.76 and 3.29 ppm are relative to H^{δ},H^{γ} and H^{α},H^{β} respectively, because the latter shows a long range coupling correlation peak with H^{12} at 6.87 ppm.

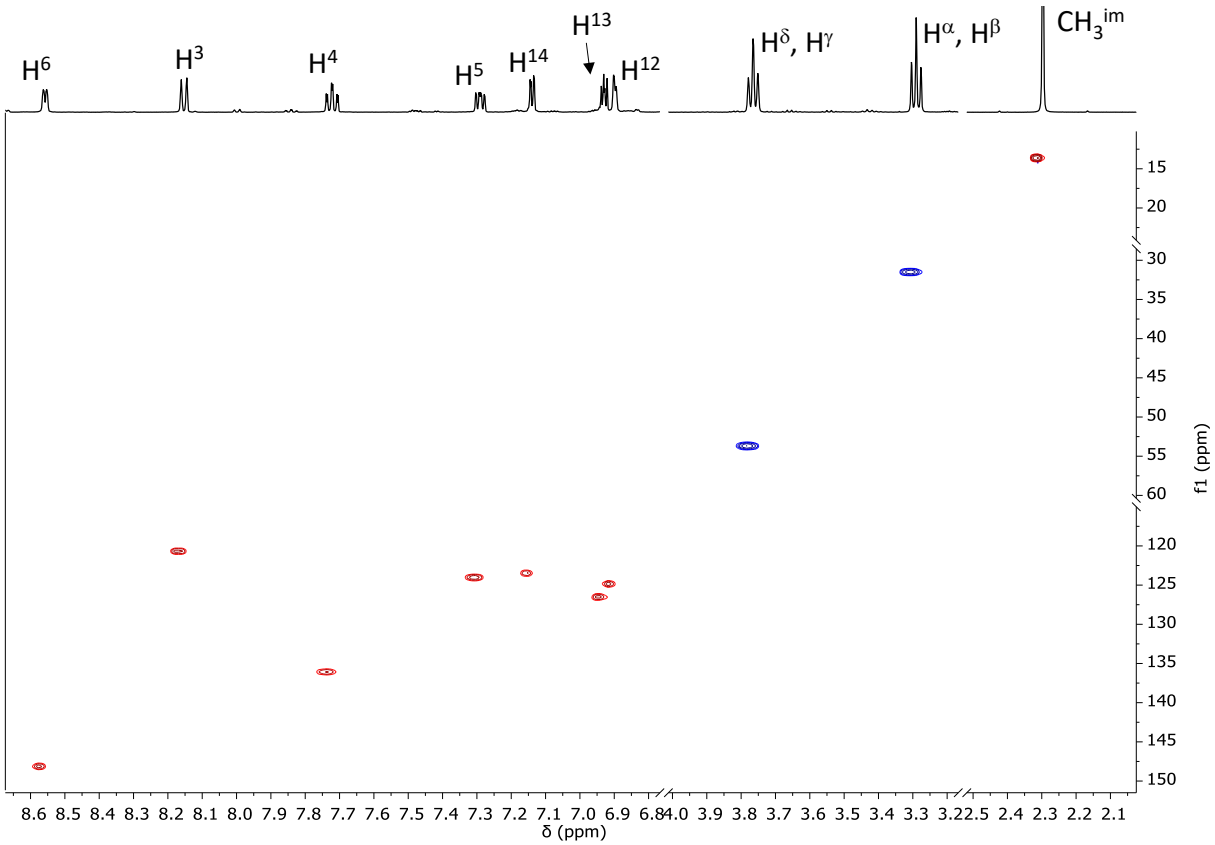

Figure 3.5. $^{1}H,^{13}C$ HSQC spectrum (CD_2Cl_2, 298 K) of **4**.

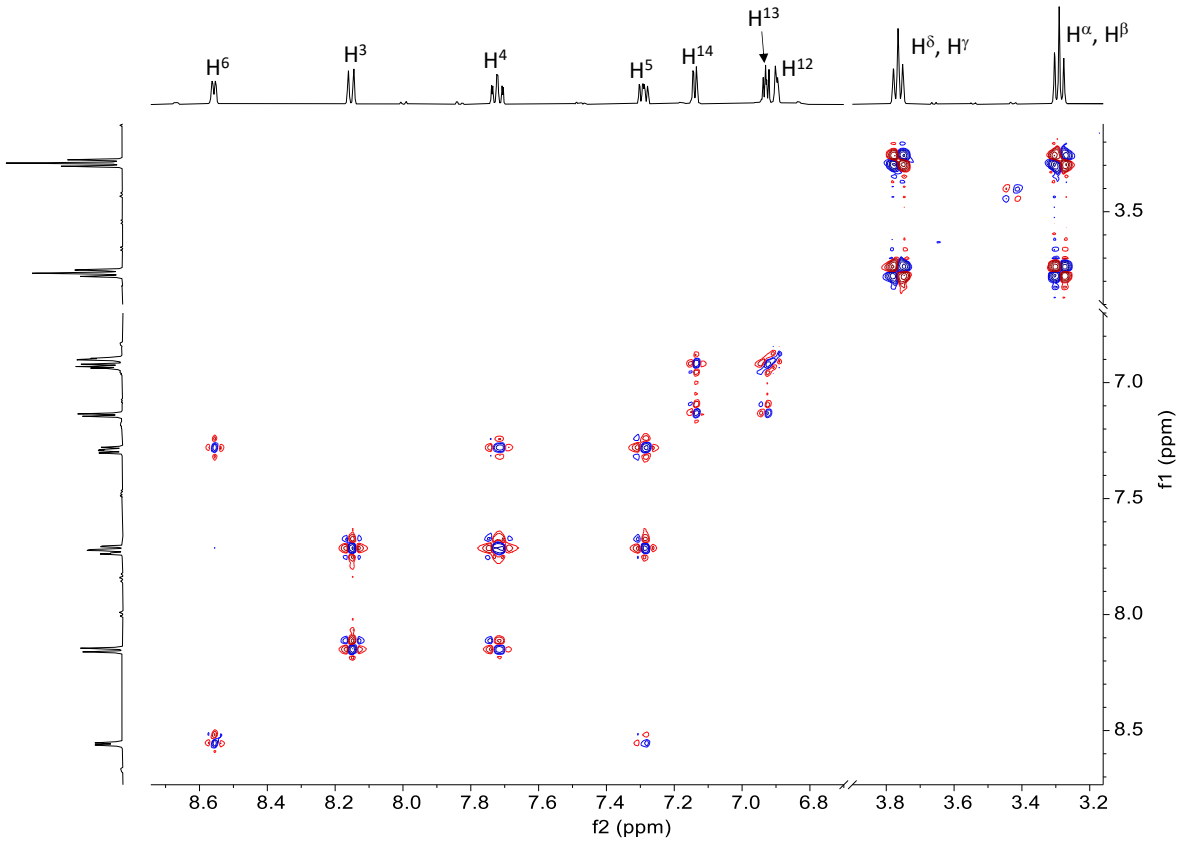

Figure 3.6. $^{1}H,^{1}H$ DQCOSY spectrum (CD_2Cl_2, 298 K) of **4**.

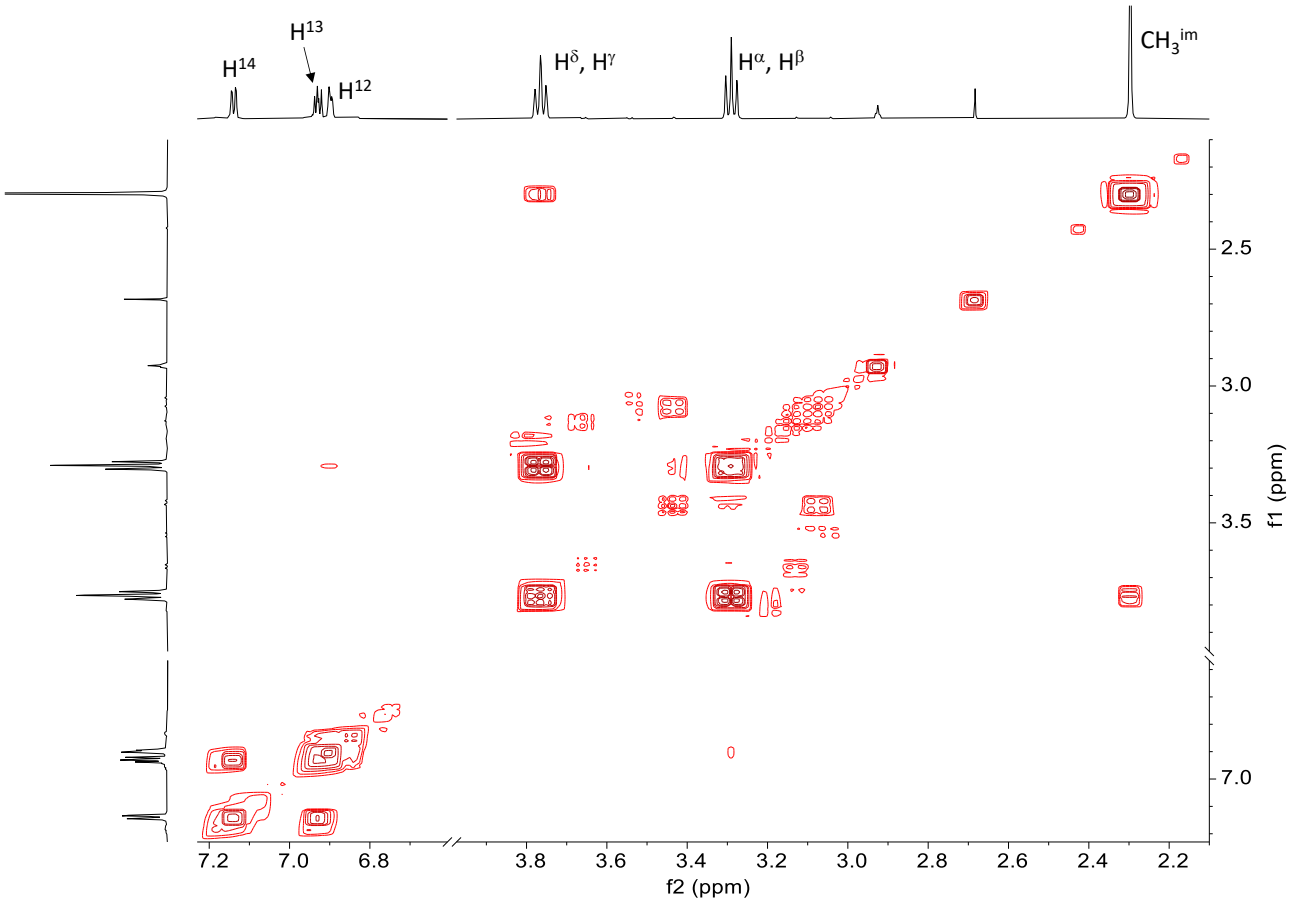

Figure 3.7. $^{1}H,^{1}H$ COSY spectrum (CD_2Cl_2, 298 K) of **4**.

*3.2.2 Synthesis and characterization of neutral Pd(II) complexes **3a** and **4a**.*

The neutral Pd(II) complexes [Pd(CH_3)Cl(N-N′-S)], **3a**[7] and **4a**, are synthesized starting from the precursor [Pd(cod)(CH_3)Cl] through the substitution reaction of the diolefin with the ligand **3** or **4**, respectively at room temperature (Scheme 3.2).

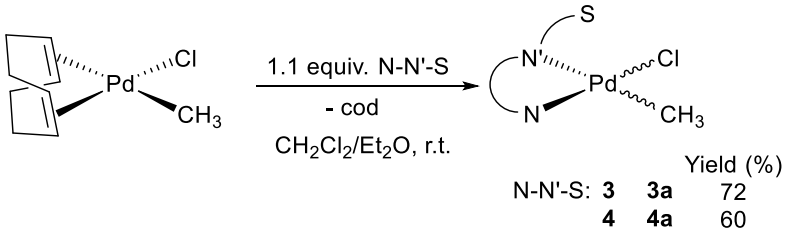

Scheme 3.2. Synthesis of neutral complexes **3a** and **4a**.

The complexes are obtained in good yields and as a yellow solid for **3a** or as an orange powder for **4a**. The inequivalent tridentate ligands N-N'-S are coordinated in a non-equivalent chemical environment, thus two geometrical isomers are possible, depending on the relative position of the Pd-CH_3 bond with respect to the two different halves of the ligand. We conventionally defined as *trans* isomer the species having the Pd-CH_3 fragment *trans* to the Pd-N bond, where the N is the iminic nitrogen atom, N^{im}. They are characterized in solution by NMR spectroscopy at room temperature (Figures S3.1-S3.3) and in the ^{1}H NMR spectra two sets of signals of different intensity are observed indicating the presence of *cis* and *trans* isomers (Figures 3.8 and S3.3).

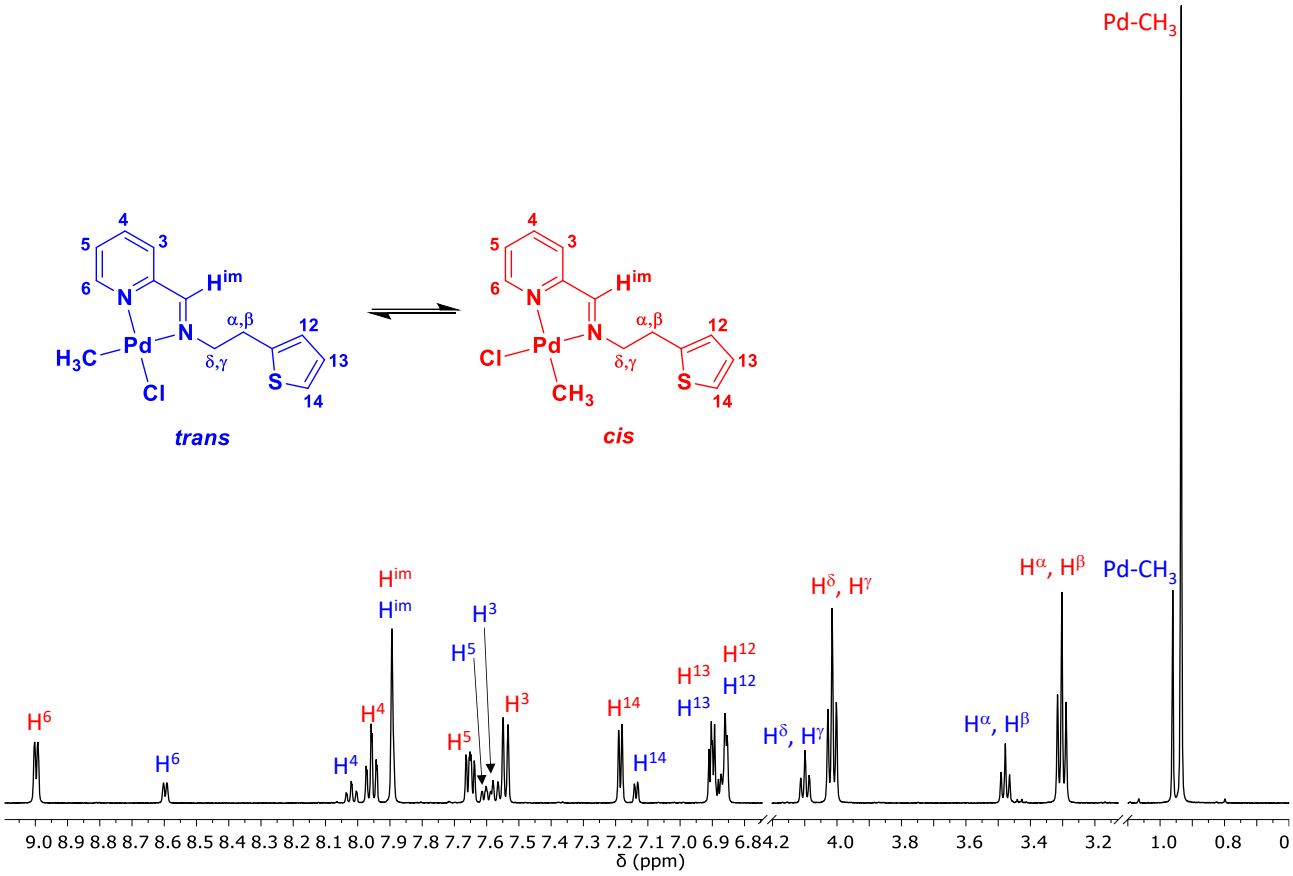

Figure 3.8. ^{1}H NMR spectrum (CD_2Cl_2, 298 K) of **3a** at t = 1 min.

Considering **3a** ^{1}H NMR spectrum (Figure 3.8), singlets at 0.93 ppm and 0.96 ppm are assigned to the Pd-CH_3 fragment and, in analogy to the assignments of **3**, the multiplets in the range 3.30 – 4.10 ppm are due to the CH_2 groups of the pendant arm. In the ^{1}H,^{1}H NOESY spectrum (Figure 3.9) a peak due to the Overhauser effect between the first singlet and the triplet at 4.02 ppm (H^{δ},H^{γ}) indicates that the major species is the *cis* isomer.

On the basis of integrals of the Pd-CH_3 signals, the ratio between *cis* and *trans* isomers at the thermodynamic equilibrium, reaching after 2 h from dissolving complex in CD_2Cl_2, is 79:21 for **3a** and 44:56 for **4a**. Thanks to bidimensional NMR analysis the proton-signal assignments are made for all resonances and the same procedure is followed for **4a**.

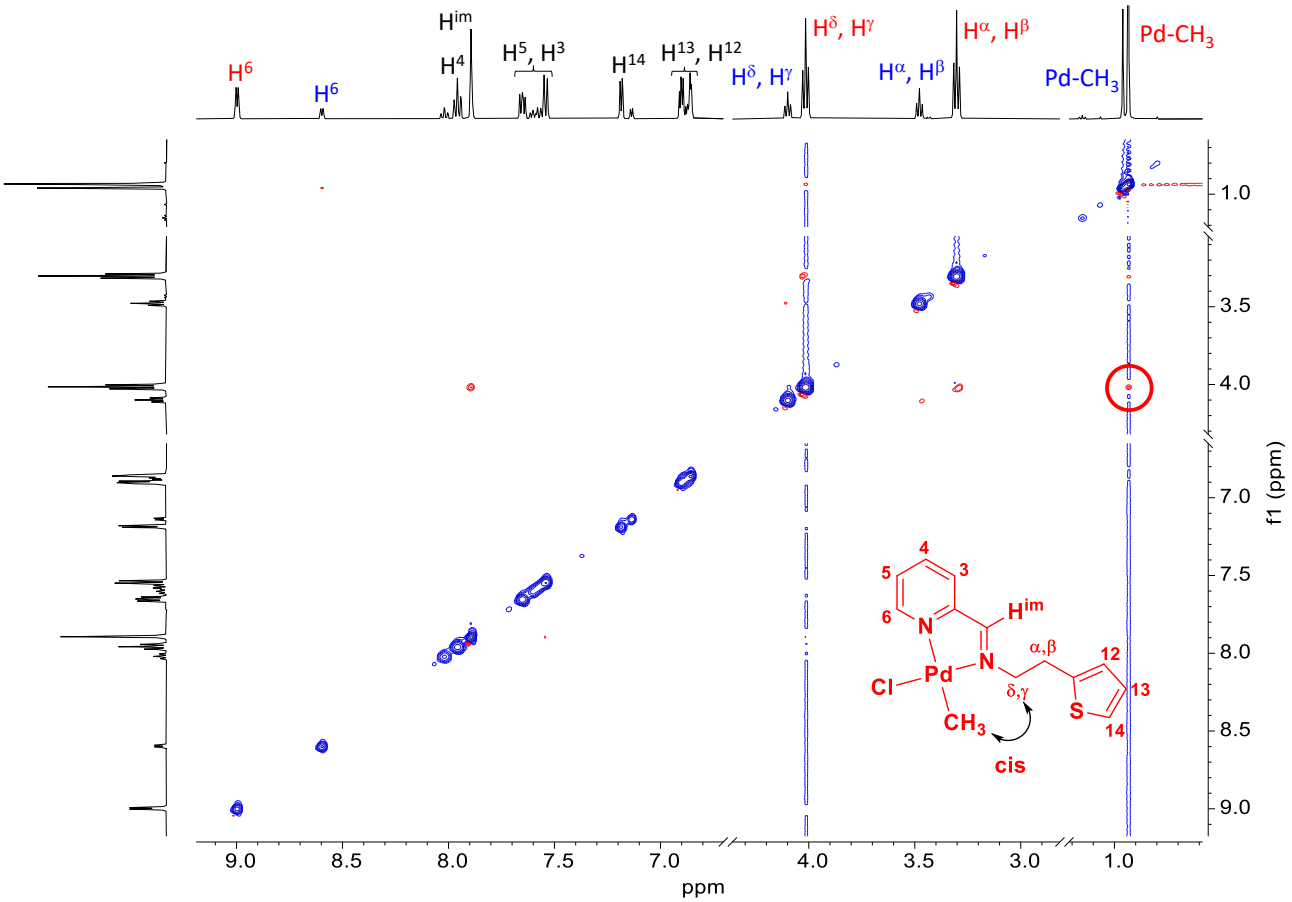

Figure 3.9. $^1H,^1H$ NOESY spectrum (CD_2Cl_2, 298 K) of **3a** at t = 2 h.

Comparing ^1H NMR spectra of **3** and **3a** (Figure 3.10), it is possible to note that H^{im} and H^3 of the neutral complex resonate at lower frequency with respect to **3**, moving from 8.30 to 7.89 ppm for H^{im} and from 8.15 to 7.54 ppm (*cis*-**3a**) and 7.57 ppm (*trans*-**3a**) for H^3, indicating that the free ligand is in *E,anti* conformation (Scheme 3.3).

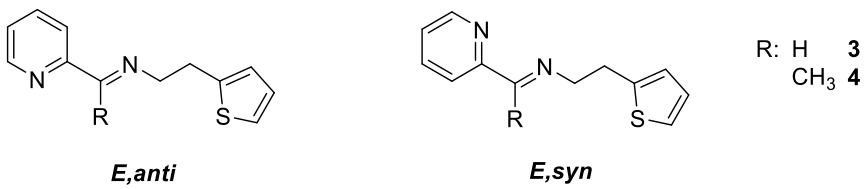

Scheme 3.3. *E,anti* and *E,syn* conformations for the N-N'-S ligands **3** and **4**.

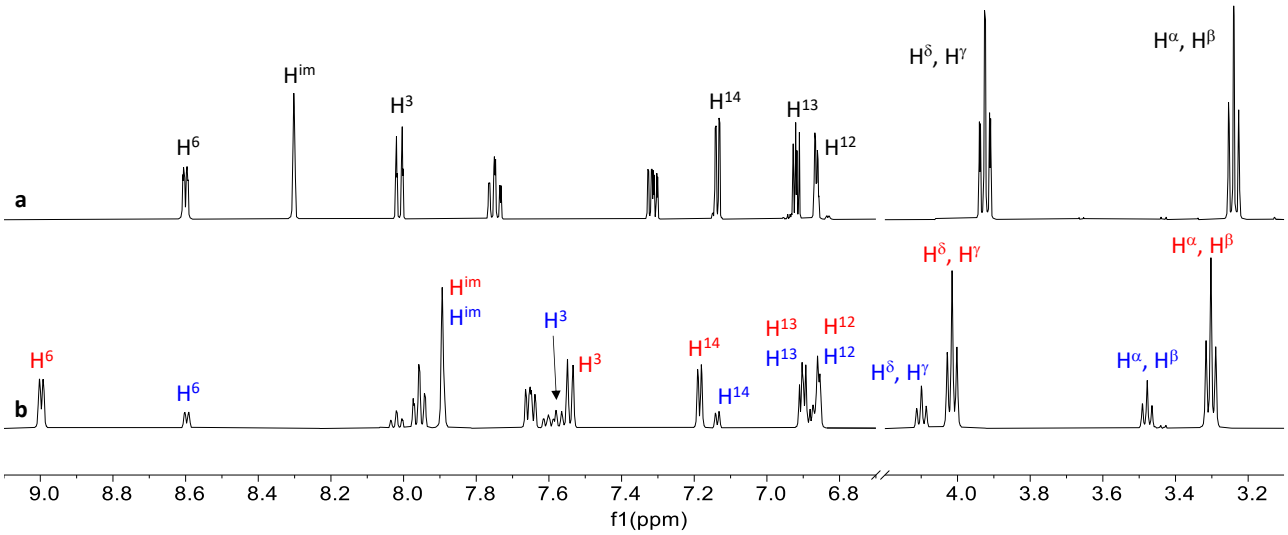

Figure 3.10. ^{1}H NMR spectra (CD_2Cl_2, 298 K) of (a) **3** and (b) **3a**.

An analogous shift to lower frequency is observed in the ^{1}H NMR spectrum moving from **4** to **4a** for the peak of CH_3^{im} (from 2.30 ppm to 2.12 ppm (*cis*-**4a**) and 1.98 ppm (*trans*-**4a**)) leading to the same conclusion as for **3** and **3a** (Figure S3.4).

Suitable crystals of both neutral complexes are obtained upon *n*-hexane slow diffusion in CD_2Cl_2 solution of each complex kept at 277 K for 3 weeks. The X-Ray structure of **3a** is in agreement with that one reported in literature.[7] In this case in the unit cell only one molecule is present and it corresponds to the *cis* isomer, the major species in solution (Figure 3.11a). Instead for **4a** two independent molecules are present: the *trans* isomer (Figure 3.11b) and a mixture of both isomers with 68 % of *trans* one (Figure S3.5). In the latter the CH_3 and Cl ligands are disordered by swapping their positions in the coordination around the Pd atom, so reported values of bond distances and angles are average values. By comparing the solid state structure of *cis*-**3a** with the *trans*-**4a**, the palladium ion shows the expected square planar geometry forming with the ligand a bite angle of 79.41(5)° for *cis*-**3a** and 78.99(9)° for *trans*-**4a**, in agreement with other values reported for Pd(II) complexes bearing pyridylimine ligand (Table S3.1).[8] In both complexes the Pd-N bond in *trans* to Pd-CH_3 bond is remarkably longer (Pd1-N2 of 2.1338(2) Å for *cis*-**3a** and Pd1-N1 of 2.126(2) Å for *trans*-**4a**) than the other Pd-N bond length (Pd1-N1 of 2.0495(1) Å for *cis*-**3a** and Pd1-N2 of 2.040(3) Å for *trans*-**4a**), in agreement with the expected higher *trans* influence of the Pd-alkyl bond with respect to that of the Pd-Cl bond. The ORTEP drawings of *cis*-**3a** and *trans*-**4a** show that the thiophene fragment is twisted out from the palladium plane forming with the latter a torsion angle of 176.1(1)° for *cis*-**3a** and 178.3(2)° for *trans*-**4a**. In both complexes no interactions between sulfur and palladium are observed.

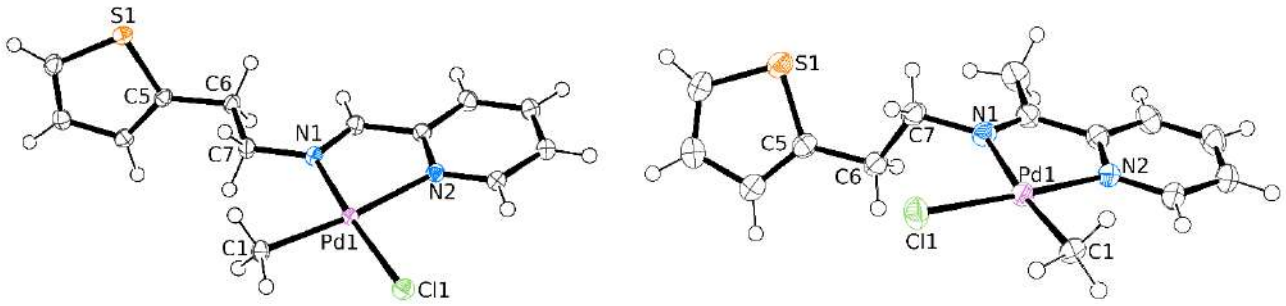

(a) (b)

Figure 3.11. ORTEP drawing (50% probability ellipsoids) of the molecule of (a) *cis*-**3a** and (b) *trans*-**4a** in the crystal structure.

*3.2.3 Synthesis and characterization of cationic Pd(II) complexes **3b**, **3c** and **4b** – **4e**.*

The monocationic complexes [Pd(CH_3)($NCCH_3$)(N-N'-S)][X], **3b** and **4b** (X = PF_6), **4d** (X = OTf) and [Pd(CH_3)(N-N'-S)][X], **3c** and **4c** (X = PF_6), **4e** (X = OTf), are synthesized according to the literature procedures,[8,9] based on the dehalogenation reaction of the corresponding neutral complexes **3a** and **4a**, by using the proper silver salt. The reaction is carried out under inert atmosphere, in dichloromethane, with the addition of a solution of AgX in dry acetonitrile for **3b**, **4b** and **4d**, while for **3c**, **4c** and **4e** the AgX salt is directly dissolved in CH_2Cl_2 (Scheme 3.4). The cationic complexes are obtained upon concentration of the reaction mixture and addition of cold diethyl ether, isolating them in good yields.

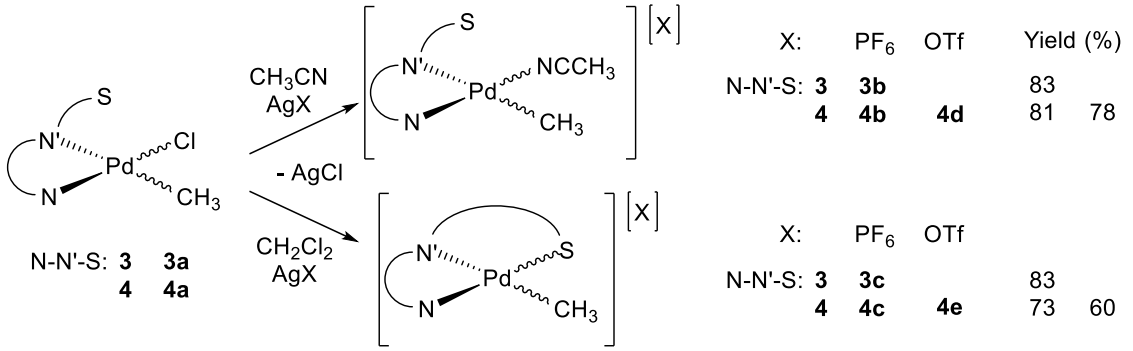

Scheme 3.4. Synthesis of cationic complexes **3b** – **3c** and **4b** – **4e**.

The complexes have all been characterized in solution by NMR spectroscopy, in CD_2Cl_2, at room temperature (Figures S3.9-S3.15). In the ^{1}H NMR spectrum of **3b** recorded immediately after the dissolution of the complex, two sets of signals are observed, meaning that both geometrical isomers are present in solution. Some resonances assigned to the major species are broad (Figure 3.12).

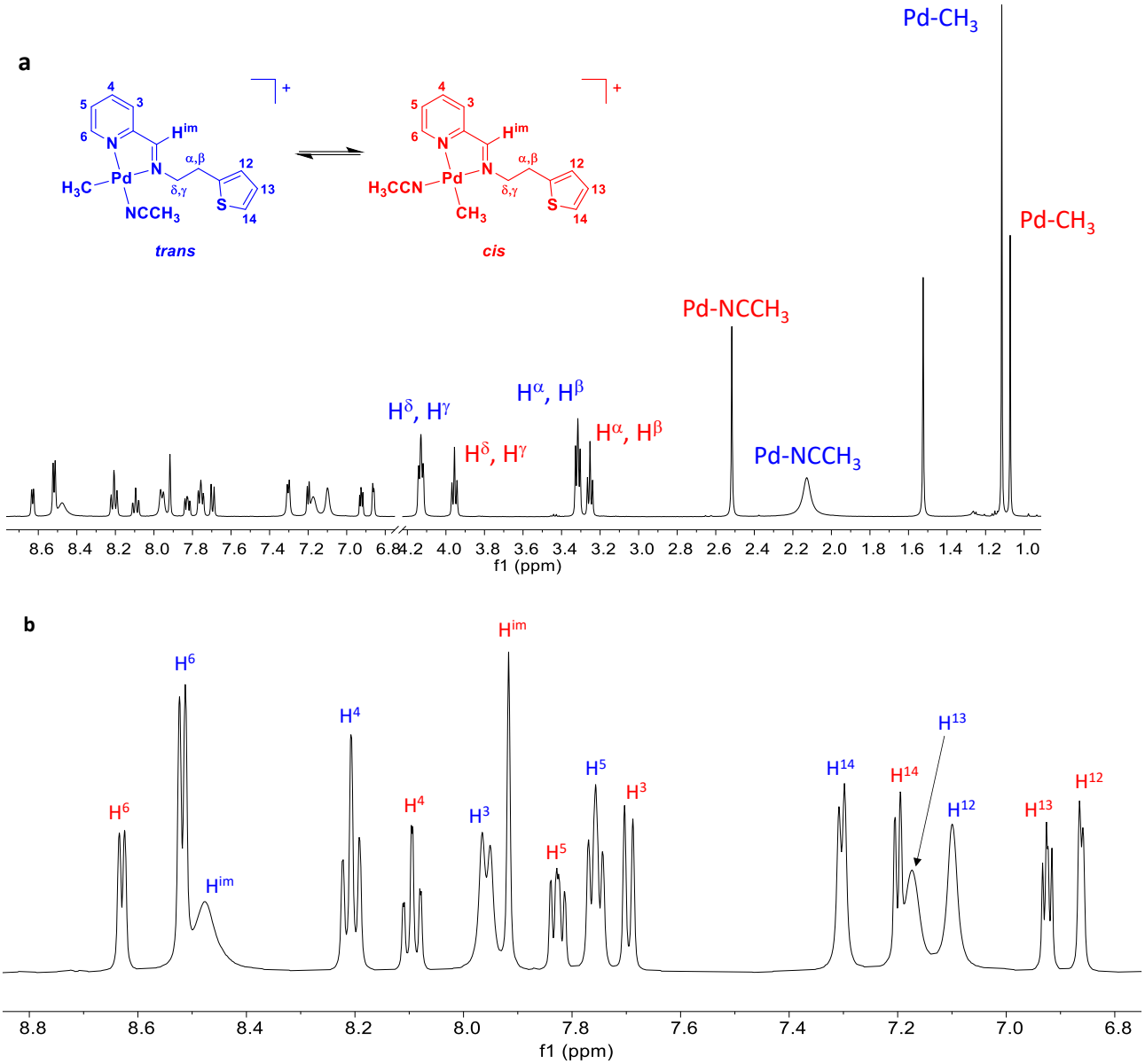

Figure 3.12. ^{1}H NMR spectrum (CD_2Cl_2, 298 K) of **3b**; (a) full spectrum, (b) aromatic region.

The characteristic signals of Pd-CH_3 fragment (1.12 and 1.07 ppm), CH_2 groups of the pendant arm, in the range from 3.10 to 4.20 ppm, and H^6 at 8.62 and 8.52 ppm are easily assigned. The *trans* isomer is recognized to be the major species (65 %) on the basis of the cross peak, due to the Overhauser effect, between the Pd-CH_3 group and H^6 of the pyridine ring, present in the $^{1}H,^{1}H$ NOESY spectrum (Figure 3.13). In addition, some exchange peaks relative to signals of Pd-$NCCH_3$, H^{δ},H^{γ} and H^6 of the two isomers indicate that the two species are in equilibrium at slow rate on the NMR time scale at room temperature.

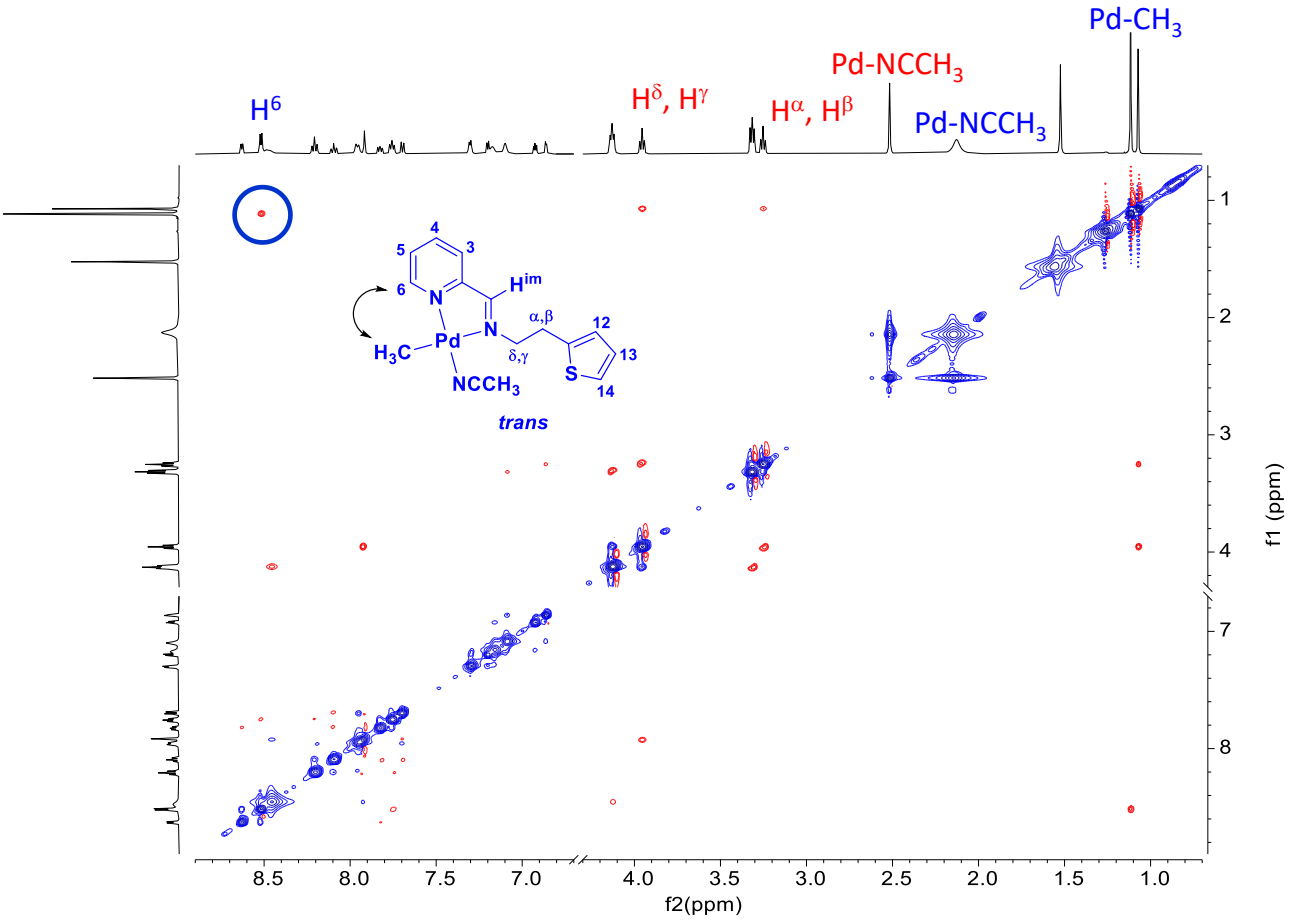

Figure 3.13. $^{1}H,^{1}H$ NOESY spectrum (CD_2Cl_2, 298 K) of **3b**.

Other proton-signal assignments are made in analogy to **3a** on the basis of the bidimensional NMR spectra. The singlet of the iminic proton of the *cis* isomer is observed at 7.92 ppm along with the characteristic chemical shift of its carbon atom at 170.8 ppm (Figure S3.7). The broad signal at 8.47 ppm is assigned to the same proton in the *trans* isomer. Indeed, in the $^{1}H,^{1}H$ NOESY spectrum it is shown an exchange peak with the sharp singlet at 7.92 ppm, confirming this attribution. NMR spectra of **4b** are similar to those of **3b** and the assignments are made similarly (Figures S3.6-S3.8). Thus, the NMR analysis of **3b** and **4b** suggests that in solution two dynamic phenomena are present: the equilibrium between the *cis* and *trans* isomers and a new process relevant to the *trans* species involving the competition between the thiophene fragment and the acetonitrile in the fourth coordination site of palladium, as suggested by the broadness of the signals of some protons of the thiophene ring. To have some additional information about the latter process, progressive amounts of acetonitrile (from 1 to 10 eq.) are added to a 10 mM CD_2Cl_2 solution of **3b** (Figure 3.14).

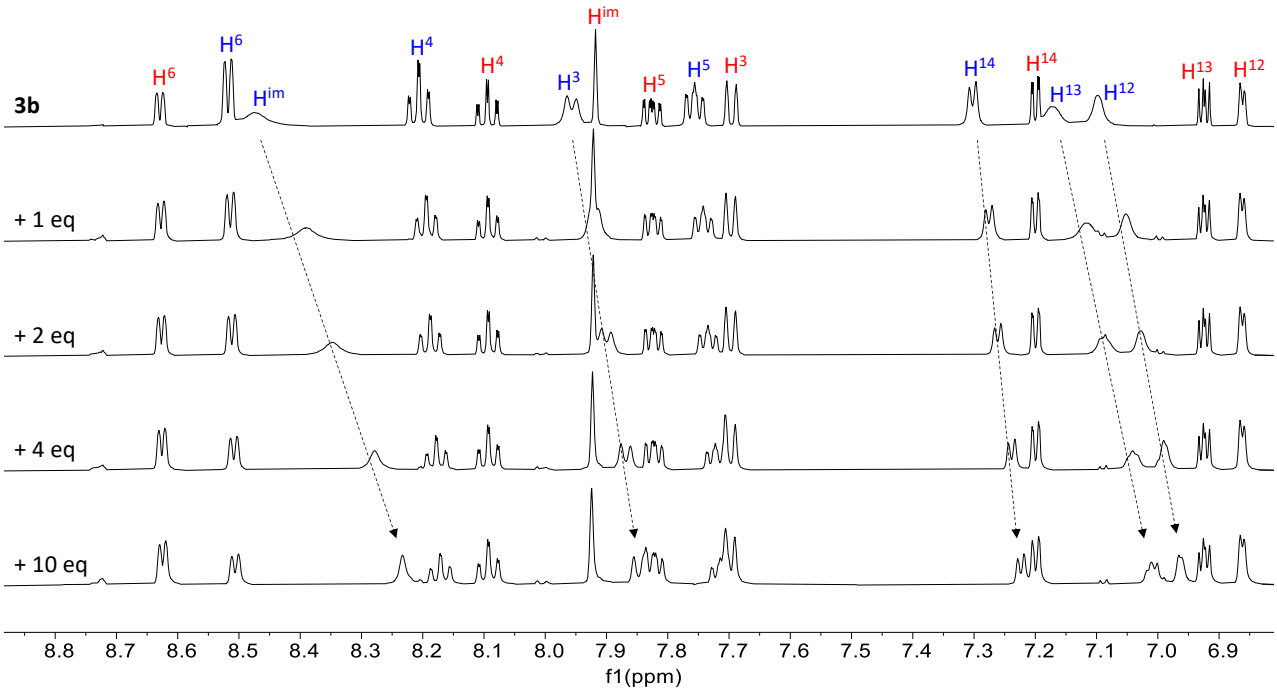

Figure 3.14. ^{1}H NMR spectra (CD_2Cl_2, 298 K) of progressive additions of acetonitrile to **3b** solution; aromatic region.

The NMR spectra show: the shift to lower frequencies of resonances of both H^{im} and the protons of the thiophene ring; the increase in intensity of the singlet of *trans* Pd-$NCCH_3$; and the variation in the relative content of the two isomers. An analogous experiment leading to analogous results is performed on a 10 mM CD_2Cl_2 solution of **4b** (Figure S3.9).

All these data suggest the presence of a third species in solution, taking part to the dynamic process. It is reasonable to assume that this species might have the sulfur atom directly bonded to the metal center in place of the acetonitrile and, in this case, N-N'-S behaves as a tridentate ligand (Scheme 3.5).

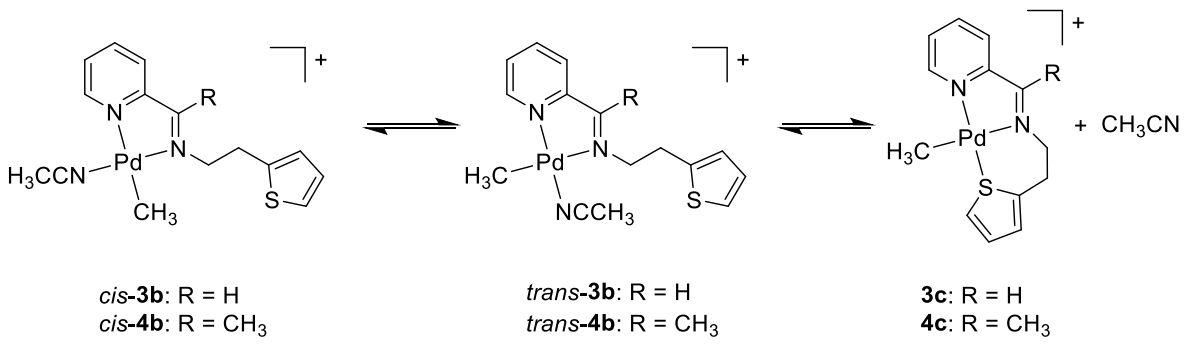

cis-**3b**: R = H
cis-**4b**: R = CH_3

trans-**3b**: R = H
trans-**4b**: R = CH_3

3c: R = H
4c: R = CH_3

Scheme 3.5. The established equilibria in the **3b** or **4b** solution.

With the aim to validate this hypothesis, monocationic Pd(II) complexes of general formula [Pd(CH_3)(N-N'-S)][PF_6], **3c** and **4c**, are synthesized (Scheme 3.4). The presence of only one species in solution is confirmed by NMR analysis and the assignments are made in analogy to other Pd(II) complexes of the same family (Figures S3.10-S3.11). All the signals are sharp. The comparison among ^{1}H NMR spectra of **3b** after the addition of 10 eq. of CH_3CN, **3b** and **3c** points out that the signals observed in the ^{1}H NMR spectrum of the solid isolated from the synthesis of **3b** are intermediate among those of the spectrum of **3b** after the addition of acetonitrile and those of **3c** (Figure 3.15). This conclusion confirms that when the solid isolated from the synthesis of **3b** is dissolved in CD_2Cl_2, two equilibria are established in solution: the *cis* isomer is in equilibrium with the *trans* isomer, which, in turn, is in equilibrium with **3c** and free acetonitrile (Scheme 3.5). Therefore, the spectrum of the solution of **3b** with the addition of an excess of acetonitrile is the closest to the real spectrum of **3b**.

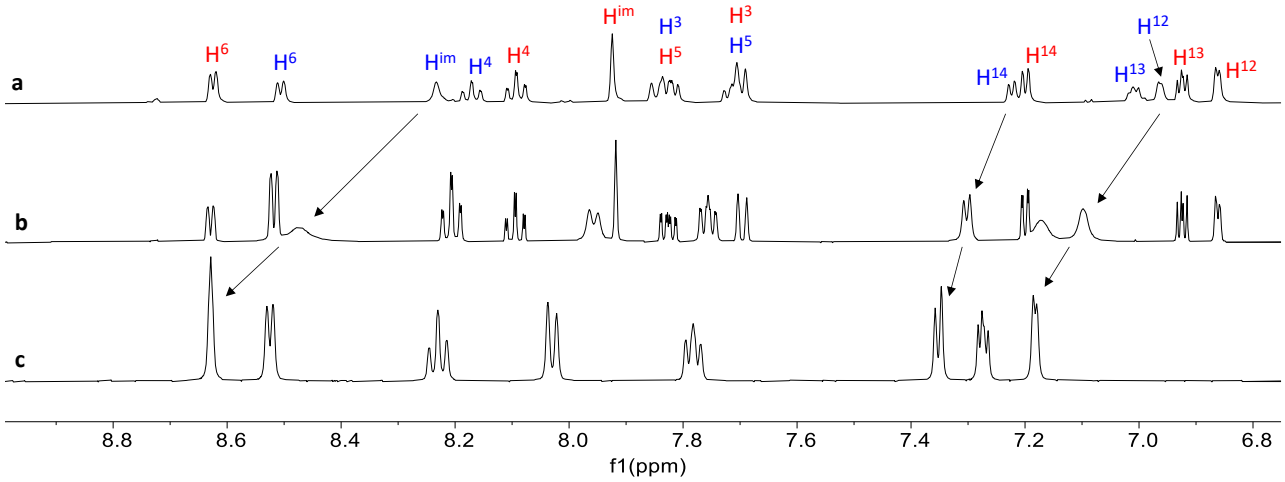

Figure 3.15. ^{1}H NMR spectra (CD_2Cl_2, 298 K) of (a) **3b** + 10 eq. of CH_3CN, (b) **3b** and (c) **3c**.

Complexes **3c** and **4c** are characterized also in solid state by X-Ray diffraction. Suitable single single crystals are obtained in the same way of those of the neutral compounds (Figure 3.16, Table S3.2). The palladium ion shows the expected square planar geometry with N-N'-S molecule bonded to the metal center as a tridentate ligand through the two nitrogen atoms and the sulfur one. The bond distances of the pyridinic half of the ligand are similar to those found in the neutral complexes, while the Pd-S bond length is 2.2683(5) Å and 2.2612(1) Å for **3c** and **4c**, respectively, in agreement with the value reported in literature for Pd(II) complexes with α-diimine bearing a thiophene moiety.[10] The bond angle N1-Pd1-S1 is 97.10(5)° for **3c** and 100.08(8)° for **4c**, higher than the ideal value of a square planar coordination geometry and this might be due to the distortion from the planarity of the six-membered metallacycle containing the iminic-thiophene moiety of the ligand.

The thiophene ring itself is twisted out with respect to the square planar plane of palladium forming with the latter a dihedral angle of 48.49(4)° for **3c** and 53.84(9)° for **4c**.

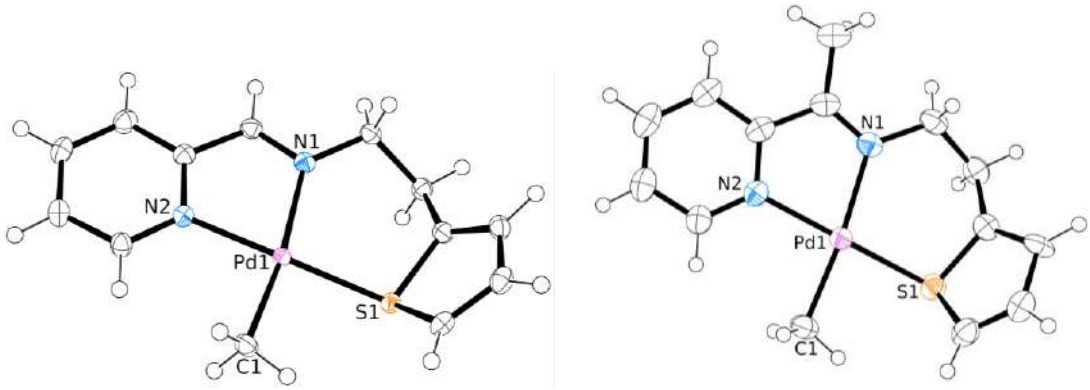

(a) (b)

Figure 3.16. ORTEP drawing (50% probability ellipsoids) of the molecule of (a) **3c** and (b) **4c** in the crystal structure; the PF_6^- anion has been omitted for the sake of clarity.

For ligand **4**, the cationic complexes with triflate (OTf) as counterion, **4d** and **4e**, are also synthesized and characterized by NMR spectroscopy (Figures S3.12-S3.13). As expected, the ^{1}H NMR spectrum of complex **4d** at the thermodynamic equilibrium is very similar to that of **4b**, except for the resonance assigned to H^6 of the *cis* isomer, that is shifted to higher frequencies going from PF_6 to OTf (8.66 ppm *vs* 8.96 ppm). This suggests that, in solution, the triflate might be preferentially located close to the H^6 of the *cis* isomer. The change of anion does not affect the chemical shift of the Pd-CH_3 singlet of both geometrical isomers. Also comparing the ^{1}H NMR spectra of **4c** and **4e** no differences are observed: only one set of sharp signals is present. Considering **4e**, in the aliphatic region of its ^{1}H NMR spectrum (Figure S3.13) the two singlets at 1.06 and 2.48 ppm are easily assigned to Pd-CH_3 and CH_3^{im}, respectively, while the triplets at 3.33 and 4.03 ppm to H^{α},H^{β} and H^{δ},H^{γ} protons. The other proton-signal assignment in the aromatic region are made in analogy with other monocationic Pd(II) complexes of the same class.

*3.2.4 Ethylene/methyl acrylate cooligomerization with the Pd(II) complexes **3b**, **3c** and **4b** – **4e**.*

The cationic complexes **3b**, **3c** and **4b** – **4e** are tested as precatalysts in the cooligomerization of ethylene with methyl acrylate carried out under the following reaction conditions: [MA]/[Pd] = 594, reaction time of 6 h, at T = 308 K, under 2.5 bar of ethylene (Table 3.1). 2,2,2-trifluoroethanol (TFE) is used as solvent thanks to its capability to stabilize the Pd-hydride intermediate.[11] The catalytic products are isolated as yellow – brown oils and characterized in $CDCl_3$ solution by NMR spectroscopy at room temperature after removal of volatile fractions at reduced pressure.

Table 3.1. Ethylene/methyl acrylate cooligomerization: effect of N-N'-S ligand and CH_3CN. Precatalyst: $[Pd(CH_3)(L)(N\text{-}N'\text{-}S)][X]$ [a]

entry	N-N'-S	X	L	yield (mg)	Productivity (g P/mol Pd)[b]	Catalytic products[c]
1	**3**	PF_6	CH_3CN	11.9	566.67	α,β- and β,γ-Unsaturated esters
2			---	15.5	738.09	
3	**4**	PF_6	CH_3CN	13.3	633.33	α,β- and β,γ-Unsaturated
4			---	18.4	876.19	esters, traces of cooligomers
5	**4**	OTf	CH_3CN	13.9	661.90	α,β- and β,γ-Unsaturated esters
6			---	27.2	1295.24	

[a] Reaction conditions: $n_{Pd} = 2.1 \cdot 10^{-5}$ mol, $V_{TFE} = 21$ mL, $V_{MA} = 1.130$ mL, [MA]/[Pd] = 594, $P_E = 2.5$ bar, T = 308 K, t = 6 h. [b] Productivity in g P/mol Pd = grams of product per mol of palladium calculated on isolated yield. [c] Determined by ^1H NMR spectroscopy on isolated product.

All complexes generate catalysts which show a low productivity (Table 3.1). Nevertheless, some trends are found. In particular, an increase in the productivity is observed moving from catalysts with the aldimine ligand to those with the corresponding ketimine (Table 3.1, entry 1 *vs* 3 and 2 *vs* 4). This trend is in agreement with the previous results reported by both Brookhart *et al.* for living alkene copolymerization and Milani and coworkers for Pd-complexes with pyridylimine ligands applied as catalysts for CO/vinyl arene coolymerization.[8,12,13] For both ligands, complexes having the N-N'-S molecule coordinated as a tridentate ligand are more productive than those with the acetonitrile, suggesting the inhibiting role of the latter (Table 3.1, entry 2 *vs* 1 and 4 *vs* 3). This trend is even more pronounced for the triflate derivatives, with **4e** showing a productivity twice as high as that of **4d** and generating the most productive catalyst of the series (Table 3.1, 6 *vs* 5). In addition, even the stability of the relevant catalysts is different: when sulfur atom is directly bonded to the metal center, no Pd(0) is observed, while in the case of the acetonitrile derivatives, the decomposition to inactive palladium metal takes place after 5 h. The higher productivity of the triflate derivative with respect to that one of the hexafluorophosphate species is counterintuitive, being triflate more coordinating than PF_6^-, however the same effect was already observed for Pd-complexes with bidentate pyridylimine ligands when used as catalysts for ethylene/MA cooligomerization.[14]

The NMR analysis of the isolated catalytic products reveals that they are formed by *trans* α,β-unsaturated esters as indicated by the characteristic doublets of triplets at 6.96 ppm assigned to the H^{β} and at 5.83 ppm of the H^{α}, together with traces of *trans* β,γ-unsaturated esters showing the typical resonances at 5.52 ppm for the H^{β} and H^{γ} and the weak signal at 3.03 ppm relative to CH_2^{α} (Figure 3.17).[15]

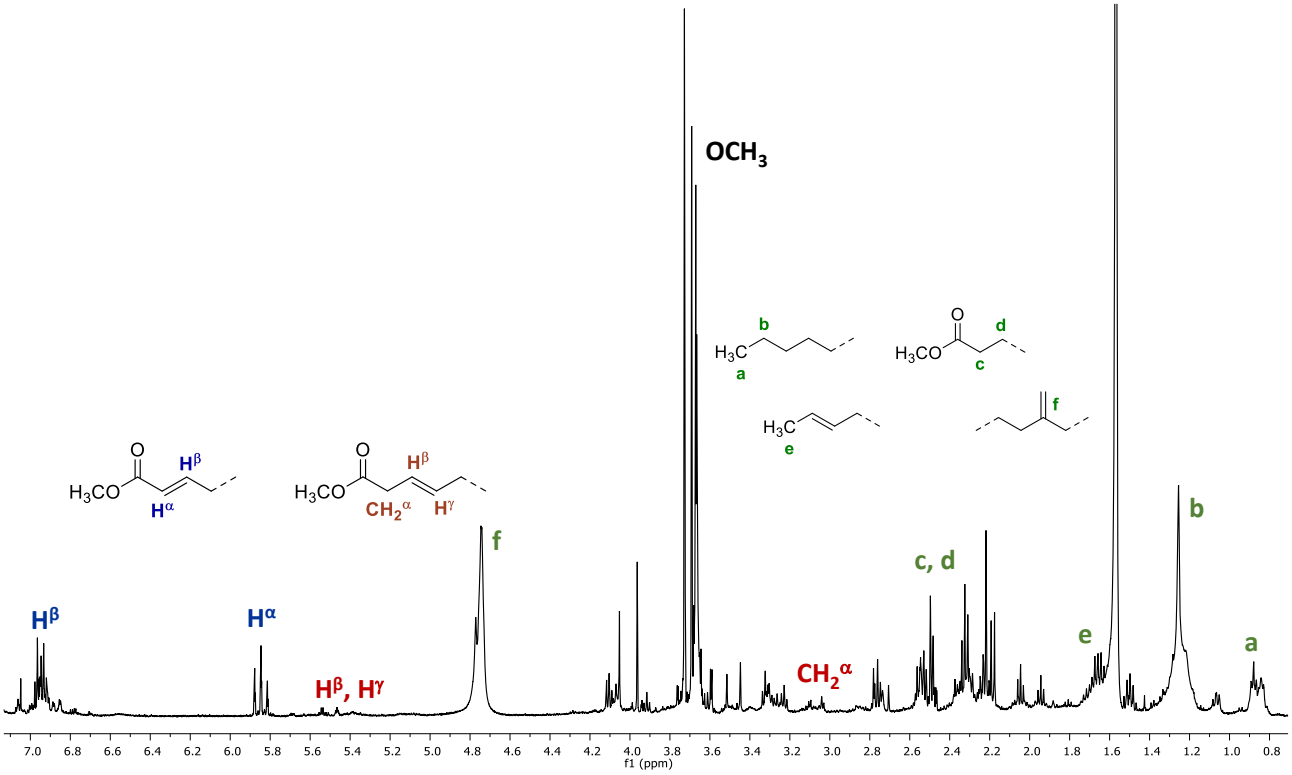

Figure 3.17. ^{1}H NMR spectrum ($CDCl_3$, 298 K) of catalytic products obtained with **4b**.

In addition weak peaks of E/MA cooligomers are observed at 1.32 ppm (CH_2 and CH of the backbone) and at 0.86 ppm (methyl moieties) together with resonances assigned to other aliphatic fragments.[16]

*3.2.5 Reaction of **4b** with the comonomers.*

In order to gain some insights into the mechanism of action of these complexes, some preliminary NMR studies are carried out about the reaction of **4b** with ethylene and with both comonomers. When the gaseous monomer is bubbled for 5 min into a CD_2Cl_2 solution of the complex, in the ^{1}H NMR spectrum recorded after 5 min, no resonances of **4b** are observed, indicating that the complex is completely converted into the active species (Figure 3.18). Some signals are broad suggesting a dynamic process between the acetonitrile and the thiophene pendant arm, but after 15 min the peaks in the aromatic region and the triplets assigned to CH_2 groups become sharp (Figure S3.14).

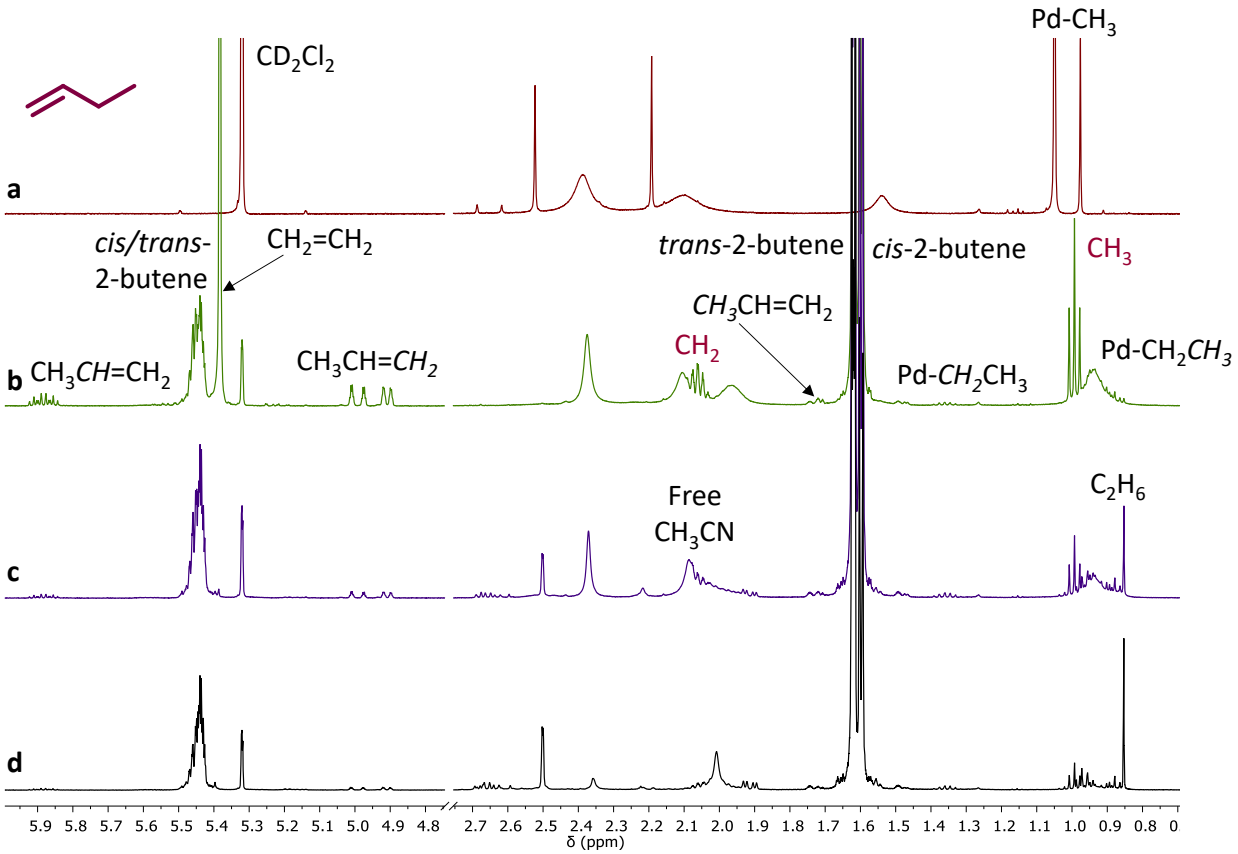

Figure 3.18. ^{1}H NMR spectra (CD_2Cl_2, 298 K) of (a) **4b** and **4b** + ethylene at (b) t = 5 min, (c) t = 30 min and (d) t = 1 h.

In the aliphatic region the triplet at 1.00 ppm (CH_3) and the multiplet at 2.06 ppm are assigned to 1-butene, according to the literature, [17,18] while signals at 1.60 and 1.62 ppm to *cis* and *trans*-2-butene respectively. During the monitoring time of 1 h the intensity of the peaks of *cis/trans*-2-butene changes and the ratio between *cis* and *trans* isomers varies moving from 47:53 at 5 min to 28:72 after 1 h, indicating that the *trans*-2-butene is preferentially formed (Figure 3.19). The weak signal at 1.74 ppm is relative to propene together with the resonances at 4.95 and 5.88 ppm in the vinylic region. In the ^{1}H NMR spectrum recorded after 30 min, together with the previous resonances, the singlet of ethane at 0.86 ppm is present, suggesting that a Pd-CH_2CH_3 intermediate is present in the reaction mixture. Thanks to ^{1}H,^{1}H COSY spectrum (Figure S3.15), a correlation peak between the broad signal at 0.88 ppm and the multiplet at 1.36 ppm is detected relative to the Pd-ethyl species. After 30 min ethylene is all consumed and the signal of free acetonitrile at 2.05 ppm is present. No resonances of free **4** are observed during all the monitoring time.

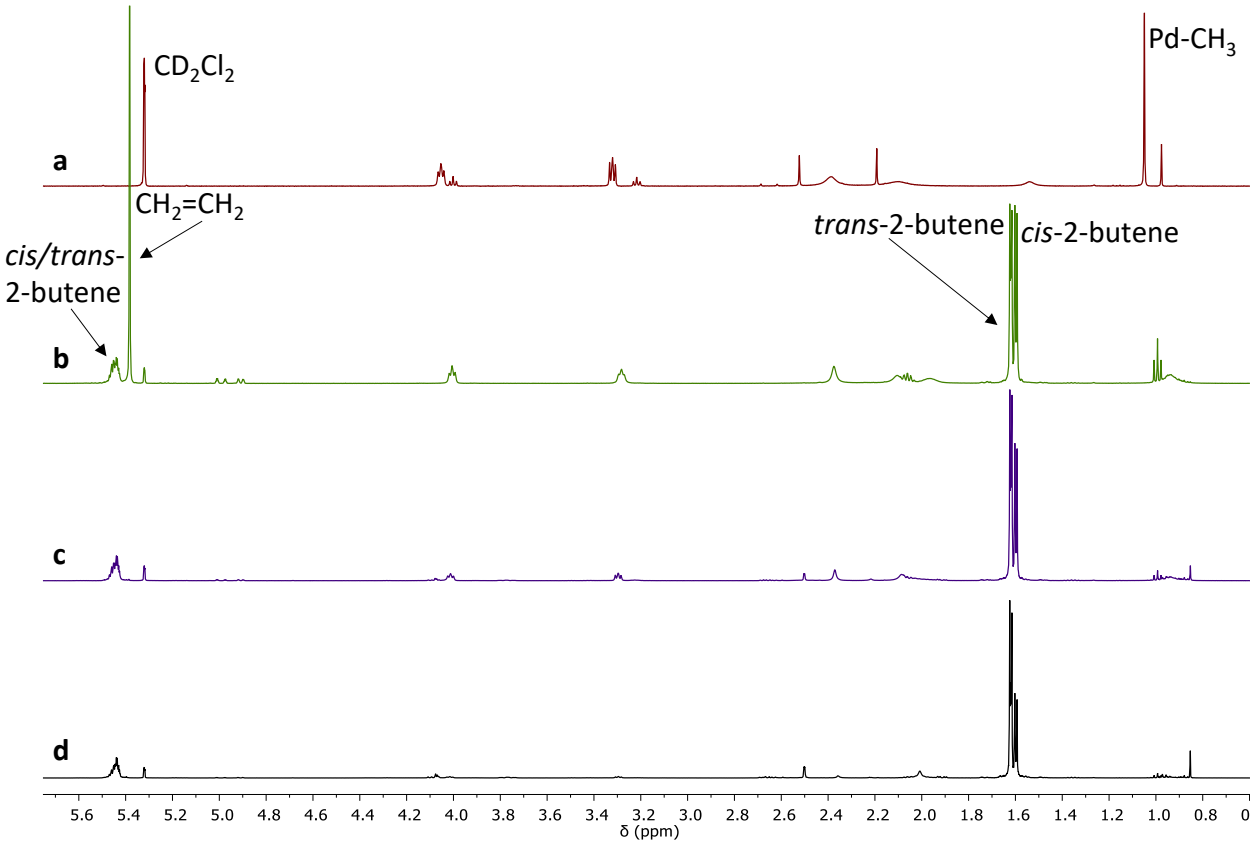

Figure 3.19. ^{1}H NMR spectra (CD_2Cl_2, 298 K) of (a) **4b** and **4b** + ethylene at (b) t = 5 min, (c) t = 30 min and (d) t = 1 h.

When both comonomers, ethylene and methyl acrylate, are added simultaneously to the same CD_2Cl_2 solution of **4b** (Figure 3.20), no resonances of the precursor are observed in the ^{1}H NMR spectrum recorded after 5 min. The reaction with ethylene takes place immediately and resonances assigned to ethane, 1-butene, *cis/trans*-2-butene and propene are observed. Very weak signals of unsaturated esters (e.g. singlets in the range from 3.60 to 3.67 ppm assigned to the OCH_3 group) are present after 15 min from the addition of both comonomers and their intensity does not increase so much for all the monitoring time of 2 h. Almost the entire amount of MA remains unreacted (singlet at 3.72 ppm). No signals of free **4** and palladacycle intermediates are observed, suggesting that the presence of the thiophene pendant arm, together with acetonitrile, disfavor their formation. Further investigations will be performed to give addition information about the role played by the ligand in the fourth coordination site of palladium, either sulfur atom or acetonitrile.

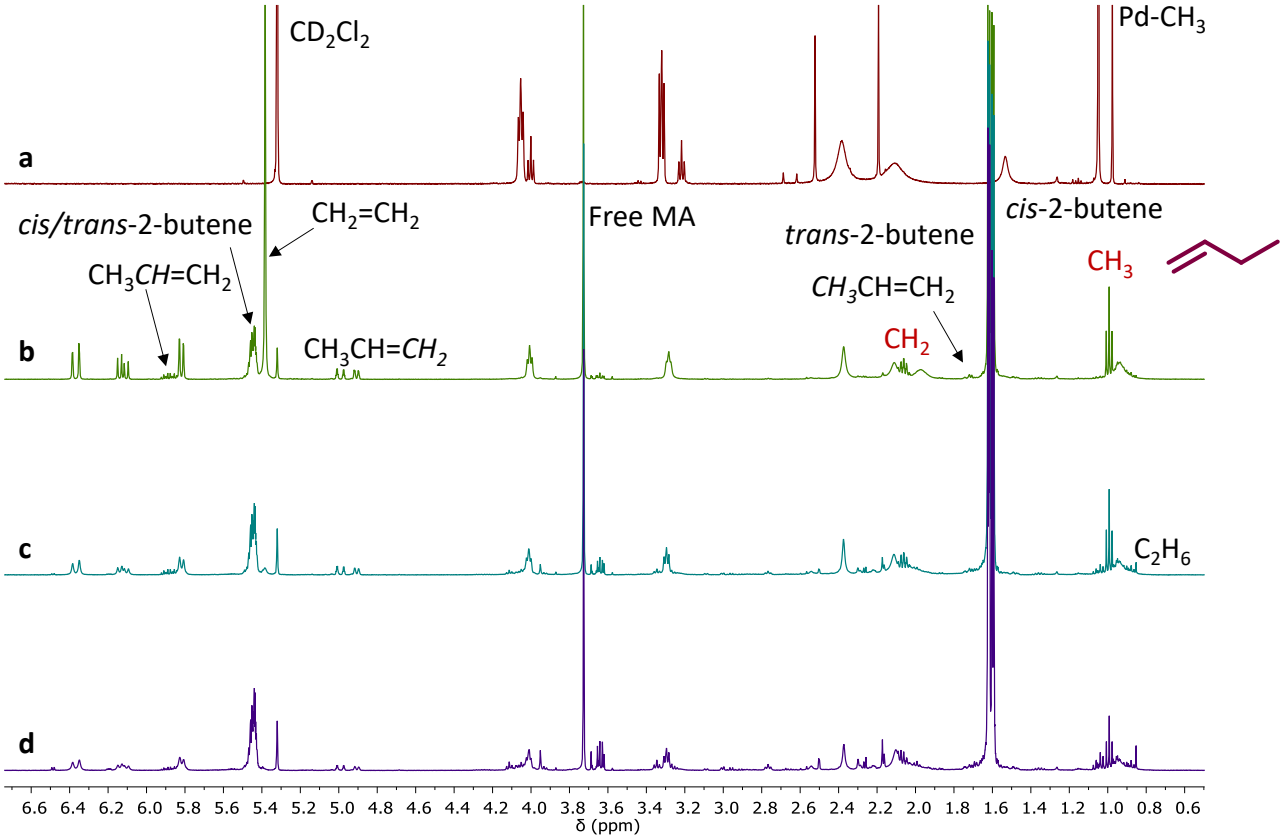

Figure 3.20. ^{1}H NMR spectra (CD_2Cl_2, 298 K) of (a) **4b**; **4b** + ethylene + MA at (b) t = 5 min, (c) t = 1 h and (d) t = 2 h.

On the basis of the NMR studies and the catalytic results a possible mechanism for the reaction of ethylene with MA using this family of Pd(II) complexes is proposed (Scheme 3.6). The Pd(II) compound is activated by the coordination/insertion of ethylene, that takes place immediately leading to propene and to the Pd-H species **II**. On this intermediate, subsequent migratory insertion reactions of ethylene molecules lead to the formation of volatile species, such as ethane, 1-butene and *cis*/*trans*-2-butene.[17] The latter being the main species formed and between the *cis/trans*-2-butene, the *trans* isomer is preferentially obtained. The Pd-ethyl intermediate **III** is detected by NMR spectroscopy at room temperature and it is recognized as the catalyst resting state. The presence in traces of unsaturated esters in both the catalytic products and the *in situ* NMR reactions suggests that when the methyl acrylate is coordinated/inserted into the Pd-alkyl bond, a subsequence β-H elimination takes place avoiding the formation of palladacycle species and generating unsaturated products.

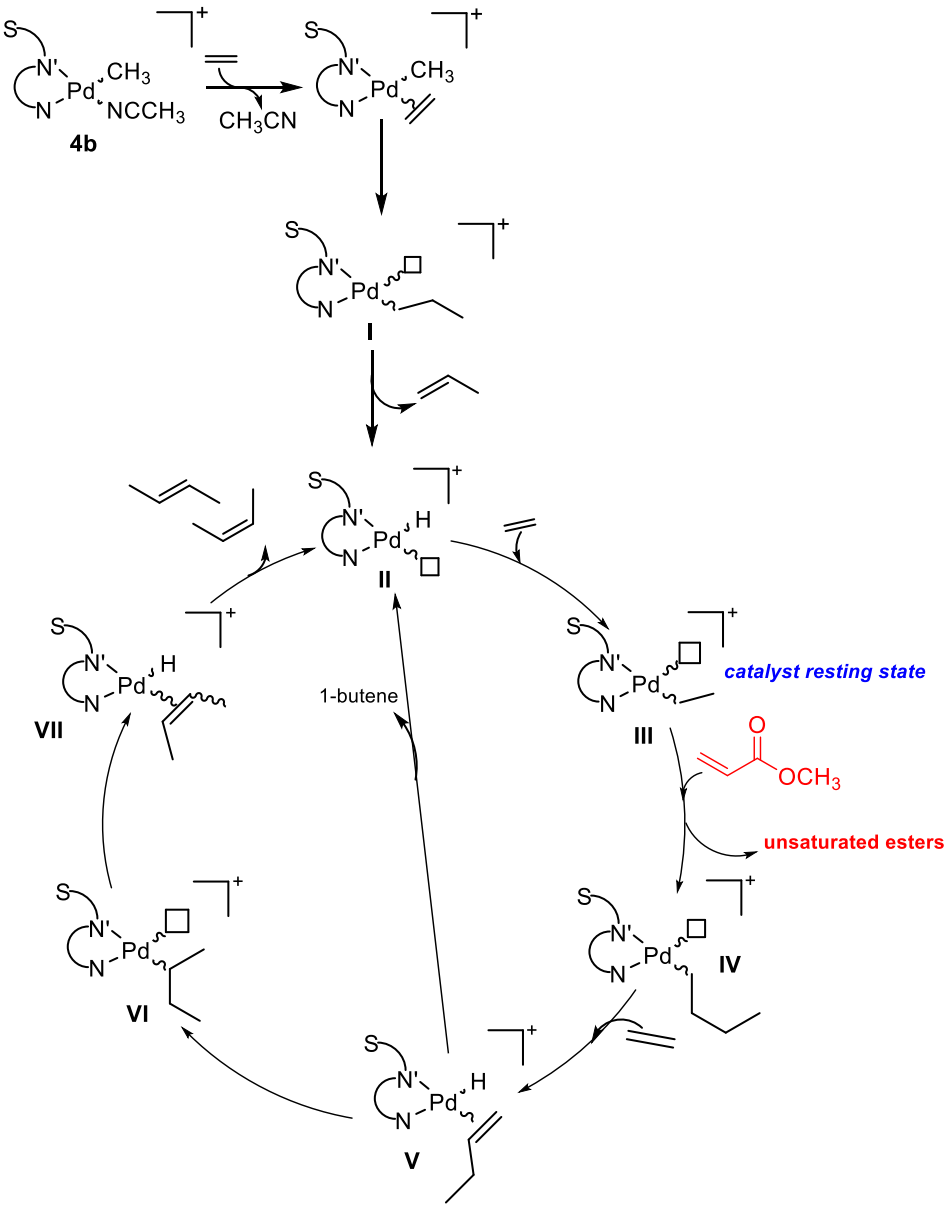

Scheme 3.6. Proposed mechanism for the reaction of Ethylene with MA using **4b**.

3.2 Results and discussion – Part B.

*3.2.6 Synthesis and characterization of aryl-thiophene-diimine ligands **5** – **7**.*

The aryl-thiophene-diimine ligands, **5** – **7**, are synthesized following a two steps procedure based on the reaction of the relevant monoketoimine species with a second amine.[19] Monoketoimines **iPrKI** and **MeKI** are obtained following a reported synthetic route with some slight modifications,[20] based on the condensation reaction of either 2,6-diisopropylaniline or 2,6-dimethylaniline, respectively, with butane-2,3-dione added in a 1:1 molar ratio in *n*-hexane solution together with a few drops of formic acid as catalyst (Scheme 3.7).

The reaction mixture is kept under stirring at room temperature for a proper time (See Experimental Section) and afterwards the solvent is removed under reduced pressure. In the yellow oil of the crude product, the desired compound is present together with the corresponding symmetric α-diimine ligand, **2** or **1** respectively, thus column chromatography purification is required to obtain the pure compound as a yellow oil in good yields (around 60 %).

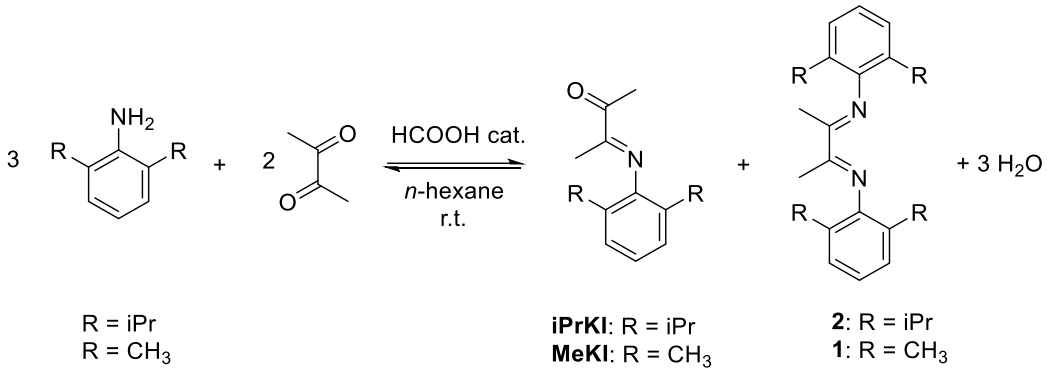

Scheme 3.7. Synthesis of the monoketoimines.

At room temperature the monoketoimines are stable compounds that are characterized by NMR spectroscopy in CD_2Cl_2 solution. Peak assignments are made on the basis of bidimensional spectra analysis. It is of interest to underline that in the ^1H NMR spectra (Figure 3.21) the singlets of the two methyl groups of the DAB skeleton resonate at remarkable different frequencies: 1.78 and 1.75 ppm for that one close to the carbonyl group for **iPrKI** and **MeKI**, respectively and 2.55 ppm in both monoketoimines for CH_3^{DAB} close to the iminic fragment, as confirmed by the cross peaks observed in the ^1H,^{13}C HMBC spectrum (Figure S3.18). The synthesized monoketoimines are also characterized by infrared spectroscopy and the two most relevant bands are due to the C=O and the C=N stretching vibrations, at 1703 and 1651 cm^{-1} respectively, confirming that the isolated species is the mono-condensation adduct (Figures S3.16 and S3.19). Furthermore, the mass spectra show peaks attributed to parent ion and its fragmentation products (Figures S3.17 and S3.20).

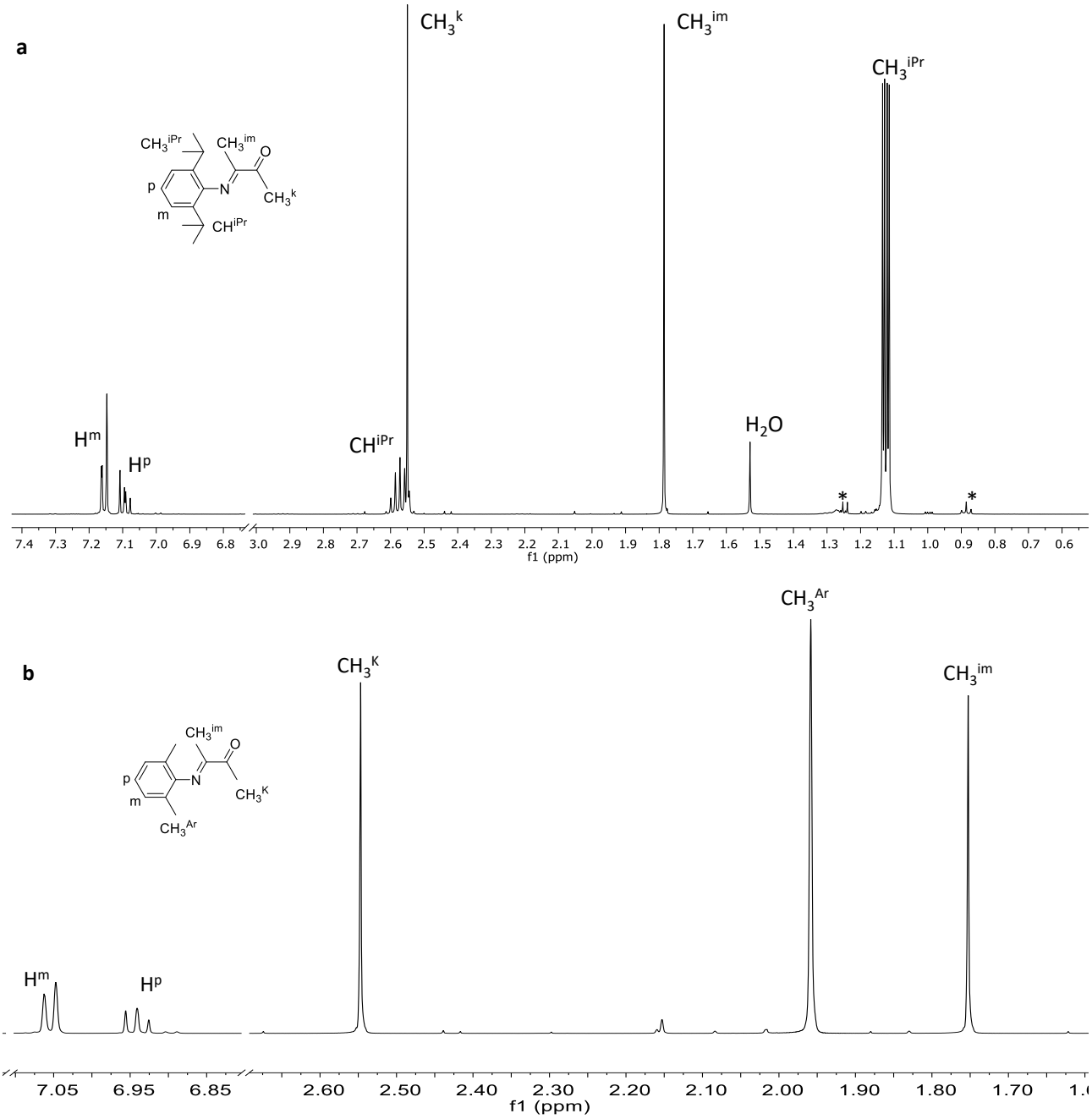

Figure 3.21. ^{1}H NMR spectra (CD_2Cl_2, 298 K) of (a) **iPrKI** and (b) **MeKI**; **n*-hexane.

Since monoketoimines are successfully isolated, the condensation reaction with 2-thiophene ethylamine or 2-thiophene methylamine is performed to obtain the nonsymmetric potentially tridentate ligands, **5**, **6** and **7**, respectively (Scheme 3.8). The synthesis is carried out in a water solution and the mixture is kept under stirring at room temperature for a proper time. After the extraction with cold Et_2O and the treatment with anhydrous sodium sulfate, the desired products are obtained as yellow oils together with an amount of either amine or the unreacted monoketoimine.

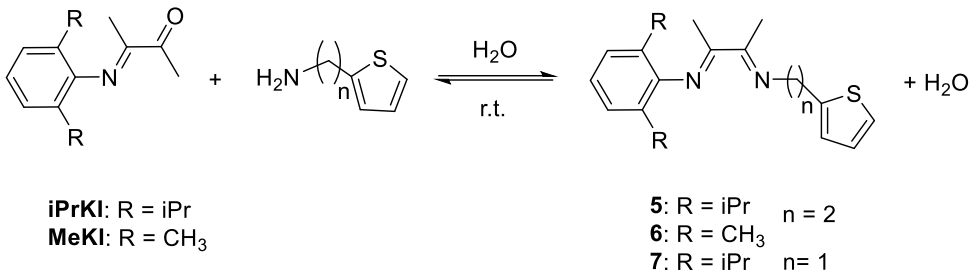

Scheme 3.8. Synthesis of N-N'-S ligands **5** – **7**.

These ligands are synthesized for the first time in this thesis work and they are characterized by mono and bidimensional NMR spectroscopy and ESI-MS (Figures S3.21-S3.26) at room temperature. As an example the ^{1}H NMR spectrum of the ligand **7** (Figure 3.22) is reported and, in addition to resonances of **7**, a set of signals of lower intensity is observed related to unreacted **iPrKI**. The proton-signal assignments are made thanks to the bidimensional NMR analysis: the signal at 1.12 ppm is assigned to the methyl groups on the isopropyl moieties, CH_3^{iPr}, in agreement with the integration and the correlation peak in the ^{1}H,^{1}H COSY spectrum (Figure S3.24) with the septet at 2.64 ppm of CH^{iPr}. In the aliphatic region the other two singlets at 1.92 and 2.33 ppm are relative to CH_3^{DAB1} and CH_3^{DAB2} for the chemical shift value of their carbon atom in the ^{1}H,^{13}C HSQC spectrum (Figure S3.25) and the *long-range* coupling correlation peak in the ^{1}H,^{1}H COSY spectrum between CH_3^{DAB2} and the singlet at 4.89 ppm, assigned to H^{α},H^{β} of the pendant arm. Focusing on the aromatic region, the protons of the thiophene ring, H^3 and H^5, resonate at 7.03 and 7.25 ppm, respectively, for the multiplicity of the signals, the correlation peaks between them and the chemical shift values of their carbon atoms.

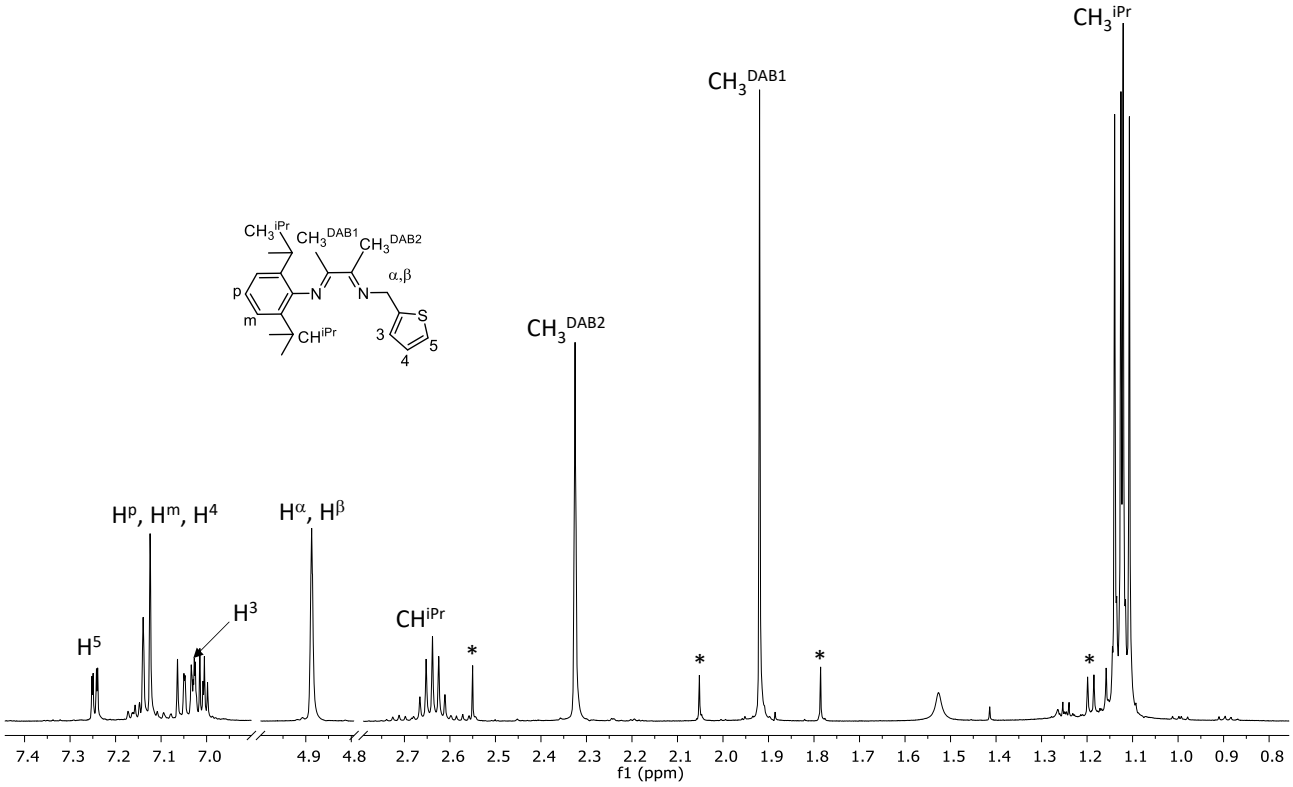

Figure 3.22. ^{1}H NMR spectrum (CD_2Cl_2, 298 K) of **7**;*unreacted **iPrKI** (7.0 mol %).

Ligands **5** and **6** assignments are made in the analogous way of that reported previously (Figures S3.39-S3.46).

Ligand **6** is not stable at room temperature, and in the ^{1}H NMR spectrum recorded after keeping it at 298 K for 24 h, resonances assigned to the symmetric ligand **L35** are observed,[10] together with those of free 2,6-dimethylaniline. The substitution of 2,6-dimethylaniline with 2-thiophene ethylamine takes place, probably due to the presence of an excess of the last one in the crude product (about 30 mol %) (Figure 3.23).

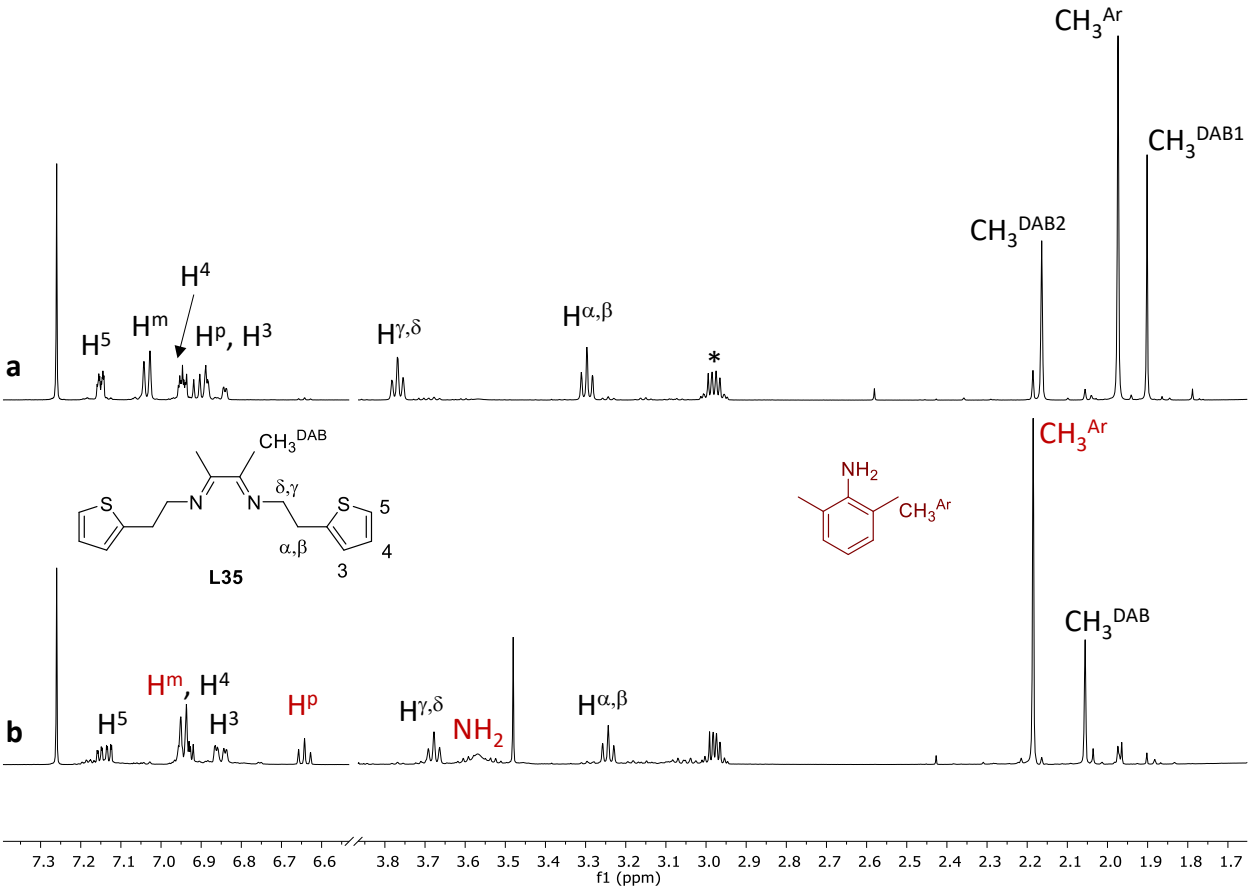

Figure 3.23. ^{1}H NMR spectra ($CDCl_3$, 298 K) of (a) **6** and (b) **6** after t = 24 h at T = 298 K. *2-thiophene ethylamine.

*3.2.7 Synthesis and characterization of neutral Pd(II) complexes **5a** – **7a**.*

The neutral Pd(II) complexes [Pd(CH_3)Cl(N-N′-S)], **5a** – **7a**, are synthesized following the same synthetic route of the previous reported Pd(II) complexes (Section 3.2.2) (Scheme 3.9).

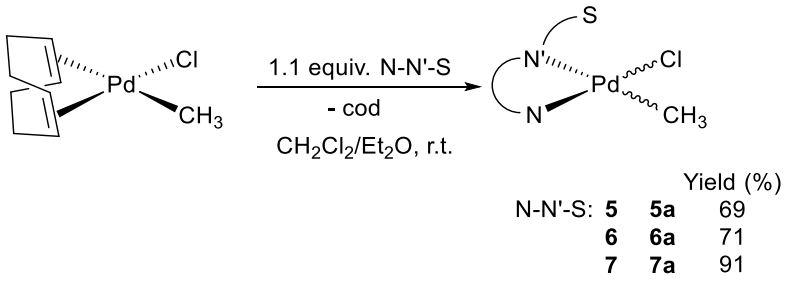

Scheme 3.9. Synthesis of neutral complexes **5a** – **7a**.

Complexes **5a** – **7a** are obtained as orange solids in good and high yields. In analogy with complexes **3a** and **4a**, the inequivalent tridentate ligands **5** – **7** coordinate in a non-equivalent chemical environment, thus two geometrical isomers are possible, depending on the relative position of Pd-CH_3 bond with respect to the two different halves of the ligand.

Conventionally the *trans* isomer is defined as the species having the Pd-CH_3 fragment *trans* to the Pd-N bond, where N is the nitrogen atom bearing the thiophene pendant arm. NMR spectroscopy is the technique of choice to characterize the neutral complexes in solution (Figures S3.26-S3.31) and in the ^{1}H NMR spectra of all complexes only one set of signals is observed, with just other peaks at very low intensity, indicating that only one geometrical isomer is almost present in solution. Thanks to the 1D NOE experiment, performed upon irradiation of the singlet of the Pd-CH_3 fragment, and observing the Overhauser effect with the peaks of the substituents on the aryl ring, the almost exclusively species present in solution is recognized to be the *trans* isomer. The signal to proton assignments are made considering the multiplicity of signals and the bidimensional NMR analysis. As an example the NMR characterization of **5a** is discussed. In the ^{1}H NMR spectrum (Figure 3.24), the singlet at 0.30 ppm is assigned to the Pd-CH_3 fragment, while the singlets at 1.83 and 1.68 ppm to CH_3^{DAB1} and CH_3^{DAB2}, respectively, for the cross peak in the ^{1}H,^{1}H COSY spectrum (Figure S3.28) between the latter and the triplet at 4.20 ppm related to H^{δ},H^{γ} of the pendant arm. As a consequence, the other triplet at 3.51 ppm is attributed to H^{α},H^{β}. Focusing on the aryl ring, the septet at 3.02 ppm, assigned to CH^{iPr}, shows correlation peaks with the doublets at 1.31 and 1.12 ppm (CH_3^{iPr}) in the ^{1}H,^{1}H COSY spectrum. Protons of the thiophene ring are assigned thanks to some correlation peaks in the ^{1}H,^{1}H COSY spectrum and the chemical shift of their carbon atoms in the ^{1}H,^{13}C HSQC spectrum (Figure S3.29): the doublet of doublets at 7.19 ppm is due to H^5, the multiplets at 6.94 ppm to H^4 and the signal at 6.90 ppm is related to H^3.

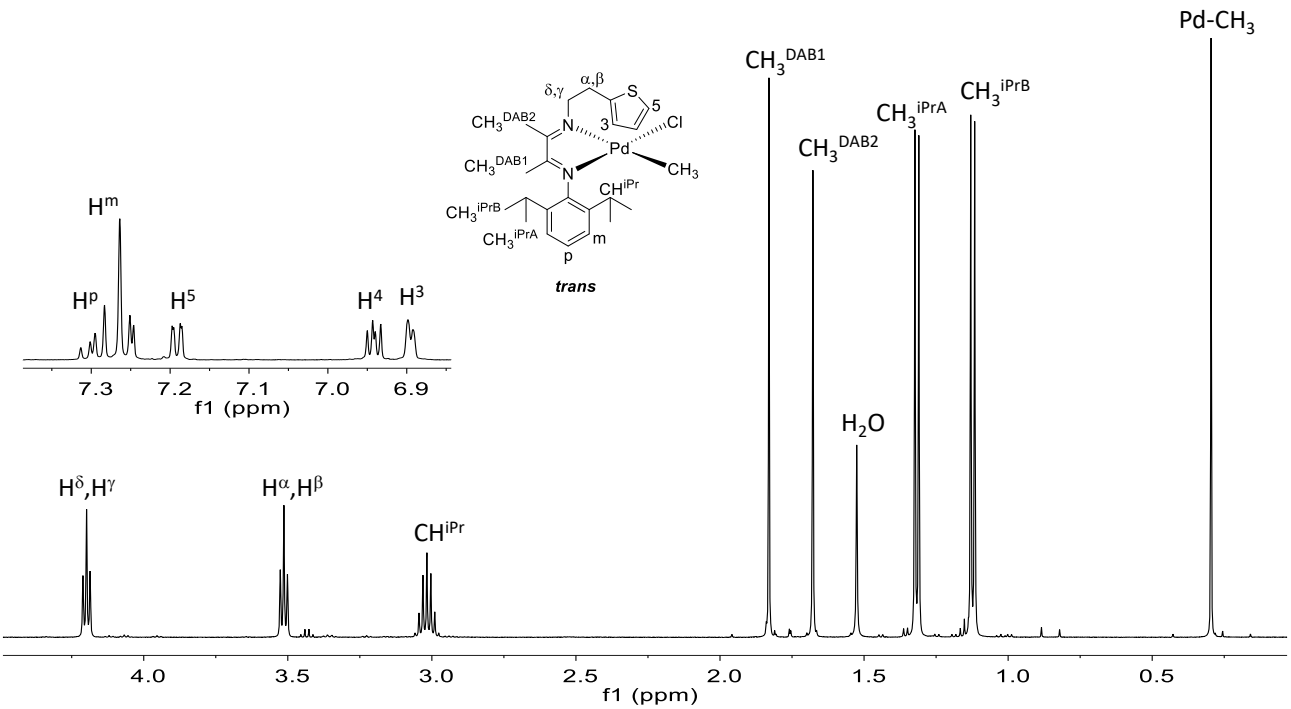

Figure 3.24. ^{1}H NMR spectrum (CD_2Cl_2, 298 K) of **5a**.

Upon stratification of *n*-hexane on the CD_2Cl_2 solution of **5a** and **7a**, after one week at 277 K, single crystals, suitable for X-ray analysis, are obtained. The structural analysis of **5a** shows the presence of only the *trans* isomer in the unit cell, corresponding to the dominant species observed in solution (Figure 3.25a). While for **7a**, two independent molecules are present in the unit cell both related to the *trans* isomer, that differ for the orientation of the sulfur atom. In one case it is opposite with respect to the metal center and in the other it points towards the palladium ion with a population distribution about 61 and 39 %, respectively (Figure 3.25b).

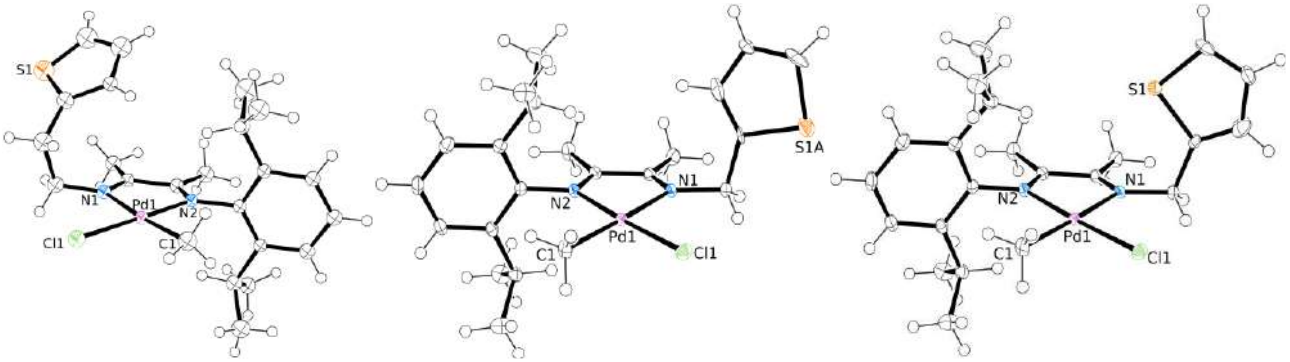

(a) (b)

Figure 3.25. ORTEP drawing (50% probability ellipsoids) of the molecule of (a) *trans*-**5a** and (b) *trans*-**7a** in the crystal structure.

The Pd(II) ions show the expected square planar geometry and the aryl-thiophene-diimine ligands are bonded as bidentate ligands through nitrogen atoms, forming with the metal center a bite angle of 78.0(2)° for *trans*-**5a** and 77.42(4)° for *trans*-**7a** (Table S3.3) in agreement with the reported values for 5-membered palladacycle.[21] According to the expected higher *trans* influence of the Pd-CH_3 bond with respect to that of the Pd-Cl bond, in both neutral complexes the Pd-N bond *trans* to Pd-CH_3 fragment is remarkably longer (Pd1-N1 of 2.125(5) Å for *trans*-**5a** and 2.1262(9) Å for *trans*-**7a**) than the other Pd-N bond length (Pd1-N2 of 2.030(5) Å and 2.0365(9) Å for *trans*-**5a** and *trans*-**7a**, respectively). The aryl ring is almost orthogonally with respect to the metal plane forming with the latter a dihedral angle of 86.0(2)° for *trans*-**5a** and of 86.31(3)° for *trans*-**7a**. In the solid structure drawings of *trans*-**5a** the thiophene fragment is less twisted out from the palladium plane with respect to that of *trans*-**7a** forming a dihedral angle with the metal plane [S1]···[Pd1] of 35.8(3)° for *trans*-**5a** and 79.6(3)° for *trans*-**7a**. This might be due to the presence of different pedant arm length either ethyl or methyl CH_2 bridge on the N-N'-S ligand. In all cases no interactions between the palladium ion and the sulfur atom are observed.

The coordination of the N-N'-S ligand to palladium ion is confirmed by some factors: the increase in number of signals relative to CH_3^{iPr} groups for **5a** and **7a** with respect to the free ligand and the shift of both CH_3^{DAB} singlets and protons of the thiophene pendant arm to higher frequencies (Figures 3.26, S3.32 and S3.33). Considering that the Pd-CH_3 signal is a probe for assessing the electron properties of ligands bonded to the metal center,[8,22] a correlation between its chemical shift and the ligands steric and electronic properties is observed.

For **5a** and **7a** the resonances of Pd-CH_3 fragments of the two geometrical isomers are very similar (0.30 ppm for *trans*-**5a** *vs* 0.33 ppm *trans*-**7a** and 0.88 *vs* 0.90 ppm for *cis*-**5a** and *cis*-**7a**, respectively), suggesting that **5** and **7** show a similar Lewis basicity. This is confirmed also by the study of the solid state structures of the Pd(II) complexes under investigation, in particular by the values of Pd-N bond distances (Table S3.3). In addition, moving from *trans* to *cis* isomer, the Pd-CH_3 singlet shifts to higher frequencies due to the fact that in the *trans* isomer it falls in the shielding cone of the aryl ring (Table 3.2).[12]

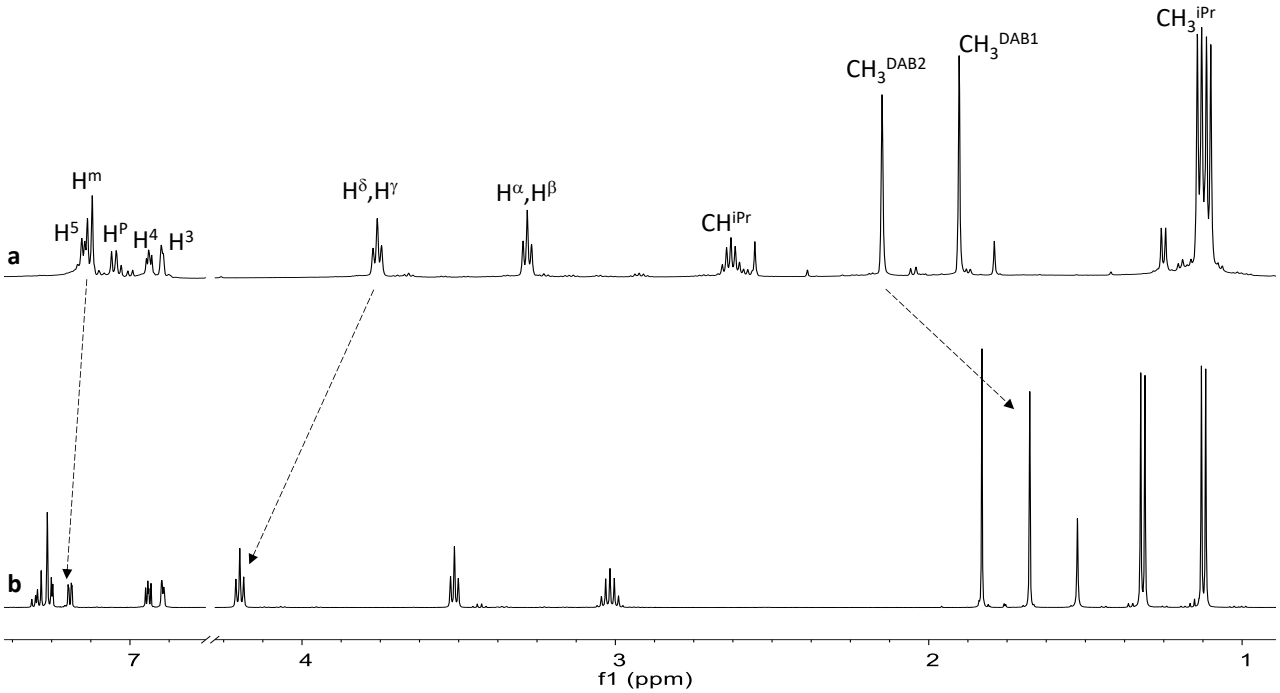

Figure 3.26. ^{1}H NMR spectra (CD_2Cl_2, 298 K) of (a) **5** and (b) **5a**.

Table 3.2. Selected chemical shifts (ppm) for free ligands and neutral complexes [a]

entry	compound	Pd-CH_3	H^{α},H^{β}	H^{δ},H^{γ}	H^3	H^5
1	**5**	---	3.28	3.79	6.90	7.12
2	**5a**	0.30(*trans*), 0.88(*cis)*	3.51	4.20	6.90	7.19
3	**6**	---	3.27	3.73	6.89	7.15
4	**6a**	0.18(*trans*)	3.48	4.18	6.91	7.19
5	**7**	---	4.89	---	7.03	7.25
6	**7a**	0.33(*trans*), 0.90(*cis)*	5.41	---	7.26	7.31

[a] ^{1}H NMR spectra in CD_2Cl_2 at 298 K, 10 mM solution of the compound.

*3.2.8 Synthesis and characterization of the cationic Pd(II) complexes **5b** – **7b** and **5c** – **7c**.*

The monocationic complexes [Pd(CH_3)($NCCH_3$)(N-N'-S)][PF_6], **5b** – **7b**, and [Pd(CH_3)(N-N'-S)][PF_6], **5c** – **7c**, are synthesized through the dehalogenation reaction of the corresponding neutral compounds **5a** – **7a** using $AgPF_6$ dissolved in either dry acetonitrile for series **b** or CH_2Cl_2 for series **c** (Scheme 3.10). They are all isolated upon concentration and precipitation with cold diethyl ether as yellow solids with yields ranging from 72 to 83 %.

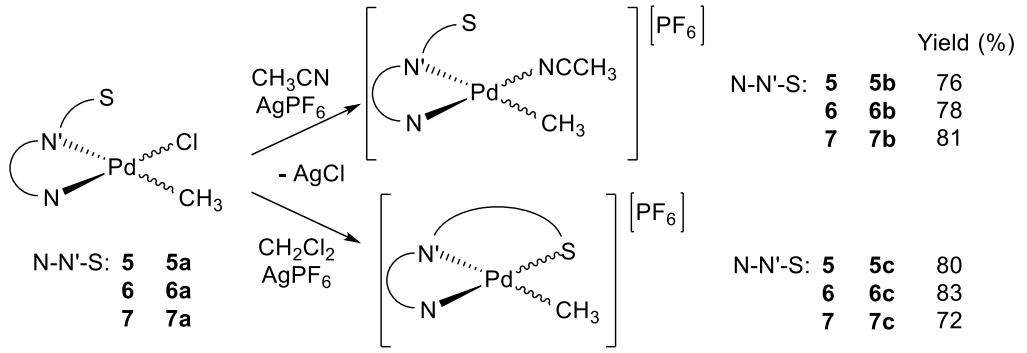

Scheme 3.10. Synthesis of cationic complexes **5b** – **7b** and **5c** – **7c**.

The cationic complexes have all been characterized in solution by NMR spectroscopy, in CD_2Cl_2, at room temperature. In the ^{1}H NMR spectrum of **5b** recorded immediately after the dissolution of the complex, two sets of signals are observed, meaning that both geometrical isomers are present in solution. Some resonances assigned to the major species are broad (Figure 3.27).

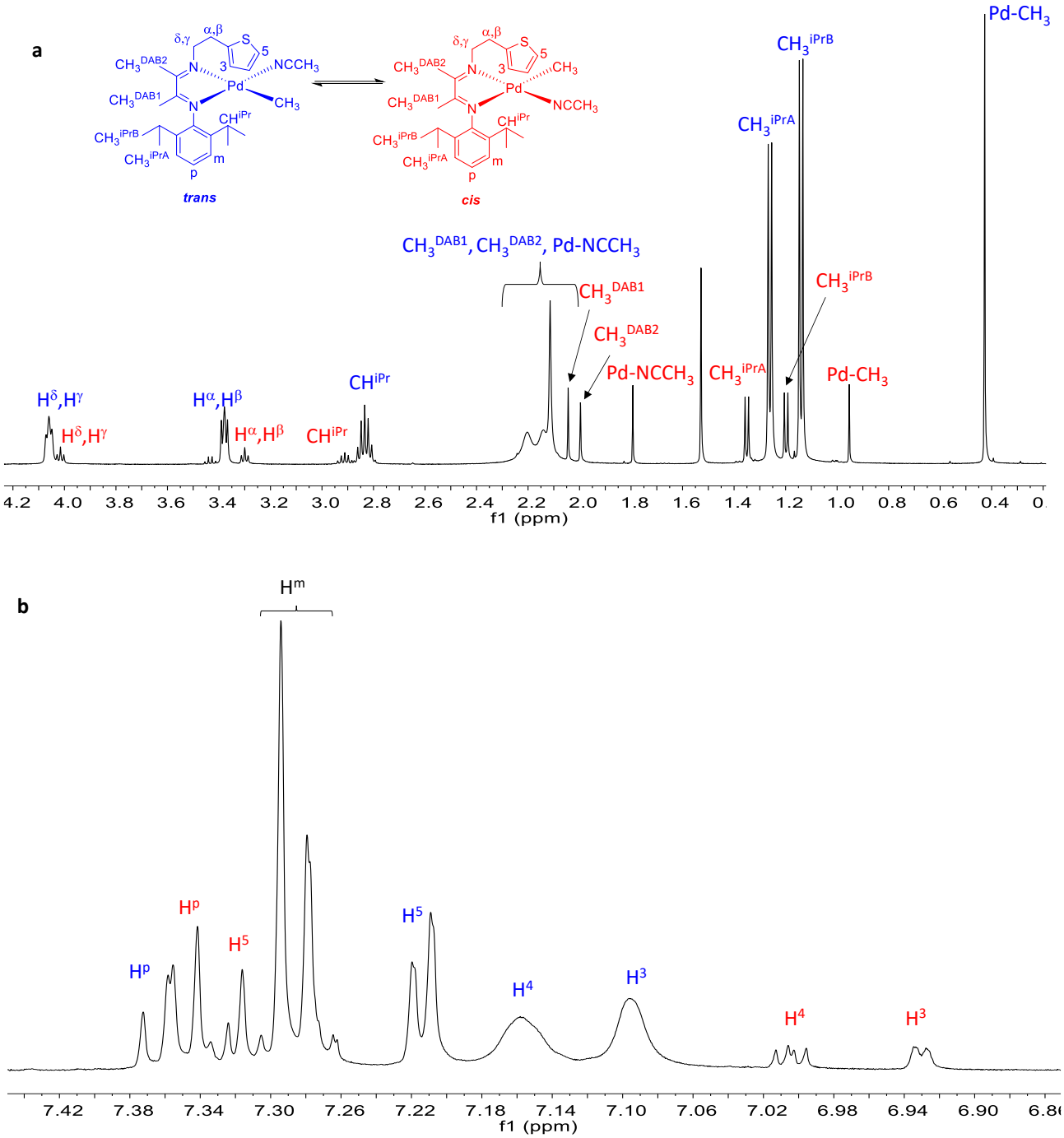

Figure 3.27. ^{1}H NMR spectrum (CD_2Cl_2, 298 K) of **5b**; (a) aliphatic and (b) aromatic region.

In the aliphatic region the characteristic signals of Pd-CH_3 fragment (0.95 ppm and 0.43 ppm), the septet of CH^{iPr} at 2.91 and 2.83 ppm and CH_2 groups of the pendant arm, in the range from 3.10 to 4.10 ppm, are easily assigned. The *trans* isomer is recognized to be the major species (86 %) present in solution on the basis of the cross peak, due to the Overhauser effect, between the Pd-CH_3 group at 0.43 ppm and the doublet of CH_3^{iPr} at 1.23 ppm, present in the $^{1}H,^{1}H$ NOESY spectrum (Figure 3.28).

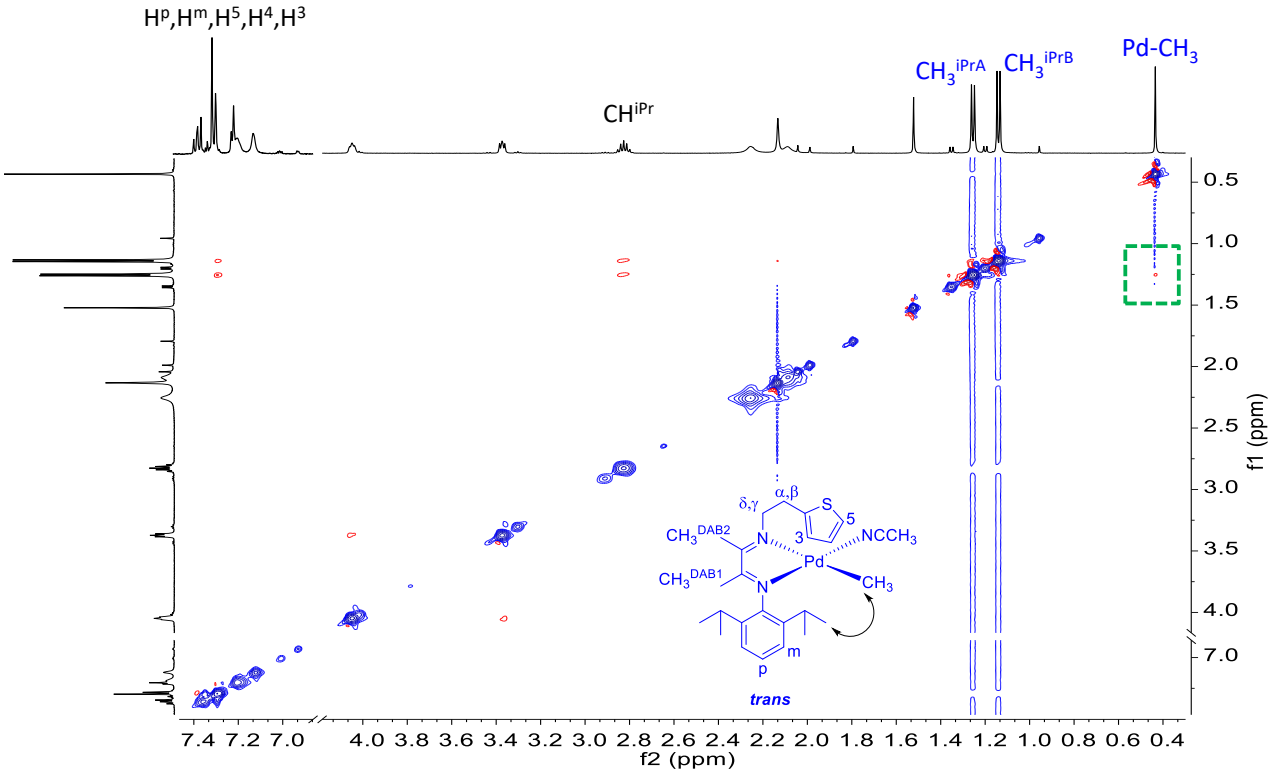

Figure 3.28. $^{1}H,^{1}H$ NOESY spectrum (CD_2Cl_2, 298 K) of **5b**.

Considering **7b** (Figure 3.29), the multiplicity and the integrals of peaks in the ^{1}H NMR spectrum allowed to assign each signal to its proton. The Pd-CH_3 fragment of the major species is associated to the singlet at 0.41 ppm, the two doublets at 1.14 and 1.28 ppm to CH_3^{iPr} moieties and the singlets at 2.13 and 2.45 ppm to the methyl groups of the DAB skeleton. The singlets assigned to the Pd-$NCCH_3$ fragment at 2.26 ppm and to H^{α},H^{β} at 5.24 ppm of the major species are a little bit broad, as resonances of H^3 and H^4 of the thiophene ring.

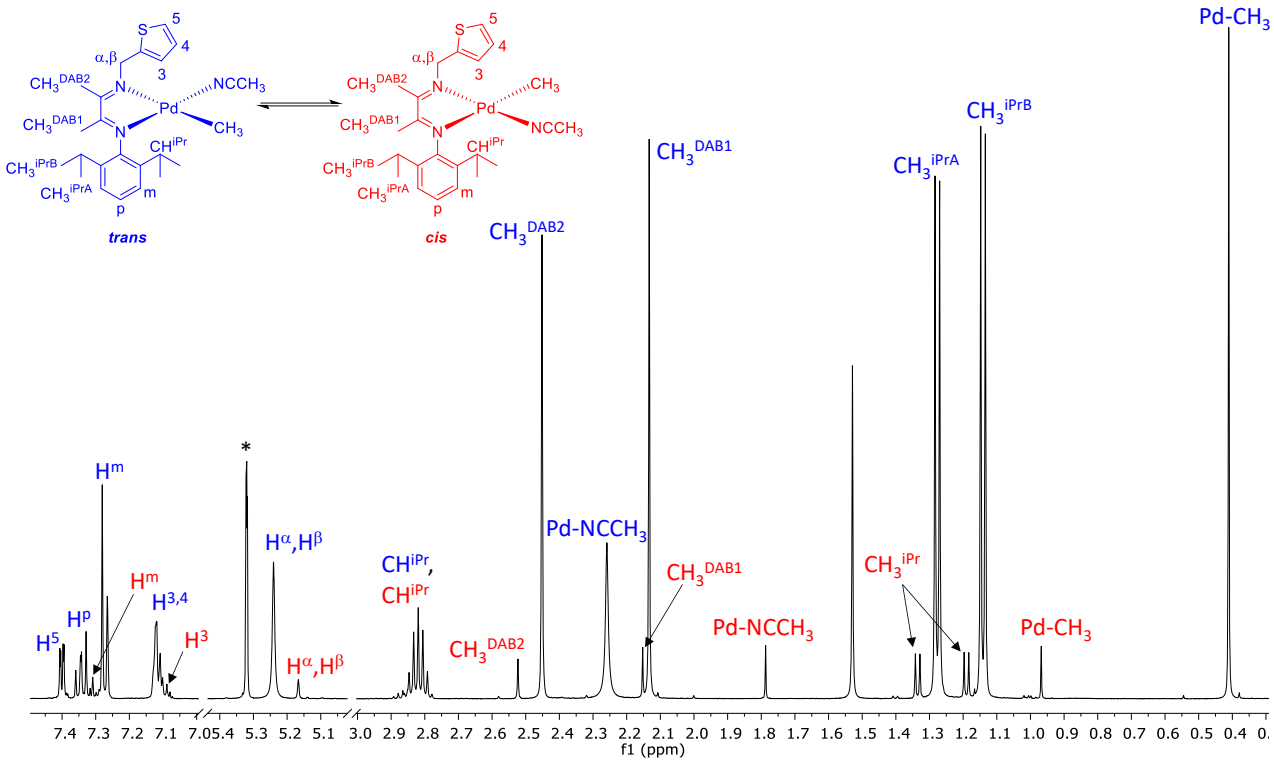

Figure 3.29. ^{1}H NMR spectrum (CD_2Cl_2, 298 K) of **7b**.

Also in this case the *trans* isomer is recognized to be the major species (93 %) present in solution on the basis of the cross peak, due the Overhauser effect, between the Pd-CH_3 group at 0.41 ppm and the doublet of CH_3^{iPr} at 1.28 ppm, present in the $^{1}H,^{1}H$ NOESY spectrum. In addition, an exchange peak relative to signals of Pd-$NCCH_3$ fragment of the two geometrical isomers indicates that the two species are in equilibrium at slow rate on the NMR time scale at room temperature (Figure 3.30).

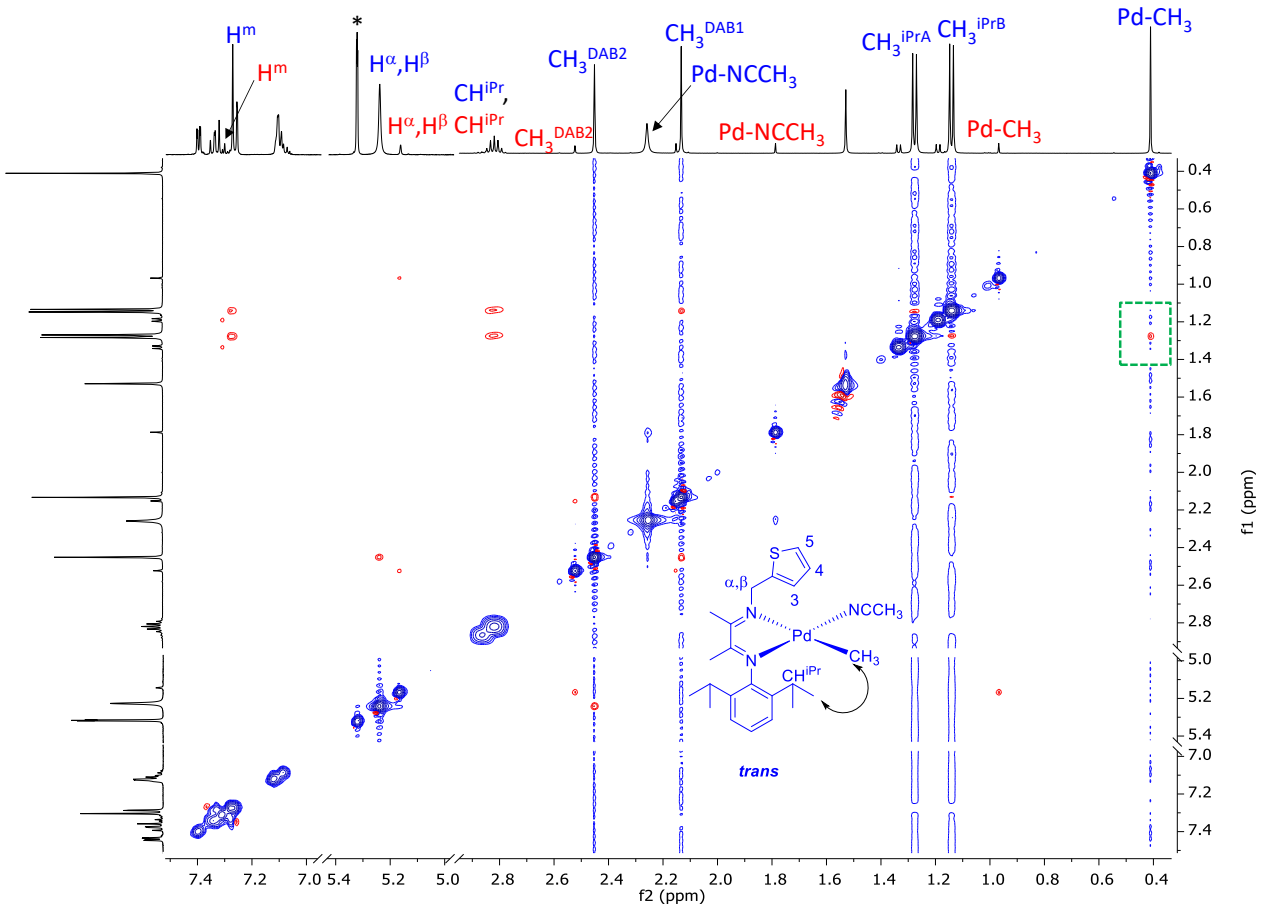

Figure 3.30. ^{1}H,^{1}H NOESY spectrum (CD_2Cl_2, 298 K) of **7b**.

The temperature is a key parameter to carry out the synthesis of **7b**, in fact when it is performed at lower temperature than 298 K, a dimeric species of palladium [Pd(CH_3)(**7**)]$_2$[μ-Cl][PF_6] is formed. Its presence is confirmed by the characterization both in solution by NMR spectroscopy and in solid state by X-ray analysis. In the ^{1}H NMR spectrum of the crude product (Figure 3.31), resonances of *cis* and *trans*-**7b** are present together with new signals at 0.18 and 4.88 ppm, assigned, thanks to bidimensional NMR analysis (Figure S3.35), to Pd-CH_3 fragment and H$^{\alpha}$,H$^{\beta}$ of the thiophene pendant arm of the dimeric species. The ratio among them is *cis*-**7b**:*trans*-**7b**:dimeric species = 21:77:2.

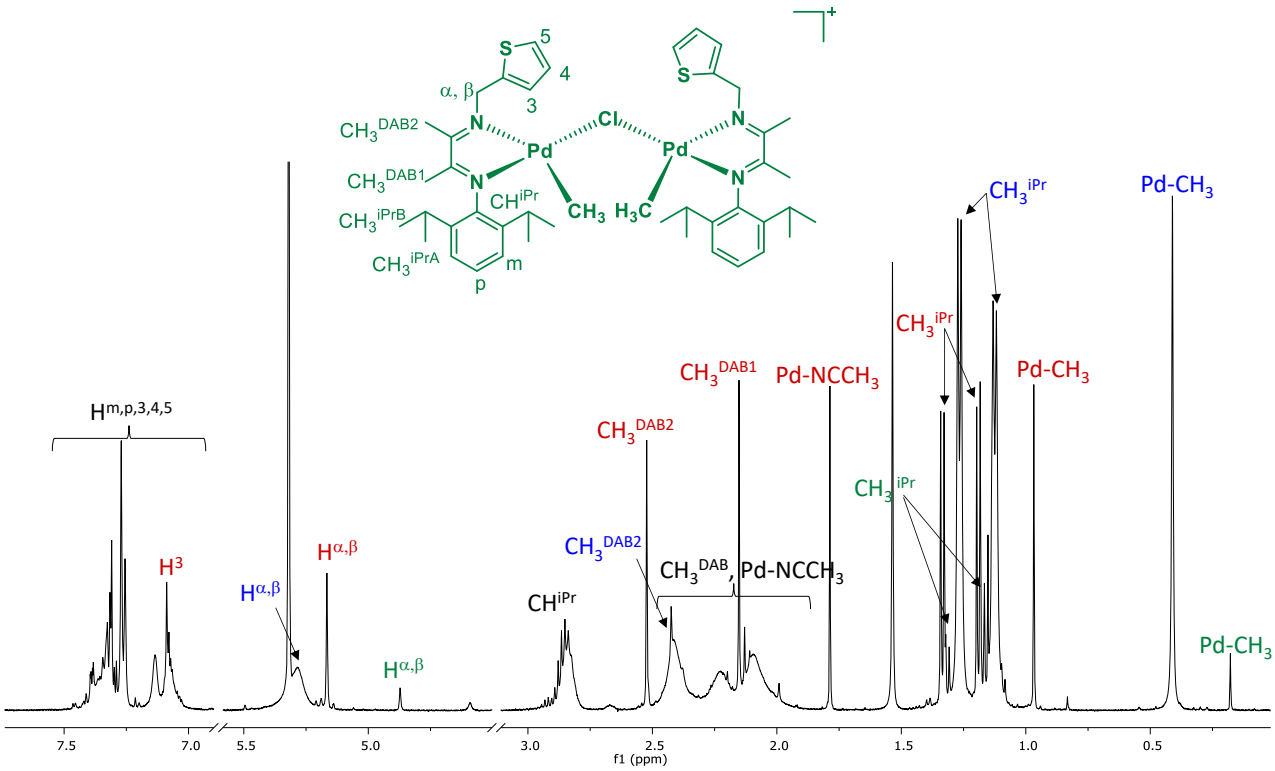

Figure 3.31. ^{1}H NMR spectrum (CD_2Cl_2, 298 K) of crude product of **7b**.

Suitable single crystals for X-Ray analysis are obtained with a double layer technique (CD_2Cl_2/*n*-hexane solution) (Figure 3.32) and in the unit cell only one molecule, relative to $[Pd(CH_3)(\mathbf{7})]_2[\mu\text{-}Cl][PF_6]$ species, is present. Its charge is confirmed by the presence of only one molecule of PF_6^-. The palladium ions show the expected square planar geometry with the N-N'-S ligands coordinate as bidentate ones through nitrogen atoms forming with the metal plane a similar bite angle of 77.75(5)° and 77.07(5)° for each halves. According to the expected higher *trans* influence of the Pd-CH_3 bond than that of the Pd-Cl bond, the Pd-N bond in *trans* to Pd-CH_3 fragment is remarkably longer than the other Pd-N bond length (Pd1-N11 of 2.1418(13) Å *vs* Pd1-N12 of 2.0420(12) Å; Pd2-N21 of 2.1464(13) Å *vs* Pd2-N22 of 2.0353(113) Å). The sulfur atom of each single fragment shows different orientation: the sulfur S21 points towards the palladium ion, while S11 towards the methyl groups of the DAB skeleton. The distance Pd2···S21 is about 3.782(11) Å suggesting no interactions between them. The aryl rings are almost orthogonally with respect to the metal plane in both fragments forming with the latter dihedral angles of 82.85(3)° and 89.61(4)°.

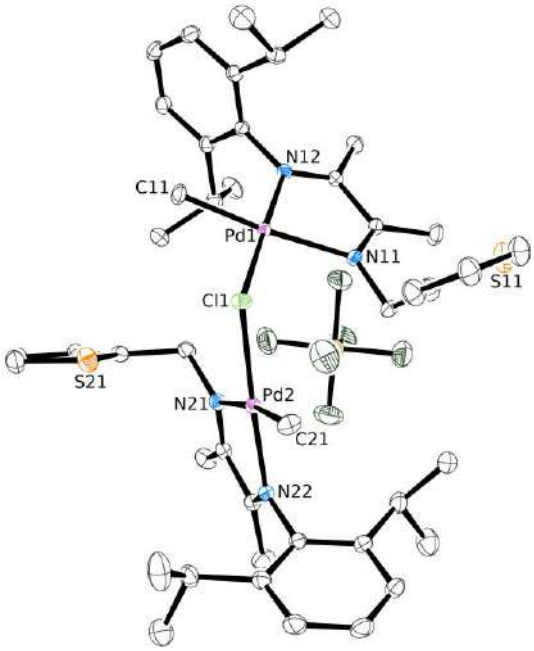

Figure 3.32. ORTEP representation (50% probability ellipsoids) of the molecule of dimeric species in the crystal structure. The hydrogen atoms have been omitted for the sake of clarity. Selected bond distances (Å) and angles (°): Pd1-C11 2.0237(16), Pd1-Cl1 2.3292(4), Pd1-N11 2.1418(13), Pd1-N12 2.0420(12), Pd2-C21 2.0284(15), Pd2-Cl1 2.3314(5), Pd2-N21 2.1464(13), Pd2-N22 2.0353(13), Pd1-S11 5.2644(15), Pd2-S21 3.782(11), C11-Pd1-Cl1 86.74(5), C11-Pd1-N11 172.02(6), C11-Pd1-N12 94.27(6), N11-Pd1-Cl1 101.24(4), N12-Pd1-Cl1 178.98(4), N12-Pd1-N11 77.75(5), C21-Pd2-Cl1 86.46(5), C21-Pd2-N21 170.94(6), C21-Pd2-N22 94.02(6), N21-Pd2-Cl1 102.52(4), N22-Pd2-Cl1 177.04(4), N22-Pd2-N21 77.07(5), Pd1-Cl1-Pd2 114.808(17); dihedral angles: [Pd1]---[Ph1] 82.85(3), [Pd1]---[S11] 65.45(6), [Pd2]---[Ph2] 89.61(4), [Pd2]---[S21] 80.69(4), [Pd1]---[Pd2] 76.01(3).

The broadness of some resonances of *trans* isomer in the ^{1}H NMR spectra of cationic Pd(II) complexes **5b** – **7b** highlights the presence of the analogues dynamic process discussed for **3b** and **4b** involving the *trans* species. It concerns the competition between the thiophene fragment and the acetonitrile in the fourth coordination site of palladium, as suggested by the broadness of the signals of some protons of the thiophene ring. It is more emphatic in **5b** and **6b**, rather than in **7b** for the length of the pendant arm and the neighbour between bonded CH_3CN and the thiophene ring. To have some additional information about this, progressive additions of acetonitrile are made to a 10 mM CD_2Cl_2 solution of **5b** and the reaction is monitored on time at room temperature (Figure 3.33).

An increase in the acetonitrile amount brings to (*i*) the shift to lower frequencies of singlets of CH_3^{DAB} and signals of H^3 and H^4 of *trans* isomer, (*ii*) the narrowing of peaks and (*iii*) a variation in the isomer distribution (from *cis*:*trans* = 14:86 for **5b** to *cis*:*trans* = 29:71 for **5b** after the addition of 3 eq. of CH_3CN). The same investigation is performed starting from a **6b** CD_2Cl_2 solution and the same results are obtained.

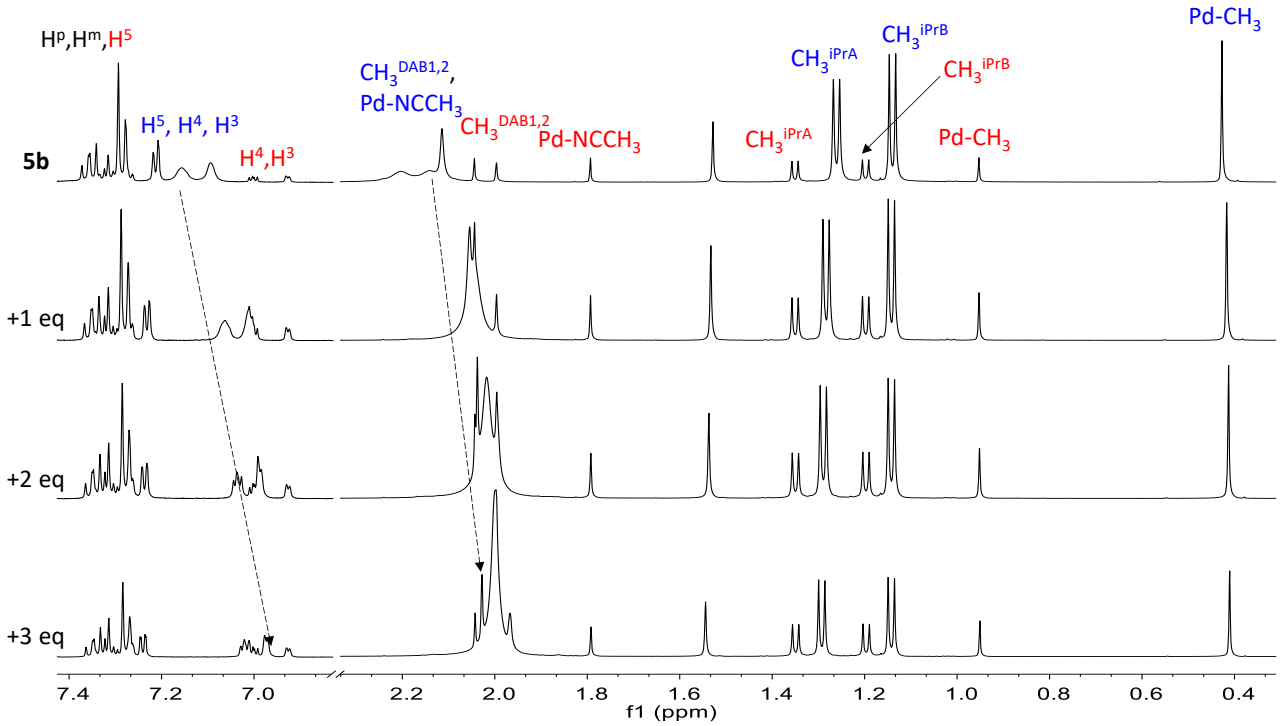

Figure 3.33. ^1H NMR spectra (CD_2Cl_2, 298 K) of progressive additions of acetonitrile to **5b** solution; aliphatic and aromatic region not on scale.

This suggests the presence of a third species in solution, in equilibrium with the *trans* isomer, characterized to have in the palladium coordination sphere the sulfur atom instead of the acetonitrile molecule leading to the cationic complexes of general formula $[Pd(CH_3)(N\text{-}N'\text{-}S)][PF_6]$.

So, Pd(II) complexes with tridentate N-N'-S ligands, **5c** – **7c**, are synthesized (Scheme 3.10), obtained as light yellow and light brown solids in good yield (72 – 83 %) and characterized in solution by NMR spectroscopy (Figures S3.72-S3.79). In the ^1H NMR spectra only one set of narrow signals is present and the proton-signal assignments are made in analogy with the previous cationic complexes of the same family and with **3c** and **4c**. As an example in the ^1H NMR spectrum of **5c** (Figure 3.34), the singlet at the lowest frequencies is assigned to Pd-CH_3 fragment (0.44 ppm), while the doublets at 1.13 and 1.25 ppm to CH_3^{iPr} and the septet at 2.81 ppm to CH^{iPr}. From bidimensional NMR analysis, the triplets at 3.36 and 4.02 ppm are related to H^{α},H^{β} and H^{δ},H^{γ}, respectively, and the latter shows a

correlation peak in the $^{1}H,^{1}H$ COSY spectrum (Figure S3.36) with the singlet at 2.37 ppm of CH_3^{DAB2}. The other singlet at 2.18 ppm is assigned to CH_3^{DAB1}.

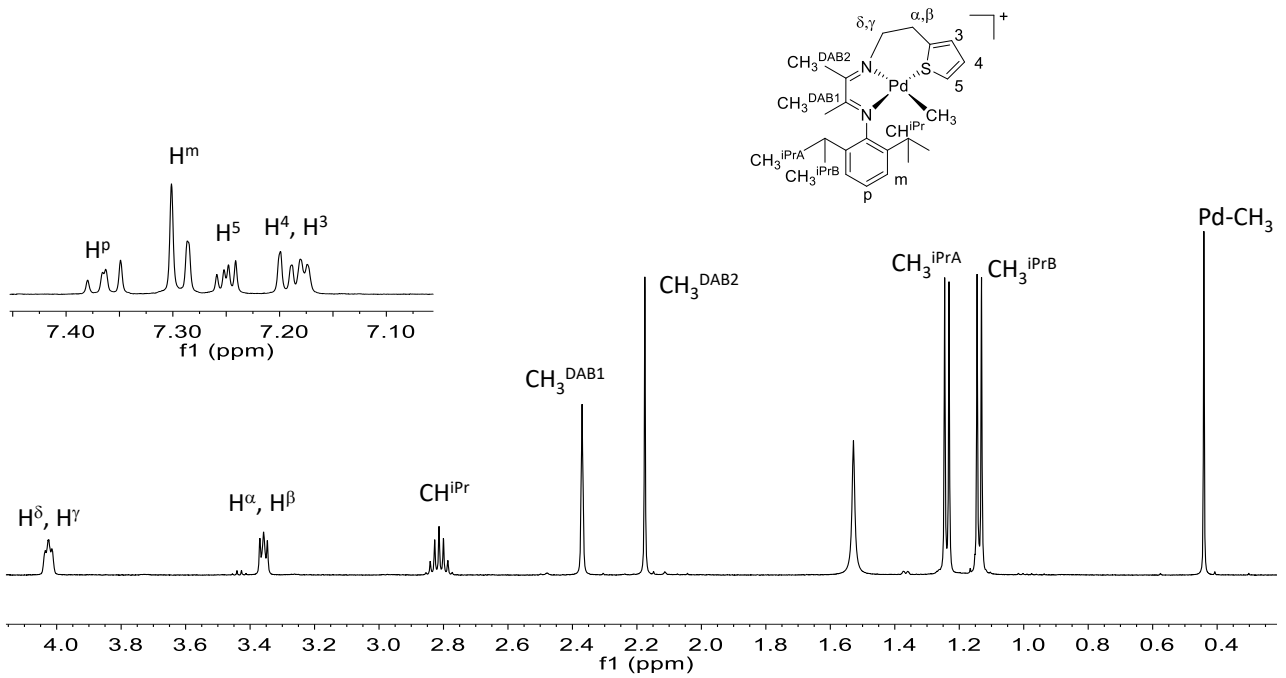

Figure 3.34. ^{1}H NMR spectrum (CD_2Cl_2, 298 K) of **5c**.

By comparing ^{1}H NMR spectra of both neutral and cationic Pd(II) complexes (Table 3.3), some considerations are explained:

- the chemical shift of the singlet of Pd-CH_3 fragment of cationic compounds is independently from the presence of the acetonitrile or the sulfur atom in the fourth coordination site of palladium; moving from neural to cationic complex, bearing the same N-N'-S ligand, a shift of the under investigation signal to higher frequencies is observed for all samples, suggesting that it is influenced exclusively by the charge of the complex. The same behaviour is observed for the resonances of the CH_3 groups of DAB skeleton;
- the signal of H^{α},H^{β} is shifted to lower frequencies moving from the neutral complex to the respective acetonitrile derivative and at the end to compound with N-N'-S as a tridentate ligand for the closer proximity of the thiophene fragment with the metal center;
- the signal of H^5, considering the chemical shift values of its proton and carbon atom, in the [Pd(CH_3)(N-N'-S)][PF_6] species resonances at higher frequencies with respect to the parent neutral compound confirming the interactions between the sulfur and the metal center (Table 3.3).

Table 3.3. Selected chemical shifts (ppm) for neutral and cationic complexes [a]

entry	compound	Pd-CH_3 [b]	H^{α},H^{β}	H^5	
				^1H	^{13}C
1	**5a**	0.30	3.51	7.19	125.0
2	**5b**	0.43	3.38	7.38	128.8
3	**5c**	0.44	3.36	7.25	134.6
4	**6a**	0.18	3.48	7.19	124.9
5	**6b**	0.32	3.35	7.20	129.1
6	**6c**	0.33	3.34	7.14	134.5
7	**7a**	0.33	5.41	7.31	127.7
8	**7b**	0.41	5.24	7.40	126.3
9	**7c**	0.43	5.01	7.43	127.8

[a] ^1H NMR spectra in CD_2Cl_2 at 298 K, 10 mM solution of the compound; [b] for series **a** and **b** only the Pd-CH_3 chemical shift of *trans* isomer is considered.

Single crystals of **5c** are obtained upon *n*-hexane slow diffusion into the CD_2Cl_2 solution of the complex and they are suitable for X-Ray analysis (Figure 3.35). The expected square planar geometry is observed for Pd ion with N-N'-S bonded as a tridentate ligand through the two nitrogen atoms and the sulfur one. By comparing the typical Pd(II) complexes bearing α-diimine bidentate ligands, the value of the bite angle N1-Pd1-N2 of 78.1(4)° is in agreement with those reported in literature.[8] Focusing on the half with thiophene pendant arm of **5**, a 6-membered metallacycle is formed and the N1-Pd1-S1 angle, about 100.7(3)°, is remarkably higher than the typical one present in the square planar geometry. It might be due to the distortion of the thiophene ring which forms a dihedral angle [S1]···[Pd1] of 59.2(3)° with the metal plane. For the higher *trans* influence of Pd-CH_3 fragment, the bond Pd1-N1 length is longer with respect to Pd1-N2 distance (2.139(9) Å *vs* 2.067(9) Å). Considering all solid state structures obtained for [Pd(CH_3)(N-N'-S)][PF_6] series, **3c** and **4c** (Figure 3.16) and **5c**, the highest value of the bond distance Pd1-S1 is reached for **5c** of 2.286(4) Å, with respect to those reported for **3c** and **4c** (2.2683(5) Å and 2.2612(1) Å, respectively). While by comparing the solid state structures of *trans*-**5a** (Figure 3.23a) with that of **5c** the bond distances Pd-C1 and Pd-N1 are similar: Pd-C1 of 2.027(8) Å for *trans*-**5a** *vs* 2.03(2) Å for **5c**; Pd-N1 of 2.139(9) Å *vs* 2.12(1) Å for *trans*-**5a** and **5c**, respectively. On the other hand, the Pd-N2 distance is higher for **5c** (2.06(6) Å) with respect to that of *trans*-**5a** (2.030(5) Å) suggesting that the coordination of the sulfur atom to the metal center produces a distortion of the entire N-N'-S ligand.

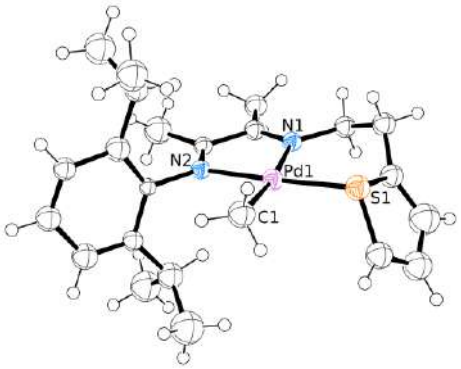

Figure 3.35. ORTEP representation (50% probability ellipsoids) of the molecule of **5c** in the crystal structure. The PF_6^- anion has been omitted for the sake of clarity. Selected bond distances (Å) and angles (°): Pd1-C1 2.03(2), Pd1-S1 2.286(4), Pd1-N1 2.139(9), Pd1-N2 2.067(9), C1-Pd1-S1 84.7(4), C1-Pd1-N1 174.4(6), C1-Pd1-N2 96.5(5), N1-Pd1-S1 100.7(3), N2-Pd1-S1 176.2(3), N2-Pd1-N1 78.1(4); dihedral angles [Ph]---[Pd1] 86.3(3), [S1]---[Pd1] 59.2(3).

*3.2.9 Ethylene/methyl acrylate cooligomerization with the Pd(II) complexes **5b** – **7b** and **5c** – **7c**.*

All cationic Pd(II) complexes **5b** – **7b** and **5c** – **7c** are tested as precatalysts in the cooligomerization reaction of ethylene with methyl acrylate (Figure 3.36, Tables 3.4 and 3.5). Catalysis are performed with the *mass flow control* device keeping constant the ethylene pressure during the reaction at 2.5 bar. The cooligomerization are performed at 308 K monitored for 6 h with a [MA]/[Pd] of 594. TFE is the solvent of choice. Their catalytic behavior is compared with that of the symmetric compounds, $[Pd(CH_3)(NCCH_3)(N\text{-}N)][PF_6]$, with N-N as **1** or **2**. Compounds $[Pd(CH_3)(N\text{-}N'\text{-}S)][PF_6]$, **5c** – **7c**, are also tested carrying out catalysis in dichloromethane (DCM) under the same reaction conditions. At the end of the catalysis, the mixture is concentrated under reduced pressure to remove volatile species and dried in vacuum. Catalytic products are isolated as yellow oils. They are characterized in $CDCl_3$ solution by NMR spectroscopy at room temperature to determinate the macromolecule microstructure and in particular the amount of inserted polar monomer and the degree of branching.

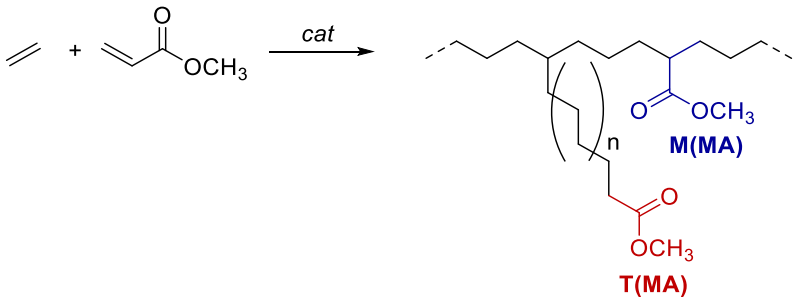

Figure 3.36. Ethylene/methyl acrylate cooligomerization reaction.

Table 3.4. Ethylene/methyl acrylate cooligomerization: effect of N-N'-S ligand and CH_3CN. Precatalyst: $[Pd(CH_3)(L)(N\text{-}N/N\text{-}N'\text{-}S)][PF_6]$ [a]

entry	N-N/ N-N'-S	L	yield (mg)	kg P/mol Pd[b]	MA (mol %)[c]	TON[d]		Bd[e]	M_n (Da)[f]
						E	MA		
1	**5**	CH_3CN	282.0	13.44	4.1	423	18	86	313
2		---	243.4	11.59	4.4	361	17	82	304
3	**6**	CH_3CN	213.9	10.18	6.2	301	20	88	294
4		---	238.6	11.40	5.9	340	21	91	304
5	**7**	CH_3CN	79.8	3.80	6.4	112	8	91	364
6		---	64.2	3.06	6.3	90	6	82	379
7	**2**	CH_3CN	2137.4	101.78	1.0	3519	35	100	81.2[g]
8	**1**	CH_3CN	1391.7	66.27	3.6	2095	79	93	24.6 [g]

[a] Reaction conditions: $n_{Pd} = 2.1 \cdot 10^{-5}$ mol, $V_{TFE} = 21$ mL, $V_{MA} = 1.130$ mL, [MA]/[Pd] = 594, $P_{Et} = 2.5$ bar, T = 308 K, t = 6 h. [b] Productivity in kg P/mol Pd = kilograms of product per mol of palladium calculated on isolated yield. [c] Amount of inserted MA in mol % calculated by ^{1}H NMR spectroscopy on isolated product. [d] Turnover number = mol of substrate converted per mol of Pd. [e] Branching degree expressed as number of branches per 1000 carbon atoms. [f] Calculated by ^{1}H NMR spectroscopy on isolated product.[16, 23] [g] Determined by GPC analysis (kDa).

Table 3.5. Ethylene/methyl acrylate cooligomerization: effect of N-N'-S ligand. Precatalyst: $[Pd(CH_3)(N\text{-}N'\text{-}S)][PF_6]$ [a]

entry	N-N'-S	yield (mg)	kg P/mol Pd[b]	MA (mol %)[c]	TON[d]		Bd[e]	Mn (Da)[f]
					E	MA		
1	**5**	238.1	11.33	4.2	356	69	69	271
2	**6**	176.7	8.41	5.9	251	16	74	269
3	**7**	54.7	2.60	4.1	82	3	80	325

[a] Reaction conditions: $n_{Pd} = 2.1 \cdot 10^{-5}$ mol, $V_{DCM} = 21$ mL, $V_{MA} = 1.130$ mL, [MA]/[Pd] = 594, $P_{Et} = 2.5$ bar, T = 308 K, t = 6 h. [b] Productivity in kg P/mol Pd = kilograms of product per mol of palladium calculated on isolated yield. [c] Amount of inserted MA in mol % calculated by ^{1}H NMR spectroscopy on isolated product. [d] Turnover number = mol of substrate converted per mol of Pd. [e] Branching degree expressed as number of branches per 1000 carbon atoms. [f] Calculated by ^{1}H NMR spectroscopy on isolated product.[16, 23]

This is the first time that Pd(II) complexes bearing an α-diimine unsymmetric ligand with an aliphatic moiety bonded to one nitrogen atom are applied as precatalysts in the ethylene/methyl acrylate copolymerization. All tested Pd(II) complexes generate active species for the target reaction under mild reaction conditions in both solvents.

The structure of the N-N'-S ligand affects the productivity and a remarkable decrease is observed moving from Pd(II) complexes with a symmetric α-diimine (Table 3.4, entries 7 and 8) to the new family of compounds. The productivity decreases moving from isopropyl to methyl substituents on the aryl ring (Table 3.4, entries 1,2 *vs* 3,4) in agreement with experimental data reported in literature for symmetric ligands **2** and **1**.[24] Moreover a decrease is observed moving from compounds with thiophene-ethyl to ones having the thiophene-methyl pendant arm: the complexes with **5** and **6** ligands are more productive than the analogues with only one CH_2-bridge (**7**). In TFE, the presence of CH_3CN in the fourth coordination site of palladium in **5b** and **7b** increases the productivity reaching the value of 13.44 kg P/mol Pd when **5b** is the precatalyst of the reaction. In DCM the Pd(II) complex with the same N-N'-S ligand, but having the sulfur atom directly bonded to the metal center, **5c**, is the most active with a productivity value of 11.33 kg P/mol Pd. No significant different in productivity is observed for **5c** moving from DCM to TFE (11.59 kg P/mol Pd).

The amount of inserted methyl acrylate is higher with respect to that reported using Brookhart catalysts and it is in the range of 4.1 – 6.4 mol % (Table 3.4). The highest values are shown when catalysis are carried out with **7b** and **7c** as precatalysts in TFE (Table 3.4, entries 5 and 6) and the presence of either CH_3CN or the sulfur atom in the fourth coordination site does not affect so much the content of MA.

The NMR characterization of the catalytic products points out that they are branched macromolecules with the values of the Bd in the range 69 – 91 per 1000 carbon atoms. When the Pd(II) complexes with N-N'-S ligands are used, the Bd is lower with respect to obtained macromolecules with **1b** and **2b**, suggesting that the chain walking process after the insertion of ethylene is slowed down. The second coordination sphere might be responsible for this: the sulfur atom competes with the gaseous monomer for the coordination on the *cis* site to the growing polymeric chain (GP) on the metal center or the thiophene pendant arm can interact with the hydrogen atoms in the beta position of GP directly bonded to the Pd ion (Figure 3.37).

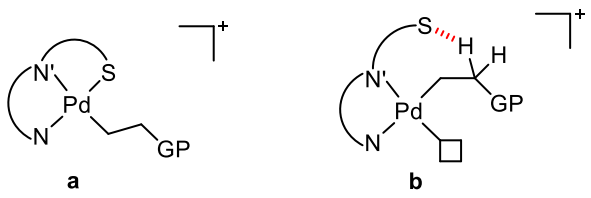

Figure 3.37. Possible mechanisms involved to slow down the chain walking process: (a) the direct coordination of the sulfur atom to Pd(II) ion or (b) the interaction between the β-H of the growing polymeric chain (GP) and the sulfur atom of the ligand.

The last interaction was supposed in the ethylene homopolymerization of Ni(II) and Pd(II) complexes bearing benzothiophene substituents on the aryl rings of the bidentate N-N ligand (**L31**) under mild reaction condition in terms of temperature (T = 293 K).[25] This suggestion is in agreement with the trend of the degree of branching of catalytic products obtained in TFE that are higher than ones relative to macromolecules produced in DCM, despite the catalyst. In the fluorinated solvent, a H-bond network might be present between the OH group of TFE and the sulfur atom preventing the involvement of the latter in an interaction with the β-H of GP, favoring the chain walking process.

The values of M_n are calculated from ^{1}H NMR spectra of isolated products and they indicate that E/MA cooligomers are obtained with respect to E/MA copolymers obtained with **1b** and **2b**.[16, 23] In TFE higher M_n values are observed with respect to those obtained in DCM and the same trend is reported for copolymers synthetized with Pd(II) complexes bearing the thiophenimine ligand in the fourth coordination site, [Pd(CH_3)(N-S)(**1**)][PF_6], (Chapter 2).[1] When **7c** is used as precatalyst, the M_n highest value is reached of 379 Da according to the literature for the presence of isopropyl groups on the aryl ring.[24]

The stability of precatalysts is monitored by the formation of Pd(0) during catalysis. An abundant amount of inactive palladium black is present in the catalysis reactor after 2 h when complexes bearing CH_3CN are used, while only traces are observed with [Pd(CH_3)(N-N'-S)][PF_6] compounds in both solvents.

In the ^{1}H NMR spectra of catalytic products a set of resonances is present with an intense broad signal in the vinylic region and a singlet of inserted methyl acrylate at 3.67 ppm, confirming the cooligomeric nature of the catalytic products, analogously to those obtained with Pd(II) complexes with either Ar-BIAN or pyridylimine ligands (Figure 3.38).[14,17,21]

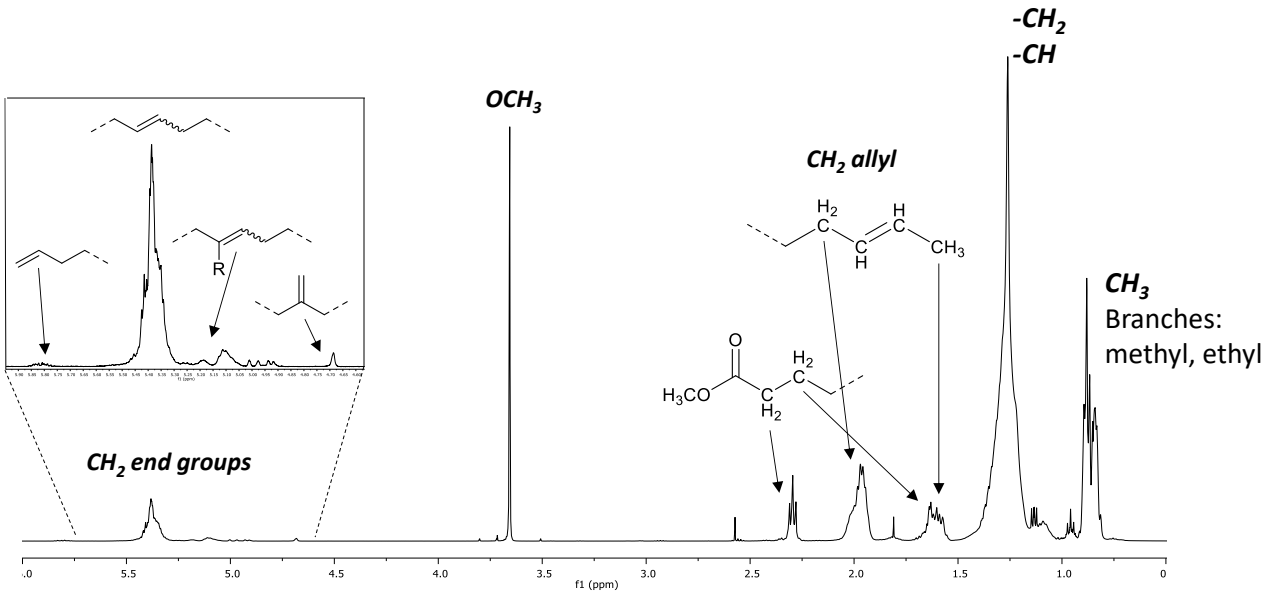

Figure 3.38. ^{1}H NMR spectrum ($CDCl_3$, 298 K) of E/MA cooligomers synthetized in TFE with **5c**.

The way of the polar monomer enchainment is detected by ^{13}C NMR spectroscopy and only one peak in the carbonyl region of the ^{13}C NMR spectra at 174.4 ppm is observed assigned to the C=O group of T(MA) (MA inserted at the end of the branches) (Figure 3.39).

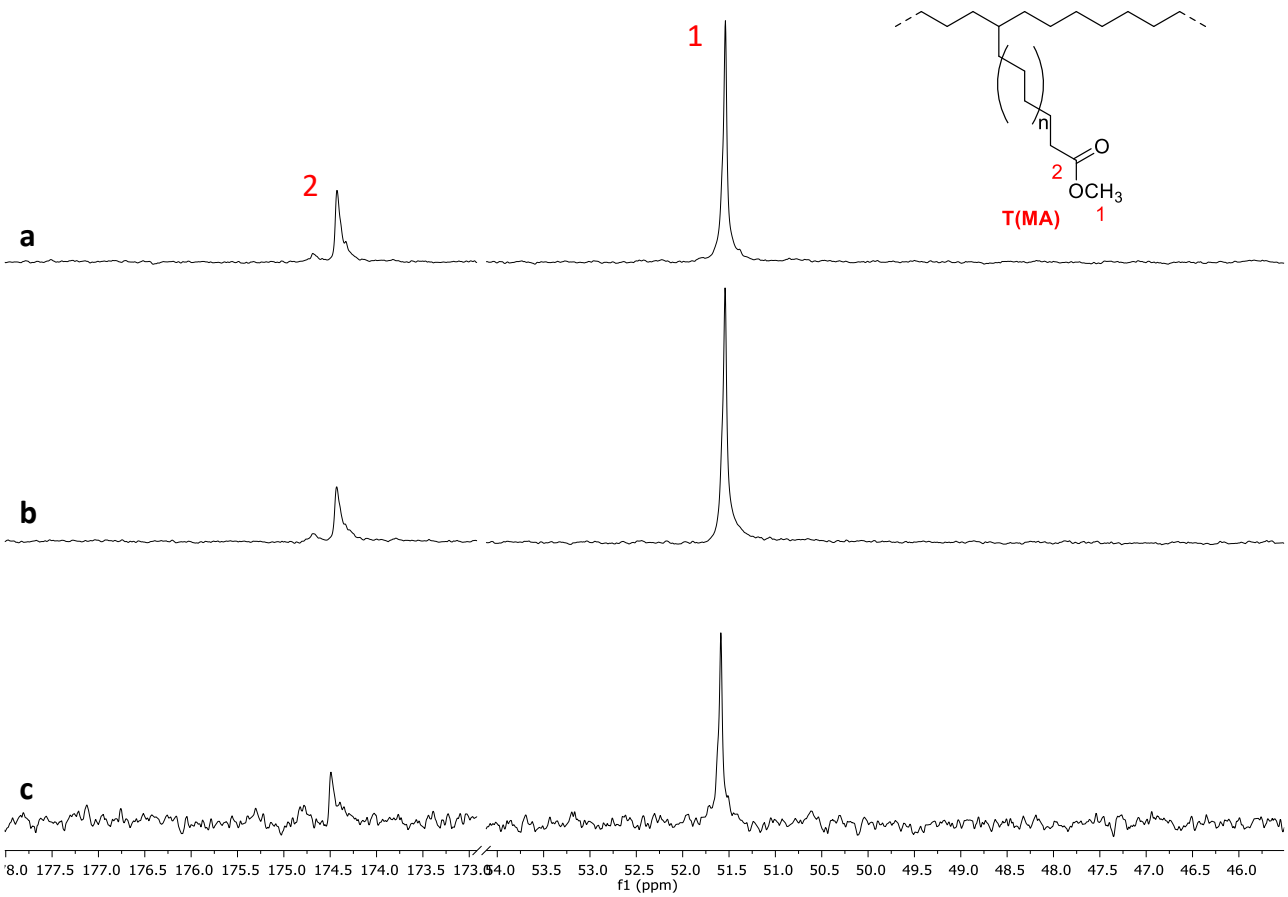

Figure 3.39. ^{13}C NMR spectra ($CDCl_3$, 298 K) of E/MA cooligomers synthetized in TFE with (a) **5b**, (b) **6b** and (c) **7b**.

The *mass flow control* device is used during catalysis to measure the consumed ethylene. For all Pd(II) complexes the induction period is comparable (about 15 min) and it is not affected by either the substitutes on the *ortho* positions of the aryl ring of the N-N'-S ligand or the presence of acetonitrile. Also the absorption of the gaseous monomer during all the monitoring time (6 h) is not as much influenced by the presence or not of CH_3CN in the palladium coordination sphere, in facts the plots recorded with complexes having the N-N'-S ligand as a bidentate or tridentate one are almost overlapped. Both series of complexes show the same TOF for the first 20 min of the reaction, afterwards, a remarkably deactivation of the Pd(II) complexes with ligand **7** is observed, suggesting the formation in solution of dinuclear inactive species (Figure 3.40).[17,26] These data are in agreement with the productivity data reported previously, where Pd(II) complexes **7b** and **7c** are the lowest productive compounds (Table 3.4, entries 5 and 6).

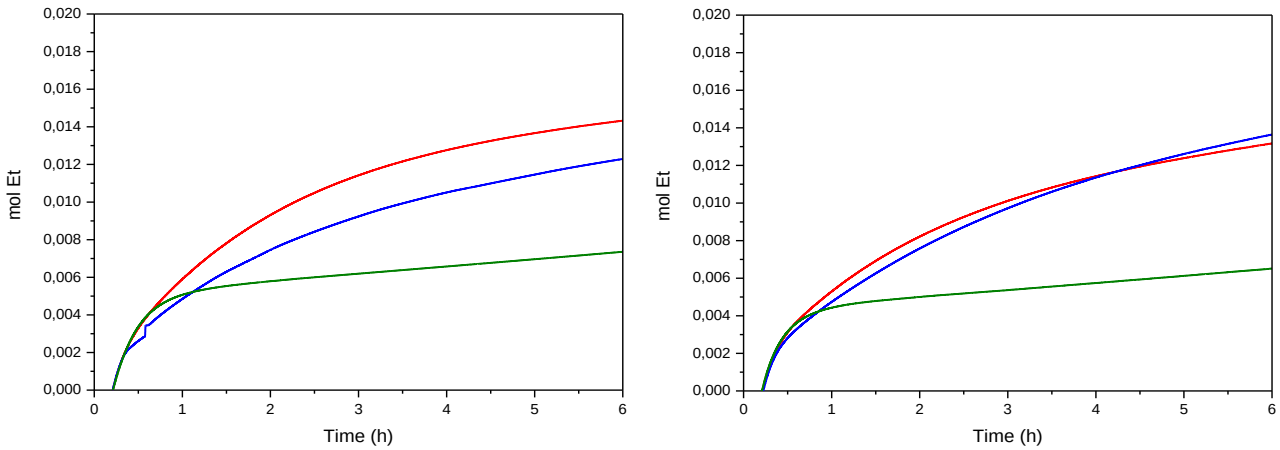

(a) (b)

Figure 3.40. Kinetic profiles of ethylene/methyl acrylate cooligomerization in TFE: effect of N-N'-S ligand. Precatalysts: (a) $[Pd(CH_3)(NCCH_3)(N\text{-}N'\text{-}S)][PF_6]$ and (b) $[Pd(CH_3)(N\text{-}N'\text{-}S)][PF_6]$ (N-N'-S: **5** (red curves), **6** (blue curves) and **7** (green curves)). Reaction conditions: see Table 3.4.

The curves recorded during catalysis performed with **1b** and **2b** under the same reaction conditions reflect the remarkable decrease in productivity and in ethylene TON values of this new series of Pd(II) complexes with respect to Pd(II) complexes bearing the symmetric α-diimine ligand, **1** or **2** (Figure S3.39).

From the analysis of kinetic profiles of the catalysis carried out in DCM (Figure 3.41), the induction time of 15 min and the TOF values for the first 20 min are similar for all the $[Pd(CH_3)(N\text{-}N'\text{-}S)][PF_6]$ compounds. Then, **7c** is strongly deactivated, while **5c** and **6c** remain active confirming the obtained experimental data.

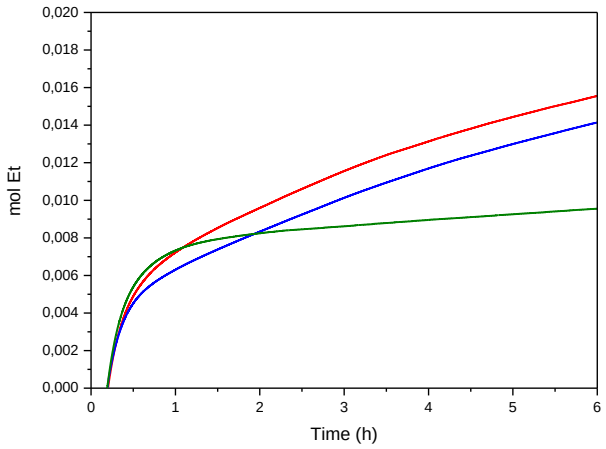

Figure 3.41. Kinetic profiles of ethylene/methyl acrylate cooligomerization in DCM: effect of N-N'-S ligand. Precatalysts: $[Pd(CH_3)(N\text{-}N'\text{-}S)][PF_6]$ (N-N'-S: **5** (red curves), **6** (blue curves) and **7** (green curves)). Reaction conditions: see Table 3.5.

The comparison between catalysis performed in TFE and DCM with **5c** and **6c** highlights that all complexes are more active and absorb more ethylene in the chloride solvent rather than in the fluorinated one (Figure 3.42). It is an opposite trend with respect to the calculated values of ethylene TON (Tables 3.4 and 3.5). The amount of absorbed ethylene by the *mass flow control* device is noted during all the monitoring time of reaction of 6 h, while reported TON is calculated by ^{1}H NMR spectra of isolated products after the removal of volatile species from the catalysis mixture under reduced pressure. This indicates that precatalysts are able to generate different active species for the production of both volatile compounds and E/MA cooligomers.

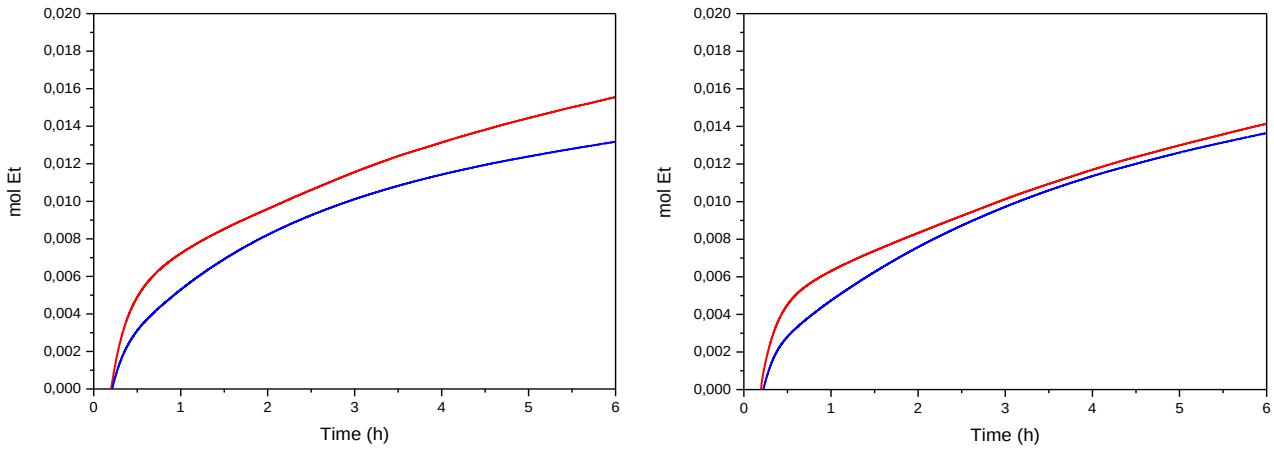

(a) (b)

Figure 3.42. Kinetic profiles of ethylene/methyl acrylate cooligomerization: effect of the solvent. Precatalysts: (a) **5c** and (b) **6c**; solvent: TFE (blue curves) and DCM (red curves). Reaction conditions: see Tables 3.4 and 3.5.

Since **5b** is the best performer precatalyst in terms of productivity, effects of variation of some reaction parameters, such as temperature and ethylene pressure, are studied carrying out the E/MA cooligomerization reaction in TFE. Temperature is investigated in the range from 298 to 318 K and a decrease in terms of the productivity moving from 13.88 kg P/mol Pd at 298 K to 7.48 kg P/mol Pd at 318 K is observed together with the formation of Pd(0) in the reactor during the catalysis. On the other hand an increase in the content of inserted MA reaching the value of 7.3 mol % is found (Figure 3.43a and Table S3.4). Keeping constant the temperature at 298 K, the effect of the ethylene pressure is studied from 2.5 to 7.0 bar. The productivity increases reaching the value of 23.76 kg P/mol Pd moving from 2.5 to 5.0 bar, while in the second variation step a decrease is observed down to 13.33 kg P/mol Pd. In agreement with the higher amount of ethylene in the reactor, the amount of inserted polar monomer decreases (1.5 mol % at 7.0 bar) (Figure 3.43b and Table S3.5).

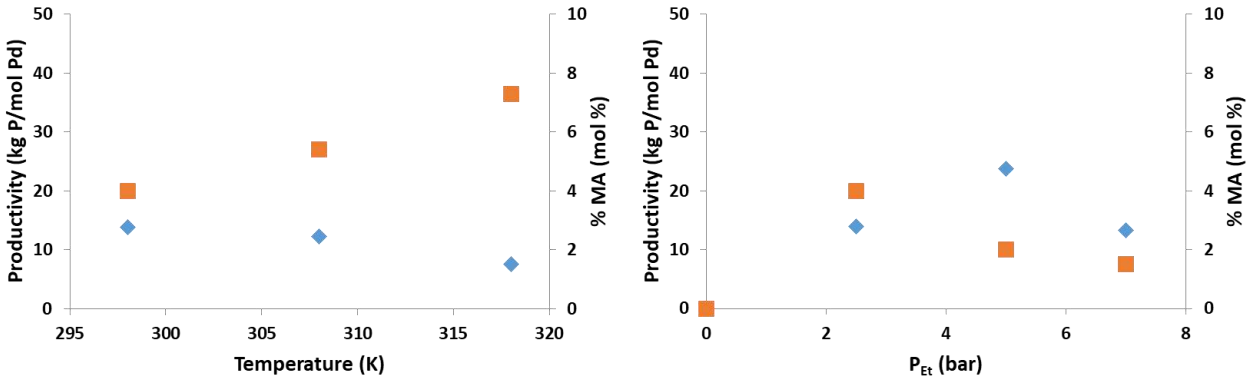

(a) (b)

Figure 3.43. Ethylene/methyl acrylate cooligomerization: effect of (a) temperature and (b) ethylene pressure on (♦) the productivity and (■) the content of inserted MA. Precatalyst: **5b**.

3.2.10 Reactivity of cationic Pd(II) complexes with ethylene and methyl acrylate.

The reaction of the cationic complexes, bearing **5** and **6** N-N'-S ligands, with ethylene and methyl acrylate is investigated by *in situ* NMR spectroscopy to give some information about the intermediates involved in the catalytic reaction.

Firstly, ethylene is bubbled for 5 min into a 10 mM CD_2Cl_2 solution of the selected complex at 298 K and the reaction is followed over time at room temperature. All the tested cationic complexes show similar behavior:

- in the ^{1}H NMR spectrum recorded after 5 min from the addition of ethylene, the singlets of Pd-CH_3 fragments of the precursor disappear indicating that the reaction with the gaseous monomer is immediate and both geometrical isomers, when they are present, react (Figures 3.44 and S3.40);
- Ethylene is totally consumed after 15 min when the starting complex is either **5b** or **6b**, while for [Pd(CH_3)(N-N'-S)][PF_6] compounds, it is totally consumed after 5 min (Figures 3.45 and S3.42). The reaction of **5c** and **6c** with ethylene is faster, suggesting that ethylene easily coordinates to the metal center in absence of acetonitrile;
- in the aliphatic and vinylic region of the ^{1}H NMR spectra typical resonances of branched polyethylene (PE) are observed together with signals assigned, according to the literature, to 3-hexene, 1-butene, propene and *cis*/*trans*-2-butene;[17,18]

- in the ^{1}H NMR spectrum of the reaction of **5b** recorded after 15 min from the addition of ethylene (Figure 3.44c), weak signals relative to Pd-ethyl intermediate, Pd-CH_2CH_3, are detected at 0.77 ppm (CH_3) and 1.96 ppm (CH_2); when **5c** is used, in the $^{1}H,^{1}H$ NOESY spectrum recorded at 273 K, a cross peak due to the Overhauser effect between the broad signal at 0.63 ppm assigned to the CH_3 group of Pd-CH_2CH_3 species and the septet of CH^{iPr} group of ligand **5** is observed, indicating that it is the *trans*-Pd-ethyl intermediate (Figure S3.41);
- broad signals around 2.00 ppm and close to the triplets of H^{α},H^{β} and H^{δ},H^{γ} are observed suggesting a dynamic exchange process that involves the thiophene pendant arm of the ligand, ethylene and the GP. No signal of free acetonitrile is detected, indicating that it takes place in the dynamic process when the reaction is carried out with either **5b** or **6b** as precatalyst.

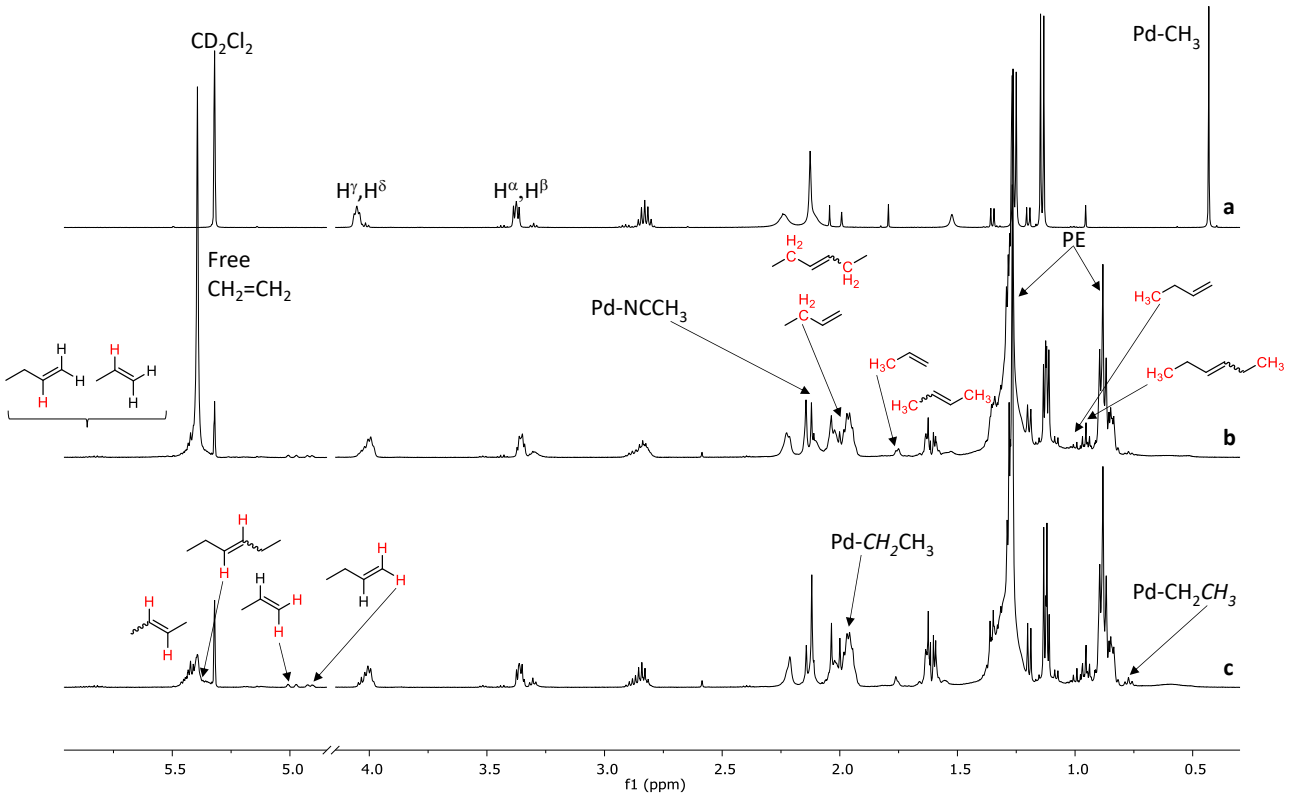

Figure 3.44. ^{1}H NMR spectra (CD_2Cl_2, 298 K) of (a) **5b**; **5b** + ethylene at (b) t = 5 min and (c) t = 15 min.

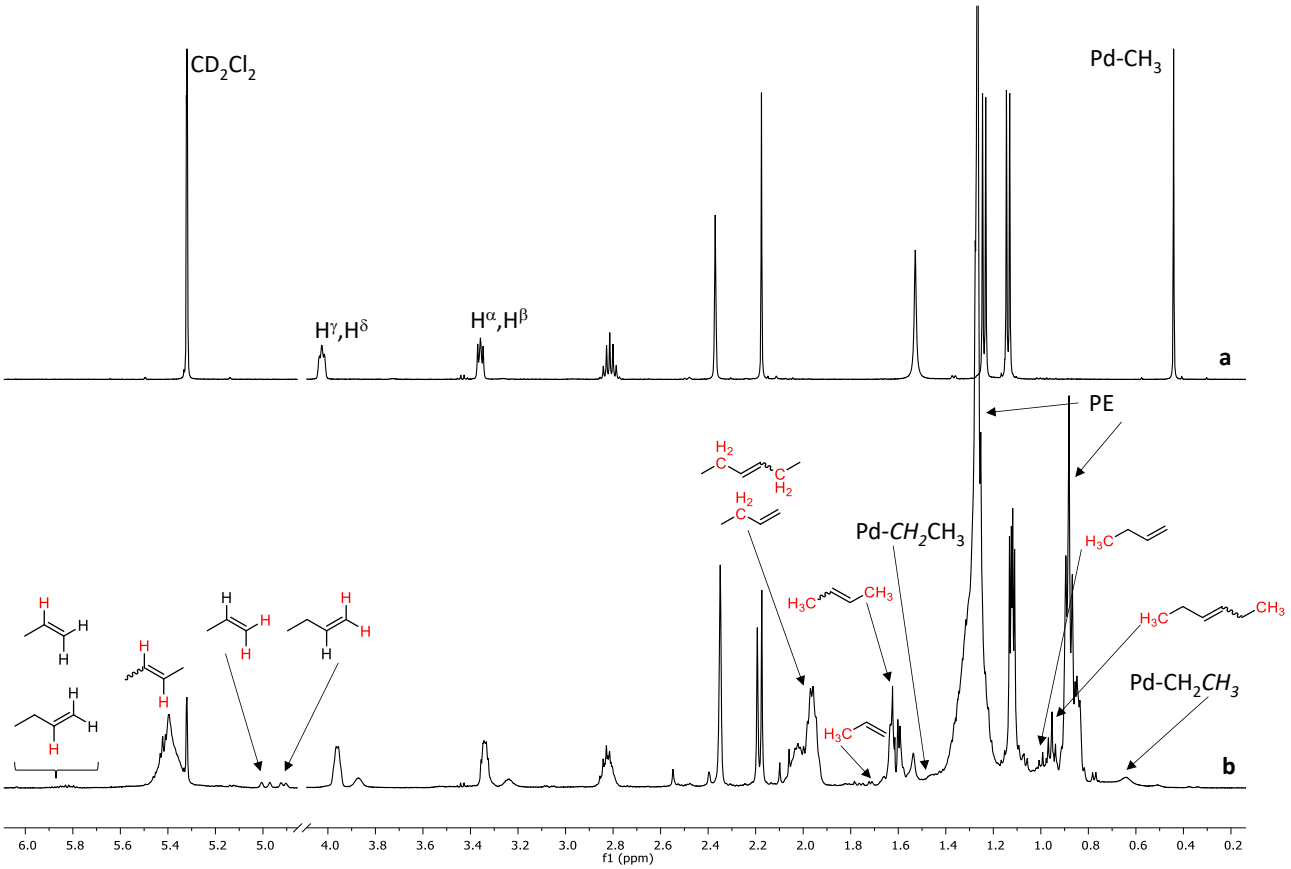

Figure 3.45. ^{1}H NMR spectra (CD_2Cl_2, 298 K) of (a) **5c** and (b) **5c** + ethylene at t = 5 min.

On the basis of the studies reported above, it is possible to state that cationic complexes of both series, bearing **5** and **6** N-N'-S ligands, are catalysts able to generate active species for both the ethylene di- and trimerization and the homopolymerization, leading to volatile products, such as butenes and hexenes, and branched PE, respectively. The mechanism for the catalytic reaction is proposed (Scheme 3.11). The activation of complex takes places by the coordination of ethylene replacing the acetonitrile in **5b** and **6b** or the sulfur atom when **5c** and **6c** are used, followed by its migratory insertion reaction into the Pd-CH_3 bond (**I**) and a subsequent β-H elimination, obtaining propylene and the Pd-hydride intermediate (**II**) as catalytic active species. Here the coordination/insertion of another incoming ethylene molecule takes place, leading to the Pd-CH_2CH_3 intermediate (**IV**), which is recognised as the catalyst resting state. From this species two different pathway are possible involving either the coordination/insertion reaction of several ethylene molecules leading to PE or the formation of Pd-*n*-butyl intermediate (**VI**). On its turn the latter species can either insert another ethylene molecule leading to the Pd-*n*-hexyl species (**VII**), which rapidly isomerizes producing 3-hexenes, or produce 1-butene as a consequence of a β-H elimination reaction in the intermediate **VIII**. In both cases the active species **II** is regenerated.

From **VIII** the reinsertion with opposite regiochemistry of the organic fragment leading to the branched intermediate (**IX**) takes place and on it the β-H elimination occurs with the formation of *cis/trans*-2-butene.

In this proposed catalytic cycle all species characterized by having 14 e^- and a Pd-H fragment might be in equilibrium with intermediates with 16 e^- having the sulfur atom directly bonded to the palladium ion (**I', II', IV', VI', VII', IX'**).

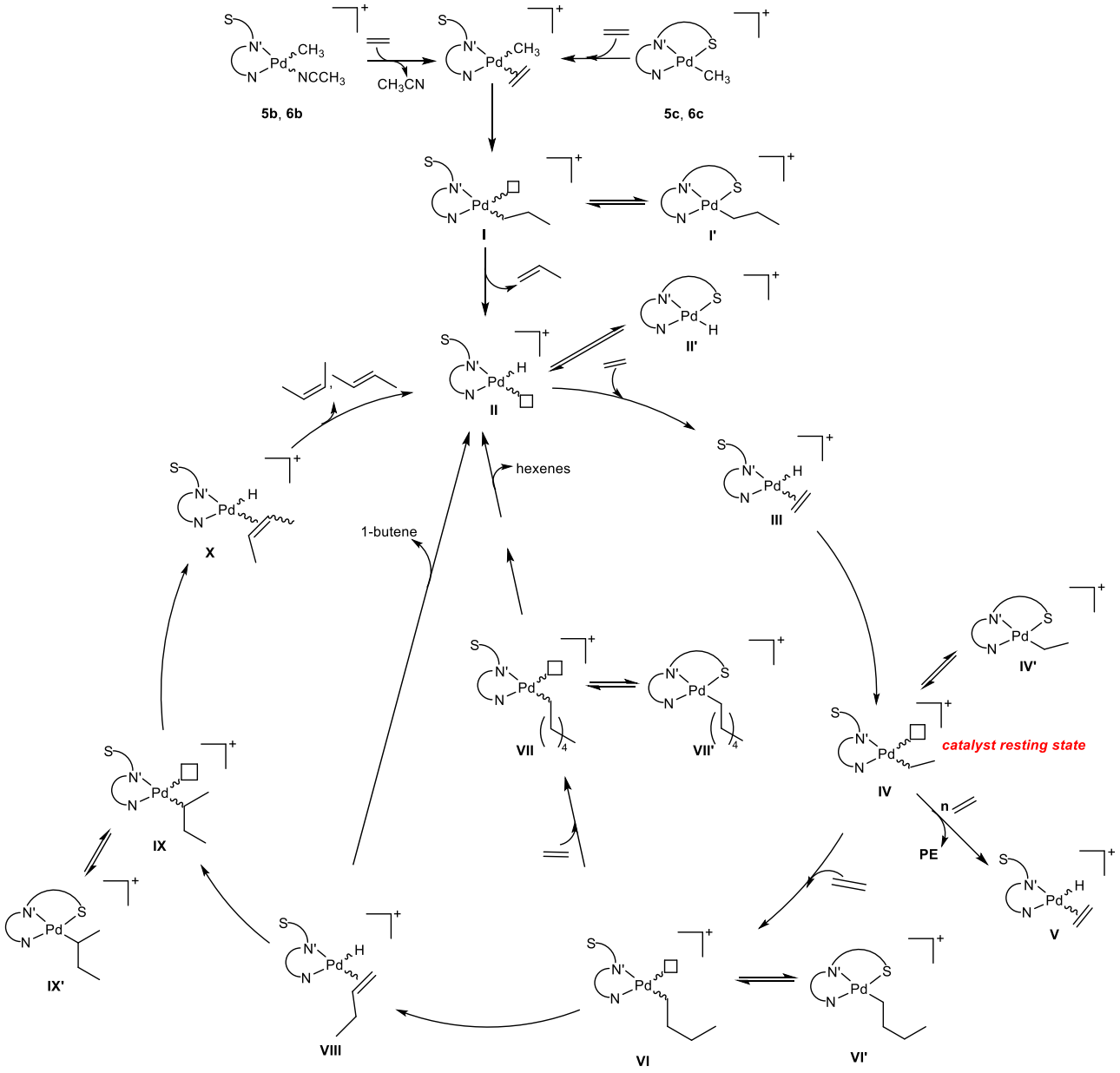

Scheme 3.11. Proposed mechanism for the reaction of Pd(II) cationic complexes with ethylene.

The reaction of **5b**, **5c** and **6c** with methyl acrylate is studied by adding to the 10 mM CD_2Cl_2 solution of the complex 2 eq. of the polar monomer. The reaction is followed on time at room temperature and the formation of metallacycle intermediates is detected by NMR spectroscopy. In the ^1H NMR spectra recorded after 15 min from the addition of the polar monomer, new resonances are observed in all *in situ* NMR investigations. The migratory insertion of MA into the Pd-CH_3 bond is slowed down with respect to that of ethylene, confirming the inhibiting behaviour of the polar monomer and the high affinity between the gaseous monomer and the palladium ion.[1,24] As the reaction of **5b** (Figure 3.46), the diagnostic singlet at 0.44 ppm of Pd-CH_3 of *trans*-**5b** is observed after 4 h, contrary to that observed in the reaction of [Pd(CH_3)(NCCH_3)(**1**)][PF_6], **1b**, with MA (Figure 2.14, Chapter 2).[1] This suggests that both acetonitrile and sulfur atom of N-N'-S ligand compete with methyl acrylate for the coordination on the metal center.

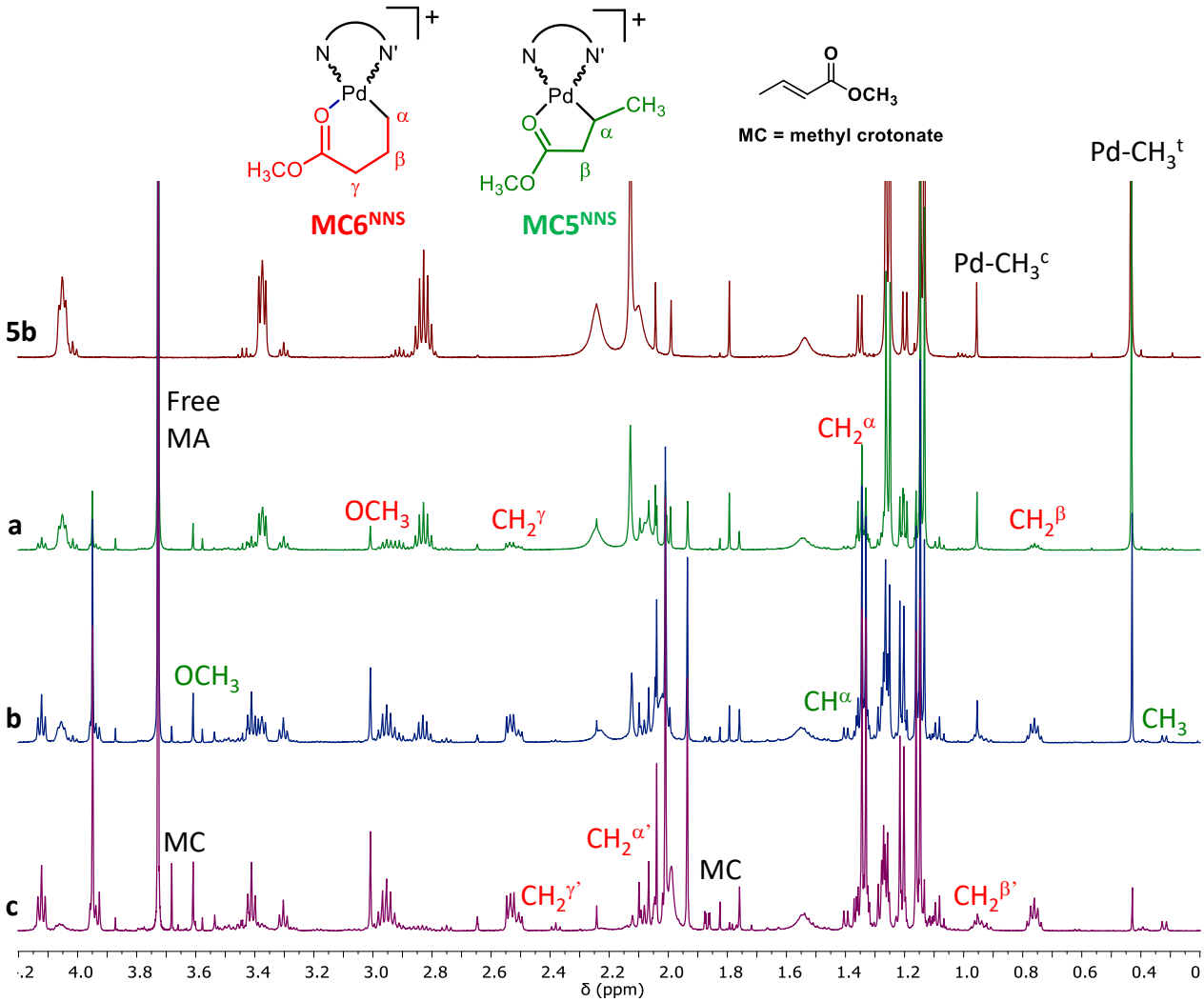

Figure 3.46. ^1H NMR spectra (CD_2Cl_2, 298 K) of the reaction of **5b** (top spectrum) with MA at (a) t = 15 min, (b) t = 60 min and (c) t = 4 h.

The proton-signal assignments of new intermediates are done thanks to bidimensional NMR analysis performed after 1 h (Figures S3.43 and S3.44) and according to the literature.[1] Resonances of the two geometrical isomers of 6-membered palladacycle (**MC6**^{NNS}), generated by the migratory insertion of MA into the Pd-CH_3 bond followed by the chain walking process, are observed together with those of **MC5**^{NNS} (5-membered metallacycle). In the ^{1}H NMR spectrum recorded after 1 h, signals of methyl crotonate (**MC**), resulted from the β-H elimination reaction, which takes place from **MC5**^{NNS}, are detected (Scheme 3.12).

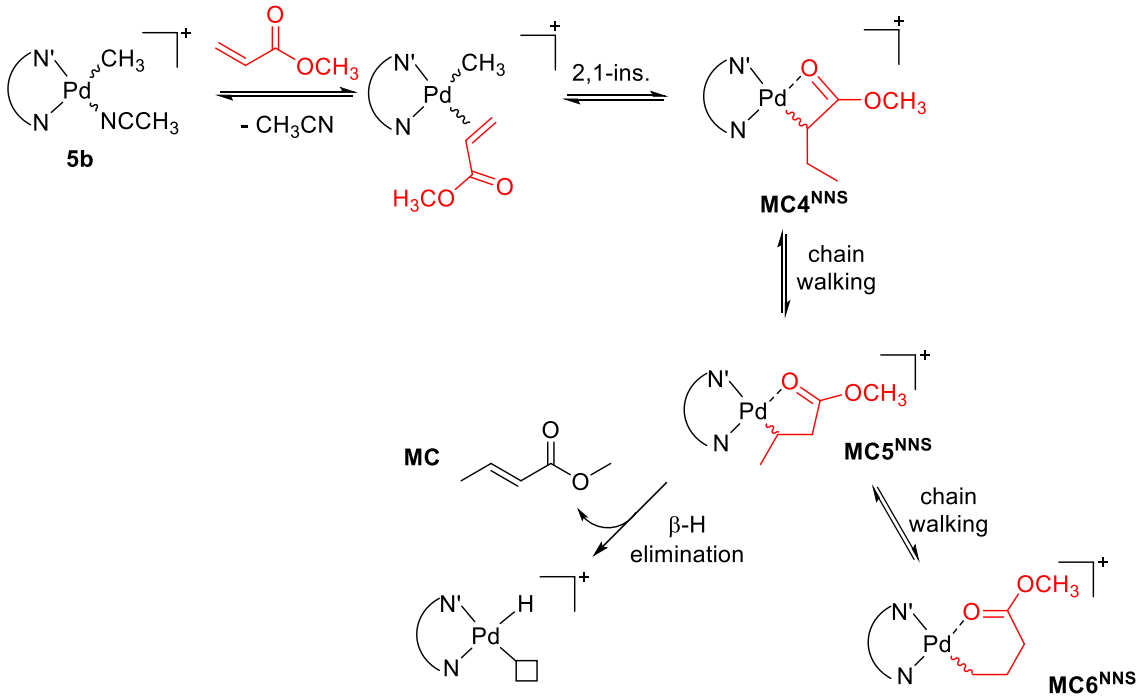

Scheme 3.12. Proposed mechanism for the reaction of **5b** with methyl acrylate.

The behaviour of **5c** are comparable with that of **5b** (Figure S3.45). In the ^{1}H NMR spectra recorded after the addition of the polar monomer, resonances of **5c** together with those of both geometrical isomers of **MC6**^{NNS} and of **MC5**^{NNS} are observed. Diagnostic peaks of **MC** are present in the ^{1}H NMR spectrum recorded after 4 h.

On the other hand, when the reaction of **6c** with MA is studied (Figures 3.47 and S3.46). In the ^{1}H NMR spectrum recorded after 15 min from the addition of the polar monomer, three sets of signals due to 4-, 5- and 6-membered metallacycles (**MC4**^{NNS}, **MC5**^{NNS}, **MC6**^{NNS}, respectively) are observed. The presence of these intermediates suggests that the chain walking process in the reaction of **6c** is slowed down with respect to **5c**, due to the less steric hindrance on the aryl ring of the N-N'-S ligand.

For this reason, the sulfur atom of **6** might be closer to the metal center during the reaction and it might compete for the coordination with the polar monomer, slowing down the chain walking process. The singlet of Pd-CH_3 at 0.33 ppm disappears after 24 h indicating that all the complex is converted into active species.

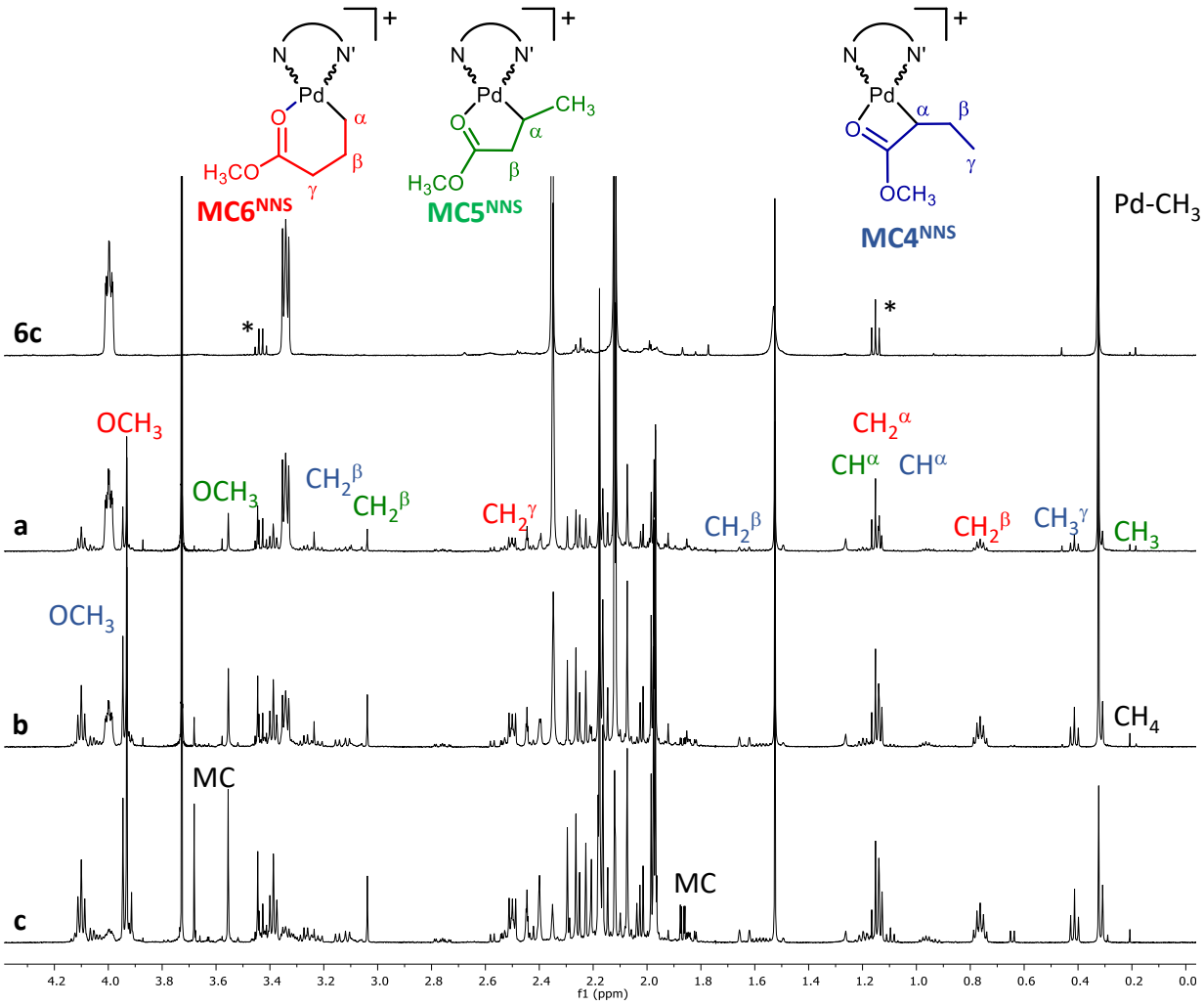

Figure 3.47. ^{1}H NMR spectra (CD_2Cl_2, 298 K) of the reaction of **6c** (top spectrum) with MA at (a) t = 15 min, (b) t = 60 min and (c) t = 4 h; *diethyl ether.

3.3 Conclusions.

With the aim to give additional information about the Pd···S interaction, two series of complexes with hemilabile potentially tridentate molecules, N-N'-S, having the thiophene group directly bonded to the N-N' fragment of the ligand itself are studied. The potentially tridentate ligands N-N'-S, with either a pyridylimine moiety or a DAB skeleton, are synthesized and characterized.

Neutral Pd(II) complexes, [Pd(CH_3)Cl(N-N'-S)], are obtained and characterized in solution by NMR spectroscopy and in solid state by X-Ray diffraction. From NMR analysis and the solid state structures, no interactions between sulfur atom and the metal center are observed. From neutral compounds through the dehalogenation reaction, monocationic complexes are synthetized of general formula [Pd(CH_3)($NCCH_3$)(N-N'-S)][X]. In their ^{1}H NMR spectra, two sets of signals are observed indicating that both geometrical isomers are present in solution. One set is composed by narrow signals, while in the other one peaks assigned to the Pd-$NCCH_3$ fragment and the protons of the thiophene pendant arm are broad. The broadness of signals suggests a dynamic process involving the two isomers and the presence of a third species in solution. To have some additional information about this phenomenon, progressive additions of CH_3CN are made to complexes solution confirming that the sulfur atom competes with the acetonitrile for the coordination on the fourth coordination site of the metal center. In this way the third species is recognised to be a Pd(II) complex where N-N'-S behaves as a tridentate ligand. So a new series of cationic complexes, of general formula [Pd(CH_3)(N-N'-S)][X], are obtained and their solid state structures confirm that the sulfur atom is directly bonded to palladium. All monocationic Pd(II) complexes are tested in the ethylene/methyl acrylate cooligomerization under mild reaction conditions and, depending on the N-N' skeleton, the catalytic products are different.

Focusing on Pd(II) complexes bearing the N-N'-S ligand with a pyridylimine backbone, catalysis are carried out using TFE as reaction medium. Active species for the target reaction are generated, producing unsaturated esters, preferentially β,γ-ones, and no Pd(0) is observed considering the acetonitrile derivatives. When the *in situ* NMR reaction of a ketoimine cationic compound, [Pd(CH_3)($NCCH_3$)(**4**)][PF_6], **4b**, with the gaseous monomer is investigated, volatile species like ethane, 1-butene and *cis/trans*-2-butene are the main species detected in ^{1}H NMR spectra. In addition the Pd-CH_2CH_3 intermediate is detected and recognized as the catalyst resting state. As the reaction of **4b** with both comonomers, the reaction with ethylene takes place immediately, leading to the same volatile species reported above, while that with the polar monomer is slowed down and only weak signal of unsaturated ester are observed.

While, the cationic complexes characterized by having a N-N'-S ligand with a DAB skeleton, produce E/MA cooligomers with the polar monomer exclusively inserted at the end of the branches (T(MA)). Surprisingly enough, the N-N'-S ligand affects the degree of branches of the products and the second coordination sphere might be responsible to slow down the chain walking process after the insertion of ethylene when catalysis are carried out in DCM. Effects of variations of some reaction parameters, such as temperature and ethylene pressure, are studied, too.

Kinetic studies are performed connecting the reactor to a *mass flow control* device. We found that the consumed ethylene is higher than that found in the isolated cooligomers, thus suggesting the formation of two catalytic species: one active in the cooligomerization and the other in ethylene di- and trimerization. The reaction with ethylene is performed at room temperature and it is monitored by *in situ* NMR spectroscopy. Resonances of volatile products, together with those relative to polyethylene, are present in the ^{1}H NMR spectra, confirming that complex is able to generate different active species. Moreover, the Pd-ethyl fragment is detected and it is assigned to *trans*-species thanks to the $^{1}H,^{1}H$ NOESY experiment. Preliminary investigations with the polar monomer are carried out and metallacycle intermediates (**MC4**^{NNS}, **MC5**^{NNS} and **MC6**^{NNS}) are detected in different ratio depending on both the precursor and the presence or not of CH_3CN in the second coordination sphere of the starting compound.

3.4 Experimental.

All complex manipulations were performed using standard Schlenk techniques under argon. Anhydrous dichloromethane was freshly obtained by distillation over CaH_2 under argon atmosphere. Deuterated solvents (Cambridge Isotope Laboratories, Inc. (CIL) and Sigma Aldrich) were stored as recommended by sellers. Ethylene (purity ≥ 99.9 %) supplied by SIAD and methyl acrylate (99.9%, with 0.02% of hydroquinone monomethyl ether) supplied by Aldrich were used as received. TFE and all the other reagents and solvents were purchased from Sigma-Aldrich/Merck and used without further purification for synthetic, spectroscopic and catalytic purposes. [$Pd(OCOCH_3)_2$] (BASF Italia) was used as source of the metal to obtain the corresponding Pd(II) complexes. Mono- and bidimensional NMR spectra of ligands and complexes were recorded on a Varian 500 spectrometer (500 MHz for ^{1}H, 125.68 MHz for ^{13}C), and of copolymers on a Varian 400 (400 MHz for ^{1}H, 100.55 MHz for ^{13}C). The resonances are reported in ppm (δ) and referenced to the residual solvent peak versus $Si(CH_3)_4$: CD_2Cl_2: at δ 5.32 (^{1}H) and δ 54.00 (^{13}C); $CDCl_3$: at δ 7.26 (^{1}H) and δ 77.16 (^{13}C). ^{19}F–NMR spectra were recorded on a Varian 400 spectrometer at 376.3 MHz and referenced with respect to CCl_3F. NMR experiments were performed employing the automatic software parameters. In the case of NOESY experiments a mixing time of 500 ms was used. Mass spectra (ESI-MS) were recorded on a Massa Esquire 4000 – Bruker in positive ion polarity (HV capillary of 4000 V and dry gas of 5.00 L/min). Samples were dissolved in methanol and the analysis was carried out immediately. Data collections were performed at the X-ray diffraction beamline (XRD1) of the Elettra synchrotron of Trieste (Italy), equipped with a Pilatus 2M image plate detector.

Collection temperature was 100 K (nitrogen stream supplied through an Oxford Cryostream 700); the wavelength of the monochromatic X-ray beam was 0.700 Å and the diffractograms were obtained with the rotating crystal method.

*3.4.1 Synthesis and characterization of thiophene-pyridylimine ligands **3** and **4**.*

To a water solution of desired pyridine (pyridun-2-aldehyde for **3**; 2-acetylpyridine for **4**) (2.34 mmol in 0.6 mL) 1.2 equiv. of 2-thiophenethylamine were added. The suspension was stirred at room temperature for 24 h, after the extraction with diethyl ether, Na_2SO_4 was added for 1 h and then the solid was filtered. The solvent was removed leading to a yellow oil for **3** and an orange oil for **4**.

3. (yellow oil, yield = 83 %); ^{1}H NMR (500 MHz, CD_2Cl_2, 298 K) δ = 8.60 (d, 1H, H^6), 8.30 (s, 1H, H^{im}), 8.01 (d, 1H, H^3), 7.75 (t, 1H, H^4), 7.32 (dd, 1H, H^5), 7.14 (dd, 1H, H^{14}), 6.92 (dd, 1H, H^{13}), 6.87 (m, 1H, H^{12}), 3.93 (t, 2H, H^{δ},H^{γ}), 3.24 (t, 2H, H^{α},H^{β}). ^{13}C NMR (500 MHz, CD_2Cl_2, 298 K, from the HSQC spectrum) δ = 163.2 (C^{im}), 149.7 (C^6), 136.6 (C^4), 127.1 (C^{13}), 125.5 (C^{12}), 124.9 (C^5), 123.9 (C^{14}), 121.2 (C^3), 62.6 (C^{δ},C^{γ}), 31.6 (C^{α},C^{β}).

4. (orange oil, yield = 86 %); ^{1}H NMR (500 MHz, CD_2Cl_2, 298 K) δ = 8.56 (d, 1H, H^6), 8.15 (d, 1H, H^3), 7.72 (dt, 1H, H^4), 7.29 (ddd, 1H, H^5), 7.14 (dd, 1H, H^{14}), 6.93 (dd, 1H, H^{13}), 6.89 (m, 1H, H^{12}), 3.77 (t, 2H, H^{δ},H^{γ}), 3.29 (t, 2H, H^{α},H^{β}), 2.30 (s, 3H, CH_3^{im}). ^{13}C NMR (500MHz, CD_2Cl_2, 298 K, from the HSQC spectrum) δ = 148.6 (C^6), 136.4 (C^4), 126.9 (C^{13}), 125.1 (C^{12}), 124.3 (C^5), 123.8 (C^{14}), 121.0 (C^3), 54.0 (C^{δ},C^{γ}), 31.8 (C^{α},C^{β}), 14.0 (CH_3^{im}).

*3.4.2 Synthesis and characterization of aryl-thiophene-diimine ligands **5**, **6** and **7**.*

To a solution of 5.6 mmol of butane-2,3-dione in 5 mL of *n*-hexane, 1.0 eq. of the desired aniline (2,6-diisopropylaniline for **5** and **7**, 2,6-dimethylaniline for **6**) in the same solvent were added. Some drops of catalytic formic acid and anhydrous sodium sulfate were introduced into the flask. The pale yellow solution was kept under stirring at room temperature. After a proper time (4 h for **iPrKI** and 2.5 h for **MeKI**), the solvent was removed under reduced pressure, obtaining yellow oils with trace amounts of symmetrical α-diimine ligand (**7** or **1**). The crude product was purified with flash chromatography on silica gel treated with 1 % NEt_3, using 50:1 hexane/ethyl acetate as elution mixture.

To a water solution of pure desired monoketoimine (**iPrKI** for **5** and **7**; **MeKI** for **6**) (0.285 mmol in 0.5 mL) 1.2 equiv. of 2-thiophenethylamine were added. The suspension was stirred at room temperature for 6 h (**5** and **7**) and for 4 h (**6**), after the extraction with diethyl ether, Na_2SO_4 was added for 1 h and then the solid was filtered. The solvent was removed leading to yellow oils.

iPrKI. (yellow oil, yield: 59 %); ^{1}H NMR (500 MHz, CD_2Cl_2, 298 K): δ = 7.16 (d, 2H, H^m), 7.09 (dd, 1H, H^p), 2.57 (sept, 2H, CH^{iPr}), 2.55 (s, 3H, $CH_3{}^k$), 1.79 (s, 3H, $CH_3{}^{im}$), 1.13-1.11 (d, 12H, $CH_3{}^{iPr}$). ^{13}C NMR (125.68 MHz, CD_2Cl_2, 298 K, from HSQC spectrum): δ = 123.4 (C^m), 124.7 (C^p), 28.6 (CH^{iPr}), 24.9 ($CH_3{}^k$), 15.0 ($CH_3{}^{im}$), 23.2-22.7 ($CH_3{}^{iPr}$). ESI-MS: m/z = 246.1 [**iPrKI** + H]$^+$, 268.1 [**iPrKI** + Na]$^+$.

MeKI. (yellow oil, yield: 63 %); ^{1}H NMR (500 MHz, CD_2Cl_2, 298 K) δ = 7.05 (d, 2H, H^m), 6.94 (t, 1H, H^p), 2.55 (s, 3H, $CH_3{}^k$), 1.96 (s, 6H, $CH_3{}^{Ar}$), 1.75 (s, 3H, $CH_3{}^{im}$). ^{13}C NMR (500 MHz, CD_2Cl_2, 298 K, from the HSQC spectrum) δ = 128.4 (C^m), 124.1 (C^p), 5.0 (C^k), 17. 9 (C^{Ar}), 14.5 (C^{im}). ^{13}C NMR (500 MHz, CD_2Cl_2, 298 K, from the HMBC spectrum) δ = 199.9 (C=O), 166.5 (C=N). ESI-MS: m/z = 190.0 [**MeKI** + H]$^+$, 204.0 [**MeKI** + CH_3]$^+$, 211.9 [**MeKI** + Na]$^+$.

5. (yellow oil, yield: 71 %); ^{1}H NMR (500 MHz, CD_2Cl_2, 298 K) δ = 7.15 (d, 1H, H^5), 7.12 (d, 2H, H^m), 7.04 (t, 1H, H^p), 6.94 (t, 1H, H^4), 6.90 (d, 1H, H^3), 3.76 (t, 2H, H^{δ},H^{γ}), 3.28 (t, 2H, H^{α},H^{β}), 2.63 (m, 2H, CH^{iPr}), 2.15 (s, 3H, $CH_3{}^{DAB2}$), 1.90 (s, 3H, $CH_3{}^{DAB1}$), 1.13 (dd, 6H, $CH_3{}^{iPr}$). ^{13}C NMR (500 MHz, CD_2Cl_2, 298 K, from the HSQC spectrum) δ = 123.6 (C^5), 122.8 (C^m), 123.3 (C^P), 126.5 (C^4), 125.0 (C^3), 54.0 (C^{δ},C^{γ}), 31.4 (C^{α},C^{β}), 28.1 (CH^{iPr}), 12.7 ($CH_3{}^{DAB2}$), 16.0 ($CH_3{}^{DAB1}$), 22.8 ($CH_3{}^{iPr}$) 22.4 ($CH_3{}^{iPr}$). ESI-MS: m/z = 228.5 [M-(CH_2-CH_2-C_4H_3S)-CH_3]$^+$, m/z = 268.5 [**5**-2iPr]$^+$, m/z = 355.3 [**5**+H]$^+$, m/z = 377.2 [**5**+Na]$^+$.

6. (yellow oil, yield: 78 %); ^{1}H NMR (500 MHz, CD_2Cl_2, 298 K) δ = 7.15 (d, 1H, H^5), 7.03 (d, 2H, H^m), 6.94 (t, 1H, H^4), 6.89 (bs, 2H, H^p, H^3), 3.75 (t, 2H, H^{δ},H^{γ}), 3.27 (t, 2H, H^{α},H^{β}), 2.16 (s, 3H, $CH_3{}^{DAB2}$), 1.95 (s, 6H, $CH_3{}^{Ar}$), 1.87 (s, 3H, $CH_3{}^{DAB1}$). ^{13}C NMR (500 MHz, CD_2Cl_2, 298 K, from the HSQC spectrum) δ = 123.9 (C^5), 128.1 (C^m), 126.9 (C^4), 125.4 (C^p), 123.1 (C^3), 54.4 (C^{δ},C^{γ}), 31.8 (C^{α},C^{β}), 13.1 ($CH_3{}^{DAB2}$), 17.9 ($CH_3{}^{Ar}$), 15.6 ($CH_3{}^{DAB1}$). ESI-MS: m/z = 299.15 [**6**+H]$^+$, m/z = 321.14 [**6**+Na]$^+$.

7. (yellow oil, yield: 65 %); ^{1}H NMR (500 MHz, CD_2Cl_2, 298 K): δ = 7.25 (dd, 1H, H^5), 7.17-7.00 (m, 4H, H^4, H^m, H^p), 7.03 (bs, 1H, H^3), 4.89 (s, 2H, $H^{\alpha,\beta}$), 2.64 (sept, 2H, CH^{iPr}), 2.33 (s, 3H, $CH_3{}^{DAB2}$), 1.92 (s, 3H, $CH_3{}^{DAB1}$), 1.12 (dd, 6H, $CH_3{}^{iPr}$). ^{13}C NMR (500 MHz, CD_2Cl_2, 298 K, from the HSQC spectrum): δ = 127.1-123.3 (C^3, C^4, C^m, C^p), 124.4 (C^5), 51.9 ($C^{\alpha,\beta}$), 28.6 (CH^{iPr}), 23.1 ($CH_3{}^{iPr}$), 16.3 ($CH_3{}^{DAB1}$), 13.5 ($CH_3{}^{DAB2}$). ESI-MS: m/z = 355.3 [**7**+H]$^+$, 377.2 [**7**+Na]$^+$.

*3.4.3 Synthesis and characterization of neutral complexes **3a** – **7a***

General procedure: To 1 eq. of [Pd(cod)(CH_3)Cl] dissolved in 3 mL of distilled dichloromethane, 1.1 equiv. of ligand were added. The solution was left to stir at room temperature for a proper time.

The solution was then concentrated under reduced pressure and diethyl ether was added to favour the precipitation of the product. The yellow and orange precipitates were then filtered and washed with additional cold diethyl ether, then dried under vacuum.

3a. (yellow solid, yield = 72 %); ^{1}H NMR (500 MHz, CD_2Cl_2, 298 K) *cis* 79.4 %, *trans* 20.6 %. *cis*: δ = 9.00 (d, 1H, H^6), 7.96 (td, 1H, H^4), 7.89 (s, 1H, H^{im}), 7.65 (ddd, 1H, H^5), 7.54 (d, 1H, H^3), 7.18 (dd, 1H, H^{14}), 6.90 (m, 1H, H^{13}), 6.86 (m, 1H, H^{12}), 4.02 (t, 2H, H^{δ},H^{γ}), 3.30 (t, 2H, H^{α},H^{β}), 0.93 (s, 3H, Pd-CH_3). *trans*: δ = 8.60 (d, 1H, H^6), 8.02 (td, 1H, H^4), 7.89 (s, 1H, H^{im}), 7.60 (m, 1H, H^5), 7.57 (d, 1H, H^3), 7.14 (dd, 1H, H^{14}), 6.91-6.85 (m, 2H, H^{13}, H^{12}), 4.10 (t, 2H, H^{δ},H^{γ}), 3.48 (t, 2H, H^{α},H^{β}), 0.96 (s, 3H, Pd-CH_3). ^{13}C NMR (500 MHz, CD_2Cl_2, 298 K, from the HSQC spectrum) *cis*: δ = 166.7 (C^{im}), 149.2 (C^6), 138.6 (C^4), 128.1 (C^5), 127.1 (C^{13}), 126.7 (C^{12}), 125.5 (C^3), 124.6 (C^{14}), 61.3 (C^{δ},C^{γ}), 30.6 (C^{α},C^{β}), -4.5 (Pd-CH_3). *trans*: δ = 161.7 (C^{im}), 148.8 (C^6), 138.6 (C^4), 127.7 (C^5), 126.9 (C^3), 125.8-127.6 (C^{13}, C^{12}), 124.0 (C^{14}), 60.5 (C^{δ},C^{γ}), 30.2 (C^{α},C^{β}), -0.8 (Pd-CH_3).

4a. (orange solid, yield = 60 %); ^{1}H NMR (500 MHz, CD_2Cl_2, 298 K) *cis* 44.4 %, *trans* 55.6 %. *cis*: δ = 9.14 (d, 1H, H^6), 8.04 (t, 1H, H^4), 7.72 (d, 1H, H^3), 7.64 (t, 1H, H^5), 7.19 (d, 1H, H^{14}), 6.95-6.82 (m, 2H, H^{13}, H^{12}), 4.07 (t, 2H, H^{δ},H^{γ}), 3.26 (t, 2H, H^{α},H^{β}), 2.12 (s, 3H, CH_3^{im}), 0.84 (s, 3H, Pd-CH_3). *trans*: δ = 8.56 (d, 1H, H^6), 8.00 (t, 1H, H^4), 7.72 (d, 1H, H^3), 7.59 (t, 1H, H^5), 7.14 (d, 1H, H^{14}), 6.95-6.82 (m, 2H, H^{13}, H^{12}), 4.22 (t, 2H, H^{δ},H^{γ}), 3.36 (t, 2H, H^{α},H^{β}), 1.98 (s, 3H, CH_3^{im}), 0.88 (s, 3H, Pd-CH_3). ^{13}C NMR (500 MHz, CD_2Cl_2, 298 K, from the HSQC spectrum) *cis*: δ = 148.8 (C^6), 138.8 (C^4), 127.7 (C^5), 125.7-124.2 (C^3), 124.7 (C^{14}), 127.7-125.9 (C^{13}, C^{12}), 54.8 (C^{δ},C^{γ}), 29.8 (C^{α},C^{β}), 15.8 (CH_3^{im}), -3.2 (Pd-CH_3). *trans*: δ = 149.1 (C^6), 138.7 (C^4), 127.5 (C^5), 125.7-124.2 (C^3), 124.3 (C^{14}), 127.7-125.9 (C^{13}, C^{12}), 53.6 (C^{δ},C^{γ}), 30.0 (C^{α},C^{β}), 14.6 (CH_3^{im}), -0.6 (Pd-CH_3).

5a. (orange solid, yield = 69 %); ^{1}H NMR (500 MHz, CD_2Cl_2, 298 K) *cis* 3.2 %, *trans* 96.8 %: *trans*: δ = 7.32-7.25 (m, 3H, H^m, H^p), 7.19 (dd, 1H, H^5), 6.94 (t, 1H, H^4), 6.90 (d, 1H, H^3), 4.20 (t, 2H, H^{δ},H^{γ}), 3.51 (t, 2H, H^{α},H^{β}), 3.02 (m, 2H, CH^{iPr}), 1.83 (s, 3H, CH_3^{DAB1}), 1.68 (s, 3H, CH_3^{DAB2}), 1.31 (d, 6H, CH_3^{iPrA}), 1.12 (d, 6H, CH_3^{iPrB}), 0.30 (s, 3H, Pd-CH_3). ^{13}C NMR (500 MHz, CD_2Cl_2, 298 K, from the HSQC spectrum): *trans*: δ = 127.9-124.2 (C^m,C^p), 125.0 (C^5), 127.4 (C^4), 126.8 (C^3), 54.1 (C^{δ},C^{γ}), 30.2 (C^{α},C^{β}), 28.5 (CH^{iPr}), 21.6 (CH_3^{DAB1}), 16.3 (CH_3^{DAB2}), 23.6 (CH_3^{iPrA}), 24.1 (CH_3^{iPrB}), 1.6 (Pd-CH_3).

6a. (orange solid, yield = 71 %); ^{1}H NMR (500 MHz, CD_2Cl_2, 298 K) *cis* 8.8 %, *trans* 91.2 %. *trans*: δ = 7.19 (dd, 1H, H^5), 7.15-7.14 (m, H^m, H^p), 6.95 (t, 1H, H^4), 6.91 (d, 1H, H^3), 4.18 (t, 2H, H^{δ},H^{γ}), 3.48 (t, 2H, H^{α},H^{β}), 2.17 (s, 6H, CH_3^{Ar}), 1.79 (s, 3H, CH_3^{DAB1}), 1.71 (s, 3H, CH_3^{DAB2}), 0.18 (s, 3H, Pd-CH_3). ^{13}C NMR (500 MHz, CD_2Cl_2, 298 K, from the HSQC spectrum): *trans*: δ = 124.9 (C^5),

128.7-126.9 (C^m,C^p), 127.5 (C^4), 126.9 (C^3), 54.2 (C^δ,C^γ), 30.2 (C^α,C^β), 18.1 (CH_3^{Ar}), 19.8 (CH_3^{DAB1}), 16.3 (CH_3^{DAB2}), -0.2 (Pd-CH_3).

7a. (orange solid, yield = 91 %); ^{1}H NMR (500 MHz, CD_2Cl_2, 298 K): *cis* 3 %, *trans* 97 %: *trans*: δ 7.31 (m, 1H, H^5), 7.26 (bs, 1H, H^3), 7.30-7.21 (m, 3H, H^m, H^p), 7.03 (dd, 1H, H^4), 5.41 (s, 2H, H^α,H^β), 2.93 (sept, 2H, CH^{iPr}), 2.30 (s, 3H, CH_3^{DAB2}), 1.93 (s, 3H, CH_3^{DAB1}), 1.29 (d, 6H, CH_3^{iPrA}), 1.09 (d, 6H, CH_3^{iPrB}), 0.33 (s, 3H, Pd-CH_3). ^{13}C NMR (500 MHz, CD_2Cl_2, 298 K, from the HSQC spectrum): *trans*: δ = 127.7 (C^3), 127.0 (C^4), 125.9 (C^5), 127.9-124.2 (C^m, C^p), 50.0 (C^α,C^β), 28.6 (CH^{iPr}), 24.1 (CH_3^{iPrB}), 23.4 (CH_3^{iPrA}), 21.5 (CH_3^{DAB1}), 17.8 (CH_3^{DAB2}), 1.6 (Pd-CH_3).

*3.4.4. Synthesis and characterization of monocationic complexes **3b** – **7b**, **3c** – **7c**, **4d** and **4e.***

General procedure: To 1 eq. of the neutral precursor dissolved in 2.0 mL of distilled dichloromethane, 1.15 eq. of the desired AgX salt dissolved in 1.0 mL of dry acetonitrile (for **3b** – **7b** and **4d**) or CH_2Cl_2 (for **3c** – **7c** and **4e**) were added. The reaction mixture was left to stir in the dark for a proper time (1 h for **3b – 7c** and 80 min for **4b – 4e**). The suspension of AgCl was filtered over Celite® and washed with dichloromethane. The solution was then concentrated under reduced pressure and diethyl ether was added to favour the precipitation of the product. The light yellow and light orange solids were then filtered under reduced pressure, washed with cold diethyl ether and dried under vacuum.

3b. (light yellow solid, yield = 83 %); ^{1}H NMR (500 MHz, CD_2Cl_2, 298 K) *cis* 35.1 %, *trans* 64.9 %. *cis*: δ = 8.62 (d, 1H, H^6), 8.09 (t, 1H, H^4), 7.92 (s, 1H, H^{im}), 7.83 (dd, 1H, H^5), 7.70 (t, 1H, H^3), 7.20 (d, 1H, H^{14}), 6.93 (dd, 1H, H^{13}), 6.86 (d, 1H, H^{12}), 3.96 (t, 2H, H^δ,H^γ), 3.25 (t, 2H, H^α,H^β), 2.52 (s, 3H, Pd-$NCCH_3$), 1.07 (s, 3H, Pd-CH_3). *trans*: δ = 8.52 (d, 1H, H^6), 8.48 (bs, 1H, H^{im}), 8.20 (t, 1H, H^4), 7.96 (bd, 1H, H^3), 7.76 (t, 1H, H^5), 7.30 (d, 1H, H^{14}), 7.17 (bs, 1H, H^{13}), 7.10 (bs, 1H, H^{12}), 4.13 (t, 2H, H^δ,H^γ), 3.32 (t, 2H, H^α,H^β), 2.13 (bs, 3H, Pd-$NCCH_3$), 1.12 (s, 3H, Pd-CH_3). ^{13}C NMR (500 MHz, CD_2Cl_2, 298 K, from the HSQC spectrum) *cis*: δ = 170.8 (C^{im}), 149.9 (C^6), 140.4 (C^4), 130.0 (C^5), 127.5 (C^{13}), 127.5 (C^3), 127.1 (C^{12}), 125.1 (C^{14}), 61.3 (C^δ,C^γ), 30.6 (C^α,C^β), 3.4 (Pd-$NCCH_3$), 0.1 (Pd-CH_3). *trans*: δ = 148.8 (C^6), 141.3 (C^4), 129.0 (C^3), 128.8 (C^5), 61.5 (C^δ,C^γ), 29.0 (C^α,C^β), 1.9 (Pd-CH_3).

4b. (light orange solid, yield = 81 %); ^{1}H NMR (500 MHz, CD_2Cl_2, 298 K) *cis* 16.7 %, *trans* 83.3 %. *cis*: δ = 8.66 (d, 1H, H^6), 8.15 (td, 1H, H^4), 7.88-7.83 (m, 2H, H^3, H^5), 7.21 (d, 1H, H^{14}), 6.93 (dd, 1H, H^{13}), 6.86 (d, 1H, H^{12}), 4.00 (t, 2H, H^δ,H^γ), 3.22 (t, 2H, H^α,H^β), 2.52 (s, 3H, Pd-$NCCH_3$), 2.19 (s, 3H, CH_3^{im}), 0.95 (s, 3H, Pd-CH_3). *trans*: δ = 8.56 (d, 1H, H^6), 8.24 (td, 1H, H^4), 8.02 (bd, 1H, H^3), 7.75 (t, 1H, H^5), 7.31 (bd, 1H, H^{14}), 7.21 (bs, 1H, H^{13}), 7.10 (bs, 1H, H^{12}), 4.05 (t, 2H, H^δ,H^γ), 3.32 (t, 2H, H^α,H^β), 2.39 (bs, 3H, CH_3^{im}), 2.11 (bs, 3H, Pd-$NCCH_3$), 1.05 (s, 3H, Pd-CH_3). ^{13}C NMR (500 MHz,

CD_2Cl_2, 298 K, from the HSQC spectrum) *cis*: δ = 149.54 (C^6), 140.36 (C^4), 129.8-125.9 (C^5, C^3), 127.5 (C^{13}), 126.7 (C^{12}), 125.1 (C^{14}), 54.8 (C^{δ},C^{γ}), 29.6 (C^{α},C^{β}), 16.3 (CH_3^{im}), 3.5 (Pd-$NCCH_3$), 1.3 (Pd-CH_3). *trans*: δ = 148.4 (C^6), 141.3 (C^4), 128.6 (C^5), 127.1 (C^3), 28.6 (C^{α},C^{β}), 14.6 (CH_3^{im}), 2.5 (Pd-CH_3).

5b. (light yellow solid, yield = 76 %); ^{1}H NMR (500 MHz, CD_2Cl_2, 298 K) *cis* 13.9 %, *trans* 86.1 %. *trans*: δ = 7.38-7.27 (m, H^5, H^m, H^p), 7.20 (bs, 1H, H^4), 7.09 (bs, 1H, H^3), 4.06 (t, 2H, H^{δ},H^{γ}), 3.38 (t, 2H, H^{α},H^{β}), 2.83 (sept, 2H, CH^{iPr}), 2.30-2.06 (bs, 9H, CH_3^{DAB1}, CH_3^{DAB2}, Pd-$NCCH_3$), 1.26 (d, 6H, CH_3^{iPrA}), 1.14 (d, 6H, CH_3^{iPrB}), 0.43 (s, 3H, Pd-CH_3); *cis*: δ = 7.38-7.27 (m, H^5, H^m, H^p), 7.00 (t, 1H, H^4), 6.93 (d, 1H, H^3), 4.02 (t, 2H, H^{δ},H^{γ}), 3.30 (t, 2H, H^{α},H^{β}), 2.91 (sept, 2H, CH^{iPr}), 2.04 (s, 3H, CH_3^{DAB1}), 1.99 (s, 3H, CH_3^{DAB2}), 1.79 (s, 3H, Pd-$NCCH_3$), 1.36 (d, 6H, CH_3^{iPrA}), 1.19 (d, 6H, CH_3^{iPrB}), 0.95 (s, 3H, Pd-CH_3). ^{13}C NMR (500 MHz, CD_2Cl_2, 298 K, from the HSQC spectrum) *trans*: δ = 128.8-124.7 (C^5, C^m, C^p, C^4, C^3), 57.0 (C^{δ},C^{γ}), 28.8 (C^{α},C^{β}), 28.8 (CH^{iPr}), 22.3-18.1 (CH_3^{DAB1}, CH_3^{DAB2}, Pd-$NCCH_3$), 23.6 (CH_3^{iPrA}), 24.1 (CH_3^{iPrB}), 4.9 (Pd-CH_3); *cis*: δ = 129.0-124.8 (C^5, C^m, C^p), 127.9 (C^4), 127.4 (C^3), 55.5 (C^{δ},C^{γ}), 29.7 (C^{α},C^{β}), 29.0 (CH^{iPr}), 20.5 (CH_3^{DAB1}), 18.7 (CH_3^{DAB2}), 2.3 (Pd-$NCCH_3$), 23.8 (CH_3^{iPrA}), 23.9 (CH_3^{iPrB}), 2.5 (Pd-CH_3).

6b. (yellow solid, yield = 78 %); ^{1}H NMR (500 MHz, CD_2Cl_2, 298 K) *cis* 4.9 %, *trans* 95.1 %. *trans*: δ = 7.20 (bs, 5H, H^p, H^m, H^4, H^5), 7.13 (bs, 1H, H^3), 4.02 (t, 2H, H^{δ},H^{γ}), 3.35 (t, 2H, H^{α},H^{β}), 2.30-2.21 (bs, 6H, Pd-$NCCH_3$, CH_3^{DAB2}), 2.12 (s, 6H, CH_3^{Ar}), 2.09 (s, 3H, CH_3^{DAB1}), 0.32 (s, 3H, Pd-CH_3). ^{13}C NMR (500 MHz, CD_2Cl_2, 298 K, from the HSQC spectrum) *trans*: δ = 129.1-128.0 (C^m, C^p), 57.5 (C^{δ},C^{γ}), 28.6 (C^{α},C^{β}), 18.2 (CH_3^{DAB2}, CH_3^{Ar}), 20.6 (CH_3^{DAB1}), 2.6 (Pd-CH_3).

7b. (yellow solid, yield = 81 %); ^{1}H NMR (500 MHz, CD_2Cl_2, 298 K): *cis* 7 %, *trans* 93 %: *trans*: δ = 7.40 (dd, 1H, H^5), 7.34 (dd, 1H, H^p), 7.28-7.27 (m, 2H, H^m), 7.12-7.09 (bs, 2H, H^3, H^4), 5.24 (br s, 2H, $H^{\alpha,\beta}$), 2.82 (sept, 2H, CH^{iPr}), 2.45 (s, 3H, CH_3^{DAB2}), 2.26 (bs, 3H, Pd-$NCCH_3$), 2.13 (s, 3H, CH_3^{DAB1}), 1.28 (d, 6H, CH_3^{iPrA}), 1.14 (d, 6H, CH_3^{iPrB}), 0.41 (s, 3H, Pd-CH_3); *cis*: δ = 7.31 (m, 2H, H^m), 7.03 (m, 1H, H^3), 5.17 (s, 2H, $H^{\alpha,\beta}$), 2.82 (sept, 2H, CH^{iPr}), 2.52 (s, 3H, CH_3^{DAB2}), 2.15 (s, 3H, CH_3^{DAB1}), 1.79 (s, 3H, Pd-$NCCH_3$), 1.34 (d, 6H, CH_3^{iPr}), 1.19 (d, 6H, CH_3^{iPr}), 0.97 (s, 3H, Pd-CH_3). ^{13}C NMR (500 MHz, CD_2Cl_2, 298 K, from the HSQC spectrum): *trans*: δ = 128.9 (C^p), 127.0 ($C^{3,4}$), 126.3 (C^5), 124.7 (C^m), 52.8 ($C^{\alpha,\beta}$), 28.7 (CH^{iPr}), 24.1 (CH_3^{iPrB}), 23.2 (CH_3^{iPrA}), 22.1 (CH_3^{DAB1}), 17.8 (CH_3^{DAB2}), 6.3 (Pd-CH_3), 3.7 (Pd-$NCCH_3$); *cis*: δ = 128.3 (C^m), 126.9 (C^3), 52.9 ($C^{\alpha,\beta}$), 28.7 (CH^{iPr}), 23.9 (CH_3^{iPr}), 23.7 (CH_3^{iPr}), 20.5 (CH_3^{DAB1}), 19.6 (CH_3^{DAB2}), 3.5 (Pd-CH_3), 2.4 (Pd-$NCCH_3$).

3c. (light yellow solid, yield = 83 %); ^{1}H NMR (500 MHz, CD_2Cl_2, 298 K) δ = 8.63 (s, 1H, H^{im}), 8.53 (d, 1H, H^6), 8.23 (t, 1H, H^4), 8.03 (d, 1H, H^3), 7.78 (dd, 1H, H^5), 7.35 (d, 1H, H^{14}), 7.27 (dd, 1H, H^{13}), 7.18 (d, 1H, H^{12}), 4.16 (m, 2H, H^{δ},H^{γ}), 3.30 (dd, 2H, H^{α},H^{β}), 1.12 (s, 3H, Pd-CH_3). ^{13}C NMR (500

MHz, CD_2Cl_2, 298 K, from the HSQC spectrum) δ = 166.72 (C^{im}), 148.4 (C^6), 141.5 (C^4), 134.1 (C^{13}), 130.2 (C^{12}), 129.2 (C^3), 129.0 (C^5), 127.1 (C^{14}), 61.5 (C^{δ},C^{γ}), 28.6 (C^{α},C^{β}), 1.3 (Pd-CH_3).

4c. (light orange solid, yield = 73 %); ^{1}H NMR (500 MHz, CD_2Cl_2, 298 K) δ = 8.55 (d, 1H, H^6), 8.25 (t, 1H, H^4), 8.06 (d, 1H, H^3), 7.79 (m, 1H, H^5), 7.35 (d, 1 H, H^{14}), 7.28 (dd, 1H, H^{13}), 7.17 (s, 1H, H^{12}), 4.03 (m, 2H, H^{δ},H^{γ}), 3.33 (dd, 2H, H^{α},H^{β}), 2.48 (s, 3H, CH_3^{im}), 1.06 (s, 3H, Pd-CH_3). ^{13}C NMR (500 MHz, CD_2Cl_2, 298 K, from the HSQC spectrum) δ = 148.0 (C^6), 141.5 (C^4), 134.3 (C^{13}), 129.0 (C^{12}), 128.8 (C^5), 127.3 (C^3), 127.1 (C^{14}), 57.4 (C^{δ},C^{γ}), 28.4 (C^{α},C^{β}), 16.7 (CH_3^{im}), 2.1 (Pd-CH_3).

5c. (light yellow solid, yield = 80 %); ^{1}H NMR (500 MHz, CD_2Cl_2, 298 K) δ = 7.36 (t, 1H, H^p), 7.29 (d, 2H, H^m), 7.25 (dd, 1H, H^5), 7.21-7.16 (m, 2H, H^3, H^4), 4.02 (t, 2H, H^{δ},H^{γ}), 3.36 (t, 2H, H^{α},H^{β}), 2.81 (sept, 2H, CH^{iPr}), 2.37 (s, 3H, CH_3^{DAB2}), 2.18 (s, 3H, CH_3^{DAB1}), 1.25 (d, 6H, CH_3^{iPrA}), 1.13 (d, 6H, CH_3^{iPrB}), 0.44 (s, 3H, Pd-CH_3). ^{13}C NMR (500 MHz, CD_2Cl_2, 298 K, from the HSQC spectrum) δ = 129.0-124.9 (C^p, C^m), 134.6 (C^5), 129.7-127.5 (C^3, C^4), 57.9 (C^{δ},C^{γ}), 28.5 (C^{α},C^{β}), 28.8 (CH^{iPr}), 18.8 (CH_3^{DAB2}), 22.4 (CH_3^{DAB1}), 23.4 (CH_3^{iPrA}), 24.2 (CH_3^{iPrB}), 3.9 (Pd-CH_3).

6c. (light orange solid, yield = 83 %); ^{1}H NMR (500 MHz, CD_2Cl_2, 298 K) δ = 7.25-7.14 (m, 6H, H^p, H^m, H^5, H^4, H^3), 4.00 (t, 2H, H^{δ},H^{γ}), 3.34 (t, 2H, H^{α},H^{β}), 2.35 (s, 3H, CH_3^{DAB2}), 2.12 (s, 9H, CH_3^{DAB1}, CH_3^{Ar}), 0.33 (s, 3H, Pd-CH_3). ^{13}C NMR (500 MHz, CD_2Cl_2, 298 K, from the HSQC spectrum) δ = 134.5-127.2 (C^p, C^m, C^7, C^6, C^5), 57.8 (C^{δ},C^{γ}), 28.3 (C^{α},C^{β}), 18.6 (CH_3^{DAB2}), 20.6-17.9 (CH_3^{Ar}, CH_3^{DAB1}), 2.1 (Pd-CH_3).

7c. (light brown solid, yield = 72 %); ^{1}H NMR (500 MHz, CD_2Cl_2, 298 K): δ = 7.43 (d, 1H, H^5), 7.36-7.27 (m, 4H, H^m, H^p, H^4), 7.20 (d, 1H, H^3), 5.01 (s, 2H, $H^{\alpha,\beta}$), 2.82 (sept, 2H, CH^{iPr}), 2.47 (s, 3H, CH_3^{DAB2}), 2.17 (s, 3H, CH_3^{DAB1}), 1.22 (d, 6H, CH_3^{iPr}), 1.14 (d, 6H, CH_3^{iPr}), 0.43 (s, 3H, Pd-CH_3). ^{13}C NMR (500 MHz, CD_2Cl_2, 298 K, from the HSQC spectrum): δ = 128.9 (C^3), 128.9-124.7 (C^4, C^m, C^p), 127.8 (C^5), 50.2 ($C^{\alpha,\beta}$), 28.8 (CH^{iPr}), 23.9 (CH_3^{iPr}), 23.5 (CH_3^{iPr}), 21.5 (CH_3^{DAB1}), 19.1 (CH_3^{DAB2}), 2.0 (Pd-CH_3).

4d. (light orange solid, yield = 78 %); ^{1}H NMR (500 MHz, CD_2Cl_2, 298 K) *cis* 13.1 %, *trans* 86.9 %. *cis*: δ = 8.76 (d, 1H, H^6), 8.16 (td, 1H, H^4), 7.88-7.83 (m, 2H, H^3, H^5), 7.21 (d, 1H, H^{14}), 6.93 (dd, 1H, H^{13}), 6.87 (d, 1H, H^{12}), 4.01 (t, 2H, H^{δ},H^{γ}), 3.21 (t, 2H, H^{α},H^{β}), 2.56 (s, 3H, Pd-$NCCH_3$), 2.21 (s, 3H, CH_3^{im}), 0.97 (s, 3H, Pd-CH_3). *trans*: δ = 8.55 (d, 1H, H^6), 8.24 (td, 1H, H^4), 8.09 (bd, 1H, H^3), 7.77 (t, 1H, H^5), 7.31 (bd, 1H, H^{14}), 7.21 (bs, 1H, H^{13}), 7.12 (bs, 1H, H^{12}), 4.07 (t, 2H, H^{δ},H^{γ}), 3.33 (t, 2H, H^{α},H^{β}), 2.43 (bs, 3H, CH_3^{im}), 2.13 (bs, 3H, Pd-$NCCH_3$), 1.05 (s, 3H, Pd-CH_3). ^{19}F NMR (400 MHz, CD_2Cl_2, 298 K) δ = -78.8 (s).

4e. (light orange solid, yield = 60 %); ^{1}H NMR (500 MHz, CD_2Cl_2, 298 K) δ = 8.55 (d, 1H, H^6), 8.27 (t, 1H, H^4), 8.12 (d, 1H, H^3), 7.79 (m, 1H, H^5), 7.35 (d, 1 H, H^{14}), 7.28 (dd, 1H, H^{13}), 7.17 (s, 1H, H^{12}), 4.05 (m, 2H, H^{δ},H^{γ}), 3.33 (dd, 2H, H^{α},H^{β}), 2.50 (s, 3H, CH_3^{im}), 1.04 (s, 3H, Pd-CH_3).

3.4.4. Ethylene/methyl acrylate cooligomerization reactions.

All catalytic experiments were carried out in a Büchi "tinyclave" reactor equipped with an interchangeable 50 mL glass vessel. The liner was loaded with the complex of choice (21 μmol), TFE (21 mL) or DCM (21 mL) and methyl acrylate ([MA]/[Pd] = 594). The vessel was then placed in a preheated oil bath (308 K), connected to the ethylene tank, and then ethylene was bubbled for 10 min. The reactor was pressurized, and the reaction mixture stirred at constant temperature and pressure. After the proper time, the reactor was cooled to room temperature and vented. The reaction mixture was poured in a 50 mL flask with dichloromethane (3 x 2 mL) used to clean the glass vessel. Volatile products were removed under reduced pressure and the residual oil was left to dry at constant weight, then analysed with NMR spectroscopy. The ethylene uptake was measured by performing the catalysis in the same Büchi "tinyclave" reactor connected to a thermal mass flow meter (Bronkhorst EL-FLOW Select model F-111B) and forward pressure controller device (Bronkhorst EL-PRESS model P-602). Gas flow needed to feed the reactor at a constant pressure was computer-recorded using the FlowPlot interface.

3.4.5 General procedures for in situ NMR reactivities.

In situ NMR progressive additions of CH_3CN to cationic complexes.

A 10 mM solution of the desired complex in CD_2Cl_2 is prepared and a first ^{1}H NMR spectrum is recorded. The reaction is followed over time at T = 298 K adding progressive equivalents of CH_3CN (from 1.0 to 10.0 eq.), as calculated with respect to *trans* isomer.

General procedure for the in situ NMR reactivity of cationic complex with ethylene.

A 10 mM solution of the desired cationic complex in CD_2Cl_2 is prepared, and a first ^{1}H NMR spectrum is recorded. Ethylene is bubbled into the NMR tube for 5 min. The reaction is followed over time, at T = 298 K.

General procedure for the in situ ^{1}H NMR reactivity of cationic complex with methyl acrylate.

A 10 mM solution of the desired cationic complex in CD_2Cl_2 is prepared, and a first ^{1}H NMR spectrum is recorded. Methyl acrylate (2 eq.) is then added to the solution. The reaction is followed over time, at T = 298 K.

General procedure for the in situ ^{1}H NMR reactivity of cationic complex with both comonomers.

A 10 mM solution of the desired cationic complex in CD_2Cl_2 is prepared, and a first ^{1}H NMR spectrum is recorded. Methyl acrylate (2 eq.) is added to the solution, followed by bubbling of ethylene into the NMR tube for 5 min. The reaction is followed over time, at T = 298 K.

3.5. References.

(1) Alberoni, C.; D'Alterio, M. C.; Balducci, G.; Immirzi, B.; Polentarutti, M.; Pellecchia, C.; Milani, B. Tunable "In-Chain" and "At the End of the Branches" Methyl Acrylate Incorporation in the Polyolefin Skeleton through Pd(II) Catalysis. *ACS Catal.* **2022**, *12*, 3430–3443.

(2) Zhang, Y.; Wang, C.; Mecking, S.; Jian, Z. Ultrahigh Branching of Main-Chain-Functionalized Polyethylenes by Inverted Insertion Selectivity. *Angew. Chemie* **2020**, *132* (34), 14402–14408.

(3) Zhang, Y.; Jian, Z. Comprehensive Picture of Functionalized Vinyl Monomers in Chain-Walking Polymerization. *Macromolecules* **2020**, *53* (20), 8858–8866.

(4) Takano, S.; Takeuchi, D.; Osakada, K.; Akamatsu, N.; Shishido, A. Dipalladium Catalyst for Olefin Polymerization: Introduction of Acrylate Units into the Main Chain of Branched Polyethylene. *Angew. Chemie - Int. Ed.* **2014**, *53* (35), 9246–9250.

(5) Dong, J.; Wang, B. Homo- And Copolymerization of Norbornene Using Tridentate IzQO Palladium Catalysts with Dimethylaminoethyl as a Side Arm. *Polym. Chem.* **2021**, *12* (32), 4736–4747.

(6) Rogness, D. C.; Markina, N. A.; Waldo, J. P.; Larock, R. C. Synthesis of Pyrido[1,2- a]Indole Malonates and Amines through Aryne Annulation. *J. Org. Chem.* **2012**, *77* (6), 2743–2755.

(7) Motswainyana, W. M.; Ojwach, S. O.; Onani, M. O.; Iwuoha, E. I.; Darkwa, J. Novel Hemi-Labile Pyridyl-Imine Palladium Complexes: Synthesis, Molecular Structures and Reactions with Ethylene. *Polyhedron* **2011**, *30* (15), 2574–2580.

(8) Rosar, V.; Dedeic, D.; Nobile, T.; Fini, F.; Balducci, G.; Alessio, E.; Carfagna, C.; Milani, B. Palladium Complexes with Simple Iminopyridines as Catalysts for Polyketone Synthesis. *Dalt. Trans.* **2016**, *45* (37), 14609–14619.

(9) Durand, J.; Zangrando, E.; Stener, M.; Fronzoni, G.; Carfagna, C.; Binotti, B.; Kamer, P. C. J.; Müller, C.; Caporali, M.; Van Leeuwen, P. W. N. M.; Vogt, D.; Milani, B. Long-Lived Palladium Catalysts for CO/Vinyl Arene Polyketones Synthesis: A Solution to Deactivation Problems. *Chem. - A Eur. J.* **2006**, *12* (29), 7639–7651.

(10) Fang, X.; Watkin, J. G.; Scott, B. L.; Kubas, G. J. Electrophilic Cationic Palladium(II) Complexes Containing a Diimine Ligand with Pendant Thienyl Groups. X-Ray Structure of {PdIIMe[1,4-Bis(2′-(2- Thienyl)Ethyl)2,3-Dimethyl-1,4-Diazabutadiene]}. *Organometallics* **2001**, *20* (15), 3351–3354.

(11) Scarel, A.; Durand, J.; Franchi, D.; Zangrando, E.; Mestroni, G.; Milani, B.; Gladiali, S.; Carfagna, C.; Binotti, B.; Bronco, S.; Gragnoli, T. Trifluoroethanol: Key Solvent for Palladium-Catalyzed Polymerization Reactions. *J. Organomet. Chem.* **2005**, *690* (8 SPEC. ISS.), 2106–2120.

(12) Canil, G.; Rosar, V.; Dalla Marta, S.; Bronco, S.; Fini, F.; Carfagna, C.; Durand, J.; Milani, B. Unprecedented Comonomer Dependence of the Stereochemistry Control in Pd-Catalyzed CO/Vinyl Arene Polyketone Synthesis. *ChemCatChem* **2015**, *7* (14), 2255–2264.

(13) Dall'Anese, A.; Fiorindo, M.; Olivieri, D.; Carfagna, C.; Balducci, G.; Alessio, E.; Durand, J.; Milani, B. Pd-Catalyzed CO/Vinyl Arene Copolymerization: When the Stereochemistry Is Controlled by the Comonomer. *Macromolecules* **2020**, *53* (18), 7783–7794.

(14) Dall'Anese, A., PhD thesis "Palladium catalyzed copolymerizations: from ligand architecture to macromolecule microstructure", University of Trieste, A.A. **2018**/**2019**.

(15) Ó Máille, G. M.; Dall'Anese, A.; Grossenbacher, P.; Montini, T.; Milani, B.; Albrecht, M. Modulation of N^N′-Bidentate Chelating Pyridyl-Pyridylidene Amide Ligands Offers Mechanistic Insights into Pd-Catalysed Ethylene/Methyl Acrylate Copolymerisation. *Dalt. Trans.* **2021**, *50* (18), 6133–6145.

(16) Cruz, T. F. C.; Figueira, C. A.; Veiros, L. F.; Gomes, P. T. Benzylnickel(II) Complexes of 2-Iminopyrrolyl Chelating Ligands: Synthesis, Structure, and Catalytic Oligo-/Polymerization of Ethylene to Hyperbranched Polyethylene. *Organometallics* **2021**, *40* (15), 2594–2609.

(17) Dall'Anese, A.; Tosolini, M.; Alberoni, C.; Balducci, G.; Polentarutti, M.; Pellecchia, C.; Tecilla, P.; Milani, B. Palladium (II) Complexes with the 4 , 5-Bis (Diphenylphosphino) Acenaphthene Ligand and Their Reactivity with Ethylene. *Eur. J. Inorg. Chem.* **2022**, *in press.*

(18) Milani, B.; Marson, A.; Scarel, A.; Mestroni, G.; Ernsting, J. M.; Elsevier, C. J. Facile Synthesis of New, Stable, Palladium-Ethyl Derivatives Containing Nitrogen-Donor Ligands. *Organometallics* **2004**, *23* (9), 1974–1977.

(19) Rosar, V.; Montini, T.; Balducci, G.; Zangrando, E.; Fornasiero, P.; Milani, B. Palladium-Catalyzed Ethylene/Methyl Acrylate Co-Oligomerization: The Effect of a New Nonsymmetrical α-Diimine with the 1,4-Diazabutadiene Skeleton. *ChemCatChem* **2017**, *9* (17), 3402–3411.

(20) Abakumov, G. A.; Cherkasov, V. K.; Druzhkov, N. O.; Kocherova, T. N.; Shavyrin, A. S. New Polydentate Ligands Based on Sterically Hindered O-Benzoquinones (Pyrocatechols) Containing the 1,4-Diazadiene Group. *Russ. Chem. Bull.* **2011**, *60* (1), 112–117.

(21) Meduri, A.; Montini, T.; Ragaini, F.; Fornasiero, P.; Zangrando, E.; Milani, B. Palladium-Catalyzed Ethylene/Methyl Acrylate Cooligomerization: Effect of a New Nonsymmetric α-Diimine. *ChemCatChem* **2013**, *5* (5), 1170–1183.

(22) Navarro, M.; Rosar, V.; Montini, T.; Milani, B.; Albrecht, M. Olefin Dimerization and Isomerization Catalyzed by Pyridylidene Amide Palladium Complexes. *Organometallics* **2018**, *37* (20), 3619–3630.

(23) Wiedemann, T.; Voit, G.; Tchernook, A.; Roesle, P.; Göttker-Schnetmann, I.; Mecking, S. Monofunctional Hyperbranched Ethylene Oligomers. *J. Am. Chem. Soc.* **2014**, *136* (5), 2078–2085.

(24) Mecking, S. Mechanistic Studies of the Palladium-Catalyzed Copolymerization of Ethylene and α-Olefins with Methyl Acrylate. *J. Am. Chem. Soc.* **1998**, *120* (5), 888–899.

(25) Wang, H.; Duan, G.; Fan, H.; Dai, S. Second Coordination Sphere Effect of Benzothiophene Substituents on Chain Transfer and Chain Walking in Ethylene Insertion Polymerization. *Polymer*. **2022**, *245* (February), 124707.

(26) Dall'Anese, A.; Rosar, V.; Cusin, L.; Montini, T.; Balducci, G.; D'Auria, I.; Pellecchia, C.; Fornasiero, P.; Felluga, F.; Milani, B. Palladium-Catalyzed Ethylene/Methyl Acrylate Copolymerization: Moving from the Acenaphthene to the Phenanthrene Skeleton of α-Diimine Ligands. *Organometallics* **2019**, *38* (19), 3498–3511.

CHAPTER 4

Moving from acetonitrile to pyridine ligand in the Pd(II) coordination sphere for the synthesis of hyperbranched ethylene/methyl acrylate copolymers.

Overview

Pd(II) complexes with α-diimine ligands are one of the main catalytic systems active for the copolymerization of ethylene with methyl acrylate (MA), leading to branched copolymers with the polar monomer inserted almost exclusively at the end of the branches. With the aim to discover highly efficient catalysts able to control the polar monomer enchainment during the copolymerization process, pursuing the alternative strategy to ligand design, we have now investigated a new class of Pd(II) complexes, of general formula $[Pd(CH_3)(L)(N\text{-}N)][PF_6]$, having a highly coordinating ligand, L, such as pyridine or its derivatives. These new complexes have been characterized both in solution by NMR spectroscopy and in solid state by X-Ray analysis. A detailed investigation of their catalytic behavior in the copolymerization of ethylene with MA was performed. The pyridine ligand is involved in the target reaction suggesting that it remains close to the metal center during the catalysis and it affects both the macromolecules microstructure and the way of MA enchainment. In addition, both DFT calculations and *in situ* NMR studies confirm that a new open-chain intermediate having both the pyridine ligand and the growing polymeric chain bonded to palladium ion is formed.

Alberoni, C., D'Alterio, M. C., Balducci, G., Polentarutti, M., Pellecchia, C., Milani, B. *manuscript in preparation*.

4.1 Introduction.

The main catalytic systems active for the copolymerization of ethylene (E) with methyl acrylate (MA) are based on Pd(II) complexes with α-diimine ligands (N-N) (Figures 1.5 – 1.8, Chapter 1) or phosphino-sulfonate derivatives (Figure 1.9, Chapter 1).[1,2] In general, to be applicable at the industrial level, the ideal catalyst, in addition to show a high productivity, has to control some parameters over the produced macromolecules, such as the molecular weight, the amount of incorporated polar monomer and its way of enchainment. The industrial target E/MA macromolecules should be linear ones with low amount of MA (less than 20 mol %) inserted in the main chain. In literature, several examples of Pd(II) complexes with different N-N ancillary ligands are reported and the study of these systems continue to expand. Some investigated structural variations are based on the ligand design, related to modify the α-diimine skeleton[3,4,5] or increase the congestion produced by a nonsymmetric ligand to tune properties of the obtained copolymers[6] or, at least, desymmetrize the ligand itself.[7] In the last years a new approach based on the studied of the secondary interactions is taking hold. It involves the introduction of specific functional group on the *ortho* positions of the aryl rings of the N-N ligand (e.g. an amide[8] or a thiophenic fragment[9]) or the replacement of the labile ligand (e.g. CH_3CN, Et_2O) in the fourth coordination site with different molecules. All these variations highlight that these groups might generate weak interactions in some intermediates involved in the copolymerization reaction and they might control the polar monomer enchainment. Moreover, they stabilize the Pd(II) complexes.

Recently, Pd(II) compounds of general formula $[Pd(CH_3)(N\text{-}N)(N\text{-}S)][PF_6]$, with the well-known N-N bidentate ligand **1** and a hemilabile potentially bidentate one, as a thiophenimine N-S, are reported as catalysts for ethylene/methyl acrylate copolymerization (Figure 4.1).[10] The N-S ligand present in the fourth coordination site of the metal center is able to affect the way of the polar monomer enchainment and the produced E/MA copolymers show MA inserted both in the main chain and at the end of the branches. Detailed *in situ* NMR studies on the reaction of the precatalyst with the two comonomers point out that the N-S ligand remains in the palladium coordination sphere during catalysis (Scheme 2.6, Chapter 2).

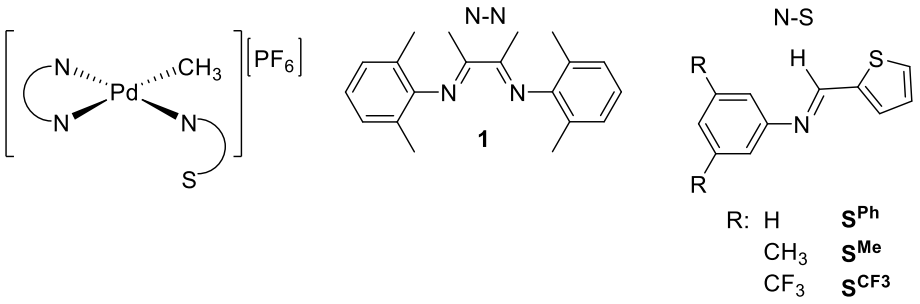

Figure 4.1. Investigated Pd(II) complexes $[Pd(CH_3)(N\text{-}N)(N\text{-}S)][PF_6]$.

Also Pd(II) complexes bearing the phosphino-sulfonate ligands are active for the ethylene/methyl acrylate copolymerization and the obtained copolymers are linear macromolecules with acrylate units incorporated in a high amount exclusively in the main chain (M(MA)).[11,12,13] On the other hand, the high percentage of inserted MA (up to 52 mol %) does not allow to maintain the thermoplastic features of pristine polyolefins and the class of these catalysts show comparable performances to those bearing N-N bidentate ligands only when the copolymerization reactions are carried out under harsh reaction conditions. In literature some investigated structural variations are reported, too.

Firstly, the introduction of Bis-Phosphine Mono-Oxide (BPMO) ligands (**L22** and **L23**, Figure 4.2) with different substituents on the *ortho* positions of the aryl rings is reported by Nozaki *et al.*.[14] Moving from methoxy to trifluoromethyl groups, the activity increases (4.1 *vs* 5.9 kg CP/mol Pd·h, respectively), while the amount of inserted MA decreases from 2.3 mol % using **L22^{Pd}** to 0.9 mol % with **L23^{Pd}**. They are the first example of Pd(II) catalysts containing the [P(III)-P(V)=O] coordination pattern, which then inspired the synthesis of new bidentate phosphino-(diethyl-phoshonate) ligand (**L24**, Figure 4.2).[15] Catalyst bearing **L24** shows an activity of 58 kg CP/mol Pd·h and the obtained linear copolymers present 1.5 mol % of MA, almost exclusively inserted as M(MA) (95 % of selectivity). The catalysis are carried out at 353 K under 28 atm of ethylene pressure. In addition Pd(II) complexes with phosphonamide (**L26**, Figure 4.2) and phosphino-phosphon(bisamide) (**L27**, Figure 4.2) ligands are tested in the target copolymerization leading to linear copolymers with either 16 or 5.4 mol %, respectively, of inserted M(MA).[16,17]

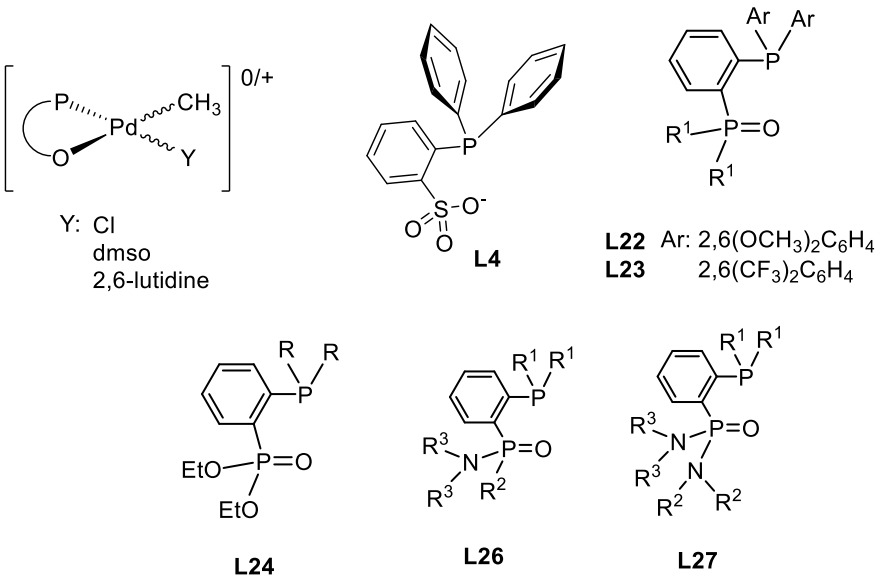

Figure 4.2 Examples of phosphino-sulfonate ligands reported in literature.

Since the bidentate ligands, N-N and P-O, are strong σ-donors, a huge portion of the metal center is in an inactive dormant state and this limits the range of comonomers incorporation. So a potentially more labile ligand in the fourth coordination site has to be present. In particular dimethyl sulfoxide (dmso), pyridine (pyr) or 2,6-lutidine (2,6lut) are the most commonly used labile ligands in P-O Pd(II) complexes.[12]

So merging the approach that studies the secondary interactions in Pd(II) α-dimmine compounds and the presence of a specific coordinating ligand in fourth site in the P-O Pd(II) complexes, we decided to introduce in the palladium coordination sphere, in addition to the α-diimine, a monodentate ligand belonging to the family of pyridines. With this aim we studied the monocationic Pd(II) complexes of general formula $[Pd(CH_3)(L)(N\text{-}N)][PF_6]$, where L is the pyridine ligand with different substituents on the positions of the pyridine ring and N-N is the symmetric ligand **1** or **2**. The catalytic behavior of these complexes in the ethylene/methyl acrylate copolymerization was investigated in detailed under mild reaction conditions and compared with that of the parent compound $[Pd(CH_3)(NCCH_3)(\mathbf{1})][PF_6]$, **1b**, and $[Pd(CH_3)(NCCH_3)(\mathbf{2})][PF_6]$, **2b**. In deep *in situ* NMR reactions of such complexes with ethylene, MA and both comonomers were also performed to gain information about the mechanism of the copolymerization reaction.

4.2 Results and Discussion.

4.2.1 Synthesis and characterization of cationic Pd(II) complexes ***1***^{pyr} – ***1***^{3,5lut} *and* ***2***^{pyr} – ***2***^{3,5lut}.

Initially, the reaction of [Pd(CH_3)($NCCH_3$)(**2**)][PF_6], **2b**, with 4-picoline is studied by *in situ* NMR spectroscopy, adding 1.2 eq. of the ligand to the 10 mM CD_2Cl_2 solution of the palladium complex, at room temperature. As observed in the ^{1}H NMR spectrum (Figure 4.3), the coordination of 4-picoline to Pd ion occurs as soon as the two species are mixed together. A new set of signals, reasonably due to [Pd(CH_3)(4pic)(**2**)][PF_6], **2**^{4pic}, appears with weak resonances assigned to the excess amount of 4-picoline. In addition the signal of free CH_3CN (singlet at 1.99 ppm) is observed.

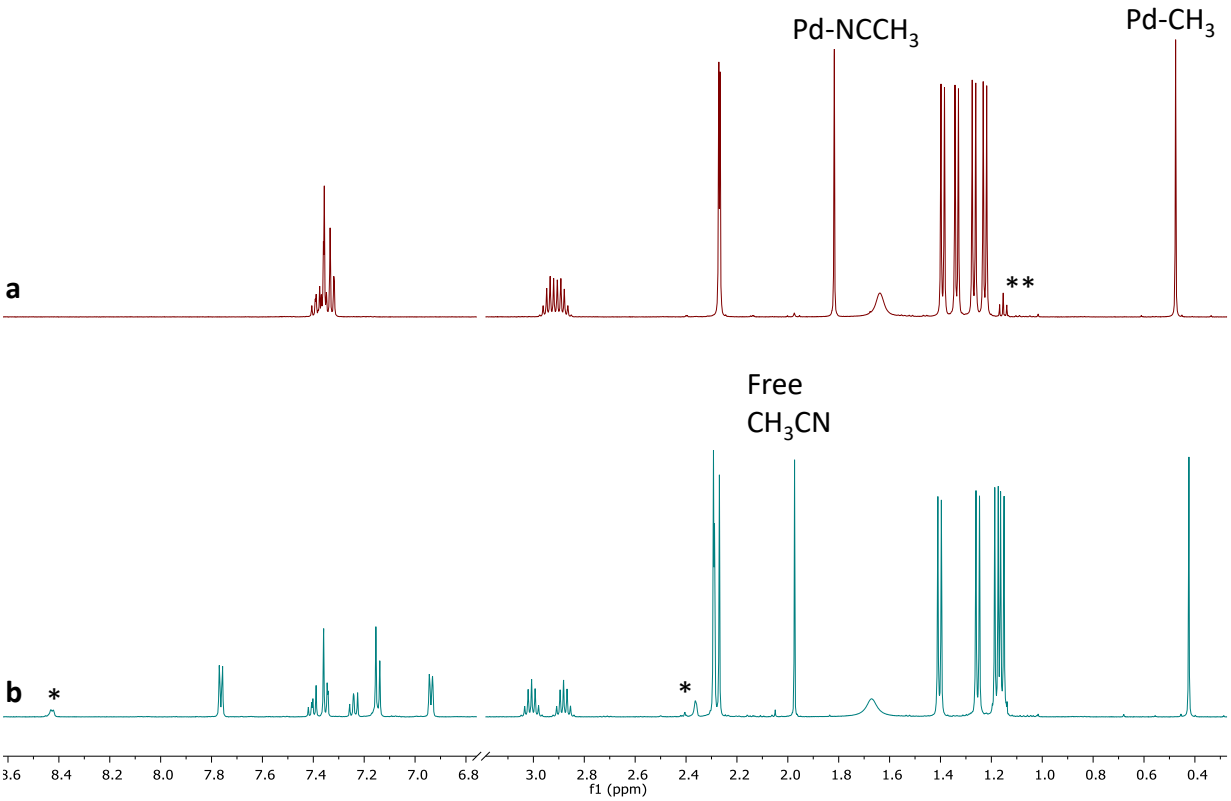

Figure 4.3. ^{1}H NMR spectra (CD_2Cl_2, 298 K) of (a) **2b** and (b) **2b** + 4pic at t = 1 min; *free 4-picoline; **diethyl ether.

So, the monocationic Pd(II) complexes are synthesized starting from the reported cationic complex bearing the acetonitrile in the fourth coordination site, [Pd(CH_3)($NCCH_3$)(**1**)][PF_6], **1b**, and [Pd(CH_3)($NCCH_3$)(**2**)][PF_6], **2b**.[18] The desired complexes are isolated as yellow solids in moderate – high yields (from 57 to 91 %) (Scheme 4.1).

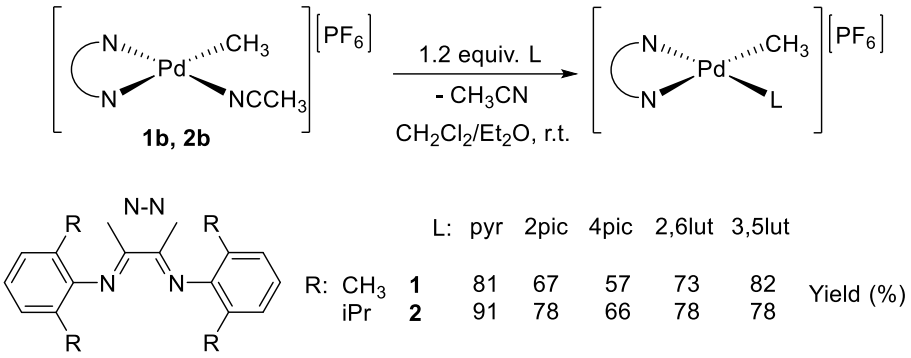

Scheme 4.1. Synthesis of Pd(II) complexes under investigation.

All monocationic complexes are characterized in solution by NMR spectroscopy recording the spectra in CD_2Cl_2 at room temperature. The proton to signal is assigned and the number of peaks and their integration are in agreement with the coordination of the monodentate ligand to palladium ion. In addition, the singlet at 1.82 ppm relative to Pd-$NCCH_3$ fragment of the precursors disappears. As an example the characterization of $\mathbf{2}^{\mathbf{pyr}}$ is discussed. In the aliphatic region of the ^1H NMR spectrum (Figure 4.4), the singlet at 0.46 ppm, the signals in the range 1.15 – 1.41 ppm and those at 2.85 – 3.05 are easily assigned to Pd-CH_3 fragment (for the diagnostic chemical shift of its carbon value at 9.8 ppm in the $^1H,^{13}C$ HSQC spectrum (Figure S4.6)), CH_3 and CH groups of isopropyl moieties on the aryl rings, respectively. On the basis of $^1H,^1H$ COSY experiment it is possible to recognize that the doublet at 7.95 ppm is due to $H^{2,6}$ of pyridine for the correlation peaks with $H^{3,5}$ at 7.13 ppm and the triplet of H^4 at 7.72 ppm (Figure 4.5). The two different halves of **2** are identified thanks to $^1H,^1H$ NOESY experiment, due some cross peaks generated by the Overhauser effect between the singlet of CH_3^{DAB} groups and the signals of substituted groups on the aryl rings (Figure S4.7).

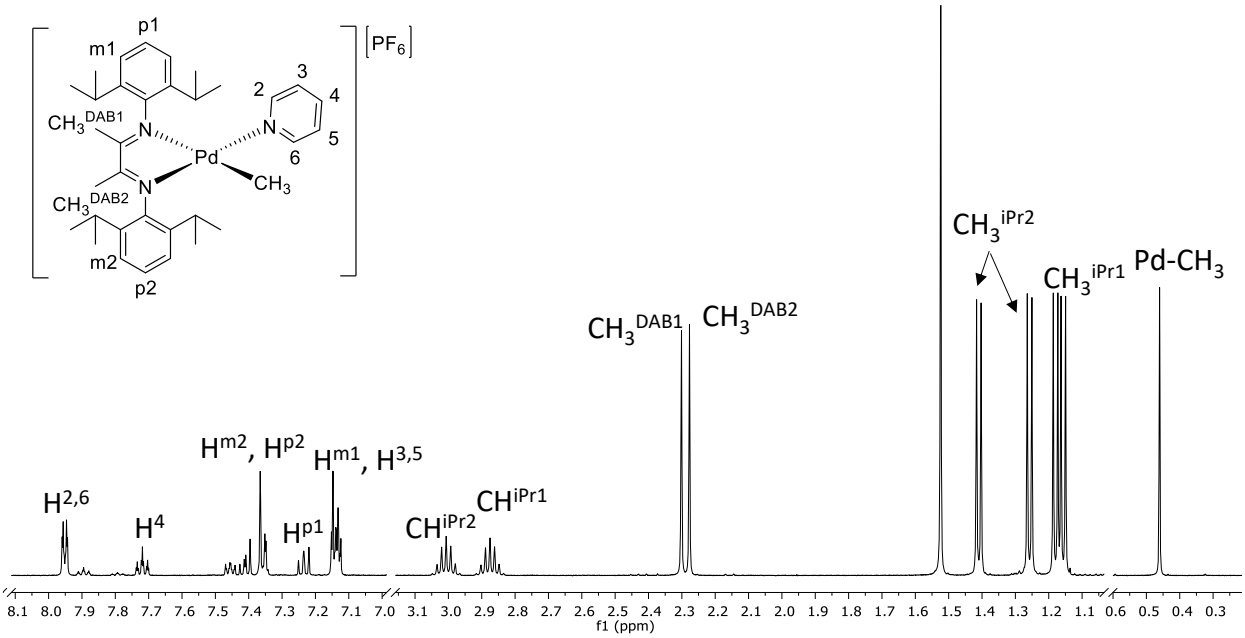

Figure 4.4. ^{1}H NMR spectrum (CD_2Cl_2, 298 K) of **2^{pyr}**.

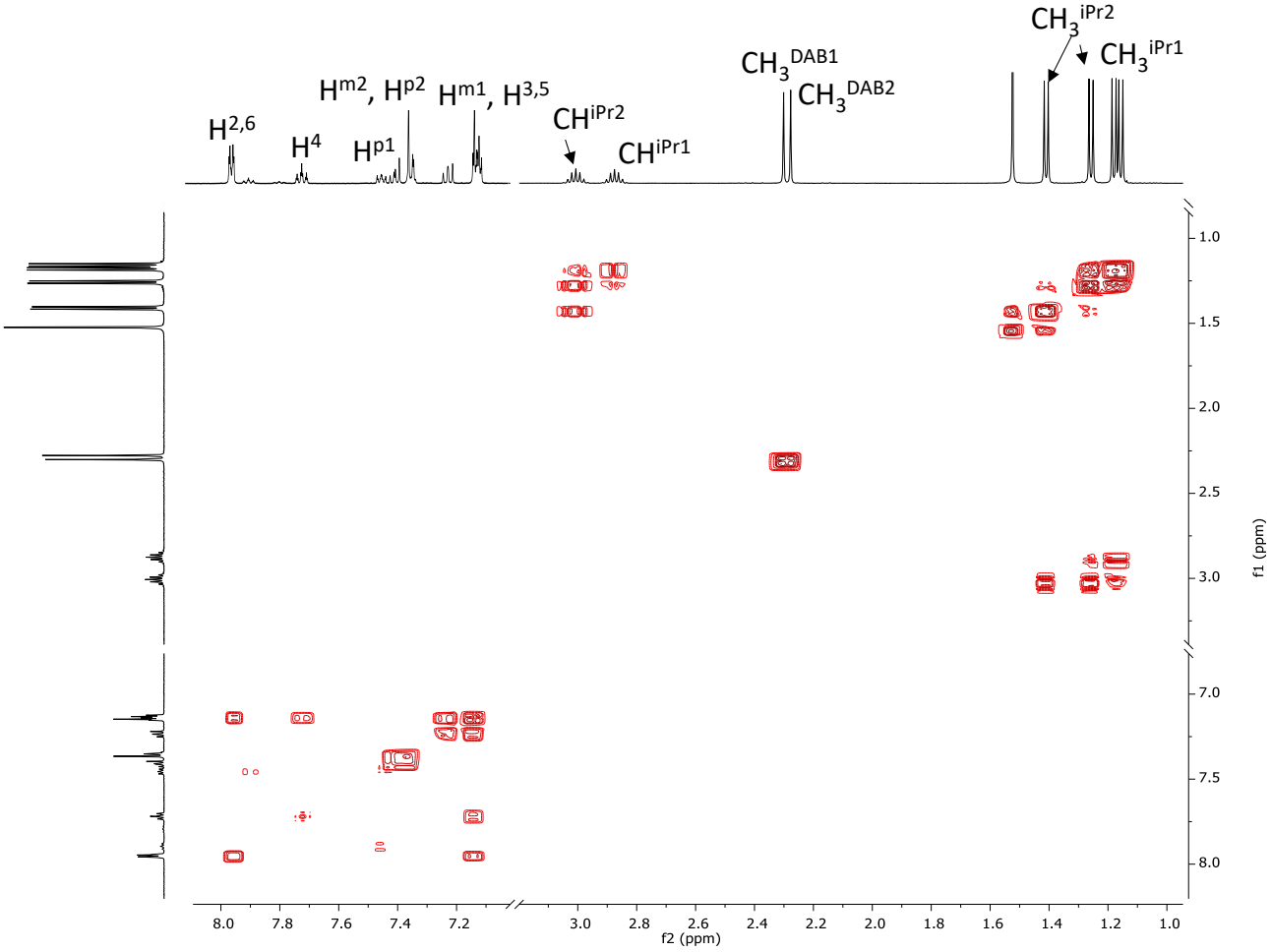

Figure 4.5. ^{1}H,^{1}H COSY spectrum (CD_2Cl_2, 298 K) of **2^{pyr}** (aliphatic and aromatic region not on scale).

Focusing on the ^{1}H NMR spectra of cationic complexes **1**$^{\mathbf{2pic}}$ and **2**$^{\mathbf{2pic}}$, the presence of different resonances assigned to DAB skeleton and the increase in the number of signals of methyl or isopropyl groups, respectively, indicate that the plane of palladium ion is not an element of symmetry any more. As for **2**$^{\mathbf{2pic}}$, in the aliphatic region of ^{1}H NMR spectrum (Figure 4.6), in addition to the diagnostic singlets at 0.27 ppm of the Pd-CH_3 fragment and at 2.83 ppm relative to CH_3^{pic}, eight doublets and four septets are observed assigned to CH_3^{iPr} and CH^{iPr}, respectively, for the presence of two different halves of **2**. Finally, the two closed singlet of CH_3^{DAB} at 2.28 and 2.29 ppm are observed. On the basis of the ^{1}H,^{1}H NOESY spectrum (Figure 4.7), the two different halves of **2** are discriminated and the doublets of CH_3^{iPr} groups can be assigned. Moreover, some exchange peaks between different doublets of CH_3^{iPr} groups are present indicating those of the same aryl ring. The same consideration might be done for the four septets of CH^{iPr} groups.

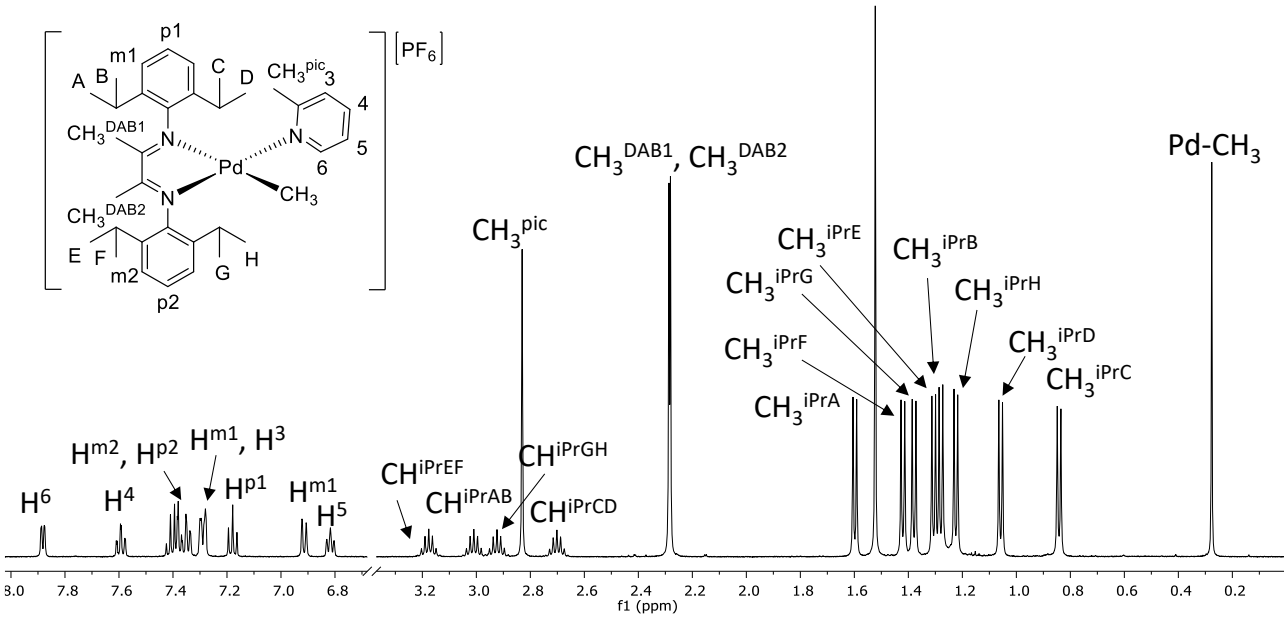

Figure 4.6. ^{1}H NMR spectrum (CD_2Cl_2, 298 K) of **2**$^{\mathbf{2pic}}$.

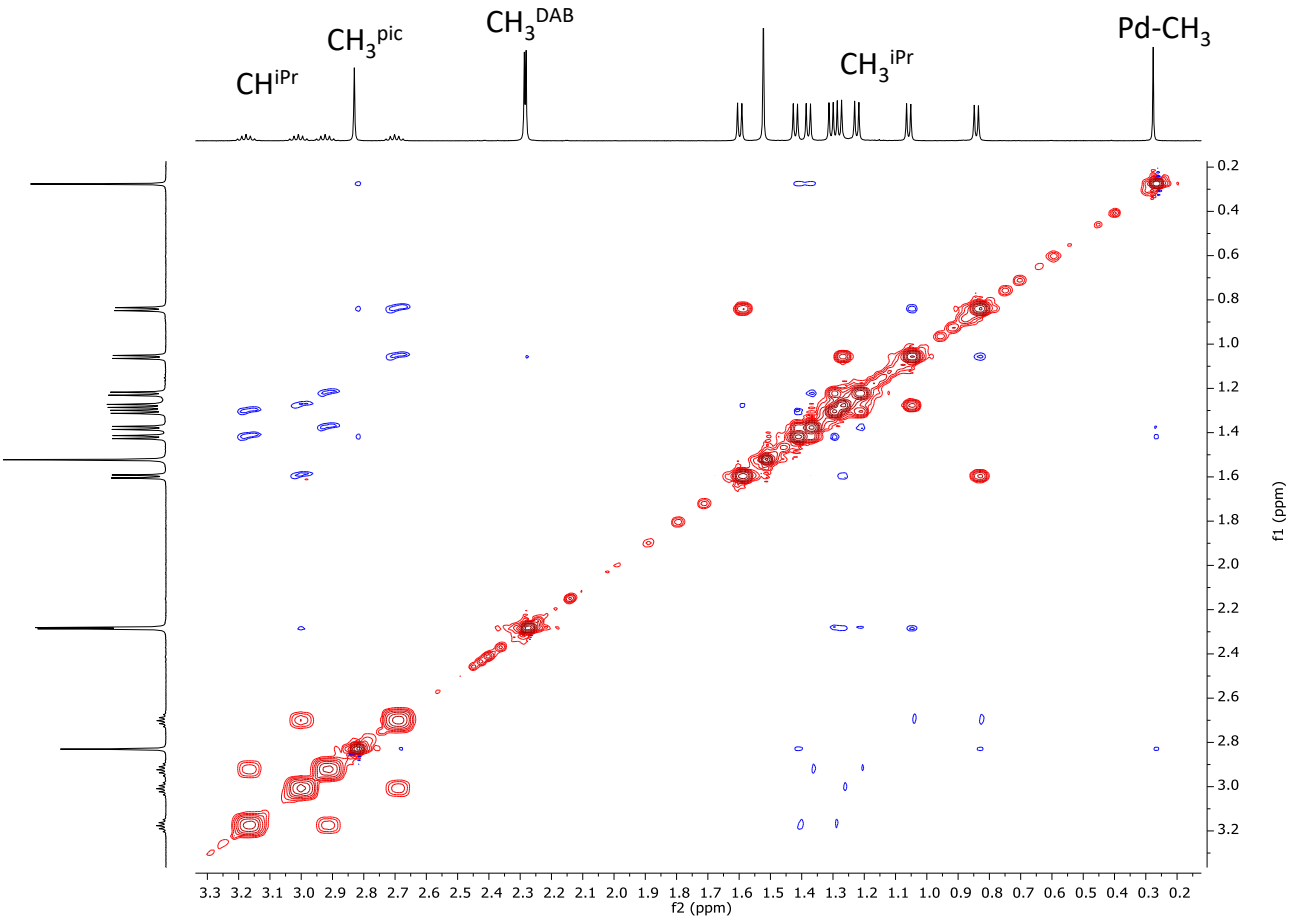

Figure 4.7. $^{1}H,^{1}H$ NOESY spectrum (CD_2Cl_2, 298 K) of **2^{2pic}**.

The $^{1}H,^{1}H$ COSY and $^{1}H,^{13}C$ HSQC experiments (Figures 4.8 and S4.8) allow to detect protons of the picoline ligand: the doublet at 7.88 ppm with the diagnostic chemical shift of its carbon atom at 151.0 ppm is assigned to H^6 and it correlates with the triplet at 6.82 ppm (H^5) that on its turn has a cross peak with the signal at 7.59 ppm relative to H^4. The latter shows another correlation peak with a broad signals at 7.29 ppm assigned to H^3 and H^{m1} of one of the aryl ring.

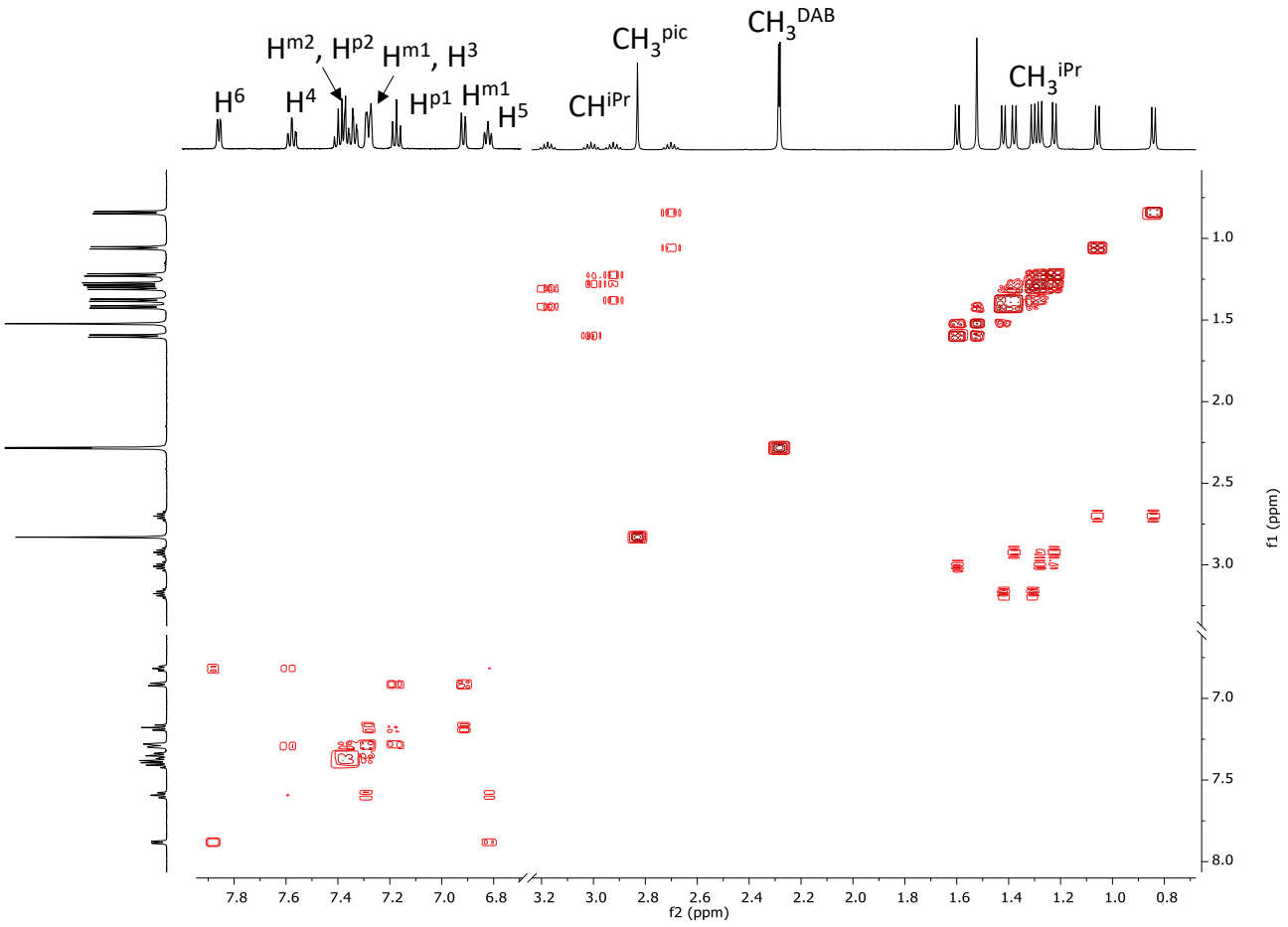

Figure 4.8. $^{1}H,^{1}H$ COSY spectrum (CD_2Cl_2, 298 K) of $\mathbf{2^{2pic}}$; aliphatic and aromatic region not on scale.

Suitable crystals are obtained by slow diffusion of *n*-hexane into a CD_2Cl_2 solution of the desired complex kept at 277 K for 2 weeks. In all solid state structures the palladium ion shows the expected square planar coordination geometry with the α-diimine **1** or **2** as a chelating ligand and the pyridine/picoline bonded as a monodentate one (Figures 4.9, 4.10 and S4.12). Recorded crystallographic data reflect different trends depending on the nature of the N-N ligand present in the coordination sphere (Table S4.1). Focusing on the series with **1** as the bidentate nitrogen donor ligand (Figure 4.9), the values of the bite angle N32-Pd1-N31 are typical of 5-membered palladacycle (77.49(5)° for $\mathbf{1^{2pic}}$ and of 77.44(8)° for $\mathbf{1^{4pic}}$) reported in literature.[10,19]

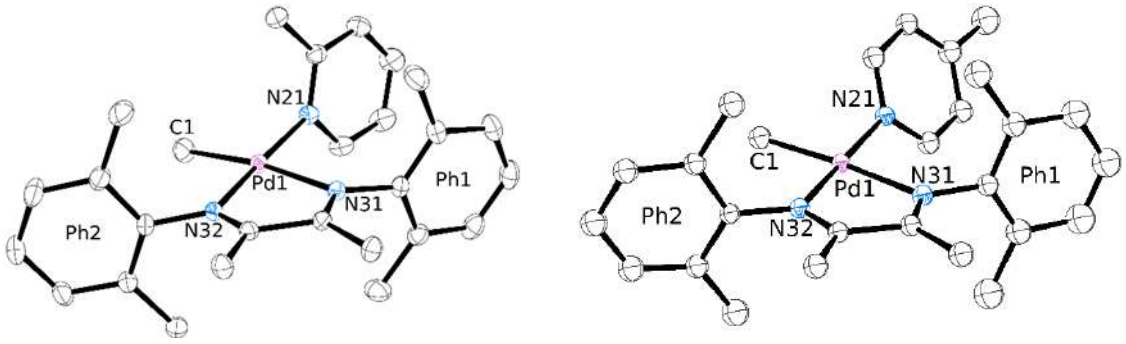

(a) (b)

Figure 4.9. ORTEP drawing (50% probability ellipsoids) of the molecule of (a) $\mathbf{1}^{\mathbf{2pic}}$ and (b) $\mathbf{1}^{\mathbf{4pic}}$. Hydrogen atoms and the PF_6^- anion have been omitted for the sake of clarity.

The aryl rings of DAB skeleton show an almost orthogonal orientation with respect to the palladium square plane forming with the latter dihedral angles of 83.03(5)° and 88.00(5)° for $\mathbf{1}^{\mathbf{2pic}}$ and 81.82(5)° and 88.14(8)° for $\mathbf{1}^{\mathbf{4pic}}$. In agreement with the higher *trans* influence of Pd-CH_3 bond with respect to Pd1-N21 fragment, the bond length Pd1-N31 is longer in both complexes (2.121(1) Å and 2.145(2) Å for $\mathbf{1}^{\mathbf{2pic}}$ and $\mathbf{1}^{\mathbf{4pic}}$, respectively) than the Pd1-N32 distance (2.033(1) Å for $\mathbf{1}^{\mathbf{2pic}}$ and 2.040(2) Å for $\mathbf{1}^{\mathbf{4pic}}$). Focusing on the picoline ligand, its aryl ring is slightly twisted out from the palladium plane, forming a dihedral angle [Pyr]---[Pd1] of 82.30(5)° in $\mathbf{1}^{\mathbf{2pic}}$ and 59.0(1)° in $\mathbf{1}^{\mathbf{4pic}}$. The higher value recorded for $\mathbf{1}^{\mathbf{2pic}}$ suggests that the 2-picoline does not remain close to the plane of the complex to reduce the steric and electronical repulsions that might be present between it and the methyl groups of **1**. In addition, the Pd1-N21 bond length of $\mathbf{1}^{\mathbf{2pic}}$ is shorter to that of $\mathbf{1}^{\mathbf{4pic}}$ (2.032(1) Å *vs* 2.039(2) Å, respectively).

Also, the solid state structures of the Pd(II) complexes $\mathbf{2}^{\mathbf{pyr}}$, $\mathbf{2}^{\mathbf{2pic}}$ and $\mathbf{2}^{\mathbf{4pic}}$ are solved (Figures 4.10 and S4.12). Structural considerations about the N-N chelating ligand **2** are analogous of those previously discussed for **1**. The values of angles and bond distances of the 5-membered palladacycle are in agreement with those reported in literature.[10,19] The bond length Pd1-N31, in *trans* position with respect to Pd-CH_3 fragment, is longer in all complexes (2.140(1) Å, 2.130(2) Å and 2.145(2) Å for $\mathbf{2}^{\mathbf{pyr}}$, $\mathbf{2}^{\mathbf{2pic}}$ and $\mathbf{2}^{\mathbf{4pic}}$, respectively) than the Pd1-N32 distance (2.031(1) Å for $\mathbf{2}^{\mathbf{pyr}}$, 2.041(1) Å for $\mathbf{2}^{\mathbf{2pic}}$ and 2.032(1) Å for $\mathbf{2}^{\mathbf{4pic}}$), in agreement with the higher *trans* influence of Pd-CH_3 bond rather than the Pd1-N21 fragment. Focusing on the picoline ligand, a different behavior moving from $\mathbf{2}^{\mathbf{2pic}}$ to $\mathbf{2}^{\mathbf{4pic}}$ with respect to the previous discussed data are observed about the dihedral angle values between the picoline ligand and the palladium square plane.

The methyl hindrance present on the *ortho* position of 2-picoline in $\mathbf{2^{2pic}}$ affects the dihedral angle between it and the complex plane reaching the value of 30.20(9)° (*vs* 52.71(7)° for $\mathbf{2^{4pic}}$) suggesting a decrease in the electronic repulsions between the methyl group of the monodentate ligand and the isopropyl groups of **2**. This trend is reflected by the value of the Pd-CH_3 bond length, which is longer for $\mathbf{2^{2pic}}$ (2.077(2) Å) than for $\mathbf{2^{4pic}}$ (2.046(2) Å).

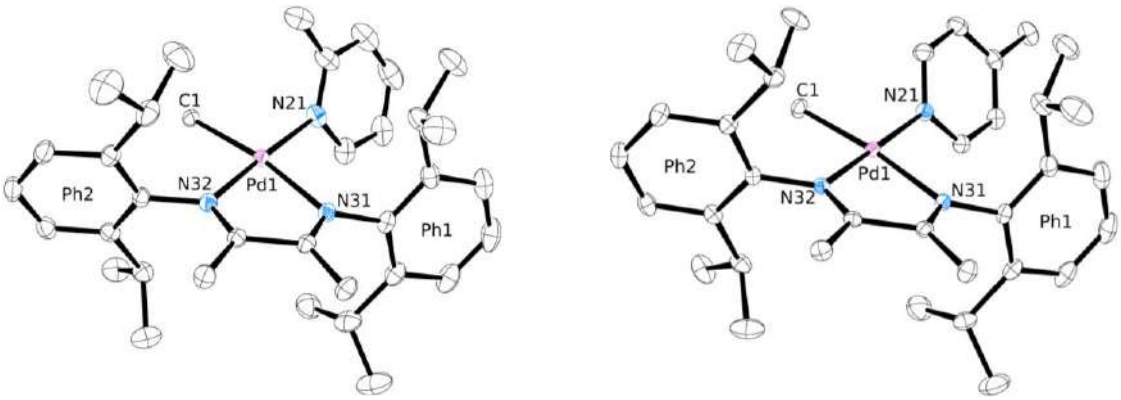

(a) (b)

Figure 4.10. ORTEP drawing (50% probability ellipsoids) of the molecule of (a) $\mathbf{2^{2pic}}$ and (b) $\mathbf{2^{4pic}}$. Hydrogen atoms and the PF_6^- anion have been omitted for the sake of clarity.

Since the signal of Pd-CH_3 fragment is a probe for assessing the electron properties of ligands bonded to the metal center,[20,21] a correlation between its chemical shift and the pyridine ligands steric and electronic properties is observed. Moving from CH_3CN to pyridine and its mono and disubstituted derivatives, a shift to lower frequencies is observed from 0.34 ppm in **1b** to 0.16 ppm in $\mathbf{1^{2,6lut}}$ and from 0.48 ppm in **2b** to 0.19 ppm in $\mathbf{2^{2,6lut}}$ (Figures 4.11 and 4.12). It is accordingly due to both the presence of electron donor methyl group on *ortho* positions and the generated steric hindrance. The strongly shielded Pd-CH_3 resonance of complexes bearing the 2-picoline (0.19 ppm for $\mathbf{1^{2pic}}$ and 0.27 ppm for $\mathbf{2^{2pic}}$) or 2,6-lutidine (0.16 ppm for $\mathbf{1^{2,6lut}}$ and 0.19 ppm for $\mathbf{2^{2,6lut}}$) indicates an increase in the donor strength of the ligands with respect to other complexes. The different coordinating capability is confirmed by the different value of pKa of each monodentate ligand (Table 4.1).

Table 4.1. pKa values and Pd-CH_3 chemical shifts (ppm) of cationic complexes.[a]

entry	L	pKa[22]	Pd-CH_3[b]	Pd-CH_3[c]
1	**CH_3CN**	-4.30	0.34	0.48
2	**Pyridine**	5.23	0.32	0.46
3	**2-picoline**	6.00	0.19	0.27
4	**4-picoline**	5.99	0.29	0.42
5	**2,6-lutidine**	6.65	0.16	0.19
6	**3,5-lutidine**	6.15	0.32	0.45

[a] ^{1}H NMR spectra in CD_2Cl_2 at 298 K, 10 mM solution of the complex; [b] [Pd(CH_3)(L)(**1**)][PF_6]; [c] [Pd(CH_3)(L)(**2**)][PF_6].

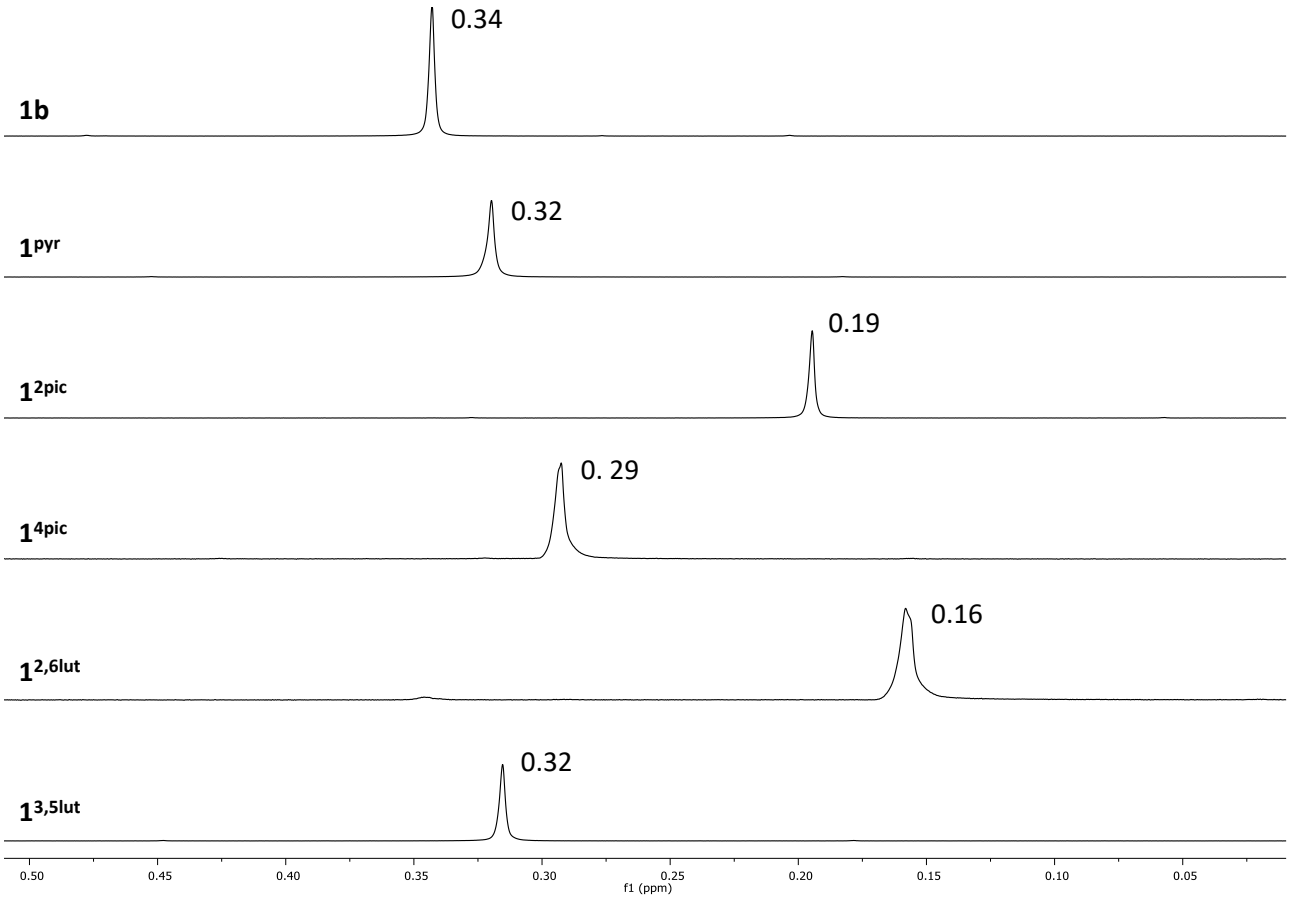

Figure 4.11. ^{1}H NMR spectra (CD_2Cl_2, 298 K) of [Pd(CH_3)(L)(**1**)][PF_6]; signal of Pd-CH_3.

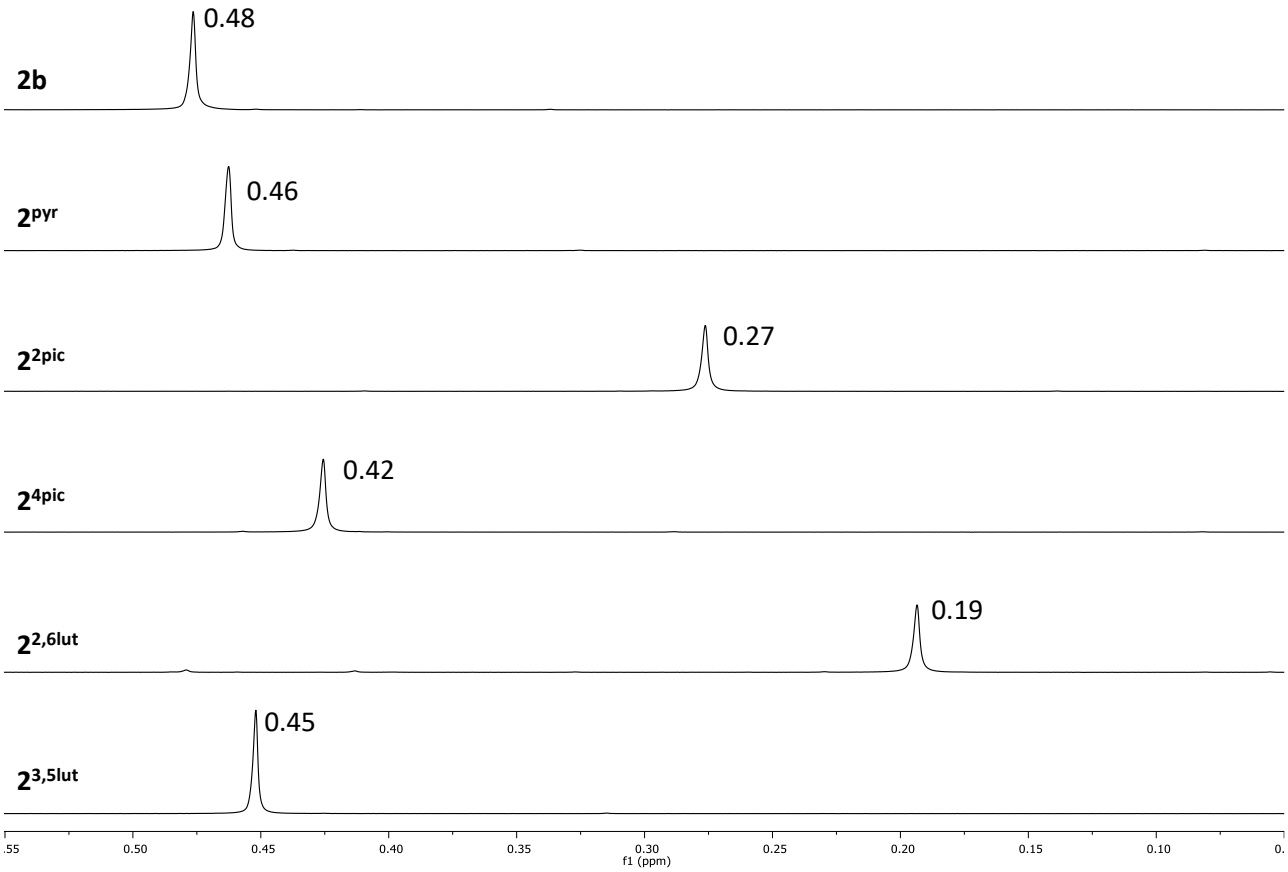

Figure 4.12. ^{1}H NMR spectra (CD_2Cl_2, 298 K) of [Pd(CH_3)(L)(**2**)][PF_6]; signal of Pd-CH_3.

4.2.2 Ethylene/methyl acrylate copolymerization with Pd-complexes ***1***^{pyr} *–* ***1***^{3,5lut} *and* ***2***^{pyr} *–* ***2***^{3,5lut}.

All complexes are tested as precatalysts for the E/MA copolymerization. They generate active species leading to E/MA branched copolymers. Catalysis are carried out in either 2,2,2-trifluoroethanol (TFE) or dichloromethane (DCM). They are monitored for a proper time of 6 h at the constant temperature of 308 K under 2.5 bar of ethylene pressure with [MA]/[Pd] of 594. Their catalytic behavior is compared to that of the parent compounds **1b** and **2b** (Tables 4.2 and 4.3). The obtained copolymers are yellow-green oils. Their microstructures and the amount of inserted polar monomer are studied in solution by NMR spectroscopy and their M_n is calculated using GPC analysis

Table 4.2. Ethylene/methyl acrylate copolymerization: effect of L and solvent.

Precatalyst: [Pd(CH$_3$)(L)(1)][PF$_6$][a]

entry	precat.	Solvent	yield (g)	kg CP/mol Pd[b]	MA (mol %)[c]	TON[d]		M_n kDa[e] (M_w/M_n)	Bd[f]
						E	MA		
1	**1b**	TFE	1.3917	66.27	3.6	2095	79	24.6 (1.88)	93
2	**1^{pyr}**	TFE	0.0799	3.80	3.0	124	4	4.2 (2.47)	107
3	**1^{2pic}**	TFE	0.1443	6.87	2.3	229	5	6.1 (1.67)	109
4	**1^{4pic}**	TFE	0.0712	3.39	3.0	110	3	3.4 (1.79)	107
5	**1^{2,6lut}**	TFE	0.0485	2.31	3.0	77	2	---	98
6	**1^{3,5lut}**	TFE	0.0334	1.59	3.4	51	2	---	117
7	**1b**	DCM	0.9692	46.15	4.8	1425	72	6.0 (2.18)	90
8	**1^{pyr}**	DCM	0.0484	2.30	6.1	67	5	1.8 (1.85)	100
9	**1^{2pic}**	DCM	0.0431	2.05	4.6	64	3	1.6 (1.82)	99
10	**1^{4pic}**	DCM	0.0450	2.14	2.2	71	2	0.4 (1.52)	107

[a] Reaction conditions: $n_{Pd} = 2.1 \cdot 10^{-5}$ mol, $V_{solvent} = 21$ mL, $V_{MA} = 1.130$ mL, [MA]/[Pd] = 594, $P_{Et} = 2.5$ bar, T = 308 K, t = 6 h. [b] Productivity in kg CP/mol Pd = kilograms of copolymer per mol of palladium calculated on isolated yield. [c] Amount of inserted MA in mol % calculated by ^{1}H NMR spectroscopy on isolated product. [d] Turnover number = mol of substrate converted per mol of Pd. [e] Determined by GPC. [f] Branching degree expressed as number of branches per 1000 carbon atoms.

Table 4.3. Ethylene/methyl acrylate copolymerization: effect of L and solvent.
Precatalyst: [Pd(CH$_3$)(L)(2)][PF$_6$][a]

entry	precat.	Solvent	yield (g)	kg CP/mol Pd[b]	MA (mol %)[c]	TON[d]		M_n kDa[e] (M_w/M_n)	Bd[f]
						E	MA		
1	**2b**	TFE	2.1374	101.78	0.9	3534	31	81.2 (1.29)	99
2	**2^{pyr}**	TFE	0.3911	18.62	0.7	650	4	23.0 (1.62)	103
3	**2^{2pic}**	TFE	0.5282	25.15	0.6	880	5	35.5 (1.90)	100
4	**2^{4pic}**	TFE	0.3532	16.82	0.5	590	3	19.9 (1.95)	103
5	**2^{2,6lut}**	TFE	0.2012	9.58	0.6	336	2	---	93
6	**2^{3,5lut}**	TFE	0.1512	7.20	0.5	252	1	---	100
7	**2b**	DCM	1.8087	86.13	1.1	2963	35	6.3 (1.65)	89
8	**2^{pyr}**	DCM	0.0711	3.38	6.6	99	7	3.0 (1.94)	85
9	**2^{2pic}**	DCM	0.0457	2.18	0.9	75	1	2.1 (1.65)	66
10	**2^{4pic}**	DCM	0.0324	1.54	1.1	53	1	0.4 (1.48)	72

[a] Reaction conditions: $n_{Pd} = 2.1 \cdot 10^{-5}$ mol, $V_{solvent} = 21$ mL, $V_{MA} = 1.130$ mL, [MA]/[Pd] = 594, $P_{Et} = 2.5$ bar, T = 308 K, t = 6 h. [b] Productivity in kg CP/mol Pd = kilograms of copolymer per mol of palladium calculated on isolated yield. [c] Amount of inserted MA in mol % calculated by ^{1}H NMR spectroscopy on isolated product. [d] Turnover number = mol of substrate converted per mol of Pd. [e] Determined by GPC. [f] Branching degree expressed as number of branches per 1000 carbon atoms.

A decrease in productivity is observed moving from **1b** or **2b** to the new family of precatalysts having the pyridine ligands, according to the highly coordinating capability of this family of ligands. Pd(II) complexes with 2-picoline are the best performers for both series when catalysis are carried out in TFE reaching values of productivity of 6.87 kg CP/mol Pd for **1^{2pic}** and 25.15 kg CP/mol Pd for **2^{2pic}**. While when DCM is the reaction medium, the most productive precatalysts are **1^{pyr}** and **2^{pyr}** (2.30 and 3.38 kg CP/mol Pd, respectively) (Tables 4.2 and 4.3).

The different substituent group on the *ortho* positions of the aryl rings of α-diimine ligand affects the content of inserted polar monomer.[23] Catalysis performed in the fluorinated solvent lead to copolymers with inserted MA in the range of 2.3 – 3.6 mol % for series with **1** as the chelate ligand and of 0.5 – 0.9 mol % when the α-diimine ligand is **2**. When catalysis are carried out in DCM, obtained macromolecules using **1^{pyr}** and **2^{pyr}** show the highest amount of inserted MA (6.1 and 6.6 mol %, respectively) (Tables 4.2 and 4.3, entry 8).

The molecular weight is determined by GPC analysis and, as general consideration, E/MA copolymers obtained by catalysis in TFE have a higher value of M_n with respect to those synthetized in DCM for all the precatalysts under investigation. The molecular weight distributions (M_w/M_n) are narrow in the range between 1.5 – 2.5. Catalysts **1b** and **2b** afford the copolymers with the highest M_n values in both solvents and the experimental data indicate that the presence of L in the palladium coordination sphere affects the growth of copolymer. Macromolecules obtained with precatalysts having 2-picoline as monodentate ligand show the highest value of M_n in both solvents: 6.1 kDa for $\mathbf{1}^{\mathbf{2pic}}$ and 35.5 kDa for $\mathbf{2}^{\mathbf{2pic}}$ in TFE, 1.8 kDa for $\mathbf{1}^{\mathbf{2pic}}$ and 3.0 kDa for $\mathbf{2}^{\mathbf{2pic}}$ in DCM.

The stability of precatalysts is monitored by the formation of Pd(0). It is observed only in traces when catalysis are carried out in dichloromethane for complexes of both series with lutidines as a monodentate ligand. In TFE no inactive palladium metal is present in the reactor thanks to the capability of the fluorinated solvent to stabilize the Pd-hydride intermediate, which is the species that leads to the deactivation of the complex.[10,19,24]

The value of the degree of branches, calculated from ^{1}H NMR spectra of isolated copolymers, is higher for both series when catalysis are carried out in TFE that goes from 93 to 117 per 1000 C atoms. In DCM $\mathbf{2}^{\mathbf{2pic}}$ and $\mathbf{2}^{\mathbf{4pic}}$ have the lowest values, 66 and 72 per 1000 C atoms respectively (Table 4.3, entries 9 and 10), suggesting that the chain walking process is slowed down in the chloride solvent after the insertion of the gaseous monomer.

In the ^{1}H NMR spectra of synthetized macromolecules, the singlet at 3.66 ppm is assigned to the methoxy group of inserted MA[5,25] and thanks to ^{13}C NMR spectroscopy, the way of MA enchainment is detected. When catalysis are carried out in TFE, the polar monomer is inserted in a small amount in the main chain (M(MA)) and preferentially at the end of the branches (T(MA)) (Figures 4.13 and S4.13). No differences in the macromolecules microstructure are present moving from the acetonitrile (**1b** and **2b**) to pyridine derivatives and this might be due to the high value of pKa of TFE about 12.46.[22] The fluorinated solvent protonates the pyridine ligand that subsequently leaves the coordination sphere of palladium. So the way of MA incorporation is affected only by the effect of the reaction medium, previously observed with other Pd(II) complexes with the N-N bidentate ligand.[5,10]

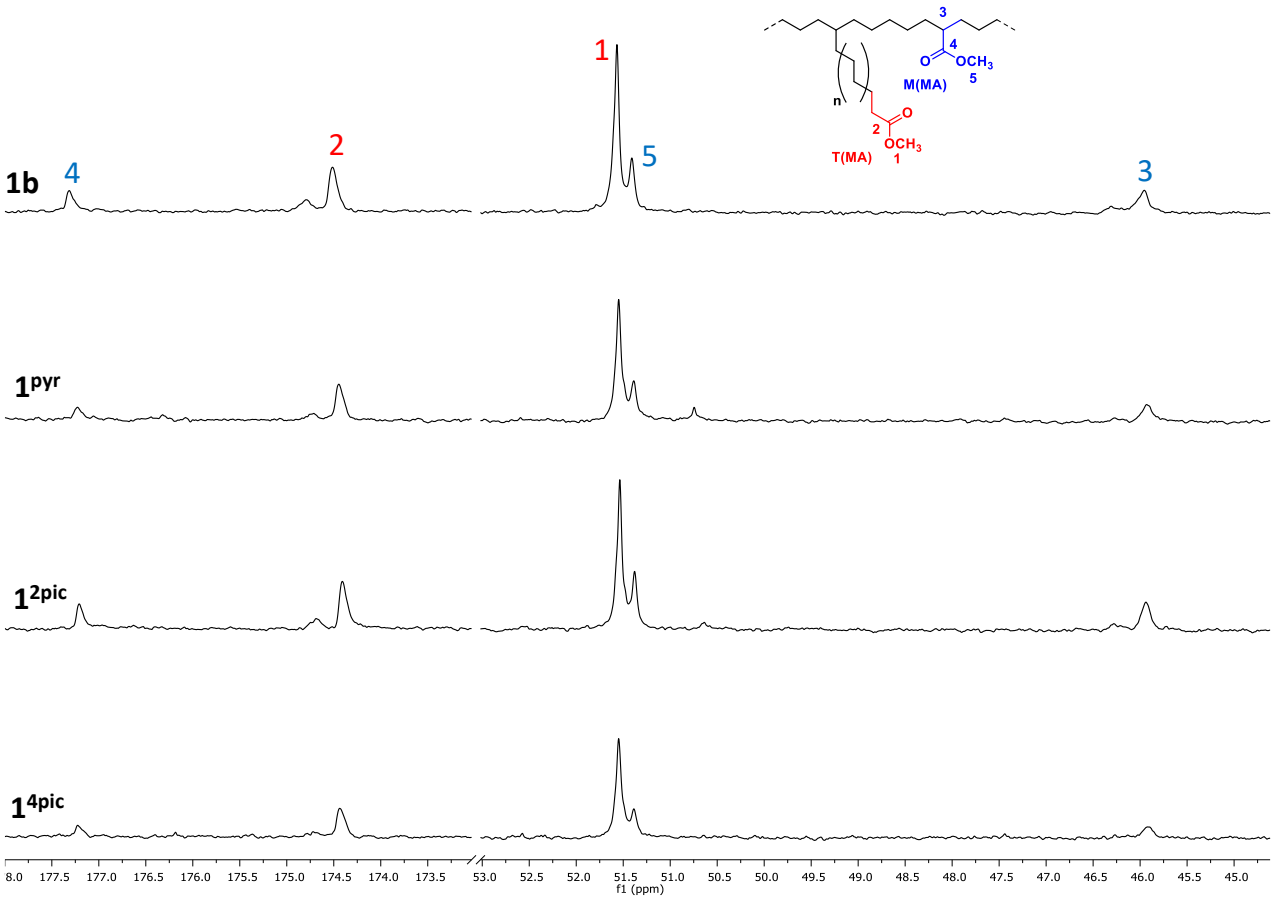

Figure 4.13. ^{13}C NMR spectra ($CDCl_3$, 298 K) of E/MA copolymers obtained with [Pd(CH_3)(L)(**1**)][PF_6] in TFE (Table 4.2, entries 1 – 4); (left) carbonyl region; (right) methoxy and methinic region.

When catalysis are carried out in distilled DCM, macromolecules microstructure changes moving from the parent compound **1b** or **2b** to the new complexes, in particular **1**^{pyr} and **2**^{pyr}. No peaks relative to M(MA) are observed in ^{13}C NMR spectra (Figures S4.14 and 4.14), but, in addition to typical resonances of T(MA), a new set of signals in the diagnostic regions is observed and in the copolymers synthesized with **2**^{pyr} and **2**^{4pic} the way of MA enchainment is almost exclusively this last one (Figure 4.14).

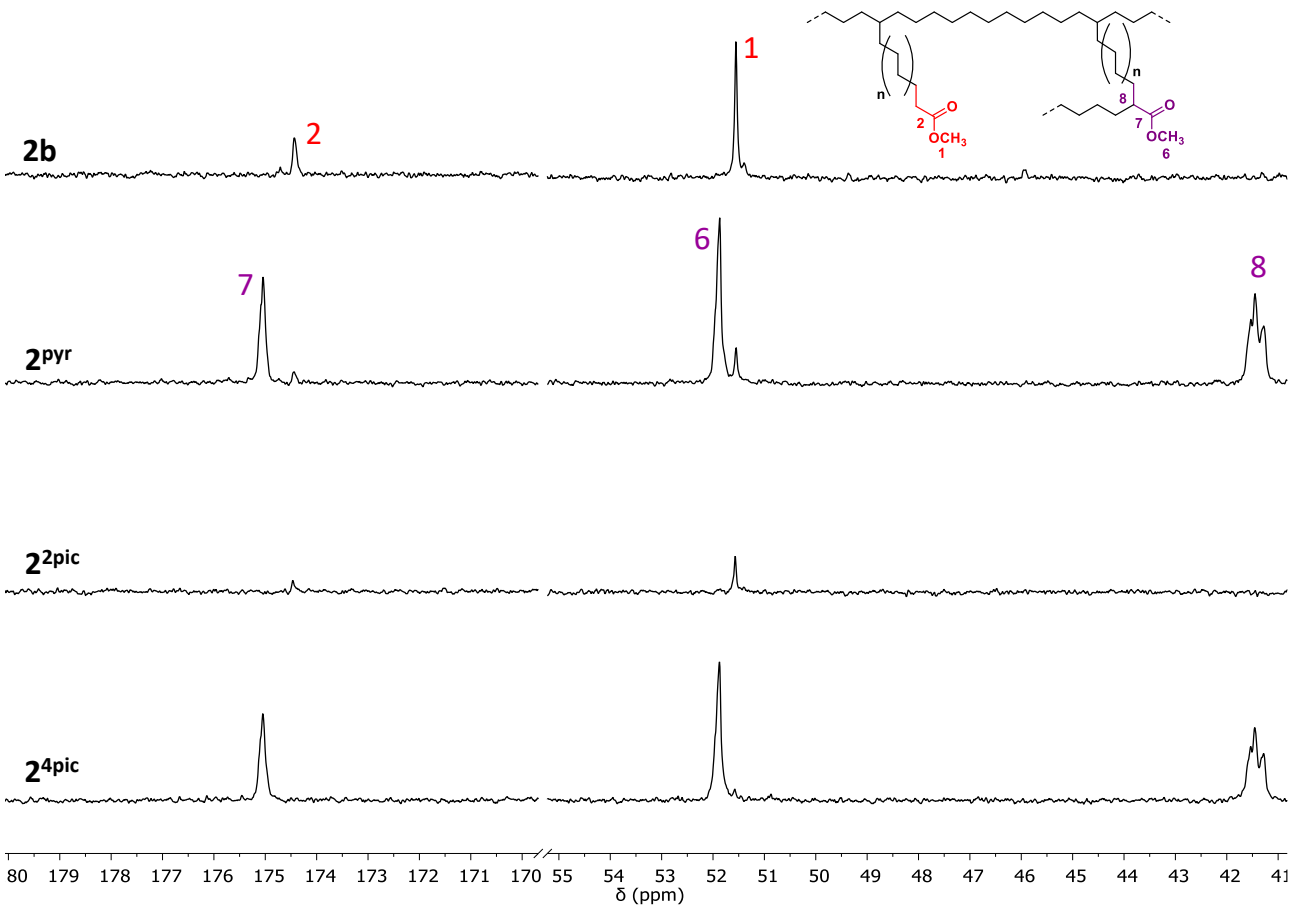

Figure 4.14. ^{13}C NMR spectra ($CDCl_3$, 298 K) of E/MA copolymers obtained with [Pd(CH_3)(L)(**2**)][PF_6] in CH_2Cl_2 (Table 4.3, entries 7 – 10); (left) carbonyl region; (right) methoxy and methinic region.

The way of growth of the polymeric chain is investigated with bidimensional NMR experiments performing on the copolymers obtained with **2^{pyr}**. In the $^{1}H,^{13}C$ HMBC spectrum (Figure 4.15), the jagged singlet of C=O carbonyl group at 175.1 ppm shows correlation peaks with the singlet of inserted MA at 3.66 ppm and broad signals at 2.30 ppm and at 1.95, 1.68 and 1.50 ppm, assigned to CH and CH_2 moieties thanks to $^{1}H,^{13}C$ HSQC spectrum (Figure S4.15), respectively. In the $^{1}H,^{1}H$ DQCOSY spectrum (Figure 4.16) correlation peaks between the previously reported signals are evidenced indicating that they are in the same polymeric chain and the polar monomer is inserted in a junction point (J(MA)) of a branch. The not define resolution of the singlet related to the carbonyl functionality of inserted MA is probably due to the way of packing of polymeric chains in the microstructure.

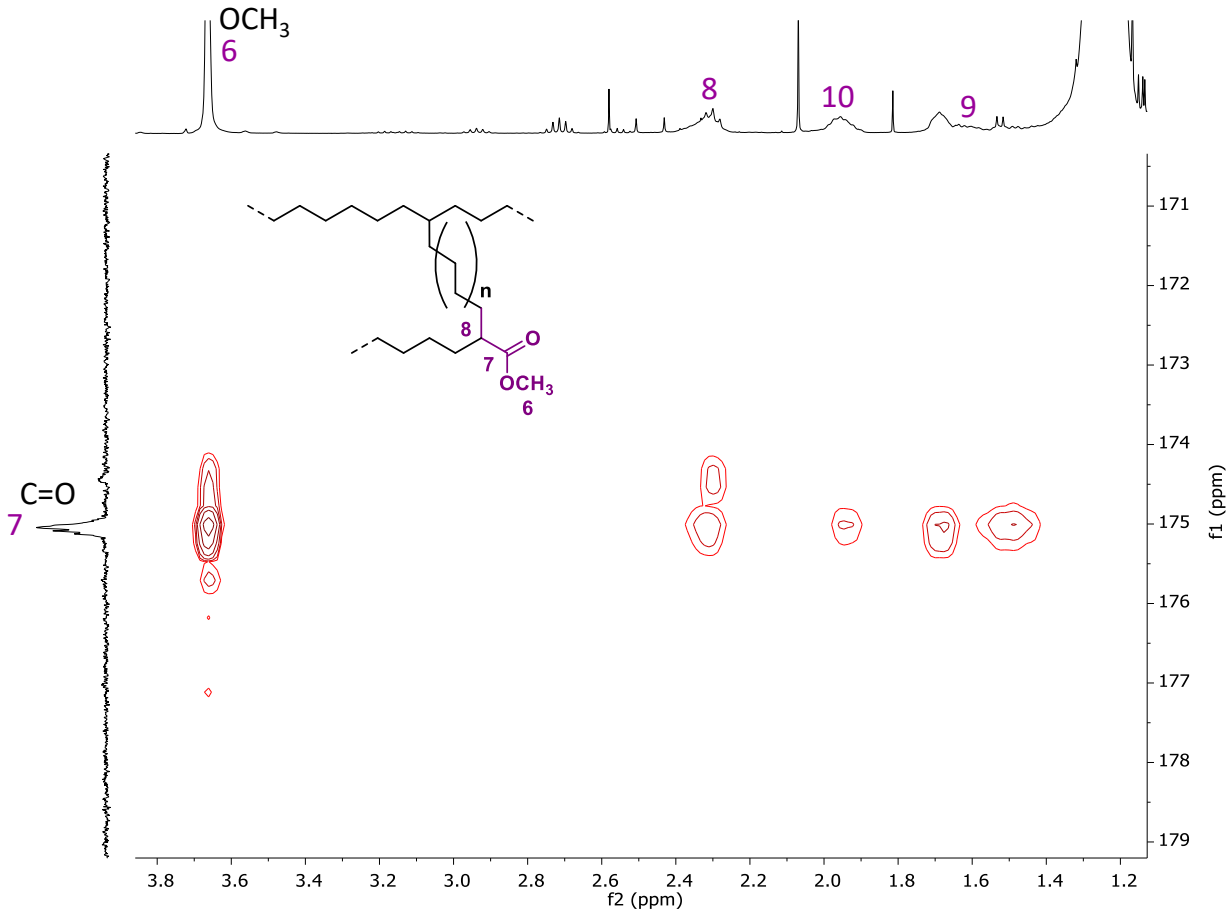

Figure 4.15. $^{1}H,^{13}C$ HMBC spectrum ($CDCl_3$, 298 K) of the E/MA copolymer obtained with **2^{pyr}** in CH_2Cl_2; carbonyl region.

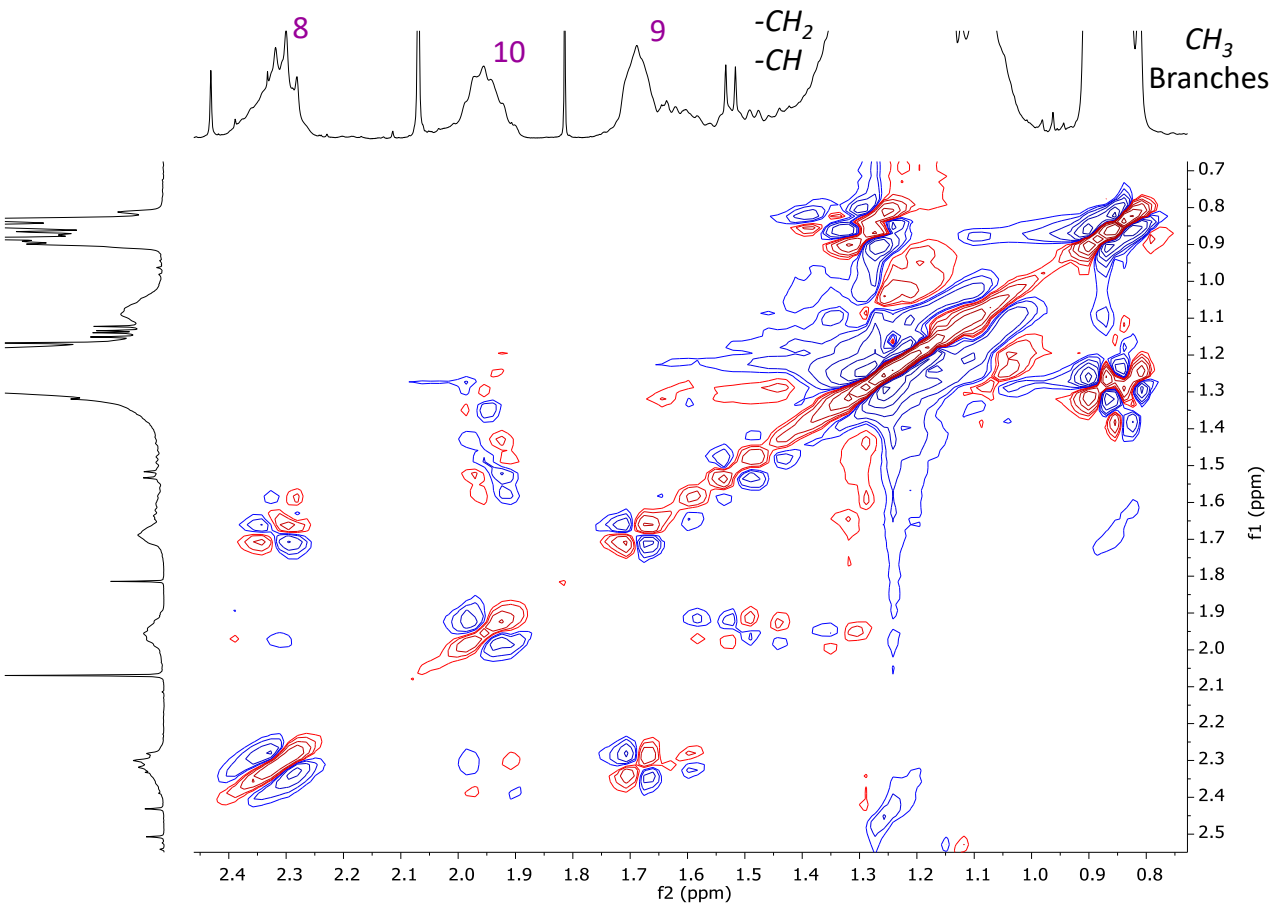

Figure 4.16. $^{1}H,^{1}H$ DQCOSY spectrum ($CDCl_3$, 298 K) of the E/MA copolymer obtained with **2**^{pyr} in CH_2Cl_2.

Since one of the desired controlled parameters of macromolecules microstructure from the industrial point of view is the branch formation and their pattern distribution,[26] a detailed study of the aliphatic region of the ^{13}C NMR spectra of the obtained copolymers is conducted in order to determine the various types of branches present in the samples microstructure (Table 4.4). Diagnostic resonances of different lengths branches, assigned according to the literature,[27,28] are evidenced and it is possible to distinguish methyl, short-chain (ethyl, propyl, and butyl) and long-chain branches (Figure 4.17). The smallest type of a branch-on-branch structure can also be assigned in the ^{13}C NMR spectrum to the resonances observed at 11.4 and 19.4 ppm, corresponding to sec-butyl groups, which is a clear indication of hyperbranched microstructures.

Table 4.4. Distribution of different branches by ^{13}C NMR spectra analysis.[29,30]

Entry	precat.	Solvent	Bd[a]	Methyl[b]	Ethyl[b]	Propyl[b]	LCB[c]	Sec-butyl[b]
1	**2b**	TFE	99	39	17	2	35	7
2	**2^{pyr}**	TFE	103	34	17	2	40	7
3	**2^{2pic}**	TFE	100	34	18	2	40	6
4	**2^{4pic}**	TFE	103	34	17	2	40	7
5	**2b**	DCM	89	31	18	1	44	6
6	**2^{pyr}**	DCM	85	26	17	1	50	6
7	**2^{2pic}**	DCM	66	23	17	2	52	6
8	**2^{4pic}**	DCM	72	23	16	1	55	5

[a] Branching degree expressed as number of branches per 1000 carbon atoms; [b] Calculated by the relative intensities of the methyl resonances $1B_1$, $1B_2$, $1B_3$, and $1B_2$-sec-Bu; [c] LCB = butyl and longer branches, calculated by the relative intensity of the methine resonance of the br-B_n.

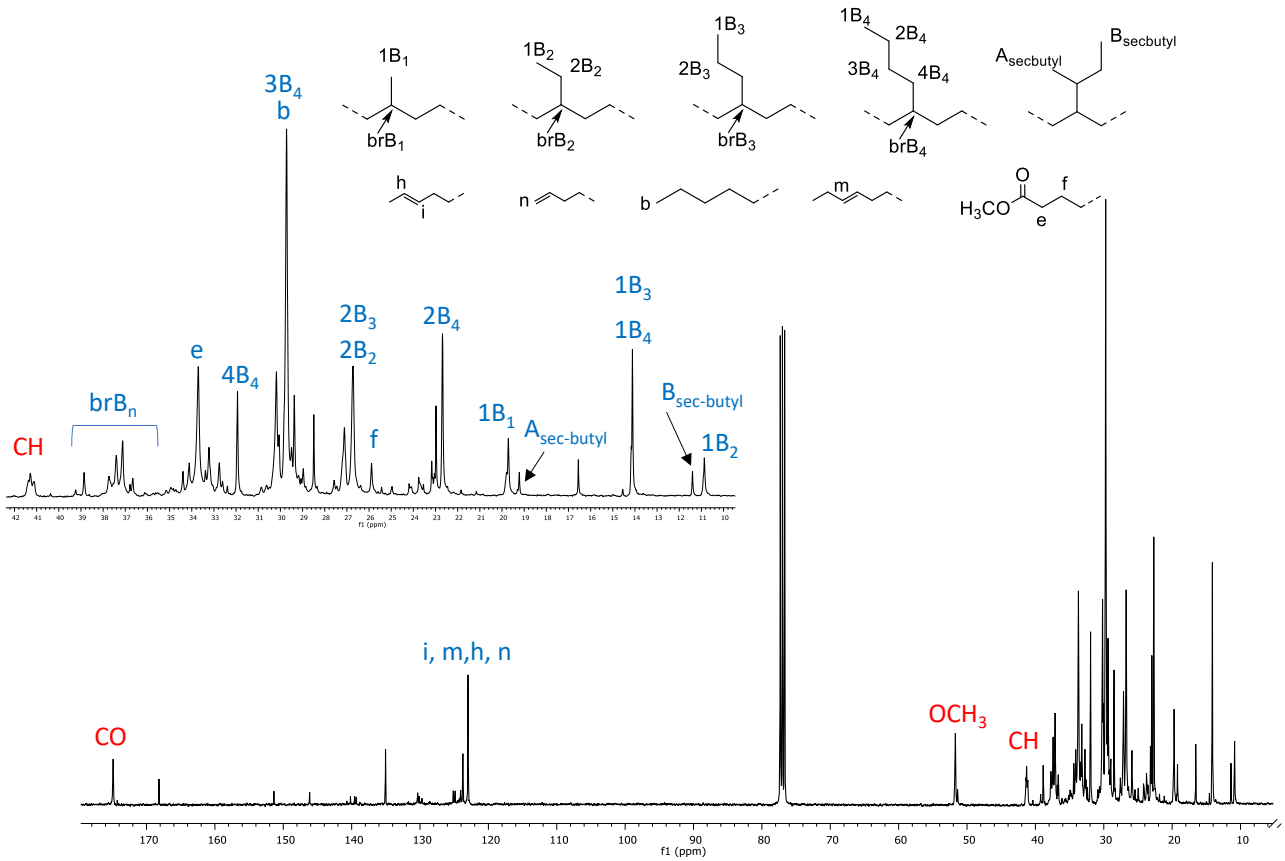

Figure 4.17. ^{13}C NMR spectrum ($CDCl_3$, 298 K) of the E/MA copolymer obtained with **2^{pyr}** in CH_2Cl_2.

In general, almost half of the branching content correspond to butyl groups and longer branches, reinforcing that macromolecules obtained with these catalytic systems are branched copolymers. Values of Bd suggest that the chain walking process is slowed down in CH_2Cl_2 only after the insertion of ethylene, while the way of MA enchainment indicates that after the insertion of the polar monomer the chain walking process is kinetically favored due to the presence of acrylate units at the end of the branches (Scheme 1.2, Chapter 1)[23] and in a junction point of a branch. This consideration is not in agreement with the percentage of LCB calculated from ^{13}C NMR spectra that is higher for macromolecules synthetized in CH_2Cl_2. This might be due to the shift of a unit of MA away from the metal center for the high congestion around Pd(II) ion for also the presence of the pyridine ligand in the palladium coordination sphere during catalysis. By comparing the ^{13}C NMR spectra of macromolecules, obtained under the same reaction conditions, using **2^{pyr}** in both TFE and DCM, variations are observed in the diagnostic regions of carbonyl and methoxy/methinic groups, while at lower frequencies the only difference is the resonance associated to a CH moiety of the junction point at 41.3 ppm (Figure 4.18).

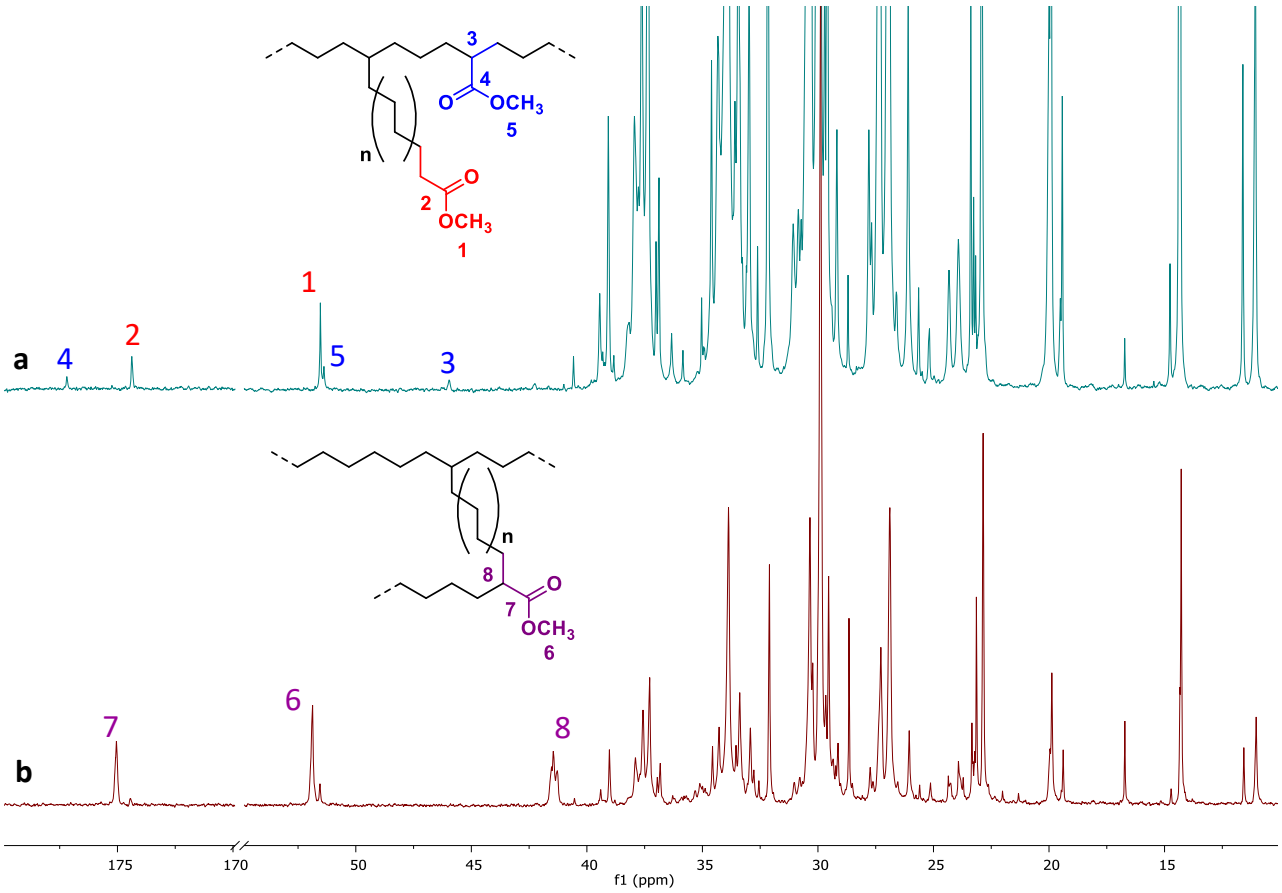

Figure 4.18. ^{13}C NMR spectra ($CDCl_3$, 298 K) of E/MA copolymers obtained with **2^{pyr}** in (a) TFE and (b) CH_2Cl_2.

On the basis of these novel catalytic results, the effect of some reaction parameters is investigated using **1**^{pyr} and **2**^{pyr} as precatalysts in order to evaluate how the new detected way of MA enchainment is affected by the reaction conditions. Catalysis are carried out in dichloromethane as reaction medium. The influence of ethylene pressure is studied from 2.5 to 7.0 bar (Figure 4.19 and Tables S4.2 and S4.3). As expecting, an increase in ethylene pressure produces a linear increase in the productivity from 2.30 to 5.13 kg CP/mol Pd with **1**^{pyr} and from 3.38 to 6.15 kg CP/mol Pd with **2**^{pyr}. On the other hand a decrease in the content of inserted MA into the obtained copolymers for both series is observed. From NMR analysis, the obtained copolymers microstructures is not affected by the variation of this parameter and the polar monomer is inserted as both T(MA) and J(MA) (Figure S4.17).

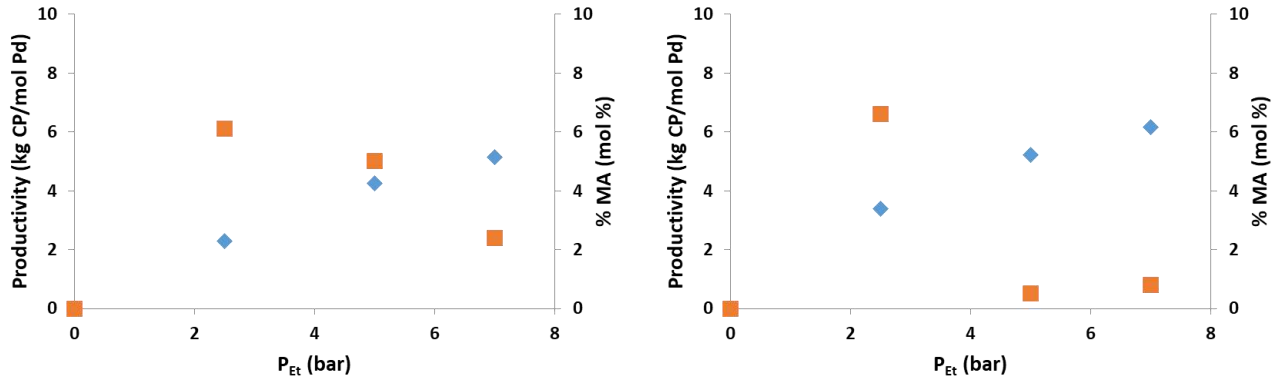

(a) (b)

Figure 4.19. Ethylene/methyl acrylate copolymerization: effect of P_{Et} on (♦) the productivity and (■) the content of MA. Precatalysts: (a) **1**^{pyr} and (b) **2**^{pyr}.
Reaction conditions: see Tables S4.2 and S4.3.

The effect of methyl acrylate to palladium ratio is investigated in the range 594 – 1782 by increasing the amount of the polar monomer and keeping constant the amount of precatalyst (Figure 4.20 and Tables S4.4 and S4.5). According to the inhibitor behavior of MA,[10,23] the productivity decreases when the ratio between the polar monomer and Pd(II) complex increases, while the percentage of inserted MA increases for both series up to 13.3 and 22.2 mol % for **1**^{pyr} and **2**^{pyr}, respectively. In the ^{13}C NMR spectra of copolymers produced by **2**^{pyr} the methyl acrylate is almost exclusively inserted as J(MA) (Figure S4.18).

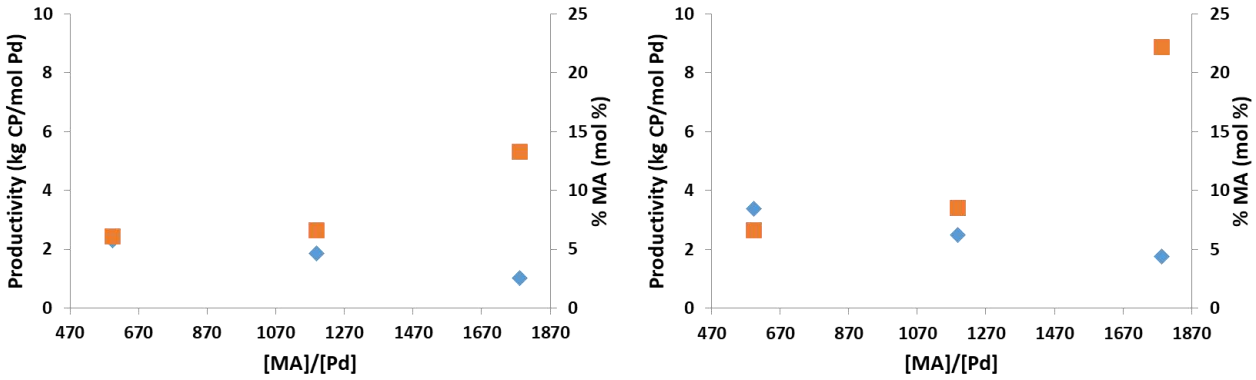

(a) (b)

Figure 4.20. Ethylene/methyl acrylate copolymerization: effect of [MA]/[Pd] on (♦) the productivity and (■) the content of MA. Precatalysts: (a) **1**^{pyr} and (b) **2**^{pyr}.
Reaction conditions: see Tables S4.4 and S4.5.

The temperature variation is performed in the range 298 – 318 K using the precatalyst **1**^{pyr} (Table 4.5). An increase in temperature value leads to an increase in the productivity, that doublets (from 1.90 to 3.99 kg CP/mol Pd) and, moving from 298 K to 308 K, an increase in the content of inserted MA (from 3.3 to 6.1 mol %) is found. Whereas at higher temperature (318 K) a decrease in the mol % of inserted polar monomer (5.2 mol %) is observed together with the formation of Pd(0) during the catalysis.

Table 4.5. Ethylene/methyl acrylate copolymerization: effect of temperature.
Precatalyst: [Pd(CH$_3$)(1)(pyr)][PF$_6$], 1^{pyr} [a]

entry	T (K)	yield (g)	kg CP/mol Pd[b]	MA (mol %)[c]	TON[d]		Bd[e]
					E	MA	
1	298	0.0400	1.90	3.3	61	2	105
2	308	0.0484	2.30	6.1	69	4	100
3	318	0.0837	3.99	5.2	122	7	96

[a] Reaction conditions: $n_{Pd} = 2.1 \cdot 10^{-5}$ mol, $V_{CH2Cl2} = 21$ mL, $P_{Et} = 2.5$ bar, $V_{MA} = 1.130$ mL, [MA]/[Pd] = 594, t = 6 h; [b] productivity in kg CP/mol Pd = kilograms of copolymer per mole of palladium; [c] calculated by ^{1}H NMR spectroscopy on isolated product; [d] Turnover number = mol of substrate converted per mol of catalyst (E = ethylene); [e] branching degree calculated by ^{1}H NMR spectroscopy on isolated product and expressed as branches per 1000 carbon atoms.

The catalytic behavior of precatalyst **1**^{pyr} is also assessed for the homopolymerization of ethylene, comparing it with the parent compound **1b** performing the reaction in both solvents (Table 4.6). It generates active species for the target reaction leading to branched polyethylene.

Table 4.6. Ethylene homopolymerization: effect of precatalyst and solvent.
Precatalyst: [Pd(CH$_3$)(L)(1)][PF$_6$][a]

entry	precat.	Solvent	yield (g)	kg PE/mol Pd[b]	Bd[c]
1	**1b**	TFE	3.0802	146.68	112
2	**1^{pyr}**	TFE	0.1007	4.79	116
3	**1b**	DCM	3.1278	148.94	105
4	**1^{pyr}**	DCM	0.1392	6.63	104

[a] Reaction conditions: $n_{Pd} = 2.1 \cdot 10^{-5}$ mol, $V_{solvent} = 21$ mL, $P_{Et} = 2.5$ bar, T = 308 K, t = 6 h. [b] Productivity in kg PE/mol Pd = kilograms of polyethylene per mol of palladium calculated on isolated yield. [c] Branching degree expressed as number of branches per 1000 carbon atoms.

In analogy to what has been found in the copolymerization, the productivity strongly decreases moving from acetonitrile to pyridine ligand, from 146.68 to 4.79 kg PE/mol Pd when catalysis are performed in TFE. While the value of degree of branches is not affected by the variation of the ligand in the coordination sphere of the metal center. In general, the degree of branching is higher when catalysis are carried out in TFE rather than in CH_2Cl_2 (for **1b**: 112 *vs* 105 and for **1^{pyr}**: 116 *vs* 104).

*4.2.3 Reaction of **1^{4pic}** with ethylene, methyl acrylate and both comonomers.*

Preliminary independent *in situ* reactions of the two comonomers with complex **1^{4pic}** are investigated with the aim to have some insights into the intermediates involved in the copolymerization reaction. At the end the reaction with both comonomers, methyl acrylate and ethylene, is studied using the same precatalyst.

A 10 mM CD_2Cl_2 solution of **1^{4pic}** is saturated with ethylene at room temperature (Figure 4.21). In the ^{1}H NMR spectrum recorded after 5 min from bubbling the gaseous monomer, signals of the precursor (e.g. singlet of Pd-CH_3 at 0.29 ppm), the singlet of free E at 5.40 ppm and new resonances in both aliphatic and aromatic regions are observed. A detailed bidimensional NMR analysis is carried out after 1 h from the addition of ethylene and in the ^{1}H NMR spectrum recorded at this time the doublets in the range 0.36 – 0.42 ppm are assigned to CH groups of short PE chains, while signals from 0.49 to 1.26 ppm to CH_2 and CH_3 moieties, respectively, thanks to ^{1}H,^{13}C HSQC experiment (Figure S4.19). The formation of junction points (CH) in the PE backbone with either CH_3 groups or the growing polymeric chain close to it is supposed.[30,31] After 2 h, ethylene still present in the solution, **1^{4pic}** is almost totally converted into active species and typical resonances of branched PE are observed.

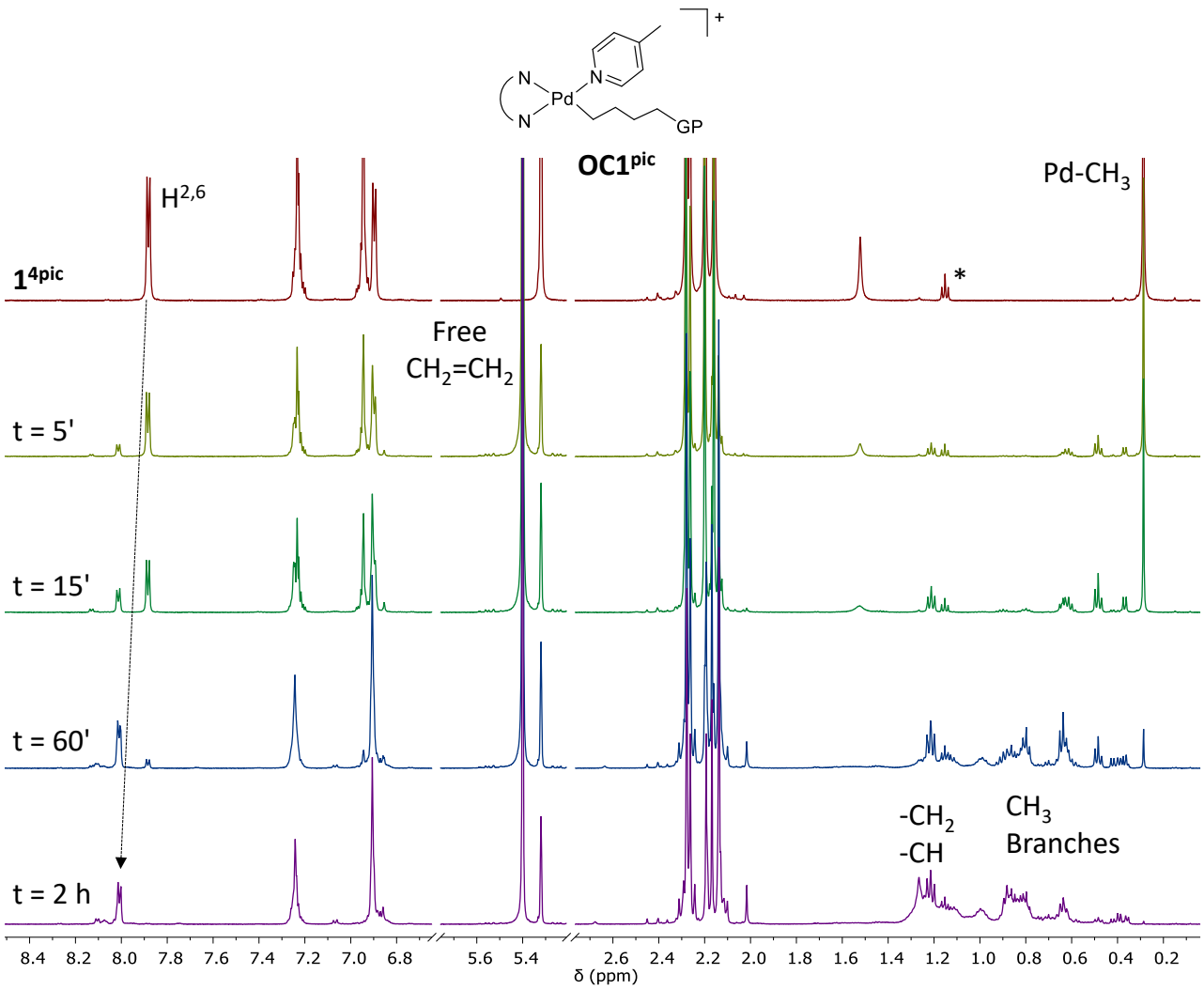

Figure 4.21. ^{1}H NMR spectra (CD_2Cl_2, 298 K) of **1^{4pic}** (top spectrum) and the mixture of **1^{4pic}** with ethylene at different reaction times; *diethyl ether.

In the aromatic region a new set of signals is observed and the presence of a new Pd species in solution that might have the growing polymeric chain and **4pic** bonded to the metal (**OC1^{pic}**) is detected. This new species is recognized to be a novel catalyst resting state of the reaction with this kind of Pd(II) complexes. The coordination of 4-picoline to the Pd(II) ion is confirmed by (*i*) the shift to higher frequencies (from 7.88 to 8.01 ppm) of the doublet assigned to $H^{2,6}$ of the monodentate ligand in the ^{1}H NMR spectrum and (*ii*) the chemical shift value of its carbon atom (150.5 ppm in **OC1^{pic}** *vs* 150.8 ppm in **1^{4pic}**) (Figure 4.22). This behavior is completely different from that typical of other Pd-α-diimine complexes.[10,23] Moreover, no signals of free **4pic** are evident as well as no formation of Pd(0) is found in the NMR tube for the whole monitoring time.

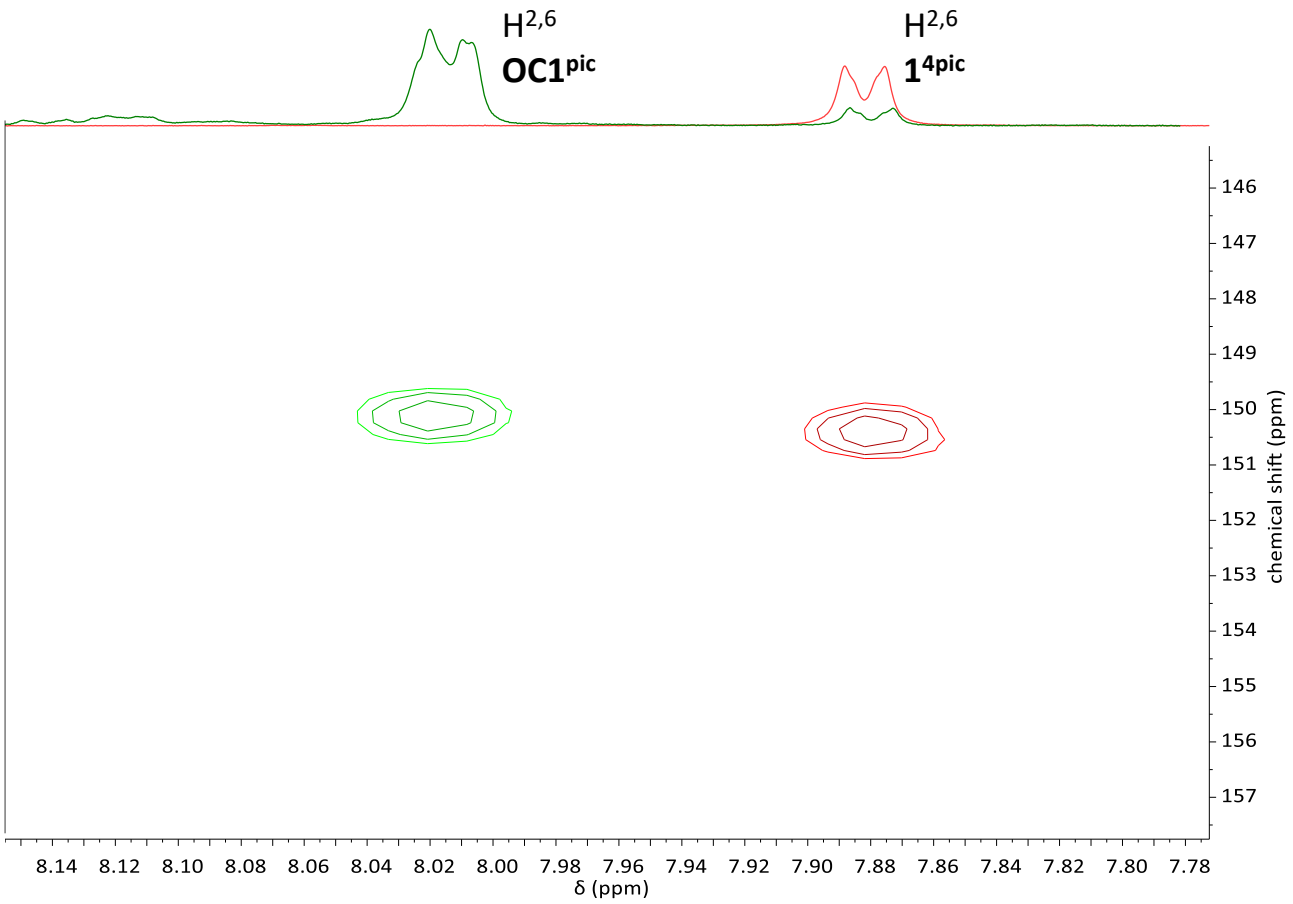

Figure 4.22. $^{1}H,^{13}C$ HSQC spectra (CD_2Cl_2, 298 K) of **1^{4pic}** (red spectrum) and the mixture of **1^{4pic}** + ethylene at t = 1 h (green spectrum); signal of $H^{2,6}$.

Considering the reactivity of **1^{4pic}** with the polar monomer in CD_2Cl_2, no reaction takes place within 1 h (Figure S4.20) and the complex shows the same behavior of Pd(II) compounds with the N-S ligand in the metal fourth coordination site, [Pd(CH_3)(N-S)(**1**)][PF_6] (Figure S2.37, Appendix Chapter 2).[10] So, this solution is saturated with ethylene. The peaks originated from its insertion into the Pd-CH_3 bond are observed after 5 min and after 90 min from the addition of the gaseous monomer the resonances of branched PE are present together with those of free ethylene, free MA and **1^{4pic}** (Figure 4.23). No resonances of free **4pic** and metallacycle intermediates are observed.

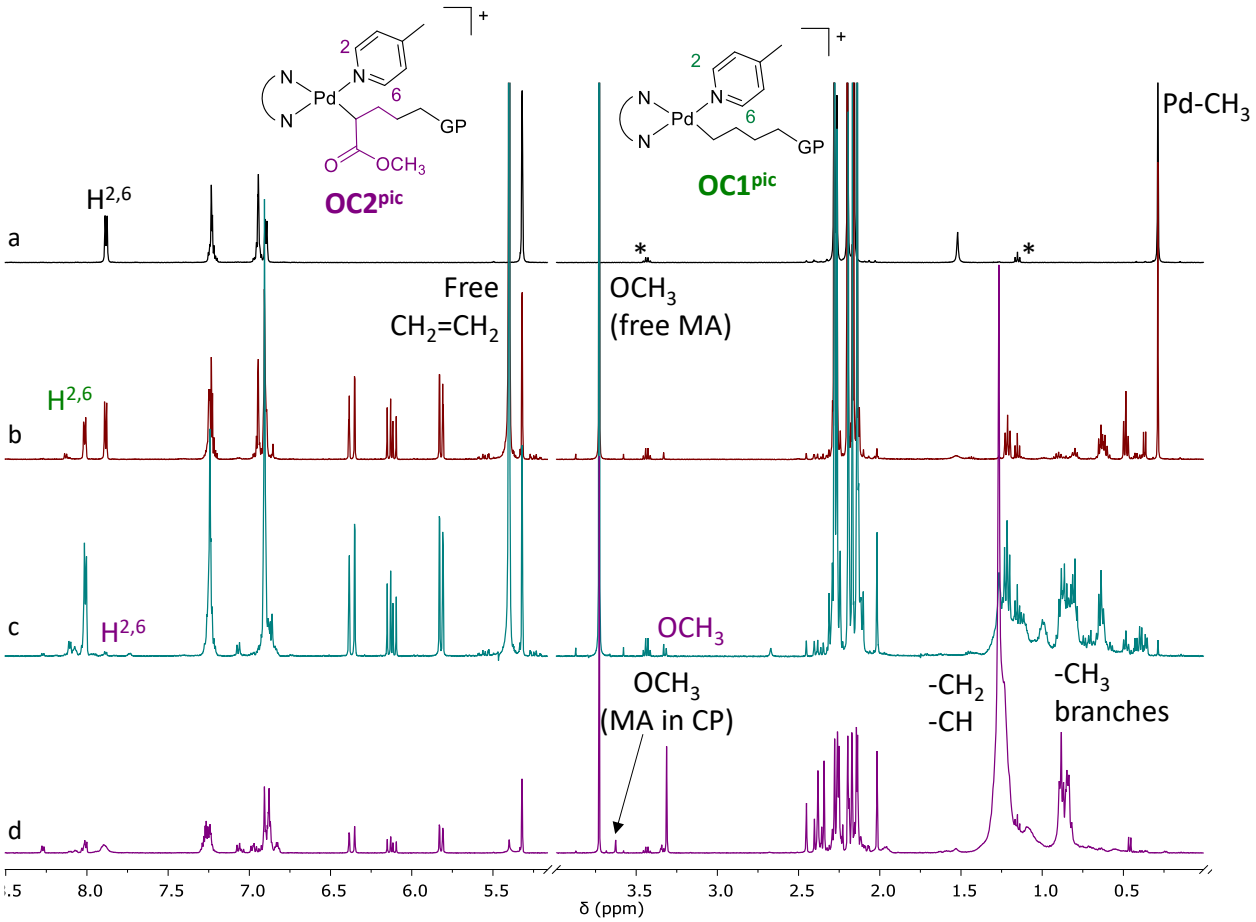

Figure 4.23. ^{1}H NMR spectra (CD_2Cl_2, 298 K) of (a) **1^{4pic}**; **1^{4pic}** + MA and ethylene at (b) t = 15 min, (c) t = 90 min and (d) t = 19 h; *diethyl ether.

A detailed bidimensional NMR analysis is performed after 90 min from the addition of ethylene to detect intermediates involved in the target reaction. The presence of **OC1^{pic}** species, also in this case, is confirmed by the NOESY experiment. In the $^{1}H,^{1}H$ NOESY spectrum cross peaks generated by the Overahuser effect between the doublet of $H^{2,6}$ and CH_2 groups of the growing polymeric chain in **OC1^{pic}** are observed (Figure S4.21), confirming that **4pic** and the growing polymer are in close spatial proximity to each other. In addition, an exchange peak between the doublet at 8.01 ppm and other weak signals, which resonate at higher frequencies, is present, suggesting the presence of other open-chain intermediates of the same nature. These species are in equilibrium at slow rate on the NMR time scale at room temperature.

In the $^{1}H,^{1}H$ NOESY spectrum (Figure 4.24) another peak due to the Oversahuer effect between the doublet at 7.89 ppm, assigned to $H^{2,6}$ of coordinated **4pic**, and the singlet at 3.31 ppm, is observed. The latter, in the $^{1}H,^{13}C$ HMBC spectrum (Figure S4.22) correlates with a C=O carbonyl group at 177.4 ppm and it is assigned to a methoxy group of inserted MA for the chemical shift of its carbon atom at 50.8 ppm in the $^{1}H,^{13}C$ HSQC spectrum (Figure S4.23).

These considerations allow to detect a new open-chain intermediate having both the growing copolymeric chain with inserted MA, produced by the coordination/insertion reactions of both comonomers in the Pd-CH_3 bond, and the **4pic** bonded to palladium ion (**OC2^{pic}**).

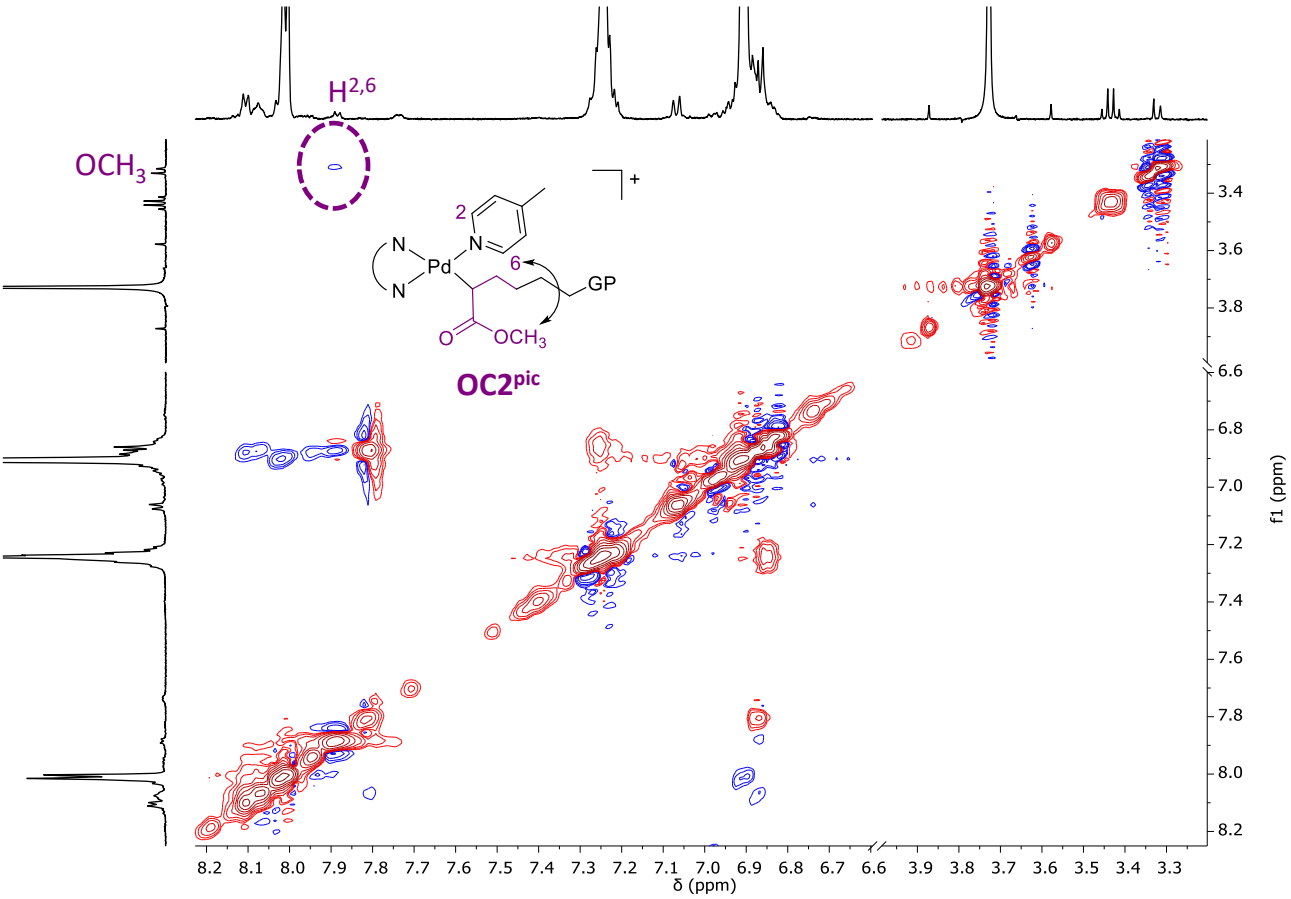

Figure 4.24. ^{1}H,^{1}H NOESY spectrum (CD_2Cl_2, 298 K) of the reaction mixture of **1^{4pic}** with MA and ethylene at t = 90 min.

After 19 h, a weak signal of free ethylene is still present together with the resonances of **OC2^{pic}** and the free methyl acrylate. In addition, the characteristic peaks of E/MA copolymer are observed, in particular the singlet of the inserted MA at 3.63 ppm, assigned to T(MA) due to its carbonyl group that resonates at 174.1 ppm (Figure 4.25).

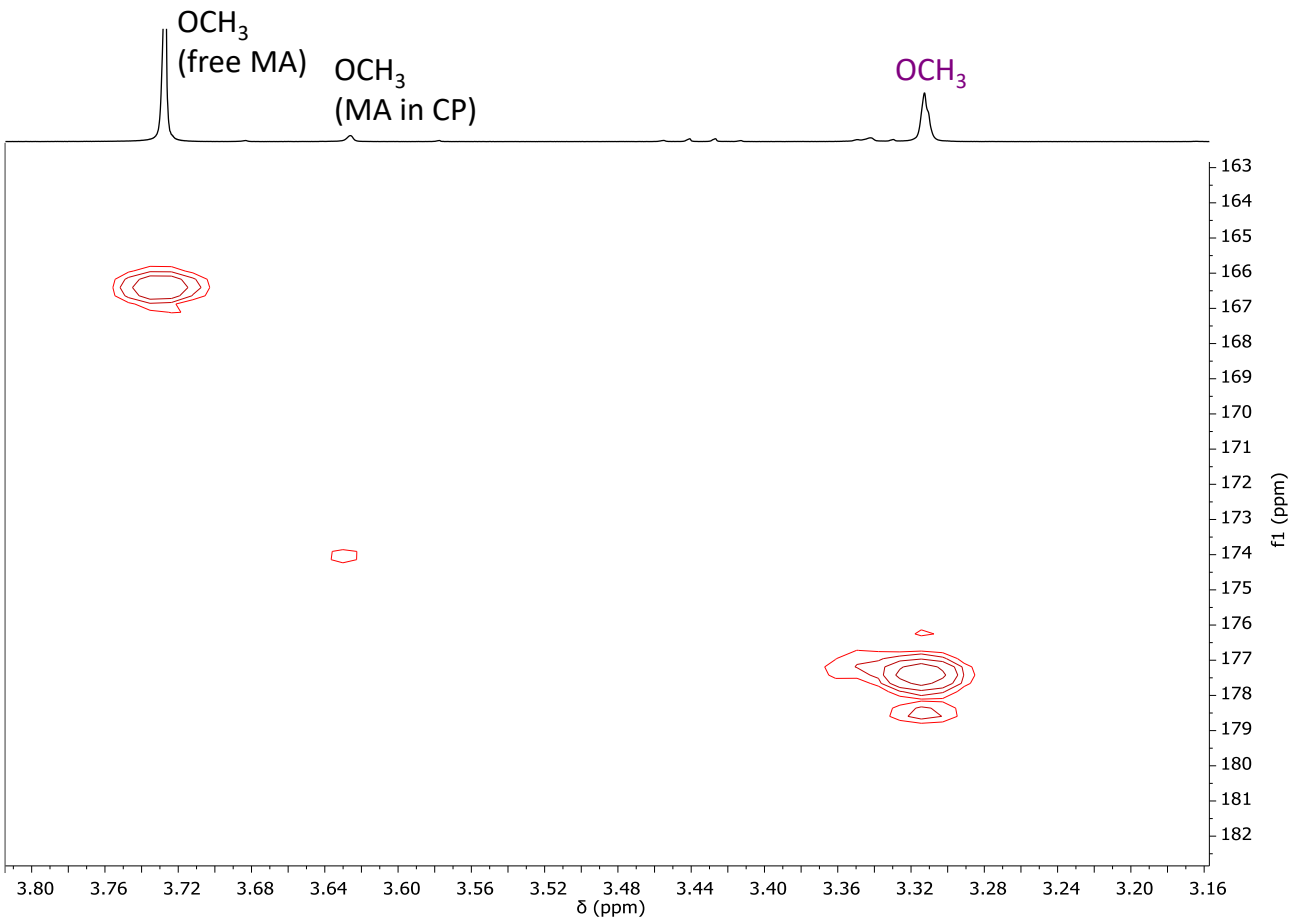

Figure 4.25. $^{1}H,^{13}C$ HMBC spectrum (CD_2Cl_2, 298 K) of the reaction mixture of **1^{4pic}** with MA and ethylene at t = 19 h.

Preliminary mechanistic insights into the copolymerization reaction by an in-depth density functional theory (DFT) calculation is elucidated. Complexes under investigation are **1^{pyr}** and **1b** and their minimum energy paths (MEPs) are compared (Figure 4.26, right and left, respectively).

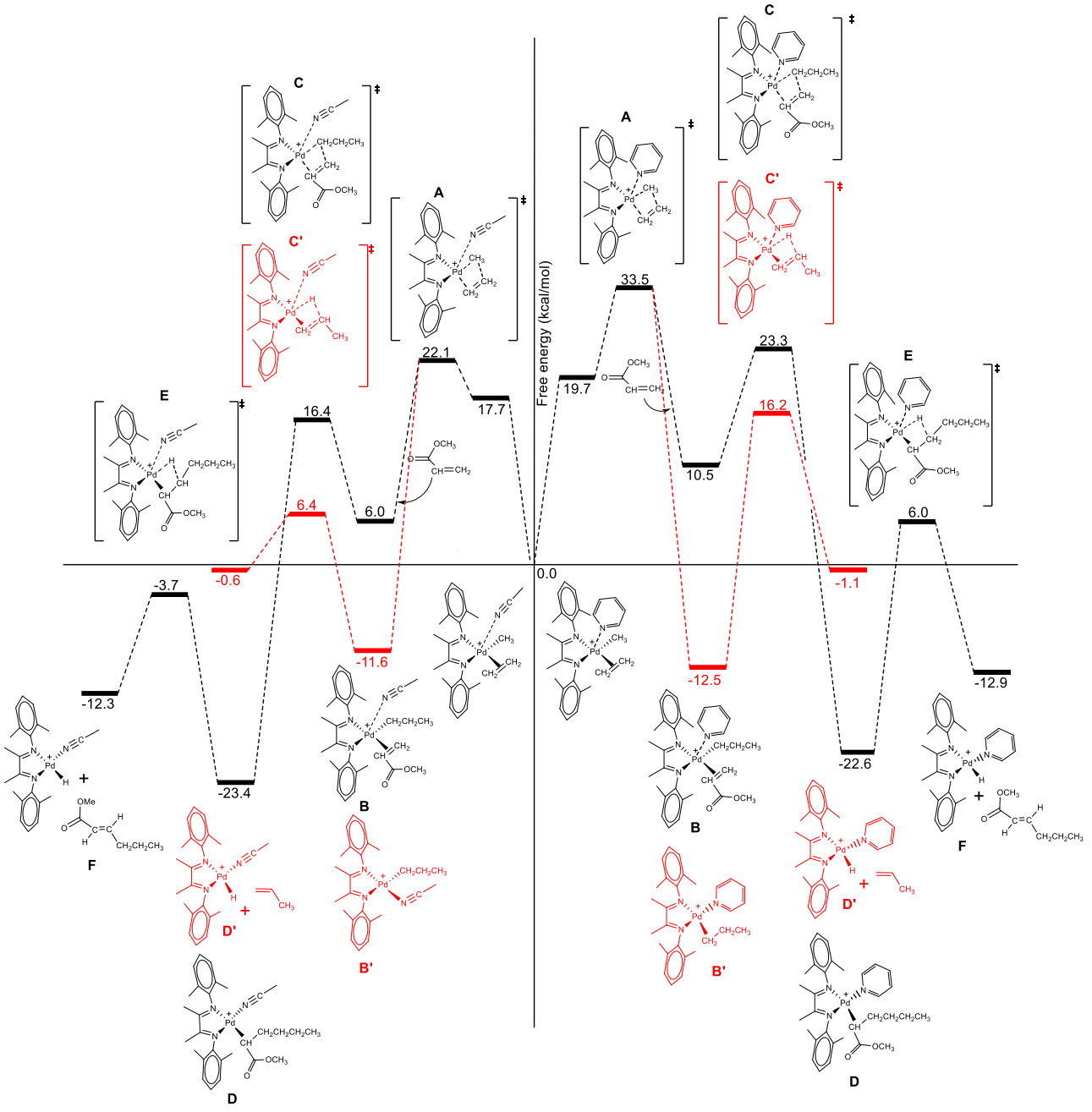

Figure 4.26. MEPs of the E/MA copolymerization mechanism for **1**^{pyr} (right) and for **1b** (left).

According to the high affinity of the metal center for the gaseous monomer[23] and the obtained results of *in situ* NMR experiments, the reaction starts with the coordination/insertion of ethylene in the Pd-CH_3 bond (**A**) that costs 22.1 kcal/mol for **1b** and 33.5 kcal/mol for **1**^{pyr}. The difference in the energetic values is in agreement with the higher coordinating capability of pyridine with respect to CH_3CN, confirmed by the decrease in the productivity moving from **1b** to **1**^{pyr} in the experimental catalytic data (Table 4.2). From this intermediate MEPs are split to give either a propylene-coordinated complex (**B'**) (red pathway) or the insertion of the polar monomer (**B**) (black pathway).

The first process is followed by the formation of Pd-H species (**D3'**) that is quite more stable for Pd(II) complex bearing pyridine ligand (-1.1 kcal/mol for **1**^{pyr} *vs* -0.6 kcal/mol for **1b**), confirmed by the absence of inactive palladium metal during catalysis with this new family of precatalysts. While when the second pathway is considered, the subsequent coordination/insertion of MA (**C2**) overcomes a free energy barrier of 10.4 kcal/mol for **1b** and 12.8 kcal/mol for **1**^{pyr} due to the inhibiting effect of the pyridine ligand. These unstable intermediates go to an open-chain Pd(II) species (**D**) having both the CH_3CN or the pyridine and the organic fragment, generated by the previous step, coordinated to the metal center. Their stability confirms that the monodentate ligand remains coordinated to palladium ion, as demonstrated by the *in situ* NMR reaction of **1**^{4pic} with both comonomers where no signals of free 4-picoline are observed, together with the presence of **OC2**^{pic} for all the monitoring time of 19 h. A new β-agostic intermediate (**E**) is generated costing 19.7 kcal/mol for **1b** and 28.6 kcal/mol for **1**^{pyr} to lead a stable Pd-H species (**F**). The higher coordinating capability of the pyridine ligand rather than the acetonitrile decreases all the barrier of the process disfavoring the formation of metallacycle intermediates. Indeed, all the attempts to optimize them for the complex **1**^{pyr} produced a failure since the pyridine displaces the oxygen atom of MA in the growing polymeric chain bonded to palladium ion (Figure 4.27). Only the 6-membered palladacycle is modelled with an energy of -3.3 kcal/mol (**INT-MC6**^{pyr}). This is in agreement with the *in situ* NMR investigation where no resonances of palladacycle intermediates are detected.

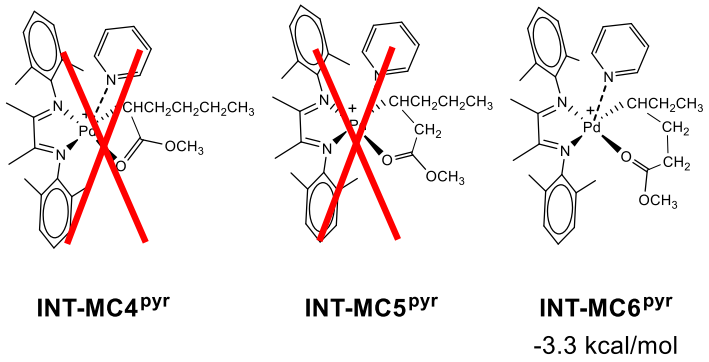

Figure 4.27. The possible metallacycles originated from the insertion of methyl acrylate into the Pd-alkyl chain from **1**^{pyr}.

By combining the catalytic data and *in situ* NMR experiments with DFT calculations, a possible pathway of the chain growth is proposed. When TFE is the solvent of choice, in all copolymers MA is inserted preferentially at the end of the branches (T(MA)), but in a small amount into the main chain (M(MA)).

This indicates that the followed mechanism is independent on the ligand in the fourth coordination site (CH_3CN or pyridine/picoline), but the role of the fluorinated solvent is crucial (Figure 2.6, Chapter 2).[10] After the coordination reaction and the migratory insertion of the polar monomer, two intermediates are possible: the undetected open-chain intermediate **b1** where the fluorinated solvent generates a H-bonds network that traps the polar monomer into the main chain (M(MA)) and the six-membered metallacycle **c1**, generated by the insertion of MA into the Pd-alkyl bond followed by the chain walking process, that leads to T(MA) (Scheme 4.2).

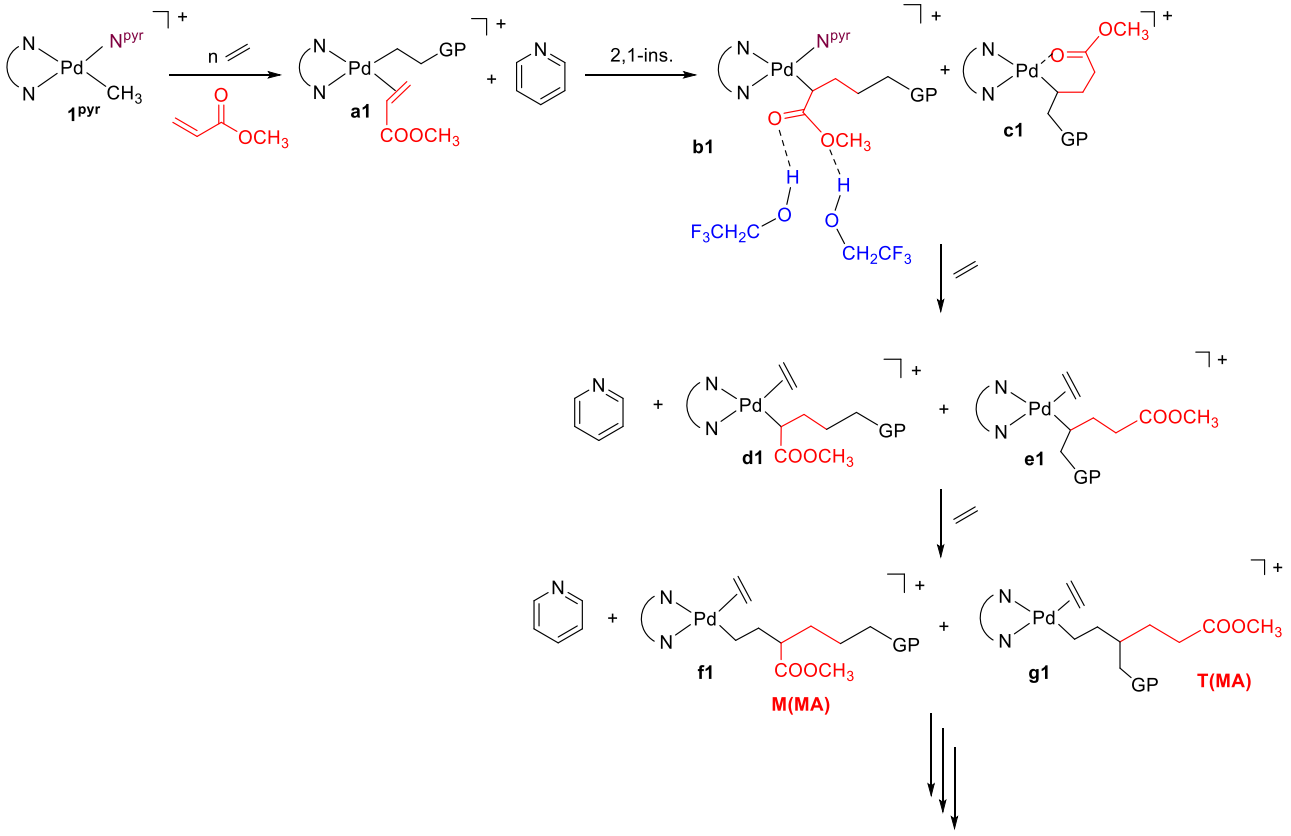

Scheme 4.2. Proposed mechanism for E/MA copolymerization with $\mathbf{1}^{pyr}$ in TFE.

In CH_2Cl_2, the new precatalysts show a different behavior with respect to the parent compounds **1b** and **2b**, resulting in a different way of the polar monomer enchainment. The mechanism for E/MA copolymerization using [Pd(CH_3)($NCCH_3$)(**1**)][PF_6], **1b**, has been elucidated in *Chapter 2* with detailed *in situ* NMR studies and DFT calculations and it follows that firstly investigated by Brookhart.[10,23] While when Pd(II) compounds with pyridine ligands are used in the copolymerization reaction, the coordination/insertion reaction of ethylene into the Pd-alkyl bond $\mathbf{a}^{pyr}$ activates the precatalyst. The subsequent insertion of the polar monomer with secondary regiochemistry leads the formation of an open-chain intermediate, $\mathbf{b}^{pyr}$, with both the pyridine ligand and the organic fragment

of growing copolymer bonded to palladium ion. This is recognized as the novel catalyst resting state. Afterwards the coordination/insertion of incoming ethylene molecules takes place with secondary and primary regiochemistry leading the formation of branches and junction points.[31] From this intermediate the chain walking process generates an hyperbranched structure $\mathbf{f}^{pyr}$ with MA in a junction point of a branches (Scheme 4.3).

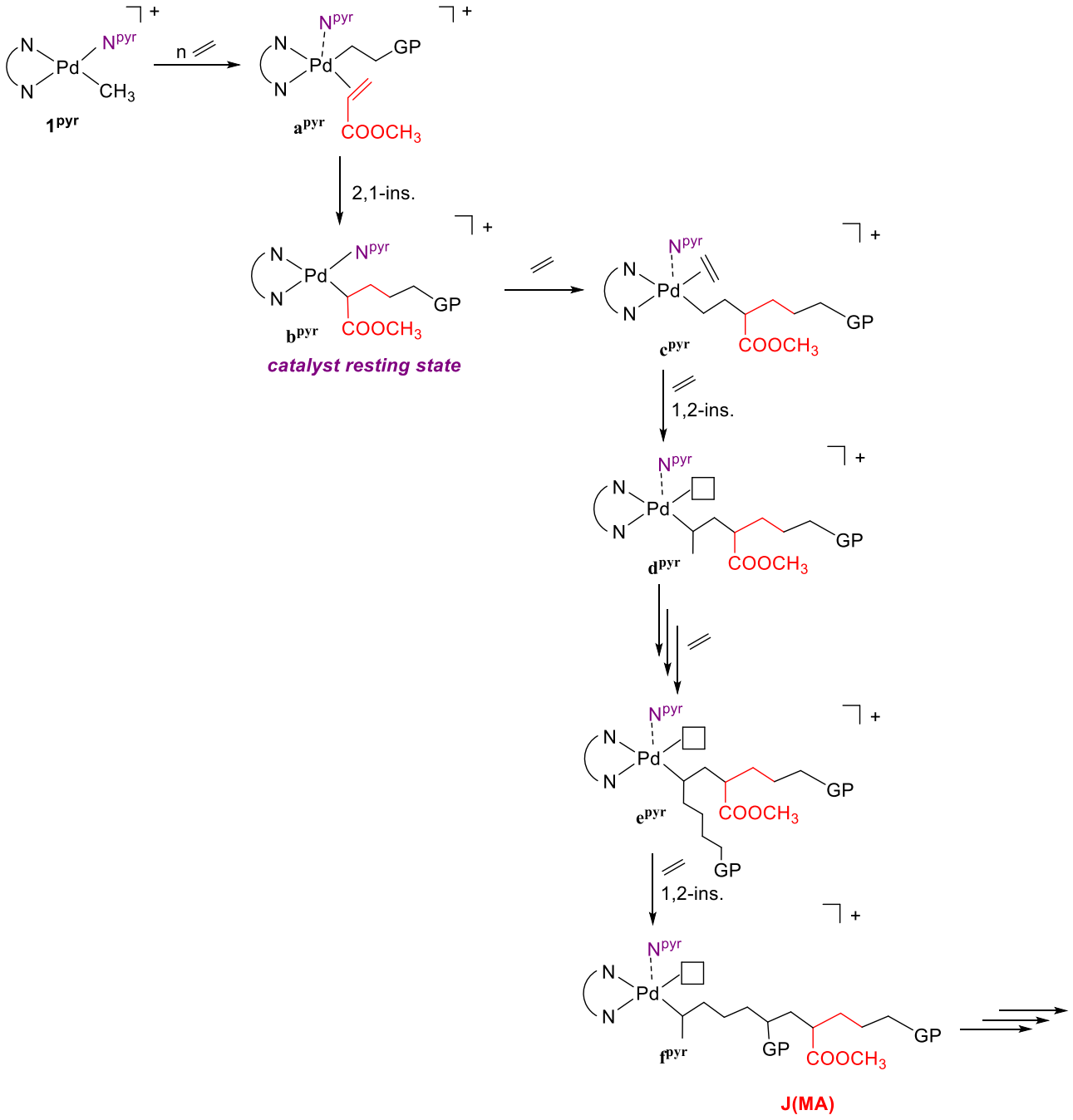

Scheme 4.3. Proposed mechanism for E/MA copolymerization with $\mathbf{1}^{pyr}$ in CH_2Cl_2.

Since a very low amount of methyl acrylate is inserted at the end of the branches (T(MA)) (Scheme 4.2), the chain walking process takes place and the 6-membered metallacycle **c1** is formed. After some insertion reaction of ethylene units, the polar monomer goes at the end of the branches (T(MA)). The metallacycle intermediates are not detected in the NMR spectra during reactivity and this is in agreement with DFT calculations.

4.3 Conclusions.

Pd(II) complexes of general formula [Pd(CH_3)(L)(**1**)][PF_6] and [Pd(CH_3)(L)(**2**)][PF_6], where L is a highly coordinating ligand belonging to the family of the pyridines, are synthesized starting from the precursor [Pd(CH_3)($NCCH_3$)(N-N)][PF_6], **1b** or **2b**. They are characterized in solution by NMR spectroscopy confirming the coordination of the pyridine ligand to the metal center and the presence of only one single species in solution. Some suitable crystals allowed to characterize them also in the solid state with X-ray diffraction. This analysis evidences that pyridine ligand is coordinated to the Pd ion forming with the metal different dihedral angles due to the steric hindrance and electronic factors between the pyridine derivatives and the substituted groups on the *ortho* positions of the aryl ring.

This new series of monocationic complexes is tested in the copolymerization of ethylene with methyl acrylate under mild reaction conditions of temperature and ethylene pressure by carrying out the catalysis in two different solvents, both trifluoroethanol and dichloromethane. These compounds generate active species for the target reaction producing branched macromolecules, characterized in solution at room temperature by NMR spectroscopy. The most relevant results are relative to the way of the polar monomer enchainment:

• when catalysis are carried out in TFE, no differences in the macromolecules microstructure are observed moving from the precursors to Pd(II) complexes with pyridine ligands. The polar monomer is preferentially inserted at the end of the branches (T(MA)) with a small amount into the main chain (M(MA)). Due to the acid nature of the fluorinated solvent that protonates the pyridine ligand, it, on its turn, leaves the palladium coordination sphere during catalysis, so the way of the polar monomer enchainment depends almost exclusively on the presence of the TFE as the solvent of catalysis;

• when catalysis are carried out in DCM, hyperbranched copolymers with MA inserted as T(MA) or J(MA), a unit of the polar monomer in a junction point of a branch, are obtained.

We performed some *in situ* NMR studies to have mechanistic insights about the species involved in the growth of copolymer chains. The reaction with ethylene is investigated. It is slowed down with respect to that of the precursor and only after 2 h the precatalyst is almost totally consumed.

Resonances of branched PE are observed during the monitoring time together with an open-chain intermediate having both the pyridine ligand and the growing polyethylene chain bond to palladium ion. No reaction with only methyl acrylate takes place. While when both comonomers are added to the solution, the complex is activated through the reaction with ethylene, followed by that with MA, leading to the formation of E/MA copolymer, the previous open-chain intermediate and another one having both the pyridine ligand and the growing copolymeric chain with inserted MA bonded to the metal center. This is recognized as a novel catalyst resting state. Bidimensional NMR analysis, in particular the $^{1}H,^{1}H$ NOESY experiment, confirms that, during the catalytic process, pyridine remains coordinated to palladium and no signals of free ligand or metallacycle intermediate are detected.
On the basis of these experimental results, supported by preliminary DFT calculations, the mechanism of E/MA copolymerization is proposed pointing out that when DCM is the solvent of choice, intermediate with coordinated pyridine ligand are responsible of both modulating the macromolecules microstructure and disfavoring the chain walking process.
These considerations evidence that the ligand present in the fourth coordination site of Pd(II) ion is not innocent and it can tune the catalytic performances of complexes.

4.4 Experimental.

All complex manipulations were performed using standard Schlenk techniques under argon. Anhydrous dichloromethane was freshly obtained by distillation over CaH_2 under argon atmosphere. Deuterated solvents (Cambridge Isotope Laboratories, Inc. (CIL) and Sigma Aldrich) were stored as recommended by sellers. Ethylene (purity ≥ 99.9 %) supplied by SIAD and methyl acrylate (99.9%, with 0.02% of hydroquinone monomethyl ether) supplied by Aldrich were used as received. TFE and all the other reagents and solvents were purchased from Sigma-Aldrich/Merck and used without further purification for synthetic, spectroscopic and catalytic purposes. $[Pd(OCOCH_3)_2]$ (BASF Italia) was used as source of the metal to obtain the corresponding Pd(II) complexes. Mono- and bidimensional NMR spectra of ligands and complexes were recorded on a Varian 500 spectrometer (500 MHz for ^{1}H, 125.68 MHz for ^{13}C), and of copolymers on a Varian 400 (400 MHz for ^{1}H, 100.55 MHz for ^{13}C). The resonances are reported in ppm (δ) and referenced to the residual solvent peak versus $Si(CH_3)_4$: CD_2Cl_2: at δ 5.32 (^{1}H) and δ 54.00 (^{13}C); $CDCl_3$: at δ 7.26 (^{1}H) and δ 77.16 (^{13}C). NMR experiments were performed employing the automatic software parameters. In the case of NOESY experiments a mixing time of 500 ms was used.
Mass spectra (ESI-MS) were recorded on a Massa Esquire 4000 – Bruker in positive ion polarity (HV capillary of 4000 V and dry gas of 5.00 L/min). Samples were dissolved in methanol and the analysis

was carried out immediately. The average molecular weights (M_n and M_w) and polydispersity (M_w/M_n) values of copolymer samples were determined by SEC in THF against polystyrene standards. Data collections were performed at the X-ray diffraction beamline (XRD1) of the Elettra synchrotron of Trieste (Italy), equipped with a Pilatus 2M image plate detector. Collection temperature was 100 K (nitrogen stream supplied through an Oxford Cryostream 700); the wavelength of the monochromatic X-ray beam was 0.700 Å and the diffractograms were obtained with the rotating crystal method.

*4.4.1 Synthesis and characterization of Pd(II) cationic complexes, **1^{pyr} – 1^{3,5lut}** and **2^{pyr} – 2^{3,5lut}**.*

The cationic complexes were synthesized starting from [Pd(CH_3)($NCCH_3$)(**1**)][PF_6], **1b**, and from [Pd(CH_3)($NCCH_3$)(**2**)][PF_6], **2b**, that, on turn, were prepared from [Pd($OCOCH_3$)$_2$] following the literature procedure.[19,32,33]

General procedure: to a stirred solution of **1b** or **2b** in CH_2Cl_2 (0.1 mmol in 5 mL), at 313 K, a 1M dichloromethane solution of pyridine derivatives (1.1 eq. in 2 mL) is added. The reaction mixture is left under stirring, in the dark, for the proper reaction time. Afterward it is concentrated to few mL of volume and upon addition of cold diethyl ether the product is precipitated. It is filtered under vacuum after a night at 277 K and washed with cold Et_2O. Products are obtained as yellow powders.

1^{pyr}. (yield = 81 %); ^{1}H NMR (500 MHz, CD_2Cl_2, 298 K) δ: 8.08-8.07 (dd, 2H, H^{2,6}), 7.66 (t, 1H, H^4), 7.26-7.23 (m, 3H, H^{m2}, H^{p2}), 7.22-7.21 (t, 2H, H^{3,5}), 7.11-6.93 (m, 3H, H^{m1}, H^{p1}), 2.29 (s, 6H, CH_3^{Ar2}), 2.21 (s, 6H, CH_3^{DAB1}, CH_3^{DAB2}), 2.16 (s, 6H, CH_3^{Ar1}), 0.32 (s, 3H, Pd-CH_3). ^{13}C NMR (125.68 MHz, CD_2Cl_2, 298 K from the ^{1}H,^{13}C HSQC spectrum) δ: 151.6 (C^2, C^6), 138.87 (C^4), 129.1-127.4 (C^m, C^p), 125.7 (C^3, C^5), 18.0-17.8 (CH_3^{Ar}), 20.1-19.3 (CH_3^{DAB}), 6.0 (Pd-CH_3).

1^{2pic}. (yield = 67 %); ^{1}H NMR (500 MHz, CD_2Cl_2, 298 K) δ = 8.21 (d, 1H, H^6), 7.54 (t, 1H, H^4), 7.26-7.21 (m, 3H, H^{p2}, H^{m2}), 7.11 (d, 1H, H^3), 6.95-6.89 (m, 4H, H^5, H^{p1}, H^{m1}), 2.77 (s, 3H, CH_3^{pic}), 2.33 (s, 3H, CH_3^{Ar2}), 2.28 (d, 6H, CH_3^{Ar1A}, CH_3^{Ar2}), 2.21 (s, 3H, CH_3^{DAB2}), 2.19 (s, 3H, CH_3^{DAB1}), 2.09 (s, 3H, CH_3^{Ar1}), 0.19 (s, 3H, Pd-CH_3). ^{13}C NMR (125.68 MHz, CD_2Cl_2, 298 K from the ^{1}H,^{13}C HSQC spectrum) δ = 151.3 (C^6), 138.5 (C^4), 129.1-127.2 (C^p, C^m), 127.1 (C^3), 122.8 (C^5), 27.6 (CH_3^{pic}), 18.2-17.8 (CH_3^{Ar}), 20.2-19.6 (CH_3^{DAB}), 3.3 (Pd-CH_3).

1^{4pic}. (yield = 57 %); ^{1}H NMR (500 MHz, CD_2Cl_2, 298 K) δ = 7.89 (d, 2H, H^{2,6}), 7.23 (m, 3H, H^{m2}, H^{p2}), 6.95 (m, 3H, H^{m1}, H^{p1}), 6.89 (d, 2H, H^{3,5}), 2.28 (s, 6H, CH_3^{Ar2}), 2.27 (s, 3H, CH_3^{pic}), 2.20 (s, 6H, CH_3^{DAB1}, CH_3^{DAB2}), 2.16 (s, 6H, CH_3^{Ar1}), 0.29 (s, 3H, Pd-CH_3). ^{13}C NMR (125.68 MHz, CD_2Cl_2, 298 K from the ^{1}H,^{13}C HSQC spectrum) δ = 150.8 (C^{2,6}), 129.1-127.3 (C^m, C^p), 126.5 (C^{3,5}), 21.2 (CH_3^{pic}), 19.4-17.1 (CH_3^{Ar}, CH_3^{DAB}), 5.8 (Pd-CH_3).

$1^{2,6lut}$. (yield = 73 %); ^{1}H NMR (500 MHz, CD_2Cl_2, 298 K) δ = 7.71 (s, 2H, $H^{2,6}$), 7.26-7.20 (m, 4H, H^4, H^{m2}, H^{p2}), 6.96 (s, 3H, H^{m1}, H^{p1}), 2.28 (s, 6H, CH_3^{Ar2}), 2.20 (d, 6H, CH_3^{DAB1}, CH_3^{DAB2}), 2.16 (s, 3H, CH_3^{Ar1}), 2.08 (s, 3H, CH_3^{lut}), 0.32 (s, 3H, Pd-CH_3). ^{13}C NMR (125.68 MHz, CD_2Cl_2, 298 K, from the ^{1}H,^{13}C HSQC spectrum) δ = 148.9 ($C^{2,6}$), 139.9 (C^4), 129.0-127.4 (C^m, C^p), 18.0 (CH_3^{lut}), 20.0-19.2 (CH_3^{DAB}), 18.3-17.9 (CH_3^{Ar}), 5.8 (Pd-CH_3).

$1^{3,5lut}$. (yield = 82 %); ^{1}H NMR (500 MHz, CD_2Cl_2, 298 K) δ = 7.50 (t, 1H, H^4), 7.28-7.24 (m, 3H, H^{m2}, H^{p2}), 6.98-6.92 (m, 5H, $H^{3,5}$, H^{m1}, H^{p1}), 2.90 (s, 6H, CH_3^{lut}), 2.33 (s, 6H, CH_3^{Ar2}), 2.23 (s, 3H, CH_3^{DAB2}), 2.20 (s, 3H, CH_3^{DAB1}), 2.14 (s, 6H, CH_3^{Ar1}), 0.18 (s, 3H, Pd-CH_3). ^{13}C NMR (125.68 MHz, CD_2Cl_2, 298 K, from the ^{1}H,^{13}C HSQC spectrum) δ = 138.8 (C^4), 129.2-127.2 (C^m, C^p), 123.1 ($C^{3,5}$), 28.3 (CH_3^{lut}), 18.0 (CH_3^{Ar}), 20.3-19.7 (CH_3^{DAB}), 1.8 (Pd-CH_3).

2^{pyr}. (yield = 91 %); ^{1}H NMR (500 MHz, CD_2Cl_2, 298 K) δ = 7.95 (d, 2H, $H^{2,6}$), 7.72 (t, 1H, H^4), 7.48-7.33 (m, 3H, H^{m2}, H^{p2}), 7.24 (m, 1H, H^{p1}), 7.16-7.13 (m, 4H, $H^{3,5}$, H^{m1}), 3.05-2.97 (sept, 2H, CH^{iPr2}), 2.92-2.83 (sept, 2H, CH^{iPr1}), 2.30 (s, 3H, CH_3^{DAB1}), 2.28 (s, 3H, CH_3^{DAB2}), 1.41 (d, 6H, CH_3^{iPr2}), 1.26 (d, 6H, CH_3^{iPr2}), 1.19-1.15 (m, 12H, CH_3^{iPr1}), 0.46 (s, 3H, Pd-CH_3). ^{13}C NMR (125.68 MHz, CD_2Cl_2, 298 K, from the ^{1}H,^{13}C HSQC spectrum) δ = 151.7 ($C^{2,6}$), 139.1 (C^4), 129.1-124.7 (C^m, C^p, $C^{3,5}$), 29.2-29.1 (CH^{iPr}), 23.7-23.2 (CH_3^{iPr}), 21.7-21.1 (CH_3^{DAB}), 9.8 (Pd-CH_3).

2^{2pic}. (yield = 78 %); ^{1}H NMR (500 MHz, CD_2Cl_2, 298 K) δ = 7.88 (d, 1H, H^6), 7.59 (t, 1H, H^4), 7.45-7.32 (m, 3H, H^{m2}, H^{p2}), 7.29 (m, 2H, H^3, H^{m1}), 7.18 (t, 1H, H^{p1}), 6.91 (d, 1H, H^{m1}), 6.82 (t, 1H, H^5), 3.18 (sept, 1H, CH^{iPrEF}), 3.01 (sept, 1H, CH^{iPrAB}), 2.92 (sept, 1H, CH^{iPrGH}), 2.83 (s, 3H, CH_3^{pic}), 2.70 (sept, 1H, CH^{iPrCD}), 2.29 (s, 6H, CH_3^{DAB1}, CH_3^{DAB2}), 1.60 (d, 3H, CH_3^{iPrA}), 1.42 (d, 3H, CH_3^{iPrF}), 1.38 (d, 3H, CH_3^{iPrG}), 1.30 (d, 3H, CH_3^{iPrE}), 1.28 (d, 3H, CH_3^{iPrB}), 1.22 (d, 3H, CH_3^{iPrH}), 1.05 (d, 3H, CH_3^{iPrD}), 0.83 (d, 3H, CH_3^{iPrC}), 0.27 (s, 3H, Pd-CH_3). ^{13}C NMR (125.68 MHz, CD_2Cl_2, 298 K, from the ^{1}H,^{13}C HSQC spectrum) δ = 151.0 (C^6), 138.7 (C^4), 129.0-124.6 (C^m, C^p), 126.7 (C^3), 122.6 (C^2), 29.9-22.4 (CH_3^{iPr}), 29.1-29.0 (CH^{iPr}), 27.7 (CH_3^{pic}), 21.6 (CH_3^{DAB}), 5.7 (Pd-CH_3). MS-ESI: m/z = 566.2 [**2b**]$^+$, m/z = 509.2 [$\mathbf{2}^{\mathbf{2pic}}$]$^+$– {$CH_3$-2pic} + {2H}.

2^{4pic}. (yield = 66 %); ^{1}H NMR (500 MHz, CD_2Cl_2, 298 K) δ: 7.77 (d, 2H, $H^{2,6}$), 7.42-7.39 (m, 3H, H^{m2}, H^{p2}), 7.24 (t, 1H, H^{m1}), 7.15 (d, 2H, H^{p1}), 6.93 (d, 2H, $H^{3,5}$), 3.05-2.96 (sept, 2H, CH^{iPr2}), 2.92-2.85 (sept, 2H, CH^{iPr1}), 2.28 (m, 9H, CH_3^{DAB1}, CH_3^{DAB2}, CH_3^{pic}), 1.40 (d, 6H, CH_3^{iPr2}), 1.26 (d, 6H, CH_3^{iPr2}), 1.19-1.15 (m, 12H, CH_3^{iPr1}), 0.42 (s, 3H, Pd-CH_3). ^{13}C NMR (500 MHz, CD_2Cl_2, 298 K, from the ^{1}H,^{13}C HSQC spectrum) δ: 150.9 ($C^{2,6}$),128.9-124.5 (C^m, C^p), 126.7 ($C^{3,5}$), 29.2-29.1 (CH^{iPr}), 23.9-16.4 (CH_3^{iPr}), 21.1-18.5 (CH_3^{DAB}, CH_3^{pic}), 9.5 (Pd-CH_3). MS-ESI: m/z = 618.2 [$\mathbf{2}^{\mathbf{4pic}}$]$^+$, m/z = 566.2 [**2b**]$^+$, m/z = 509.2 [$\mathbf{2}^{\mathbf{4pic}}$]$^+$ – {CH_3 - 4pic} + {2H}, m/z = 507.2 [$\mathbf{2}^{\mathbf{4pic}}$]$^+$ – {CH_3 - 4pic}, m/z = 216.1 [$\mathbf{2}^{\mathbf{4pic}}$]$^+$ – {**2**} + {2H}.

$2^{2,6lut}$. (yield = 88 %); ^{1}H NMR (500 MHz, CD_2Cl_2, 298 K) δ: 7.55 (t, 1H, H^4), 7.42-7.32 (m, 3H, H^{p2}. H^{m2}), 7.23 (t, 1H, H^{p1}), 7.14 (d, 2H, H^{m1}), 7.06 (d, 2H, $H^{3,5}$), 3.12-3.02 (sept, 2H, CH^{iPr2}), 2.80-2.76 (m, 8H, CH_3^{lut}, CH^{iPr1}), 2.28 (s, 3H, CH_3^{DAB2}), 2.27 (s, 3H, CH_3^{DAB1}), 1.39 (d, 6H, CH_3^{iPrG}), 1.27 (d, 6H, CH_3^{iPrE}), 1.13 (d, 6H, CH_3^{iPrA}), 1.05 (d, 6H, CH_3^{iPrC}), 0.19 (s, 3H, Pd-CH_3). ^{13}C NMR (500 MHz, CD_2Cl_2, 298 K, from the ^{1}H,^{13}C HSQC spectrum) δ: 139.2 (C^4), 129.0-124.7 (C^m, C^p), 123.5 ($C^{3,5}$), 29.0-28.2 (CH^{iPr}), 28.2 (CH_3^{lut}), 25.1-18.7 (CH_3^{iPr}), 22.2 (CH_3^{DAB}), 5.7 (Pd-CH_3).

$2^{3,5lut}$. (yield = 78 %); ^{1}H NMR (500 MHz, CD_2Cl_2, 298 K) δ: 7.58 (s, 2H, $H^{2,6}$), 7.42-7.34 (m, 3H, H^{p2}, H^{m2}), 7.30 (s, 1H, H^4), 7.26-7.15 (m, 3H, H^{p1}, H^{m1}), 3.03-2.98 (sept, 2H, CH^{iPr2}), 2.90-2.85 (sept, 2H, CH^{iPr1}), 2.31 (s, 3H, CH_3^{DAB1}), 2.27 (s, 3H, CH_3^{DAB2}), 2.06 (s, 6H, CH_3^{lut}), 1.42 (d, 6H, CH_3^{iPrG}), 1.26 (d, 6H, CH_3^{iPrE}), 1.18 (d, 6H, CH_3^{iPrA}), 1.15 (d, 6H, CH_3^{iPrC}), 0.45 (s, 3H, Pd-CH_3). ^{13}C NMR (500 MHz, CD_2Cl_2, 298 K, from the ^{1}H,^{13}C HSQC spectrum) δ: 148.9 (C^2), 140.2 (C^4), 128.5-124.5 (C^m, C^p), 30.0-29.1 (CH^{iPr}), 26.0-21.2 (CH_3^{iPr}), 21.8-18.3 (CH_3^{DAB}), 18.4 (CH_3^{lut}), 9.7 (Pd-CH_3).

4.4.2 Ethylene/methyl acrylate copolymerization reaction.

All catalytic experiments are carried out in a Büchi "tinyclave" reactor equipped with an interchangeable 50 mL glass vessel. The vessel is loaded with the desired complex (21 μmol), TFE (21 mL) or distilled CH_2Cl_2 (21 mL) and methyl acrylate. The reactor is placed in a preheated oil bath and connected to the ethylene tank. The ethylene is bubbled for 10 min, then the reactor is pressurized. After the proper time (6 h), the reactor is cooled to room temperature and vented. The reaction mixture is poured in a 50 mL round flask, together with dichloromethane (3 x 2 mL) used to wash the glass vessel. Volatiles were removed under reduced pressure and the residual oil is dried at constant weight and analyzed by NMR spectroscopy at room temperature.

4.4.3 General procedures for in situ NMR reactivities.

*General procedure for the in situ NMR reactivity of **1^{4pic}** with ethylene.*

A 10 mM solution of **1^{4pic}** in CD_2Cl_2 is prepared, and a first ^{1}H NMR spectrum is recorded. Ethylene is bubbled into the NMR tube for 5 min. The reaction is followed over time, at T = 298 K.

*General procedure for the in situ ^{1}H NMR reactivity of **1^{4pic}** with methyl acrylate.*

A 10 mM solution of **1^{4pic}** in CD_2Cl_2 is prepared, and a first ^{1}H NMR spectrum is recorded. Methyl acrylate (2 eq.) is then added to the solution. The reaction is followed over time, at T = 298 K.

*General procedure for the in situ ^{1}H NMR reactivity of **1^{4pic}** with both comonomers.*

A 10 mM solution of **1^{4pic}** in CD_2Cl_2 is prepared, and a first ^{1}H NMR spectrum is recorded. Methyl acrylate (2 eq.) is added to the solution, immediately followed by bubbling of ethylene into the NMR tube for 5 min. The reaction is followed over time, at T = 298 K.

4.5 References.

(1) Tan, C.; Chen, C. Emerging Palladium and Nickel Catalysts for Copolymerization of Olefins with Polar Monomers. *Angew. Chemie - Int. Ed.* **2019**, *58* (22), 7192–7200.

(2) Drent, E.; Van Dijk, R.; Van Ginkel, R.; Van Oort, B.; Pugh, R. I. Palladium Catalysed Copolymerisation of Ethene with Alkylacrylates: Polar Comonomer Built into the Linear Polymer Chain. *Chem. Commun.* **2002**, *2* (7), 744–745.

(3) Guo, L.; Gao, H.; Guan, Q.; Hu, H.; Deng, J.; Liu, J.; Liu, F.; Wu, Q. Substituent Effects of the Backbone in α-Diimine Palladium Catalysts on Homo- and Copolymerization of Ethylene with Methyl Acrylate. *Organometallics* **2012**, *31* (17), 6054–6062.

(4) Zhong, S.; Tan, Y.; Zhong, L.; Gao, J.; Liao, H.; Jiang, L.; Gao, H.; Wu, Q. Precision Synthesis of Ethylene and Polar Monomer Copolymers by Palladium-Catalyzed Living Coordination Copolymerization. *Macromolecules* **2017**, *50* (15), 5661–5669.

(5) Dall'Anese, A.; Rosar, V.; Cusin, L.; Montini, T.; Balducci, G.; D'Auria, I.; Pellecchia, C.; Fornasiero, P.; Felluga, F.; Milani, B. Palladium-Catalyzed Ethylene/Methyl Acrylate Copolymerization: Moving from the Acenaphthene to the Phenanthrene Skeleton of α-Diimine Ligands. *Organometallics* **2019**, *38* (19), 3498–3511.

(6) Zhang, Y.; Wang, C.; Mecking, S.; Jian, Z. Ultrahigh Branching of Main-Chain-Functionalized Polyethylenes by Inverted Insertion Selectivity. *Angew. Chemie* **2020**, *132* (34), 14402–14408.

(7) Lu, W.; Wang, H.; Fan, W.; Dai, S. Exploring the Relationship between the Polyethylene Microstructure and Spatial Structure of α-Diimine Pd(II) Catalysts via a Hybrid Steric Strategy. *Inorg. Chem.* **2022**, *61* (18), 6799–6806.

(8) Zhai, F.; Solomon, J. B.; Jordan, R. F. Copolymerization of Ethylene with Acrylate Monomers by Amide-Functionalized α-Diimine Pd Catalysts. *Organometallics* **2017**, *36* (9), 1873–1879.

(9) Fan, H.; Xu, G.; Wang, H.; Dai, S. Direct Synthesis of Hyperbranched Ethene Oligomers and Ethene-MA Co-Oligomers Using Iminopyridyl Systems with Weak Neighboring Group Interactions. *J. Polym. Sci.* **2022**, *60* (13), 1944–1953.

(10) Alberoni, C.; D'Alterio, M. C.; Balducci, G.; Immirzi, B.; Polentarutti, M.; Pellecchia, C.; Milani, B. Tunable "In-Chain" and "At the End of the Branches" Methyl Acrylate Incorporation in the Polyolefin Skeleton through Pd(II) Catalysis. *ACS Catal.* **2022**, *12*, 3430–3443.

(11) Kochi, T.; Yoshimura, K.; Nozaki, K. Synthesis of Anionic Methylpalladium Complexes with Phosphine-Sulfonate Ligands and Their Activities for Olefin Polymerization. *Dalt. Trans.* **2006**, No. 1, 25–27.

(12) Guironnet, D.; Roesle, P.; Rünzi, T.; Göttker-Schnetmann, I.; Mecking, S. Insertion Polymerization of Acrylate. *J. Am. Chem. Soc.* **2009**, *131* (2), 422–423.

(13) Nakamura, A.; Anselment, T. M. J.; Claverie, J.; Goodall, B.; Jordan, R. F.; Mecking, S.; Rieger, B.; Sen, A.; Van Leeuwen, P. W. N. M.; Nozaki, K. Ortho-Phosphinobenzenesulfonate: A Superb Ligand for Palladium-Catalyzed Coordination-Insertion Copolymerization of Polar Vinyl Monomers. *Acc. Chem. Res.* **2013**, *46* (7), 1438–1449.

(14) Mitsushige, Y.; Carrow, B. P.; Ito, S.; Nozaki, K. Ligand-Controlled Insertion Regioselectivity Accelerates Copolymerisation of Ethylene with Methyl Acrylate by Cationic Bisphosphine Monoxide-Palladium Catalysts. *Chem. Sci.* **2016**, *7* (1), 737–744.

(15) Contrella, N. D.; Sampson, J. R.; Jordan, R. F. Copolymerization of Ethylene and Methyl Acrylate by Cationic Palladium Catalysts That Contain Phosphine-Diethyl Phosphonate Ancillary Ligands. *Organometallics* **2014**, *33* (13), 3546–3555.

(16) Sui, X.; Dai, S.; Chen, C. Ethylene Polymerization and Copolymerization with Polar Monomers by Cationic Phosphine Phosphonic Amide Palladium Complexes. *ACS Catal.* **2015**, *5* (10), 5932–5937.

(17) Zhang, W.; Waddell, P. M.; Tiedemann, M. A.; Padilla, C. E.; Mei, J.; Chen, L.; Carrow, B. P. Electron-Rich Metal Cations Enable Synthesis of High Molecular Weight, Linear Functional Polyethylenes. *J. Am. Chem. Soc.* **2018**, *140* (28), 8841–8850.

(18) Johnson, L. K.; Mecking, S.; Brookhart, M. Copolymerization of Ethylene and Propylene with Functionalized Vinyl Monomers by Palladium(II) Catalysts. *J. Am. Chem. Soc.* **1996**, *118* (1), 267–268.

(19) Rosar, V.; Montini, T.; Balducci, G.; Zangrando, E.; Fornasiero, P.; Milani, B. Palladium-Catalyzed Ethylene/Methyl Acrylate Co-Oligomerization: The Effect of a New Nonsymmetrical α-Diimine with the 1,4-Diazabutadiene Skeleton. *ChemCatChem* **2017**, *9* (17), 3402–3411.

(20) Rosar, V.; Dedeic, D.; Nobile, T.; Fini, F.; Balducci, G.; Alessio, E.; Carfagna, C.; Milani, B. Palladium Complexes with Simple Iminopyridines as Catalysts for Polyketone Synthesis. *Dalt. Trans.* **2016**, *45* (37), 14609–14619.

(21) Navarro, M.; Rosar, V.; Montini, T.; Milani, B.; Albrecht, M. Olefin Dimerization and Isomerization Catalyzed by Pyridylidene Amide Palladium Complexes. *Organometallics* **2018**, *37* (20), 3619–3630.

(22) Haynes, W. M. *CRC Handbook of chemistry and physics*, 97th edition, , **2016-2017**.

(23) Mecking, S. Mechanistic Studies of the Palladium-Catalyzed Copolymerization of Ethylene and α-Olefins with Methyl Acrylate. *J. Am. Chem. Soc.* **1998**, *120* (5), 888–899.

(24) Scarel, A.; Durand, J.; Franchi, D.; Zangrando, E.; Mestroni, G.; Milani, B.; Gladiali, S.; Carfagna, C.; Binotti, B.; Bronco, S.; Gragnoli, T. Trifluoroethanol: Key Solvent for Palladium-Catalyzed Polymerization Reactions. *J. Organomet. Chem.* **2005**, *690* (8 SPEC. ISS.), 2106–2120.

(25) Takano, S.; Takeuchi, D.; Osakada, K.; Akamatsu, N.; Shishido, A. Dipalladium Catalyst for Olefin Polymerization: Introduction of Acrylate Units into the Main Chain of Branched Polyethylene. *Angew. Chemie - Int. Ed.* **2014**, *53* (35), 9246–9250.

(26) Zhang, Y.; Kang, X.; Jian, Z. Selective Branch Formation in Ethylene Polymerization to Access Precise Ethylene-Propylene Copolymers. *Nat. Commun.* **2022**, *13* (1), 1–9.

(27) Cotts, P. M.; Guan, Z.; McCord, E.; McLain, S. Novel Branching Topology in Polyethylenes as Revealed by Light Scattering and 13C NMR. *Macromolecules* **2000**, *33* (19), 6945–6952.

(28) Galland, G. B.; De Souza, R. F.; Mauler, R. S.; Nunes, F. F. 13C NMR Determination of the Composition of Linear Low-Density Polyethylene Obtained with [H3-Methallyl-Nickel-Diimine]PF6 Complex. *Macromolecules* **1999**, *32* (5), 1620–1625.

(29) Cruz, T. F. C.; Figueira, C. A.; Veiros, L. F.; Gomes, P. T. Benzylnickel(II) Complexes of 2-Iminopyrrolyl Chelating Ligands: Synthesis, Structure, and Catalytic Oligo-/Polymerization of Ethylene to Hyperbranched Polyethylene. *Organometallics* **2021**, *40* (15), 2594–2609.

(30) D'Auria, I.; Milione, S.; Caruso, T.; Balducci, G.; Pellecchia, C. Synthesis of Hyperbranched Low Molecular Weight Polyethylene Oils by an Iminopyridine Nickel(II) Catalyst. *Polym. Chem.* **2017**, *8* (41), 6443–6454.

(31) Ittel, S. D.; Johnson, L. K.; Brookhart, M. Late-Metal Catalysts for Ethylene Homo- and Copolymerization. *Chem. Rev.* **2000**, *100* (4), 1169–1203.

(32) Brookhart, M.; Johnson, L. K.; Killian, C. M. New Pd(II)- and Ni(II)-based catalysts for polymerization of ethylene and α-olefins. *J. Am. Chem. Soc.* **1995**, *117*, 6414–6415.

(33) Durand, J.; Zangrando, E.; Stener, M.; Fronzoni, G.; Carfagna, C.; Binotti, B.; Kamer, P. C. J.; Müller, C.; Caporali, M.; Van Leeuwen, P. W. N. M.; Vogt, D.; Milani, B. Long-Lived Palladium Catalysts for CO/Vinyl Arene Polyketones Synthesis: A Solution to Deactivation Problems. *Chem. - A Eur. J.* **2006**, *12* (29), 7639–7651.

CHAPTER 5

Crucial role of acetonitrile on the mechanism of Pd(II)-catalyzed activation of polar vinyl monomers.

Overview

Considering Pd(II) catalysts for the synthesis of functionalized polyolefins through coordination/insertion polymerization, the migratory insertion reaction of the polar vinyl monomer into the Pd-alkyl bond is one of the key steps of the catalytic cycle. Following the recent paper where Pd(II) complexes with a N-N' bidentate pyridyl-pyridylidene amide (PYA) ligand were reported as catalysts for ethylene/methyl acrylate (MA) cooligomerization, we have now performed a detailed NMR investigation about the reactivity of two Pd-PYA complexes with either MA or *N*,*N*-dimethylacrylamide (DMA). The neutral complex [Pd(CH_3)Cl(PYA)], activated *in situ* with NaBArF, and the cationic derivative [Pd(CH_3)($NCCH_3$)(PYA)][BArF] show distinct reactivity with the two polar monomers. Palladacycle intermediates, resulting from the migratory insertion reaction of the polar monomer into the Pd-CH_3 bond, are always detected, but in different amount depending on both the precursor and the polar monomer. The presence, or not, of acetonitrile in the palladium coordination sphere affects the reactivity of the complexes, suggesting that it plays a crucial role in the chain walking process.

The studies reported in this chapter are the result of a collaboration with Prof. Martin Albrecht of University of Bern (CH).

5.1. Introduction.

Pd(II) catalysts with unsymmetrical ligands have been reported in literature with either P-O donor molecules (Figure 1.9 – Chapter 1) or N-N' α-diimines differing for the substituents on the two aryl rings (Figure 1.6 – Chapter 1).[1,2,3,4,5] In general, in the copolymerization of ethylene with polar vinyl monomers, they show higher productivity than their symmetrical analogues.

With the aim to extend examples of N-bidentate unsymmetrical ligands, pyridyl-pyridyldene amide (PYA) derivatives have been investigated as ancillary ligands for Pd-catalysts in the copolymerization of ethylene with methyl acrylate, leading to low molecular weight products with a high amount of inserted MA, up to 32 mol % (Figure 5.1).[6] A clear relationship between the electronic property of the PYA ligand and the catalytic behavior (productivity and stability) of the complexes is observed. In particular, Pd(II) compounds bearing *o*-PYA ligand show higher catalytic activity, reaching the highest value of ethylene TON about 153 mol of converted gaseous monomer per mol of Pd, than *m*- and *p*-PYA ones. A strong correlation between the catalytic outcome and the ligand setting, as the presence of N-CH_3 on the *ortho* position of the PYA ring and the carbonyl group, that forces this half of ligand to be twisted out from the complex plane, is shown and the coordination/insertion of olefins (like ethylene) is favored leading to the formation of butenes within 30 min. In addition, the insertion of methyl acrylate as a polar monomer is more efficient with stronger donor PYA units.

Since the productivity of these Pd(II)-PYA compounds is low and the increase of the steric hindrance around the metal center might be an advantageous approach to obtain better performing catalysts, a new ligand is synthesized introducing a methyl group on the 3-position of PYA ring, obtaining ligand **8**. The relevant Pd(II) cationic complexes might increase the catalyst productivity (Figure 5.1).[7]

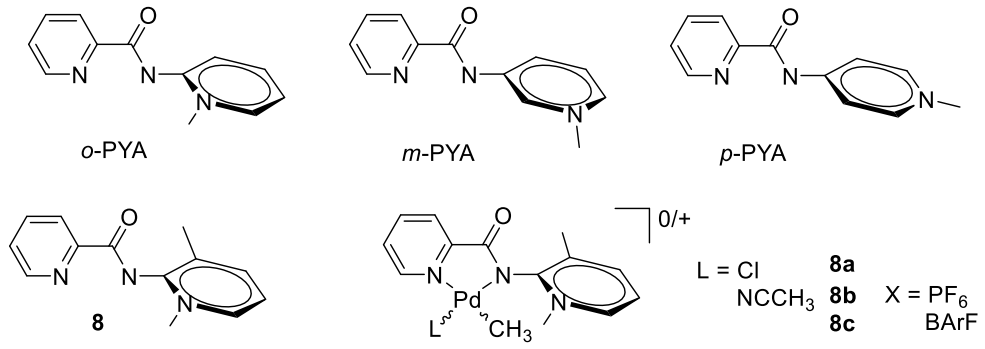

Figure 5.1. The investigated PYA ligands and the relevant neutral and monocationic Pd(II) complexes.

Complex **8b** was tested as catalyst in the cooligomerization of ethylene with methyl acrylate under mild reaction conditions of temperature and ethylene pressure. Productivity remains low (26.6 g P per g Pd) and unsaturated esters, like pentenoic and heptanoic esters, are present together with significant amount of E/MA cooligomers. A detailed *in situ* NMR investigation was carried out to have additional insights about the cooligomerization mechanism. A 10 mM CD_2Cl_2 solution of **8b** was saturated with ethylene and the reaction followed over time, at room temperature. The precatalyst was fully converted into active species immediately after the saturation of the solution with the gaseous monomer, producing propene, *cis/trans*-2-butenes and the Pd-ethyl intermediate, Pd-CH_2CH_3, recognized as the catalyst resting state. In the reaction of **8b** with the polar monomer, the 4-membered palladacycle (**MC4^{PYA}**) was detected for the first time at room temperature (Figure 5.2). Since **8** is a nonsymmetric molecule, which coordinates to Pd(II) ion in a nonsymmetric chemical environment, two different geometrical isomers are possible. We conventionally define the *cis* isomer as the complex bearing the Pd-CH_3 (or more general the Pd-alkyl) bond of the same side of the PYA ring, while the *trans* isomer is the complex bearing the Pd-CH_3 (or more general the Pd-alkyl) bond on the opposite side of the PYA ring. The signals of **MC4^{PYA}** were assigned through a bidimensional NMR characterization and, in particular, the peak due to the Overhauser effect between γCH_3 and the resonance of N-CH_3 of the PYA ring indicated that the detected **MC4^{PYA}** is the *cis* isomer.

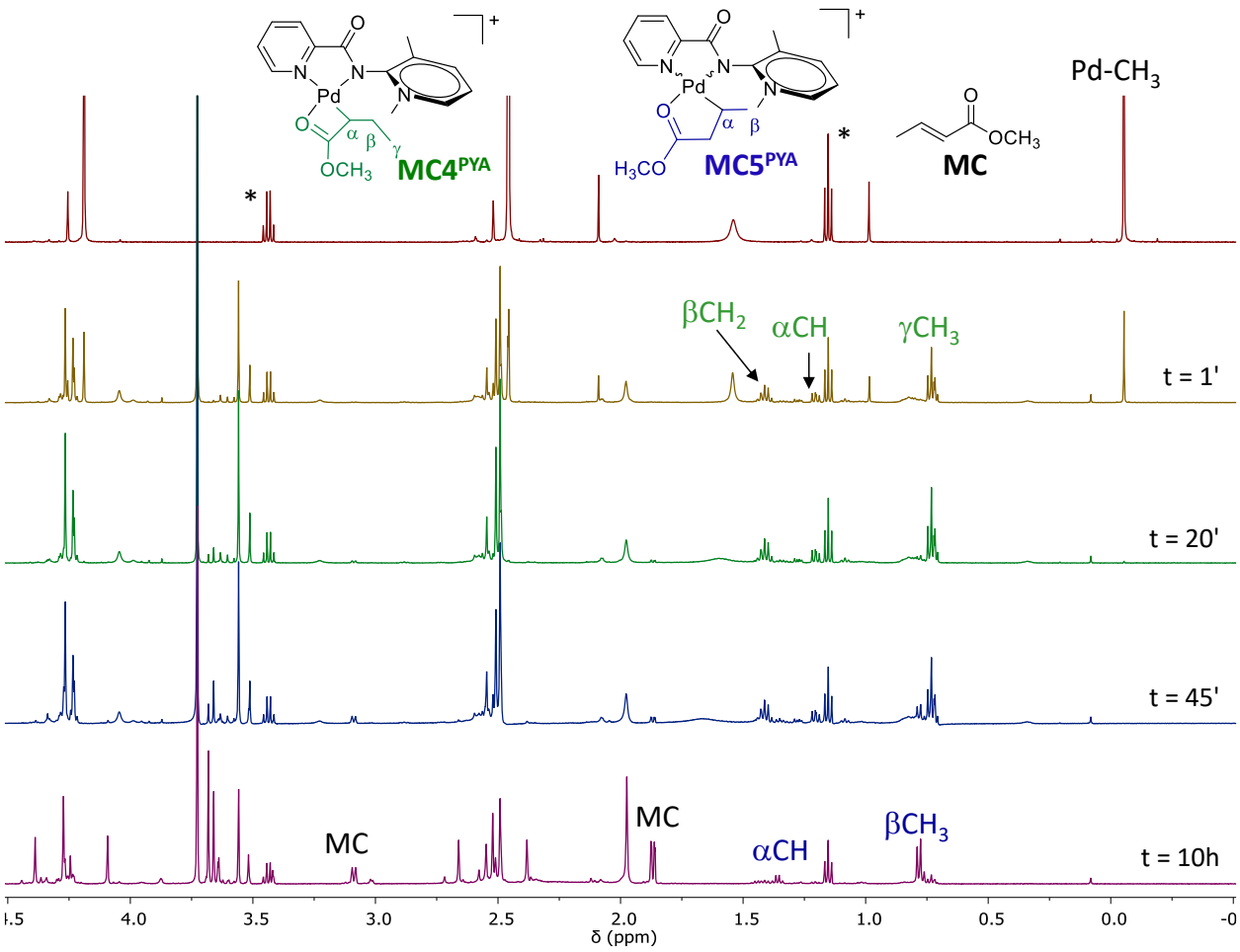

Figure 5.2. ^{1}H NMR spectra (CD_2Cl_2, 298 K) of **8b** (top spectrum) and **8b** after the addition of MA at different reaction times; *diethyl ether.[7]

MC4^{PYA} slowly evolves to the 5-membered palladacycle, **MC5^{PYA}**, that is the main species present in solution after 10 h together with methyl crotonate (**MC**). These data confirm the high stability of **MC4^{PYA}**, that might be the reason of the low productivity of **8b** during E/MA cooligomerization. The absence of resonances of the 6-membered palladacycle (**MC6^{PYA}**) during all the monitoring time indicates that the chain walking process is very slow and it is in competition with the formation of methyl crotonate.

In the last decade there has been a considerable industrial interest in functionalized polyolefins containing amide moieties. Indeed, the hydrogen-bonding capability of the amide functionality can improve the surface properties of the composite materials.[8,9] Examples of direct, controlled, homogeneously catalyzed copolymerization of alkenes with polar vinyl monomers containing the amide functional group are rare. In particular, when Pd(II) catalysts with α-diimine ligands are used no reaction takes place, whereas when phosphino-sulfonate derivatives are the spectator ligands, ethylene/acrylamide copolymers are obtained.

N-isopropylacrylamide (NIPAM) and *N*,*N*-dimethylacrylamide (DMA) are the most investigated polar monomers of this class. In the E/DMA macromolecules obtained with Pd(II) precatalysts bearing a di-(2-methoxyphenyl)phosphino-benzenesulfonate ligand (**L4^{Pd}**), the amount of inserted DMA is about 3.5 mol % and it is present both in the main chain and in unsaturated chain ends, suggesting that the β-H elimination reaction occurs preferentially after the insertion reaction of the polar monomer (Figure 5.3).[8] Also neutral Ni(II) phoshino-phenolate complexes (**L7^{Ni}**) having a bulky axial substituent on the bidentate ligand, such as 2′,6′-dimethoxybiphenyl-2-yl-phenylphosphine, were tested in the copolymerization of ethylene with *N*,*N*-dimethylacrylamide.[10] The presence of a high steric hindrance around the metal center can facilitate the catalytic reaction increasing both the activity of the catalyst and the molecular weight of the obtained copolymers, disfavouring the β-H elimination and the formation of dinuclear species that might cause the complex deactivation. In these obtained macromolecules DMA is efficiently incorporated into the main chain (3.3 mol %) (Figure 5.3).

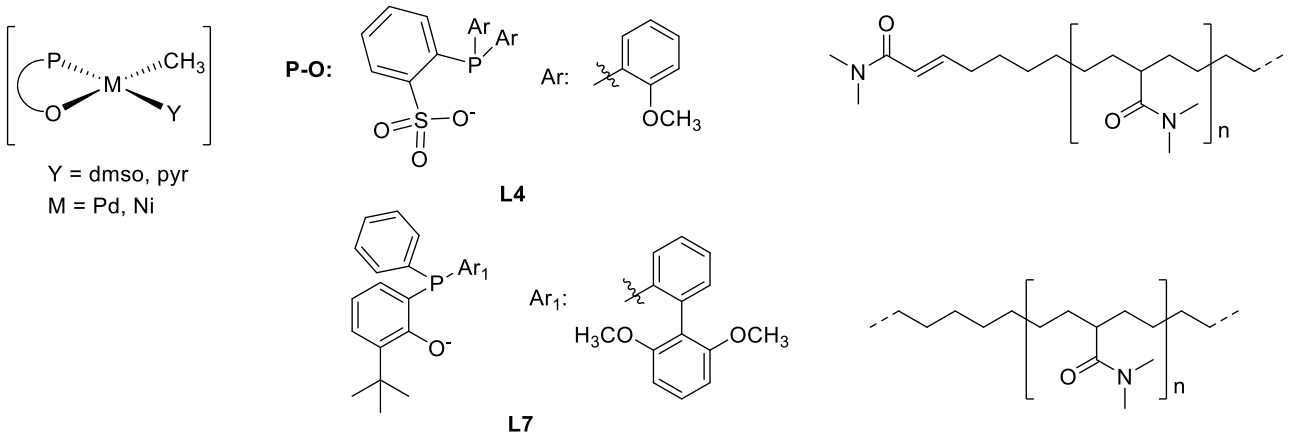

Figure 5.3. Pd(II) and Ni(II) catalysts active in the ethylene/*N*,*N*-dimethylacrylamide copolymerization and the produced copolymers.

The previous results about the stability of the detected **MC4^{PYA}** and the interest in polar monomers with the amide group prompted us to carry out a detailed *in situ* NMR investigation on the reaction of the neutral complex [Pd(CH_3)Cl(**8**)], **8a**, activated *in situ* with NaBArF (sodium tetrakis[3,5-bis(trifluoromethyl)phenyl]borate), and the cationic derivative [Pd(CH_3)($NCCH_3$)(**8**)][BArF], **8c**, with both methyl acrylate and *N*,*N*-dimethylacrylamide.

5.2. Results and discussion.

*5.2.1. Synthesis and characterization of [Pd(CH₃)(NCCH₃)(**8**)][BArF], **8c**.*

The synthesis of **8c** is performed starting from the neutral compound **8a**, synthesized in the laboratories of Prof. Albrecht's group, and following the dehalogenation reaction.[3,11] To a dichloromethane solution of the neutral complex, a solution of NaBArF in anhydrous acetonitrile is added under inert atmosphere, leading to the immediate precipitation of AgCl. The reaction is kept under magnetic stirring, at room temperature, for 1 h. **8c** is obtained in a good yield (78 %) as a white powder and it is characterized in solution by NMR spectroscopy. In the ^{1}H NMR spectrum the number of signals and their integration indicate the presence of both possible geometrical isomers (Figure 5.4). By comparing the chemical shifts of the Pd-CH_3 peaks of **8c** with those of **8b**, it is proposed that, also in this case, the main species is the *cis* isomer (95 %). The ^{19}F NMR spectrum shows a singlet at - 62.89 ppm assigned to the counterion.

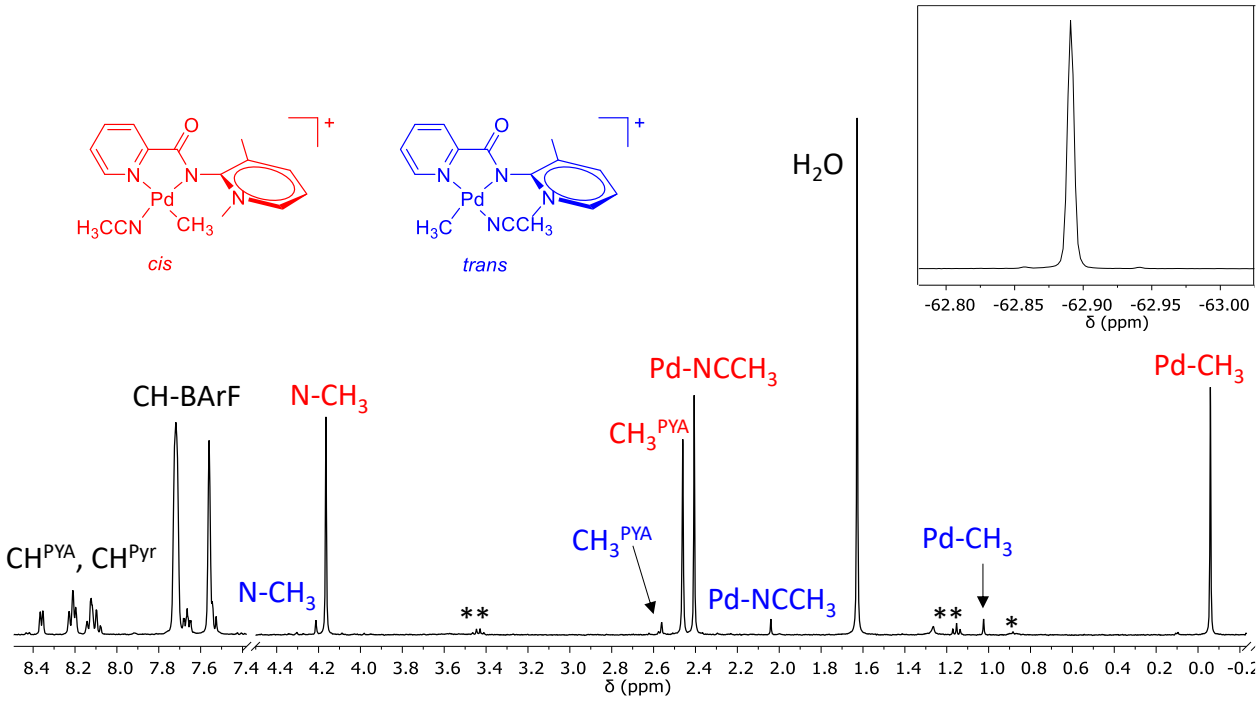

Figure 5.4. ^{1}H NMR spectrum (CD_2Cl_2, 298 K) of **8c**; inset: ^{19}F NMR spectrum; **n*-hexane; **diethyl ether.

*5.2.2. Reaction of **8a** and **8c** with methyl acrylate.*

The reaction of **8a** with methyl acrylate is studied at room temperature by adding to the 10 mM CD_2Cl_2 solution of the complex 2 eq. of the polar monomer simultaneously with 1 eq. of NaBArF (Scheme 5.1). As soon as the three species are mixed together the precipitation of NaCl is observed.

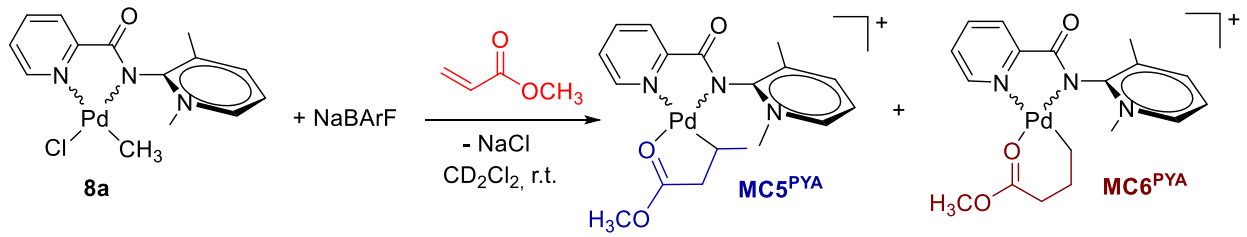

Scheme 5.1. *In situ* NMR reaction of **8a** with methyl acrylate.

In the ^{1}H NMR spectrum recorded immediately after the addition, no signals of **8a** are present, indicating that all the complex is converted into new species, and both isomers react (Figure 5.5). During the reaction in the NMR tube the solution remains yellow and no Pd(0) is formed. The proton-signal assignments are based on integration, signal multiplicity and bidimensional NMR experiments. Resonances of the metallacycles are present. **MC4^{PYA}** is observed only in traces in the spectra recorded after 1 and 5 min. Afterwards **MC4^{PYA}** disappears. The assignments of **MC4^{PYA}** are made in following experiments, reported below. **MC5^{PYA}** and **MC6^{PYA}** are also detected and they are present for all the monitoring time. In the ^{1}H,^{1}H DQCOSY spectrum recorded at 30 min (Figure S5.1), the two overlapped doublets (βCH_3) at 0.30 ppm show correlation peaks with the multiplets (αCH) at 0.98 ppm and 1.07 ppm, that correlate with four signals of CH_2 groups. All these resonances are assigned to **MC5^{PYA}** and the number of signals and their multiplicity suggest the presence of two different diasteroisomers rather than the two geometrical isomers, *cis* and *trans*. This is also confirmed by the similar chemical shift values for the carbon atom of βCH_3 in the ^{1}H,^{13}C HSQC spectrum (Figure S5.2) at 22.03 and 23.04 ppm. The multiplets at 0.75, 0.81 and 2.56 ppm relative to CH_2 groups are assigned to **MC6^{PYA}**, which should be present as one isomer. The methoxy group of this species is the singlet at 3.16 ppm. The ratio among the three intermediates goes from **MC4^{PYA}**:**MC5^{PYA}**:**MC6^{PYA}** = 18:15:67, immediately after the addition of NaBArF and MA, to 0:15:85, after 150 min. In the spectrum recorded at this time the typical resonances of methyl crotonate (**MC**) are also present.

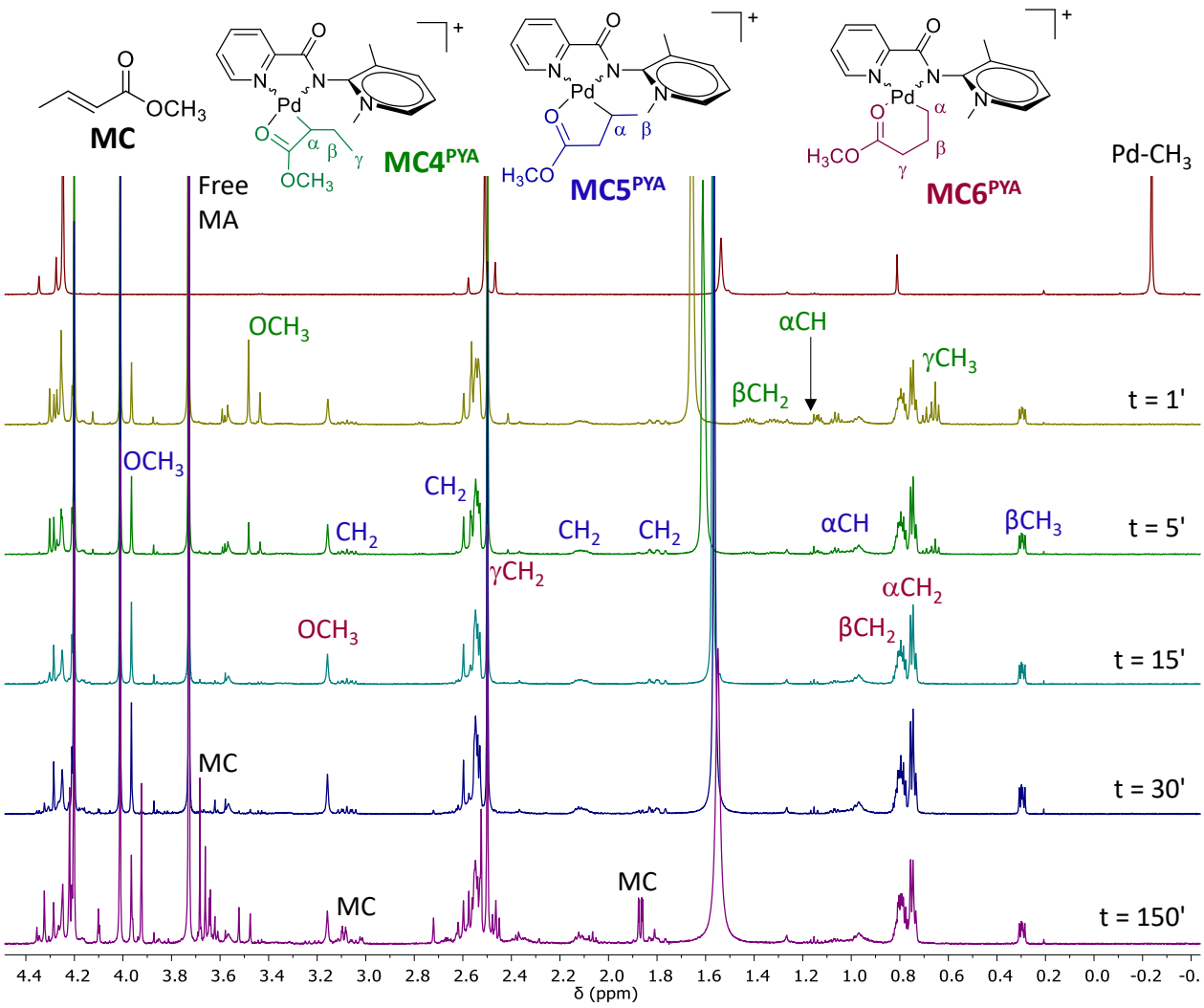

Figure 5.5. ^{1}H NMR spectra (CD_2Cl_2, 298 K) of **8a** (top spectrum) and **8a** after the addition of NaBArF and MA at different reaction times.

The reaction of **8c** with MA is studied upon addition of 2 eq. of the polar monomer to the 10 mM CD_2Cl_2 solution of the complex, at room temperature (Scheme 5.2).

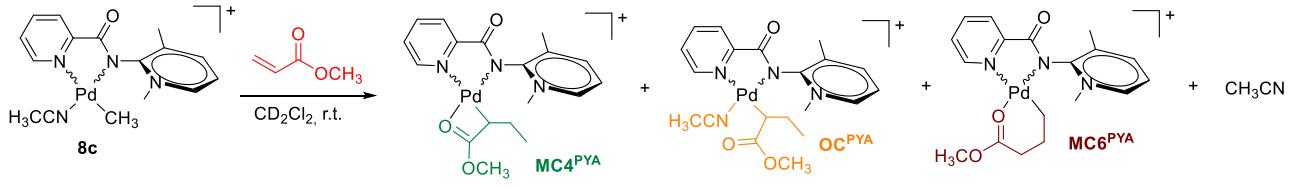

Scheme 5.2. *In situ* NMR reaction of **8c** with methyl acrylate.

In this case in the ^{1}H NMR spectrum, the disappearance of the Pd-CH_3 signals of **8c** takes place after 30 min from the addition of the polar monomer (Figure 5.6).

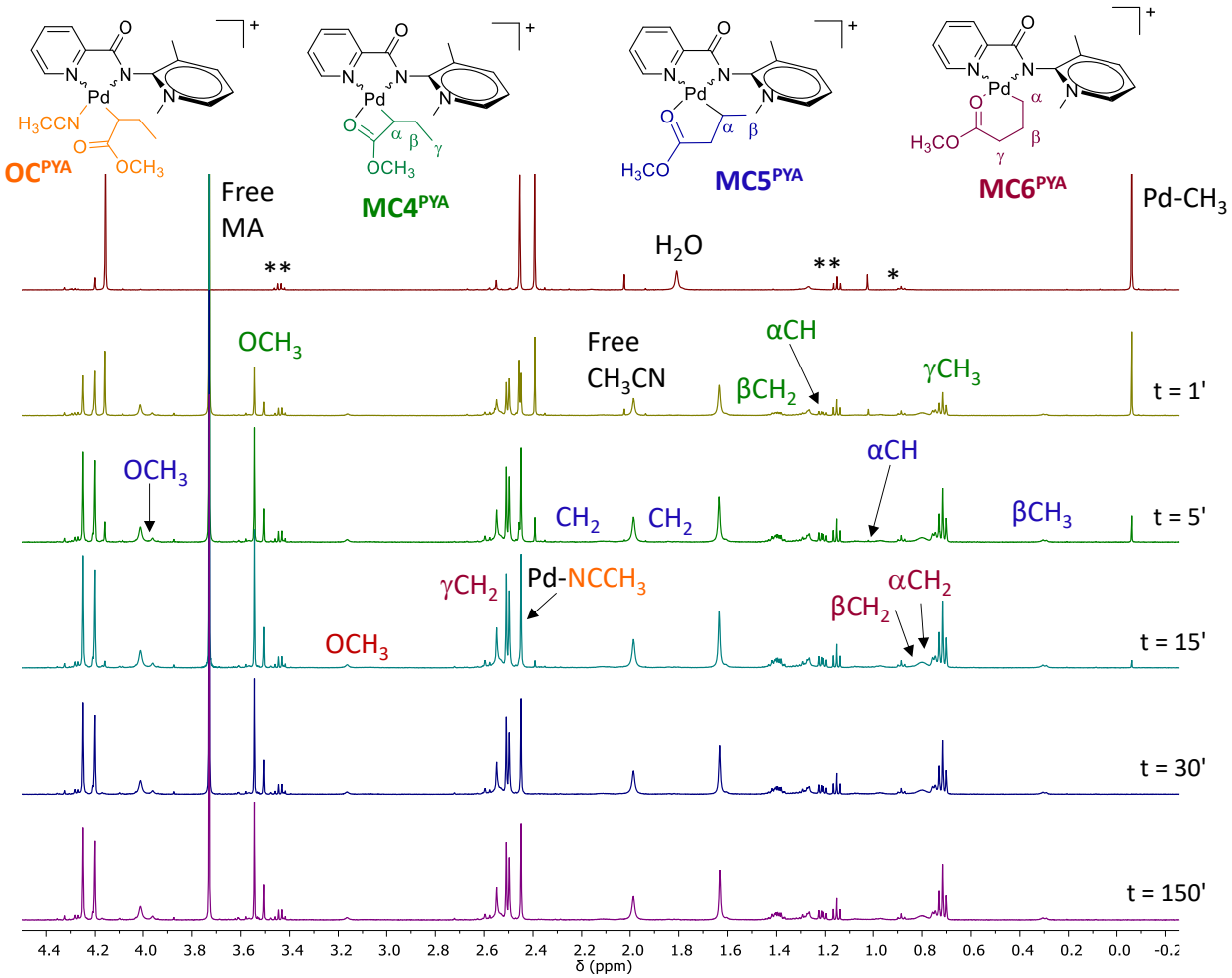

Figure 5.6. ^{1}H NMR spectra (CD_2Cl_2, 298 K) of **8c** (top spectrum) and **8c** after the addition of MA at different reaction times; **n*-hexane; ***diethyl ether.

In the ^{1}H NMR spectrum recorded immediately after the addition of the polar monomer, the peak of free CH_3CN is present at 1.99 ppm confirming that it dissociates from the metal center. Following over time, a new signal is observed at 2.45 ppm, unambiguously assigned from the chemical shift of its carbon atom at 4.20 ppm to coordinated acetonitrile (Figure S5.3). In the ^{1}H,^{1}H NOESY spectrum (Figure S5.4) an exchange peak between it and the singlet of free acetonitrile, suggests that an open-chain species **OC^{PYA}** having both the organic fragment, generated by the insertion of MA into the Pd-CH_3 bond, and CH_3CN coordinated to Pd ion, might be present in solution and that this species is in equilibrium with **MC4^{PYA}** with a slow rate on the NMR timescale at room temperature.

The NMR analysis indicates that the main intermediate present in solution is **MC4^{PYA}**, while the intensity of signals of **MC5^{PYA}** and **MC6^{PYA}** is very weak and, after 150 min, the ratio among **MC4^{PYA}**:**MC5^{PYA}**:**MC6^{PYA}** is 69:8:23 (Figure 5.7).

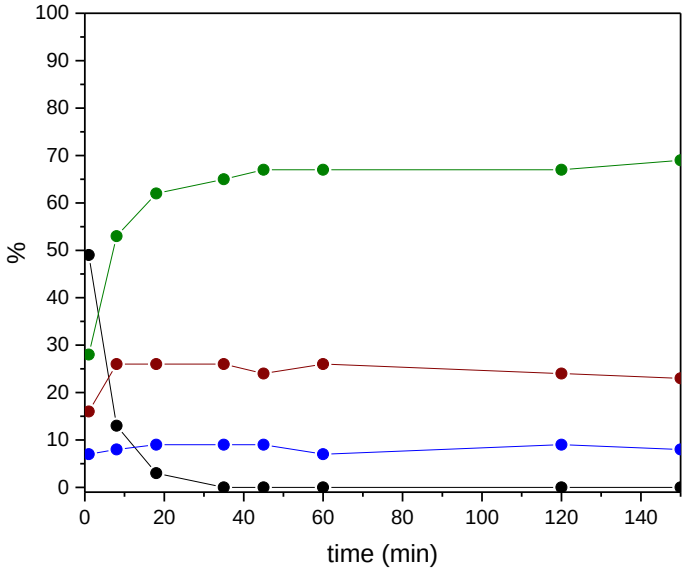

Figure 5.7. The evolution over time of the percentage amount of **8c** (black circles), **MC4^{PYA}** (green circles), **MC5^{PYA}** (blue circles) and **MC6^{PYA}** (red circles).

By comparing the reaction with MA of the cationic complexes **8b**[7] and **8c**, that differ only for the anion (PF_6^- and $BArF^-$, respectively), it is evident that the conversion of the precursor into the active species occurs with different rate, and that the ratio between the metallacycles is different. As for **8b**, it disappears after 10 min from the addition of MA and **MC4^{PYA}** is the only species present in solution, while when **8c** is the precursor, it reacts completely after 30 min and, in addition to **MC4^{PYA}** and the **OC^{PYA}**, traces of **MC5^{PYA}** and **MC6^{PYA}** are observed, too. This suggests that by just changing the anion, the coordination/insertion reaction of the polar monomer becomes slower and this might be due to the fact that for the $BArF^-$ derivative the acetonitrile remains closer to the palladium coordination sphere, whereas when PF_6^- is the counterion the acetonitrile is far away from palladium. This might be related to the steric hindrance of the counterion: the bulky $BArF^-$ is more tight ion pairing rather than PF_6^-, thus leaving enough space for the acetonitrile to coordinate.

While considering the same reaction using the two complexes **8a** and **8c**, it points out that on the neutral compound **8a**, the coordination of MA, the migratory insertion reaction and the chain walking process are faster than on the cationic complex **8c**, thus suggesting that for **8c** the acetonitrile competes for one coordination site of palladium and it slows down the reactions (Figure 5.8).

In both cases Pd(0) is not observed during the monitoring time indicating the high stability of these palladacycles.

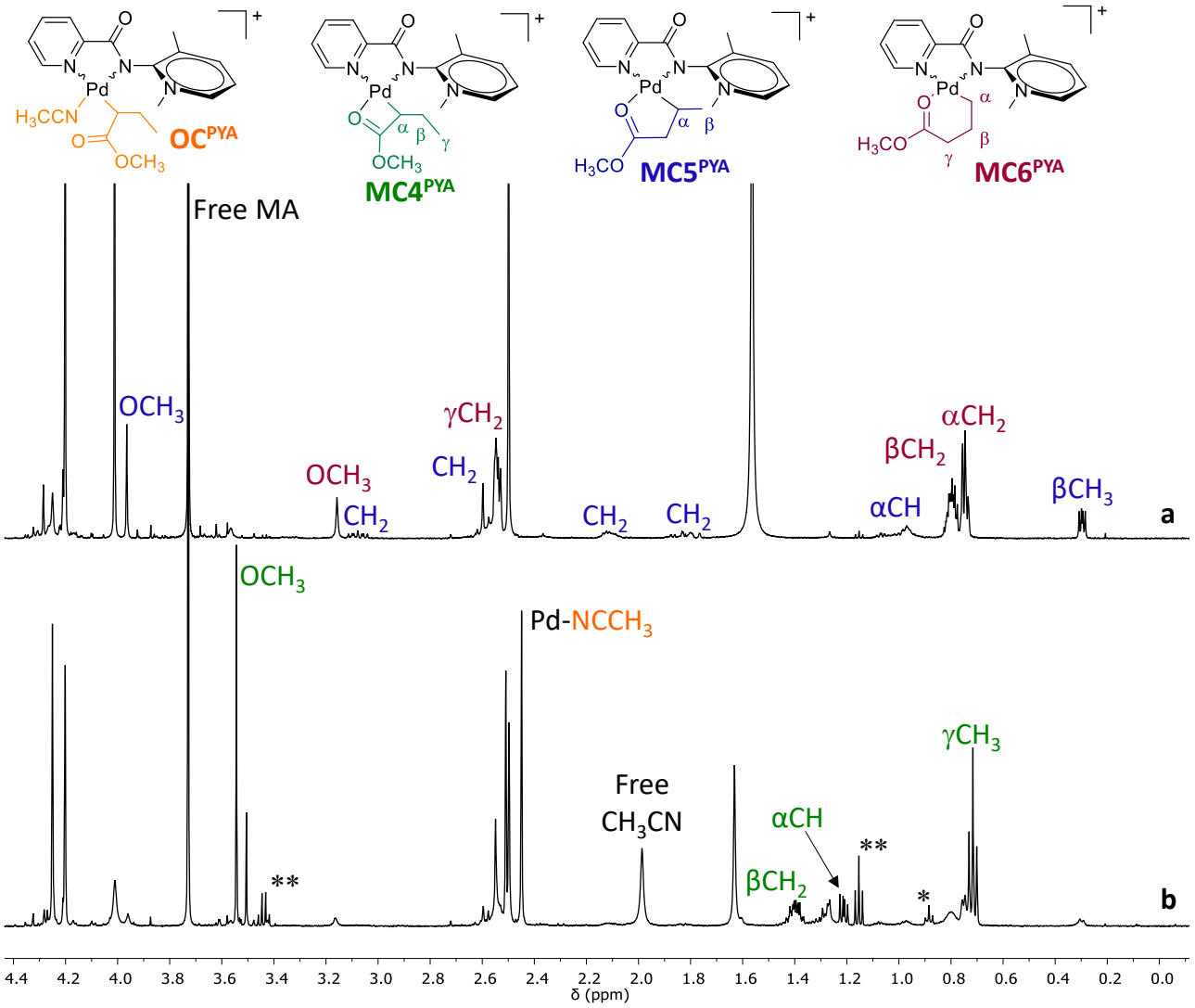

Figure 5.8. ^{1}H NMR spectra (CD_2Cl_2, 298 K) of the reaction mixture at t = 30 min of (a) **8a** with NaBArF and MA and (b) **8c** and MA; **n*-hexane; ***diethyl ether.

To have some additional information about the role played by the acetonitrile other experiments are performed using **8a**. When to the 10 mM solution of the neutral complex in CD_2Cl_2, 1 eq. of NaBArF, 2 eq. of MA and 1 eq. of acetonitrile are added at the same time, no resonances of **8a** are present in the spectrum recorded after 1 min and the new observed signals are due to both geometrical isomers of **8c** (e.g. the singlet of Pd-CH_3 at -0.06 ppm and at 1.02 ppm of *cis*-**8c** and *trans*-**8c**, respectively), **MC4^{PYA}** and traces of **MC5^{PYA}** and **MC6^{PYA}** together with the singlet at 1.99 ppm of free acetonitrile (Figure 5.9). No variations in the signal intensity of **MC5^{PYA}** and **MC6^{PYA}** is observed within 150 min.

The proton-signal assignments for **MC4^{PYA}** is done thanks to bidimensional NMR analysis: considering the triplet at 0.72 ppm (γCH_3), it shows a correlation peak with the signal at 1.40 ppm, that on its turn correlates with the peak at 1.20 ppm, assigned to βCH_2 and αCH respectively from the $^{1}H,^{13}C$ HSQC spectrum (Figures S5.5 and S5.6).

The $^{1}H,^{1}H$ NOESY experiment allows to recognize the **MC4^{PYA}** to be the *cis* isomer on the basis of the peak due to the nuclear Overhauser effect between γCH_3 and the singlet at 2.51 ppm relative to N-CH_3 group of PYA ring (Figure S5.4). Also in this case the signal of Pd-$NCCH_3$ is observed at 2.45 ppm suggesting the presence in solution of the open-chain species.

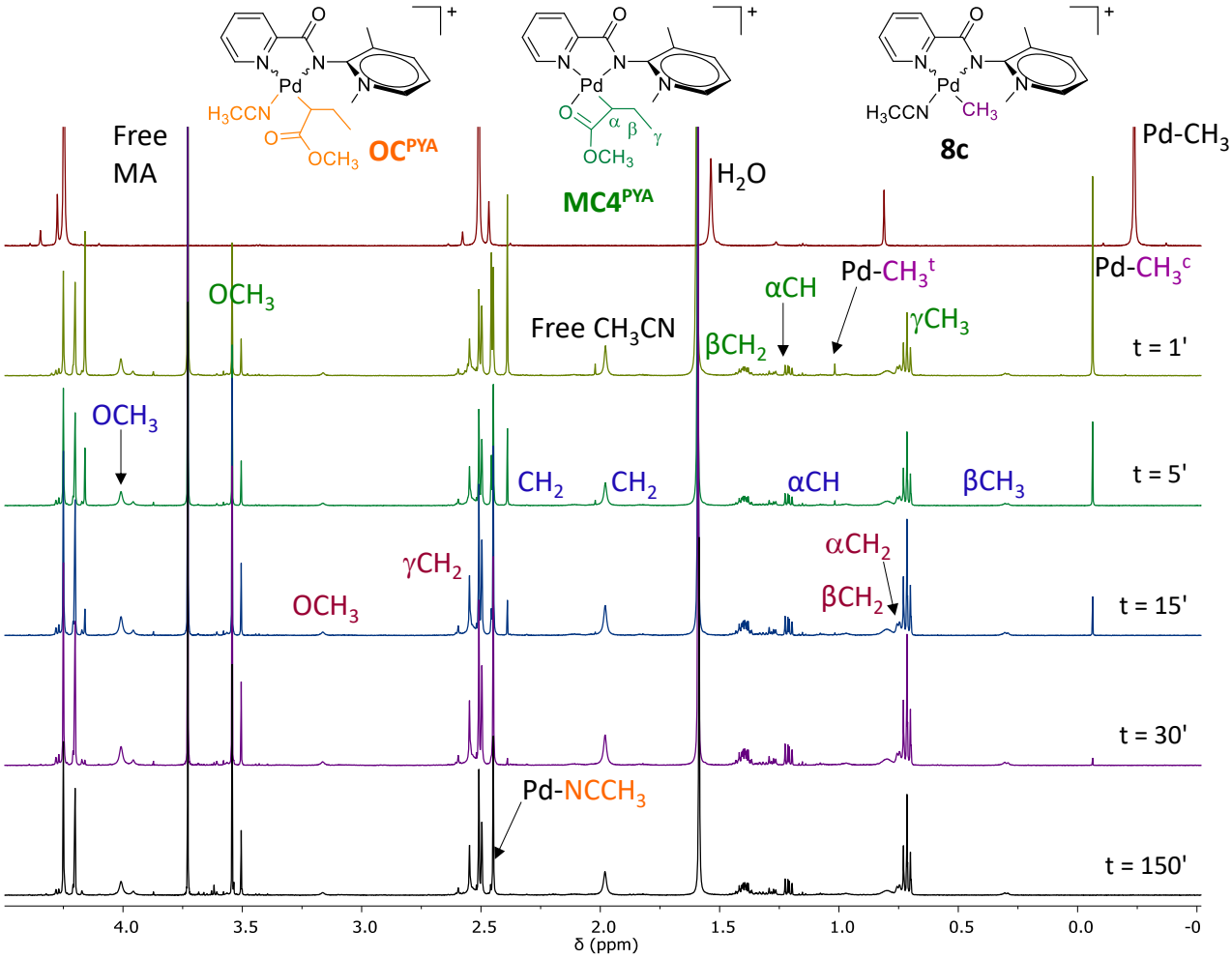

Figure 5.9. ^{1}H NMR spectra (CD_2Cl_2, 298 K) of **8a** (top spectrum) and **8a** after the addition of NaBArF, MA and CH_3CN (1 eq.) at different reaction times.

When the same experiment is performed upon addition of 2 eq. of acetonitrile, the immediate formation of **8c** is observed together with **MC4^{PYA}**, no traces of **MC5^{PYA}** and **MC6^{PYA}** are present (Figure 5.10). **MC4^{PYA}** and **OC^{PYA}** remain the only species present in solution at 150 min.

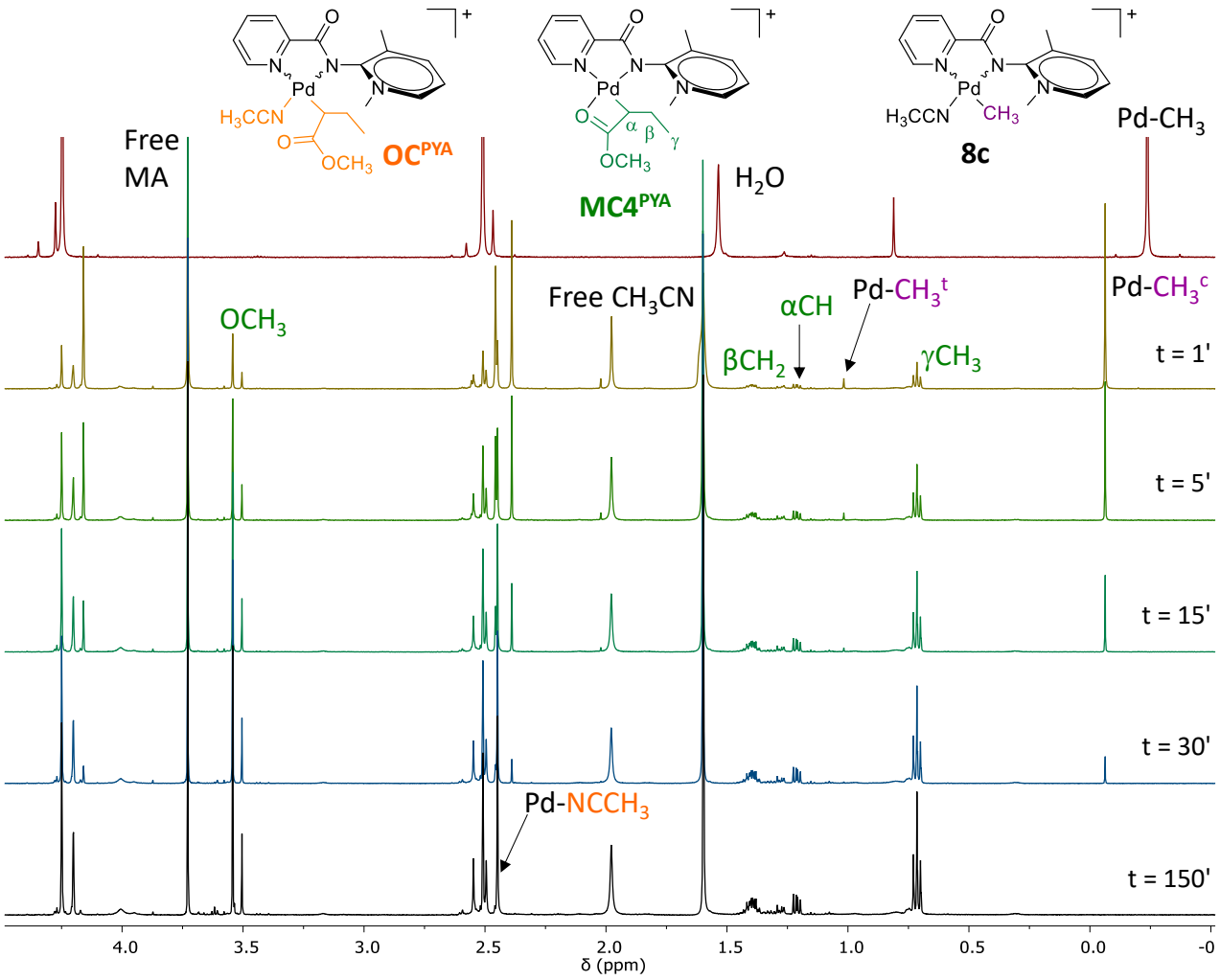

Figure 5.10. ^{1}H NMR spectra (CD_2Cl_2, 298 K) of **8a** (top spectrum) and **8a** after the addition of NaBArF, MA and CH_3CN (2 eq.) at different reaction times.

These experiments confirm the competing effect of acetonitrile with respect to MA. When acetonitrile is added to the solution of **8a** together with MA and NaBArF, the formation of **8c** and **MC4^{PYA}** is observed (Scheme 5.3). Then **8c** is consumed and metallacycles species are present in the reaction mixture. **8c** reacts with a different rate depending if it is the starting compound (t = 30 min), or it is produced starting from **8a** plus 1 eq. of CH_3CN (t = 45 min) or from **8a** plus 2 eq. of CH_3CN (t = 60 min). Since free acetonitrile is present in solution, **MC4^{PYA}** might be opened and the **OC^{PYA}** intermediate is formed.

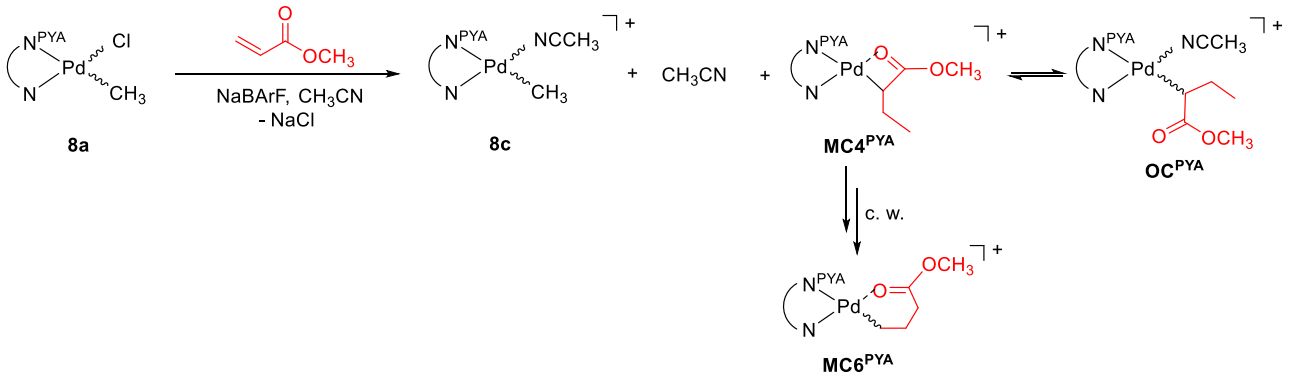

Scheme 5.3. Reaction of **8a** with NaBArF and methyl acrylate in presence of acetonitrile.

Considering the investigated reactions, it is possible to state that: when the reaction with MA is catalyzed by neutral compound, **MC5^{PYA}** and **MC6^{PYA}** are present in solution, with the predominantly formation of the latter species (85 %) indicating that the chain walking process takes place. While in all the reactions where acetonitrile is present either in the starting compound **8c** or in addition to **8a**, **MC4^{PYA}** is the major species formed. It is 62 % starting from **8c**, 71 % considering the reaction with the addition of 1 eq. of acetonitrile to **8a** solution and it reaches the value of 92 % when 2 eq. of CH_3CN are added to the neutral compound solution (Figure 5.11). For all the monitoring time no **MC** is detected when **8c** is the precursor of the reaction, thus confirming that traces of **MC5^{PYA}** evolve to **MC6^{PYA}** and **MC** is not formed. Finally traces of Pd(0) are present in the NMR tube only after 4 days at room temperature, confirming the high stability of **MC4^{PYA}** for Pd-PYA complexes.[7]

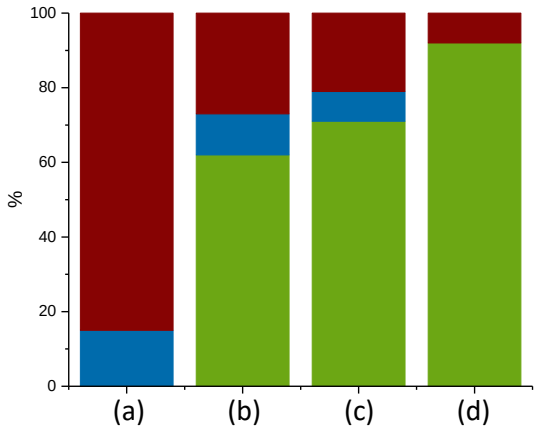

Figure 5.11. Percentages of detected intermediates in the *in situ* NMR reaction with methyl acrylate calculated after 2 h from the addition of the polar monomer of: (a) **8a** with NaBArF, (b) **8c**, (c) **8a** with NaBArF and CH_3CN (1 eq.) and (d) **8a** with NaBArF and CH_3CN (2 eq.); **MC4^{PYA}** (green bars), **MC5^{PYA}** (blue bars) and **MC6^{PYA}** (red bars).

*5.2.3. Reaction of **8a** and **8c** with N,N-dimethylacrylamide.*

The neutral complex **8a** is also tested in the reaction with *N,N*-dimethylacrylamide upon addition of 2 eq. of the polar monomer simultaneously with 1 eq. of NaBArF to the 10 mM CD_2Cl_2 solution of the complex at room temperature (Scheme 5.4).

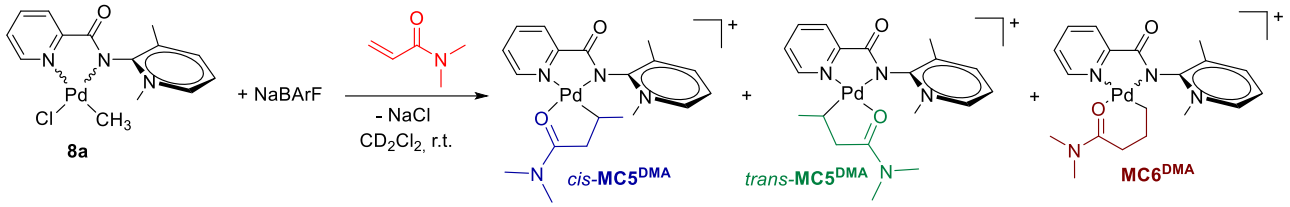

Scheme 5.4. *In situ* NMR reaction of **8a** with *N,N*-dimethylacrylamide.

The reaction is followed for 5 h (Figure 5.12). In the ^{1}H NMR spectrum recorded immediately after the addition of NaBArF and the polar monomer, all the signals are broad. In the ^{1}H NMR spectrum recorded after 15 min no signal of **8a** is observed, whereas new sharp resonances are present, indicating that all complex is converted into new species and both isomers react.

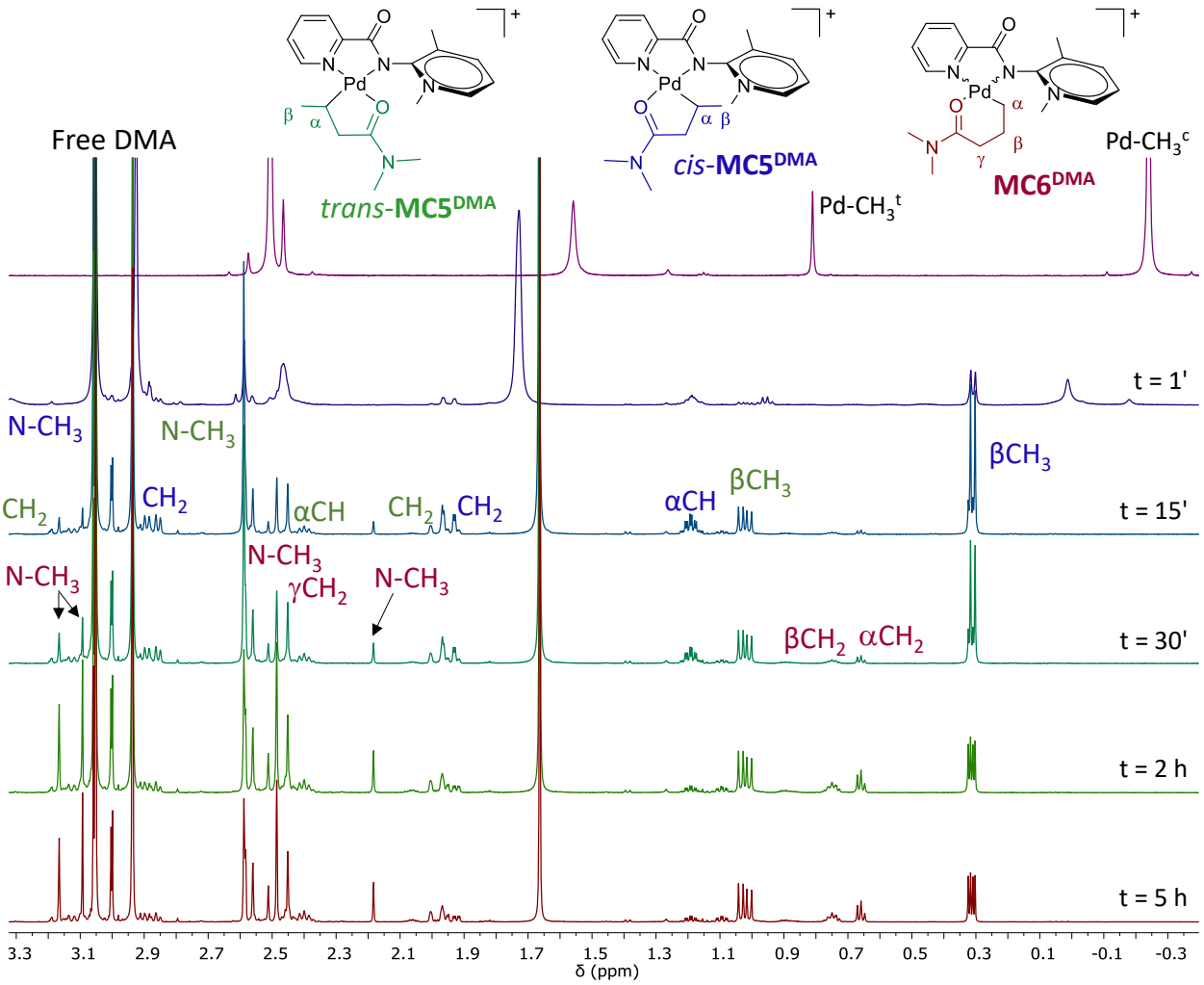

Figure 5.12. ^{1}H NMR spectra (CD_2Cl_2, 298 K) of **8a** (top spectrum) and **8a** after the addition of NaBArF and DMA at different reaction times.

To identify the species present in solution, after half an hour a detailed NMR analysis is performed that allows to recognize the two main species as the two isomers of the five-membered metallacycle **MC5^{DMA}** originated by the insertion of DMA into the Pd-CH_3 bond with secondary regiochemistry followed by the chain walking process (Scheme 5.5).

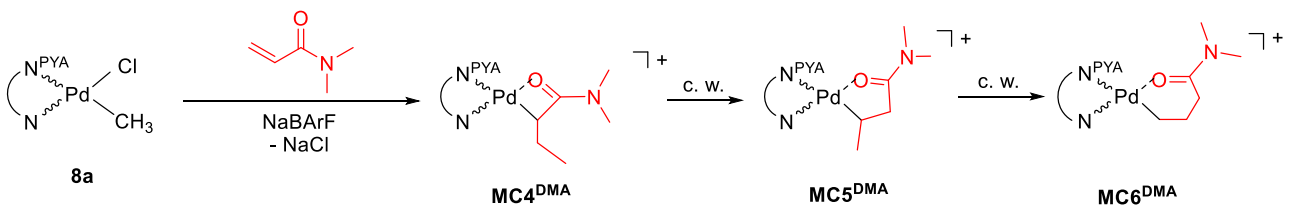

Scheme 5.5. Chain walking process after the insertion of *N*,*N*-dimethylacrylamide into the Pd-CH_3 bond.

In particular, on the basis of the 1D NOE spectrum recorded upon irradiation of the two overlapped doublets at 0.32 ppm an Overhauser effect with the singlet of N-CH_3 of PYA ring at 4.21 ppm is evident, indicating that this is the *cis* isomer, *cis*-**MC5^{DMA}** (Figure S5.7). Focusing the attention on the resonances of this metallacycle, in the $^1H,^1H$ COSY spectrum (Figure S5.8) the signal of βCH_3 has a correlation peak with the multiplet at 1.19 ppm assigned to αCH. The latter shows two extradiagonal peaks with the resonances at 1.95 and 2.88 ppm due to the CH_2 group. The $^1H,^{13}C$ HSQC spectrum (Figure 5.13) confirms the assignment and the diastereotopic nature of the two protons of the CH_2 group. The multiplicity of the signal at 0.32 ppm indicates that two diastereoisomers are present, because the square planar plane of the complex is not a plane of symmetry.

The signal at 1.02 ppm is assigned to the βCH_3 group of the *trans* isomer. Also for this intermediate, the multiplicity of this signal indicates that two diasteroisomers are present and this and other signals are assigned in a similar way to *trans*-**MC5^{DMA}**. Starting from the peak of βCH_3 at 1.02 ppm, it is possible to assign the signal at 2.40 ppm to αCH and the resonances at 1.99 and 3.14 ppm to the CH_2 group on the basis of $^1H,^{13}C$ HSQC and $^1H,^1H$ COSY spectra, respectively. In agreement with the above signal to proton assignments, the βCH_3 group of *cis*-**MC5^{DMA}** resonates at lower frequency than the same group in *trans*-**MC5^{DMA}** due to the fact that it falls in the shielding cone of the PYA ring *cis* to it. In the spectrum recorded after 15 min from the addition the ratio between *cis*-**MC5^{DMA}** and *trans*-**MC5^{DMA}** is 75:25 and the two isomers show a different behaviour in terms of diasteroisomer distribution. At the beginning for *cis*-**MC5^{DMA}** one species is preferentially formed, while for *trans*-**MC5^{DMA}** both diastereoisomers are present in equal amount. After 2 h the intensity of the peaks of the two diasteroisomers is comparable for both geometrical isomers. **MC5^{DMA}** slowly evolves to **MC6^{DMA}**, whose most diagnostic signals, those of CH_2 groups, are detected on the basis of the $^1H,^{13}C$ HSQC experiment: in particular αCH_2 is at 0.66 ppm, while βCH_2 and γCH_2 are at 0.75 and 2.45 ppm, respectively.

After 2 h the ratio between the intermediates is *cis*-**MC5^{DMA}**: *trans*-**MC5^{DMA}**:**MC6^{DMA}** = 43:36:21. No difference in the relative intensity of the signals is observed after 5 h, indicating that the equilibrium is reached in 2 h. The solution in the NMR tube remains yellow for 1 week at room temperature and during this time no Pd(0) is formed.

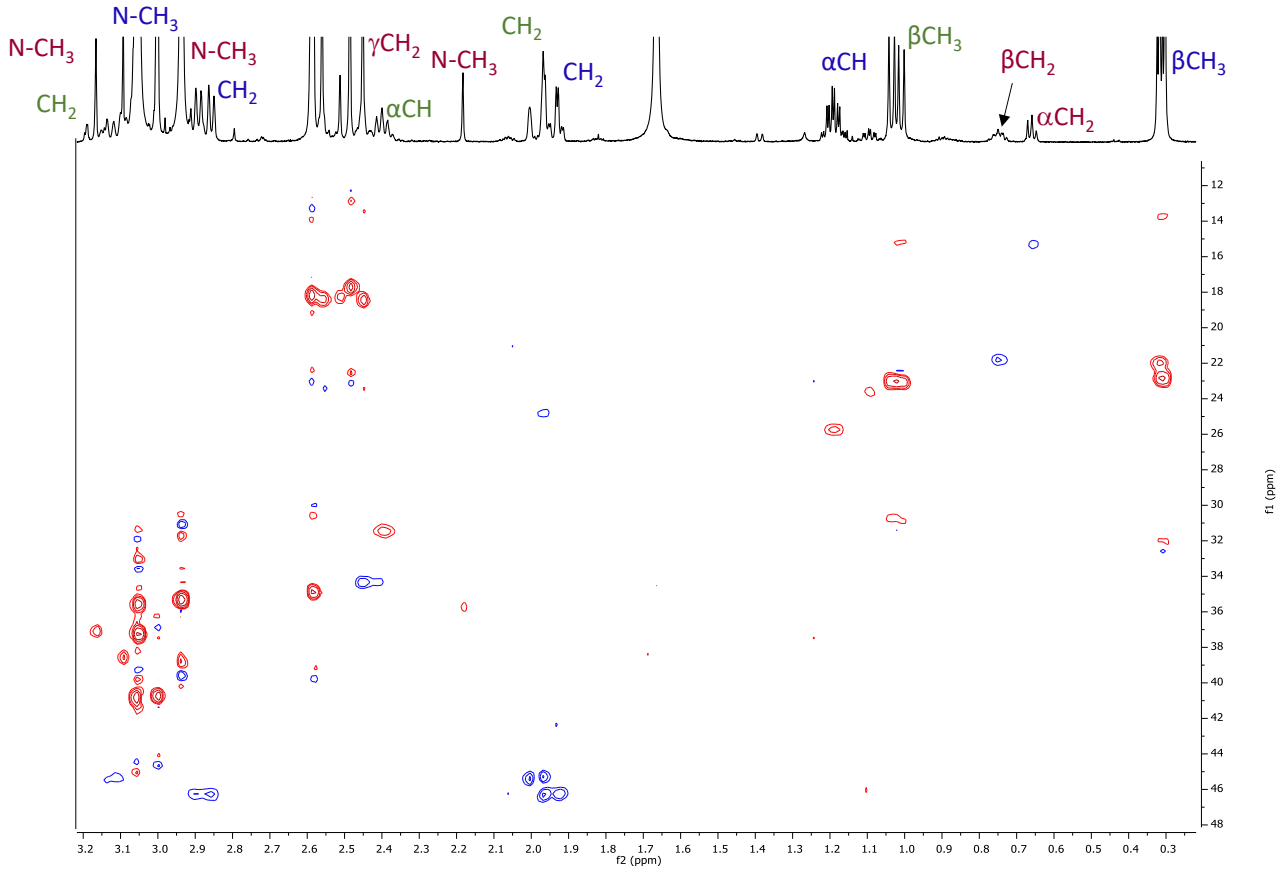

Figure 5.13. $^{1}H,^{13}C$ HSQC spectrum (CD_2Cl_2, 298 K) of the mixture of **8a** with NaBArF and DMA at t = 30 min.

The N-CH_3 groups of the inserted DMA for each metallacycle are assigned thanks to the correlation peaks in the $^{1}H,^{13}C$ HMBC spectrum with the signals of the CH_2 groups close to the carbonyl moiety (Figure 5.14). The carbon atom of the C=O group resonates at similar values in all metallacycles, **MC5^{DMA}** (185.3 ppm for *cis* and 186.3 ppm for *trans*) and **MC6^{DMA}** (176.6 ppm). For the latter the presence of four signals for the N-CH_3 groups of inserted DMA indicates that even for **MC6^{PYA}** both geometrical isomers are present.

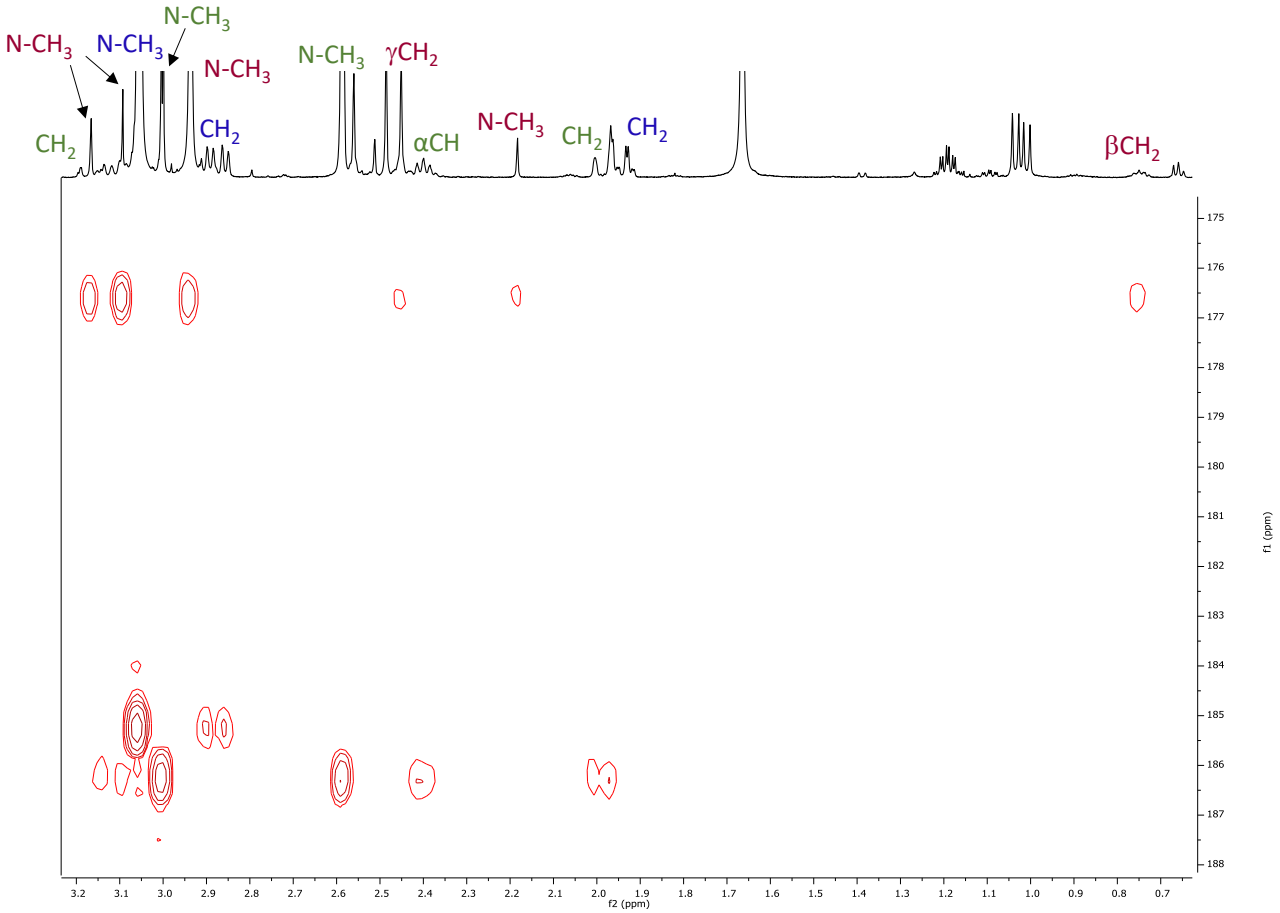

Figure 5.14. $^{1}H,^{13}C$ HMBC spectrum (CD_2Cl_2, 298 K) of the mixture of **8a** with NaBArF and DMA at t = 30 min; carbonyl region.

In literature an example of open-chain *N*-isopropylacrylamide (NIPAM)-inserted intermediate solid state structure is reported.[8] Crystals are obtained by layering pentane to a methanolic solution of [Pd(CH_3)(dmso)(**L4**)], **L4^{Pd}** (Figure 5.3) at room temperature. The metal center shows a distorted square planar coordination geometry with both methanol-d_4 coordinated *trans* to the phosphorus atom and the organic fragment, generated by the 2,1-insertion of NIPAM into the Pd-CH_3 bond, bonded to it. No solid state structures are solved of DMA-inserted intermediates, till now.

From the *in situ* NMR reaction of **8a** with NaBArF and DMA, yellow crystals, suitable for X-ray diffraction analysis, are obtained upon slow diffusion of *n*-hexane into the CD_2Cl_2 solution kept at 277 K for two weeks. The structure in solid state is that of the *trans*-**MC5^{DMA}** with $BArF^-$ as counterion and this is the first solved solid state structure of chelate DMA-inserted palladacycle on a Pd(II) complex (Figure 5.15 and Table S5.1).

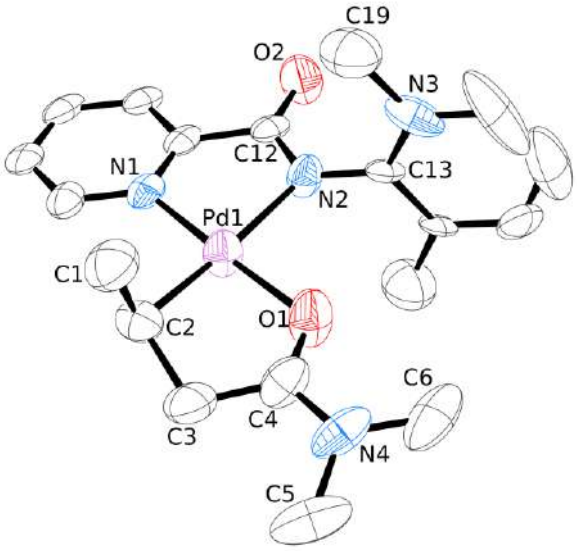

Figure 5.15. ORTEP drawing (50% probability ellipsoids) of *trans*-**MC5^{DMA}**. Hydrogen atoms and the $BArF^{-}$ anion have been omitted for the sake of clarity.

The typical square planar coordination geometry is shown for the palladium ion with both the N-N' chelating PYA ligand and the organic fragment, originated by the insertion of DMA into the Pd-CH_3 bond followed by the chain walking process, bonded to it, the latter through the oxygen atom. The bond lengths and angles around the metal center are within expectation for Pd(II) complexes containing a N-N' bidentate ligand.[4] The Pd1-N2 bond in *cis* to Pd1-O1 bond is remarkably longer (2.121(8) Å) than the Pd1-N1 bond length (2.027(7) Å), in agreement with the expected higher *trans* influence of the Pd-alkyl bond with respect to that of the Pd-O bond. The steric hindrance produced by the presence of both the N^{PYA}-CH_3 groups and carbonyl group of the ligand itself influences the orientation of the PYA ring, that is twisted almost orthogonally with respect to the palladium coordination plane with a dihedral angle [N^{PYA}] --- [Pd1] of 86.1(3)°. The exocyclic C-N bond is remarkably shorter than the classical C-N single bond (C13-N2 = 1.353(1) Å *vs* C-N = 1.475(6) Å). These two considerations suggest that the PYA ligand is in an intermediate situation between the zwitterionic and neutral form (Figure 5.16).[6]

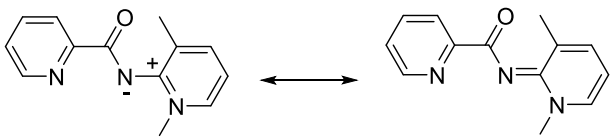

Figure 5.16. Resonance structures of PYA ligand: neutral (left) and zwitterionic form (right).

Considering the organic fragment of the DMA-inserted metallacycle, the crystal analysis confirms that it is coordinated through the oxygen atom and it is in the Pd(II) plane forming with the latter a dihedral angle [N^{DMA}] --- [Pd1] of 8.9(5)°.

The bond length of the carbonyl group is longer than both that present in the ligand (C4-O1 = 1.259(1) Å *vs* C12-O2 = 1.200(1) Å) and that of free DMA about 1.238(1) Å (Deposition Numbers CCDC 1418571), while the C-N is shorter (C4-N4 = 1.305(1) Å *vs* C12-N2 = 1.335(1) Å), suggesting a delocalization of charge between the C=O double bond and the single one C-N. Indeed, the nitrogen atom of DMA shows an sp^2 hybridization with C-N-C angles about 120°. The C1-C2-Pd angle of 105.4(7)° is in agreement with the sp^3 hybridization of these carbon atoms.

Since it is known that the Pd(II) metallacycle derivatives with P-O ancillary ligand originated by the mixture of the 2,1- and 1,2-insertion of DMA into the Pd-CH_3 bond are activated by the coordination/insertion of ethylene under mild reaction conditions in terms of ethylene pressure (from 2.5 to 7.5 bar)[8] and thanks to the high stability of the metallacycles obtained from the reaction of **8a** with NaBArF and DMA, the CD_2Cl_2 solution of **MC5^{DMA}** and **MC6^{DMA}** mixture is saturated with ethylene at room temperature. No reaction is observed within 1 h and the color of the solution remains pale yellow. In the ^{1}H NMR spectrum recorded after this time the peak of free ethylene (singlet at 5.40 ppm) is still present together with the resonances of **MC5^{DMA}** and **MC6^{DMA}** (Figure 5.17c).

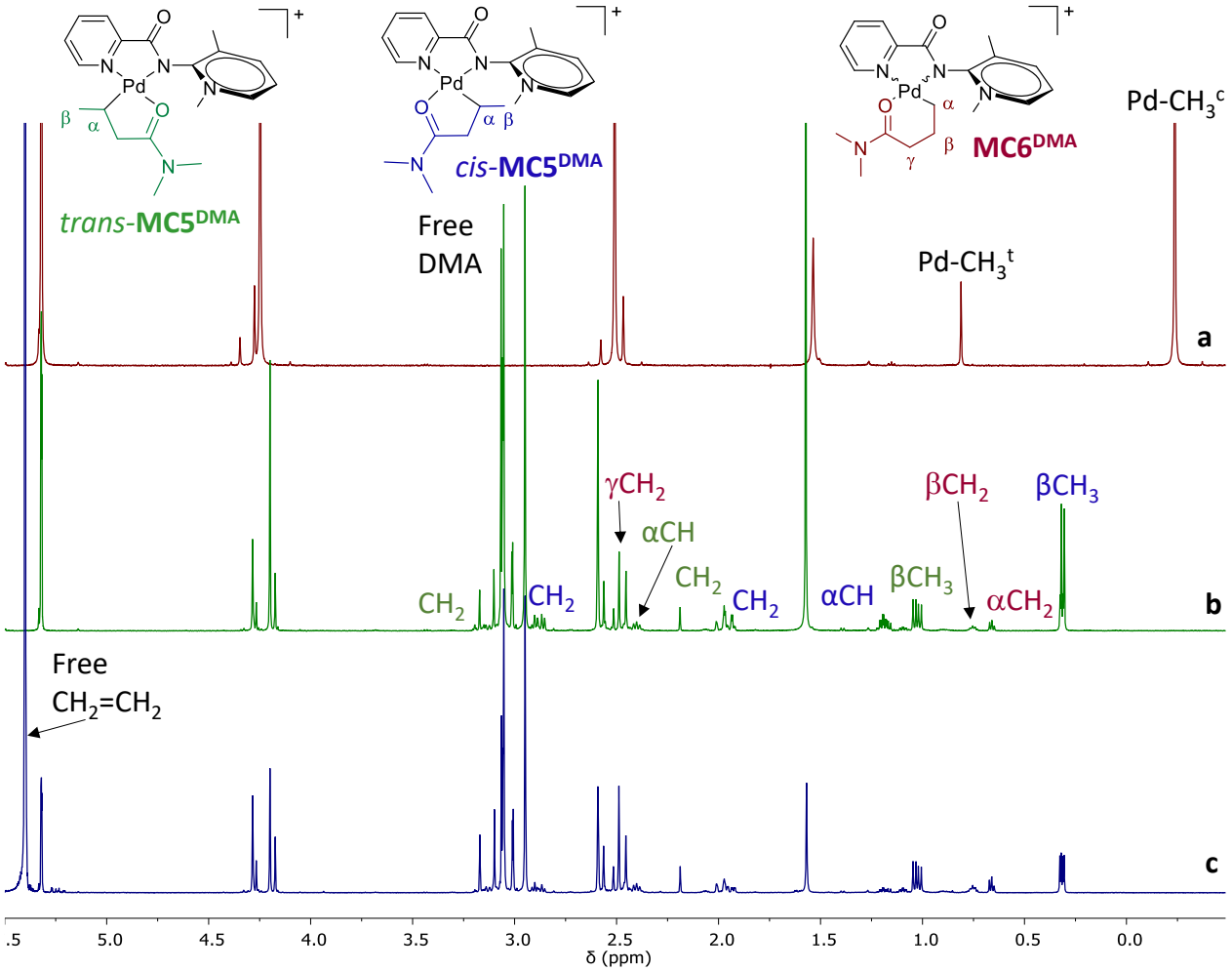

Figure 5.17. ^{1}H NMR spectra (CD_2Cl_2, 298 K) of (a) **8a**, (b) **8a** with NaBArF and DMA at t = 2 h and (c) **8a** with NaBArF, DMA and ethylene at t = 1 h.

Several research groups focused on the study of the insertion reaction of the carbon monoxide in Pd-alkyl bond used Pd(II) complexes containing N-N bidentate ligands because it is considered a key step in the synthesis of alternating polyketones, that are produced by the Pd(II)-catalyzed carbon monoxide/olefins copolymerization.[12,13] These considerations and the high affinity of CO for the palladium ion prompted us to investigate the reaction of the **MC5^{DMA}** and **MC6^{DMA}** mixture with CO. Immediately after carbon monoxide is bubbled into the reaction mixture, the latter changes its color from yellow to pink and no Pd(0) is observed. In the ^{1}H NMR spectrum recorded after 5 min, the signals of traces of **MC5^{DMA}** and **MC6^{DMA}** are observed together with new resonances in both the aliphatic and aromatic region (Figure 5.18). The metallacycle intermediates are totally converted after 30 min from the addition of CO.

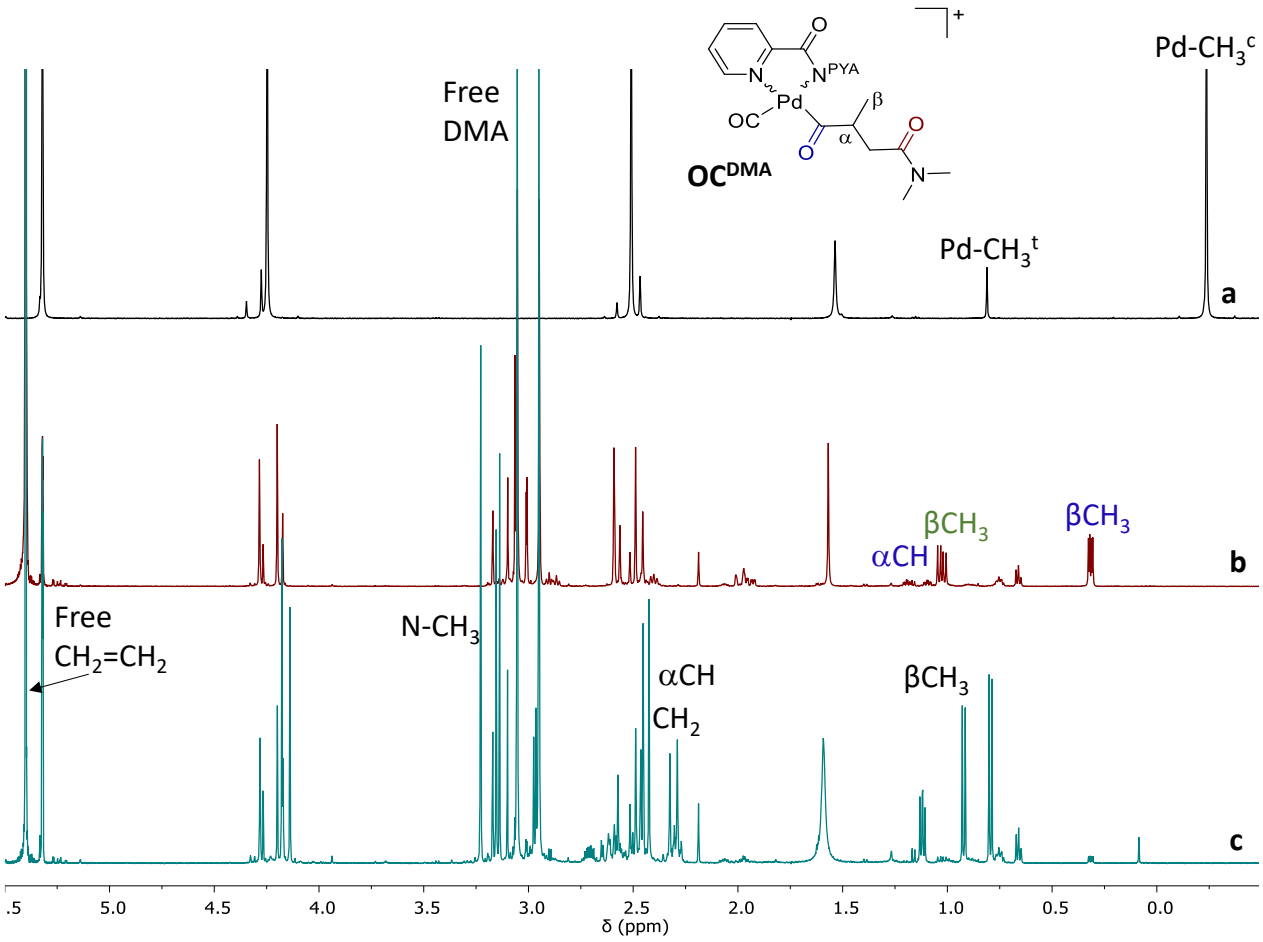

Figure 5.18. ^{1}H NMR spectra (CD_2Cl_2, 298 K) of (a) **8a**, (b) **8a** with NaBArF, DMA and ethylene at t = 1h and (c) **8a** with NaBArF, DMA, ethylene and CO at t = 5 min.

The newly formed species are characterized by NMR spectroscopy (Figure 5.19 and Figures S5.9 and S5.10). In the $^{1}H,^{13}C$ HMBC spectrum (Figure 5.20) the signal of a ketonic group originated by the insertion of CO into the Pd-alkyl bond[12] at 219.9 ppm shows correlation peaks with the two new doublets at 0.79 and 0.92 ppm, assigned to the methyl groups βCH_3, and with signals in the range of 2.29 – 2.66 ppm, assigned to CH_2 groups. In addition these peaks show other correlation peaks with the signals of the carbonyl group of inserted DMA at 175.2 ppm, that also correlates to N-CH_3 moieties of the polar monomer. These sets of signals are assigned to one of the possible geometrical isomer of the open-chain intermediate, $[Pd(\mathbf{9})(CO)(C(O)CH(CH_3)CH_2C(O)N(CH_3)_2]^+$, **OC^{DMA}**, resulting from the insertion of carbon monoxide into the Pd-alkyl bond of **MC5^{DMA}** with the fourth coordination site being completed by CO.

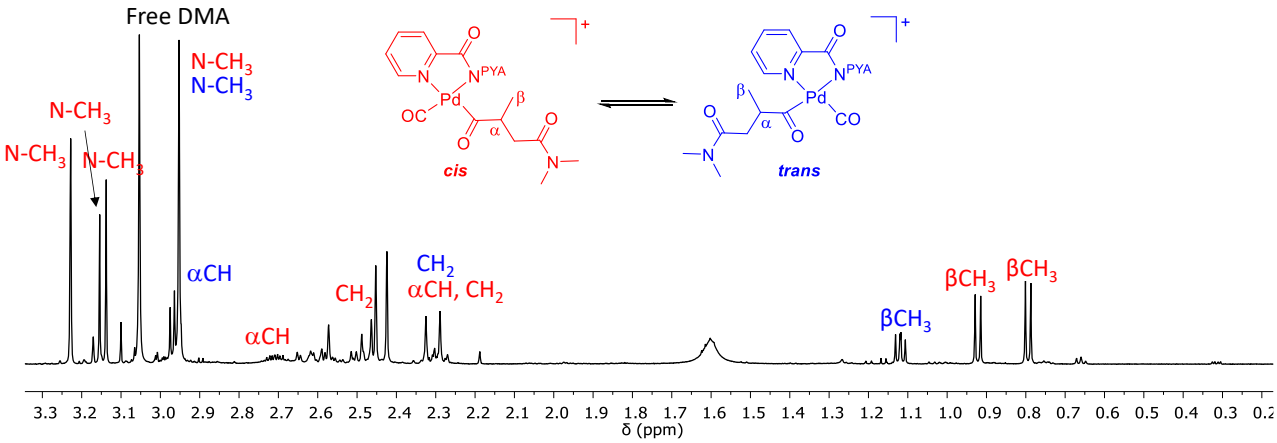

Figure 5.19. ^{1}H NMR spectrum (CD_2Cl_2, 298 K) of the mixture of **8a** with NaBArF, DMA, ethylene and CO at t = 5 min; aliphatic region.

The proton to signal assignments are done in the similar way for the other set of signals. In the $^{1}H,^{13}C$ HMBC spectrum (Figure 5.20) signal of the ketonic group at 218.4 ppm correlates with the two overlapped doublets at 1.11 ppm (βCH_3), that in the $^{1}H,^{1}H$ COSY spectrum correlates with the resonances of CH_2 groups and αCH, that are between 2.31 and 2.58 ppm and at 2.97 ppm, respectively. This species should be the other geometrical isomer of the open-chain intermediate **OC^{DMA}**. In the $^{1}H,^{1}H$ NOESY spectrum no NOE signal is evident between any signals of the PYA ligand and either the doublets at 0.79 and 0.92 ppm or the overlapped doublets at 1.11 ppm. Nevertheless, it is reasonable to assign the doublets at 0.79 and 0.92 ppm, that are the most shifted at lower frequency among the three signals, to the *cis* isomer.

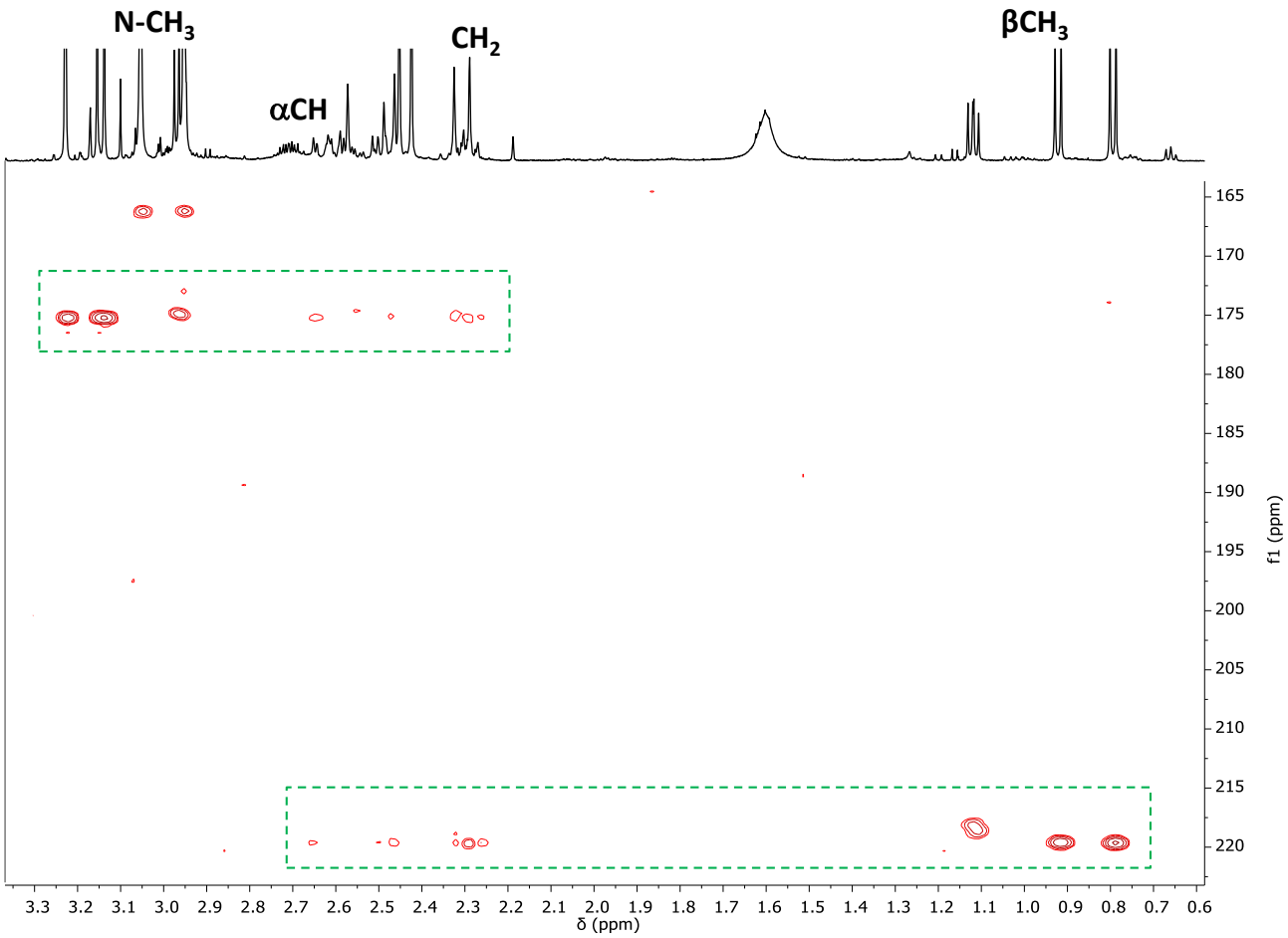

Figure 5.20. $^{1}H,^{13}C$ HMBC (CD_2Cl_2, 298 K) of the mixture of **8a** with NaBArF, DMA, ethylene and CO at t = 5 min; carbonyl region.

For both geometrical isomers the presence of two doublets for βCH_3 and four singlets for inserted DMA N-CH_3 groups (between 2.97 and 3.22 ppm) are due to the presence of the two different diastereoisomers (Figure 5.21).

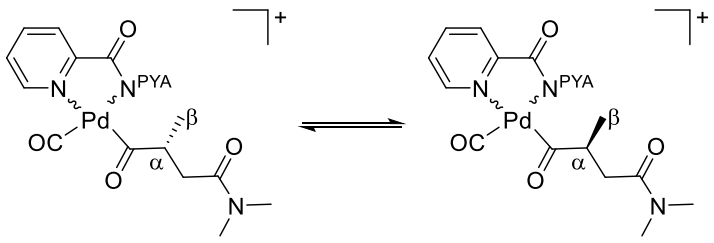

Figure 5.21. The two different diastereoisomers for both geometrical isomers of **OC^{DMA}**.

In the $^{1}H,^{1}H$ NOESY spectrum exchange peaks between doublets of βCH_3 are observed indicating that the two diastereoisomers of each geometrical isomer are in equilibrium at low rate on the NMR time scale at room temperature (Figure 5.22). The ratio between geometrical isomers is of *cis*:*trans* = 72:28, calculated considering the signals of βCH_3.

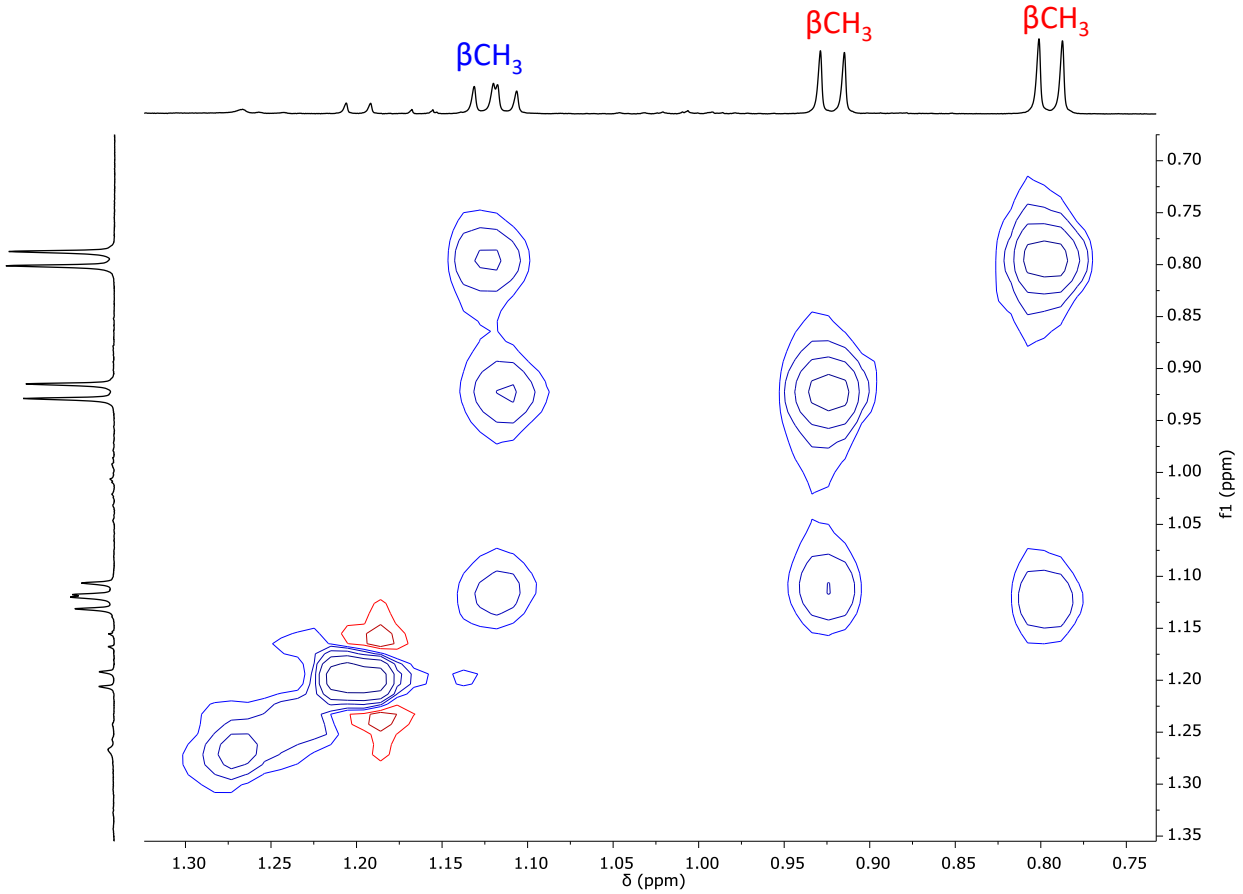

Figure 5.22. $^{1}H,^{1}H$ NOESY spectrum (CD_2Cl_2, 298 K) of the mixture of **8a** with NaBArF, DMA, ethylene and CO at t = 5 min; aliphatic region.

For all the investigated time the intensity of the peak of free ethylene remains constant and no signals derived from the insertion reaction of this molecule on one of the palladium species present in solution is observed. Pd(0) is formed after 19 h at room temperature, but no signal of *N*,*N*-dimethylcrotoneamide is observed.[8]

The reaction of the cationic complex **8c** with DMA is also studied by adding 2 eq. of the polar monomer to the 10 mM CD_2Cl_2 solution of the complex (Scheme 5.6).

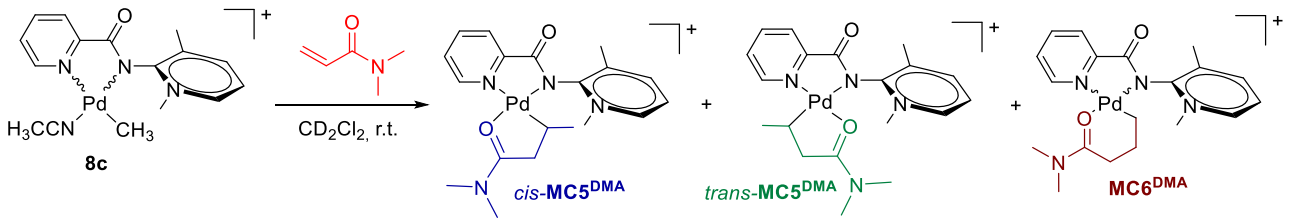

Scheme 5.6. *In situ* NMR reaction of **8c** with *N*,*N*-dimethylacrylamide.

The *cis*-Pd-CH_3 signal of **8c** at -0.06 ppm is present after 5 h from the addition in an amount about 4 %, while the *trans*-Pd-CH_3 resonance disappears after 15 min (Figure 5.23). The NMR analysis indicates that the main intermediates present in solution are *cis*-**MC5^{DMA}**, *trans*-**MC5^{DMA}** and **MC6^{DMA}** in 42:37:21 ratio, calculated at 5 h.

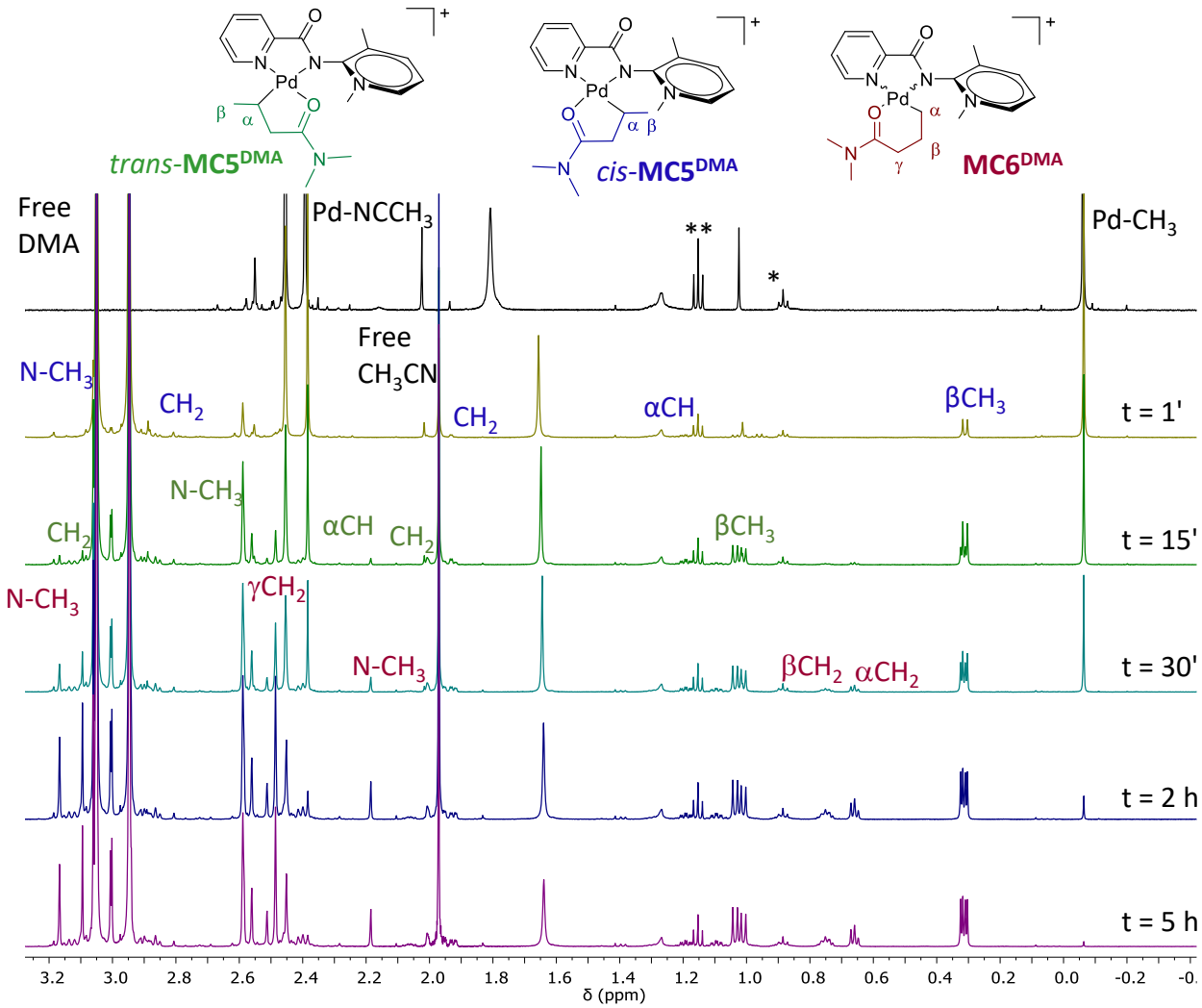

Figure 5.23. ^{1}H NMR spectra (CD_2Cl_2, 298 K) of **8c** (top spectrum) and **8c** after the addition of DMA at different reaction times; **n*-hexane; ***diethyl ether.

In the spectrum recorded after 3 days keeping the NMR tube at room temperature, the major species are **MC5^{DMA}** and **MC6^{DMA}** in the same ratio of that calculated after 5 h from the addition of the polar monomer to **8c** solution (*cis*-**MC5^{DMA}**:*trans*-**MC5^{DMA}**:**MC6^{DMA}** = 42:37:21) and no Pd(0) is observed.

By comparing the reaction with DMA starting from either **8a** or **8c** at t = 30 min (Figure 5.24), the detected intermediates, **MC5^{DMA}** and **MC6^{DMA}**, are the same, present in a different ratio (**MC5^{DMA}**:**MC6^{DMA}** = 93:7 starting from **8a** and 89:11 starting from **8c**), confirming that the migratory insertion of DMA into the Pd-CH_3 bond and the chain walking process are faster when **8a** is used. The main difference deals with the presence of *cis*-**8c** (26 %) at t = 30 min. This clearly indicate that, as already observed for the reaction with methyl acrylate, even in the case of *N*,*N*-dimethylacrylamide the presence of acetonitrile in the precursor slows down the coordination/insertion of the polar monomer into the Pd-CH_3 bond.

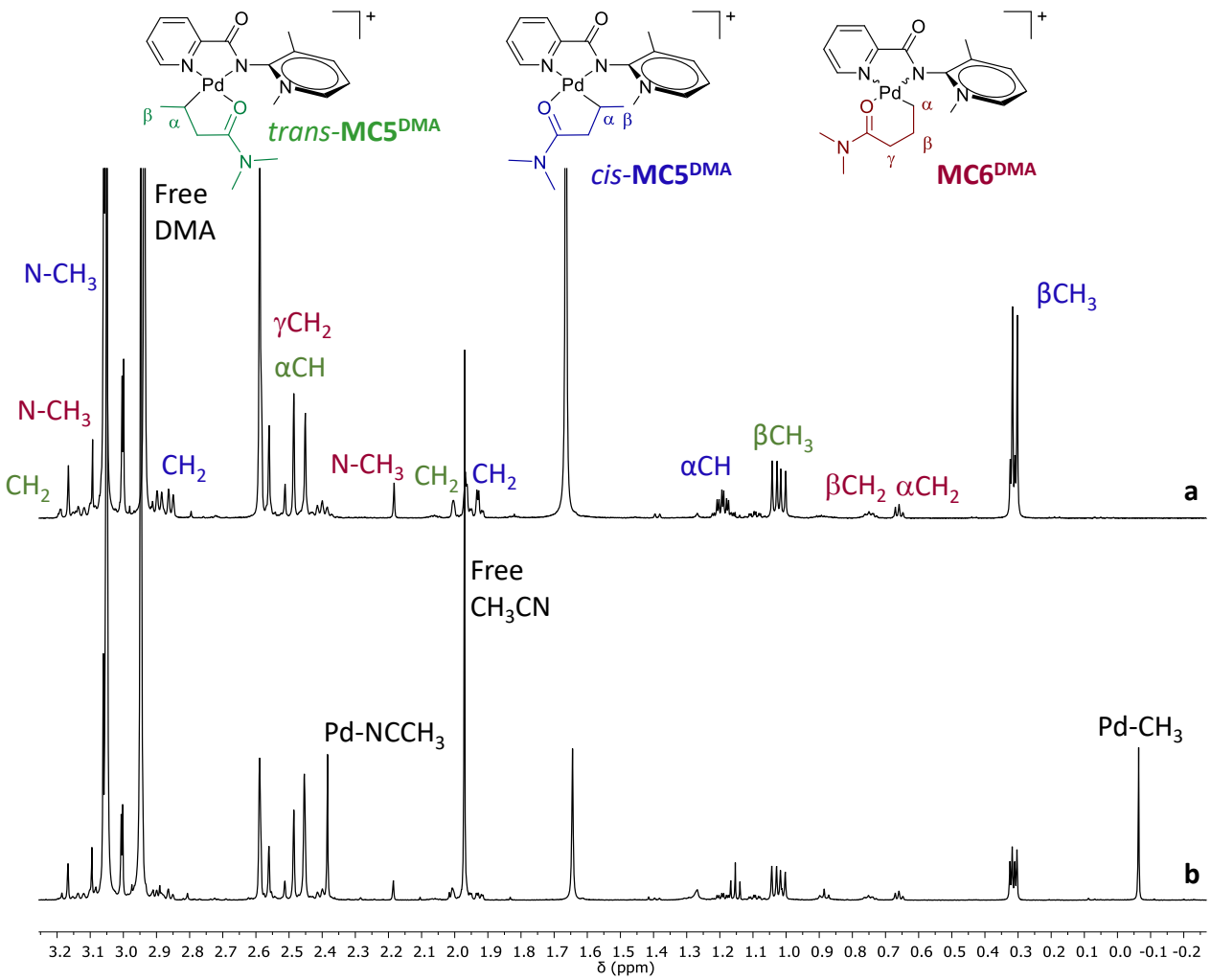

Figure 5.24. ^{1}H NMR spectra (CD_2Cl_2, 298 K) of the mixture of (a) **8a** with NaBArF and DMA and (b) **8c** and DMA at t = 30 min; **n*-hexane; **diethyl ether.

Considering **8c** and its *in situ* NMR studies with either MA or DMA, the coordination/insertion of *N*,*N*-dimethylacrylamide into the Pd-CH_3 bond is slower than that of MA (Figure 5.25), in agreement with the literature data,[8] suggesting that the delocalization of charge between the C=O and C-N group of DMA, together with a higher steric hindrance present in the amide polar monomer, disfavor its coordination. Signals of the precursor **8c** are observed in the ^{1}H NMR spectra for 30 min in the reaction with MA, while when DMA is added to **8c** solution, a weak signal of Pd-CH_3 is observed after 5 h. However, the observed conversion rate of Pd-CH_3 signals into active species include not only the insertion of the polar monomer, but also the insertion of acetonitrile, that competes for the coordination on palladium.

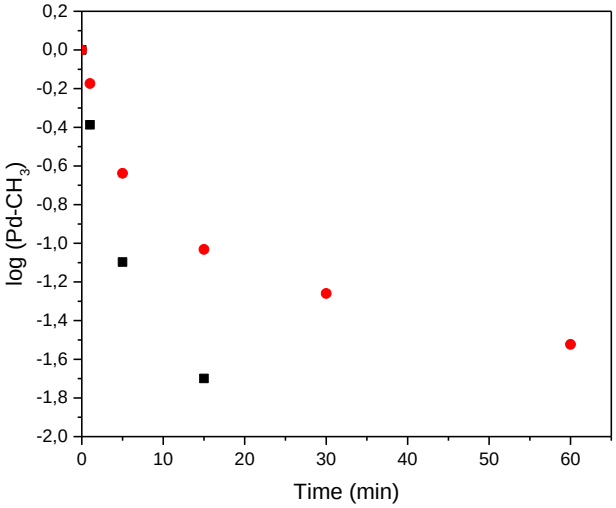

Figure 5.25. Plots of the time-dependent decrease of the Pd-CH_3 signal of *cis*-**8c** at 298 K in the reaction with MA (black squares) and DMA (red circles).

5.3. Conclusions.

Neutral Pd(II) complex containing a PYA ligand, **8a**, [Pd(CH_3)Cl(**8**)], activated *in situ* with NaBArF, and the monocationic derivative, **8c**, [Pd(CH_3)($NCCH_3$)(**8**)][BArF], are used to investigate their reaction with polar vinyl monomers of industrial interest, such as methyl acrylate (MA) and *N*,*N*-dimethylacrylamide (DMA). The technique of choice used for this study is the *in situ* NMR spectroscopy. The cationic compound **8c** is synthesized for the first time in this work and characterized in solution by NMR spectroscopy. The two expected isomers, differing for the relative position of the Pd-CH_3 fragment with respect to the two inequivalent halves of the ligand, are present in solution and the *cis* isomer is the major species (95 %). The NMR studies are performed from a 10 mM CD_2Cl_2 solution of the desired complex and the reaction is followed by recording the NMR spectra at different reaction time at room temperature.

When the neutral compound **8a** is reacted with either MA or DMA upon contemporary addition of NaBArF, all the complex is immediately converted into the 5- and 6-membered metallacycles, originated by the migratory insertion reaction of the polar monomer into the Pd-CH_3 bond, followed by the chain walking process.

Instead, when the cationic complex **8c** is the precursor in the reaction with MA, the 4-membered palladacycle is the main species observed together with traces of the 5- and 6-membered metallacycles. The migratory insertion reaction of MA into the Pd-CH_3 bond of the neutral compound is faster as well as the chain walking process than on the cationic complex, suggesting that the acetonitrile competes with the polar monomer for the coordination on palladium. When progressive equivalents of the acetonitrile are added to the solution of the neutral complex containing also NaBArF and MA, **MC4^{PYA}** becomes the main species confirming the role of the acetonitrile in slowing down the chain walking process.

When the cationic complex is used in the reaction with DMA, its signals are still observed after 5 h (e.g. the singlet of Pd-CH_3 fragment of the *cis*-**8c**) together with the resonances of the 5- and 6-membered metallacycles, originated by the migratory insertion reaction of DMA into the Pd-CH_3 bond. A detailed bidimensional NMR analysis suggests that these metallacycles are O-bonded to the metal center and the solved solid state structure of *trans*-5-membered metallacycle confirms it.

When the reaction mixture of the metallacycles, originated by the insertion reaction of DMA, is saturated with ethylene, no reaction takes place. While when carbon monoxide is bubbled into the same solution, a stable open-chain intermediate deriving from the migratory insertion reaction of carbon monoxide into the Pd-alkyl bond of the metallacycles is formed.

These mechanistic investigations underline both the crucial role played by acetonitrile in the migratory insertion reaction of the polar monomer and the high stability of the produced metallacycles. As for the reaction of these N-N' Pd-complexes with DMA, the obtained results point out that the insertion of this polar monomer into the Pd-CH_3 takes place leading to the formation of a stable 5-membered palladacycle that, under mild reaction conditions, can be opened by carbon monoxide, but not by ethylene. This might give the possibility of using these complexes in the copolymerization of DMA with CO and/or in the terpolymerization reaction with the addition of also ethylene into the reaction mixture, under more drastic reaction conditions.

5.4. Experimental.

All complex manipulations were performed using standard Schlenk techniques under argon. Anhydrous dichloromethane was freshly obtained by distillation over CaH_2 under argon atmosphere.

Deuterated solvent (Cambridge Isotope Laboratories, Inc. (CIL)) was stored as recommended by sellers. Ethylene (purity ≥ 99.9 %) supplied by SIAD, methyl acrylate (99.9%, with 0.02% of hydroquinone monomethyl ether) and *N,N*-dimethylacrylamide (99%, with 500 ppm of hydroquinone monomethyl ether) supplied by Aldrich were used as received. Mono- and bidimensional NMR spectra of complexes and reactivities were recorded on a Varian 500 spectrometer (500 MHz for ^{1}H, 125.68 MHz for ^{13}C). The resonances are reported in ppm (δ) and referenced to the residual solvent peak versus $Si(CH_3)_4$: CD_2Cl_2: at δ 5.32 (^{1}H) and δ 54.00 (^{13}C). ^{19}F–NMR spectra were recorded on a Varian 400 spectrometer at 376.3 MHz and referenced with respect to CCl_3F. NMR experiments were performed employing the automatic software parameters. In the case of NOESY experiments a mixing time of 500 ms was used.

*5.4.1. Synthesis and characterization of [Pd(CH₃)(NCCH₃)(**8**)][BArF], **8c**.*

The cationic complex is synthesized starting from [Pd(CH_3)Cl(**8**)], **8a**, that, on turn, was prepared following the literature procedure.[7]

To a stirred solution of **8a** in CH_2Cl_2 (0.1 mmol in 5 mL), at room temperature, a solution of CH_3CN (1 mL) and NaBArF (1.15 eq.) was added. The reaction mixture was left under stirring, in the dark, for the 1 h. Afterward, it was filtered on Celite®, concentrated to a few milliliters of volume and upon addition of cold diethyl ether and *n*-hexane the product was precipitated as a white solid. It was filtered under vacuum after a night at 277 K and washed with cold Et_2O.

8c. (white solid, yield = 78 %); ^{1}H NMR (500 MHz, CD_2Cl_2, 298 K) *cis* 95 % *trans* 5 %. Major species (*cis*): δ = 8.40-7.50 (m, CH^{PYA}, CH^{Pyr}), 7.72 (s, 2H, H^{o}-BArF), 7.56 (s, 1H, H^{m}-BArF), 4.16 (s, 3H, N-CH_3), 2.46 (s, 3H, CH_3^{PYA}), 2.41 (s, 3H, Pd-$NCCH_3$), -0.06 (s, 3H, Pd-CH_3); minor species (*trans*): δ = 8.40-7.50 (m, CH^{PYA}, CH^{Pyr}), 7.72 (s, 2H, H^{o}-BArF), 7.56 (s, 1H, H^{m}-BArF), 4.21 (s, 3H, N-CH_3), 2.56 (s, 3H, CH_3^{PYA}), 2.04 (s, 3H, Pd-$NCCH_3$), 1.02 (s, 3H, Pd-CH_3). ^{19}F NMR (400 MHz, CD_2Cl_2, 298 K) δ = - 62.89 (s).

5.4.2. General procedures for in situ NMR reactivity.

*General procedure for the in situ NMR reactivity of **8a** with polar vinyl monomer.*

A 10 mM CD_2Cl_2 solution of **8a** is prepared and a first NMR spectrum is recorded. Then to this pale yellow solution, a solution of 1 eq. of NaBArF in 2 eq. of the polar monomer (MA or DMA) is added. The reaction is followed on time, at room temperature, by NMR spectroscopy.

*General procedure for the in situ NMR reactivity of **8c** with polar vinyl monomer.*

To a 10 mM CD_2Cl_2 solution of **8c**, 2 eq. of the polar monomer (MA or DMA) are added. The reaction is followed on time, at room temperature, by NMR spectroscopy.

*General procedure for the in situ NMR reactivity of **8a** with NaBArF, DMA and gaseous monomer.* The reaction with ethylene is studied by bubbling the gaseous monomer in a 10 mM CD_2Cl_2 solution of **9a** after 2 h from the addition of NaBArF and DMA. After 1 h from the addition of ethylene, this solution is saturated with carbon monoxide. Its colour changes from pale yellow to pale pink. The reaction is followed on time, at room temperature, by NMR spectroscopy.

5.5. References.

(1) Birajdar, R. S.; Chikkali, S. H. Insertion Copolymerization of Functional Olefins: Quo Vadis? *Eur. Polym. J.* **2021**, *143* (November 2020).

(2) Luckham, S. L. J.; Nozaki, K. Toward the Copolymerization of Propylene with Polar Comonomers. *Acc. Chem. Res.* **2021**, *54* (2), 344–355.

(3) Rosar, V.; Montini, T.; Balducci, G.; Zangrando, E.; Fornasiero, P.; Milani, B. Palladium-Catalyzed Ethylene/Methyl Acrylate Co-Oligomerization: The Effect of a New Nonsymmetrical α-Diimine with the 1,4-Diazabutadiene Skeleton. *ChemCatChem* **2017**, *9* (17), 3402–3411.

(4) Meduri, A.; Montini, T.; Ragaini, F.; Fornasiero, P.; Zangrando, E.; Milani, B. Palladium-Catalyzed Ethylene/Methyl Acrylate Cooligomerization: Effect of a New Nonsymmetric α-Diimine. *ChemCatChem* **2013**, *5* (5), 1170–1183.

(5) Chen, Z.; Brookhart, M. Exploring Ethylene/Polar Vinyl Monomer Copolymerizations Using Ni and Pd α-Diimine Catalysts. *Acc. Chem. Res.* **2018**, *51* (8), 1831–1839.

(6) Navarro, M.; Rosar, V.; Montini, T.; Milani, B.; Albrecht, M. Olefin Dimerization and Isomerization Catalyzed by Pyridylidene Amide Palladium Complexes. *Organometallics* **2018**, *37* (20), 3619–3630.

(7) Ó Máille, G. M.; Dall'Anese, A.; Grossenbacher, P.; Montini, T.; Milani, B.; Albrecht, M. Modulation of N^N′-Bidentate Chelating Pyridyl-Pyridylidene Amide Ligands Offers Mechanistic Insights into Pd-Catalysed Ethylene/Methyl Acrylate Copolymerisation. *Dalt. Trans.* **2021**, *50* (18), 6133–6145.

(8) Friedberger, T.; Wucher, P.; Mecking, S. Mechanistic Insights into Polar Monomer Insertion Polymerization from Acrylamides. *J. Am. Chem. Soc.* **2012**, *134* (2), 1010–1018.

(9) Gaikwad, S. R.; Deshmukh, S. S.; Koshti, V. S.; Poddar, S.; Gonnade, R. G.; Rajamohanan, P. R.; Chikkali, S. H. Reactivity of Difunctional Polar Monomers and Ethylene Copolymerization: A Comprehensive Account. *Macromolecules* **2017**, *50* (15), 5748–5758.

(10) Zhang, Y.; Mu, H.; Pan, L.; Wang, X.; Li, Y. Robust Bulky [P,O] Neutral Nickel Catalysts for Copolymerization of Ethylene with Polar Vinyl Monomers. *ACS Catal.* **2018**, *8* (7), 5963–5976.

(11) Durand, J.; Zangrando, E.; Stener, M.; Fronzoni, G.; Carfagna, C.; Binotti, B.; Kamer, P. C. J.; Müller, C.; Caporali, M.; Van Leeuwen, P. W. N. M.; Vogt, D.; Milani, B. Long-Lived Palladium Catalysts for CO/Vinyl Arene Polyketones Synthesis: A Solution to Deactivation Problems. *Chem. - A Eur. J.* **2006**, *12* (29), 7639–7651.

(12) Milani, B.; Scarel, A.; Mestroni, G.; Gladiali, S.; Taras, R.; Carfagna, C.; Mosca, L. Very Stable Palladium(II)-(N-N) Catalysts for the Synthesis of High-Molecular-Weight CO/Styrene Polyketones. *Organometallics* **2002**, *21* (7), 1323–1325.

(13) Dall'Anese, A.; Fiorindo, M.; Olivieri, D.; Carfagna, C.; Balducci, G.; Alessio, E.; Durand, J.; Milani, B. Pd-Catalyzed CO/Vinyl Arene Copolymerization: When the Stereochemistry Is Controlled by the Comonomer. *Macromolecules* **2020**, *53* (18), 7783–7794.

CHAPTER 6

General conclusions and future perspectives

The research activity carried out for this PhD thesis deals with the development of homogeneous catalysts, based on palladium(II) complexes, for the synthesis of functionalized polyolefins. A particular focus is addressed to the study of the effects of the secondary interactions between the spectator ligands present on the catalyst and the copolymer growing chain. Taking into account that the ideal catalyst, in addition to show a high productivity, has to be stable and able to control the copolymer microstructure, as an alternative strategy to ligand design, three new families of organometallic Pd(II) complexes have been synthesized and tested in the ethylene/methyl acrylate copolymerization. They differ for one of the ligand bonded to the metal center.

Regardless the Pd(II) compounds with the thiophenimine ligand, $[Pd(CH_3)(N\text{-}N)(N\text{-}S)][PF_6]$, the obtained copolymers show inserted MA both in the main chain and at the end of the branches in a ratio about 1:1 in particular reaction conditions in terms of solvent and nature of the N-S ligand. Thanks to *in situ* NMR investigations, an open-chain intermediate having both the N-S ligand and an organic fragment, generated by the insertion of both comonomers into the Pd-alkyl bond, bonded to Pd ion is detected. In addition, a network of hydrogen bonds between the oxygen atom of the ester group of the inserted polar monomer and the hydroxyl groups of the fluorinated solvent is observed and this is supposed to be responsible to trap MA into the main chain of the copolymer.

When the Pd(II) complexes with hemilabile potentially tridentate molecules $[Pd(CH_3)(NCCH_3)(N\text{-}N'\text{-}S)][X]$ and $[Pd(CH_3)(N\text{-}N'\text{-}S)][X]$ are tested in the target reaction, they lead to either unsaturated esters or cooligomers depending on the N-N' fragment. The thiophene pendant arm contributes to affect the branching degree of the obtained macromolecules, that is slowed down after the insertion of a ethylene unit. This phenomenon highlights that the sulfur atom and/or acetonitrile compete with the comonomers for the coordination on the metal center during catalysis.

Moreover, the catalytic results obtained by the Pd(II) complexes bearing a highly coordinating monodentate ligand beloging to the family of pyridine, $[Pd(CH_3)(N\text{-}N)(N^{pyr})][PF_6]$, outline that in particular reaction conditions hyperbranched copolymers are obtained and the pyridine ligand remains bonded to the metal center during the reaction.

These results might open the way to the discovery of new, efficient catalytic systems for the synthesis of functionalized polyolefins, for example by introducing on the spectator ligand functional groups able to establish non covalent, weak interactions with specific atoms on the growing copolymer chain with the aim to slow down the chain walking process after the insertion of both comonomers.

For instance the introduction of an hydroxyl group on the aryl ring of the α-diimine ligand might lead to an hydrogen bond with the oxygen atom of the ester group of the inserted acrylate, limiting its availability for the chain walking process and the formation of metallacycle intermediates. A similar effect might be obtained introducing a trifluoromethyl group, which might establish the hydrogen bond interaction with β–hydrogen atoms of the growing copolymeric chain, hampering the chain walking process after the insertion of ethylene. As a consequence, the combination of these two functional groups on the same ligand might result in catalysts able to lead to the desire linear copolymer.

ACKNOWLEDGEMENTS

The research project of this PhD thesis involves some collaborations related to specific aspects.
In particular, I want to thank:
Dr. Gabriele Balducci of University of Trieste and Dr. Maurizio Polentarutti of Elettra Sincrotrone for the X-ray structure analysis;
Dr. Fabio Hollan of University of Trieste for the ESI-Mass analysis of the ligands and Pd(II) complexes;
Prof. Claudio Pellecchia and Dr. Massimo C. D'Alterio of University of Salerno for the measurement of the molecular weight of the synthesized ethylene/methyl acrylate copolymers and the DFT calculations (Chapter 2 and 4);
Prof. Martin Albrecht of University of Bern for the synthesis of the neutral complex used in Chapter 5.

LIST OF PUBLICATIONS

1. Dall'Anese, A., Tosolini, M., Alberoni, C., Balducci, G., Polentarutti, M., Pellecchia, C., Tecilla, P., Milani, B.
"Palladium(II) complexes with the 4,5-bis(diphenylphosphino)acenaphtene ligand and their reactivity with ethylene"
Eur. J. Inorg. Chem., **2022**, in press. I.F. = 2.551
DOI: 10.1002/ejic.202200481

2. Alberoni, C., D'Alterio, M. C., Balducci, G., Immirzi, B., Polentarutti, M., Pellecchia, C., Milani, B.
"Tunable "*in chain"* and "*at the end of the branches"* methyl acrylate incorporation in polyolefin skeleton through Pd(II) catalysis"
ACS Catalysis, **2022**, *12*, 3430 . I.F. = 13.084.
DOI: 10.1021/acscatal.1c05326

3. Alberoni, C., Barroso-Martin, I., Infantes-Molina, A., Rodriguez-Castellon, E., Talon, A., Zhao, H., You, S., Vomiero, A., Moretti, E.
"Ceria doping boosts methylene blue photodegradation in titania nanostructures"
Mater. Chem. Front., **2021**, *5*, 4138. Advanced article. I.F. = 6.482.
DOI: 10.1039/D1QM00068C

4. Barroso-Martin, I., Alberoni, C., Rodriguez-Castellon, E., Infantes-Molina, A., Moretti, E.
"Recent advances in photo-assisted preferential CO oxidation in H_2-rich stream"
Current Opinion in green and sustainable chemistry, **2020**, *21*, 9. I.F. = 6.457.
DOI: 10.1016/j.cogsc.2019.07.008

CONFERENCE PARTECIPATION

1. C. Alberoni, G. Balducci, B. Milani

"The effect of potentially terdentate ligands in Pd(II) catalysts for functionalized polyolefin synthesis" – Poster communication, presented by B. Milani.

44th International Conference on Coordination Chemistry (ICCC)

Rimini, August 28th – September 2nd 2022.

Book of abstract: P003

2. C. Alberoni, E. Reusser, B. Milani, M. Albrecht

"Mechanistic insights into reactiviteies of Pd(II)-pyridylidene amide complexes with polar vynil monomers" – Poster presentation.

XXII international Symposium on Homogeneous Catalysis (ISHC)

Lisbon, July 24th – 29th 2022.

Book of abstract: P4

3. B. Milani, C. Alberoni, M. C. D'Alterio, G. Balducci, B. Immirzi, M. Polentarutti, C. Pellecchia

"Novel mechanistic insights on Pd(II)-catalysts for functionalized polyolefin synthesis" – Oral communication, presented by B. Milani

XXII international Symposium on Homogeneous Catalysis (ISHC)

Lisbon, July 24th – 29th 2022.

Book of abstract: O15

4. C. Alberoni, G. Balducci, B. Milani

"Moving from acetonitrile to a pyridine in the fourth coordination site of Pd(II) catalysts for the synthesis of functionalized polyolefins" – Poster presentation.

4th International Green Catalysis Symposium (GreenCat2022)

Rennes, April 19th – 22nd 2022.

Book of abstract: P52

5. C. Alberoni, G. Balducci, B. Milani

“Functionalized polyolefins: from pristine polyolefins to better performing macromolecules” – Oral presentation.

I giovani e la chimica in Friuli Venezia Giulia

Trieste, September 30th 2021

6. C. Alberoni, G. Balducci, C. Pellecchia, B. Milani

“Pd(II) catalysts for the synthesis of functionalized polyolefins: the control of polar monomer enchainment” – Poster presentation.

XXVII Congresso Nazionale della Società Chimica Italiana

Milano, September 14th – 23rd 2021.

Book of abstract: INO PO003

7. C. Alberoni, G. Balducci, B. Milani, M. Polentarutti

“Ethylene/methyl acrylate copolymerization: effect of palladium catalyst on methyl acrylate enchainment” – Poster communication, presented by B. Milani.

XXVII Congresso Nazionale della Società Chimica Italiana

Milano, September 14th – 23rd 2021.

Book of abstract: INO PO054

8. C. Alberoni, G. Balducci, M. Polentarutti, B. Milani

“Pd(II) catalysts for the synthesis of functionalized polyolefins: the effect of a fourth monodentate ligand” – Flash and oral presentation.

XIII International School of Organometallic Chemistry (ISOC)

Camerino, September 1st – 3rd 2021 (web edition).

9. C. Alberoni, G. Balducci, C. Pellecchia, B. Milani

“Pd(II) catalysts for the synthesis of functionalized polyolefins: the control of polar monomer enchainment” – Oral presentation.

XVII PhD-Chem Day of CIRCC (Consorzio Interuniversitario per la Reattività Chimica e la Catalisi)

Venezia, April 29th – 30th, 2021 (web edition).

Appendix chapter 2.

NMR characterization of ligands and complexes.

NMR characterization of S^{Ph} (CD_2Cl_2, 298 K).

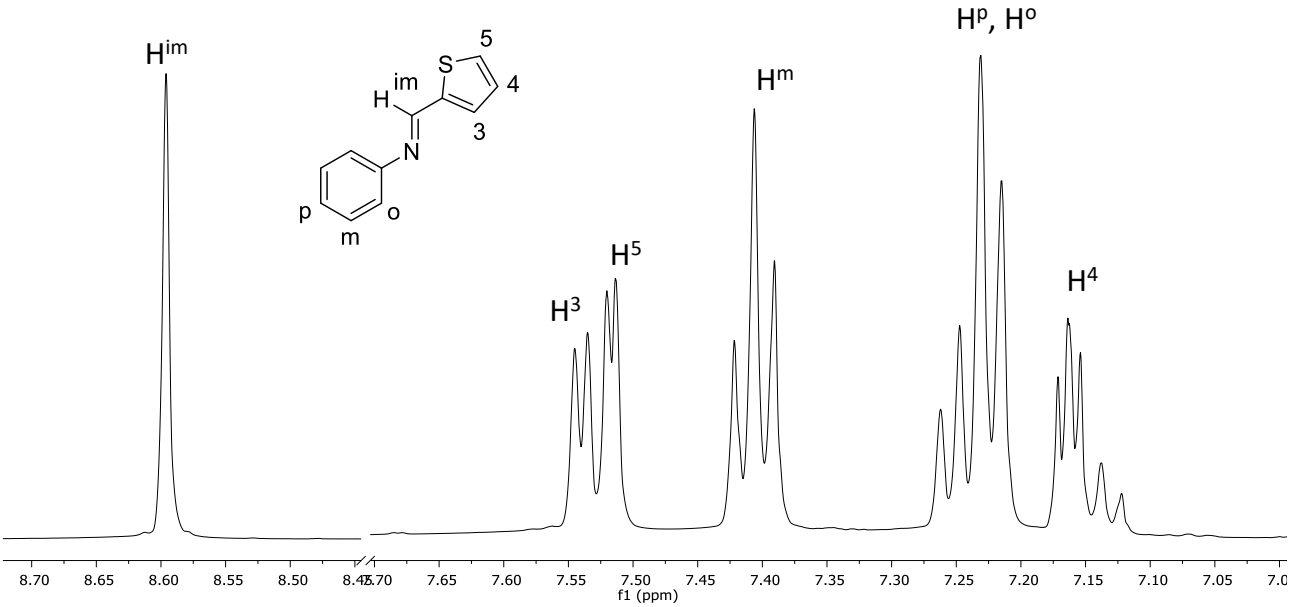

Figure S2.1. ^{1}H NMR spectrum (CD_2Cl_2, 298 K) of $\mathbf{S^{Ph}}$.

NMR characterization of S^{Me} (CD_2Cl_2, 298 K).

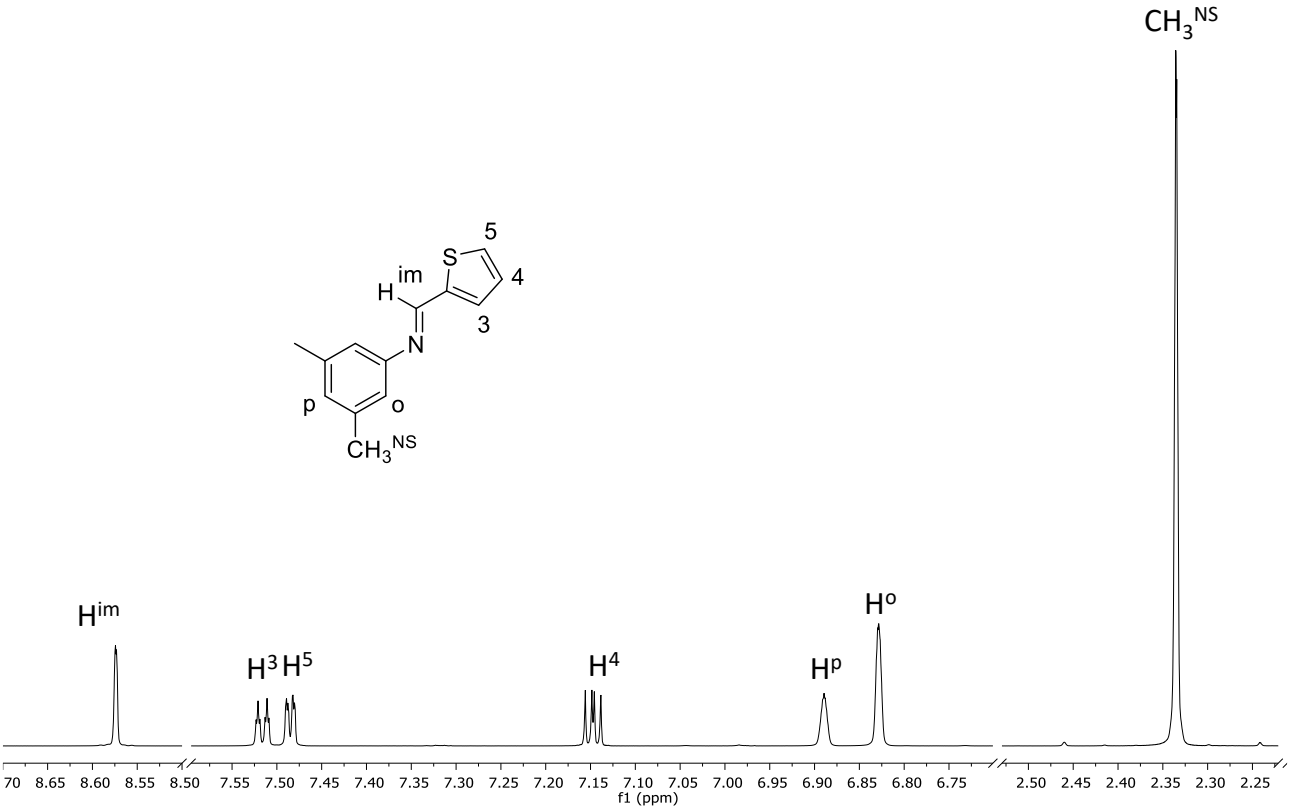

Figure S2.2. ^{1}H NMR spectrum (CD_2Cl_2, 298 K) of $\mathbf{S^{Me}}$.

NMR characterization of $1S^{Ph}$ (CD_2Cl_2, 298 K).

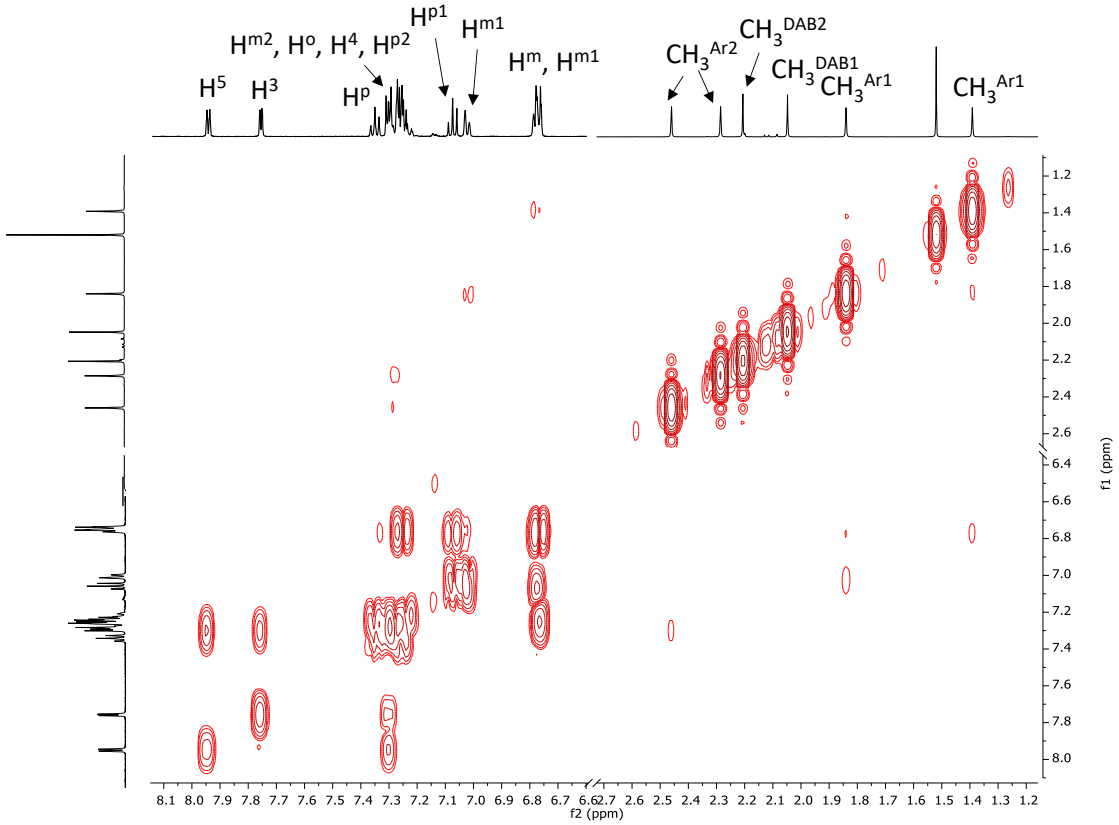

Figure S2.3. $^1H,^1H$ COSY spectrum (CD_2Cl_2, 298 K) of **$1S^{Ph}$** (aromatic and aliphatic region not on scale).

NMR characterization of $1S^{Me}$ (CD_2Cl_2, 298 K).

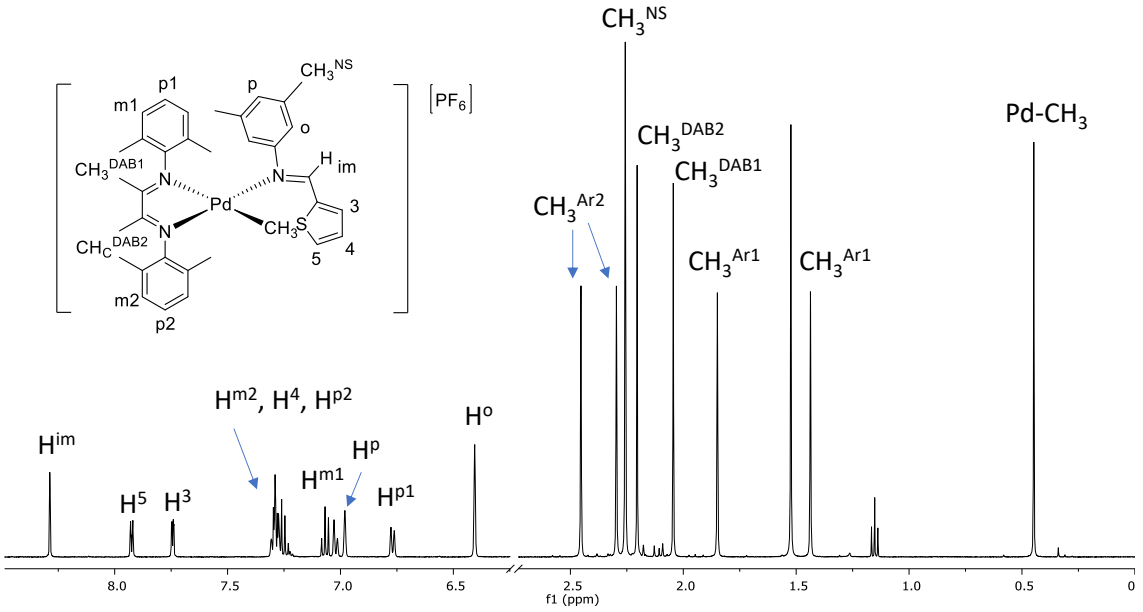

Figure S2.4. ^{1}H NMR spectrum (CD_2Cl_2, 298 K) of **1S^{Me}**.

NMR characterization of 1S^{CF3} (CD_2Cl_2, 298 K)

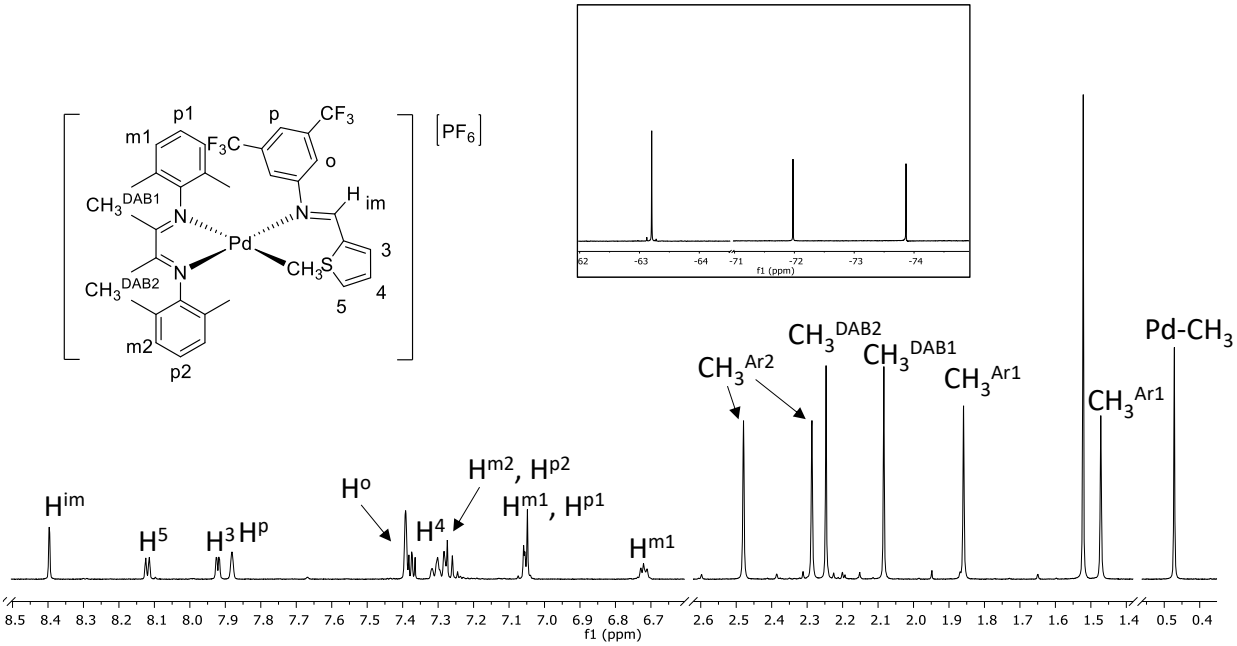

Figure S2.5. ^{1}H NMR spectrum (CD_2Cl_2, 298 K) of **1S^{CF3}**; inset: ^{19}F NMR spectrum.

X-Ray crystallography.

Table S2.1. Most significant distances and angles for complexes **1S^{Ph}** and **1S^{Me}**.

	1S^{Ph}	**1S^{Me}**			
	Distance (Å)				
Pd-C1	2.035(3)	**Pd1-C1**	2.036(4)	**Pd2-C2**	2.051(5)
Pd-N21	2.042(2)	**Pd1-N11**	2.034(3)	**Pd2-N31**	2.034(4)
Pd-N22	2.147(2)	**Pd1-N12**	2.142(3)	**Pd2-N32**	2.139(3)
Pd-N31	2.026(2)	**Pd1-N21**	2.029(3)	**Pd2-N41**	2.033(4)
Pd---S31	3.100(1)	**Pd1---S1**	3.328(2)	**Pd2---S2**	3.125(2)
	Angle (°)				
C1-Pd1-N21	95.3(1)	**C1-Pd1-N11**	94.0(2)	**C2-Pd2-N32**	171.2(2)
C1-Pd1-N22	171.2(1)	**C1-Pd1-N12**	171.4(2)	**N31-Pd2-C2**	93.4(2)
N21-Pd1-N22	77.6(1)	**N11-Pd1-N12**	77.4(2)	**N31-Pd2-N32**	77.9(1)
N31-Pd1-C1	87.99(1)	**N21-Pd1-C1**	89.1(2)	**N41-Pd2-C2**	89.6(2)
N31-Pd1-N21	175.8(1)	**N21-Pd1-N11**	173.1(1)	**N41-Pd2-N31**	176.8(1)
N31-Pd1-N22	99.5(1)	**N21-Pd1-N12**	99.4(1)	**N41-Pd2-N32**	99.1(1)

	Dihedral angle (°)				
[Ar22]-[Pd1]	82.19(9)	**[Ar11]-[Pd1]**	84.0(1)	**[Ar31]-[Pd2]**	89.2(1)
[Ar21]-[Pd1]	83.72(9)	**[Ar12]-[Pd1]**	83.40(9)	**[Ar32]-[Pd2]**	89.4(1)
[Ar22]-[Ph]	9.0(2)	**[Ar12]-[Ar21]**	17.8(2)	**[Ar32]-[Ar41]**	16.5(2)
[Ph]-[S31]	54.3(1)	**[Ar21]-[S1]**	38.6(2)	**[Ar41]-[S2]**	59.5(2)

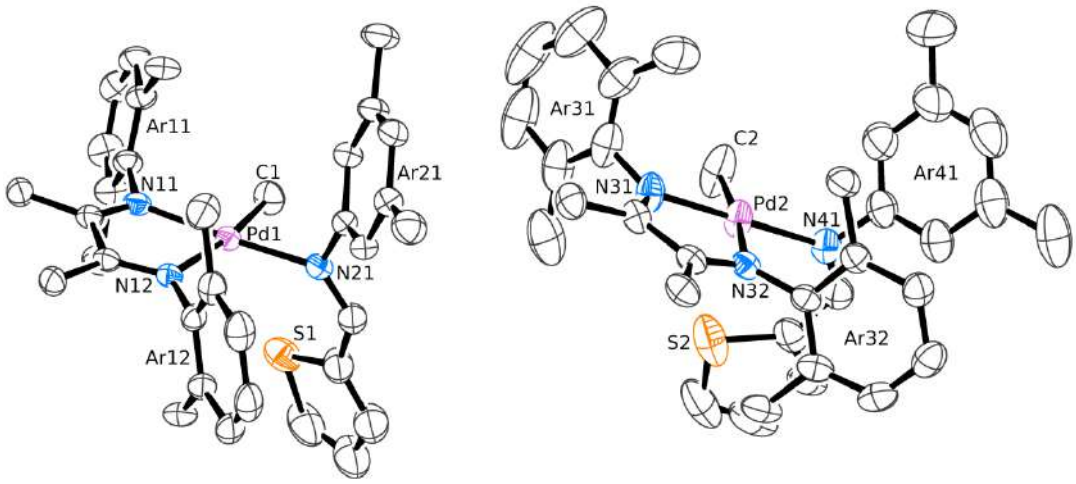

Figure S2.6. ORTEP drawing (50% probability ellipsoids) of the two independent molecules of compound **1S^{Me}** in the crystal structure. Hydrogen atoms, two disordered PF_6^- anions and a cocrystallized CH_2Cl_2 solvent molecule have been omitted for the sake of clarity.

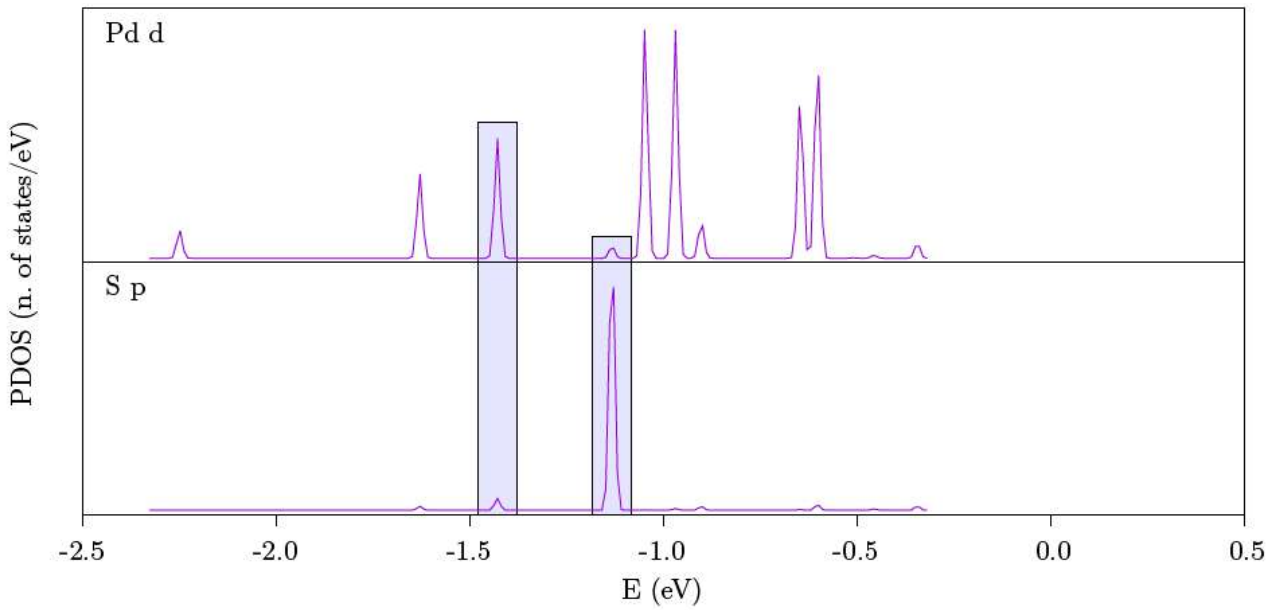

Figure S2.7. A portion of the projection of the Density of States calculated for complex **1S^{Ph}** onto Pd-d (upper) and S-p (lower) atomic orbitals. The zero of the energy axis has been set at the HOMO level. The overlap of atomic states at -1.13 eV and -1.43 eV has been evidenced.

Ethylene/methyl acrylate copolymerization reaction.

Table S2.2. Ethylene/methyl acrylate copolymerization: effect of precatalyst and solvent. Precatalyst: [Pd(CH$_3$)(N-S/L)(1)][PF$_6$][a]

entry	precat.	solvent	M_n kDa (M_w/M_n)[b]	M(MA)[c]	T(MA)[c]	M(MA): T(MA)	Bd[d]
1	**1b**	TFE	24.6 (1.88)	24	76	0.32	93
2	**1S^{CF3}**	TFE	27.0 (2.12)	27	73	0.37	98
3	**1S^{Ph}**	TFE	20.0 (1.64)	32	68	0.47	101
4	**1S^{Me}**	TFE	14.7 (1.77)	26	74	0.35	103
5	**1b**	CH_2Cl_2	6.0 (2.18)	12	88	0.14	90
6	**1S^{CF3}**	CH_2Cl_2	8.2 (2.11)	9	91	0.10	87
7	**1S^{Ph}**	CH_2Cl_2	10.0 (2.03)	13	87	0.15	92
8	**1S^{Me}**	CH_2Cl_2	12.4 (2.00)	10	90	0.11	95

[a] Reaction conditions: Set A: see Table 2.2; [b] determined by GPC; [c] way of MA enchainment, as calculated by ^{13}C NMR spectroscopy on isolated product (M(MA) = methyl acrylate in chain; T(MA) = methyl acrylate at the end of the branches); [d] branching degree calculated by ^{1}H NMR spectroscopy on isolated product and expressed as branches per 1000 carbon atoms.

Table S2.3. Ethylene/methyl acrylate copolymerization: effect of precatalyst and solvent. Precatalyst: [Pd(CH$_3$)(N-S/L)(1)][PF$_6$][a]

entry	precat.	solvent	M_n (M_w/M_n)[b]	M(MA)[c]	T(MA)[c]	M(MA): T(MA)	Bd[d]
1	**1b**	TFE	23.4 (1.19)	40	60	0.67	93
2	**1S^{CF3}**	TFE	30.4 (1.81)	32	68	0.47	100
3	**1S^{Ph}**	TFE	18.0 (1.98)	41	59	0.69	98
4	**1S^{Me}**	TFE	12.3 (1.89)	45	55	0.82	97
5	**1b**	CH_2Cl_2	5.0 (2.00)	12	88	0.14	93
6	**1S^{CF3}**	CH_2Cl_2	5.4 (1.94)	15	85	0.18	93
7	**1S^{Ph}**	CH_2Cl_2	11.0 (2.22)	21	79	0.26	90
8	**1S^{Me}**	CH_2Cl_2	9.0 (1.89)	15	85	0.18	88

[a] Reaction conditions: Set B: see Table 2.3; [b] determined by GPC; [c] way of MA enchainment, as calculated by ^{13}C NMR spectroscopy on isolated product (M(MA) = methyl acrylate in chain; T(MA) = methyl acrylate at the end of the branches); [d] branching degree calculated by ^{1}H NMR spectroscopy on isolated product and expressed as branches per 1000 carbon atoms.

Table S2.4. Ethylene/methyl acrylate copolymerization: effect of [1S^{Ph}].

Precatalyst: [Pd(CH$_3$)(S^{Ph})(1)][PF$_6$][a].

entry	n_{Pd} (10^{-5} mol)	yield (g)	kg CP/mol Pd[b]	MA (mol %)[c]	M(MA)[d]	T(MA)[d]	M(MA): T(MA)	Bd[e]
1	1.05	0.3068	29.22	2.4	30	70	0.43	104
2	2.10	0.5130	24.43	3.1	32	68	0.47	101
3	4.20	0.7441	17.72	3.0	23	68[f]	0.34	101

[a] Reaction conditions: V_{TFE} = 21 mL, V_{MA} = 1.130 mL, P_E = 2.5 bar, T = 308 K, t = 6 h; [b] productivity in kg CP/mol Pd = kilograms of copolymer per mol of palladium; [c] calculated by ^{1}H NMR spectroscopy on isolated product; [d] way of MA enchainment, as calculated by ^{13}C NMR spectroscopy on isolated product (M(MA) = methyl acrylate in chain; T(MA) = methyl acrylate in terminus); [e] branching degree calculated by ^{1}H NMR spectroscopy on isolated product and expressed as branches per 1000 carbon atoms; [f] the integral value of the additional, not assigned, peak at 175.0 (9 %) present in the carbonyl region is not considered.

Table S2.5. Ethylene/methyl acrylate copolymerization: effect of [MA]/[Pd].

Precatalyst: [Pd(CH$_3$)(S^{Ph})(1)][PF$_6$][a].

entry	[MA]/[Pd]	yield (g)	kg CP/mol Pd[b]	MA (mol %)[c]	M(MA)[d]	T(MA)[d]	M(MA): T(MA)	Bd[e]
1	297	0.8397	39.98	1.3	20	80	0.25	108
2	594	0.5130	24.43	3.1	32	68	0.47	101
3	1188	0.3620	17.24	5.0	20	70[f]	0.28	96
4	1782	0.3240	15.43	7.9	20	70[f]	0.28	91

[a] Reaction conditions: $n_{Pd} = 2.1 \cdot 10^{-5}$ mol, V_{TFE} = 21 mL, P_E = 2.5 bar, T = 308 K, t = 6 h; [b] productivity in kg CP/mol Pd = kilograms of copolymer per mol of palladium; [c] calculated by ^{1}H NMR spectroscopy on isolated product; [d] way of MA enchainment, as calculated by ^{13}C NMR spectroscopy on isolated product (M(MA) = methyl acrylate in chain; T(MA) = methyl acrylate in terminus); [e] branching degree calculated by ^{1}H NMR spectroscopy on isolated product and expressed as branches per 1000 carbon atoms; [f] the integral value of the additional, not assigned, peak at 175.0 (10 %) present in the carbonyl region is not considered (Figure S2.26).

***In situ* NMR reactivity.**

***In situ* NMR reactivity of 1b with ethylene (CD_2Cl_2, 298 K).**

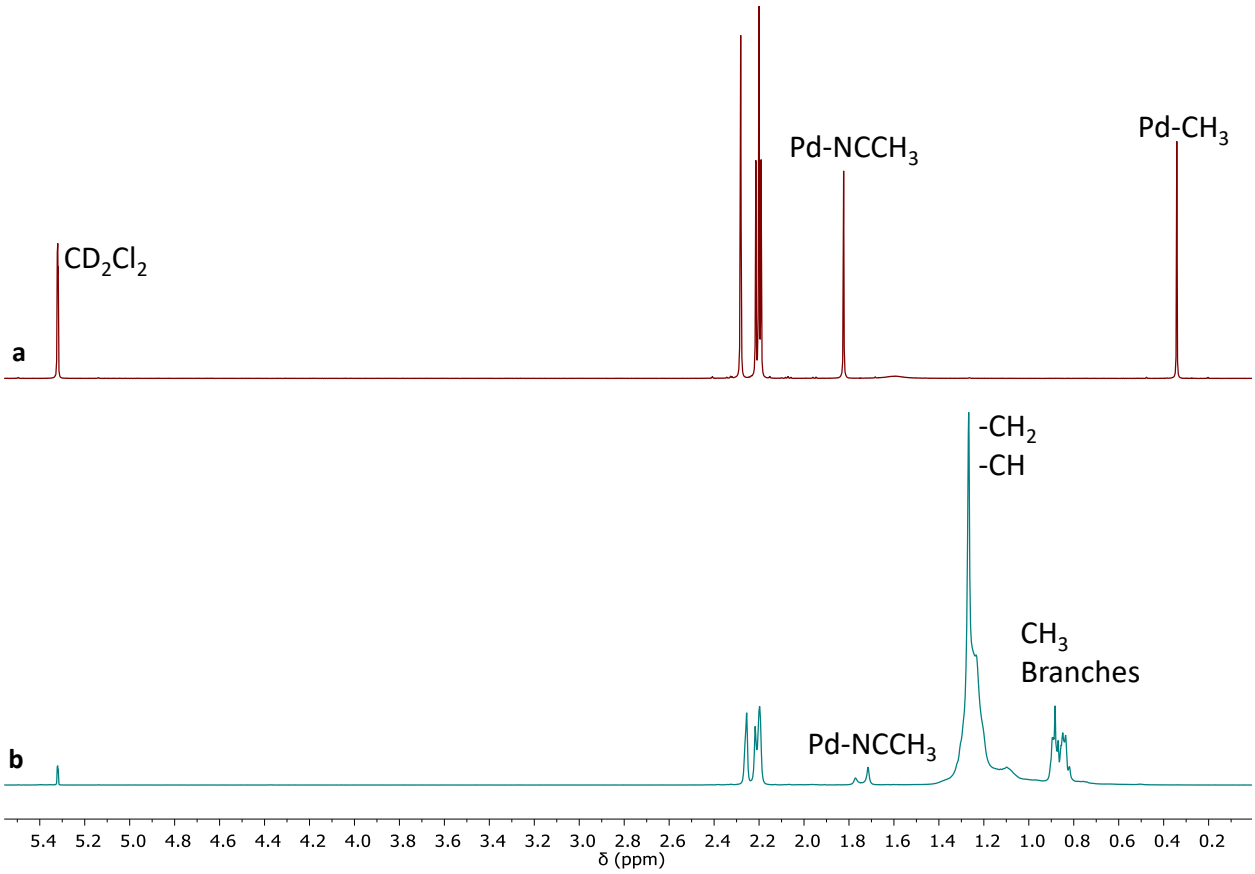

Figure S2.8. ^{1}H NMR spectra (CD_2Cl_2, 298 K) of: (a) **1b** and (b) **1b** + ethylene at t = 5 min.

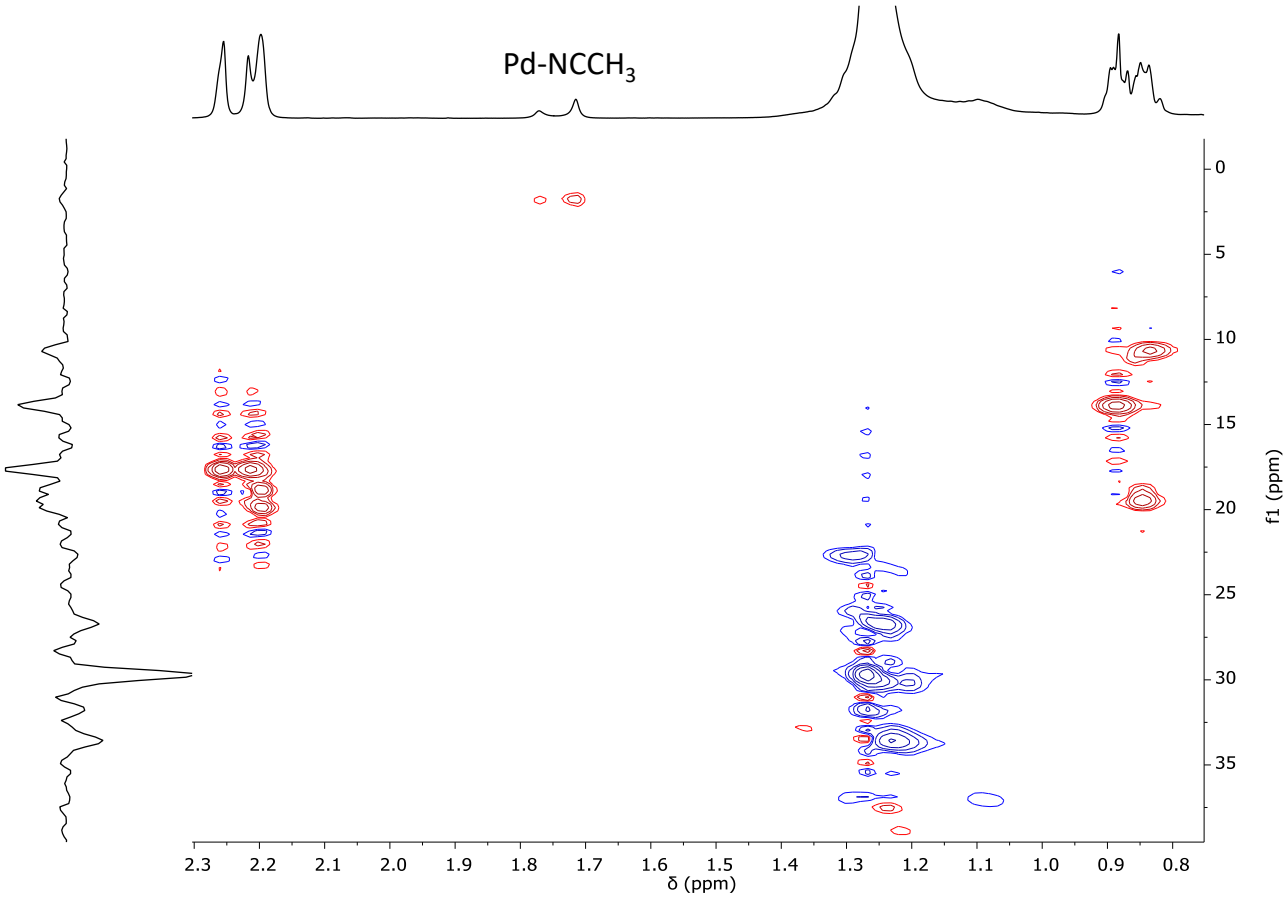

Figure S2.9. $^{1}H,^{13}C$ HSQC spectrum (CD_2Cl_2, 298 K) of the reaction mixture of **1b** with ethylene at t = 5 min.

***In situ* NMR reactivity of 1b with methyl acrylate (CD_2Cl_2, 298 K).**

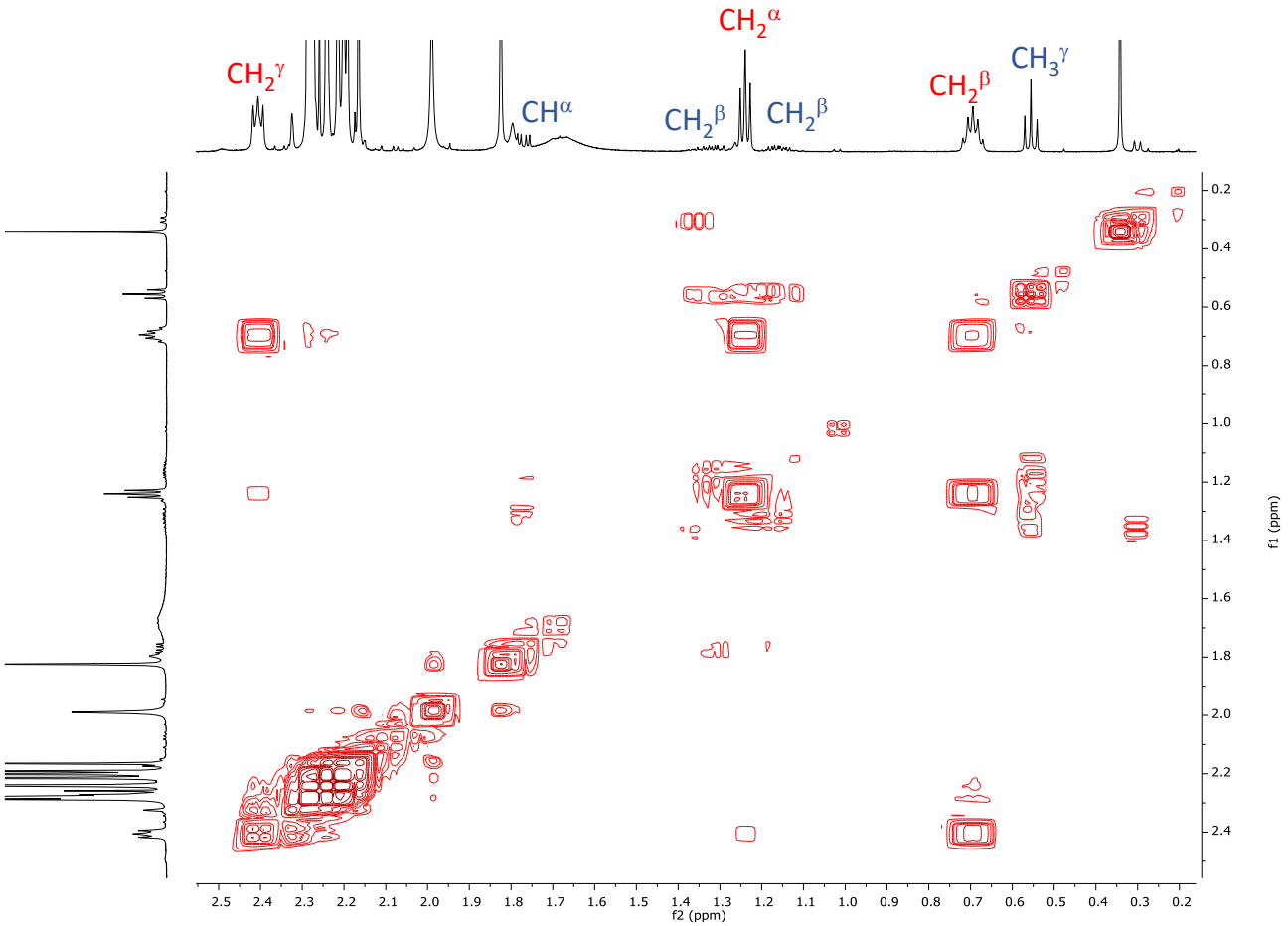

Figure S2.10. $^1H,^1H$ COSY spectrum (CD_2Cl_2, 298 K) of the reaction mixture of **1b** with methyl acrylate at t = 5 min.

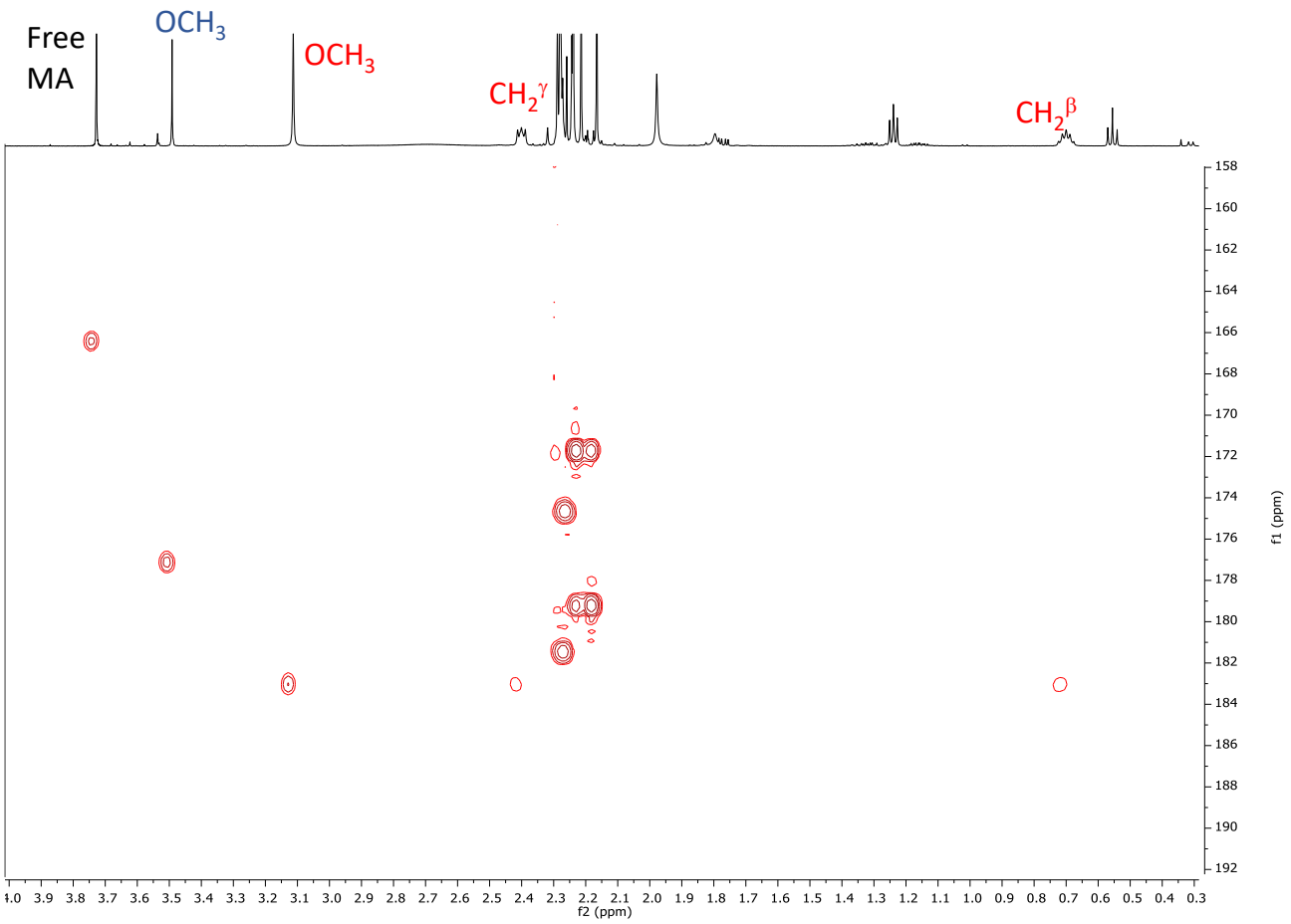

Figure S2.11. $^{1}H,^{13}C$ HMBC spectrum (CD_2Cl_2, 298 K) of the reaction mixture of **1b** with methyl acrylate at t = 120 min.

***In situ* NMR reactivity of 1b with ethylene (TFE-d_3, 298 K).**

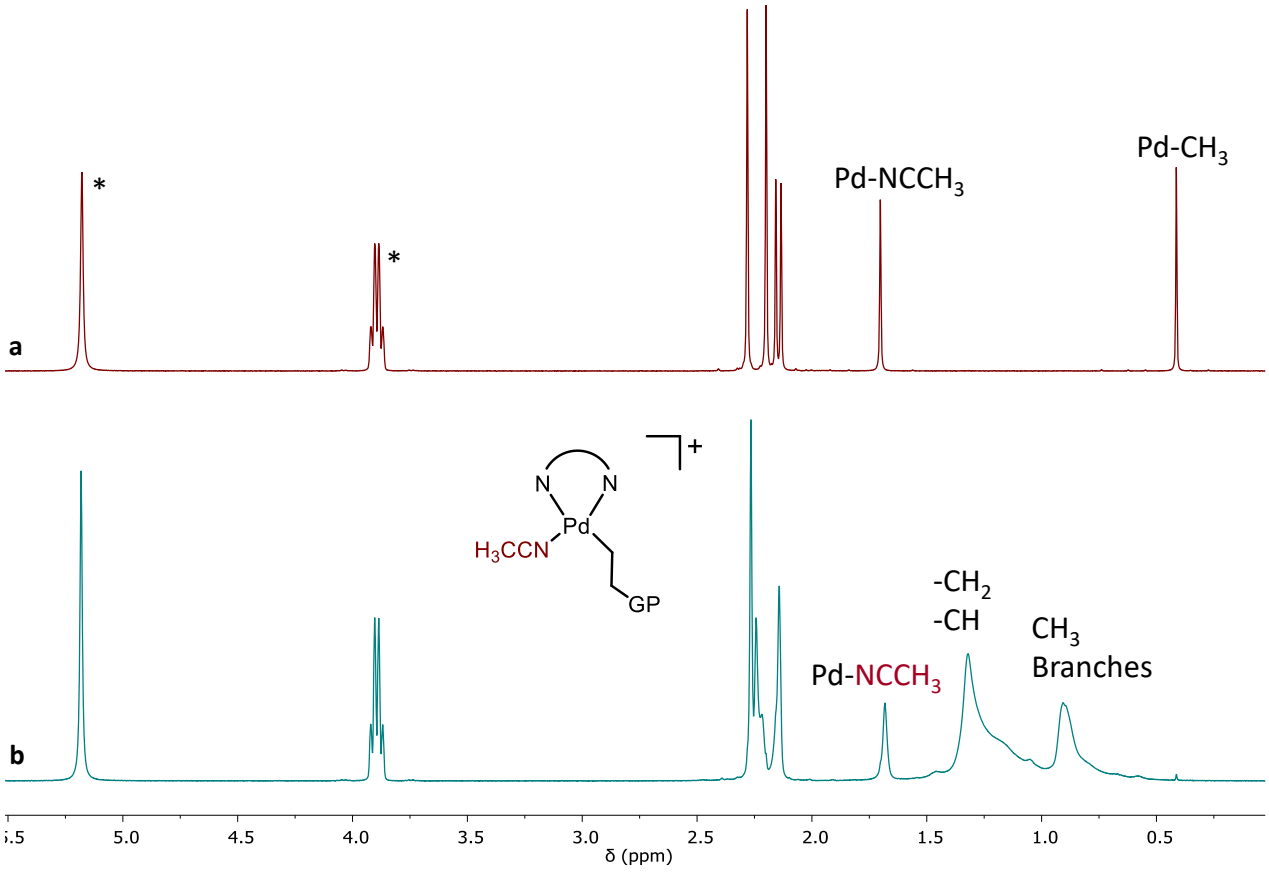

Figure S2.12. ^{1}H NMR spectra (TFE-d_3, 298 K) of (a) **1b** and (b) **1b** + ethylene at t = 5 min; *residual TFE. GP = growing polymer.

***In situ* NMR reactivity of 1b with methyl acrylate (TFE-d_3, 298 K).**

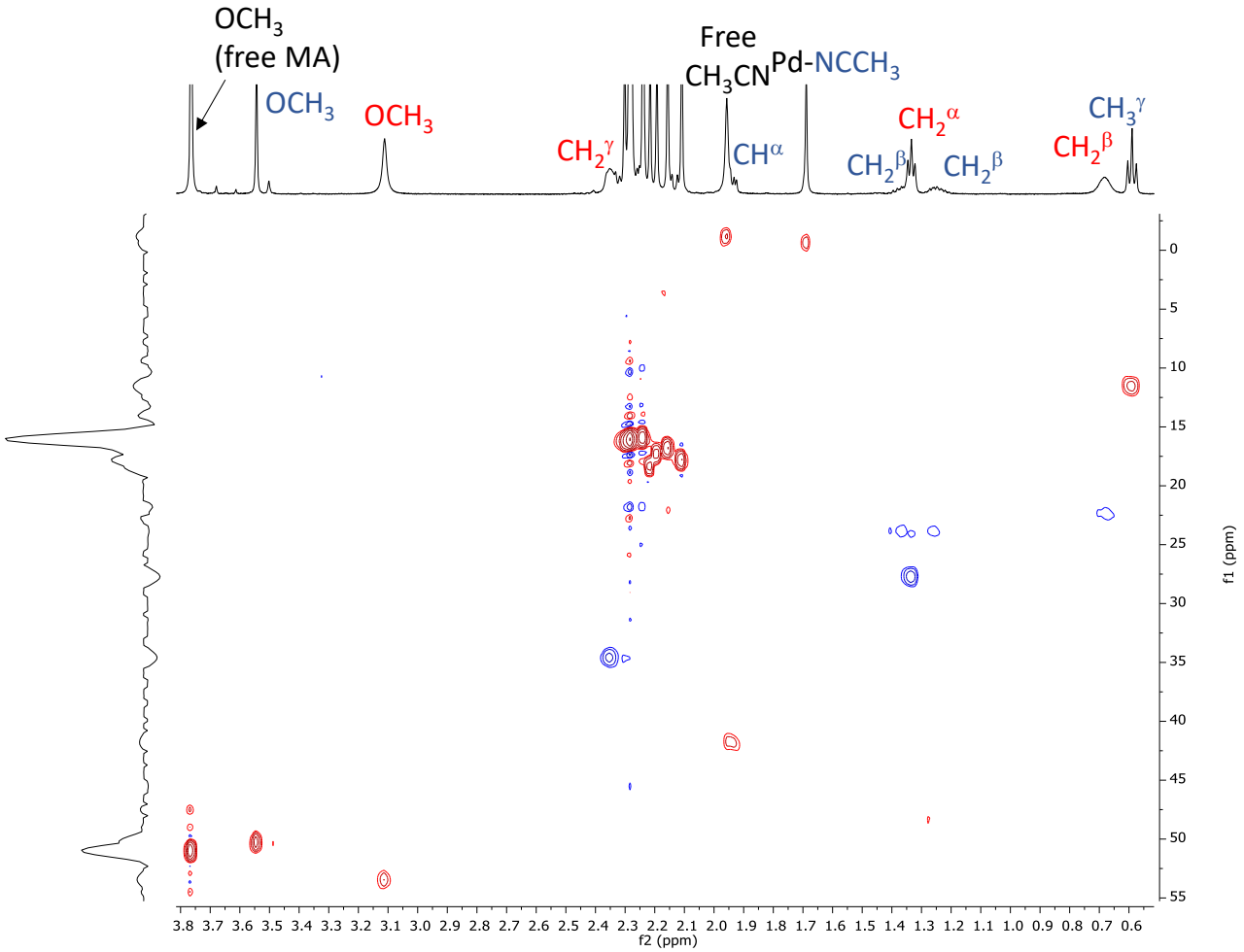

Figure S2.13. $^{1}H,^{13}C$ HSQC spectrum (TFE-d_3, 298 K) of the reaction mixture of **1b** with methyl acrylate at t = 30 min.

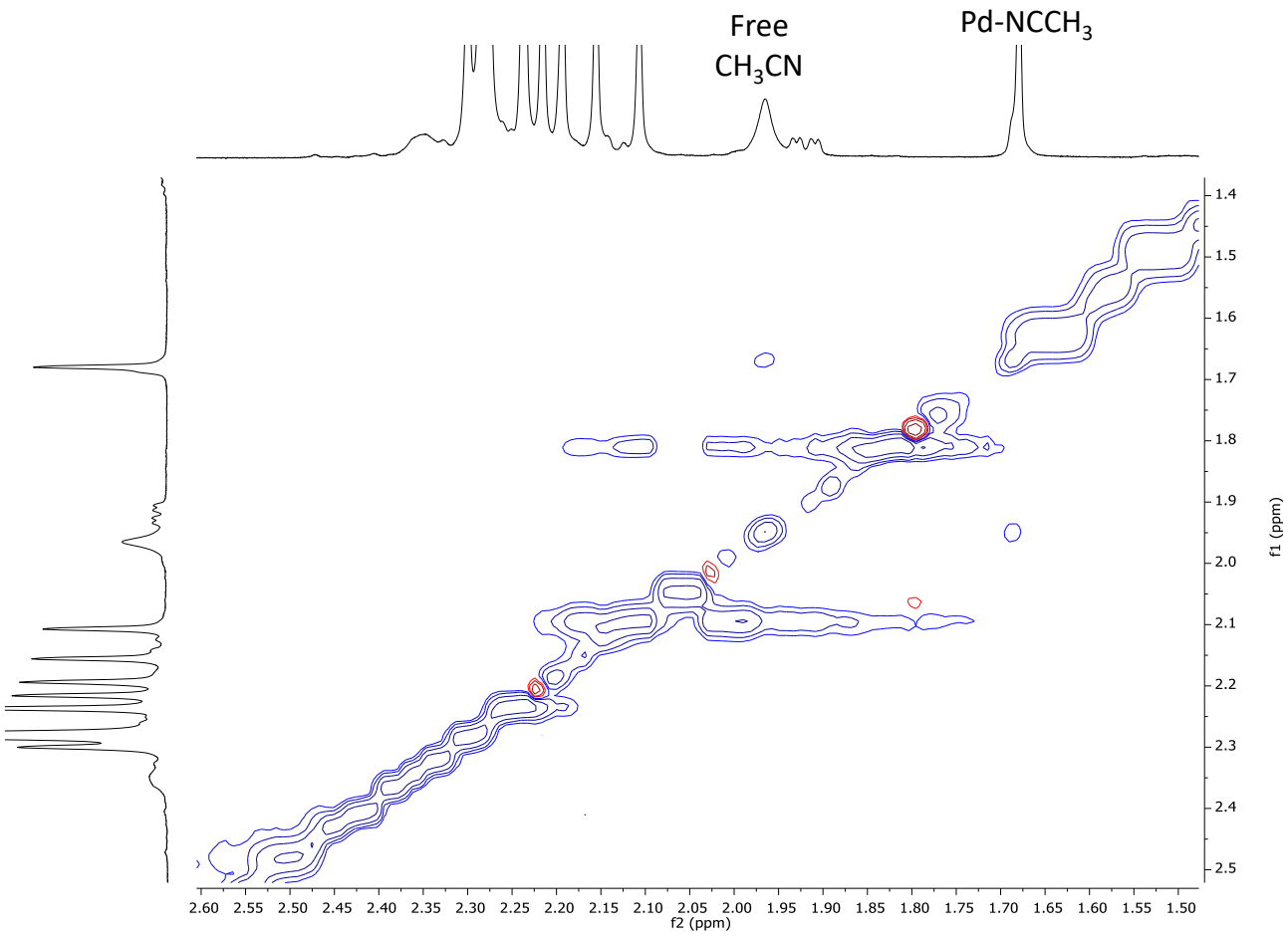

Figure S2.14. ^{1}H,^{1}H NOESY spectrum (TFE-d_3, 288 K) of the reaction mixture of **1b** with methyl acrylate at t = 120 min.

***In situ* NMR reactivity of 1b with methyl acrylate and ethylene (TFE-d_3, 298 K).**

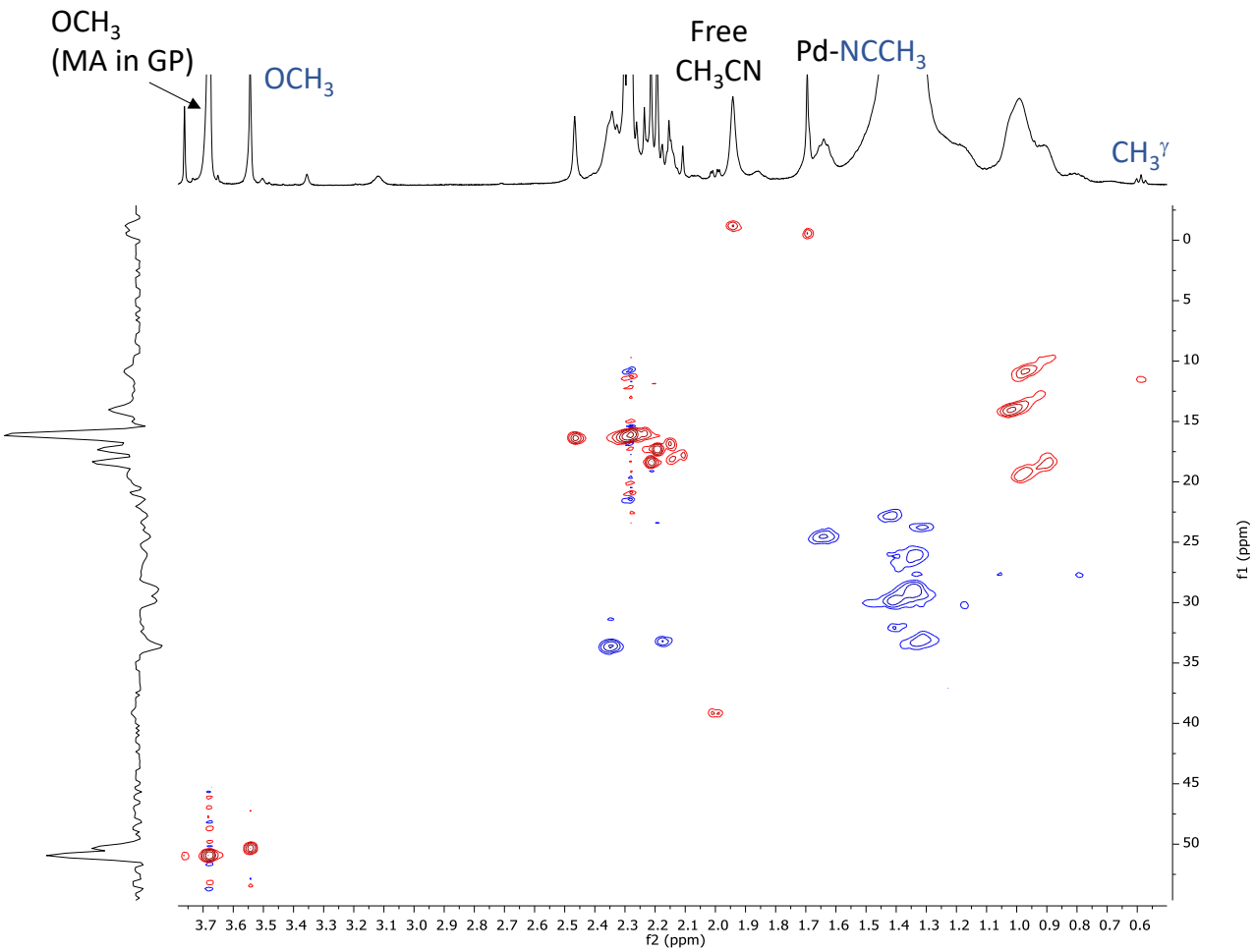

Figure S2.15. $^{1}H,^{13}C$ HSQC spectrum (TFE-d_3, 298 K) of the reaction mixture of **1b** with methyl acrylate and ethylene at t = 3 days.

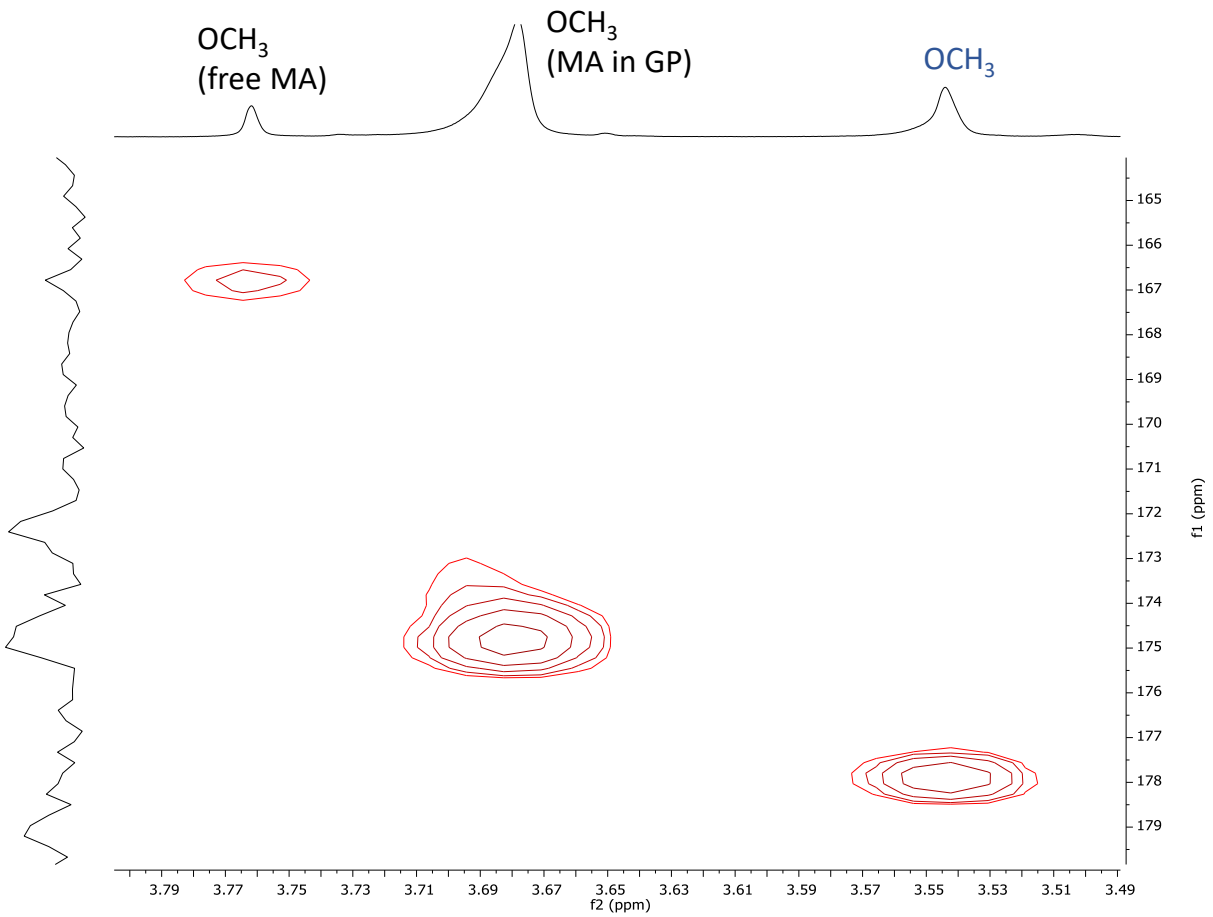

Figure S2.16. $^{1}H,^{13}C$ HMBC spectrum (TFE-d_3, 298 K) of the reaction mixture of **1b** with methyl acrylate and ethylene at t = 3 days.

***In situ* NMR reactivity of 1S^{Ph} with ethylene (CD_2Cl_2, 298 K).**

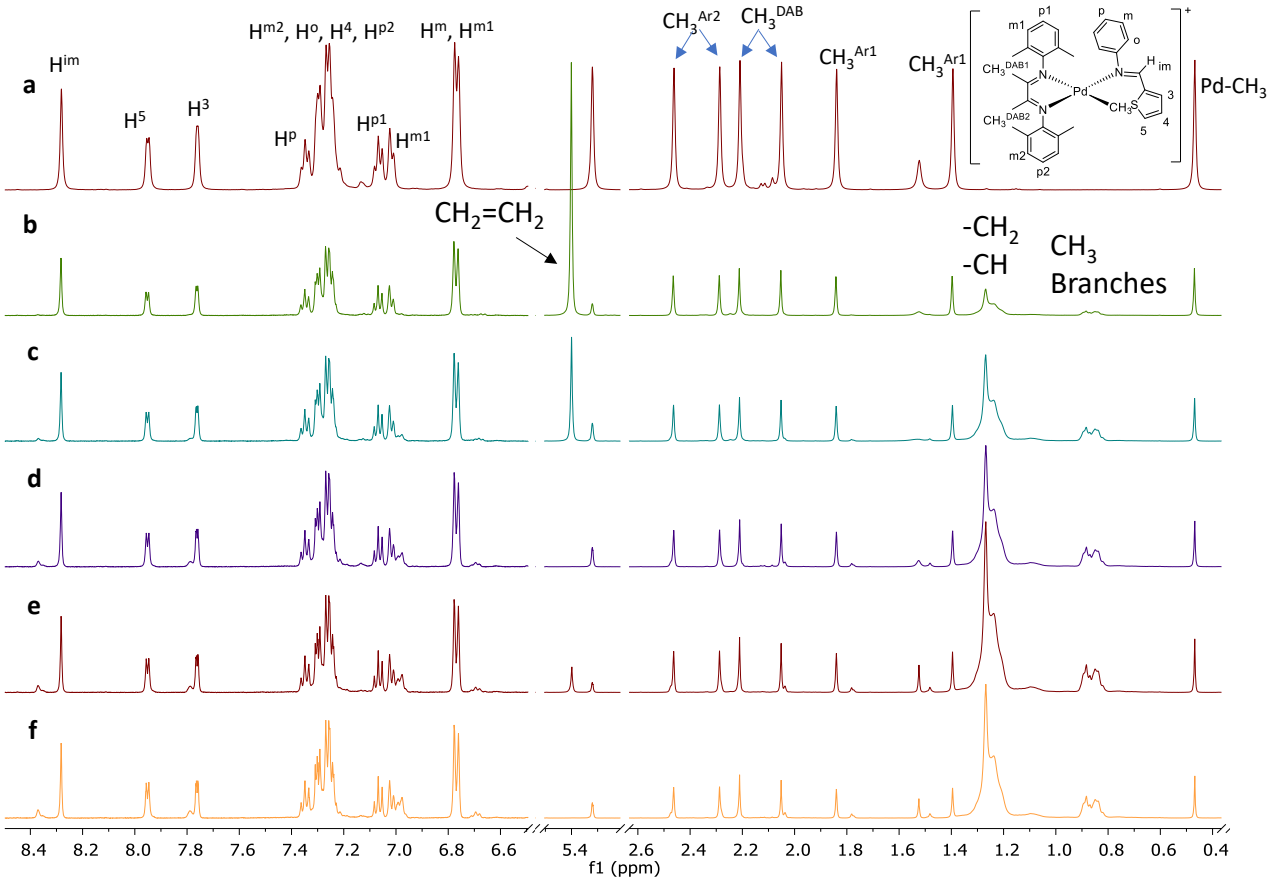

Figure S2.17. ^{1}H NMR spectra (CD_2Cl_2, 298 K) of: (a) **1S^{Ph}**; **1S^{Ph}** + ethylene at (b) t = 5 min, (c) t = 15 min, (d) t = 45 min; **1S^{Ph}** + second addition of ethylene at (e) t = 5 min and (f) t = 45 min; aromatic and aliphatic region not on scale.

***In situ* NMR reactivity of 1S^{Ph} with methyl acrylate (CD_2Cl_2, 298 K).**

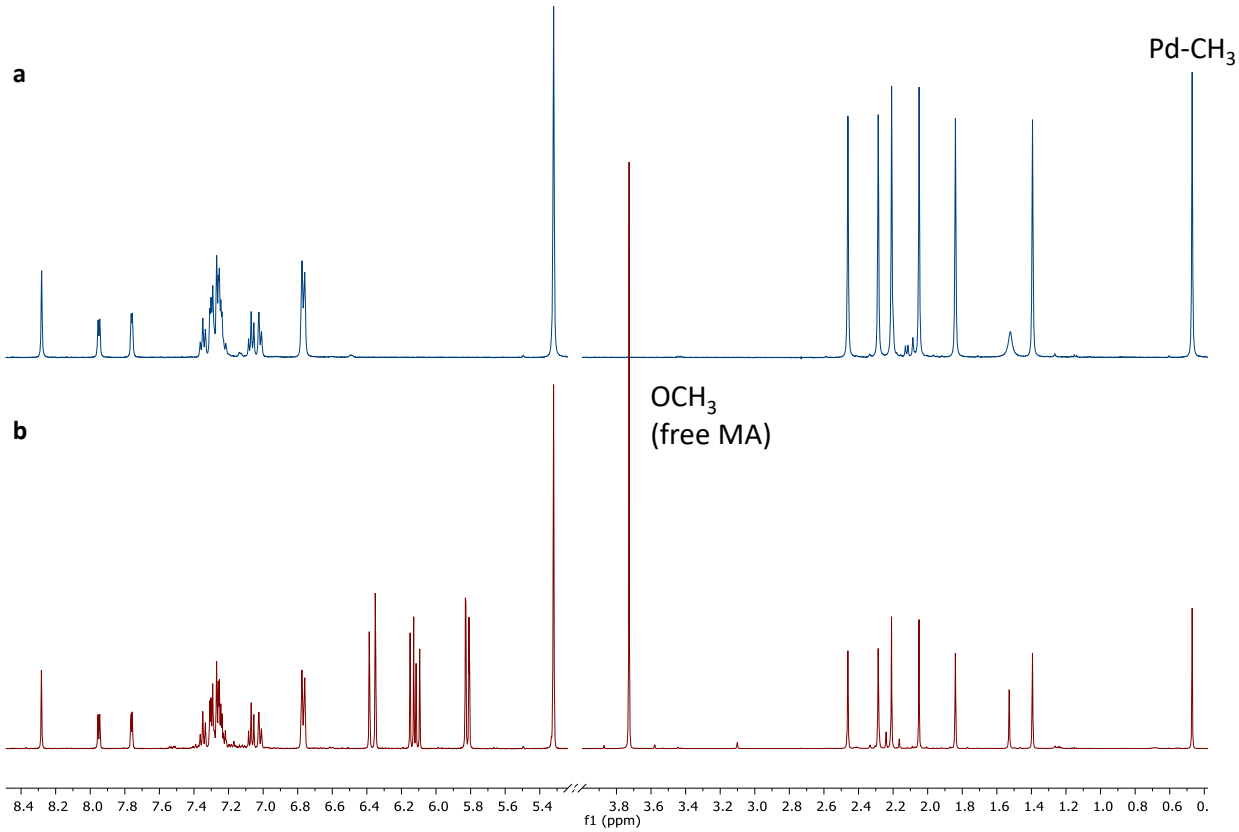

Figure S2.18. ^{1}H NMR spectra (CD_2Cl_2, 298 K) of (a) **1S^{Ph}** and (b) **1S^{Ph}** + MA at t = 2 h; aromatic and aliphatic region not on scale.

***In situ* NMR reactivity of 1S^{Ph} with methyl acrylate and ethylene (CD_2Cl_2, 298 K).**

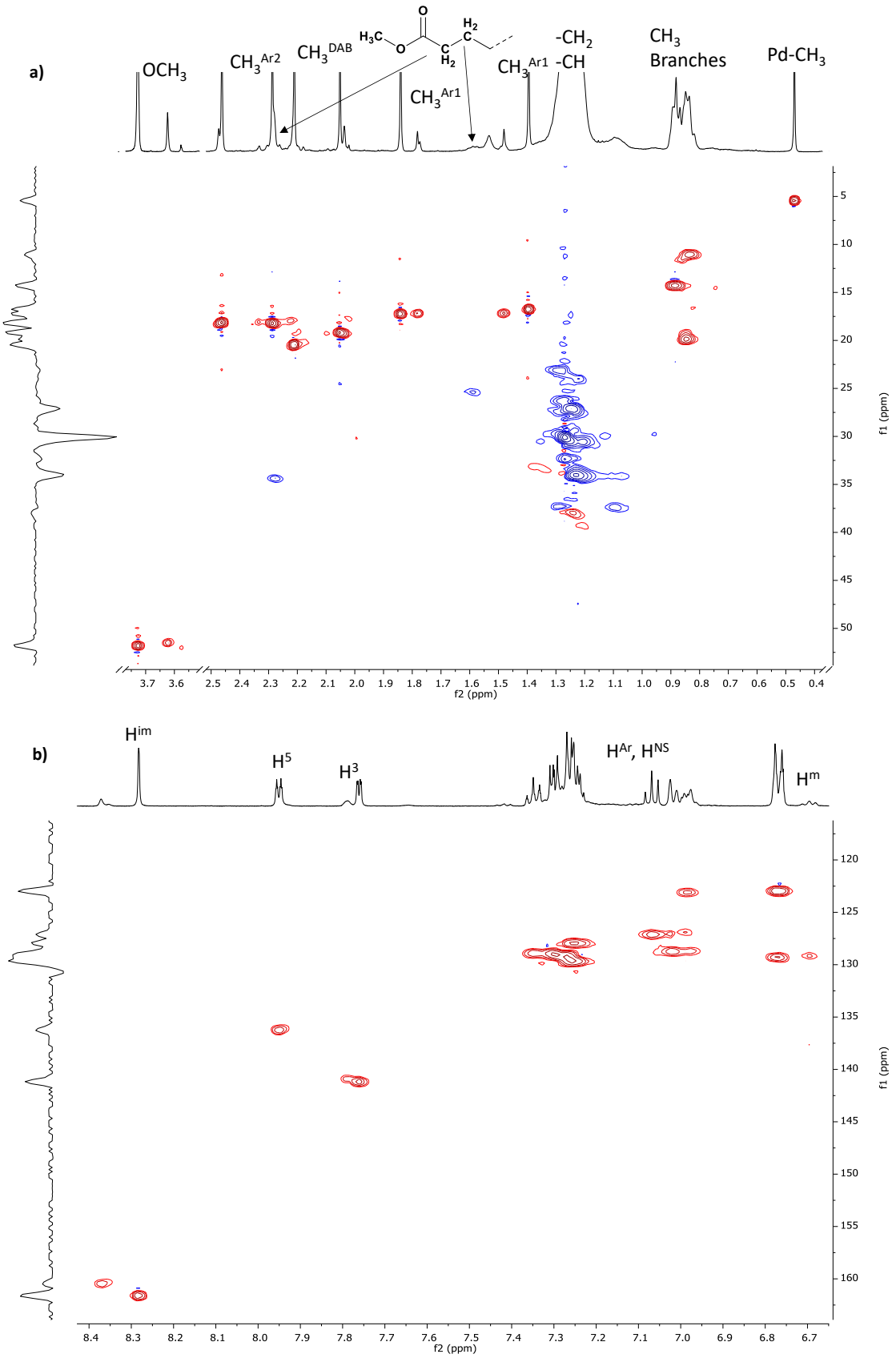

Figure S2.19. $^{1}H,^{13}C$ HSQC spectrum (CD_2Cl_2, 298 K) of reaction mixture of **1S^{Ph}** with methyl acrylate and ethylene at t = 90 min: a) region of aliphatic signals; b) region of aromatic signals.

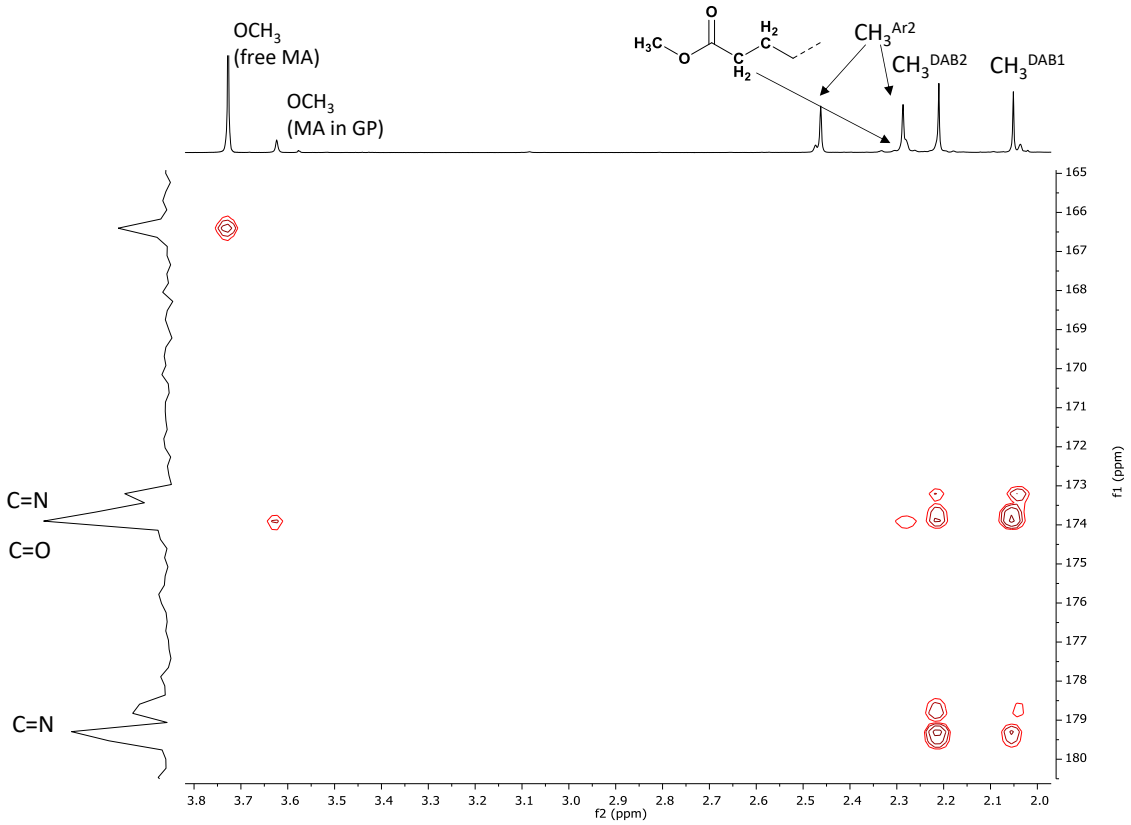

Figure S2.20. $^{1}H,^{13}C$ HMBC spectrum (CD_2Cl_2, 298 K) of reaction mixture of **1S^{Ph}** with methyl acrylate and ethylene at t = 90 min: region of carbonyl and iminic carbon signals. GP = growing polymer.

***In situ* NMR reactivity of 1S^{Ph} with methyl acrylate (TFE-d$_3$, 298 K).**

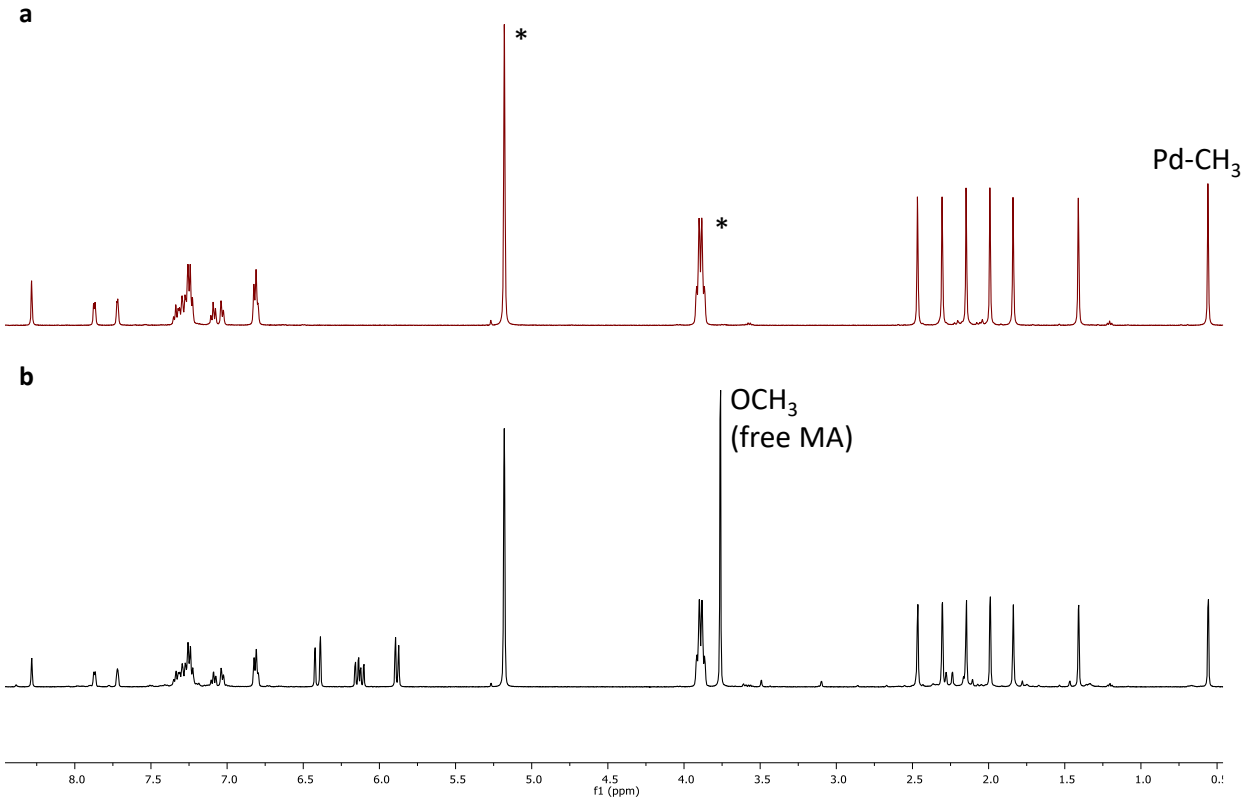

Figure S2.21. ^{1}H NMR spectra (TFE-d$_3$, 298 K) of (a) **1S^{Ph}** and (b) **1S^{Ph}** + MA at t = 2h; *residual TFE.

***In situ* NMR reactivity of 1S^{Ph} with methyl acrylate and ethylene (TFE-d$_3$, 298 K).**

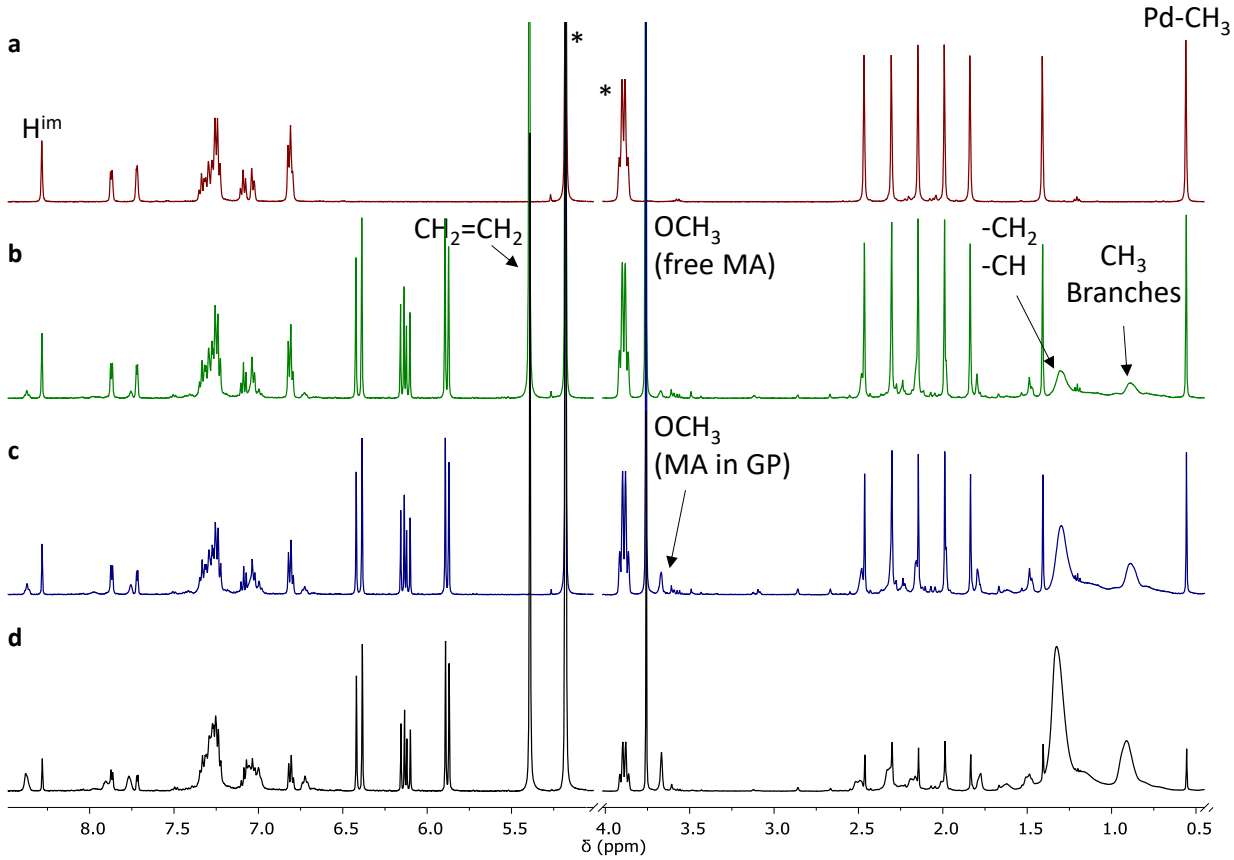

Figure S2.22. ^{1}H NMR spectra (TFE-d$_3$, 298 K) of: (a) **1S^{Ph}**; **1S^{Ph}** + MA + ethylene at (b) t = 5 min, (c) t = 45 min and (d) t = 2 h recorded immediately after the second addition of ethylene (aromatic and aliphatic region not on scale); *residual TFE. GP = growing polymer.

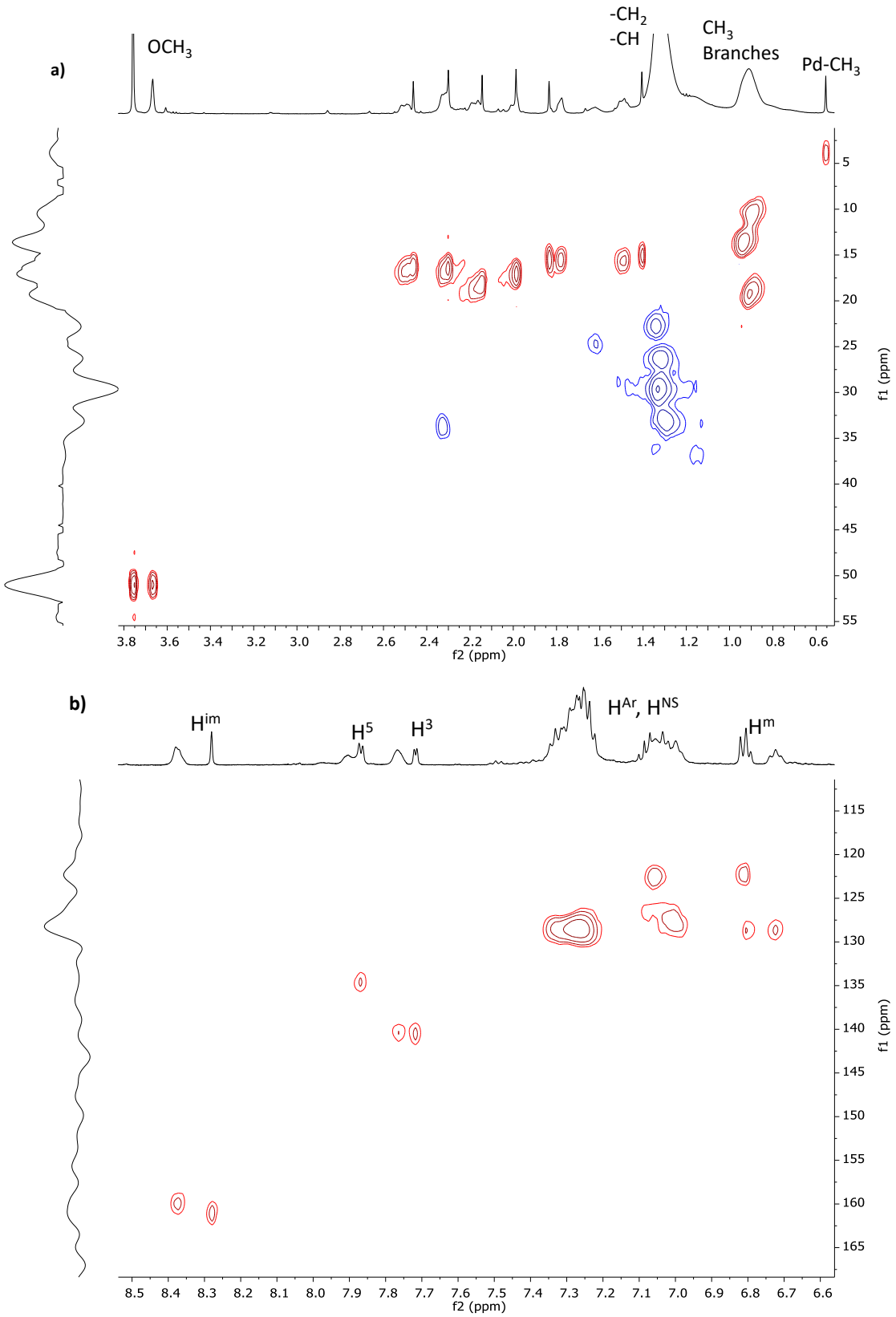

Figure S2.23. $^{1}H,^{13}C$ HSQC spectrum (TFE-d_3, 298 K) of reaction mixture of **1S^{Ph}** with methyl acrylate and ethylene at t = 2 h: a) region of aliphatic signals; b) region of aromatic signals.

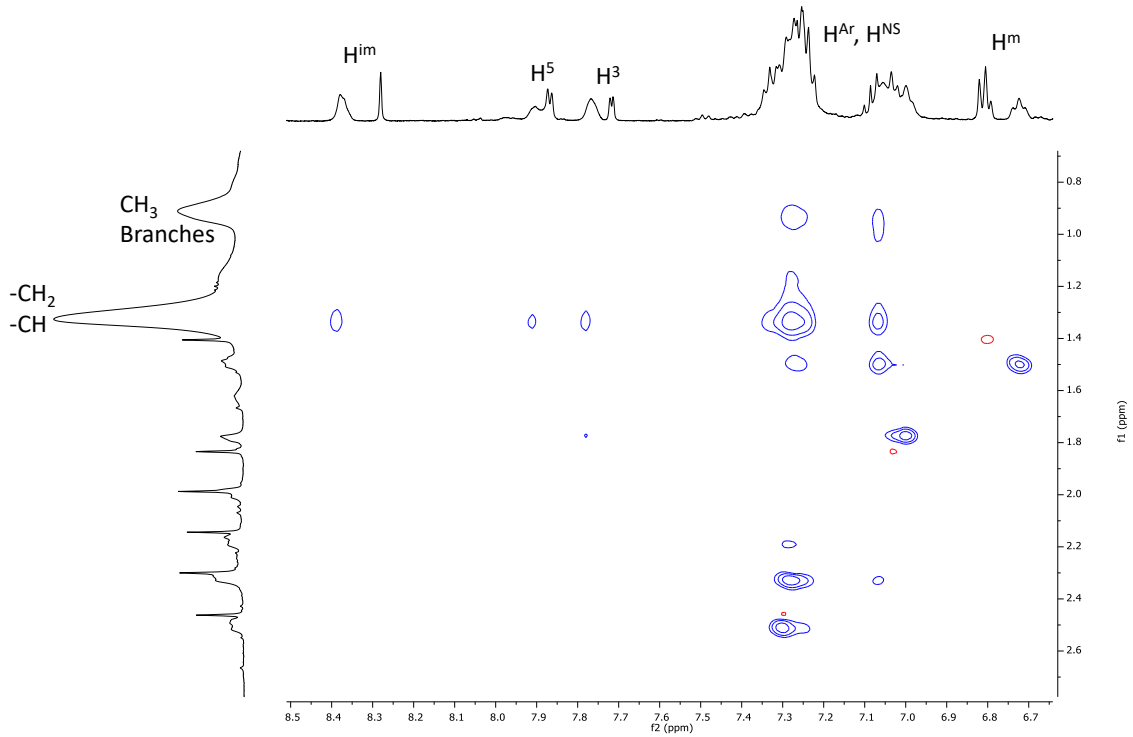

Figure S2.24. $^{1}H,^{1}H$ NOESY spectrum (TFE-d_3, 298 K) of reaction mixture of **1S^{Ph}** with methyl acrylate and ethylene at t = 2 h: region of cross peaks among aromatic and aliphatic signals.

Computational details

Chart S2.1. The possible metallacycles originated from the insertion of MA into the Pd-alkyl chain respectively from **1b** (on top) or **1S^{Ph}** (on bottom) and their computed free energy.

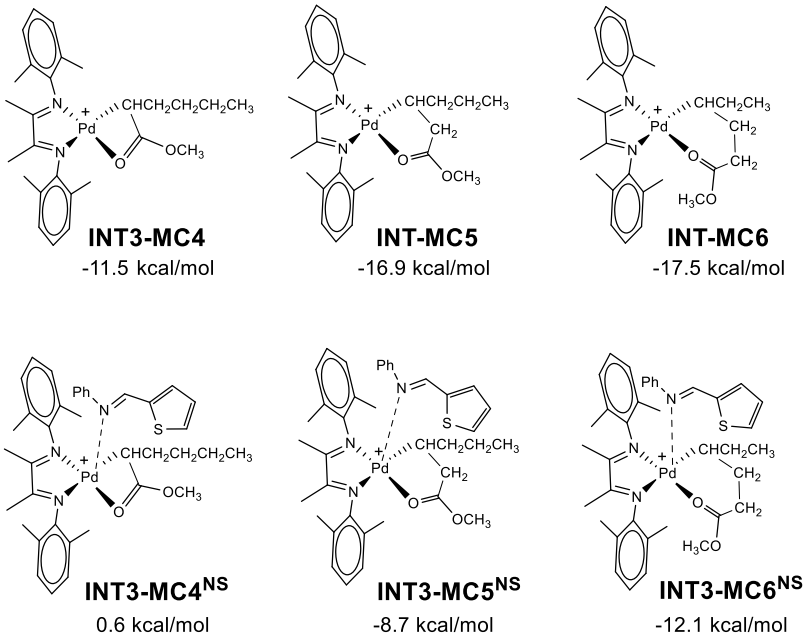

Appendix Chapter 3.

NMR characterization of neutral complexes.

NMR characterization of 3a (CD_2Cl_2, 298 K).

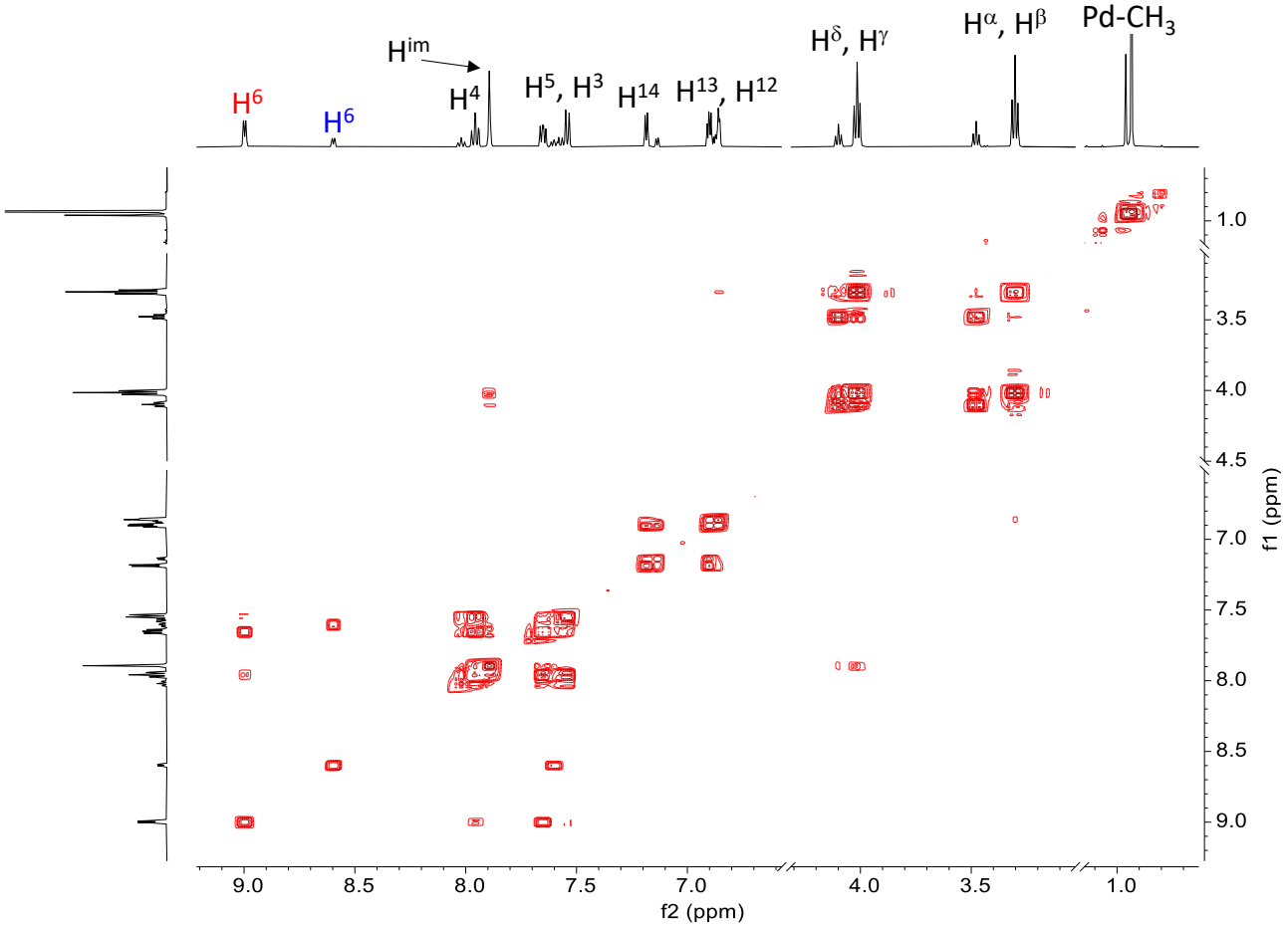

Figure S3.1. $^1H,^1H$ COSY spectrum (CD_2Cl_2, 298 K) of **3a** at t = 2 h.

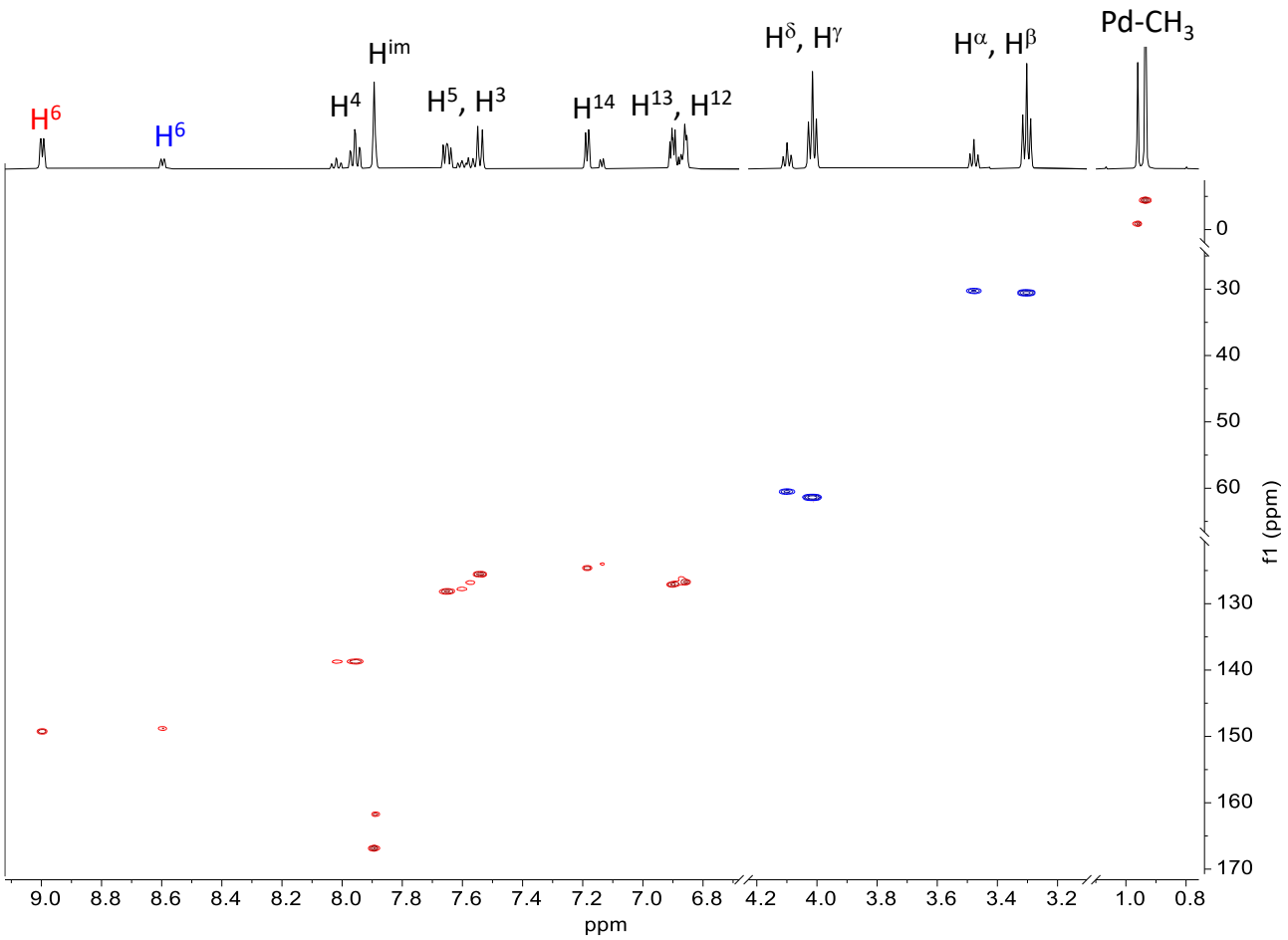

Figure S3.2. $^{1}H,^{13}C$ HSQC spectrum (CD_2Cl_2, 298 K) of **3a** at t = 2 h.

NMR characterization of 4a (CD_2Cl_2, 298 K).

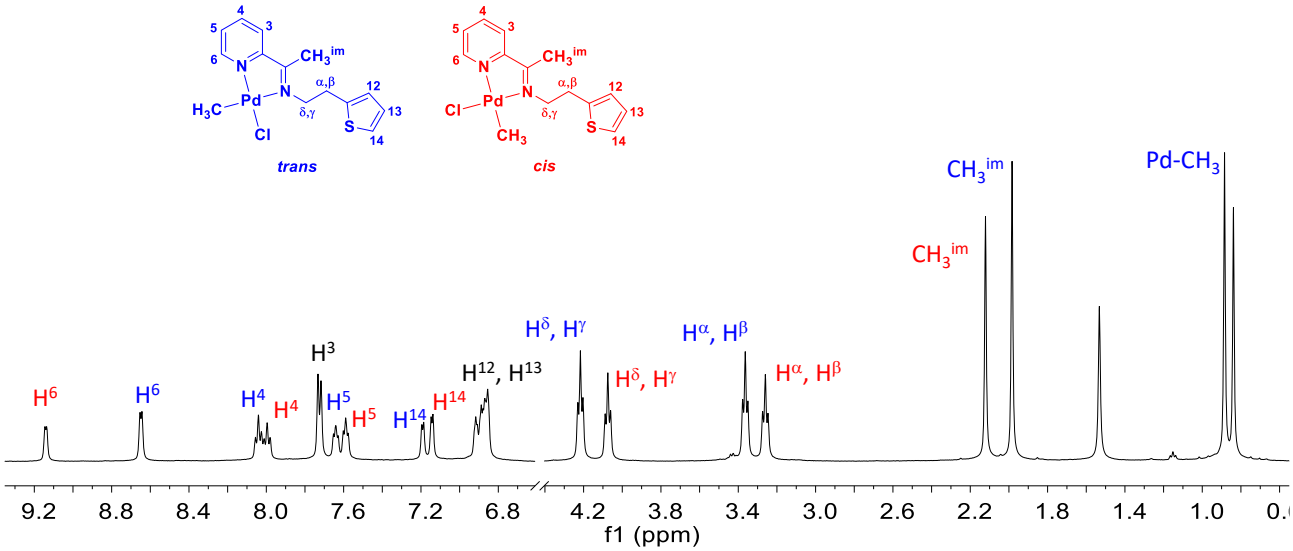

Figure S3.3. ^{1}H NMR spectrum (CD_2Cl_2, 298 K) of **4a** at = 1 min.

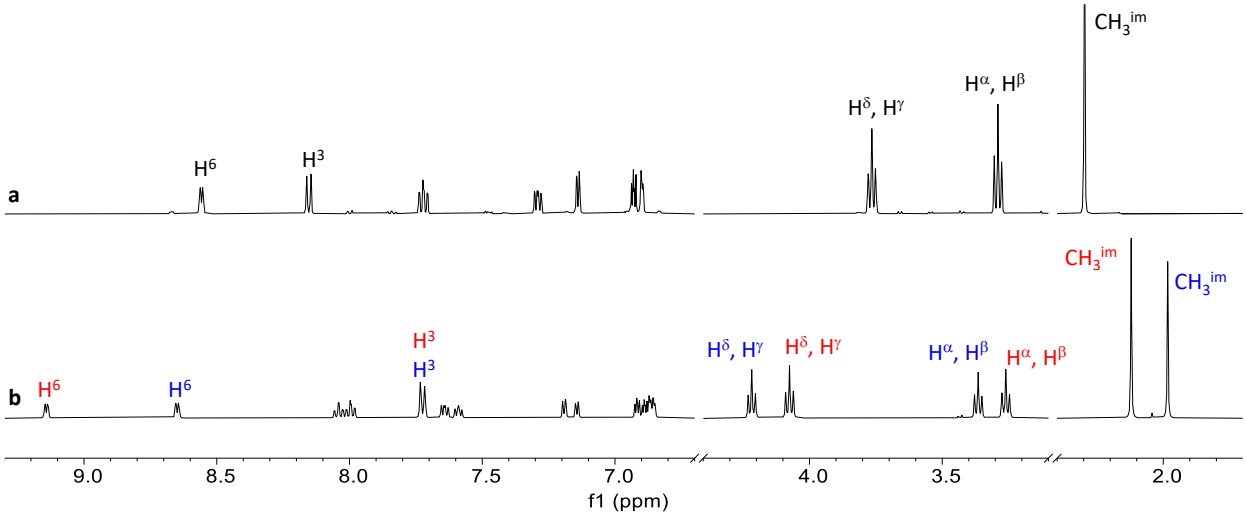

Figure S3.4. ^{1}H NMR spectra (CD_2Cl_2, 298 K) of (a) **4** and (b) **4a** at t = 2 h.

X-Ray crystallography.

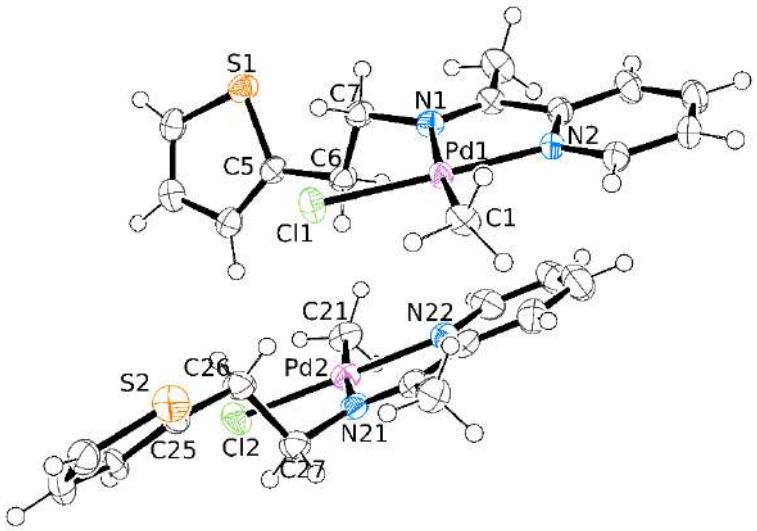

Figure S3.5. ORTEP drawing (50% probability ellipsoids) of the two independent molecules of compound **4a** in the crystal structure. Two PF_6^- anions have been omitted for the sake of clarity.

Table S3.1. Most significant distances and angles for complexes *cis*-**3a** and *trans*-**4a**.

	cis-**3a**	*trans*-**4a**			
	Distances (Å)				
Pd1-C1	2.0587(2)	**Pd1-C1**	2.056(3)	**Pd2-C21**	2.111(2)
Pd1-Cl1	2.3001(7)	**Pd1-Cl1**	2.297(2)	**Pd2-Cl2**	2.279(3)
Pd1-N1	2.0495(1)	**Pd1-N1**	2.126(2)	**Pd2-N21**	2.096(3)

Pd1-N2	2.1338(2)	**Pd1-N2**	2.040(3)	**Pd2-N22**	2.064(3)
	Angles (°)				
C1-Pd1-Cl1	90.66(4)	**C1-Pd1-Cl1**	88.04(9)	C21-Pd2-Cl2	87.5(4)
C1-Pd1-N2	173.88(5)	**C1-Pd1-N1**	173.74(1)	N21-Pd2-C21	172.4(4)
N1-Pd1-C1	95.01(6)	**N1-Pd1-Cl1**	97.39(7)	N21-Pd2-Cl2	98.96(1)
N1-Pd1-Cl1	173.50(4)	**N2-Pd1-C1**	95.61(1)	N22-Pd2-C21	94.5(4)
N1-Pd1-N21	79.41(5)	**N2-Pd1-Cl1**	176.37(7)	N22-Pd2-Cl2	177.43(1)
N2-Pd1-Cl1	95.06(3)	**N2-Pd1-N1**	78.99(9)	N22-Pd2-N21	78.88(1)
	Dihedral angle (°)				
[S1]-[Pd1]	76.12(5)	**[S1]-[Pd1]**	59.0(1)	**[S2]-[Pd2]**	26.7(3)
	Torsion angles (°)				
Pd1–N1–C7–C6	178.39(1)	**Pd1–N1–C7–C6**	92.1(3)	**Pd2–N21–C27–C26**	83.6(3)
N1-C7-C6-C5	176.1(1)	**N1-C7-C6-C5**	178.3(2)	**N21-C17-C26-C25**	175.5(3)

NMR characterization of cationic complexes.

NMR characterization of 3b (CD_2Cl_2, 298 K).

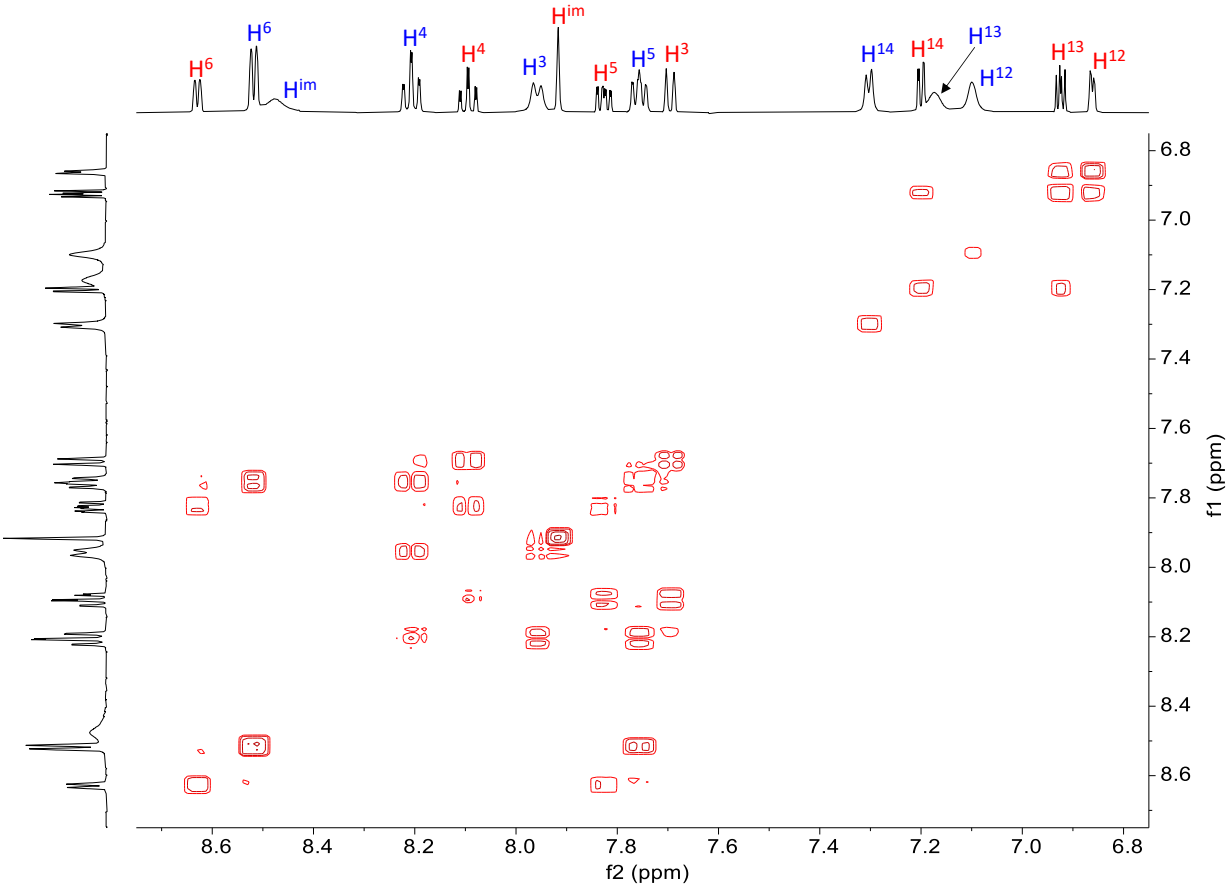

Figure S3.6. $^1H,^1H$ COSY spectrum (CD_2Cl_2, 298 K) of **3b**; aromatic region.

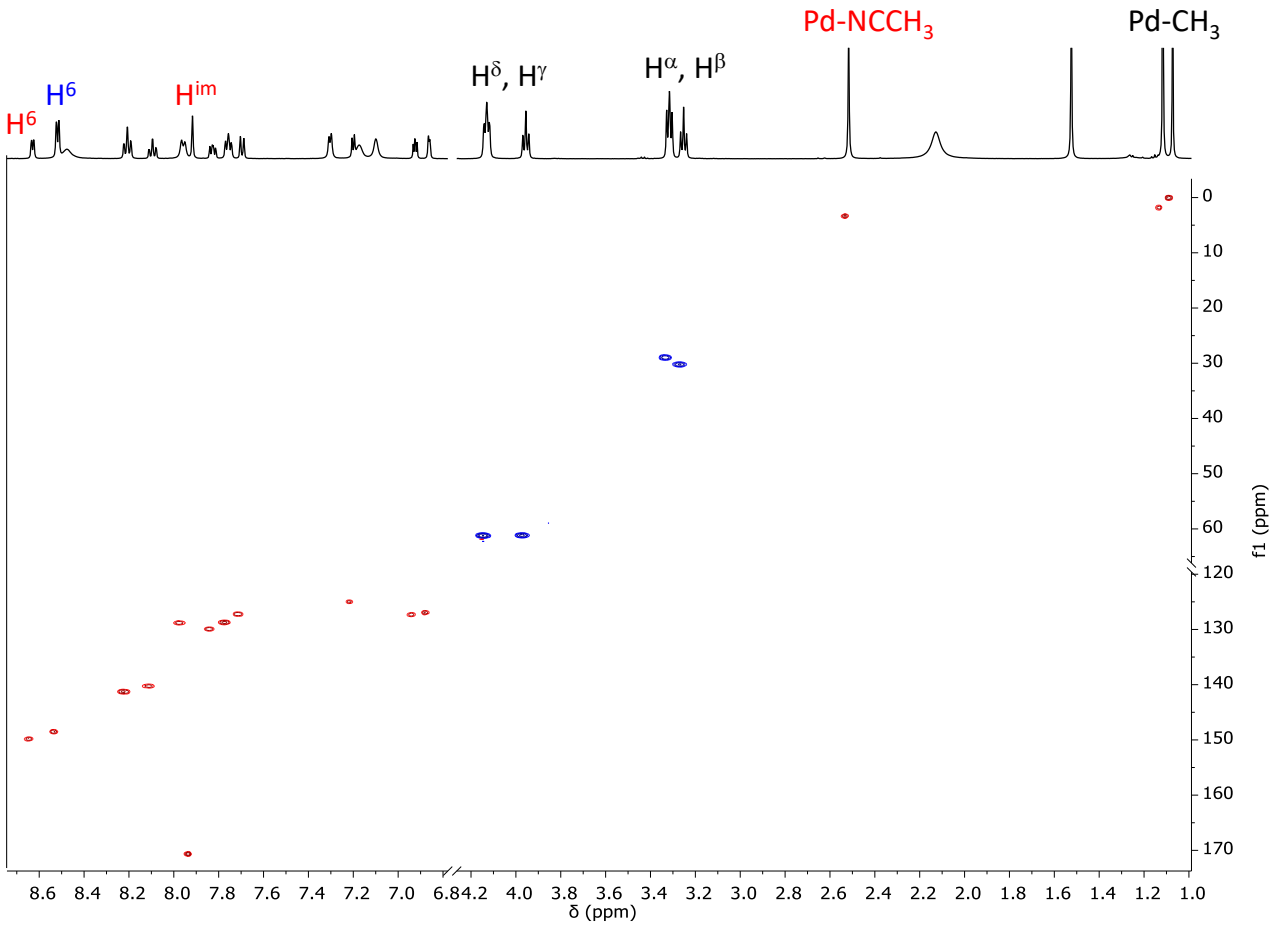

Figure S3.7. $^{1}H,^{13}C$ HSQC spectrum (CD_2Cl_2, 298 K) of **3b**.

NMR characterization of 4b (CD_2Cl_2, 298 K).

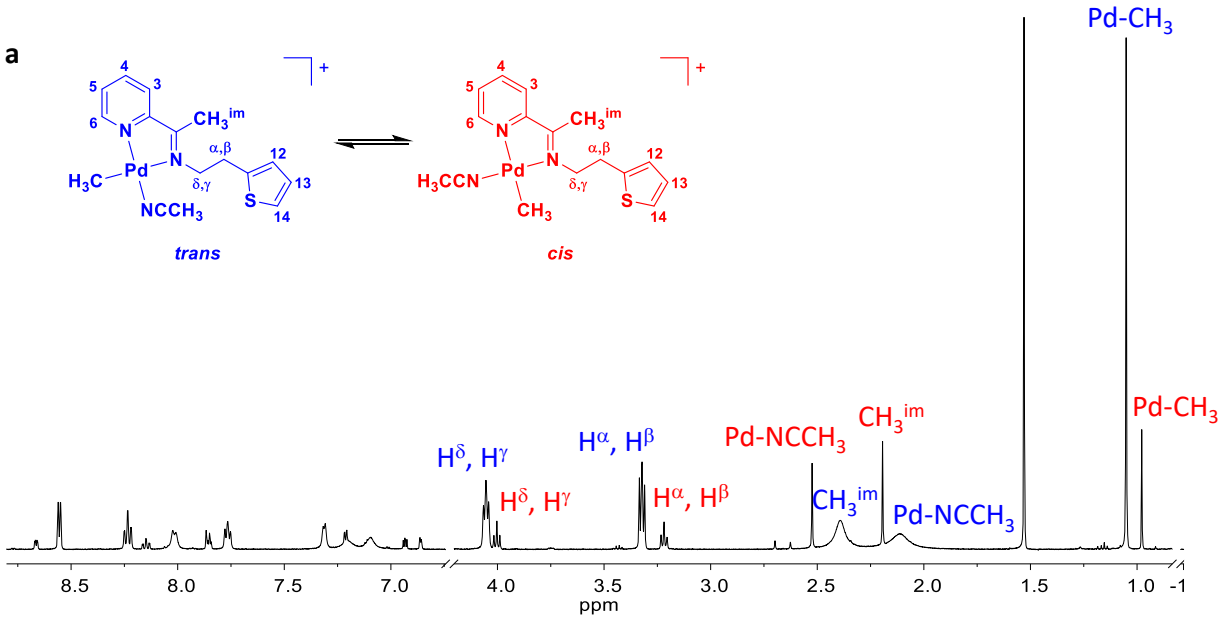

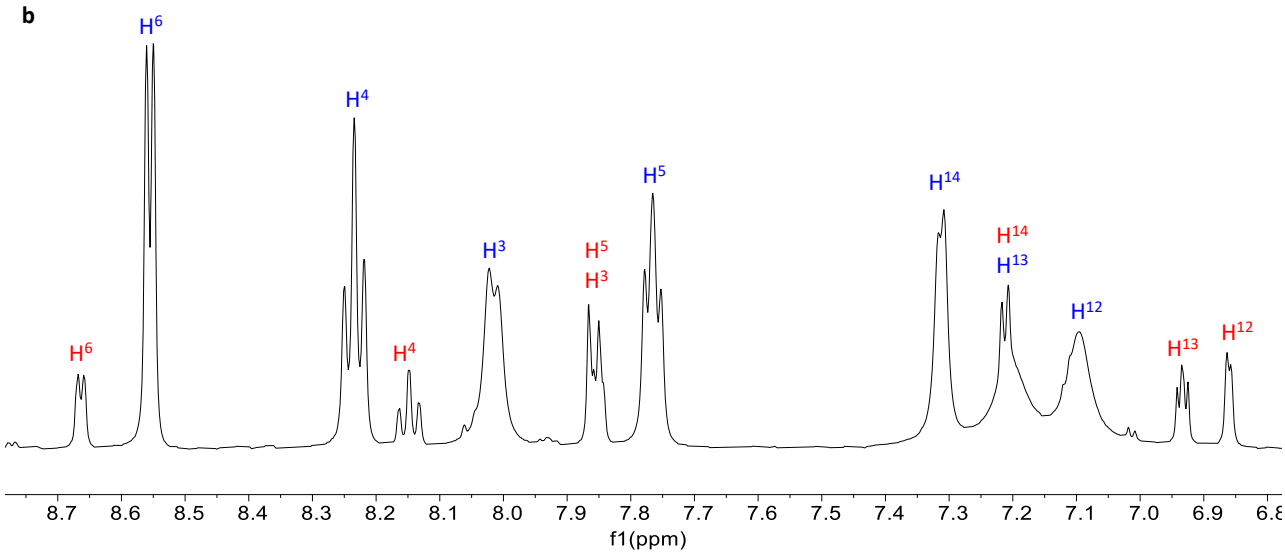

Figure S3.8. ^{1}H NMR spectrum (CD_2Cl_2, 298 K) of **4b**; (a) full spectrum, (b) aromatic region.

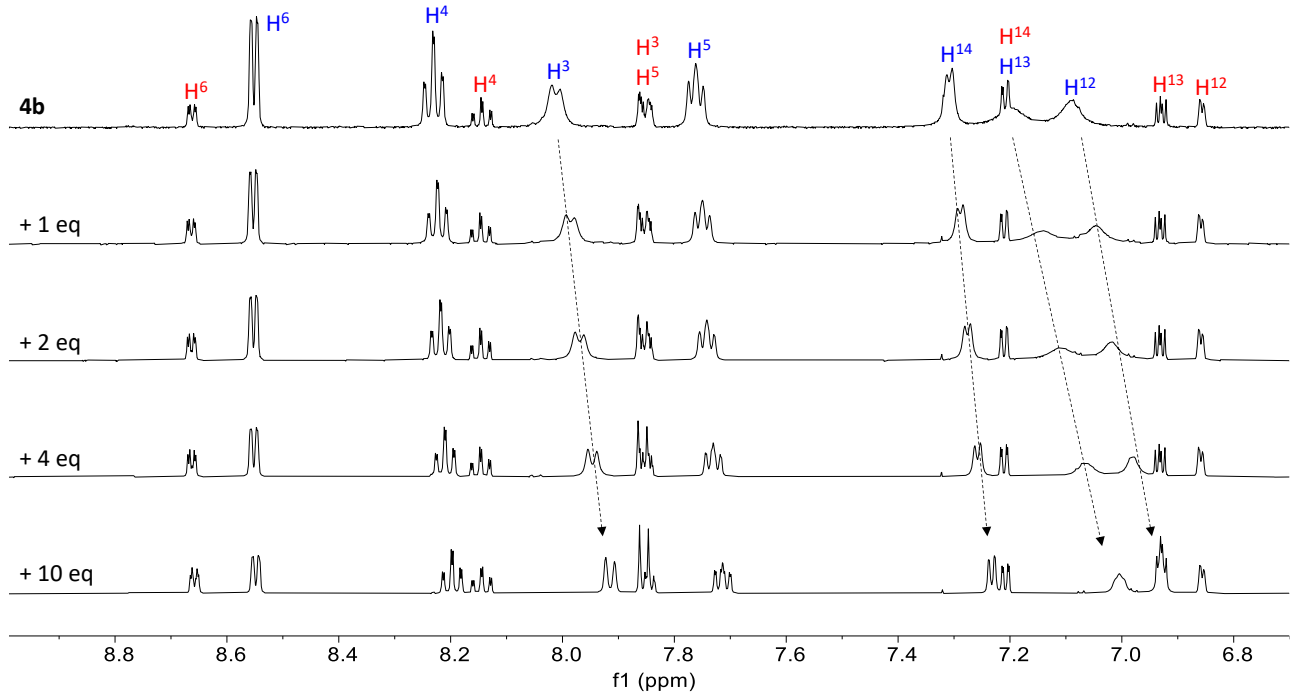

Figure S3.9. ^{1}H NMR spectra (CD_2Cl_2, 298 K) of progressive additions of acetonitrile to **4b** solution; aromatic region.

NMR characterization of 3c (CD_2Cl_2, 298 K).

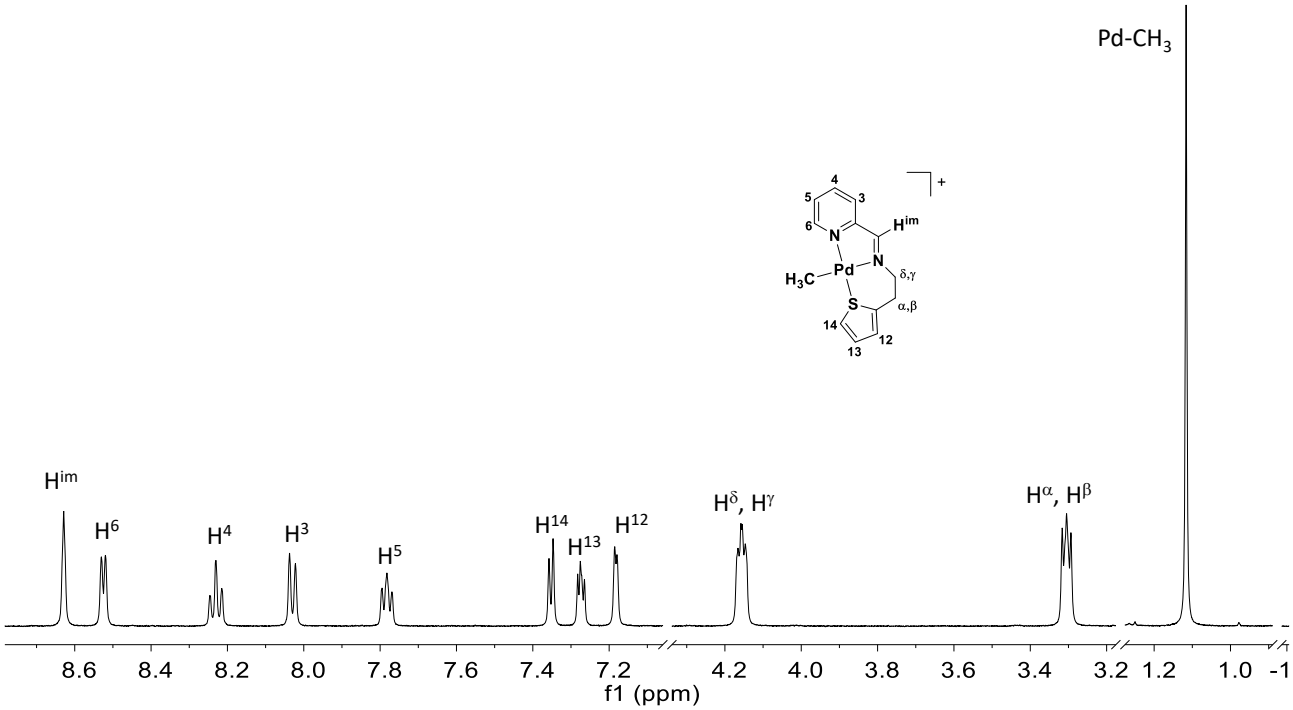

Figure S3.10. ^{1}H NMR spectrum (CD_2Cl_2, 298 K) of **3c**.

NMR characterization of 4c (CD_2Cl_2, 298 K).

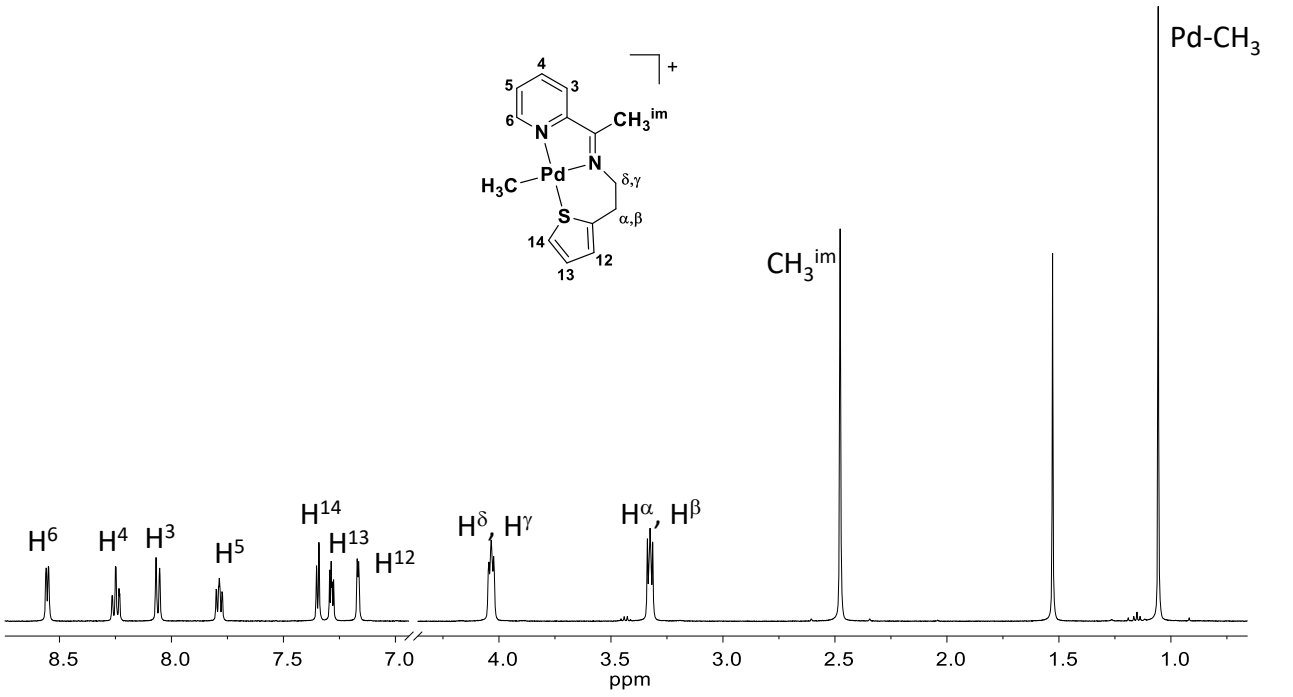

Figure S3.11. ^{1}H NMR spectrum (CD_2Cl_2, 298 K) of **4c**.

X-Ray crystallography.

Table S3.2. Most significant distances and angles for complexes **2c** and **3c**.

	3c	**4c**
	Distances (Å)	
Pd1-C1	2.0372(2)	2.039(3)
Pd1-N1	2.1387(2)	2.114(3)
Pd1-N2	2.0625(2)	2.061(3)
Pd1-S1	2.2683(5)	2.2612(1)
	Angles (°)	
C1-Pd1-N1	172.53(7)	174.21(1)
C1-Pd1-N2	93.60(7)	95.03(1)
C1-Pd1-S1	90.28(6)	85.50(1)
N1-Pd1-S1	97.10(5)	100.08(8)
N1-Pd1-N2	79.26(6)	79.31(1)
N2-Pd1-S1	171.00(5)	175.64(8)
	Dihedral angle (°)	
[S1]-[Pd1]	48.49(4)	53.84(9)
	Torsion angle (°)	
S1–Pd1–N1–C7	11.7(2)	

NMR characterization of cationic complexes.

NMR characterization of 4d (CD_2Cl_2, 298 K).

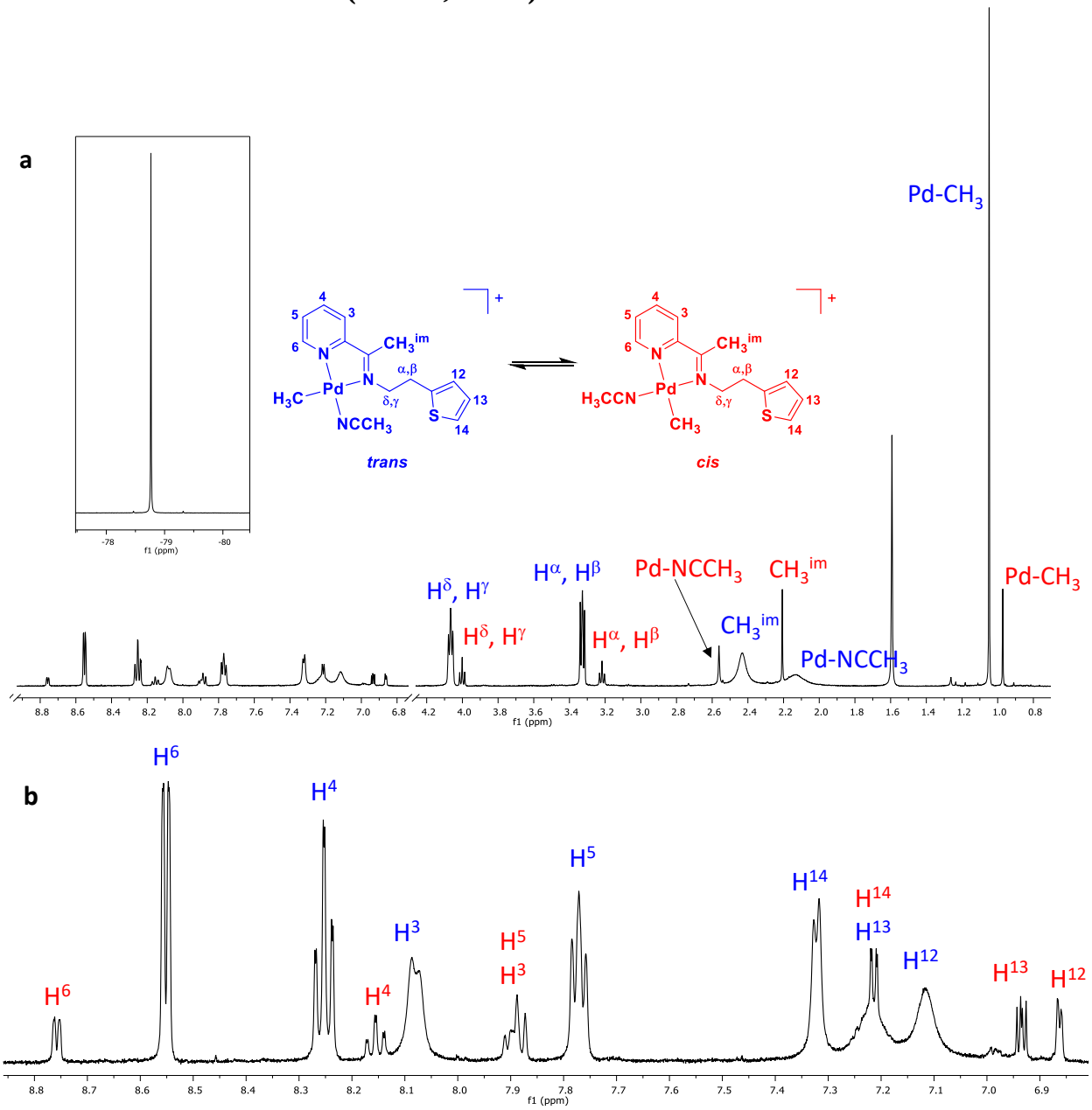

Figure S3.12. ^{1}H NMR spectrum (CD_2Cl_2, 298 K) of **4d**; (a) full spectrum (inset: ^{19}F NMR spectrum), (b) aromatic region.

NMR characterization of 4e (CD_2Cl_2, 298 K).

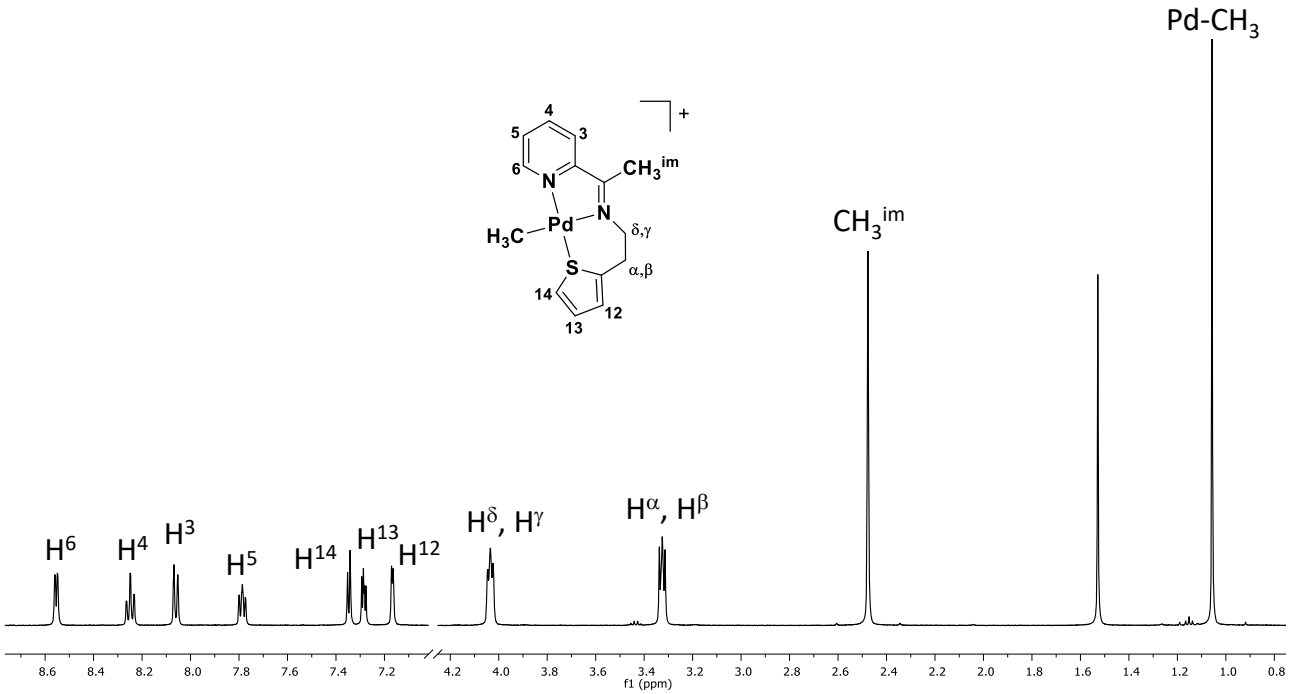

Figure S3.13. ^{1}H NMR spectrum (CD_2Cl_2, 298 K) of **4e**.

***In situ* NMR reactivity.**

***In situ* NMR reactivity of 4b with ethylene (CD_2Cl_2, 298 K).**

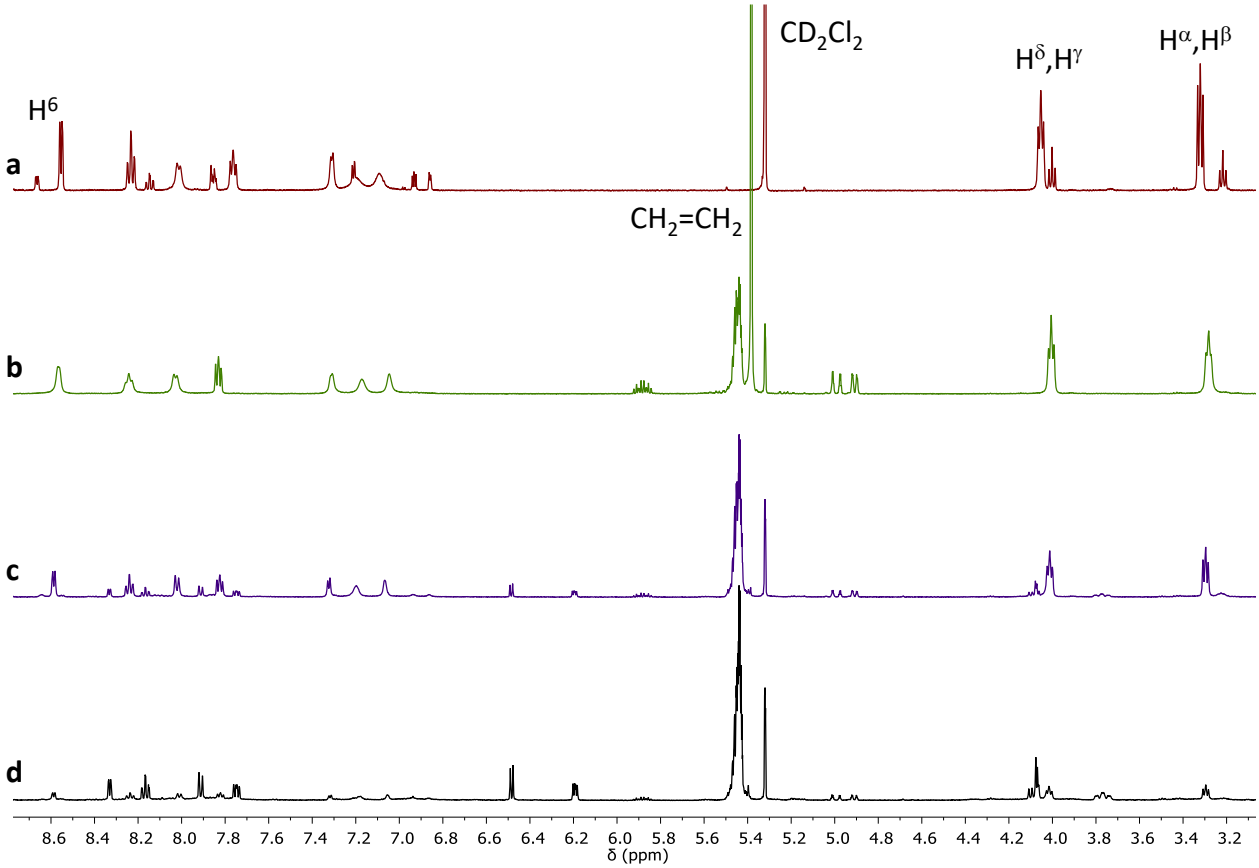

Figure S3.14. ^{1}H NMR spectra (CD_2Cl_2, 298 K) of (a) **4b**; **4b** + ethylene at (b) t = 5 min, (c) t = 30 min and (d) t = 1 h.

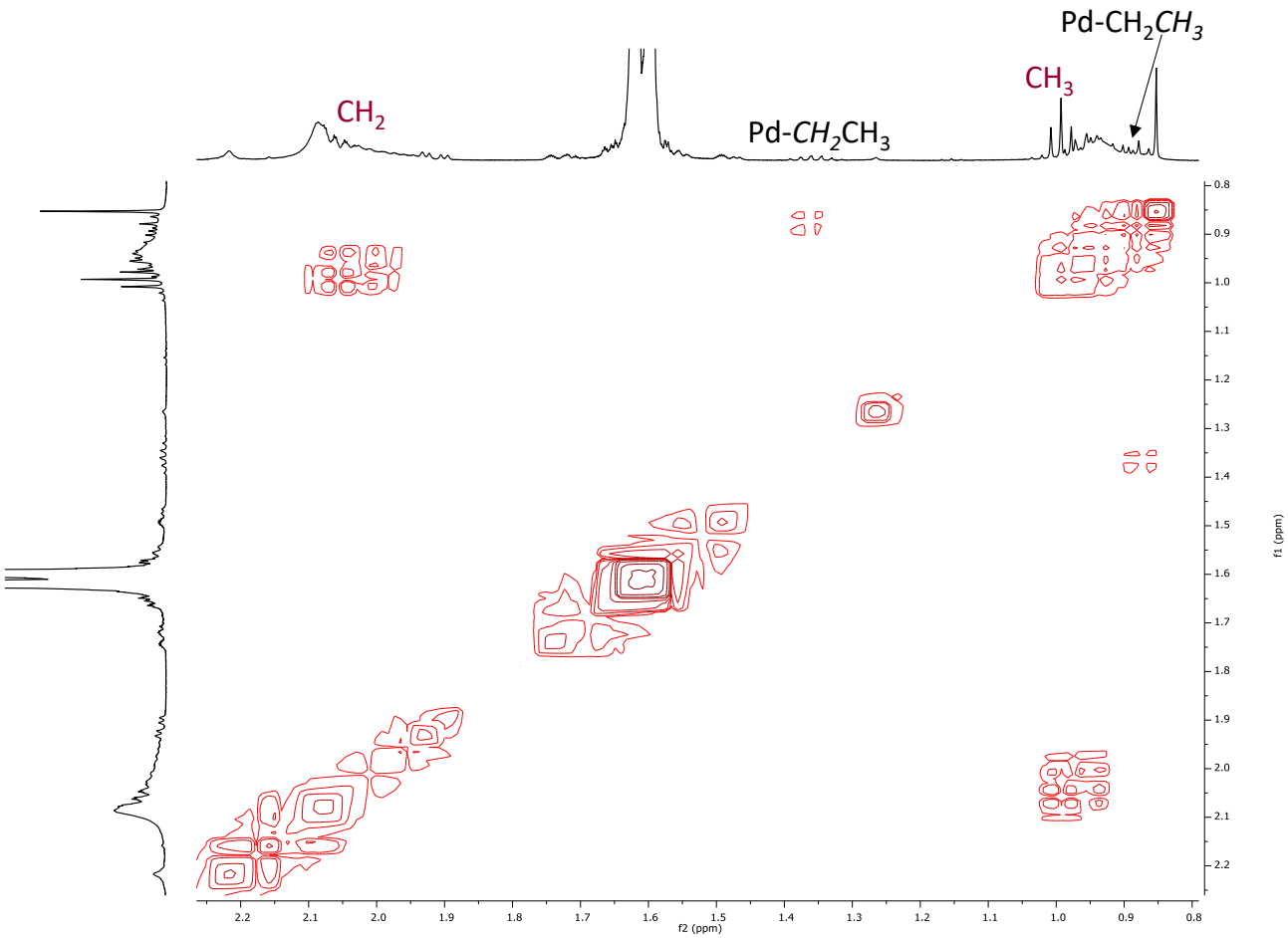

Figure S3.15. ^{1}H, ^{1}H COSY spectrum (CD_2Cl_2, 298 K) of **4b** + ethylene at t = 30 min.

NMR characterization of ligands and neutral complexes.

Characterization of iPrKI (298 K).

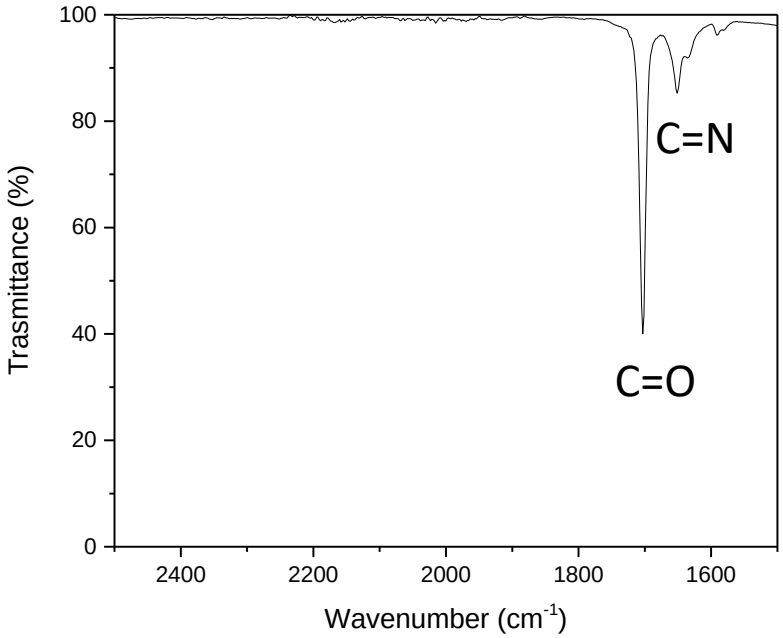

Figure S3.16. IR spectrum (298 K) of **iPrKI**.

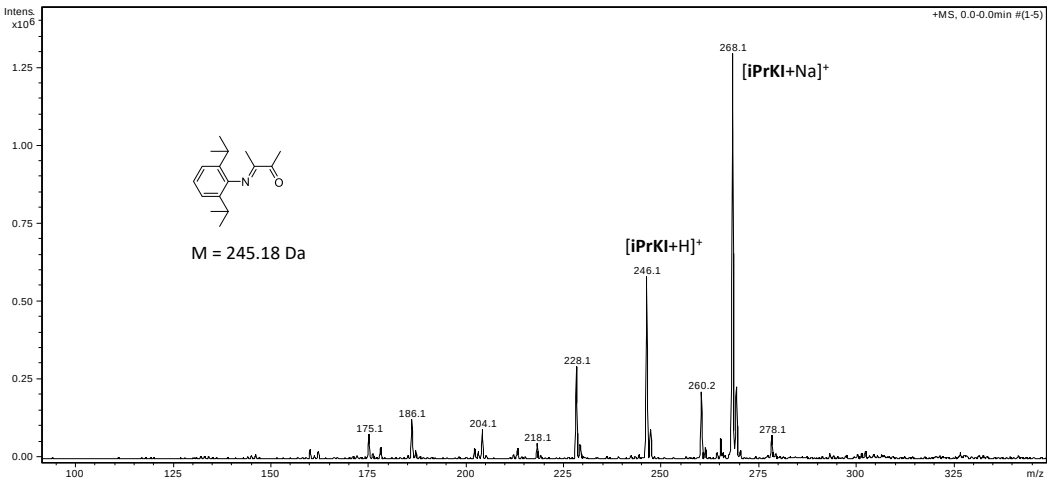

Figure S3.17. ESI-MS spectrum (positive mode, MeOH, 298 K) of **iPrKI.**

Characterization of MeKI (298 K).

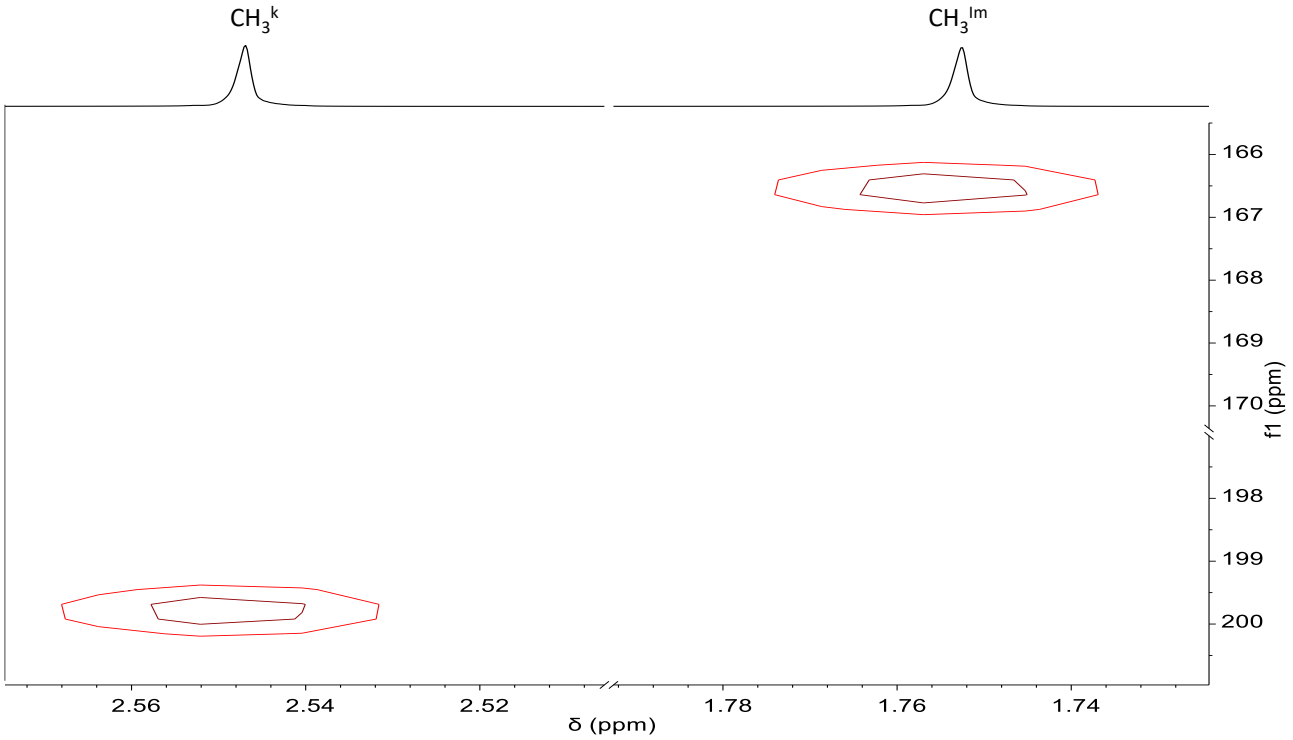

Figure S3.18. $^{1}H,^{13}C$ HMBC spectrum (CD_2Cl_2, 298 K) of **MeKI**.

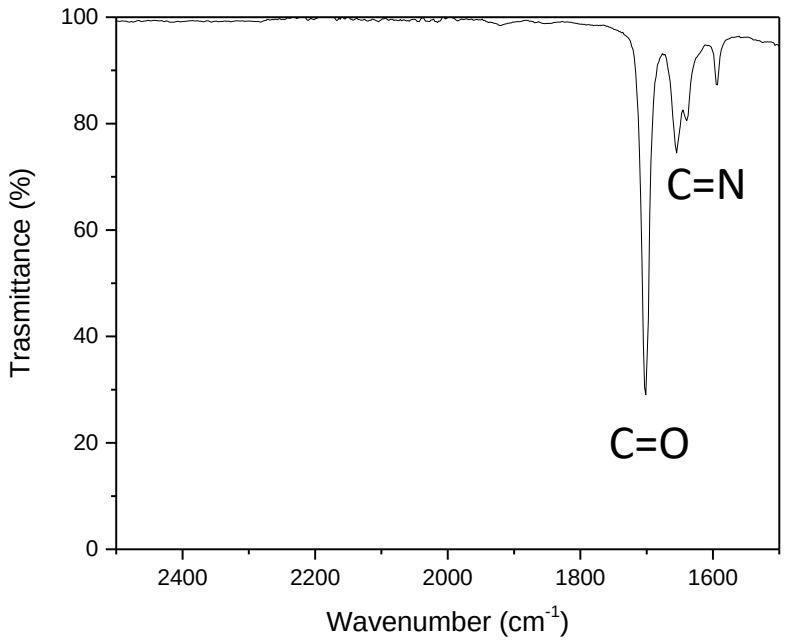

Figure S3.19. IR spectrum (298 K) of **MeKI**.

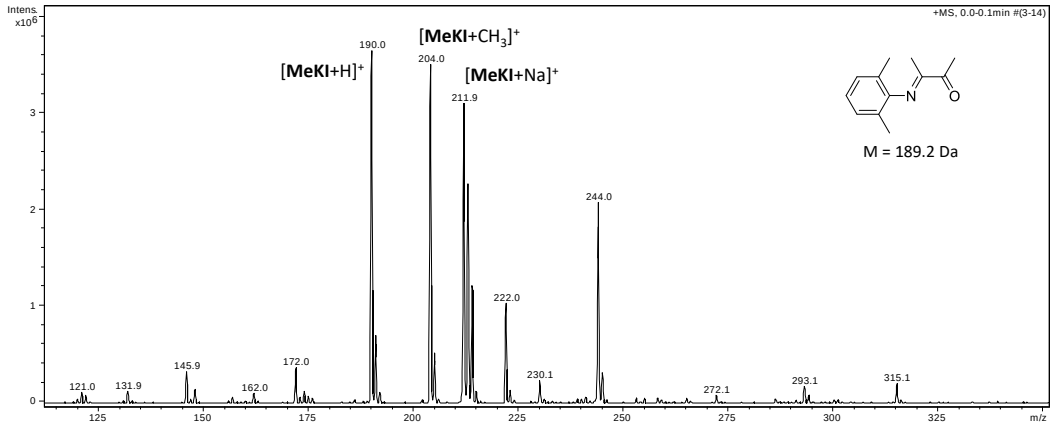

Figure S3.20. ESI-MS spectrum (positive mode, MeOH, 298 K) of **MeKI.**

Characterization of 5 (298 K).

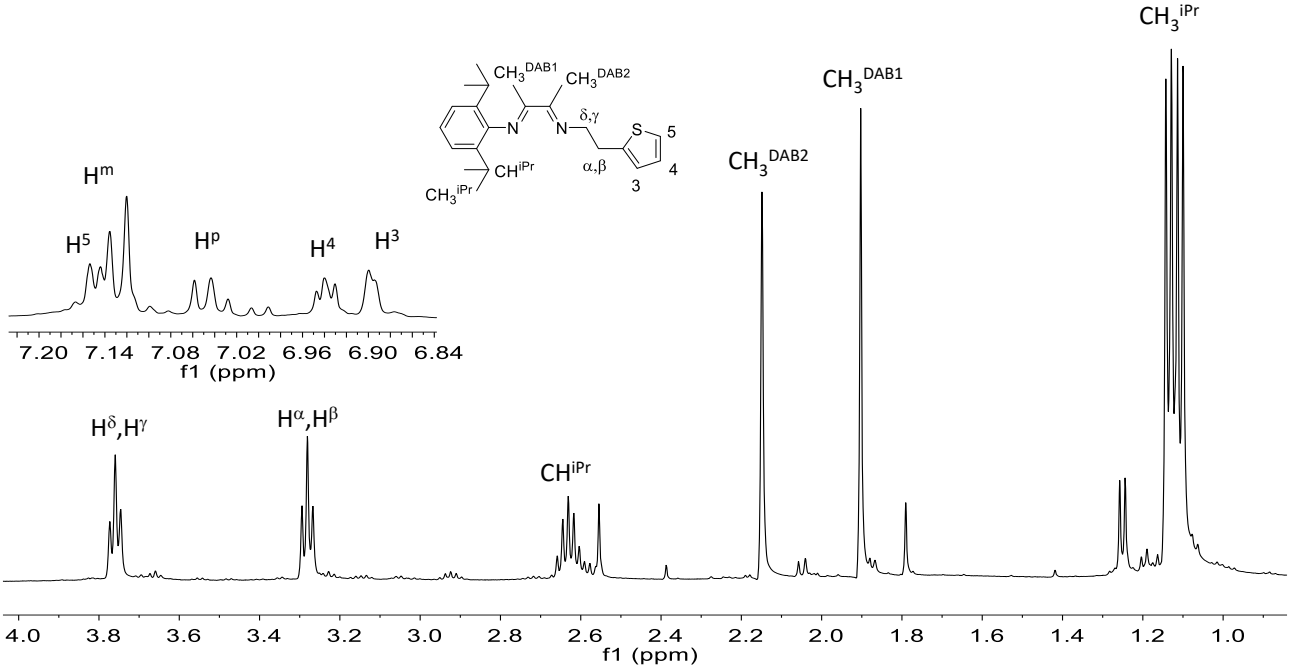

Figure S3.21. ^{1}H NMR spectrum (CD_2Cl_2, 298 K) of **5**.

Characterization of 6 (298 K).

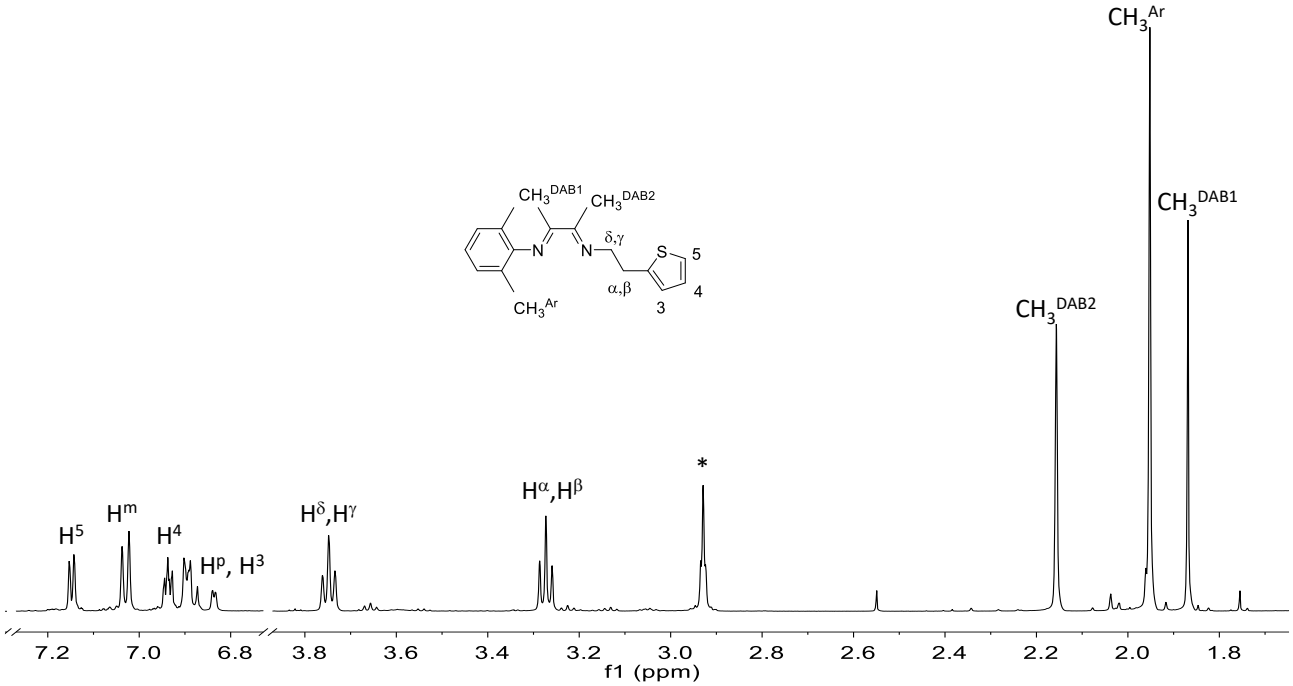

Figure S3.22. ^{1}H NMR spectrum (CD_2Cl_2, 298 K) of **6**.

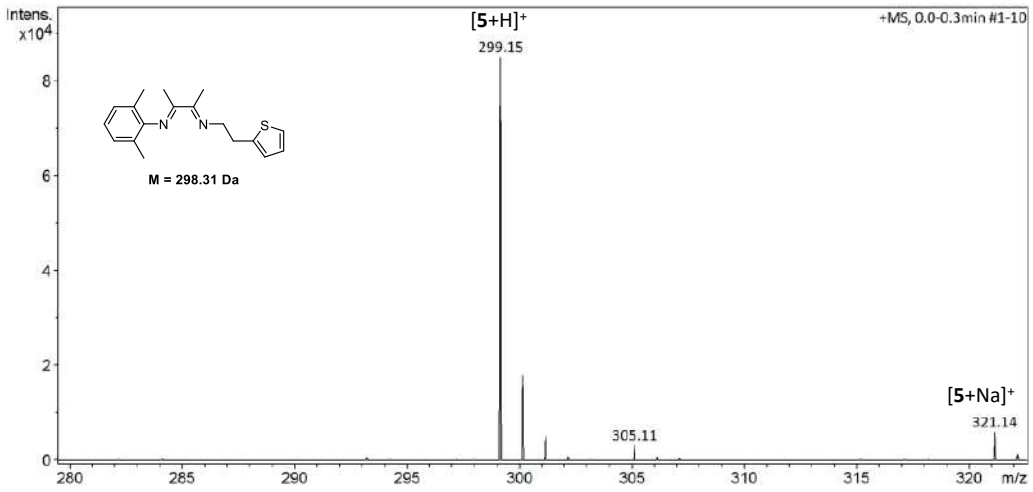

Figure S3.23. ESI-MS spectrum (positive mode, MeOH, 298 K) of **6**.

Characterization of 7 (298 K).

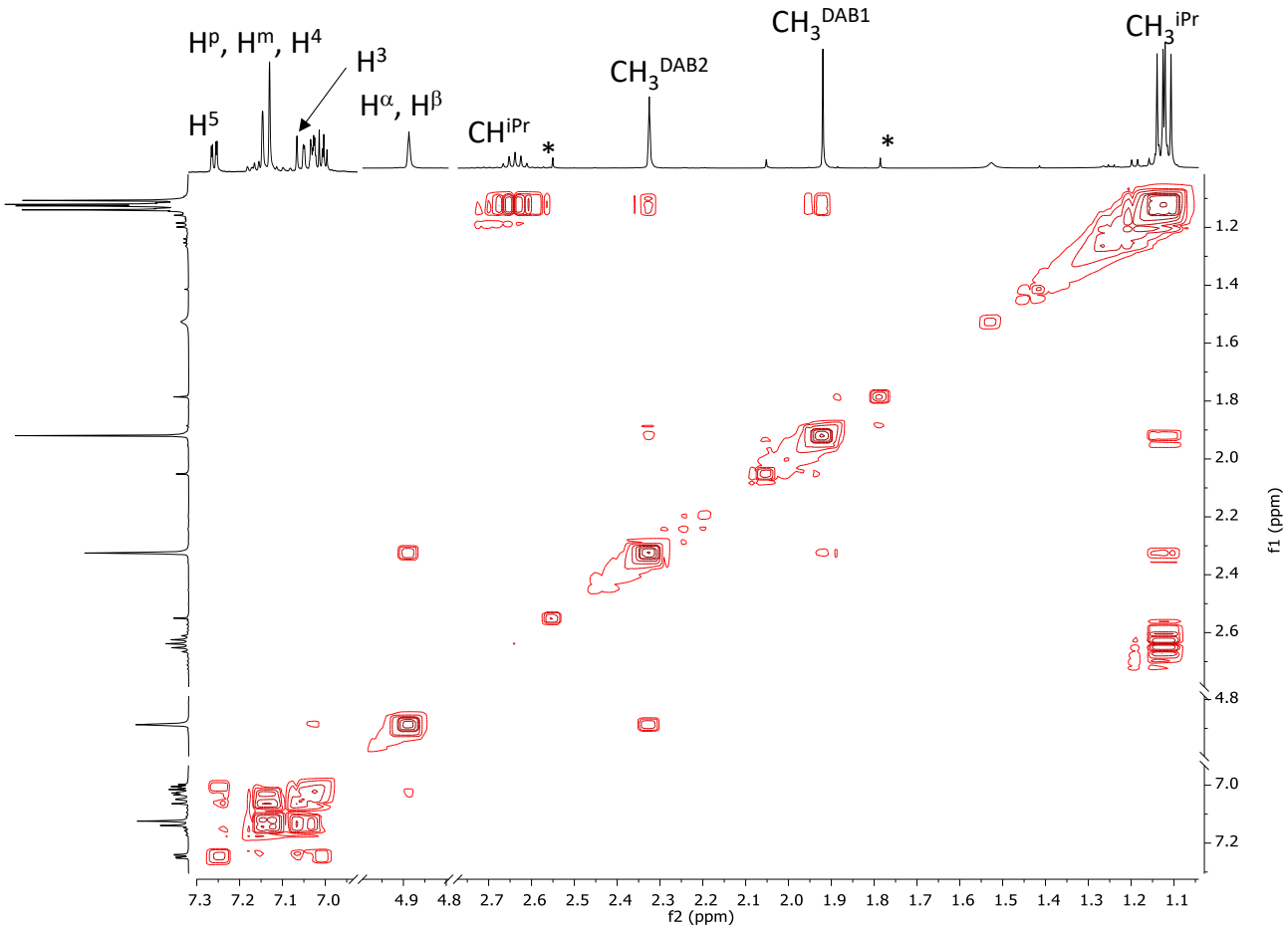

Figure S3.24. $^{1}H,^{1}H$ COSY spectrum (CD_2Cl_2, 298 K) of **7**; aliphatic and aromatic region not on scale; ***iPrKI**.

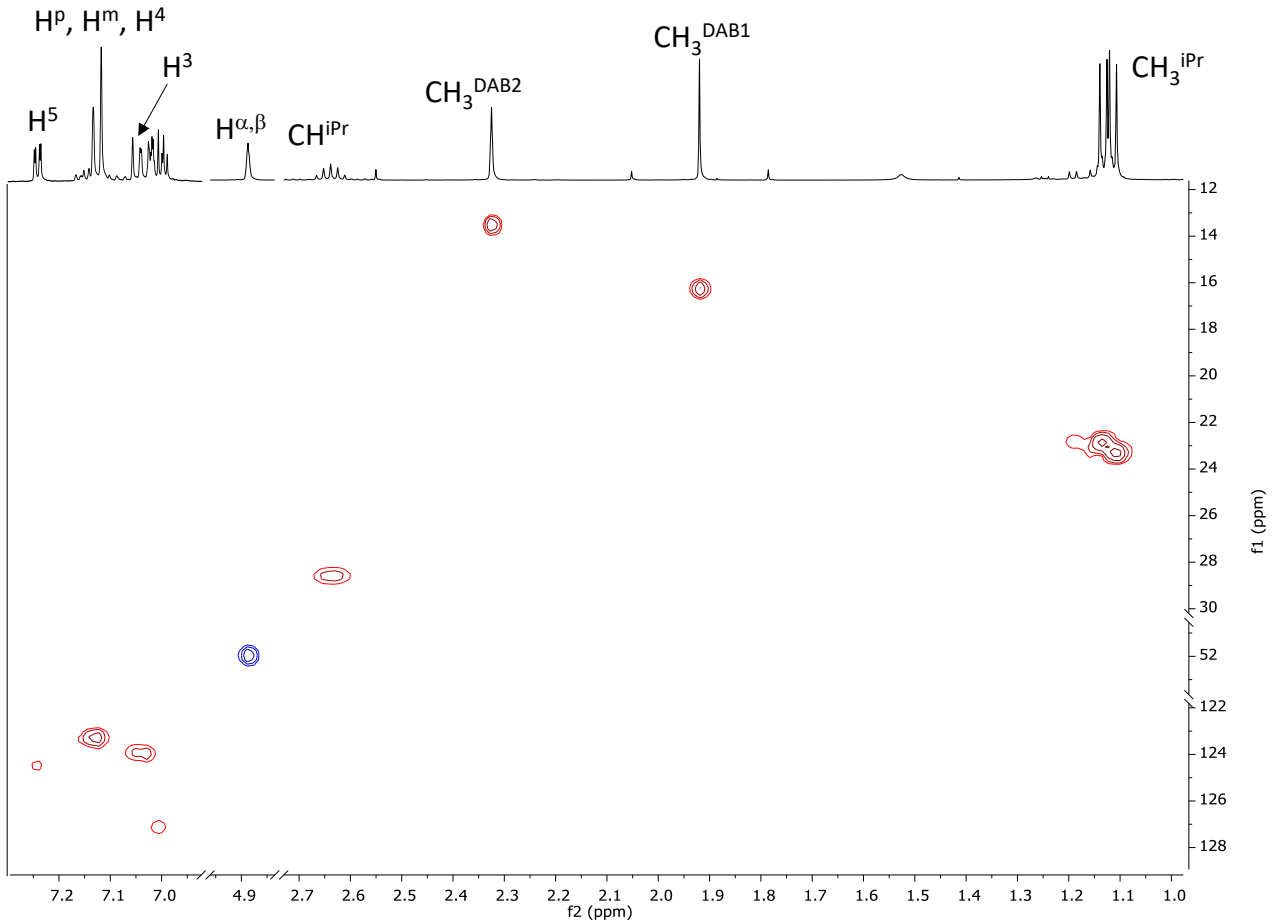

Figure S3.25. $^{1}H,^{13}C$ HSQC spectrum (CD_2Cl_2, 298 K) of **7**; aliphatic and aromatic region not on scale.

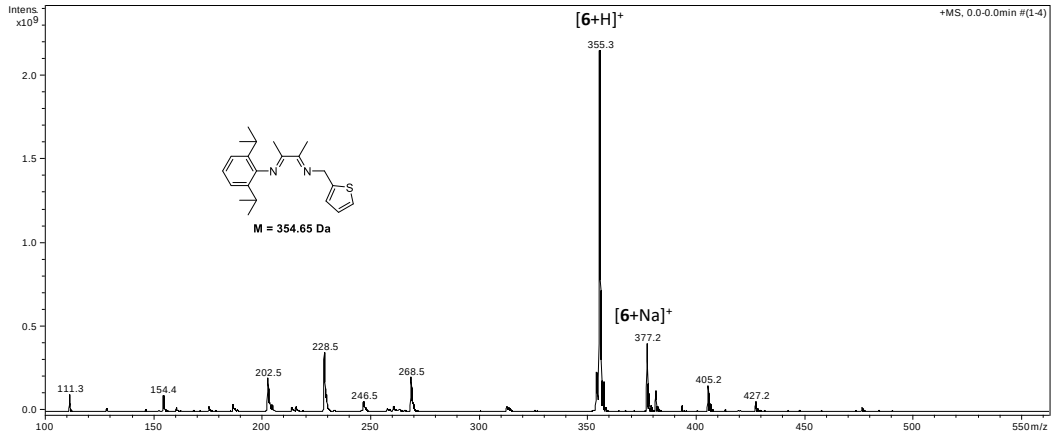

Figure S3.26. ESI-MS spectrum (positive mode, MeOH, 298 K) of **7**.

NMR characterization of 5a (CD_2Cl_2, 298 K).

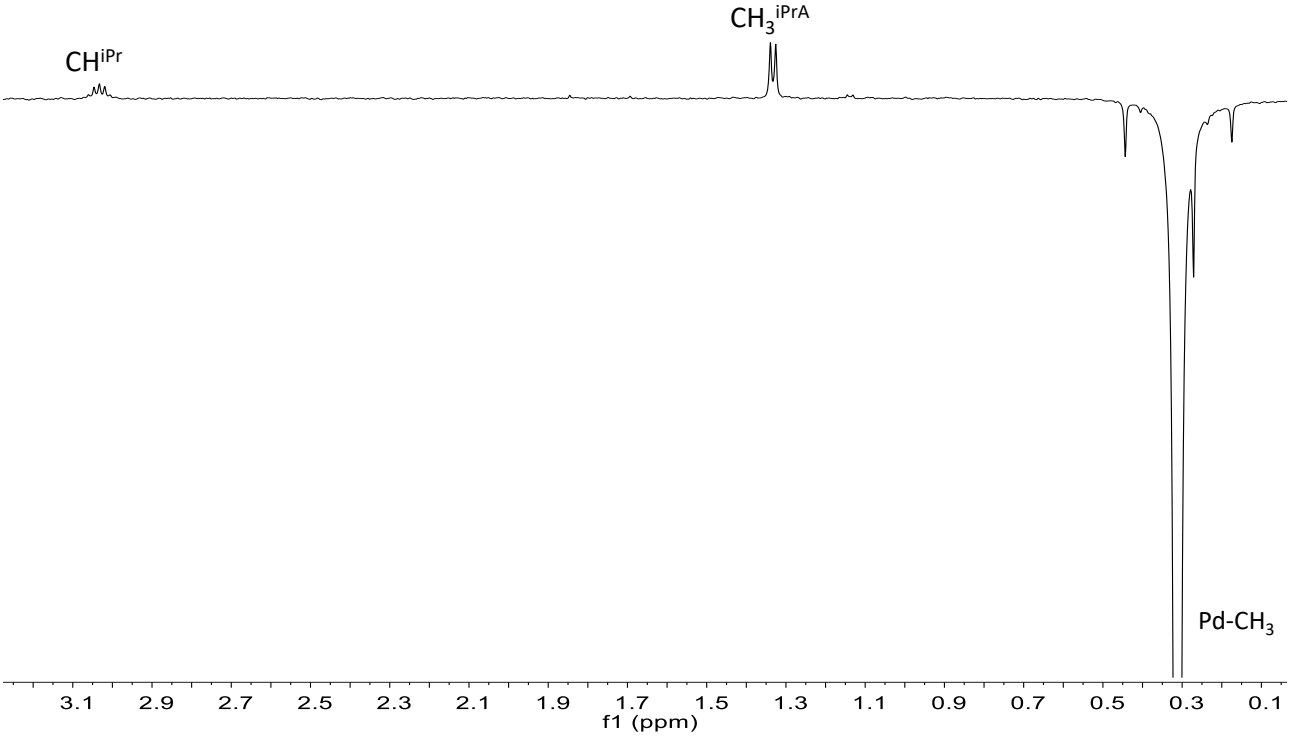

Figure S3.27. 1D NOE spectrum (CD_2Cl_2, 298 K) of **5a**.

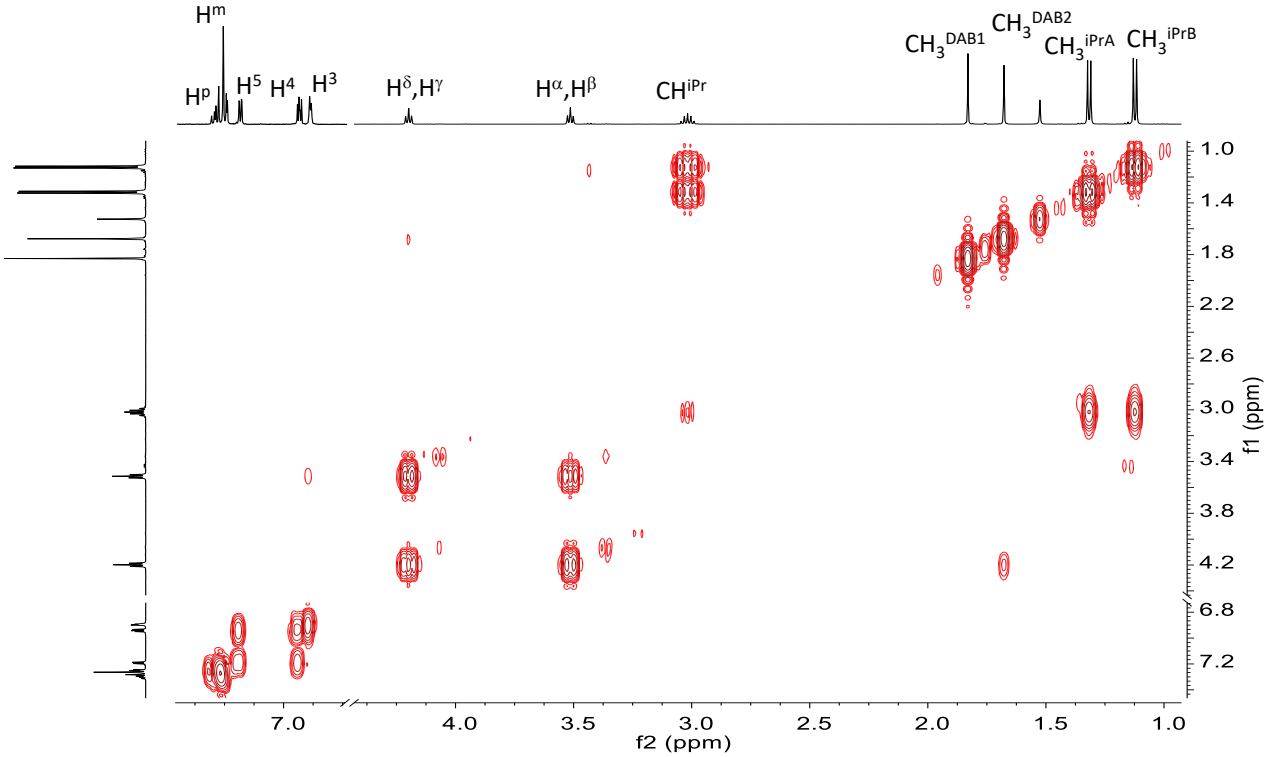

Figure S3.28. $^1H,^1H$ COSY spectrum (CD_2Cl_2, 298 K) of **5a**; aliphatic and aromatic region not on scale.

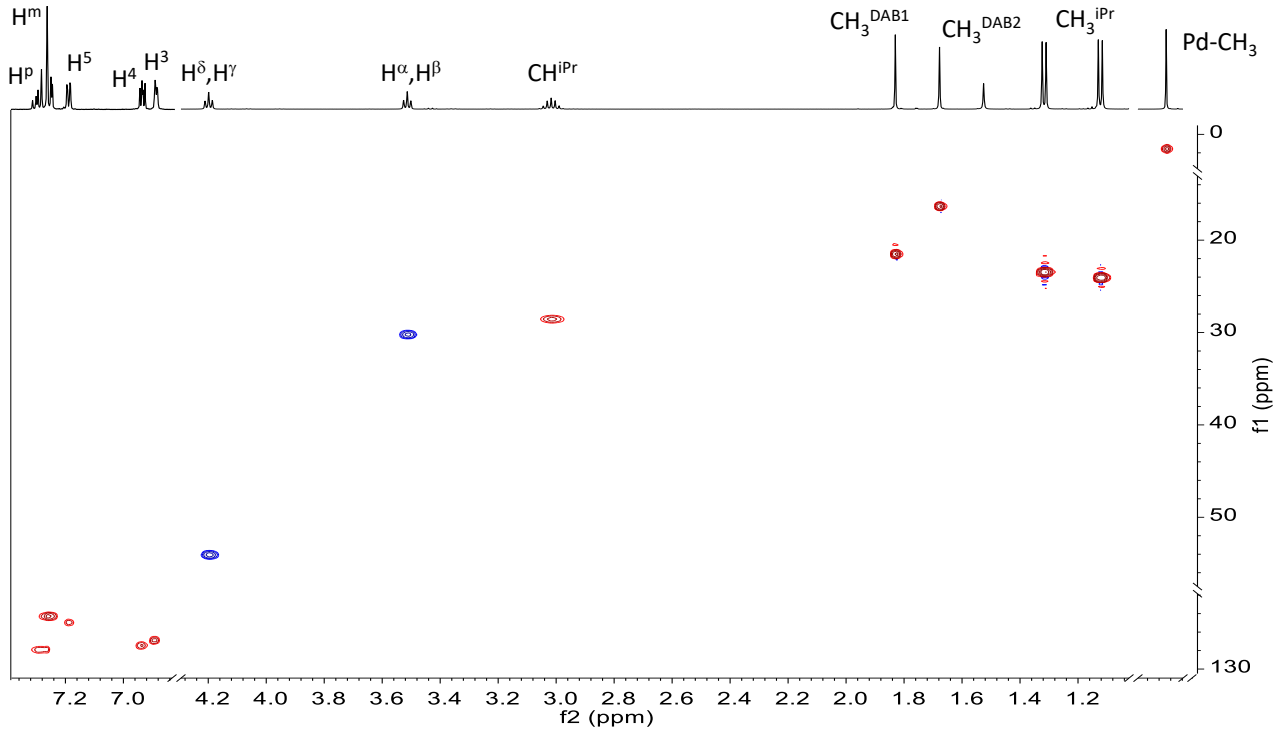

Figure S3.29. $^{1}H,^{13}C$ HSQC spectrum (CD_2Cl_2, 298 K) of **5a**; aliphatic and aromatic region not on scale.

NMR characterization of 6a (CD_2Cl_2, 298 K).

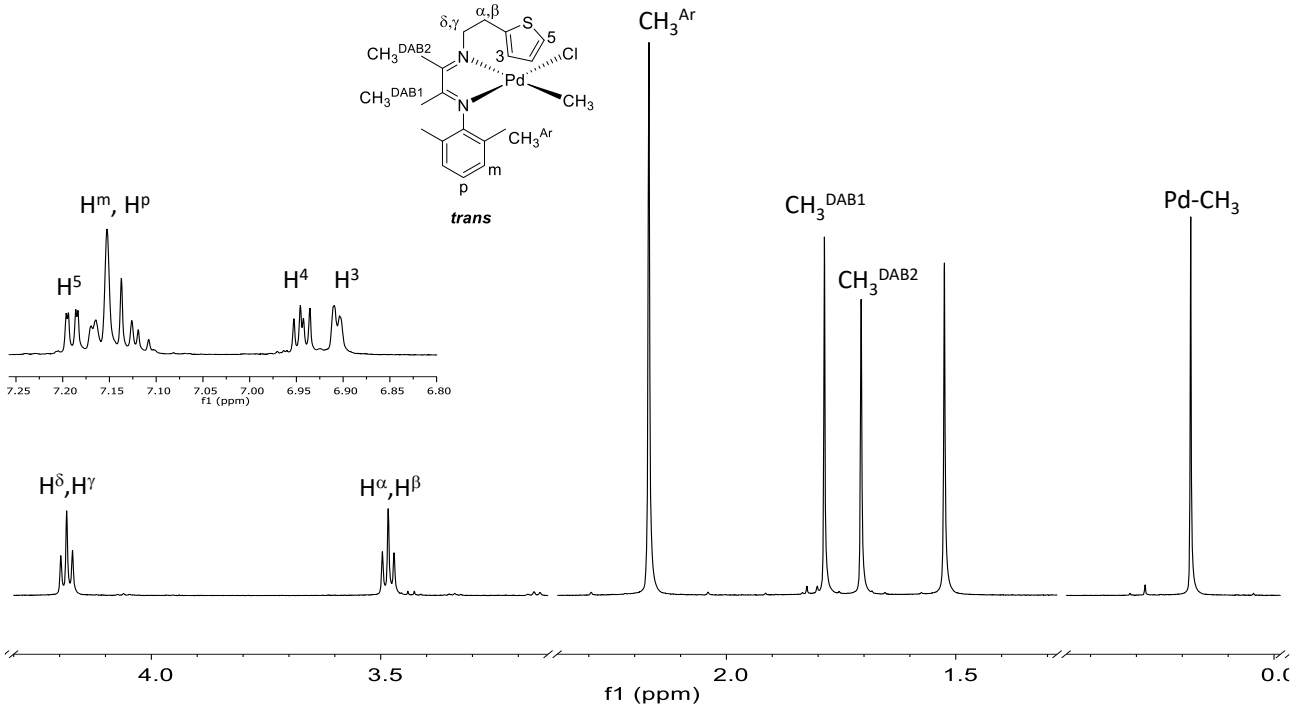

Figure S3.30. ^{1}H NMR spectrum (CD_2Cl_2, 298 K) of **6a**.

NMR characterization of 7a (CD_2Cl_2, 298 K).

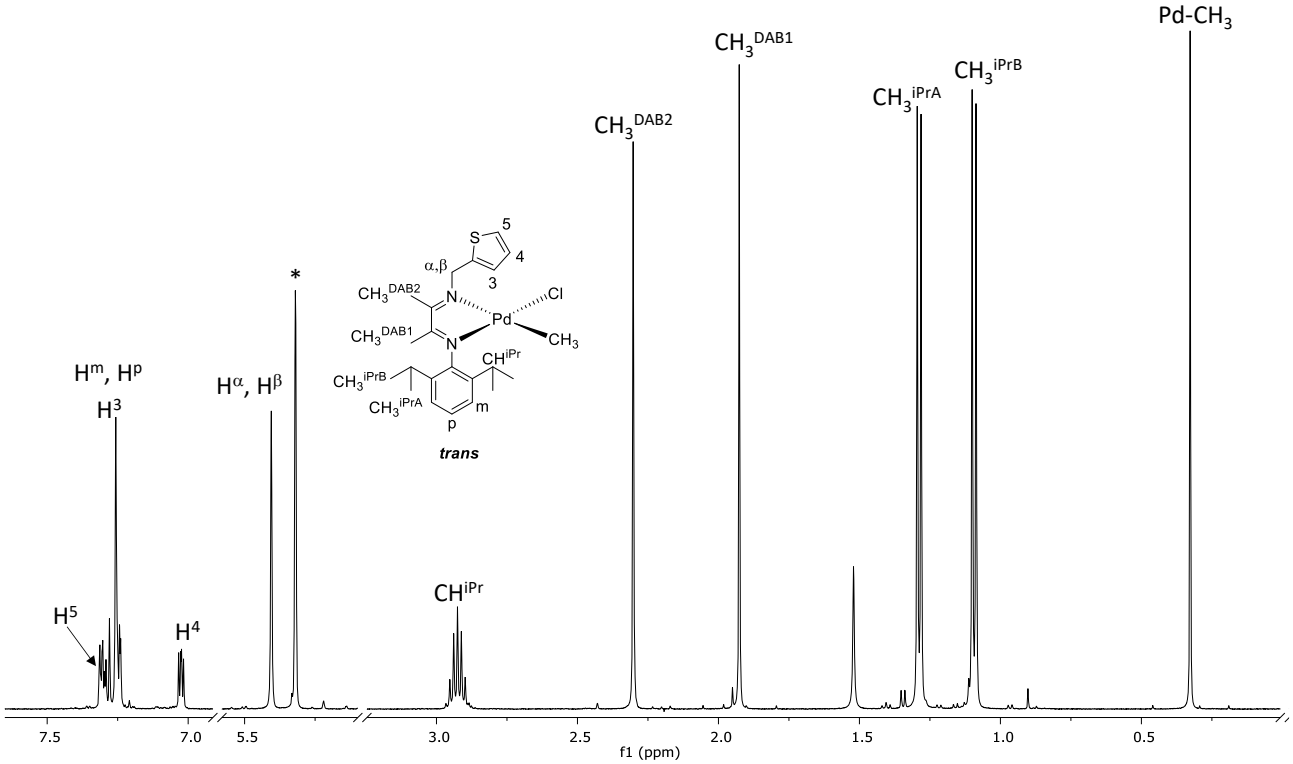

Figure S3.31. ^{1}H NMR spectrum (CD_2Cl_2, 298 K) of **7a**.

X-Ray crystallography.

Table S3.3. Most significant distances and angles for complexes *trans*-**5a** and *trans*-**7a**.

	trans-**5a**	*trans*-**7a**
	Distances (Å)	
Pd1-C1	2.027(8)	2.0336(1)
Pd1-Cl1	2.298(2)	2.2950(3)
Pd1-N1	2.125(5)	2.1262(9)
Pd1-N2	2.030(5)	2.0365(9)
	Angles (°)	
C1-Pd1-Cl1	89.5(2)	87.81(3)
C1-Pd1-N1	172.9(3)	173.85(4)
C1-Pd1-N2	95.0(3)	96.89(4)
N1-Pd1-Cl1	97.6(2)	97.88(3)
N2-Pd1-Cl1	175.13(2)	175.30(3)
N2-Pd1-N1	78.0(2)	77.42(4)
	Dihedral angles (°)	

[Ph]-[Pd1]	86.0(2)	86.31(3)
[S1]-[Pd1]	35.8(3)	79.6(3)

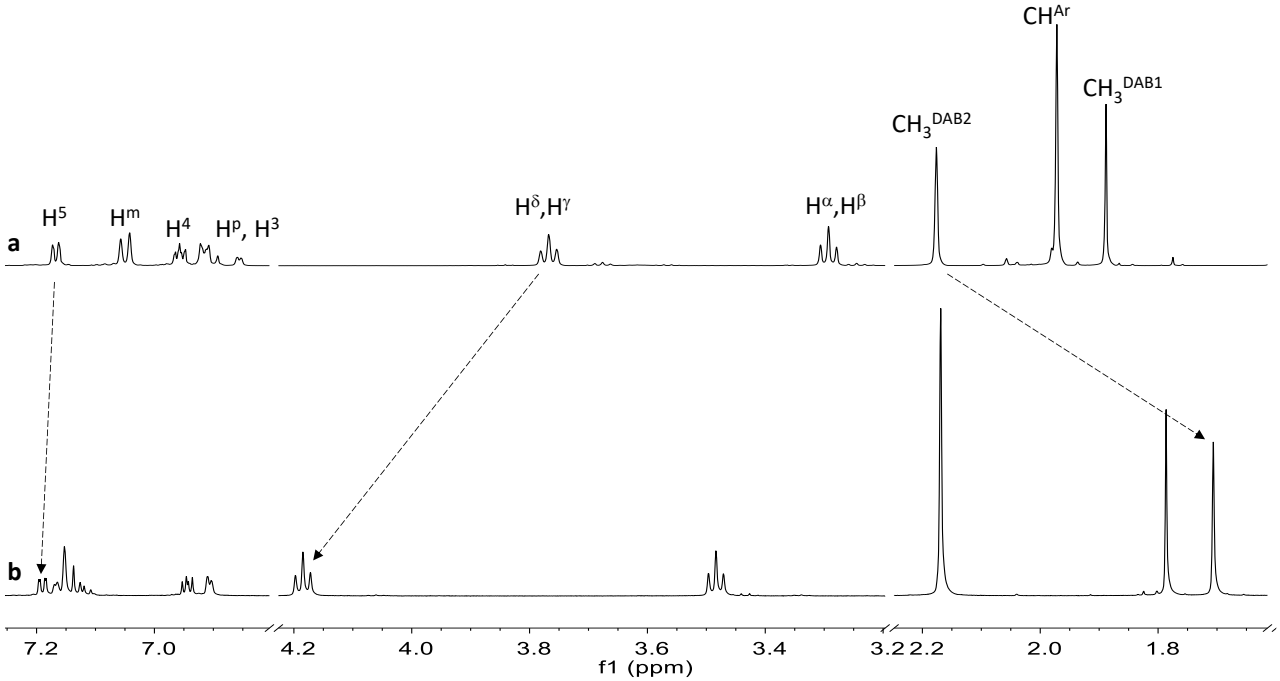

Figure S3.32. ^{1}H NMR spectra (CD_2Cl_2, 298 K) of: (a) **6** and (b) **6a**.

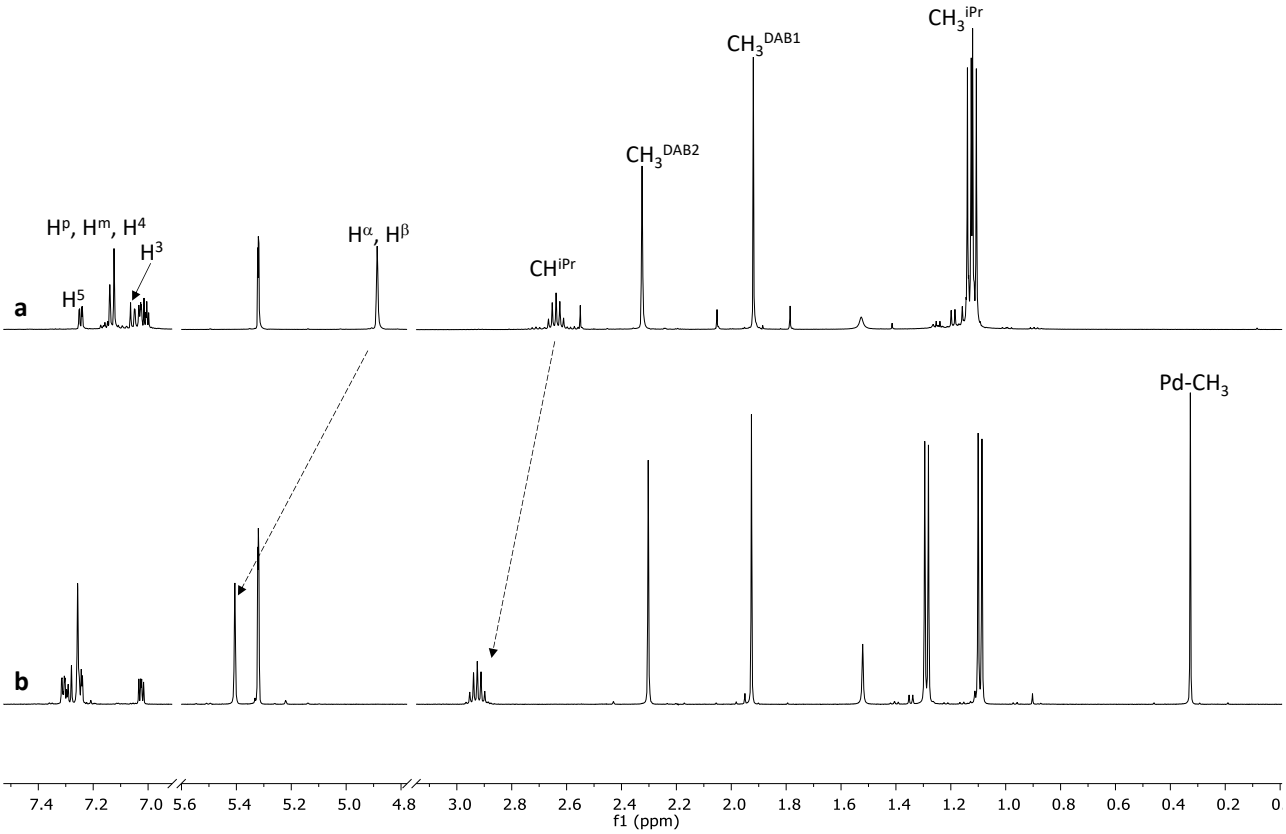

Figure S3.33. ^{1}H NMR spectra (CD_2Cl_2, 298 K) of: (a) **7** and (b) **7a**.

NMR characterization of cationic complexes.

NMR characterization of 6b (CD_2Cl_2, 298 K).

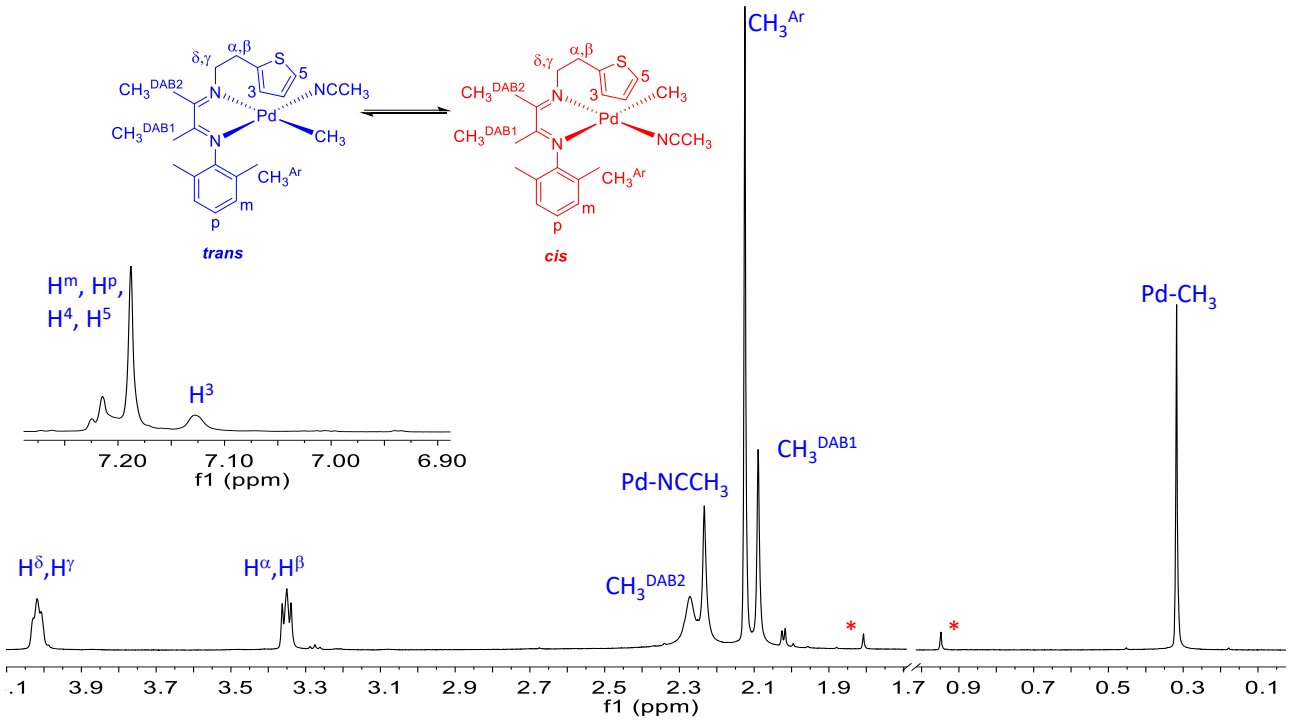

Figure S3.34. ^{1}H NMR spectrum (CD_2Cl_2, 298 K) of **6b**.

NMR characterization of dimeric species [Pd(CH3)(7)]2[μ-Cl][PF6] (CD2Cl2, 298 K).

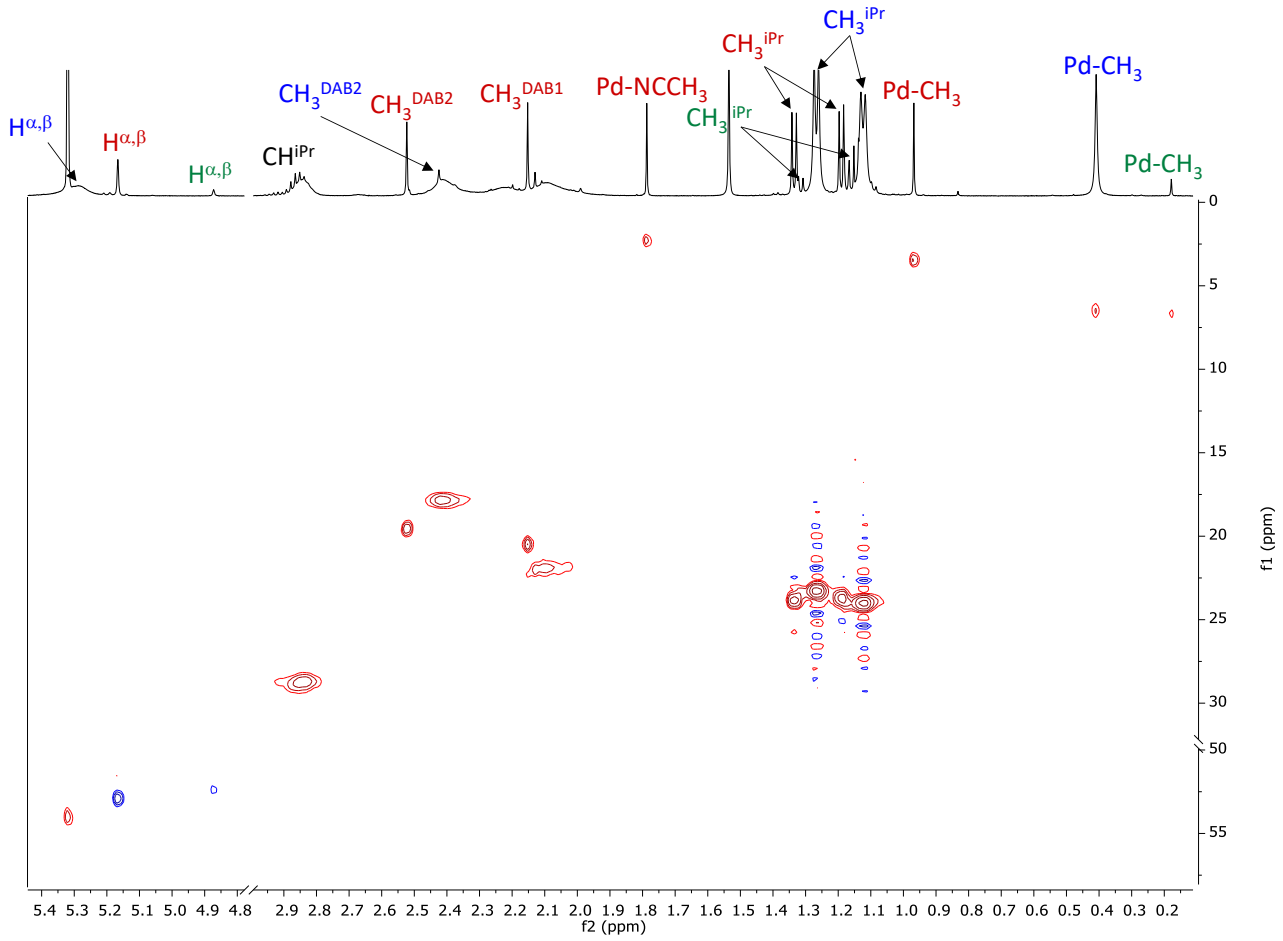

Figure S3.35. $^{1}H,^{13}C$ HSQC spectrum (CD_2Cl_2, 298 K) of [Pd(CH_3)(**7**)]$_2$[μ-Cl][PF_6].

NMR characterization of 5c (CD_2Cl_2, 298 K).

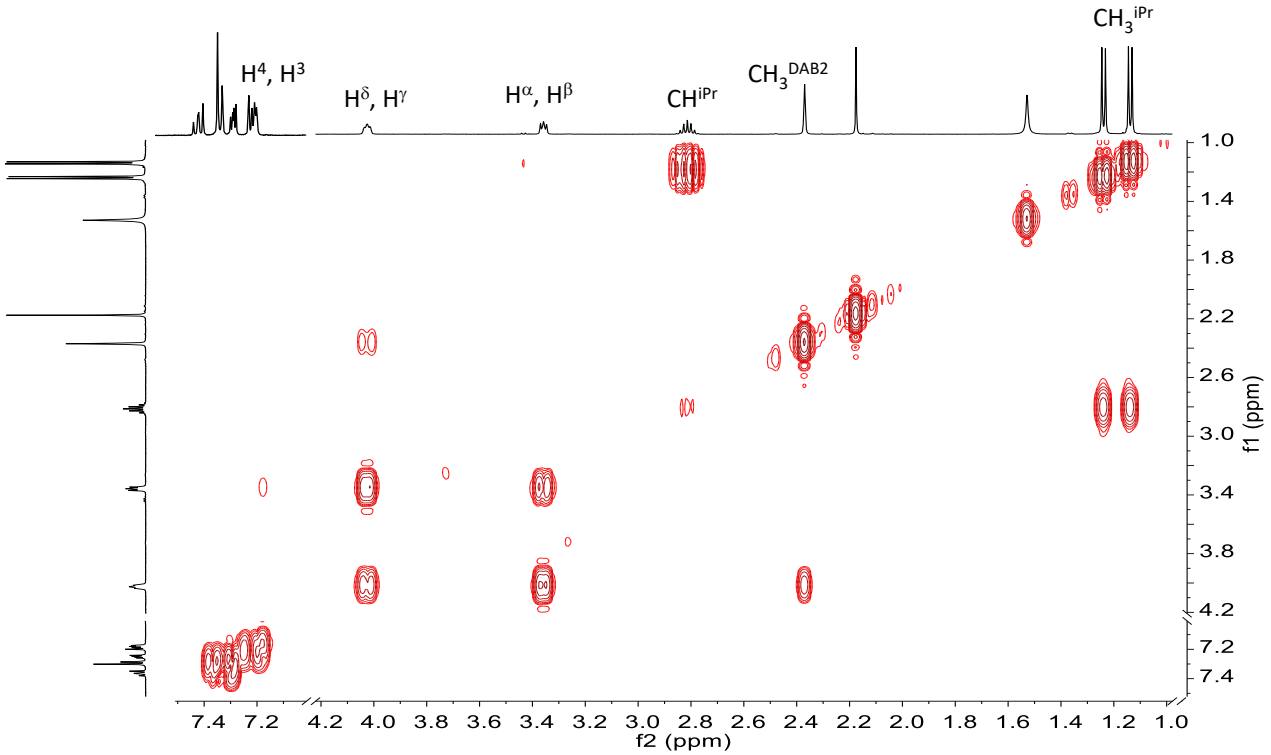

Figure S3.36. $^1H,^1H$ COSY spectrum (CD_2Cl_2, 298 K) of **5c**; aliphatic and aromatic region not on scale.

NMR characterization of 6c (CD_2Cl_2, 298 K).

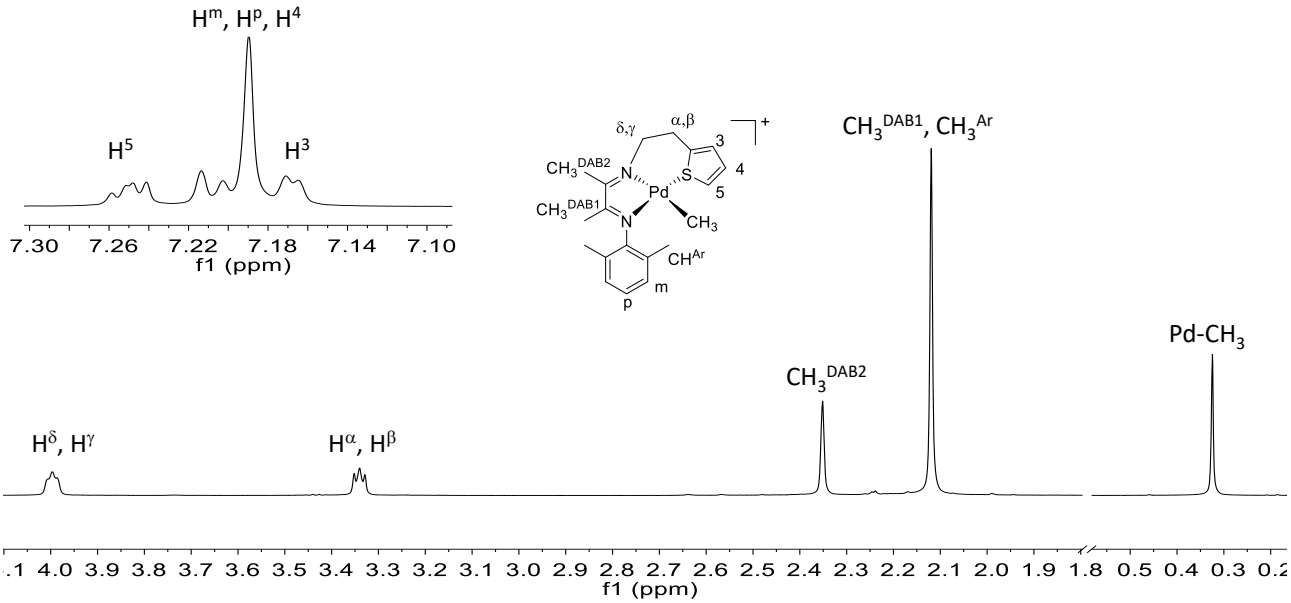

Figure S3.37. ^1H NMR spectrum (CD_2Cl_2, 298 K) of **6c**.

NMR characterization of 7c (CD_2Cl_2, 298 K).

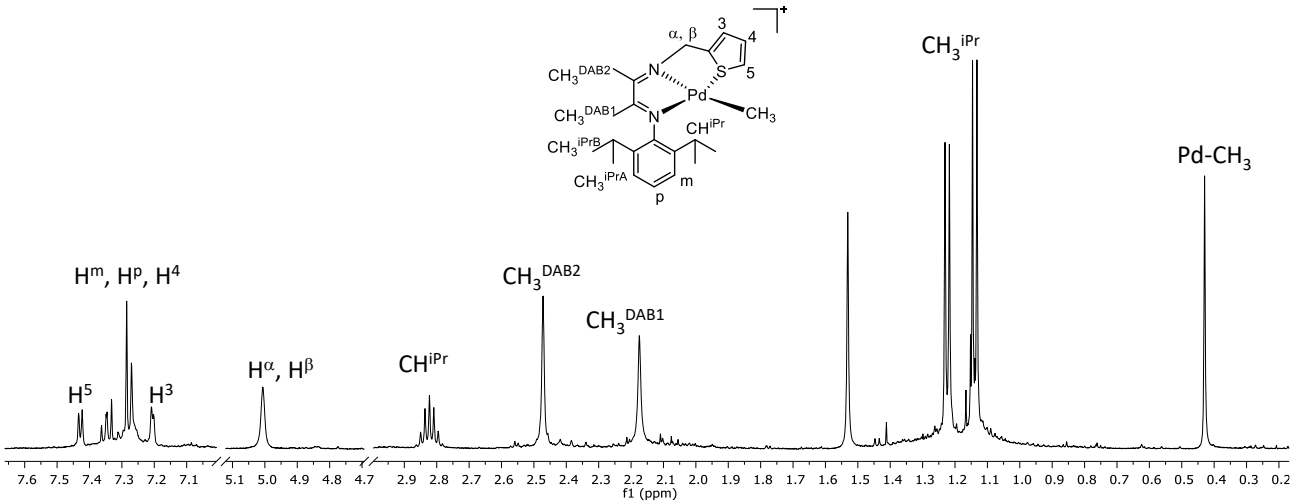

Figure S3.38. ^1H NMR spectrum (CD_2Cl_2, 298 K) of **7c**.

Ethylene/methyl acrylate cooligomerization reaction.

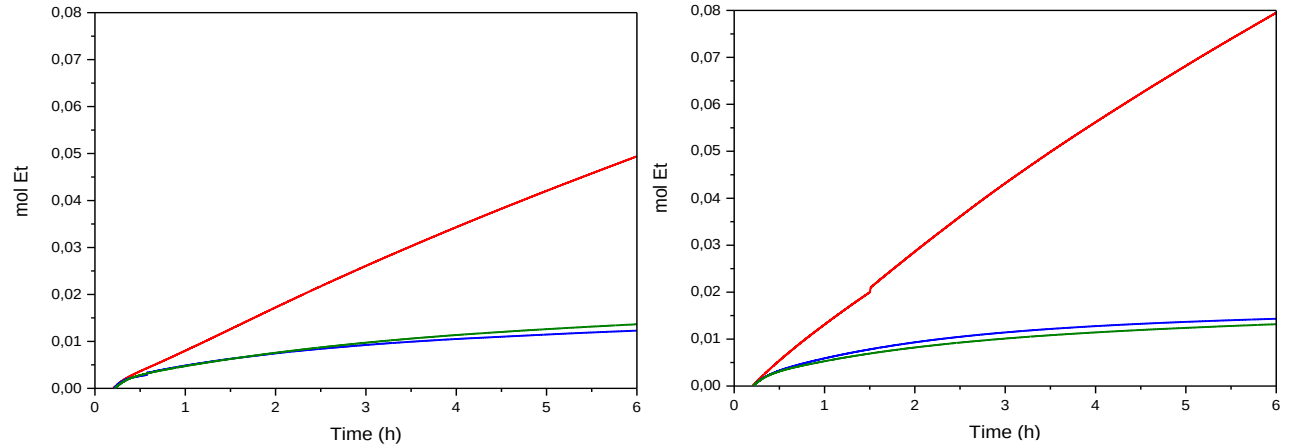

(a) (b)

Figure S3.39. Kinetic profiles of ethylene/methyl acrylate cooligomerization: effect of ligand. Precatalysts: [Pd(CH_3)($NCCH_3$)(N-N)][PF_6] (red curves), [Pd(CH_3)($NCCH_3$)(N-N'-S)][PF_6] (blue curves) and [Pd(CH_3)(N-N'-S)][PF_6] (green curves); (a) N-N: **1** and N-N'-S: **6**, (b) N-N: **2** and N-N'-S: **5**. Reaction conditions: see Table 3.4.

Table S3.4. Ethylene/methyl acrylate cooligomerization: effect of temperature.

Precatalyst: [Pd(CH$_3$)(NCCH$_3$)(5)][PF$_6$] [a]

entry	T (K)	yield (mg)	kg P/mol Pd[b]	MA (mol %)[c]	TON[d]		Bd[e]
					E	MA	
1	298	291.6	13.88	4.0	438	18	100
2	308	258.1	12.29	5.4	373	22	81
3	318	157.0	7.48	7.3	214	17	84

[a] Reaction conditions: $n_{Pd} = 2.1 \cdot 10^{-5}$ mol, V_{TFE} = 21 mL, V_{MA} = 1.130 mL, [MA]/[Pd] = 594, P_{Et} = 2.5 bar, t = 6 h. [b] Productivity in kg P/mol Pd = kilograms of product per mol of palladium calculated on isolated yield. [c] Amount of inserted MA in mol % calculated by ^{1}H NMR spectroscopy on isolated product. [d] Turnover number = mol of substrate converted per mol of Pd. [e] Branching degree expressed as number of branches per 1000 carbon atoms.

Table S3.5. Ethylene/methyl acrylate cooligomerization: effect of ethylene pressure.

Precatalyst: [Pd(CH$_3$)(NCCH$_3$)(5)][PF$_6$] [a]

entry	P_{Et} (bar)	yield (mg)	kg P/mol Pd[b]	MA (mol %)[c]	TON[d]		Bd[e]
					E	MA	
1	2.5	291.6	13.88	4.0	438	18	100
2	5.0	499.0	23.76	2.0	796	16	110
3	7.0	280.0	13.33	1.5	454	7	108

[a] Reaction conditions: $n_{Pd} = 2.1 \cdot 10^{-5}$ mol, V_{TFE} = 21 mL, V_{MA} = 1.130 mL, [MA]/[Pd] = 594, T = 298 K, t = 6 h. [b] Productivity in kg P/mol Pd = kilograms of product per mol of palladium calculated on isolated yield. [c] Amount of inserted MA in mol % calculated by ^{1}H NMR spectroscopy on isolated product. [d] Turnover number = mol of substrate converted per mol of Pd. [e] Branching degree expressed as number of branches per 1000 carbon atoms.

***In situ* NMR reactivity.**

***In situ* NMR reactivity of 6b with ethylene (CD_2Cl_2, 298 K).**

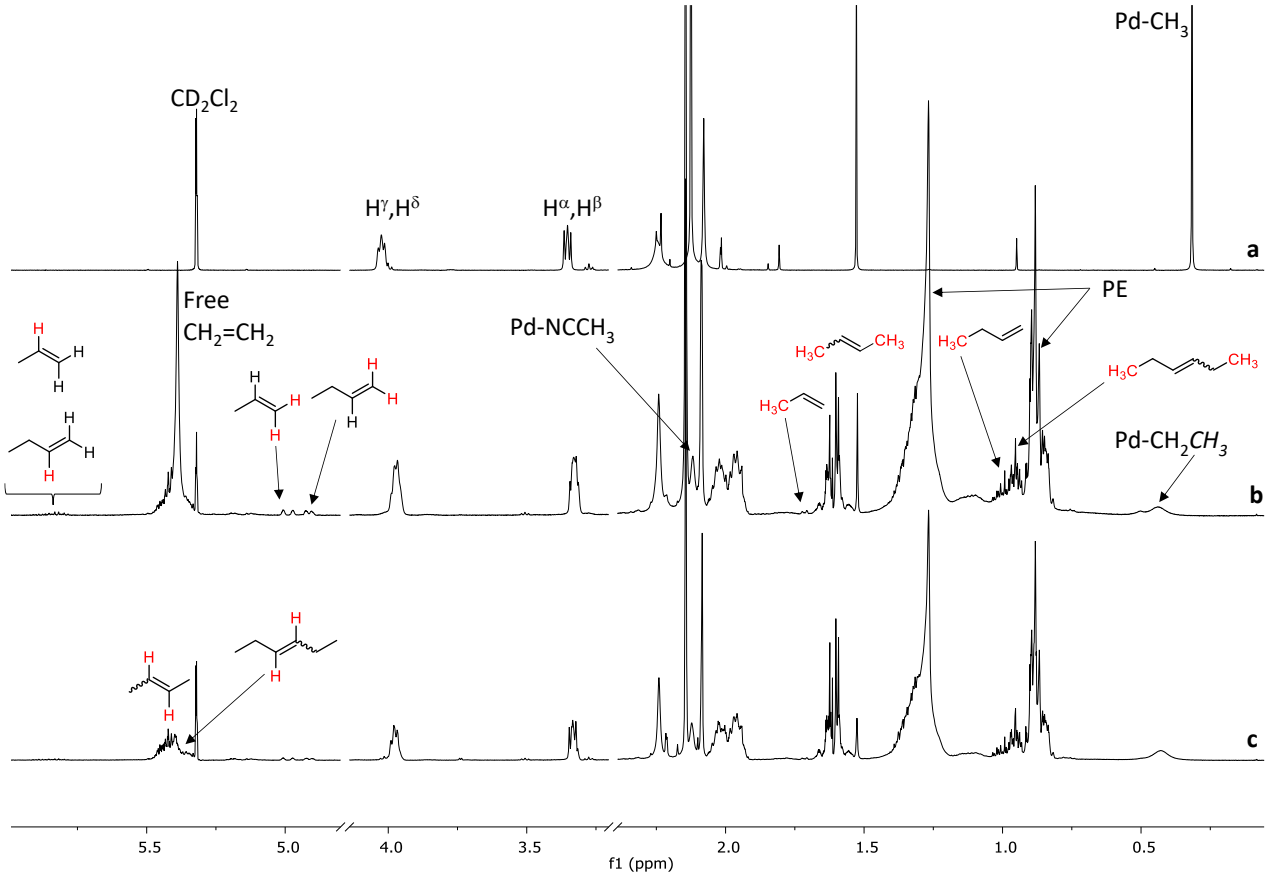

Figure S3.40. ^{1}H NMR spectra (CD_2Cl_2, 298 K) of (a) **6b**; **6b** + ethylene at (b) t = 5 min and (c) t = 15 min.

***In situ* NMR reactivity of 5c with ethylene (CD_2Cl_2, 298 K).**

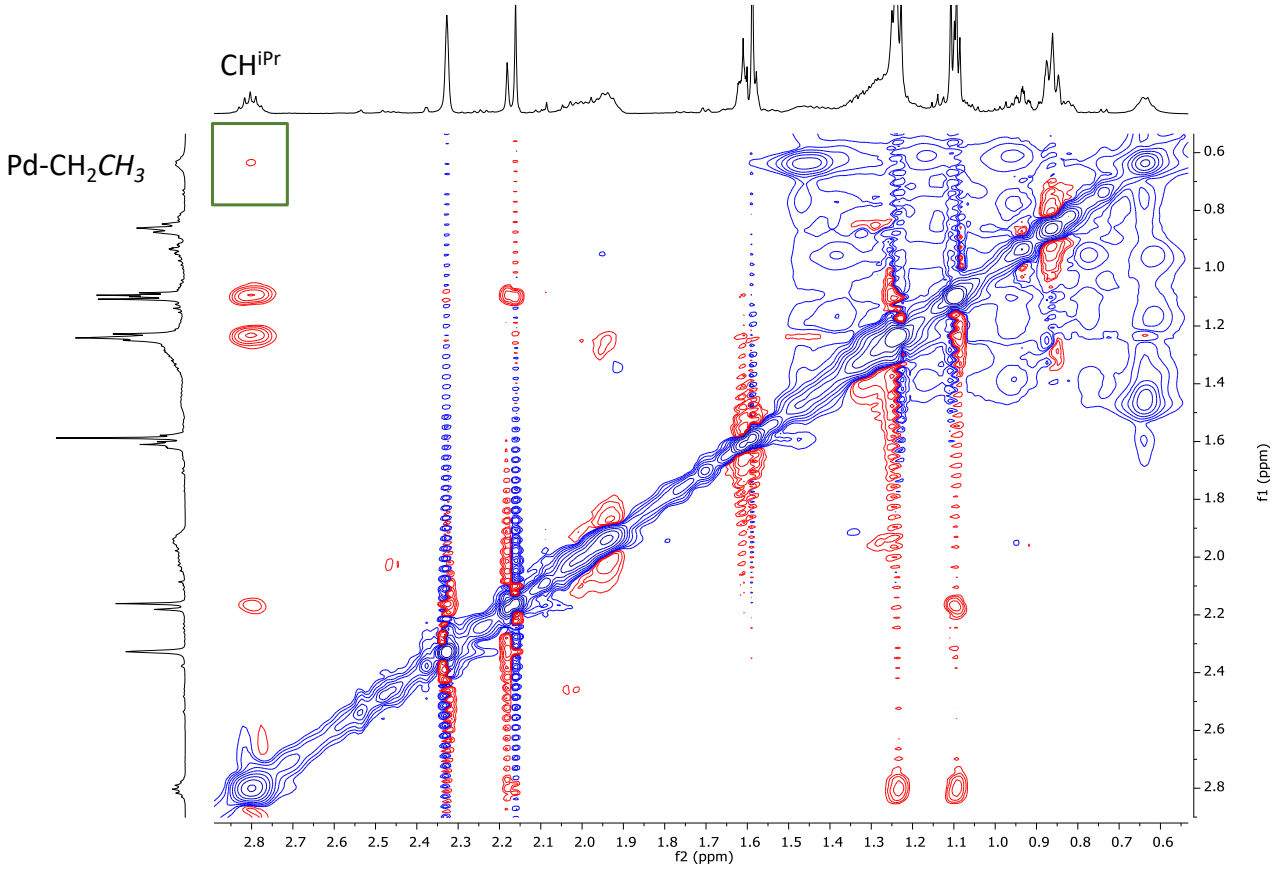

Figure S3.41. ^{1}H,1H NOESY spectrum (CD_2Cl_2, 273 K) of **5c** + ethylene at t = 1 h.

***In situ* NMR reactivity of 6c with ethylene (CD_2Cl_2, 298 K).**

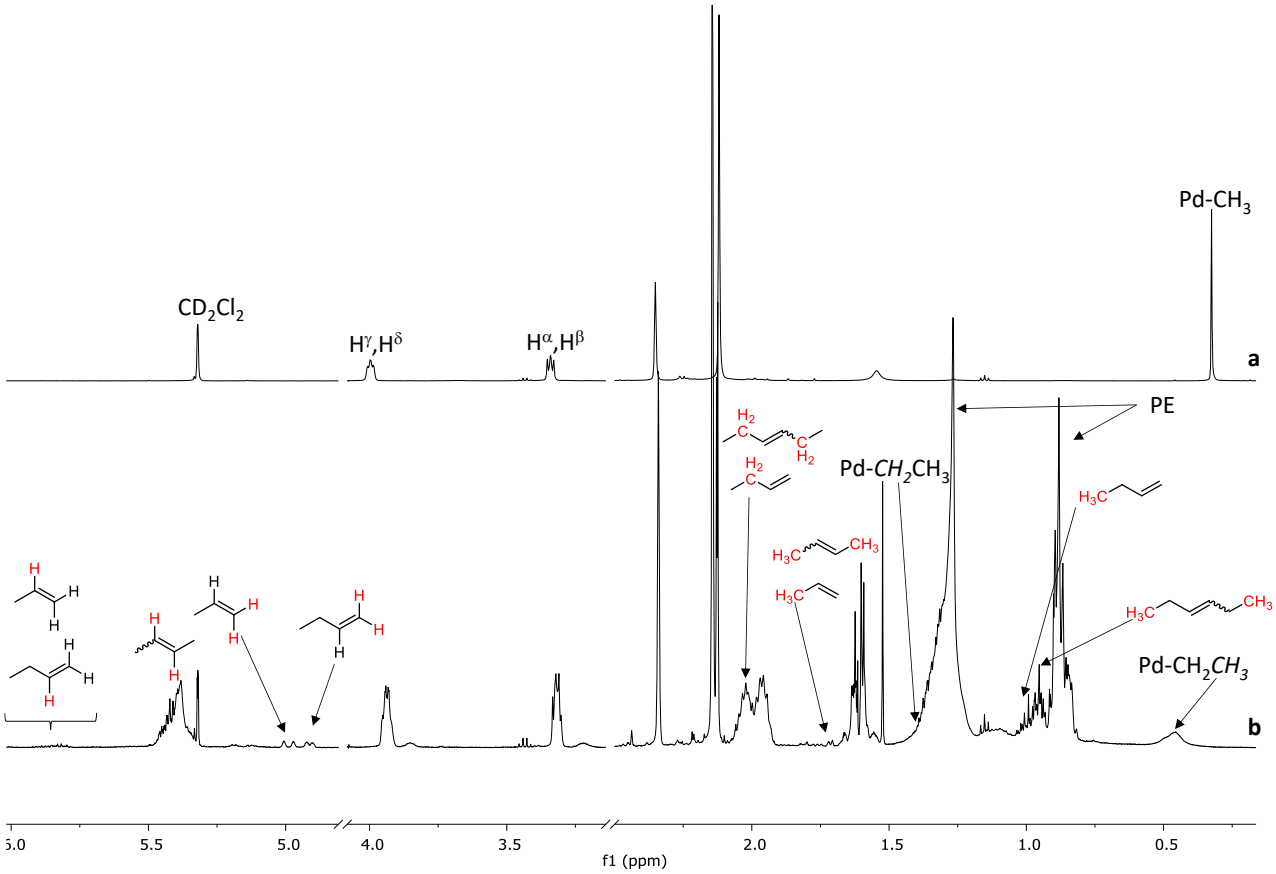

Figure S3.42. ^{1}H NMR spectra (CD_2Cl_2, 298 K) of (a) **6c** and (b) **6c** + ethylene at t = 5 min.

***In situ* NMR reactivity of 5b with methyl acrylate (CD_2Cl_2, 298 K).**

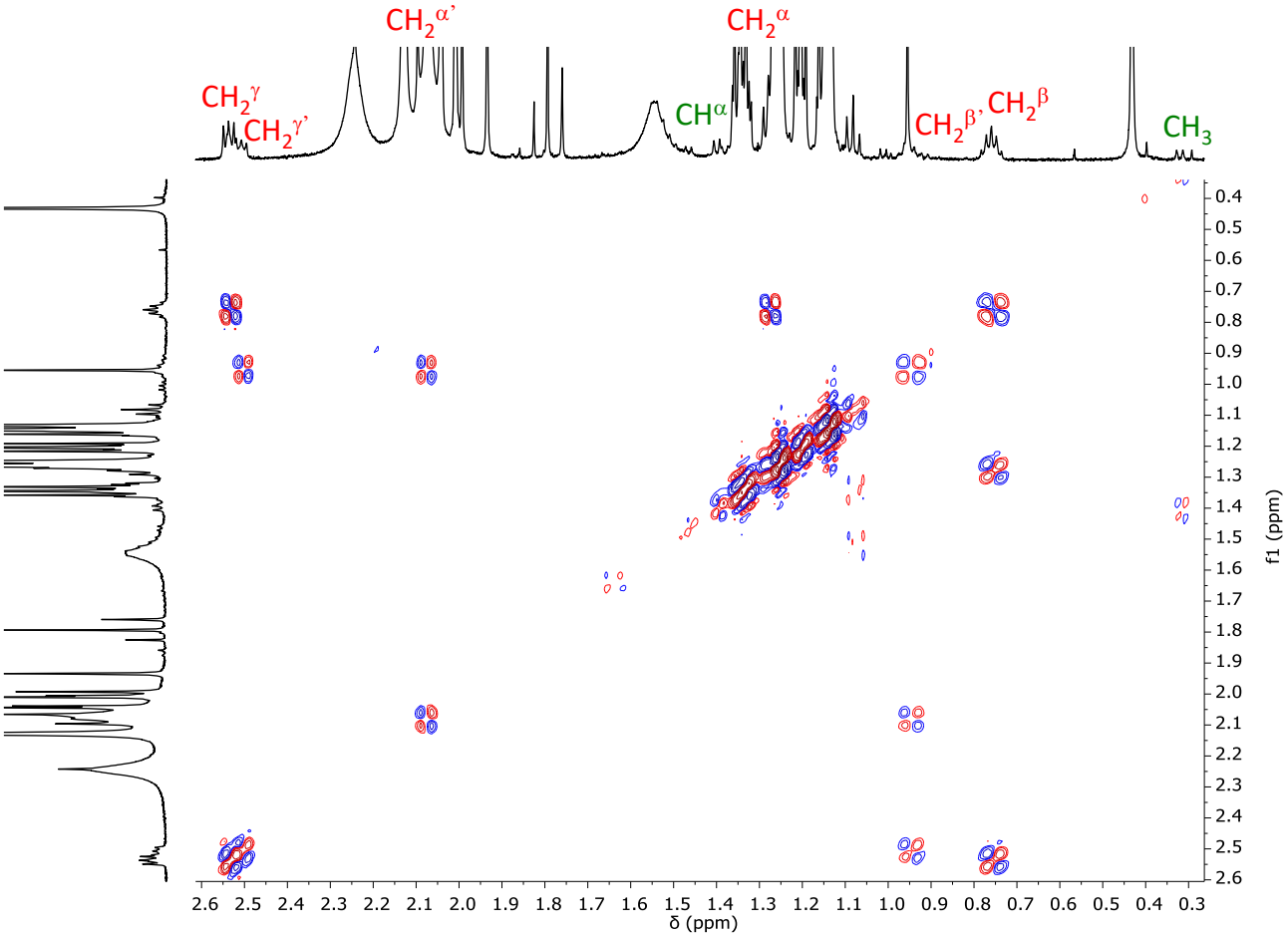

Figure S3.43 $^1H,^1H$ DQCOSY spectrum (CD_2Cl_2, 298 K) of the reaction of **5b** with MA at t = 60 min.

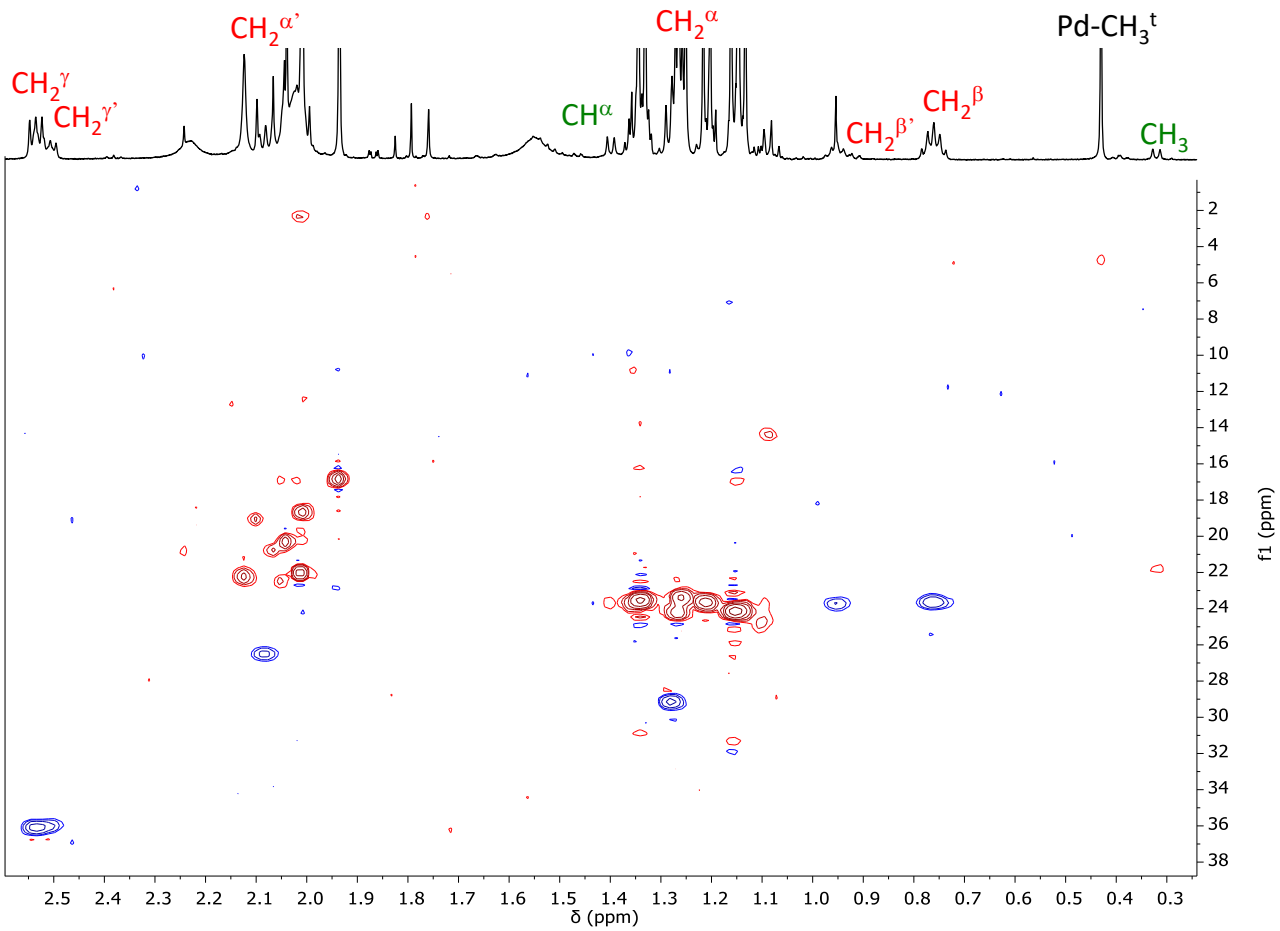

Figure S3.44. $^{1}H,^{13}C$ HSQC spectrum (CD_2Cl_2, 298 K) of the reaction of **5b** with MA at t = 60 min.

***In situ* NMR reactivity of 5c with methyl acrylate (CD_2Cl_2, 298 K).**

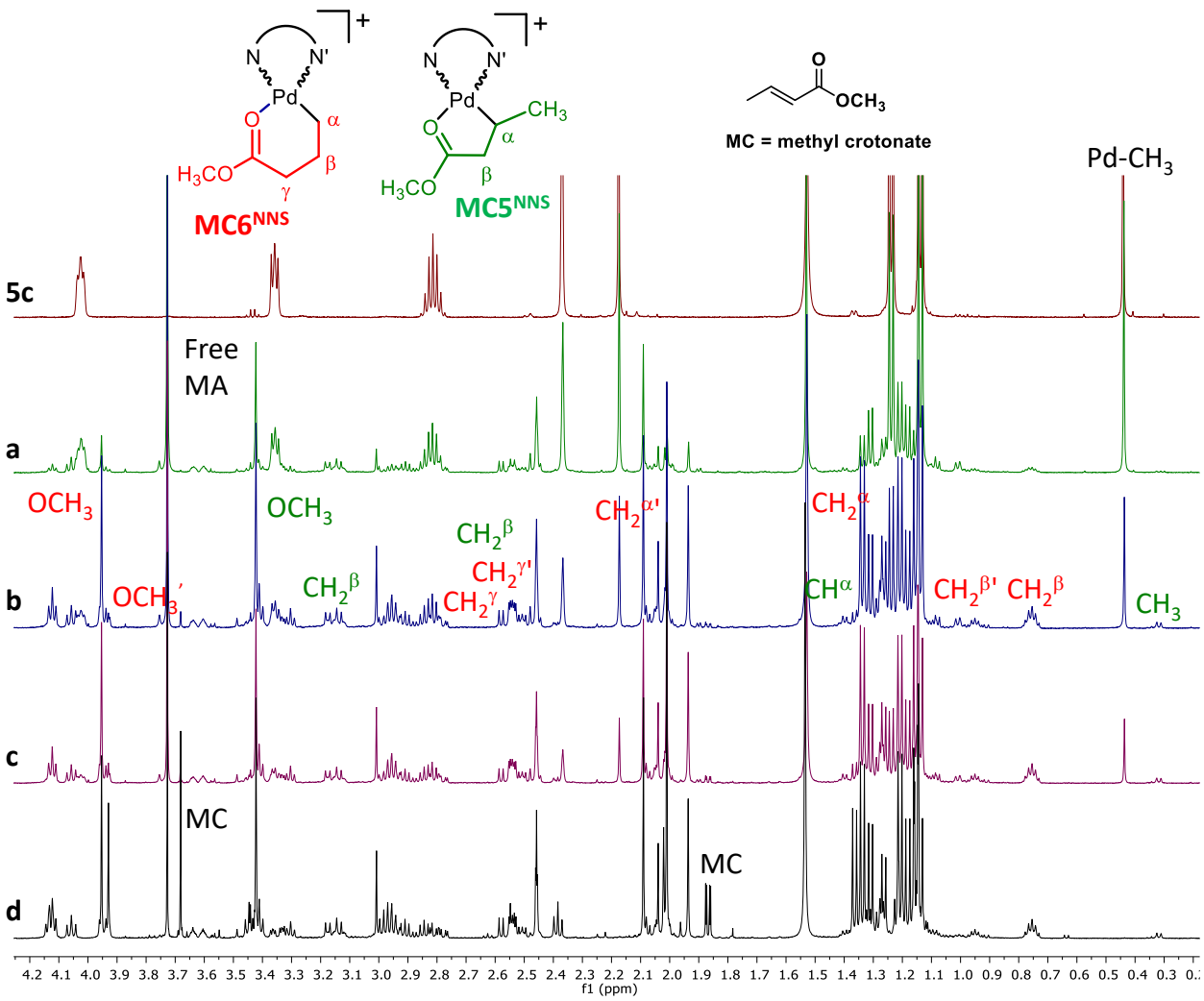

Figure S3.45. ^{1}H NMR spectra (CD_2Cl_2, 298 K) of the reaction of **5c** (top spectrum) with MA at (a) t = 15 min, (b) t = 60 min, (c) t = 4 h and (d) t = 19 h.

***In situ* NMR reactivity of 6c with methyl acrylate (CD_2Cl_2, 298 K).**

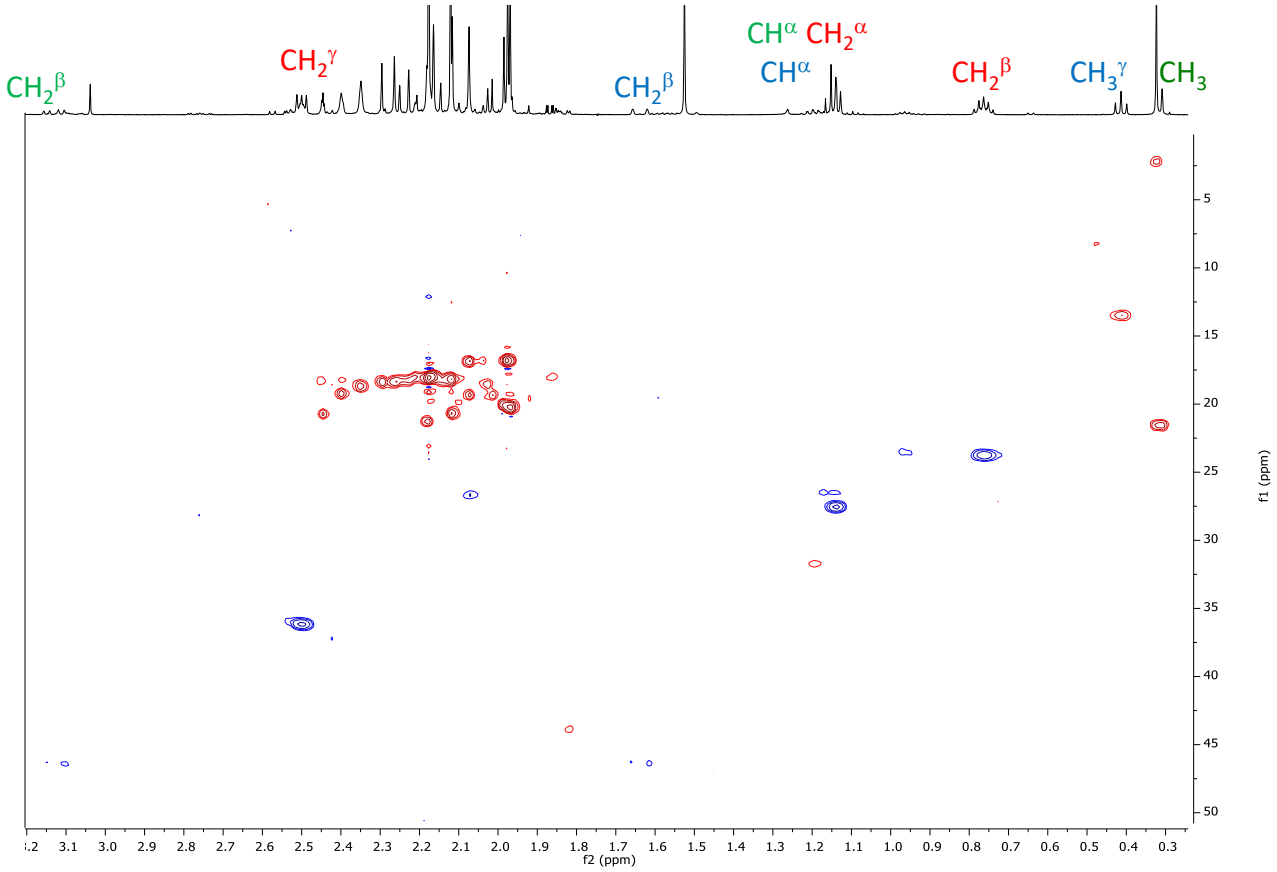

Figure S3.46. $^{1}H,^{13}C$ HSQC spectrum (CD_2Cl_2, 298 K) of the reaction of **6c** with MA at t = 2 h.

Appendix Chapter 4.

NMR characterization of complexes.

NMR characterization of 1^{pyr} (CD_2Cl_2, 298 K).

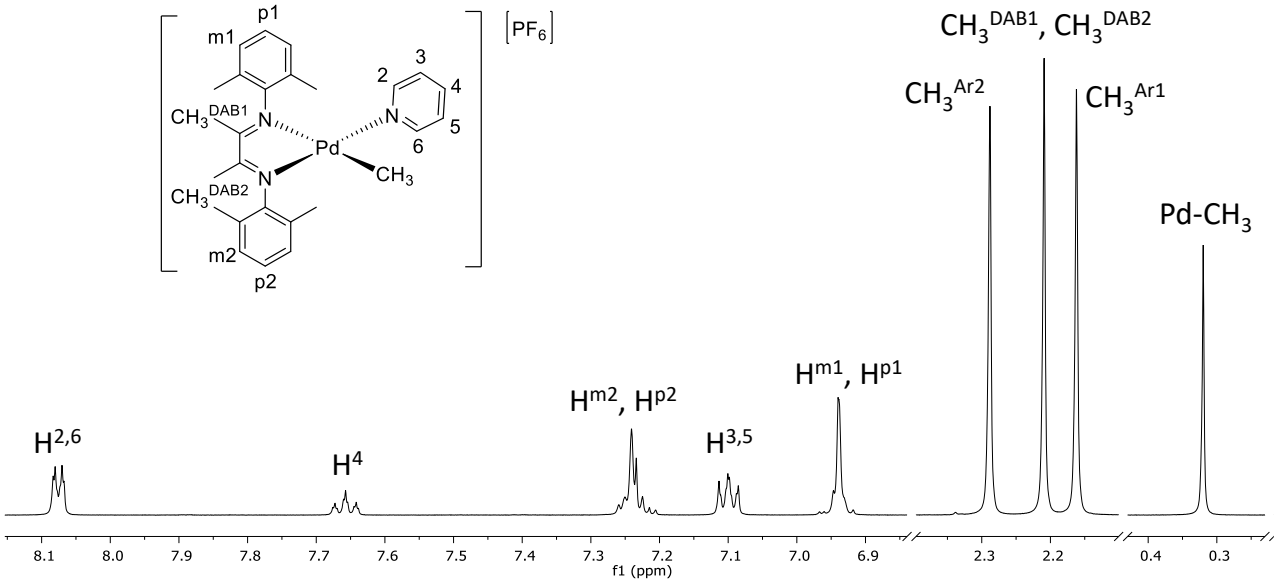

Figure S4.1. ^{1}H NMR spectrum (CD_2Cl_2, 298 K) of $\mathbf{1^{pyr}}$.

NMR characterization of 1^{2pic} (CD_2Cl_2, 298 K).

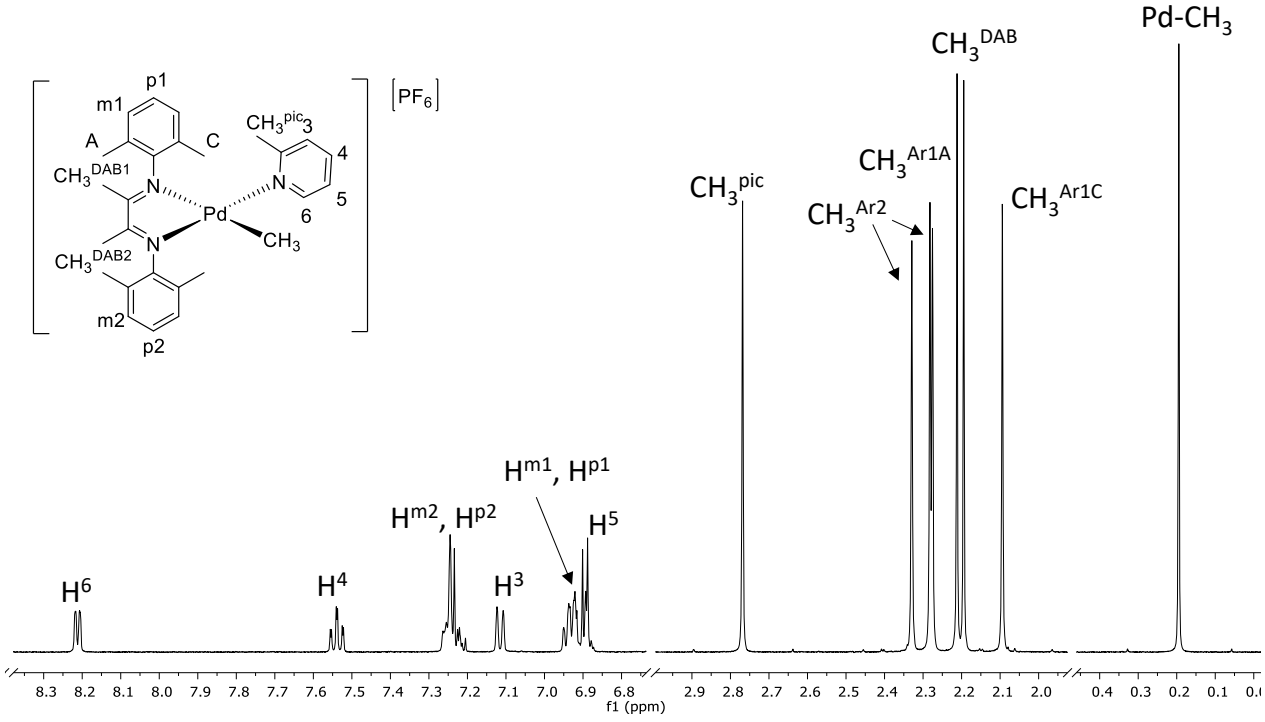

Figure S4.2. ^{1}H NMR spectrum (CD_2Cl_2, 298 K) of $\mathbf{1^{2pic}}$.

Figure S4.6. ^{1}H,^{1}H COSY spectrum (CD_2Cl_2, 298 K) of $\mathbf{1^{2pic}}$.

NMR characterization of 1^{4pic} (CD_2Cl_2, 298 K).

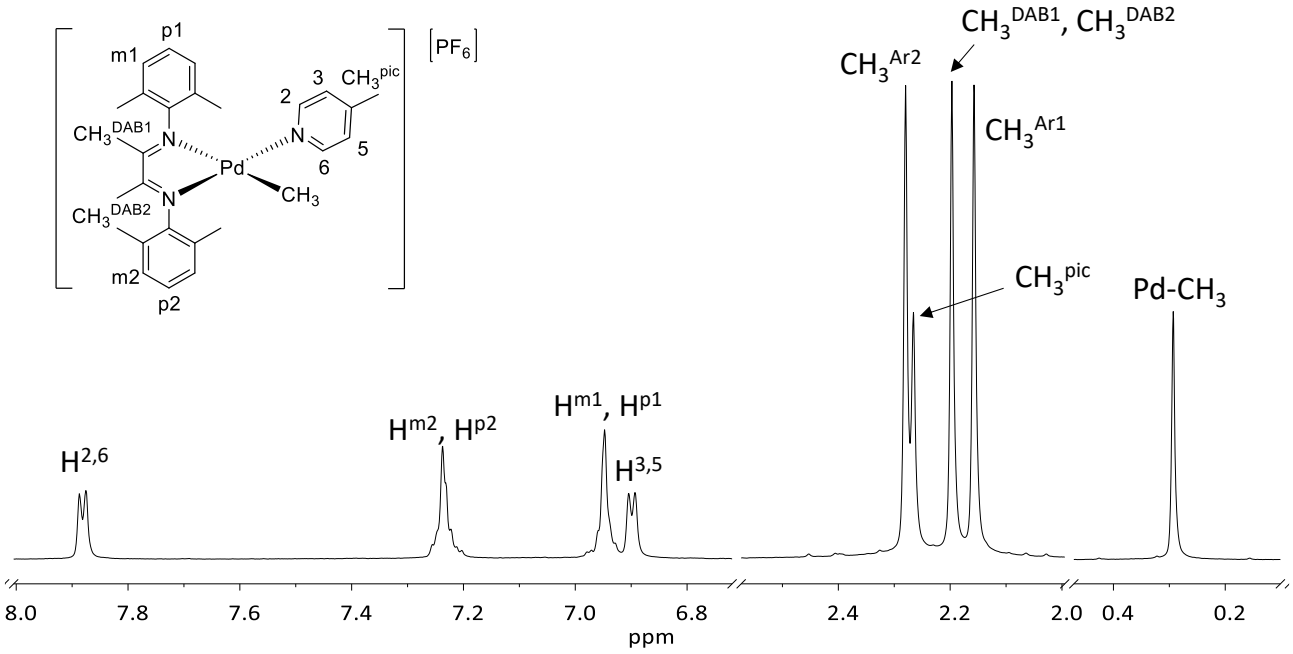

Figure S4.3. ^{1}H NMR spectrum (CD_2Cl_2, 298 K) of $\mathbf{1^{4pic}}$.

NMR characterization of $1^{2,6lut}$ (CD_2Cl_2, 298 K).

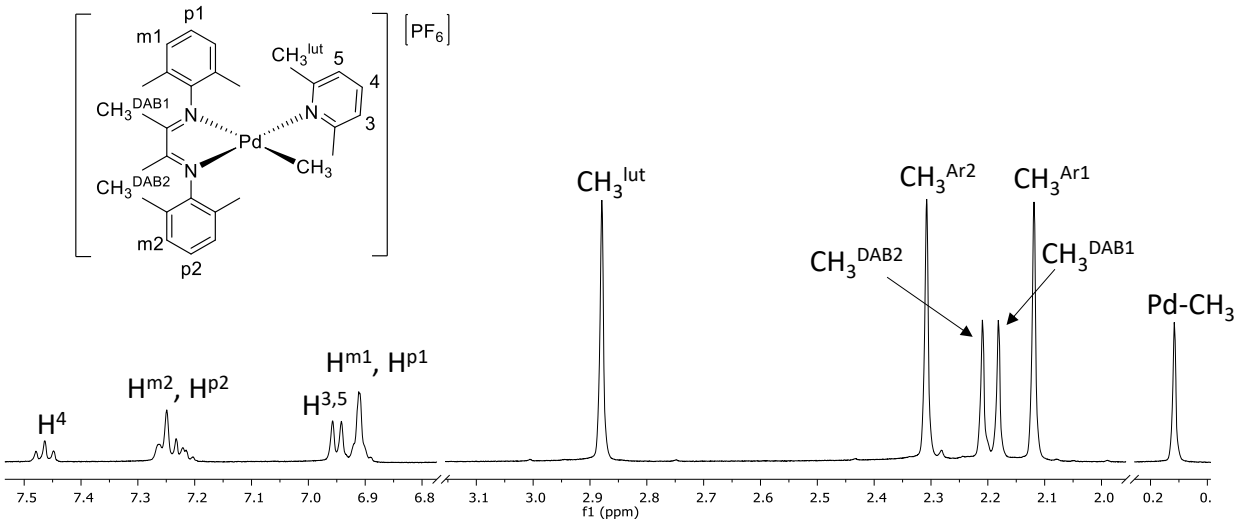

Figure S4.4. ^{1}H NMR spectrum (CD_2Cl_2, 298 K) of $\mathbf{1^{2,6lut}}$.

NMR characterization of $1^{3,5lut}$ (CD_2Cl_2, 298 K).

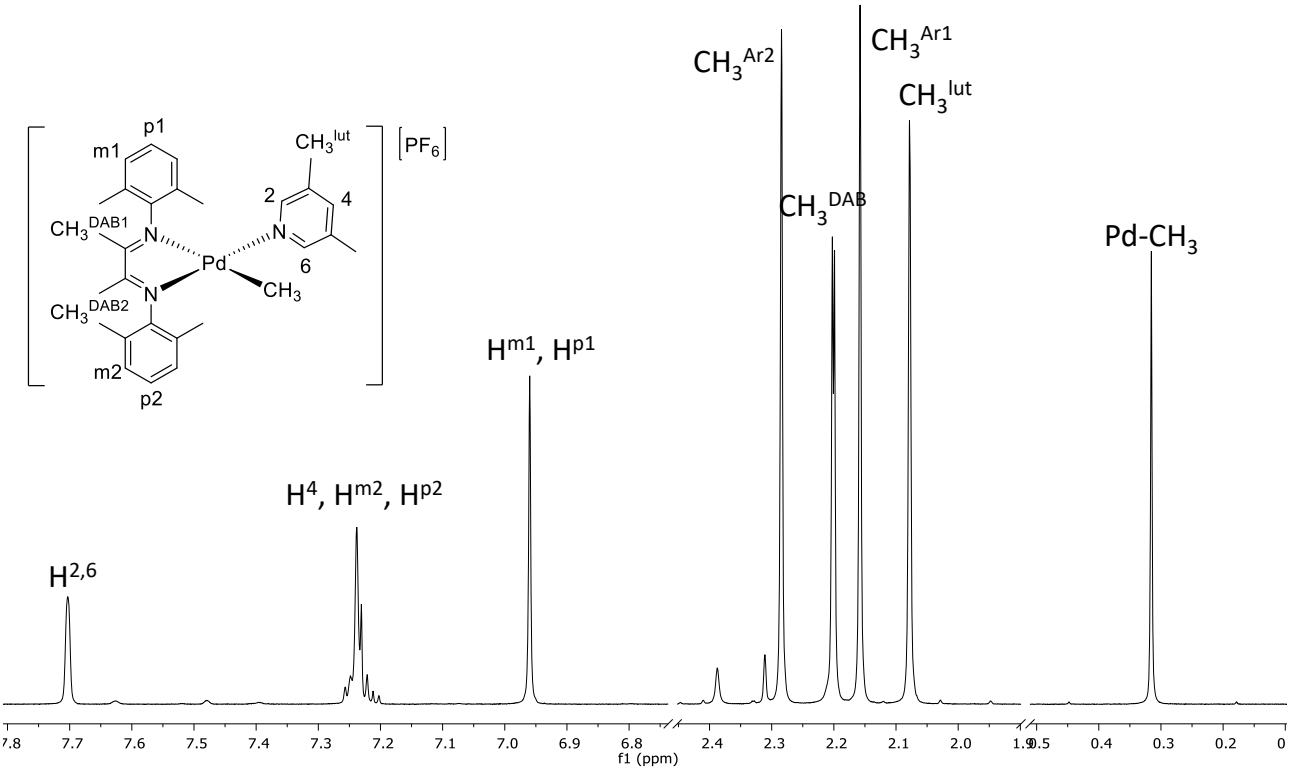

Figure S4.5. ^{1}H NMR spectrum (CD_2Cl_2, 298 K) of $\mathbf{1^{3,5lut}}$.

NMR characterization of 2^{pyr} (CD_2Cl_2, 298 K).

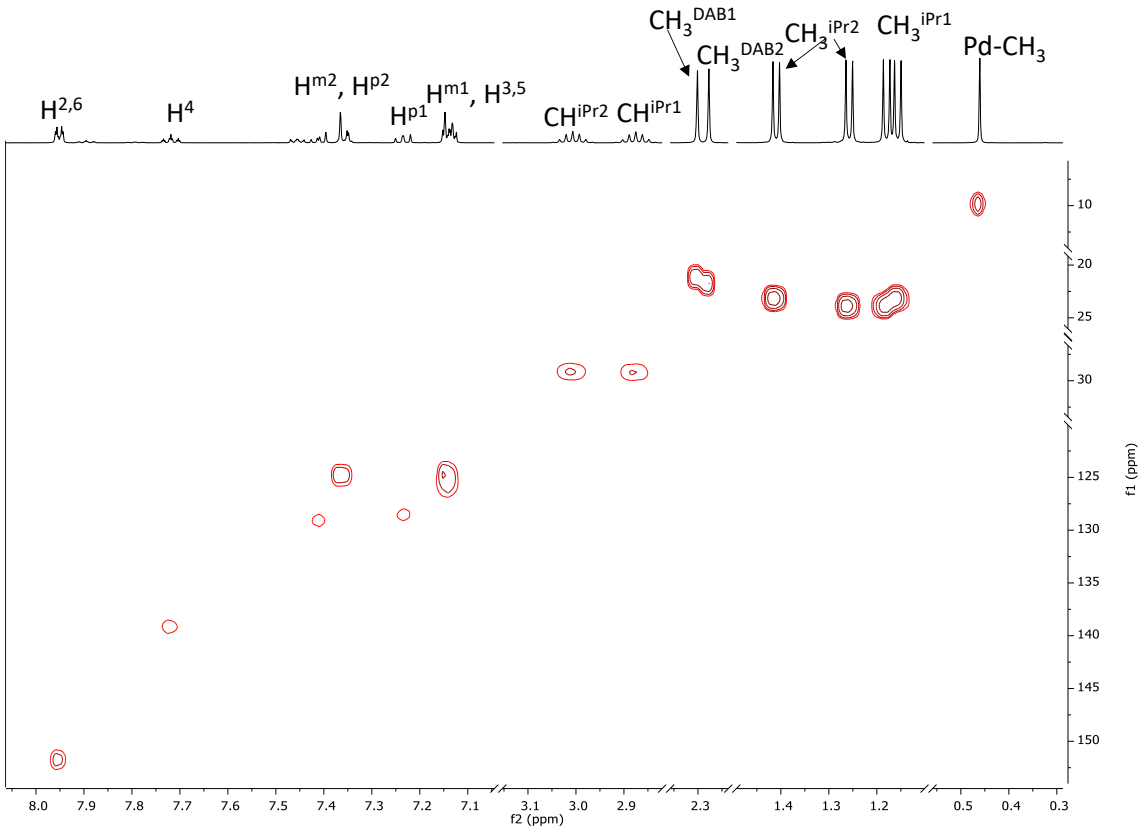

Figure S4.6. $^{1}H,^{13}C$ HSQC spectrum (CD_2Cl_2, 298 K) of $\mathbf{2^{pyr}}$.

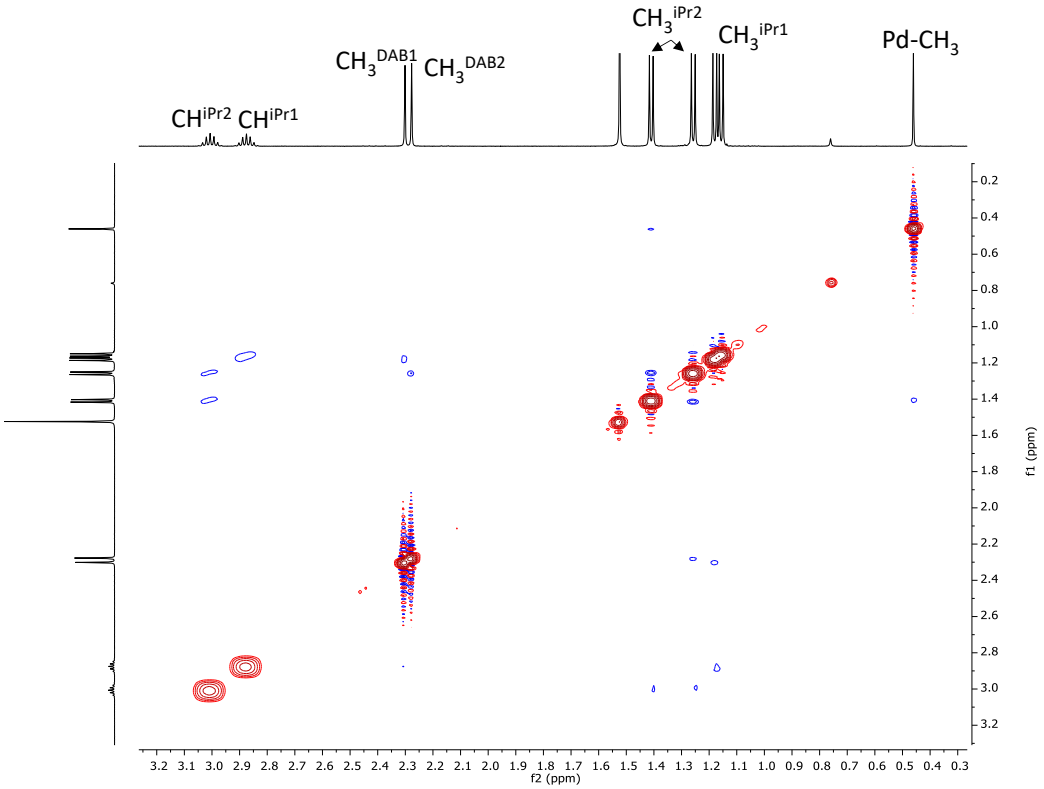

Figure S4.7. ^{1}H,^{1}H NOESY spectrum (CD_2Cl_2, 298 K) of **2^{pyr}**.

NMR characterization of 2^{2pic} (CD_2Cl_2, 298 K).

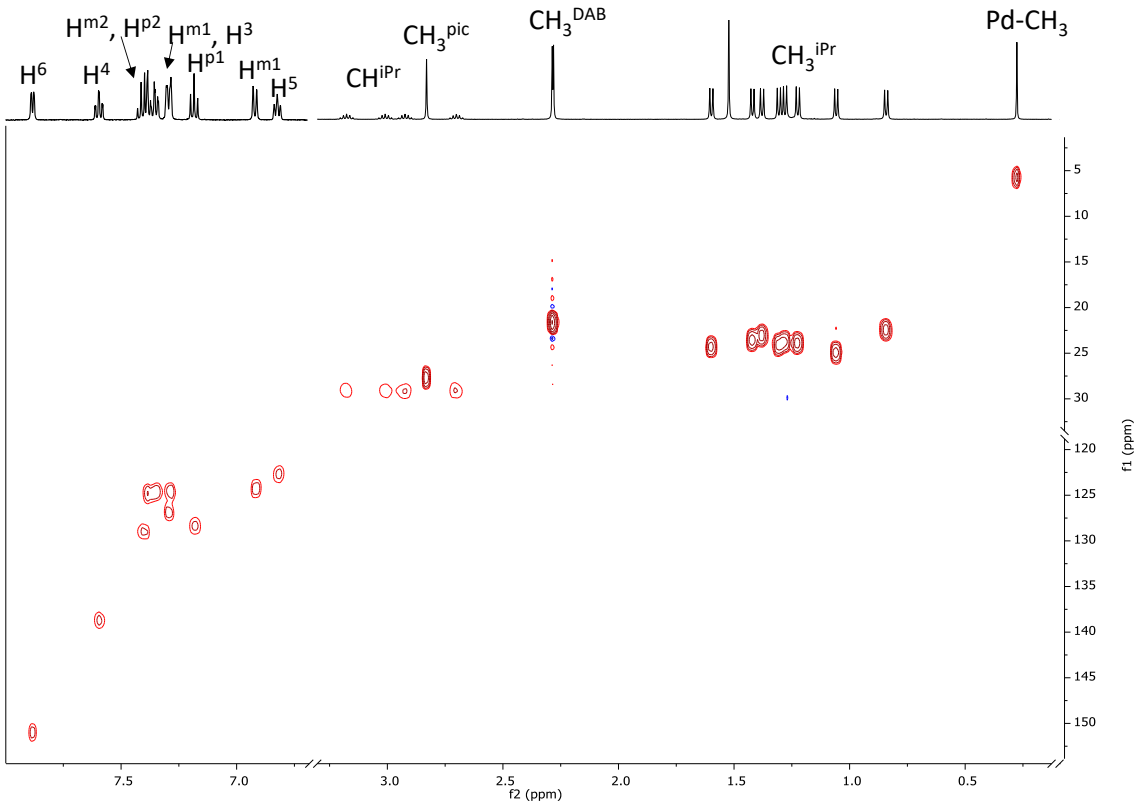

Figure S4.8. ^{1}H,^{13}C HSQC spectrum (CD_2Cl_2, 298 K) of **2^{2pic}** (aliphatic and aromatic region not on scale).

NMR characterization of 2^{4pic} (CD_2Cl_2, 298 K).

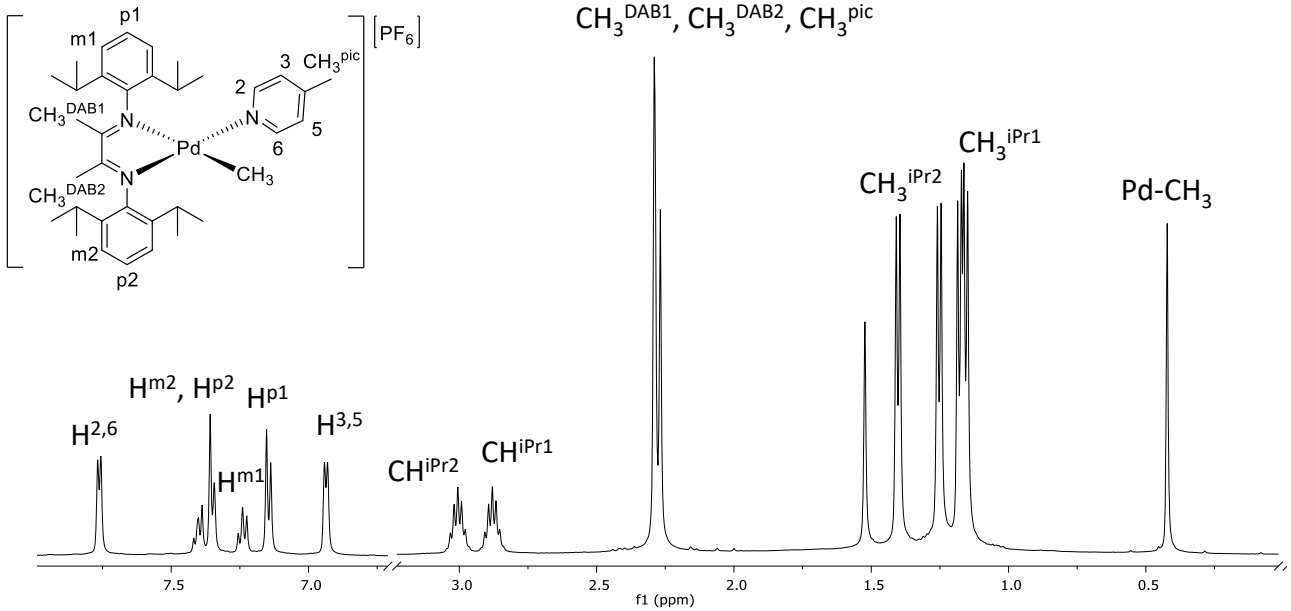

Figure S4.9. ^{1}H NMR spectrum (CD_2Cl_2, 298 K) of $\mathbf{2^{4pic}}$.

NMR characterization of $2^{2,6lut}$ (CD_2Cl_2, 298 K).

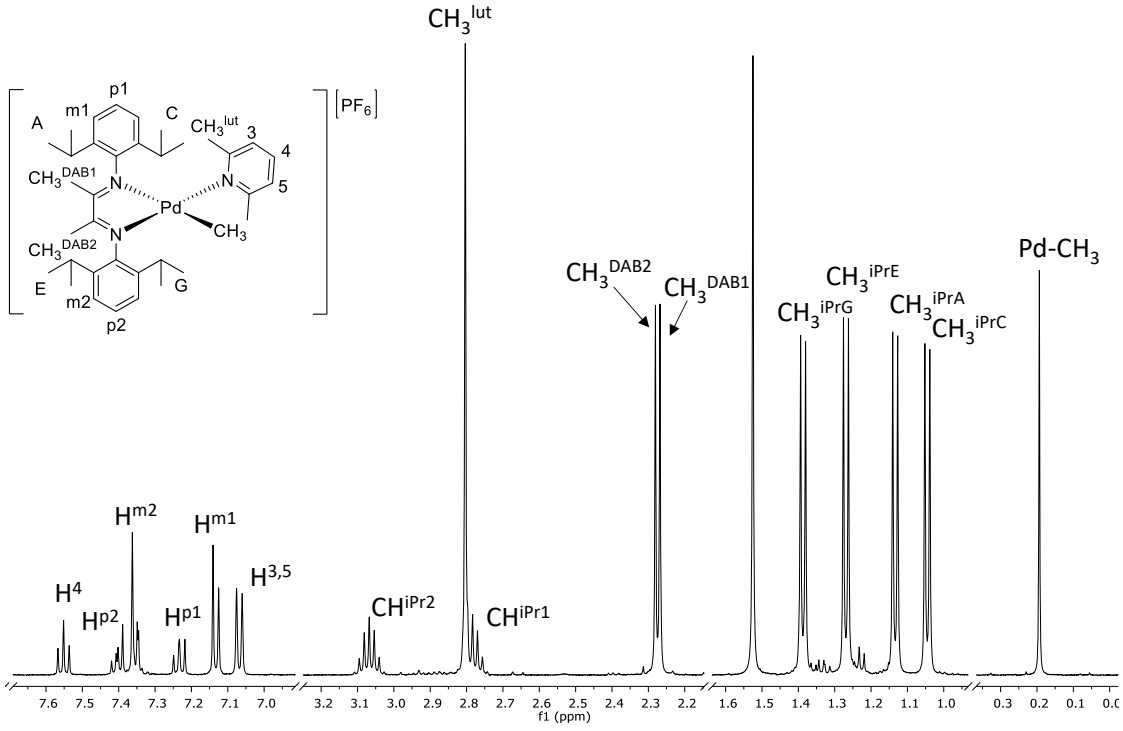

Figure S4.10. ^{1}H NMR spectrum (CD_2Cl_2, 298 K) of $\mathbf{2^{2,6lut}}$.

NMR characterization of $2^{3,5lut}$ (CD_2Cl_2, 298 K).

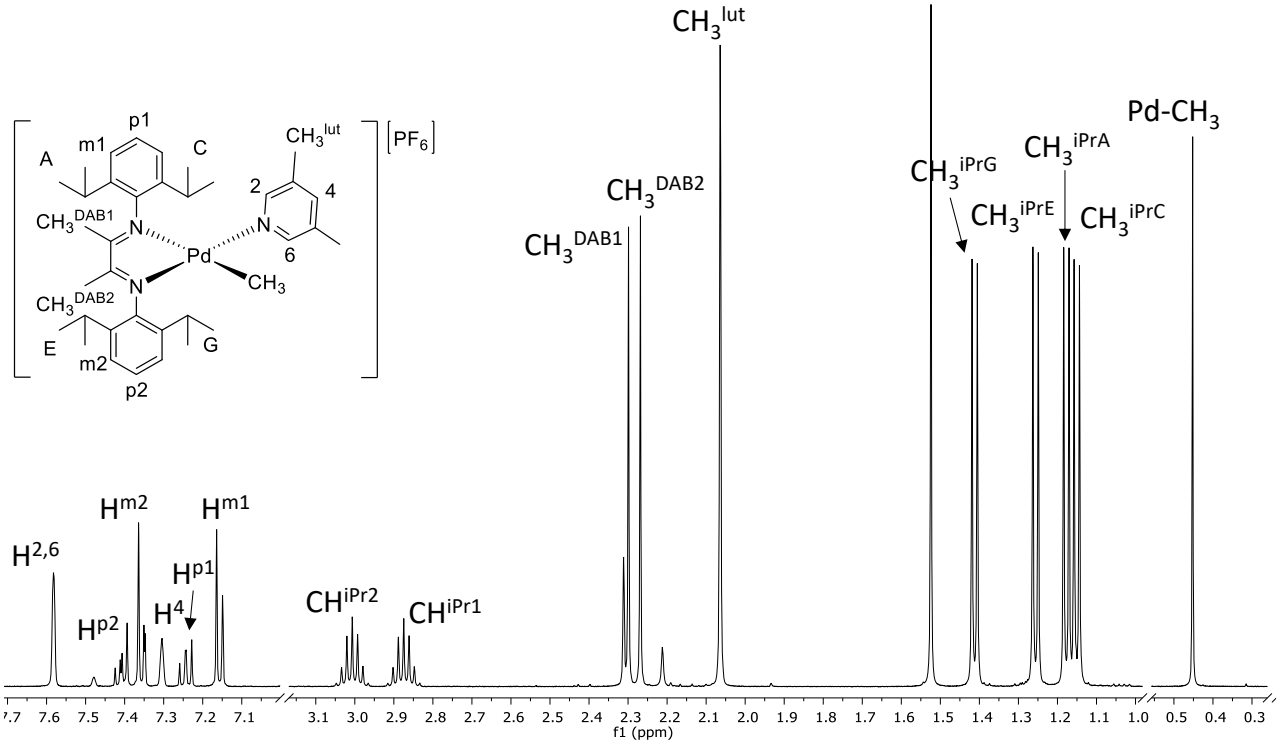

Figure S4.11. ^{1}H NMR spectrum (CD_2Cl_2, 298 K) of $\mathbf{2^{3,5lut}}$.

X-ray crystallography

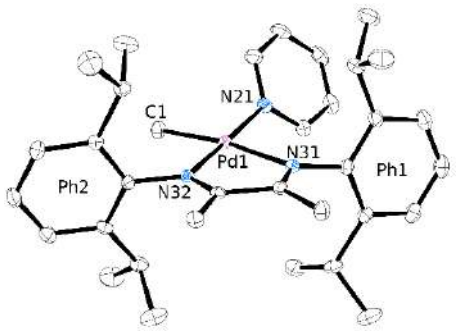

Figure S4.12. ORTEP drawing (50% probability ellipsoids) of the molecule of $\mathbf{2^{pyr}}$. Hydrogen atoms and the PF_6^- anion have been omitted for the sake of clarity.

Table S4.1. Most significant distances (Å) and angles (°) of $\mathbf{1}^{\mathbf{2pic}}$, $\mathbf{1}^{\mathbf{4pic}}$ and $\mathbf{2}^{\mathbf{pyr}}$ – $\mathbf{2}^{\mathbf{4pic}}$.

	$\mathbf{1}^{\mathbf{2pic}}$	$\mathbf{1}^{\mathbf{4pic}}$	$\mathbf{2}^{\mathbf{pyr}}$	$\mathbf{2}^{\mathbf{2pic}}$	$\mathbf{2}^{\mathbf{4pic}}$
Distances (Å)					
Pd1-C1	2.025(2)	2.029(3)	2.033(2)	2.077(2)	2.046(2)
Pd1-N21	2.032(1)	2.039(2)	2.042(1)	2.053(2)	2.041(2)
Pd1-N31	2.121(1)	2.145(2)	2.140(1)	2.130(2)	2.145(2)
Pd1-N32	2.033(1)	2.040(2)	2.031(1)	2.041(1)	2.032(1)
Angles (°)					
C1-Pd1-N31	171.98(6)	172.6(1)	170.89(6)	170.92(6)	171.70(6)
N21-Pd1-C1	90.14(6)	88.5(1)	89.27(6)	89.80(7)	88.37(7)
N21-Pd1-N31	96.19(5)	98.91(9)	99.12(5)	98.30(6)	99.86(6)
N32-Pd1-C1	96.54(6)	95.1(1)	94.50(6)	94.71(6)	94.53(7)
N32-Pd1-N21	172.36(5)	174.57(8)	174.09(5)	174.77(6)	174.66(6)
N32-Pd1-N31	77.49(5)	77.44(8)	77.42(5)	77.39(6)	77.35(6)
Dihedral angles (°)					
[Ph1]-[Pd1]	88.00(5)	88.14(8)	85.70(6)	83.44(6)	85.72(6)
[Ph2]-[Pd1]	83.03(5)	81.82(9)	78.96(6)	76.06(6)	76.71(6)
[Pyr]-[Pd1]	82.30(5)	57.0(1)	55.68(7)	30.20(9)	52.71(7)

Ethylene/methyl acrylate copolymerization reaction.

NMR Characterization of the synthesized E/MA copolymers.

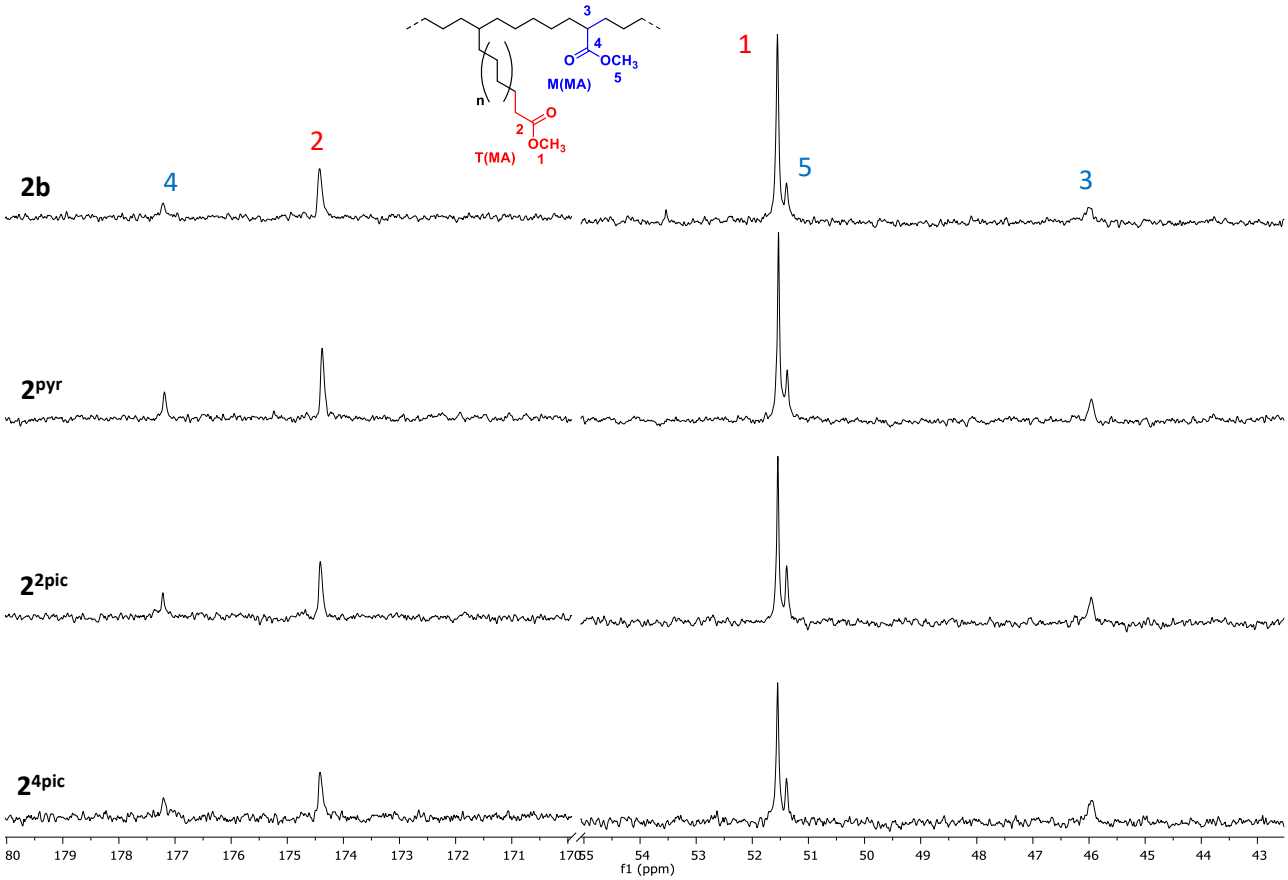

Figure S4.13. ^{13}C NMR spectra ($CDCl_3$, 298 K) of E/MA copolymers obtained with [Pd(CH_3)(L)(**2**)][PF_6] in TFE (Table 4.3, entry 1 – 4); (left) carbonyl region; (right) methoxy and methinic region;* ligand.

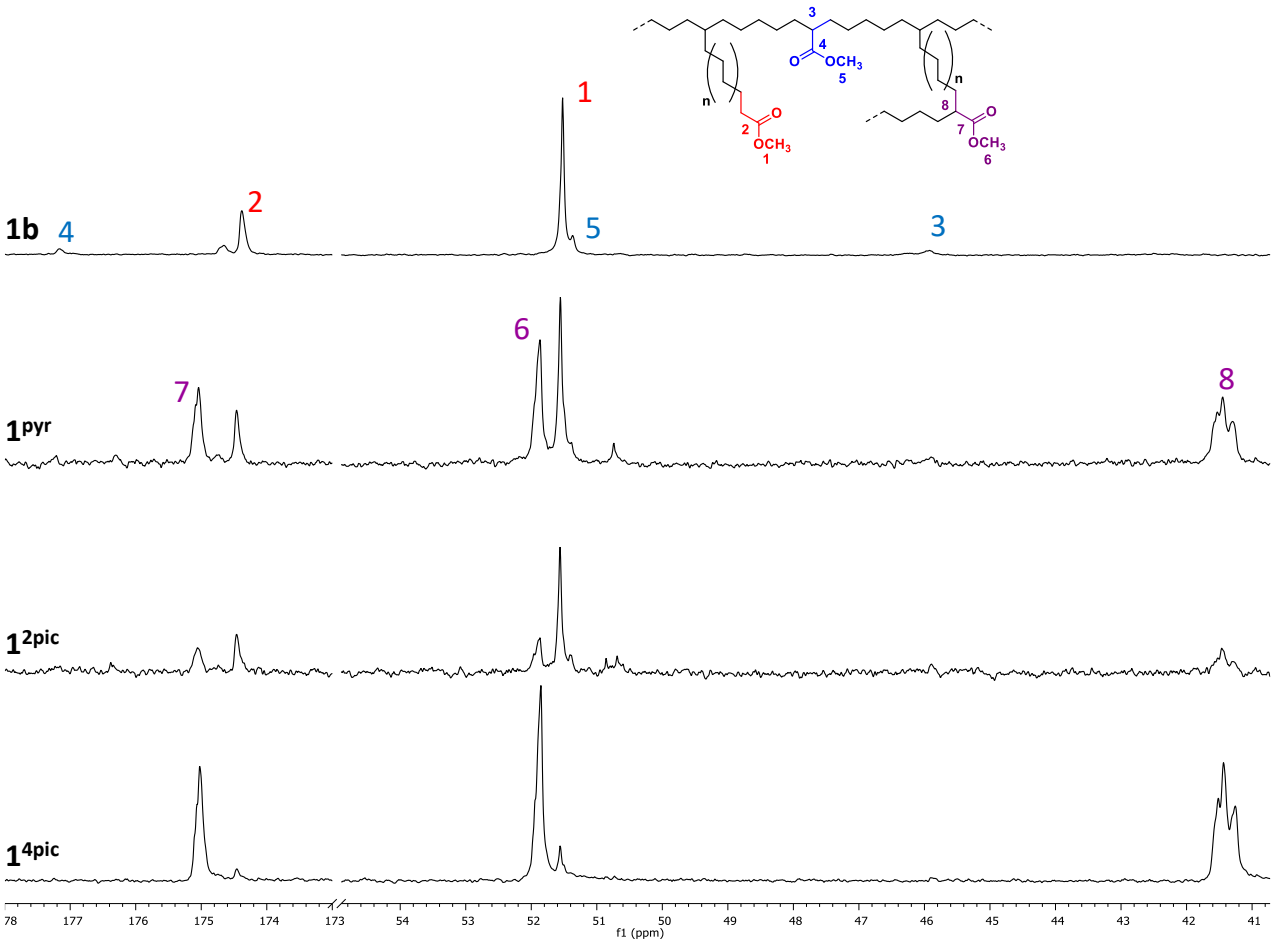

Figure S4.14. ^{13}C NMR spectra ($CDCl_3$, 298 K) of E/MA copolymers obtained with $[Pd(CH_3)(L)(\mathbf{1})][PF_6]$ in CH_2Cl_2 (Table 4.2, entries 7 – 10); (left) carbonyl region; (right) methoxy and methinic region.

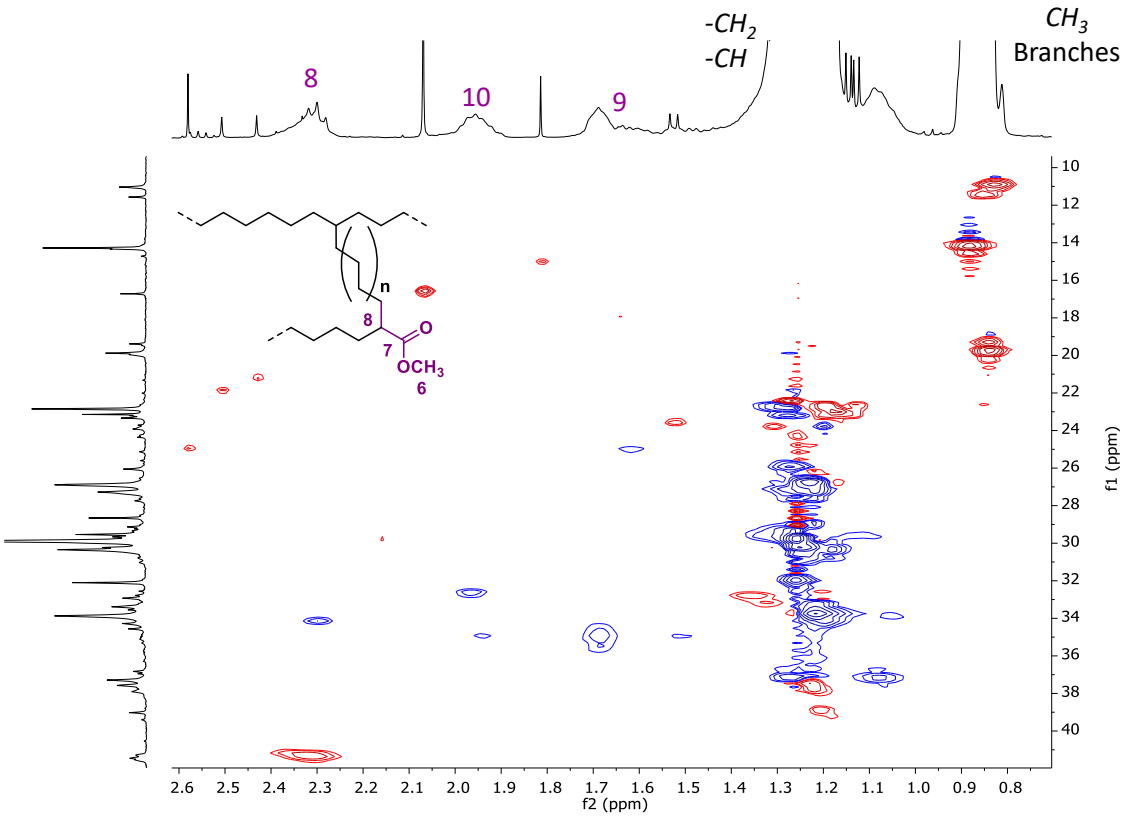

Figure S4.15. $^{1}H,^{13}C$ HSQC spectrum ($CDCl_3$, 298 K) of E/MA copolymer obtained with **2^{pyr}** in CH_2Cl_2.

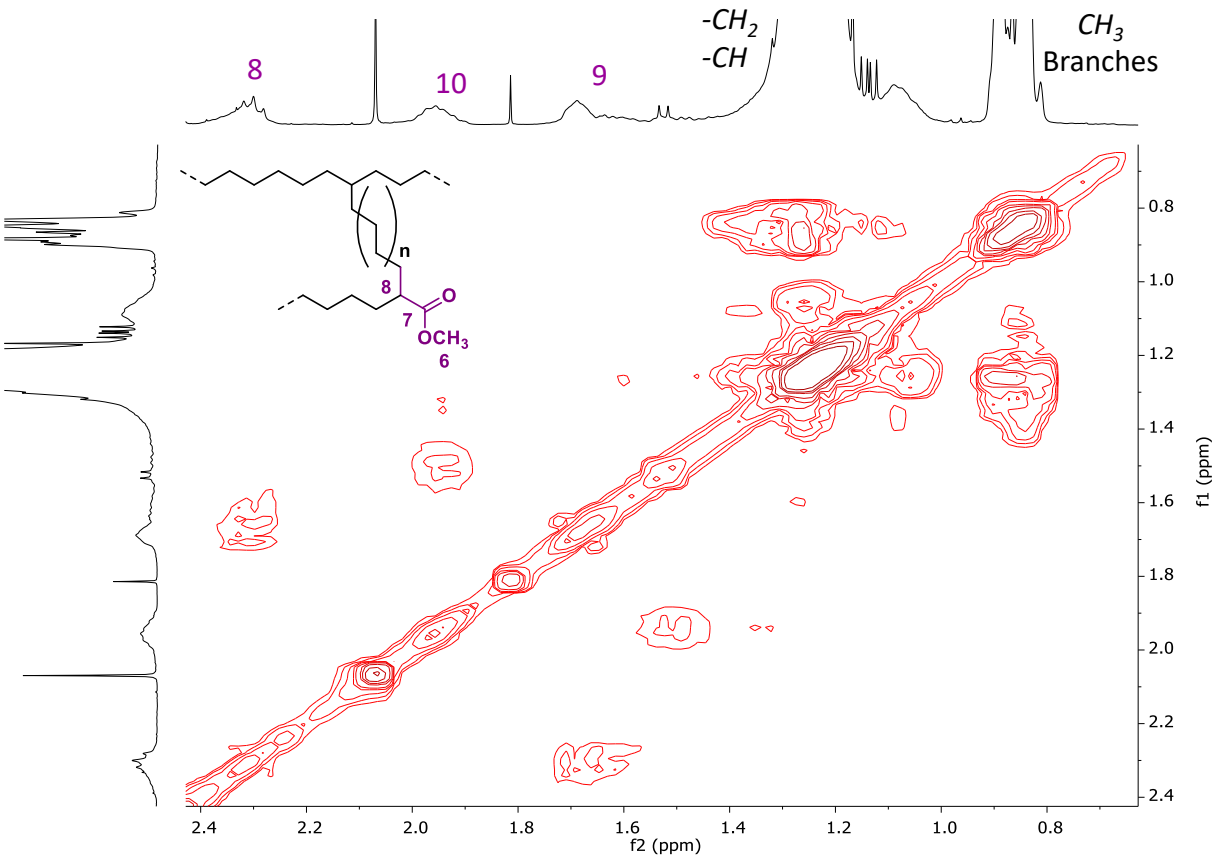

Figure S4.16. ^{1}H,^{1}H COSY spectrum ($CDCl_3$, 298 K) of E/MA copolymer obtained with **2^{pyr}** in DCM.

Calculation of branching degree[1]

The determination of branching degree (branches/1000C atoms) was estimated by ^{1}H NMR following Equations 4a and 4b.

$$\frac{Branches}{1000C} = \frac{I_{CH} \times 1000}{\frac{I_{CH3}}{3} + \frac{I_{CH_2/CH} + I_{CH}}{2} + \frac{I_{CH_2(allyl)}}{2} + I_{CH_2(vinyl)} + I_{CH_2(vinylene)}} \quad \textbf{(4a)}$$

$$I_{CH} = \frac{I_{CH3} - \frac{3I_{CH_2(vinyl)}}{2} - 3I_{CH_2(vinylene)}}{3} \quad \textbf{(4b)}$$

Determination of the branches distribution (%)[2]

The integration areas (I) used to quantify the different types of branches correspond to the area of the methyl group of each type of branch in the ^{13}C NMR spectrum following Equations:

I_{Methyl} = I6 – I4 (where I4 = I7)

I_{Ethyl} = I1

I_{Propyl} = I4

I_{Butyl} = I3 – [(I8 + I17)/2]

$I_{Sec\text{-}Butyl}$ = (I2 + I5)/2

I_{Longer} = (I8 + I17)/2

The total intensity of methyl groups, $I_{total\ CH3}$, is given by: $I_{total\ CH3}$ = (I2 + I5)/2 + I1 + I3 + I6 where I6 is the total integral I6 + I7, with I7 = I4.

The branches distribution (%) was estimated by Equation 4c:

$$Branch\ type\ (\%) = \frac{I_{branch\ type}}{I_{total\ CH3}} \cdot 100 \qquad \textbf{(4c)}$$

Table S4.2. Ethylene/methyl acrylate copolymerization: effect of ethylene pressure. Precatalyst: [Pd(CH$_3$)(pyr)(1)][PF$_6$], 1^{pyr} [a]

entry	P_{Et} (bar)	yield (g)	kg CP/mol Pd[b]	MA (mol %)[c]	TON[d]		Bd[e]
					E	MA	
1	2.5	0.0484	2.30	6.1	69	4	100
2	5.0	0.0894	4.26	5.0	131	7	102
3	7.0	0.1078	5.13	2.4	170	4	102

[a] Reaction conditions: n_{Pd} = 2.1·10^{-5} mol, V_{CH2Cl2} = 21 mL, V_{MA} = 1.130 mL, [MA]/[Pd] = 594, T = 308 K, t = 6 h; [b] productivity in kg CP/mol Pd = kilograms of copolymer per mole of palladium; [c] calculated by ^{1}H NMR spectroscopy on isolated product; [d] Turnover number = mol of substrate converted per mol of catalyst (E = ethylene); [e] branching degree calculated by ^{1}H NMR spectroscopy on isolated product and expressed as branches per 1000 carbon atoms.

Table S4.3. Ethylene/methyl acrylate copolymerization: effect of ethylene pressure. Precatalyst: [Pd(CH$_3$)(pyr)(2)][PF$_6$], 2^{pyr} [a]

entry	P_{Et} (bar)	yield (g)	kg CP/mol Pd[b]	MA (mol %)[c]	TON[d]		Bd[e]
					E	MA	
1	2.5	0.0711	3.38	6.6	99	7	85
2	5.0	0.1098	5.23	0.5	183	1	92
3	7.0	0.1292	6.15	0.8	214	2	91

[a] Reaction conditions: n_{Pd} = 2.1·10^{-5} mol, V_{CH2Cl2} = 21 mL, V_{MA} = 1.130 mL, [MA]/[Pd] = 594, T = 308 K, t = 6 h; [b] productivity in kg CP/mol Pd = kilograms of copolymer per mole of palladium; [c] calculated by ^{1}H NMR spectroscopy on isolated product; [d] Turnover number = mol of substrate converted per mol of catalyst (E = ethylene); [e] branching degree calculated by ^{1}H NMR spectroscopy on isolated product and expressed as branches per 1000 carbon atoms.

Table S4.4. Ethylene/methyl acrylate copolymerization: effect of [MA]/[Pd] ratio.

Precatalyst: [Pd(CH$_3$)(pyr)(1)][PF$_6$], 1^{pyr} [a]

entry	[MA]/[Pd]	yield (g)	kg CP/mol Pd[b]	MA (mol %)[c]	TON[d]		Bd[e]
					E	MA	
1	594	0.0484	2.30	6.1	69	4	100
2	1188	0.0390	1.86	6.6	54	4	97
3	1782	0.0216	1.03	13.3	25	4	109

[a] Reaction conditions: $n_{Pd} = 2.1 \cdot 10^{-5}$ mol, $V_{CH2Cl2} = 21$ mL, $P_{Et} = 2.5$ bar, T = 308 K, t = 6 h; [b] productivity in kg CP/mol Pd = kilograms of copolymer per mole of palladium; [c] calculated by ^{1}H NMR spectroscopy on isolated product; [d] Turnover number = mol of substrate converted per mol of catalyst (E = ethylene); [e] branching degree calculated by ^{1}H NMR spectroscopy on isolated product and expressed as branches per 1000 carbon atoms.

Table S4.5. Ethylene/methyl acrylate copolymerization: effect of [MA]/[Pd] ratio.

Precatalyst: [Pd(CH$_3$)(pyr)(2)][PF$_6$], 2^{pyr} [a]

entry	[MA]/[Pd]	yield (g)	kg CP/mol Pd[b]	MA (mol %)[c]	TON[d]		Bd[e]
					E	MA	
1	594	0.0711	3.38	6.6	99	7	85
2	1188	0.0520	2.48	8.5	69	6	87
3	1782	0.0368	1.75	22.2	33	10	79

[a] Reaction conditions: $n_{Pd} = 2.1 \cdot 10^{-5}$ mol, $V_{CH2Cl2} = 21$ mL, $P_{Et} = 2.5$ bar T = 308 K, t = 6 h; [b] productivity in kg CP/mol Pd = kilograms of copolymer per mole of palladium; [c] calculated by ^{1}H NMR spectroscopy on isolated product; [d] Turnover number = mol of substrate converted per mol of catalyst (E = ethylene); [e] branching degree calculated by ^{1}H NMR spectroscopy on isolated product and expressed as branches per 1000 carbon atoms.

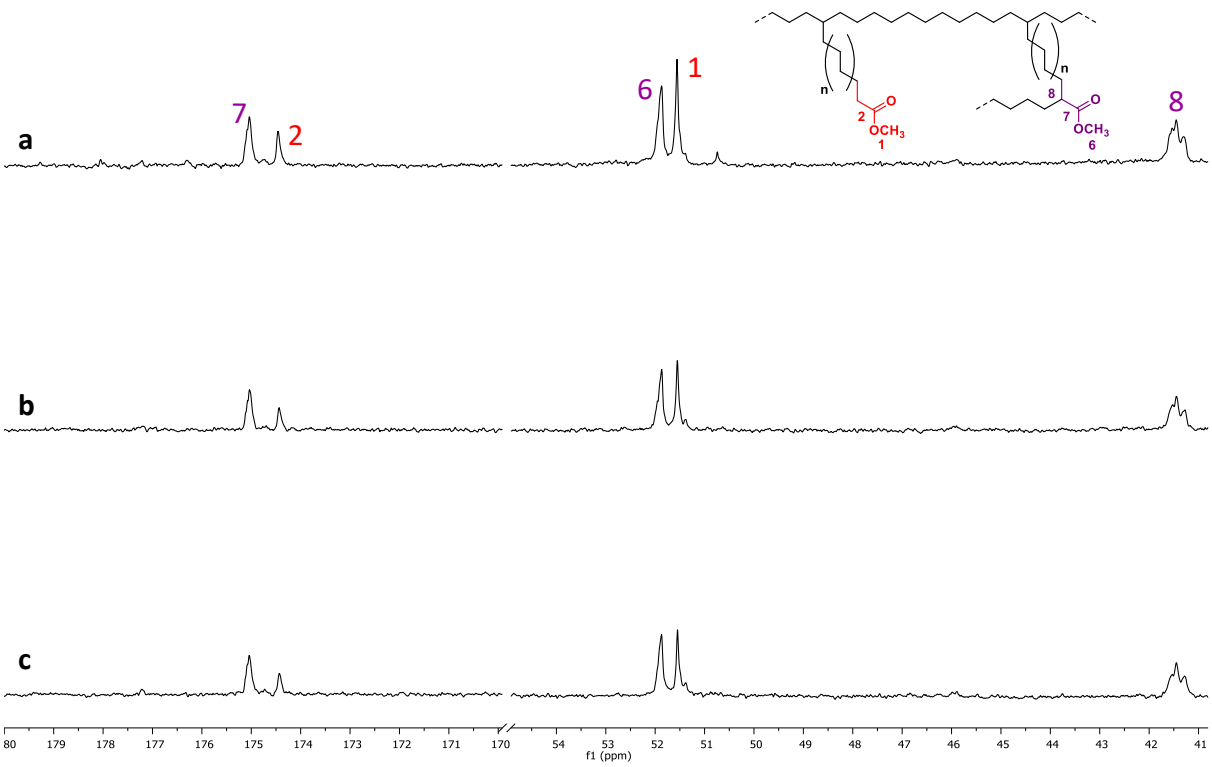

Figure S4.17. ^{13}C NMR spectra ($CDCl_3$, 298 K) of E/MA copolymers obtained with **1**^{pyr} in CH_2Cl_2 with increasing ethylene pressure (Table S4.2): (a) 2.5 bar, (b) 5.0 bar and (c) 7.0 bar); (left) carbonyl region; (right) methoxy and methinic region.

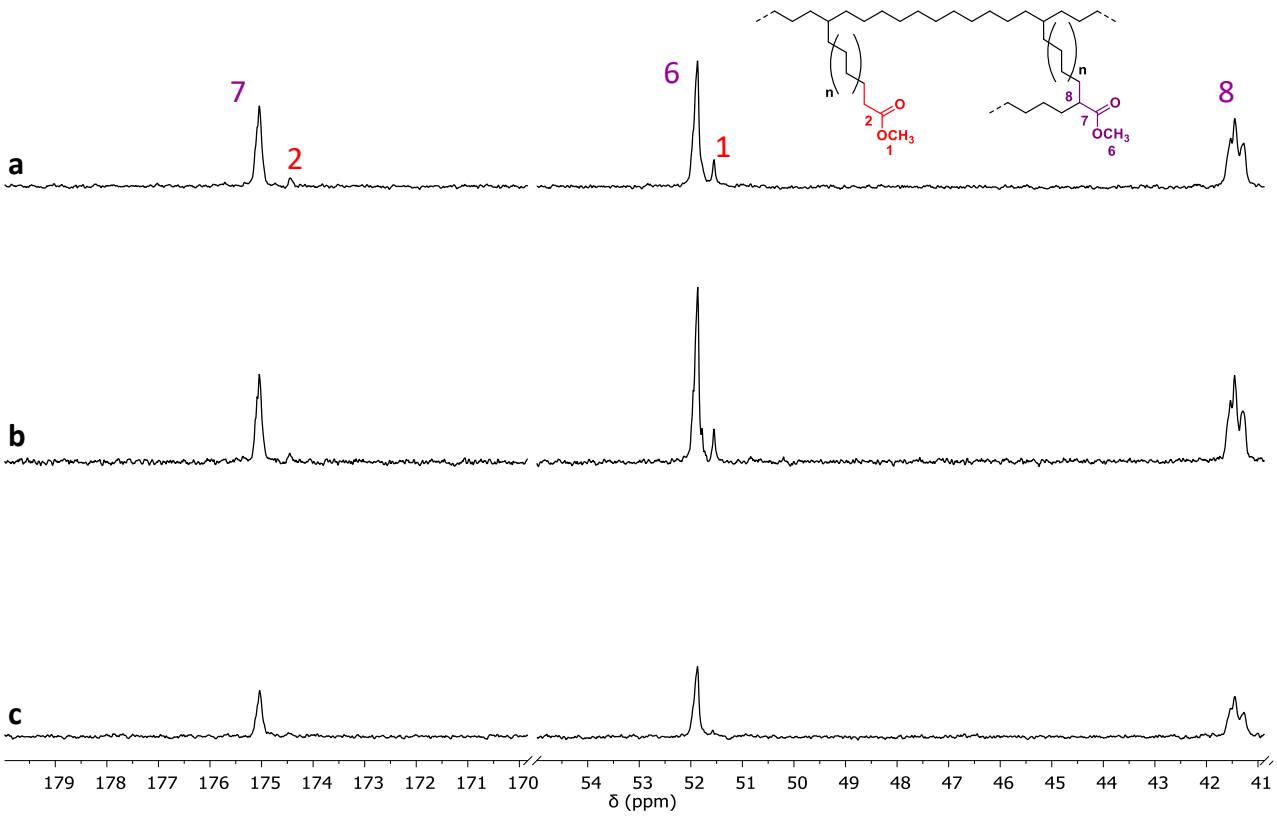

Figure S4.18. ^{13}C NMR spectra ($CDCl_3$, 298 K) of E/MA CP obtained with **2^{pyr}** in CH_2Cl_2 with increasing [MA]/[Pd] ratio (Table S4.5): (a) 594, (b) 1188 and (c) 1782); (left) carbonyl region; (right) methoxy and methinic region.

***In situ* NMR reactivity.**

***In situ* NMR reactivity of 1^{4pic} with ethylene (CD_2Cl_2, 298 K).**

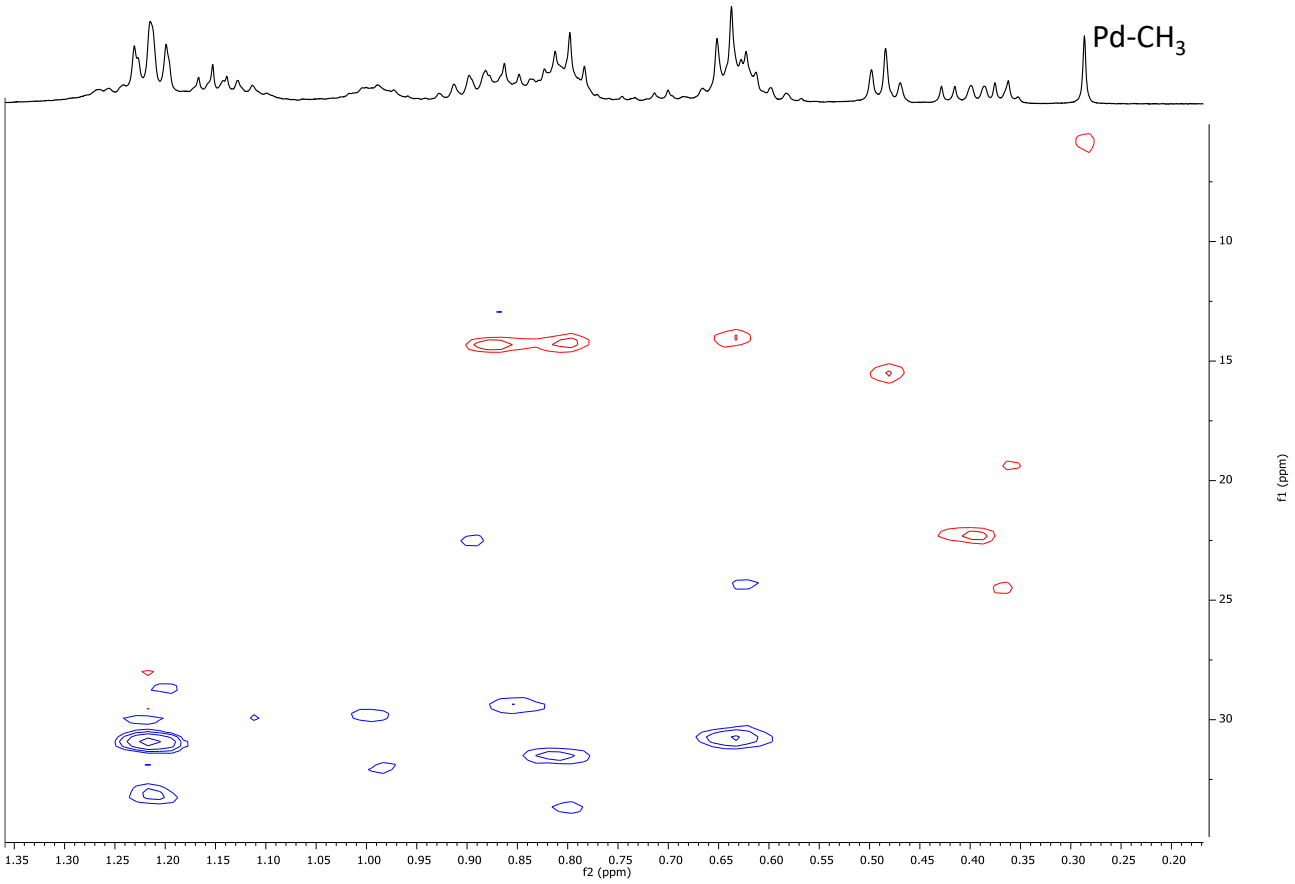

Figure S4.19. $^{1}H,^{13}C$ HSQC spectrum (CD_2Cl_2, 298 K) of the reaction mixture of $\mathbf{1^{4pic}}$ + ethylene at t = 1 h; aromatic region.

***In situ* NMR reactivity of 1^{4pic} with methyl acrylate (CD_2Cl_2, 298 K).**

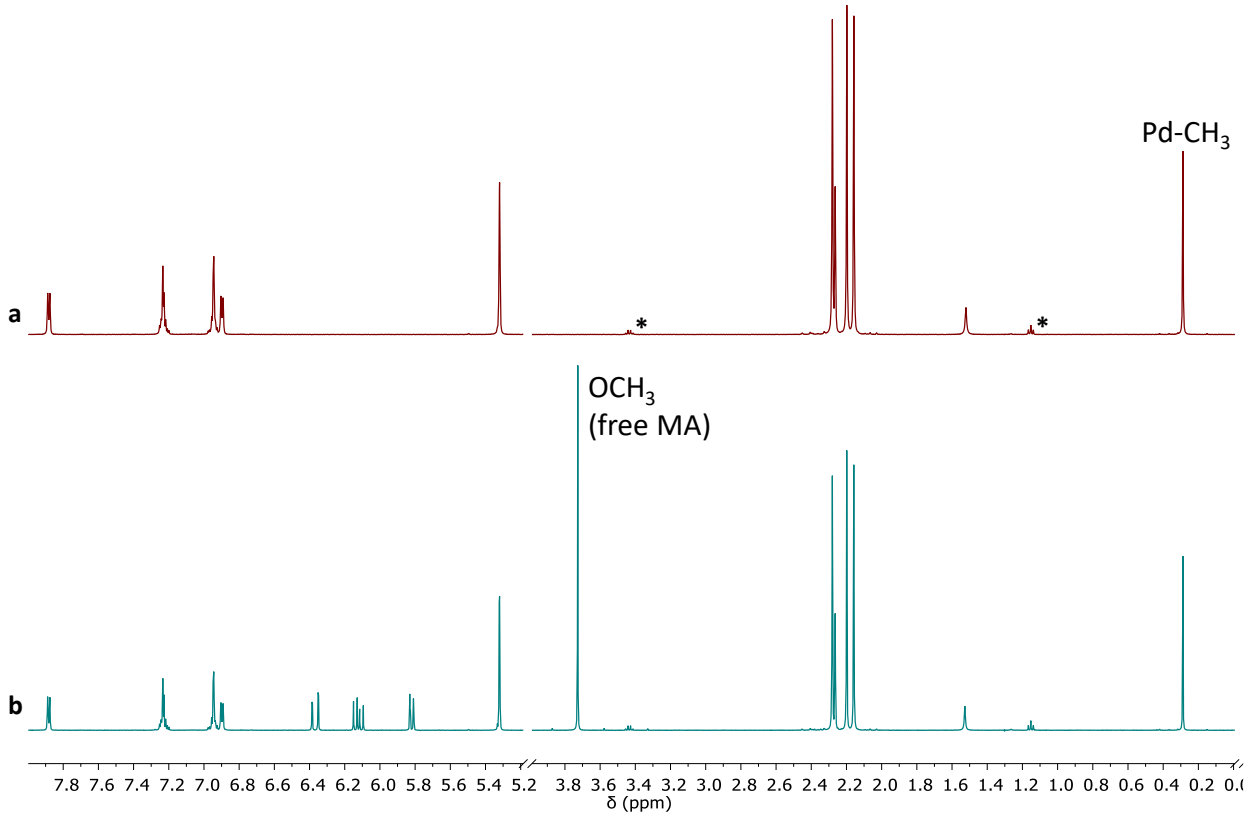

Figure S4.20. ^{1}H NMR spectra (CD_2Cl_2, 298 K) of (a) $\mathbf{1^{4pic}}$ and (b) $\mathbf{1^{4pic}}$ + MA at t = 1 h; *diethyl ether.

***In situ* NMR reactivity of 1^{4pic} with methyl acrylate and ethylene (CD_2Cl_2, 298 K).**

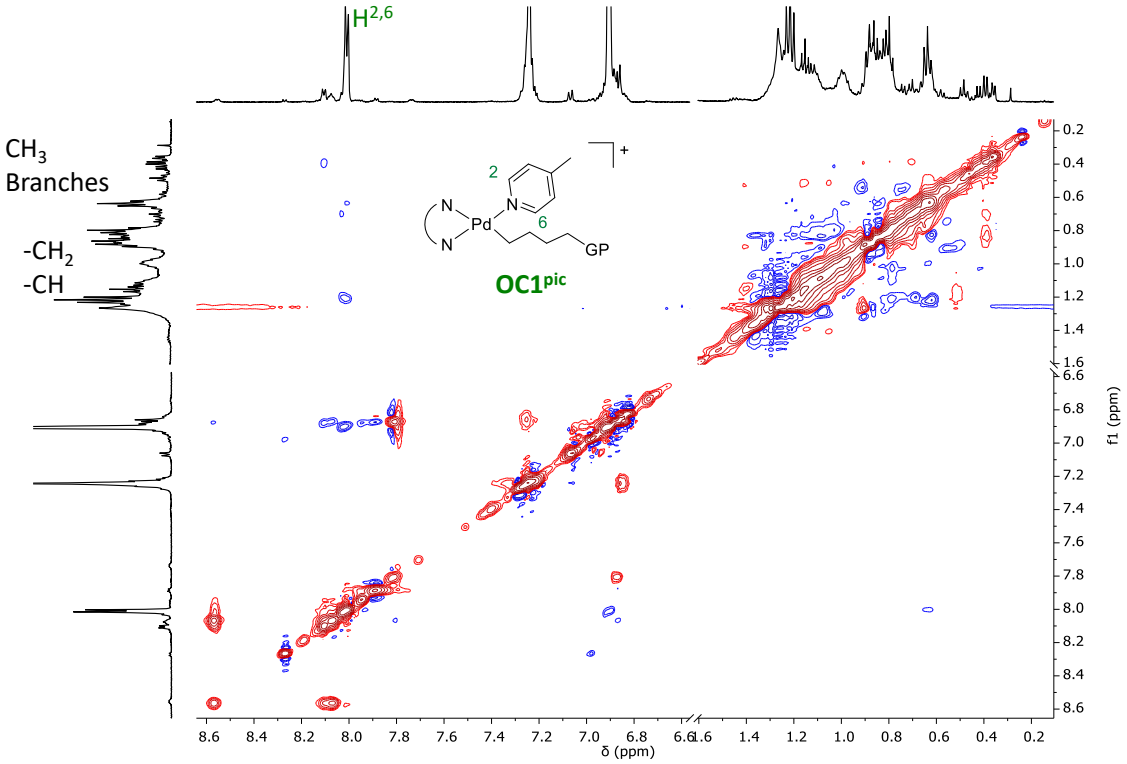

Figure S4.21. $^{1}H,^{1}H$ NOESY spectrum (CD_2Cl_2, 298 K) of the reaction mixture of $\mathbf{1^{4pic}}$ with MA and ethylene at t = 90 min.

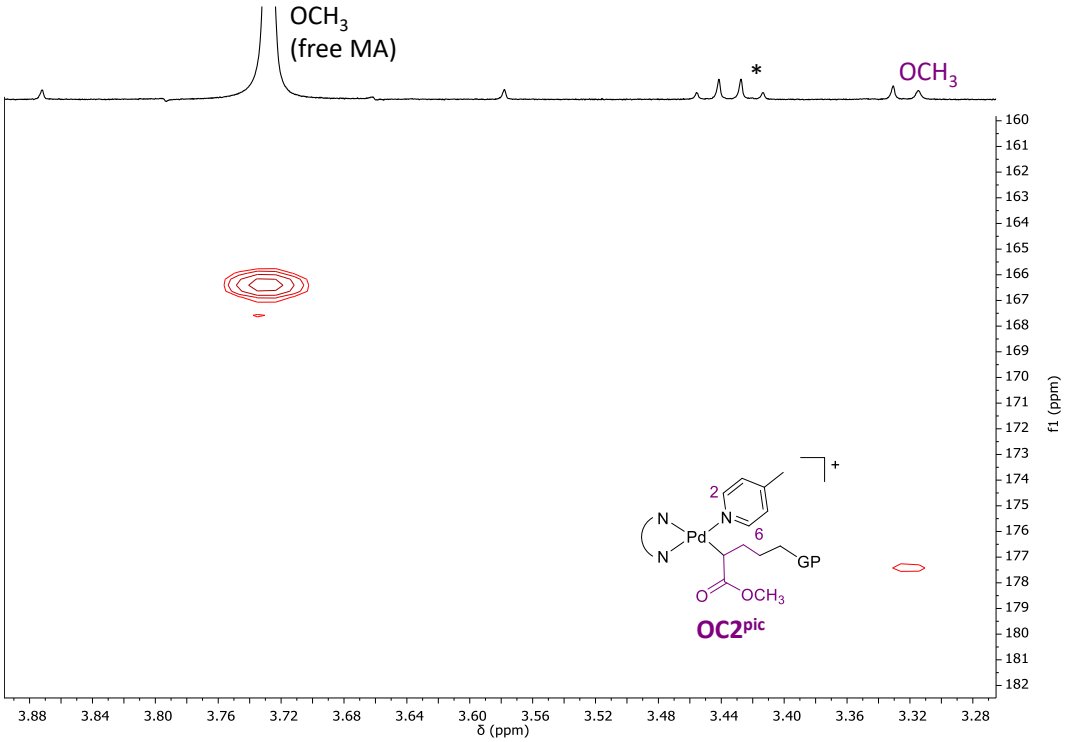

Figure S4.22. $^{1}H,^{13}C$ HMBC spectrum (CD_2Cl_2, 298 K) of the reaction mixture of $\mathbf{1^{4pic}}$ with MA and ethylene at t = 90 min; carbonyl region; *diethyl ether.

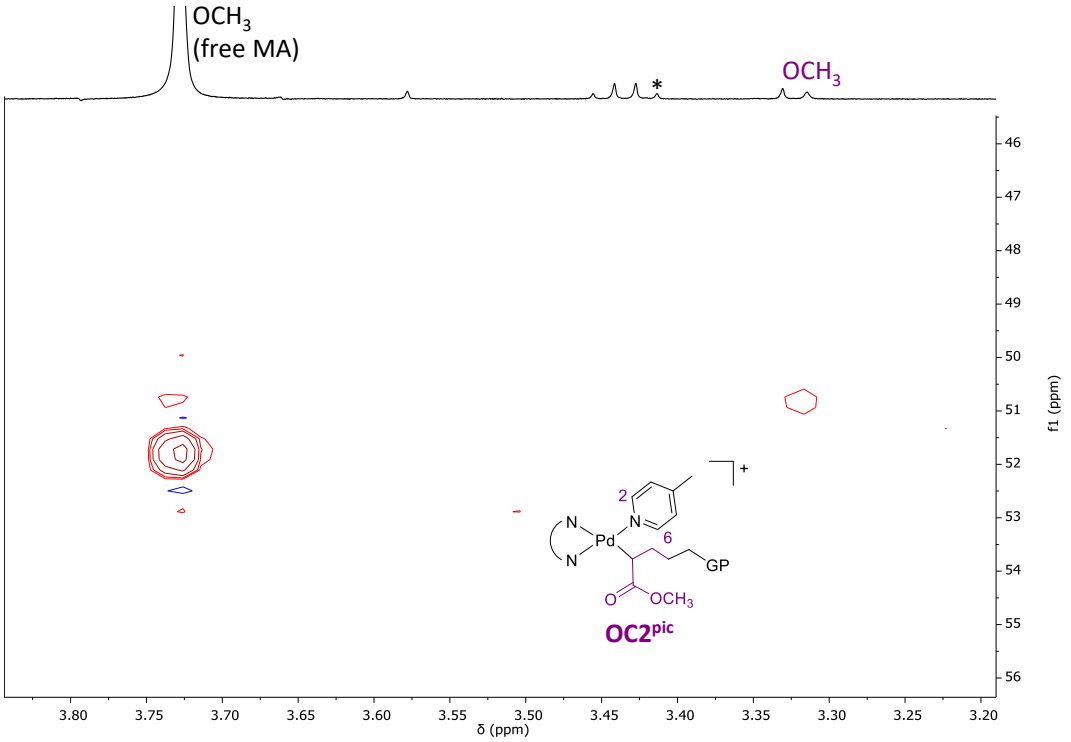

Figure S4.23. $^{1}H,^{13}C$ HSQC spectrum (CD_2Cl_2, 298 K) of the reaction mixture of **1^{4pic}** with MA and ethylene at t = 90 min; methoxy region; *diethyl ether.

Computational details.

Chart S4.1. The possible metallacycles originated from the insertion of methyl acrylate into the Pd-alkyl chain from **1b**.

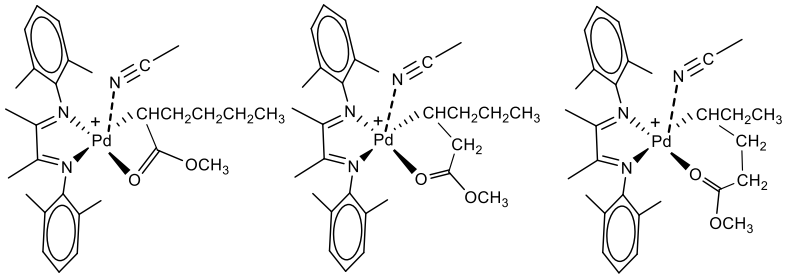

References

(1) Takano, S.; Takeuchi, D.; Osakada, K.; Akamatsu, N.; Shishido, A. *Angew. Chemie - Int. Ed.* **2014**, *53* (35), 9246–9250.

(2) Cruz, T. F. C.; Figueira, C. A.; Veiros, L. F.; Gomes, P. T. *Organometallics* **2021**, *40* (15), 2594–2609.

Appendix Chapter 5.

***In situ* NMR reactivity.**

***In situ* NMR reactivity of 8a with NaBArF and methyl acrylate (CD_2Cl_2, 298 K).**

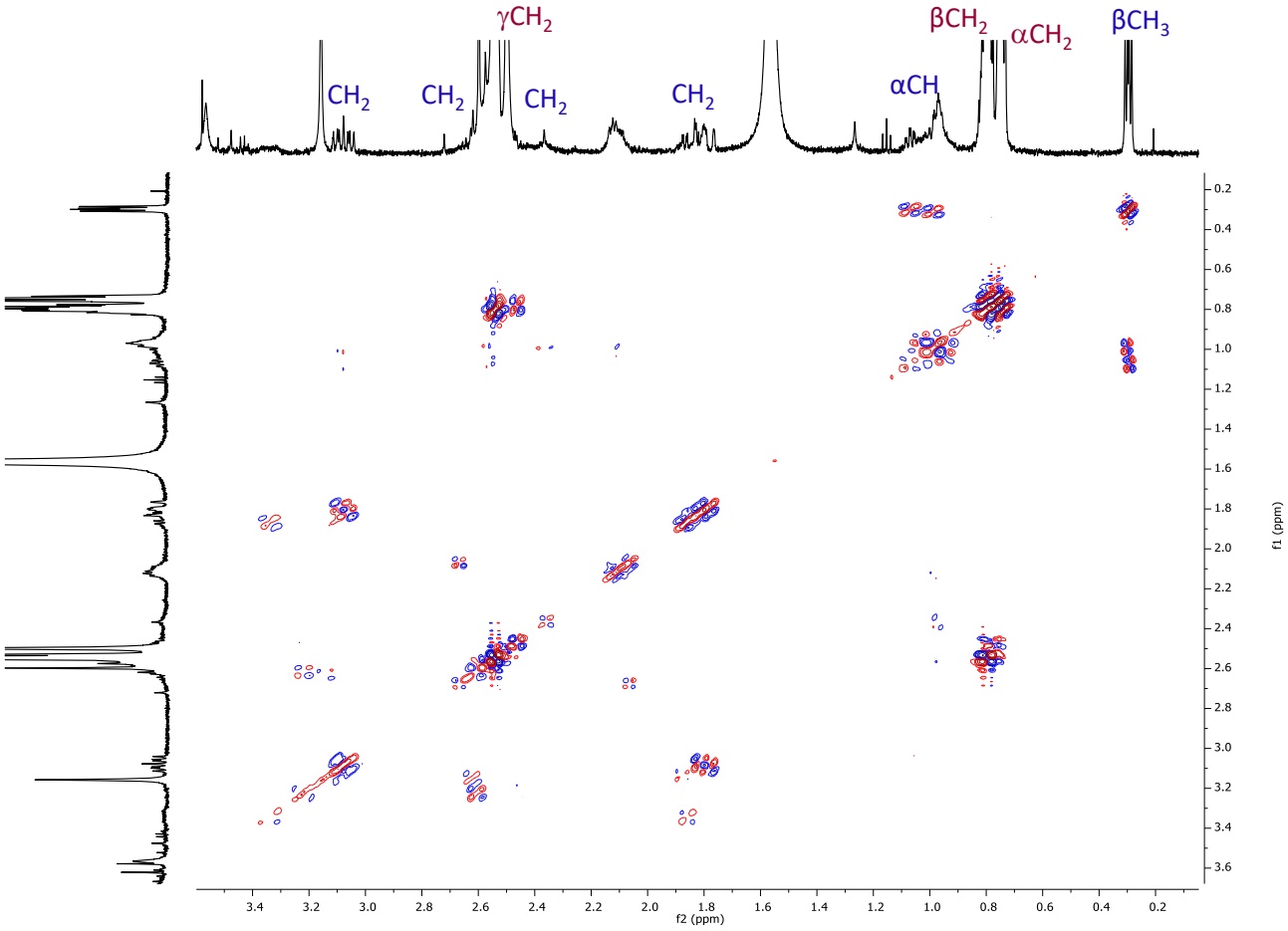

Figure S5.1. $^1H,^1H$ DQCOSY (CD_2Cl_2, 298 K) of the mixture of **8a**, NaBArF and MA at t = 30 min; aliphatic region.

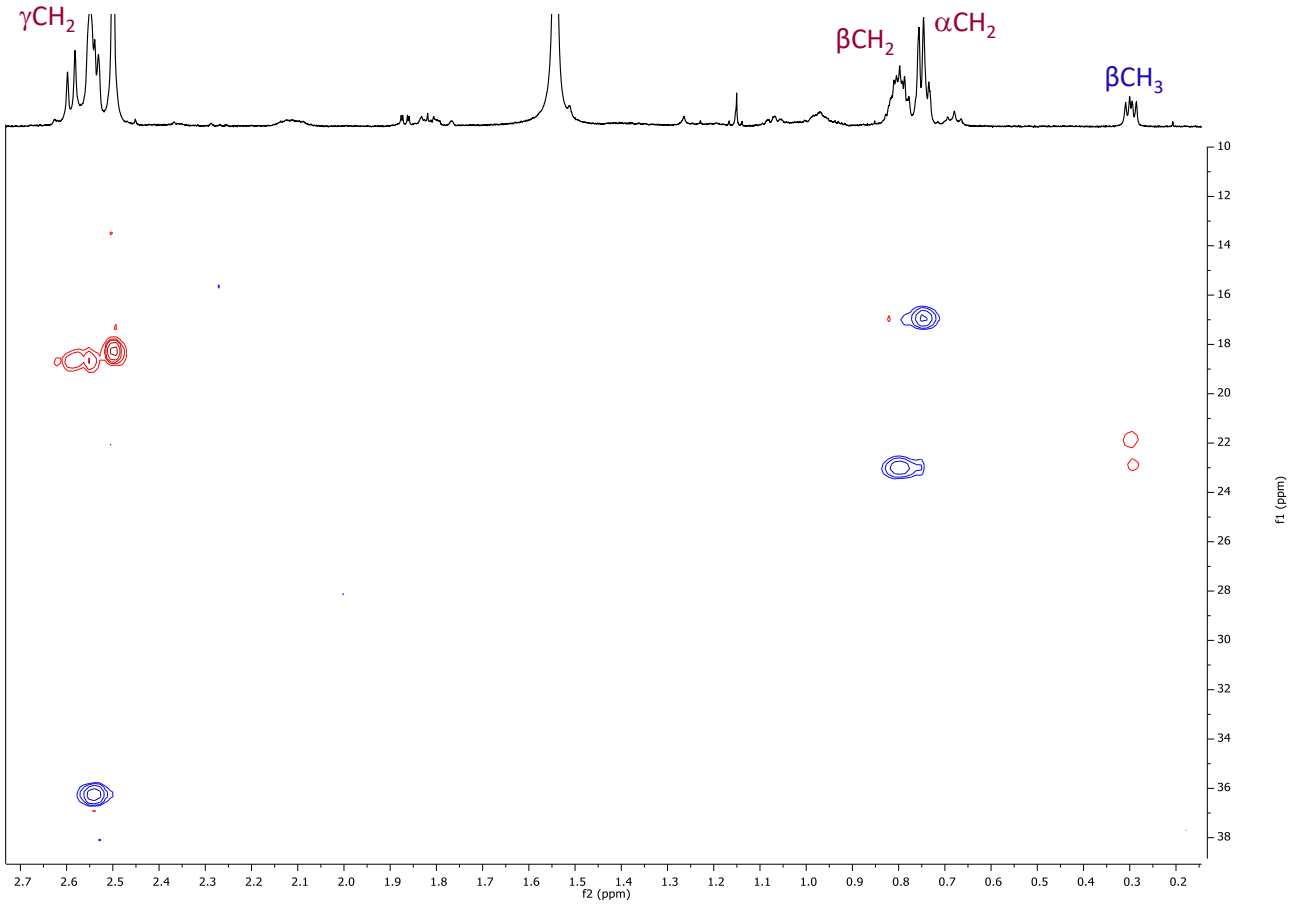

Figure S5.2. $^{1}H,^{13}C$ HSQC (CD_2Cl_2, 298 K) of the mixture of **8a**, NaBArF and MA at t = 30 min; aliphatic region.

***In situ* NMR reactivity of 8c with methyl acrylate (CD_2Cl_2, 298 K).**

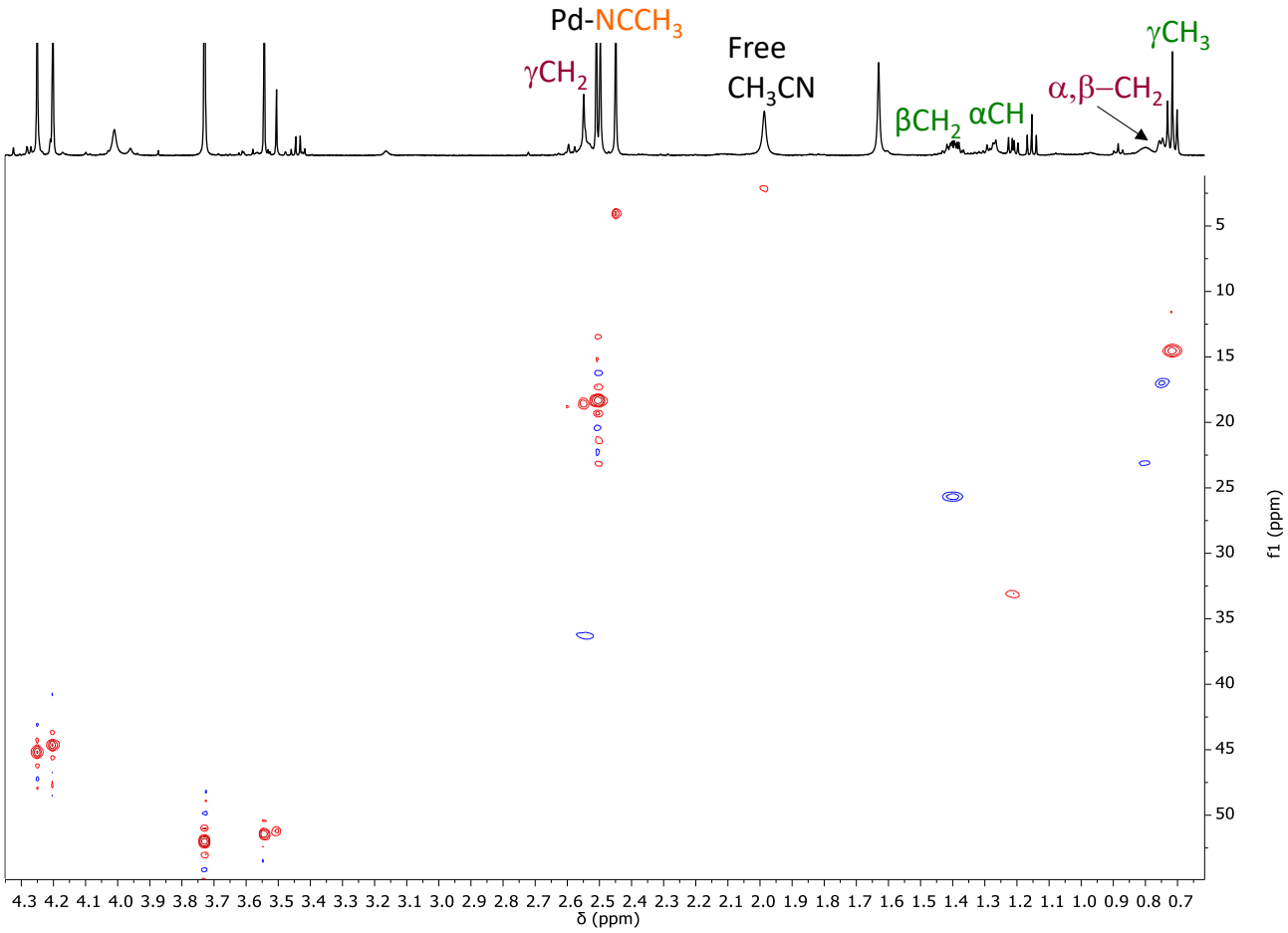

Figure S5.3. $^{1}H,^{13}C$ HSQC (CD_2Cl_2, 298 K) of the mixture of **8c** and MA at t = 30 min; aliphatic region.

***In situ* NMR reactivity of 8a with NaBArF, methyl acrylate and acetonitrile (CD_2Cl_2, 298 K).**

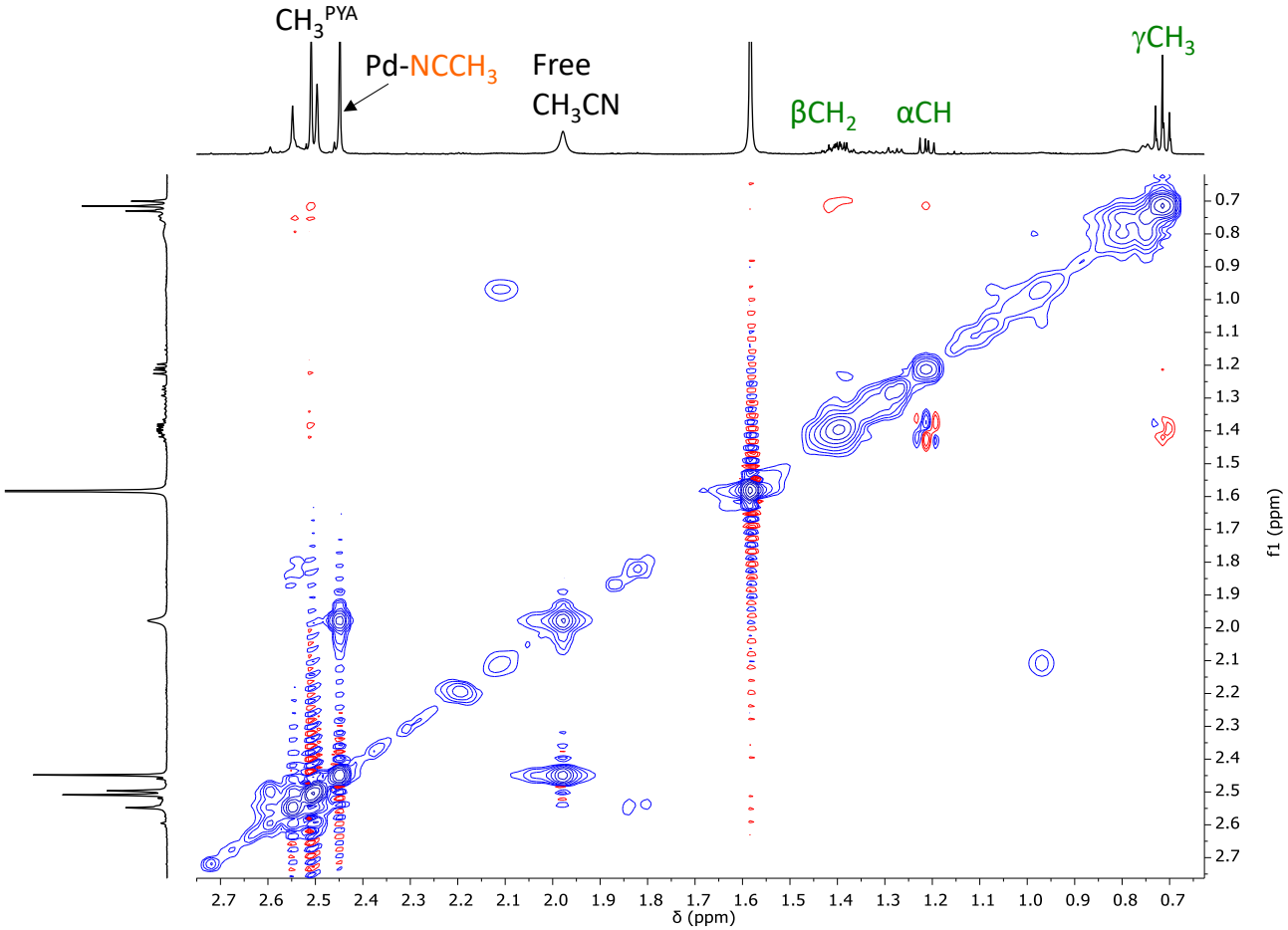

Figure S5.4. $^1H,^1H$ NOESY (CD_2Cl_2, 298 K) of reaction of **8a** with NaBArF, MA and CH_3CN (1 eq.) at t = 30 min.

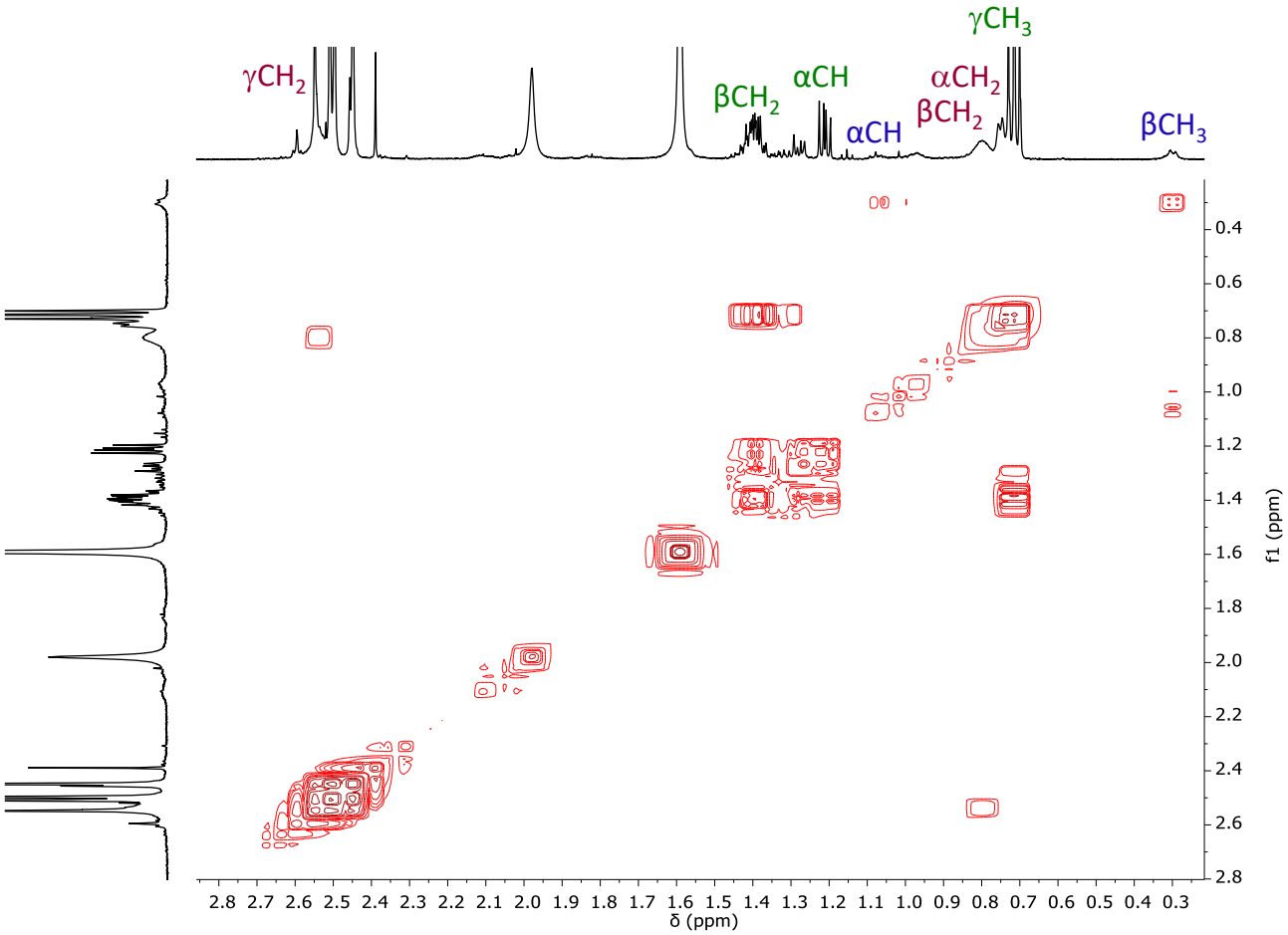

Figure S5.5. $^{1}H,^{1}H$ COSY (CD_2Cl_2, 298 K) of reaction of **8a** with NaBArF, MA and CH_3CN (1 eq.) at t = 30 min.

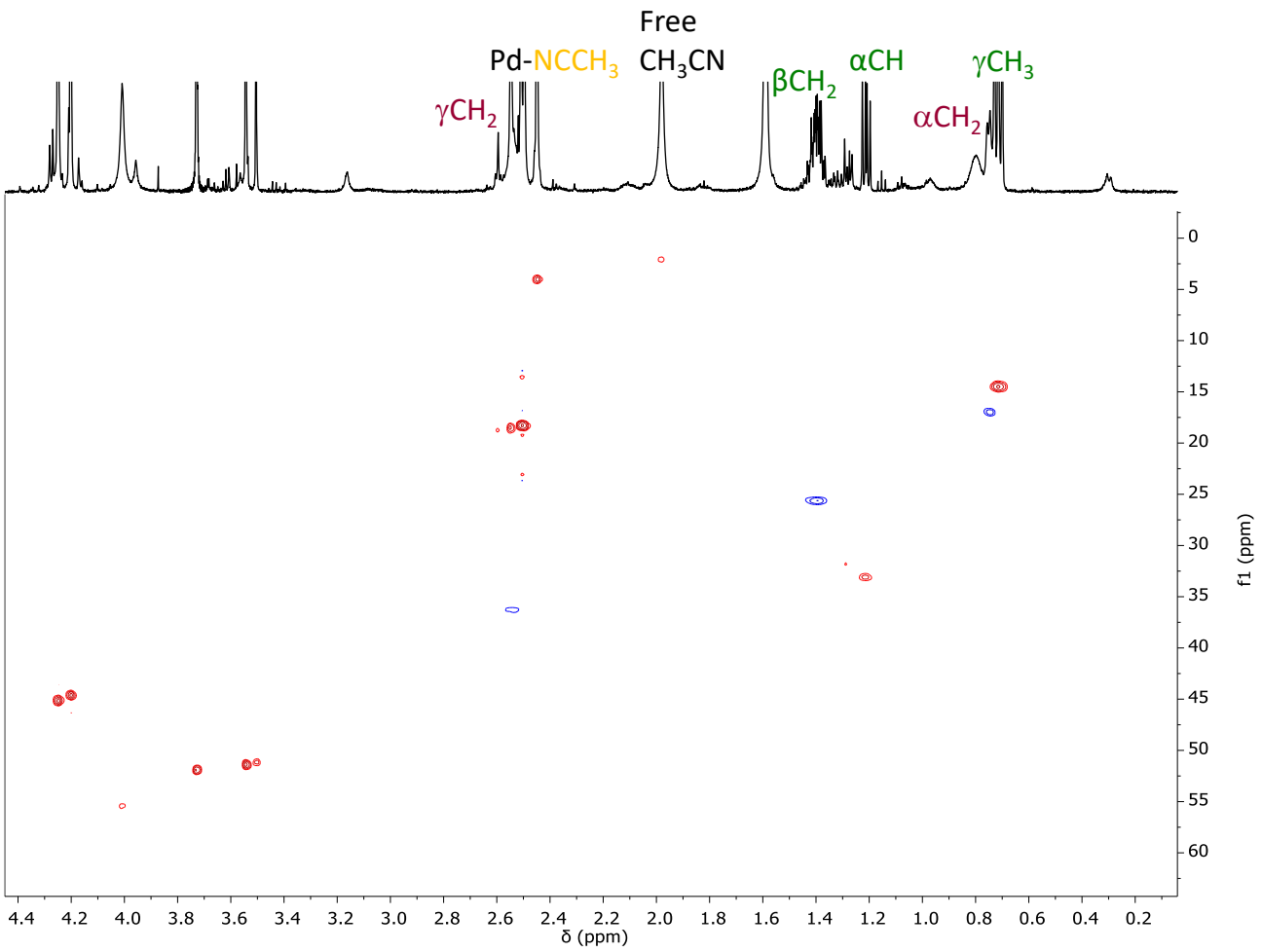

Figure S5.6. $^{1}H,^{13}C$ HSQC (CD_2Cl_2, 298 K) of reaction of **8a** with NaBArF, MA and CH_3CN (1 eq.) at t = 30 min.

***In situ* NMR reactivity of 8a with NaBArF and *N,N*-dimethylacrylamide (CD_2Cl_2, 298 K).**

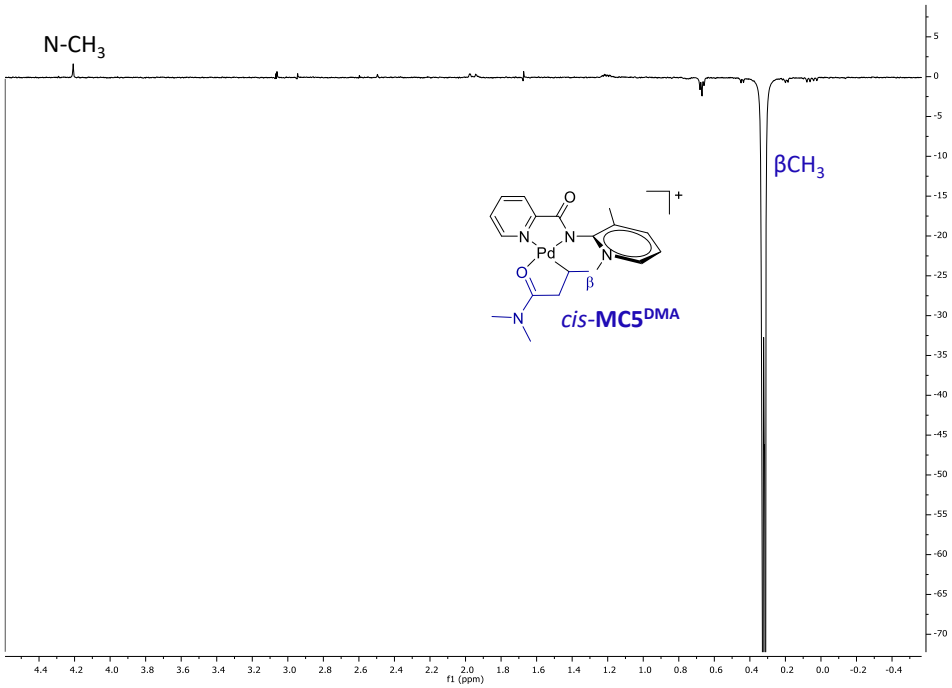

Figure S5.7. 1D NOE (CD_2Cl_2, 298 K) of reaction of **8a** with NaBArF and DMA at t = 30 min.

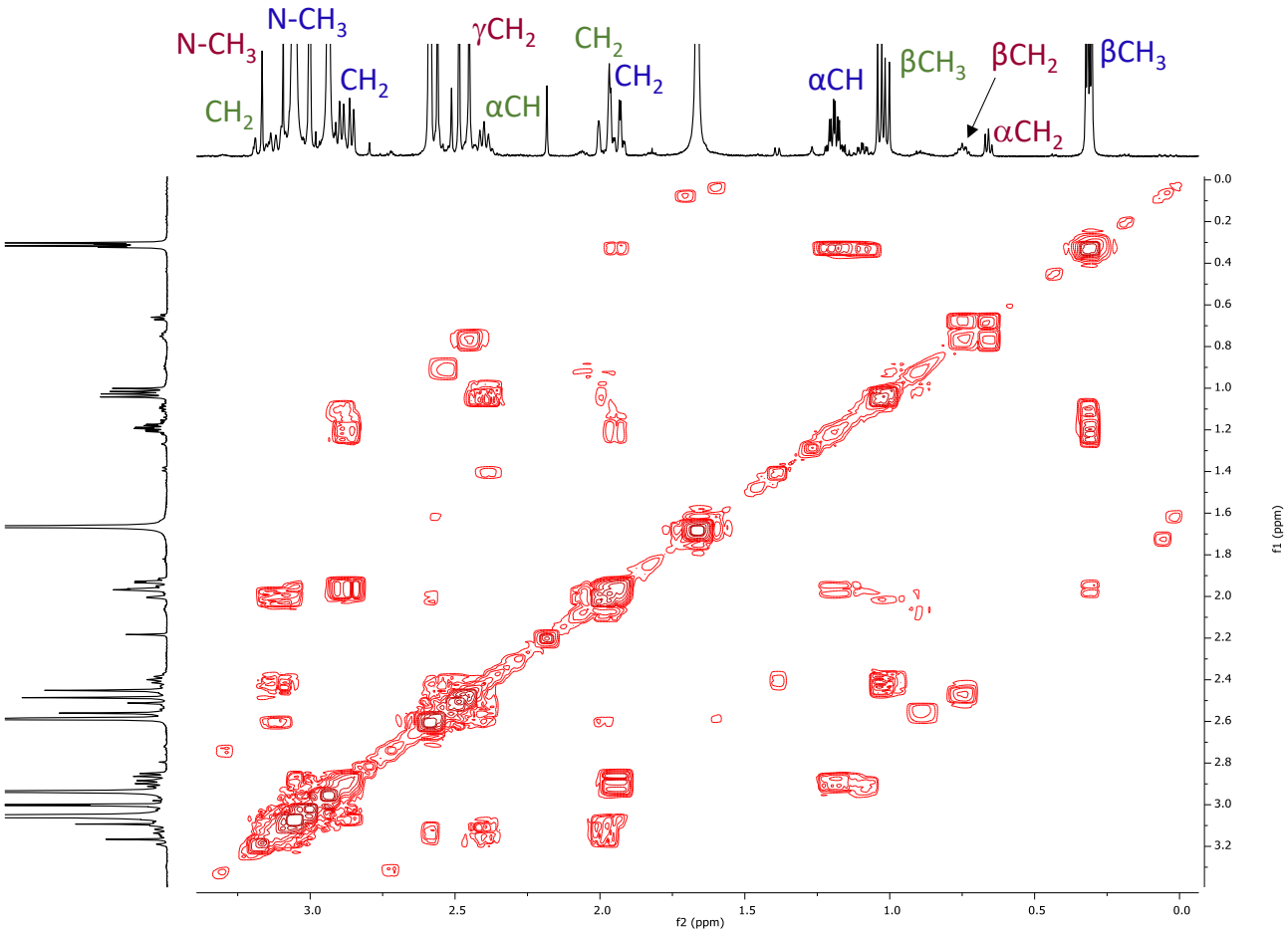

Figure S5.8. $^1H,^1H$ COSY (CD_2Cl_2, 298 K) of the mixture of **8a**, NaBArF and DMA at t = 30 min.

X-ray crystallography

Table S5.1. Selected distances, angles and dihedral angles of the *trans*-MC5^{DMA}.

Selected distances (Å)	
Pd1-C2	1.998(9)
Pd1-N1	2.027(7)
Pd1-N2	2.121(8)
Pd1-O1	2.032(7)
C1-C2	1.511(1)
C2-C3	1.608(1)
C3-C4	1.490(2)
C4-O1	1.259(1)
C4-N4	1.305(1)
C5-N4	1.505(2)
C6-N4	1.416(2)
C12-O2	1.200(1)
C12-N2	1.335(1)
C13-N2	1.353(1)
C13-N3	1.362(1)
C17-N3	1.330(2)
C19-N3	1.541(2)
Selected angles (°)	
C2-Pd1-O1	83.5(4)
N1-Pd1-N2	79.7(3)
C1-C2-C3	106.5(9)
C1-C2-Pd1	105.4(7)
C4-N4-C5	119.8(1)
C4-N4-C6	121.0(1)
C5-N4-C6	119.0(1)
Selected dihedral angles (°)	
[N^{PYA}] --- [Pd1]	86.1(3)
[N^{DMA}] --- [Pd1]	8.9(5)

***In situ* NMR reactivity of 8a with NaBArF, *N*,*N*-dimethylacrylamide, ethylene and carbon monoxide (CD_2Cl_2, 298 K).**

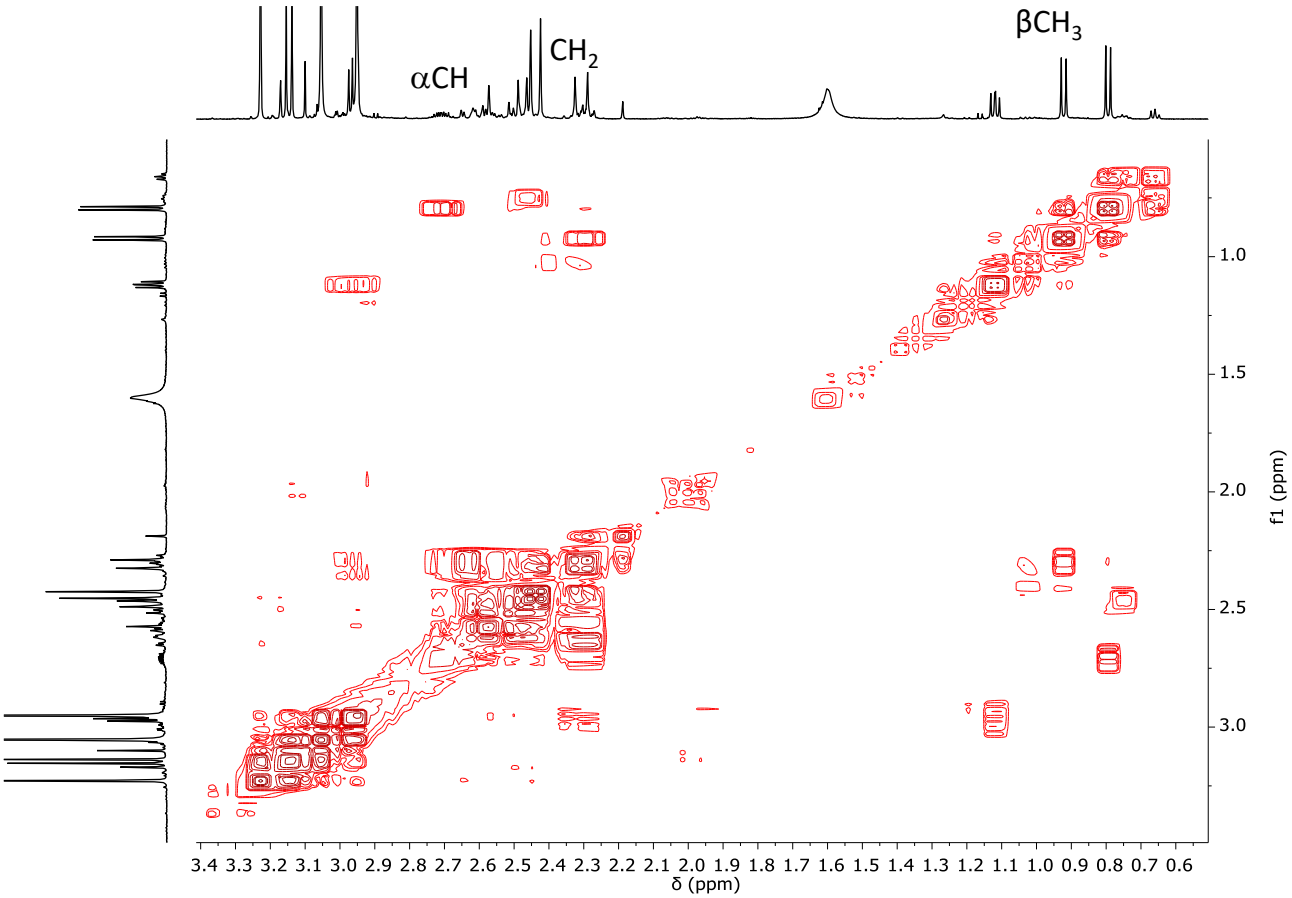

Figure S5.9. $^1H,^1H$ COSY (CD_2Cl_2, 298 K) of the mixture of **8a**, NaBArF, DMA, ethylene and CO at t = 5 min.

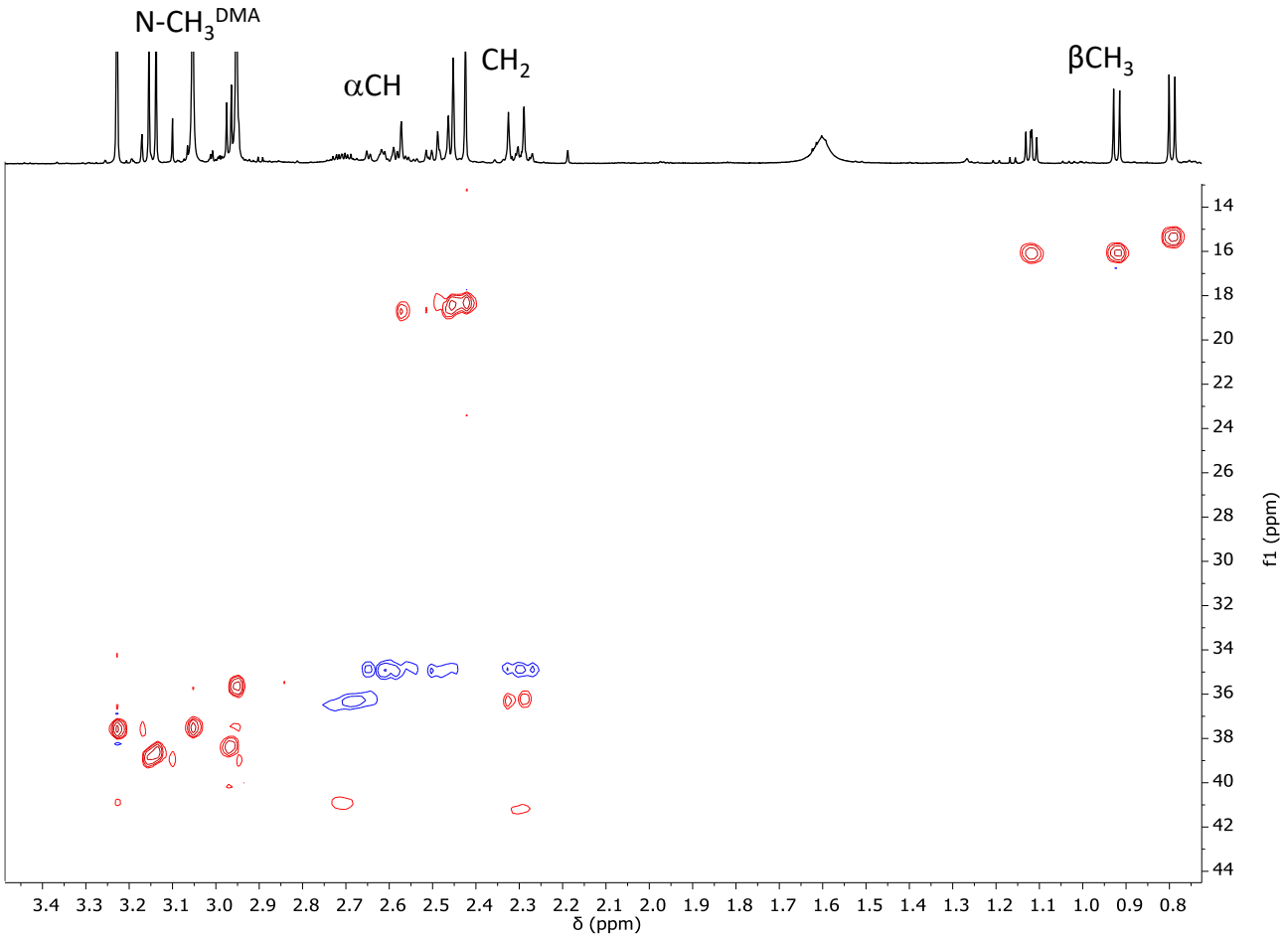

Figure S5.10. $^{1}H,^{13}C$ HSQC (CD_2Cl_2, 298 K) of the mixture of **8a**, NaBArF, DMA, ethylene and CO at t = 5 min.